UNIVERSITEIT GENT

FACULTEIT WETENSCHAPPEN

Vakgroep Geologie en Bodemkunde

Laboratorium voor Toegepaste Geologie en Hydrogeologie

Saltwater intrusion in the coastal strip of Dar es Salaam Quaternary aquifer, Tanzania

MTONI Yohana Enock

Thesis submitted in fulfillment of the requirements for the award of the degree of Doctor in Sciences: Geology

2012-2013

Promoter: Prof. Dr. K. Walraevens

The photo cover is for the area covering the main part of Dar es Salaam City Centre (source of photo: http://www.tatancasafaris.co.tz/circuit_coast.html)

To refer to this thesis:

Mtoni, Y. (2013). Saltwater intrusion in the coastal strip of Dar es Salaam Quaternary aquifer, Tanzania. PhD thesis, Ghent University, Faculty of Sciences, Belgium, 395 pp.

DEDICATION

This thesis and all of the years spent working to complete this work is dedicated to:

i) my lovely wife "Zainab", my daughter "Lizbeth" and my son "Albert"

ii) the memory of my father "Enock Mtoni "(1922-2002) and my mother "Elizabeth Nyakarungu" (1933-2013). Their words of inspiration in pursuit of excellence still remain.

ACKNOWLEDGEMENTS

Firstly, I thank God the mighty for giving me the strength and endurance to complete this research. Much praise is extended to Him, for He made heaven and earth, the sea and springs of water (Revelation 14:7).

I am highly indebted to my promoter Prof. Dr. Kristine Walraevens (Head of the Laboratory for Applied Geology and Hydrogeology, Ghent University "UGent") for her supervision both prior (during MSc. studies) and during my PhD research. Her unreserved guidance, support, fruitful suggestions, constructive criticism have given me more insight in this research. Likewise, I would like to express my deepest appreciation to my co-promoter Dr. Ibrahimu C. Mjemah (Head of the Department of Physical Science, Sokoine University of Agriculture (SUA), Tanzania) for his advices during the formulation of research proposal, guidance in the execution of the research, critical review and suggestions during thesis preparation.

Financial support was central to the success of this study. I would like to express my special gratitude to the Belgian Technical Cooperation (BTC) for sponsoring my PhD study. My sincere thanks goes to Liesbet and Nicolas (BTC in Belgium) and Victor (BTC in Tanzania) for their close collaboration and financial arrangements throughout the study time. Similarly, I am very grateful to my employer, National Environment Management Council (NEMC) for granting me a study leave and for the support provided during the fieldwork in Tanzania. My special thanks goes to NEMC Director General, Eng. B.T. Baya, NEMC Ag. Director for Research and Planning, Dr. Fadhila Khatibu, Ag. Chief Administrative Officer, Suma Mwakabalile, Ag. Director Finance and Administration, Charles Wangwe and my fellow staff for their assistance during this study.

I am also grateful for the opportunity of participating in groundwater research project in Dar es Salaam under Research Initiatives Programme (RIP) of VLIR (The Interuniversity Council), undertaken in collaboration between the Ghent University (Belgium) and Sokoine University of Agriculture (Tanzania).

I would like to thank my fellow researchers, Niels Dejager and Ine De Witte who conducted their MSc thesis research in the same study area: their participation contributed much success to the data collection process. Many thanks go to my fellow authors, Kristine Walraevens,

Ibrahimu Mjemah, Kristine Martens, the Late Kristoko Msindai, Marc Van Camp and Charles Bakundukize: their discussion and ideas were absolutely significant for producing good articles. I also take this moment to give my sincere thanks to the Geology Department, University of Dar es Salaam (UDSM) for the in-depth information about the study area that I received from Dr. Msindai (who passed away on 29th July 2011). His support and many thoughts and ideas about the subject of research during my fieldwork were very great. It was indeed a sad moment to see a friend/supervisor and my BSc (Geology) teacher dying at the moment nobody expected. I will remember him always for his invaluable and tireless effort in advising and supporting me in my study.

I would like to express my deepest and sincere appreciation to Marc Van Camp for his expertise and invaluable time spent in assisting to develop a conceptual model for understanding the saltwater transport processes occurring in the study area. I am grateful to Jill Van Reybrouck, the laboratory chemist of the Laboratory for Applied Geology and Hydrogeology (UGent) for her great effort spent in analyzing water samples. I wish to extend thanks to Dr. Kristine Martens (UGent) for her valuable comments to this study and for travelling from Belgium to Tanzania to give assistance in carrying out the geophysical survey. Dr. Flora Magige (UDSM) is thanked for encouragement and provision of materials and relevant books for my research topic.

Thanks are due to the Drilling and Dam Construction Agency (DDCA) and Ministry of Water and Irrigation (MoWI) for giving access to borehole/well drilling reports and sharing their in-depth experience and knowledge of the study area. Additional thanks go to Jovit Josephat and Arnold Kessy for their guidance during the field work mainly for identifying boreholes. Resident and boreholes owners are thanked for the cooperation given for accessing their boreholes. The fieldwork campaign for data collection would have not been successful without great help from Dar es Salaam Municipalities: Temeke, Kinondoni, and Ilala for the assistance provided during the field campaign while visiting the boreholes/wells and for providing data and useful suggestions. Many thanks go to Gymkhana Golf Club for giving the permission to conduct geophysical survey at their premises and providing boreholes which enabled groundwater monitoring. Likewise the management and staff of Coca-Cola Company, Zanaki Secondary school, Mnazi Mmoja Primary school, Bunge Dar es Salaam offices, and other institutions are all thanked for allowing access to their boreholes/wells during data collection.

I am indebted to the other members of the Jury: Prof. Dr. Jacques Verniers (UGent, Belgium), Dr. Maurizio Polemio (CNR-IRPI, Italy), Prof. Dr. Morgan De Dapper (UGent, Belgium), Dr. Alexander Vandenbohede (UGent, Belgium), Dr. Kristine Martens (UGent, Belgium), Dr. Ibrahimu Mjemah (SUA, Tanzania) and Prof. Dr. Kristine Walaraevens (UGent, Belgium) for their acceptance to be members of the jury of my PhD thesis as well as reading the manuscript. Their thoughtful review and keen comments were fundamental for the completion of this work.

I wish to express my sincere thanks goes to all my sisters and brothers who supported and encouraged me throughout my study. My brother Dr. Paul Mtoni (SUA) is acknowledged for his invaluable comments during the formulation of my research proposal and also for providing me his car for fieldwork the moment my car broke down. I would like to express my special thanks and appreciation to my brother Mussa Mtoni and his family members for their love and especially for being close to my family the moment I was away. Dr. Isaac Mtoni is thanked for his plenty friendly encouragement and to his frequent calls (especially on the weekends) and important updates of what was happening in Tanzania.

Last but not least, I owe much to my wife Zainab and my daughter Lizbeth for their support and encouragements. Every year for the period of 4 years, I had to travel and stay in Belgium for some months for laboratory analysis, data analysis and thesis write-up. My son Albert was born (on 28th March 2012) in Tanzania the moment I'm in Belgium and it passed 4 months to meet him physically. Many thanks to my family for tolerating and accepting my apologies for my absence and for unconditional support and love throughout my academic endeavors.

Finally, many thanks to Ghent Seventh Day Adventist Church members and the Tanzania community in Ghent (Tz Ghent) for their encouragements that have served as an important source of inspiration and motivation.

Thank you all!!

Mtoni, Y.E Ghent, March, 2013

SUMMARY

The main objective of this research was to assess the current state of water quality in the coastal strip of Dar es Salaam Quaternary coastal aquifer (DQCA), especially in view of sea water intrusion. Dar es Salaam City, a home of over 4 million people, is located above productive DQCA. The fact that the city receives inadequate surface water supplies, the use of groundwater has become increasingly important for domestic, irrigation and industrial purposes. However, threat exists associated with groundwater over-exploitation that leads to the intrusion of seawater. Water balance for DQCA was calculated according to the method of Thornthwaite and Mather. The groundwater replenishment under natural infiltration is about 186 mm (72.17 x 10^6 m^3 $year^{-1}$) indicating that only 16.7% of the long term average annual precipitation of 1114 mm ends up as groundwater recharge. Estimated total groundwater abstraction is approximately 69.3 x 10^6 m^3 $year^{-1}$. The water balance suggests an average sustainable yield of 28.67 x 10^6 m^3 $year^{-1}$ (calculated as 40% of natural groundwater recharge). This indicates DQCA is clearly over-exploited.

The hydraulic parameters were evaluated based on the analysis of constant-rate pumping tests. The average transmissivity (T) and hydraulic conductivity (K) deduced from curve fitting methods is 138.52 m^2/d and 4.27 m/d for unconfined aquifer respectively: the average T and K values obtained for semi-confined aquifer is 79.0 m^2/d and 1.7 m/d respectively. T and K values for the unconfined aquifer range from 24.45 m^2/d to 296.58 m^2/d and from 0.76 m/d to 8.47 m/d respectively. T and K values for the semi-confined aquifer range from 13.75 m^2/d to 130.44 m^2/d and from 0.43 m/d to 2.61 m/d respectively. T and K values vary reflecting the type of lithology in which the well is constructed. Piezometric maps indicate a general lowering of the piezometric level especially in areas close to the coastline. The lowest values are located along the coast at areas such as Kawe, City Centre and Msasani. The highest water levels are found in the west (in the direction to Pugu Hills) and southwest (towards Mbagala) of the study area. Interpretation of data for daily fluctuation of groundwater level identified changes in water levels are due to natural phenomena such as rainfall, tides (strong near the coastline) and evapotranspiration (more important at Mnazi Mmoja Primary School and Temeke Municipal Garden), and to human influences (i.e. pumping).

Geophysical data supported by groundwater hydrogeochemical data and groundwater hydrochemical/lithological sections, have enabled to draw a map showing the depth of the freshwater/saltwater interface. Vertical electrical soundings (VES) curves and resistivity profiles have shown a decrease of resistivity (thus increasing salinity) with depth and towards the coastline. Cross-sections have shown the presence of salt water in the aquifer near the coastline and the boundary between fresh and saline waters is marked. Salt water was found mostly in the area within 2 km of the coastline, and the depth to the interface is ranging from 1.3 m to 20 m. Away from the coastline, the interface (if present) is at greater depth that could not be reached. However, in the south of the study area, the VES executed at Kurasini (located 4 km from the sea), showed the freshwater/interface at a greater depth (43 m). Depth variation of resistivity logs was as well observed. In the west of the study area (about 2.7 km from the coastline) the resistivity logging was conducted up to the depth of 37 m but the saltwater interface (if present) was not reached.

The hydrogeochemical processes operating in DQCA system have been investigated through 196 groundwater samples sampled between 2009 and 2012 and analysed for major cations and anions. Piper diagrams for groundwater samples show changes towards seawater. A large proportion of the groundwater is classified as Na–Cl. The Durov diagram undoubtedly shows the modification of water types from fresh recharge-$CaHCO_3$ end member to saline-NaCl end member, where the end members are mixed in different proportions. Stuyfzand classification clearly shows the significant geochemical differences between the area near the coastline and the area away from the coastline. Groundwater types are from the inland toward the coast: CaMix, NaMix, and NaCl, showing increasing influence of salinity. Maps of Cl^-/HCO_3^- ratio, Cl^- and electrical conductivity (EC) show chlorides and EC increasing towards the coast. ΔNa^+ for analysed samples indicates areas showing deficit of Na^+. Large number of samples with negative values is found north of Msimbazi River, at Kawe, Msasani, Masaki and Oysterbay: these samples are particularly those indicating highly saline water. South of Msimbazi River, large number of samples has positive values. Few samples indicate negative values located in City Centre at southern tip of peninsula in Mzinga estuary. Results from the hydrogeochemical investigation in the study area indicate that the DQCA is experiencing contamination primarily by seawater intrusion and the use of on-site sewage disposal systems, in particular pit latrines and septic tanks. Dissolution of calcite/dolomite minerals in the aquifer matrix as well as cation exchange also modify the concentration of ions in groundwater.

In this study, a conceptual model was established for understanding the saltwater transport processes occurring as the effect of pumping in the DQCA. In the situation where a semi-pervious layer is not present in the aquifer system, pumping in the upper part of the aquifer close to the shoreline, above the saline wedge, will cause upconing of the deep saline wedge. On the other hand, pumping in the upper part of the aquifer inland from the deep saline wedge, will first cause a further inland penetration of the saline wedge near the bottom, and then an upward upconing of the pronounced wedge. If no semi-pervious layer is present and pumping is conducted in the lower part of the aquifer, inland from the deep saline wedge, this will cause a further inland penetration of the saline wedge towards the pumping wells. In the situation where a semi-pervious layer is present, halfway the aquifer, pumping in the upper aquifer above the seawater wedge (near the bottom of the lower aquifer), will cause lateral intrusion of seawater. The semi-pervious layer prevents upconing of the deep saline wedge.

Several indications for saltwater intrusion were perceived and attributed to the overutilization of the aquifer. Most boreholes located close to the coastline, due to their high solute concentrations, are not suitable for domestic and irrigation use. These research results are useful for making better groundwater protection and exploitation plans for limiting the increasing saltwater intrusion and anthropogenic aquifer contamination. Enhancing and empowering the National Water Policy (NAWAPO, 2002) and the National Environmental Policy (NEP, 1997) objectives, providing appropriate sanitation, application of rational groundwater management practices, including the decrease of pumping rates, is crucial in attaining the sustainability of groundwater resources in the study area.

SAMENVATTING

Zoutwaterintrusie in de kuststrook van de Dar es Salaam Quaternary Aquifer, Tanzania

De hoofddoelstelling van dit onderzoek was de huidige toestand van de waterkwaliteit in de kuststrook van de Dar es Salaam Quaternary Coastal Aquifer (DQCA) te onderzoeken, vooral in het licht van zeewaterintrusie. Dar es Salaam City, met meer dan 4 miljoen inwoners, bevindt zich boven de productieve DQCA. Doordat de stad ontoereikende bevoorrading vanuit oppervlaktewater ontvangt, is het gebruik van grondwater in toenemende mate belangrijk geworden voor huishoudelijke, irrigatie- en industriële doeleinden. Nochtans bestaat de dreiging van grondwateroverexploitatie, die leidt tot de intrusie van zeewater. De waterbalans van DQCA werd berekend met de methode van Thornthwaite & Mather. De grondwatervoeding onder natuurlijke infiltratie bedraagt ongeveer 186 mm (72.17 x 10^6 m³ per jaar), zodat slechts 16.7% van de lange-termijn gemiddelde neerslag van 1114 mm bijdraagt tot de grondwatervoeding. De geschatte totale grondwateronttrekking bedraagt 69.3 x 10^6 m³ per jaar. De waterbalans suggereert een gemiddeld duurzaam onttrekkingspotentieel van 28.67 x 10^6 m³ per jaar (berekend als 40% van de natuurlijke grondwatervoeding). Dit geeft duidelijk aan dat de DQCA overgeëxploiteerd wordt.

De hydraulische parameters werden geëvalueerd op basis van de analyse van pompproeven met een constant debiet. De gemiddelde transmissiviteit (T) en hydraulische conductiviteit (K) afgeleid met curve-fitting methoden bedragen 138.52 m²/dag en 4.27 m/dag voor de niet-afgesloten aquifer en 79.0 m²/dag en 1.7 m/dag voor de halfafgesloten aquifer. T voor de niet-afgesloten aquifer varieert tussen 24.45 m²/dag en 296.58 m²/dag, terwijl K tussen 0.76 m/dag en 8.47 m/dag bedraagt. Voor de halfafgesloten aquifer varieert T tussen 13.75 m²/dag en 130.44 m²/dag en K tussen 0.43 m/dag en 2.61 m/dag. T en K waarden variëren naargelang van de lithologie waarin de put zich bevindt. Stijghoogtekaarten duiden op een algemene verlaging van de stijghoogte vooral in gebieden dicht bij de kust. De laagste waarden bevinden zich langs de kust in zones zoals Kawe, City Centre en Msasani. De hoogste stijghoogten worden in het westen aangetroffen (richting Pugu Hills) en zuidwestelijk (richting Mbagala) van het studiegebied. Interpretatie van gegevens van dagelijkse stijghoogteschommelingen liet toe deze fluctuaties toe te schrijven aan natuurlijke verschijnselen, zoals neerslag, getijden (sterk dichtbij de kustlijn) en evapotranspiratie

(belangrijker t.h.v. Mnazi Mmoja Primary School en Temeke Municipal Garden), en aan menselijke invloeden (vnl. pomping).

Geofysische gegevens ondersteund door hydrogeochemische data en hydrochemisch/lithologische doorsneden, hebben toegelaten een kaart op te stellen van de diepte van het zoet/zoutwater grensvlak. Verticale elektrische sondering (VES) curven en resistiviteitsprofielen tonen een afname van de resistiviteit (dus toenemende saliniteit) met de diepte en naar de kustlijn toe. Doorsneden tonen de aanwezigheid van zout water in de aquifer nabij de kustlijn en de grens tussen zoet en zout water werd aangeduid. Zout water wordt vooral aangetroffen in de zone binnen 2 km van de kustlijn, terwijl het grensvlak zich tussen 1.3 m tot 20 m diepte bevindt. Verder van de kustlijn bevindt het grensvlak zich (indien aanwezig) op een grotere diepte, die niet bereikt werd. Nochtans werd in het zuiden van het studiegebied, in de VES uitgevoerd te Kurasini (op 4 km van de zee), het grensvlak aangetroffen op grotere diepte (43 m). Dieptevariatie werd eveneens vastgesteld in de resistiviteitsloggings. In het westen van het studiegebied (op ca. 2.7 km van de kustlijn) werd de resisitiviteitslogging uitgevoerd tot op een diepte van 37 m, maar het zoet/zoutwater grensvlak (indien aanwezig) werd niet bereikt.

De hydrogeochemische processen die optreden in het DQCA systeem werden onderzocht aan de hand van 196 grondwaterstalen die bemonsterd werden tussen 2009 en 2012 en geanalyseerd op hoofdkationen en –anionen. Piper diagrammen voor de grondwaterstalen tonen veranderingen naar zeewater toe. Een groot deel van het grondwater wordt geklasseerd als Na-Cl. Het Durov diagram toont duidelijk de evolutie van watertypes van zoet voedingswater van het $CaHCO_3$ type naar de zoute NaCl bronterm, waarbij beide brontermen in wisselende proporties gemengd worden. De Stuyfzand classificatie toont duidelijk de belangrijke geochemische verschillen tussen de zone nabij de kust en het gebied meer landinwaarts. Grondwatertypes zijn, vanaf het binnenland tot de kust: CaMix, NaMix en NaCl, en tonen de toenemende zoutwaterinvloed. Kaarten van de Cl^-/HCO_3^- verhouding, Cl^- en elektrische conductiviteit (EC) tonen dat Cl^- en EC toenemen in de richting van de kust. ΔNa^+ voor de geanalyseerde stalen toont gebieden met een Na^+ deficiet. Een groot aantal stalen met negatieve waarden voor deze parameter wordt aangetroffen ten noorden van de Msimbazi Rivier, in Kawe, Msasani, Masaki en Oysterbay: deze monsters worden gekenmerkt door hun hoge saliniteit. Ten zuiden van de Msimbazi Rivier vertoont een groot aantal stalen positieve waarden. Enkele stalen in City Centre ter hoogte van de zuidelijke uitloper van het schiereiland in Mzinga estuarium, vertonen negatieve waarden. Resultaten

van het hydrogeochemisch onderzoek geven aan dat de DQCA verontreiniging vertoont, vnl. door zeewaterintrusie en het gebruik van on-site afvalwaterlozingssystemen, met name putlatrines en septische putten. Oplossing van calciet/dolomiet mineralen in de aquifermatrix, evenals kationuitwisseling, wijzigen eveneens de ionenconcentraties in grondwater.
In deze studie werd een conceptueel model opgesteld voor een beter begrip van de zoutwater transportprocessen die optreden ten gevolge van pumping in de DQCA. In het geval waarbij geen slechtdoorlatende laag aanwezig is in het aquifersysteem, zal pomping in het bovenste deel van de aquifer dichtbij de kustlijn, boven de zoutwaterwig, resulteren in upconing van het diepe zoute water. Anderzijds zal pomping in het bovenste deel van de aquifer, landinwaarts van de zoute wig, eerst een verdere landinwaartse penetratie van de zoutwaterwig veroorzaken nabij de onderkant van de aquifer, en dan een opwaartse upconing van het zoute water. Als geen slechtdoorlatende laag aanwezig is en er wordt gepompt in het onderste deel van de aquifer, landinwaarts van de zoutwaterwig, zal dit een verdere landinwaartse penetratie van de zoutwaterwig veroorzaken, naar de pompputten toe. In het geval er wel een slechtdoorlatende laag aanwezig is, halverwege de aquifer, dan zal pomping in het bovenste deel van de aquifer boven de zeewaterwig (die zich nabij de basis van de onderste aquifer bevindt), laterale zeewaterintrusie met zich meebrengen. De slechtdoorlatende laag verhindert upconing van de diepe zoute wig.

Verschillende indicaties van zoutwaterintrusie werden vastgesteld en toegeschreven aan de overexploitatie van de aquifer. De meeste boorputten nabij de kustlijn zijn niet geschikt voor huishoudelijk of irrigatiegebruik, door hun hoog zoutgehalte. De resultaten van deze studie zijn nuttig om betere grondwaterbeschermings- en grondwateronttrekkingsplannen op te maken, met het oog op de beperking van de zeewaterintrusie en de anthropogene verontreiniging. Het bereiken en versterken van de doelstellingen van de National Water Policy (NAWAPO, 2002) en de National Environmental Policy (NEP, 1997), waarin de noodzakelijke sanering wordt opgelegd, evenals de toepassing van rationele grondwaterbeheerspraktijken, met inbegrip van de beperking van de onttrokken debieten, is cruciaal voor het bereiken van de duurzaamheid van de grondwatervoorraden in het studiegebied.

List of Figures

LIST OF TABLES

LIST OF APPENDICES

LIST OF ABBREVIATIONS AND ACRONYMS

AET: Actual Evapotranspiration

APWL: Accumulated potential water loss

BIF: Banded Iron Formation

BOD: Biological Oxygen Demand

BTC: Belgian Technical Cooperation

CBOs: Community Based Organizations

CEC: Cation Exchange Capacity

CNP: Coastal Neogene Province

CNR-IRPI: National Research Council- Research Institute for Geo-Hydrological Protection

DAWASA: Dar es Salaam Water and Sewerage Authority

DAWASCO: Dar es Salaam Water and Sewerage Corporation

DCC: Dar es Salaam City Council

DDCA: Drilling and Dam Construction Agency

DO: Dissolved Oxygen

DQCA: Dar es Salaam Quaternary coastal aquifer

DUCE: Dar es Salaam University College of Education

DWL: Dynamic Water Level

EC: Electrical Conductivity

ET: Evapotranspiration

EIAs: Environmental Impact Assessments

EMA: Environmental Management Act

EPA: Environmental Protection Agency

FAO: Food and Agriculture Organisation

GIS: Geographical Information System

GPS: Global Positioning System

GST: Geological Survey of Tanzania

HM: Hamon

HS: Hargreaves

IWRM: Integrated Water Resources Management

KFR: Kazimzumbwi Forest Reserve

LULCC: Land use and land cover changes

NAWAPO: National Water Policy

NEMC: National Environment Management Council

NEP: National Environment Policy

NGOs: Non-Government Organizations

MDG: Millenium Development Goal

MoWI: Ministry of Water and Irrigation

PAW: Plant Available Water

PET: Potential evapotranspiration

PFR: Pugu Forest Reserve

PFS: Pugu Forest Station

PM: Penman-Monteith

PWP: Permanent Wilting Point

RH: Relative Humidity (%)

SUA: Sokoine University of Agriculture

SWL: Static Water Level

SEAs: Strategic Environmental Assessments

SEAMIC: Southern and Eastern African Mineral Centre

TDS: Total Dissolved Solids

TH: Thornthwaite

TMA: Tanzania Meteorological Agency

TPCCL: Tanzania Portland Cement Company Ltd

TPDC: Tanzania Petroleum Development Cooperation

UDSM: University of Dar es Salaam

UGent: University of Gent

UNEP: United Nations Environment Programme

UHSLC: University of Hawaii Sea Level Center

URT: United Republic of Tanzania

US: United States

USSL: US Salinity Laboratory

USDA: United States Department of Agriculture

VES: Vertical Electrical Sounding

WPWP: Water content at Permanent Wilting Point

WHO: World Health Organisation

1 INTRODUCTION

1.1 General background

Around the world fresh water scarcity is an increasing problem caused by several factors such as ecosystem service degradation, overpopulation, pollution, overdrawing, climate change and water misuse (Rosegrant et al., 2002). This chapter introduces the research on salinization of the coastal aquifer conducted in Dar es Salaam City between 2008 and 2012. It gives a general overview of water resources management in Tanzania and associated environmental challenges. Furthermore, it outlines research objectives, research questions, research motivation, thesis layout and description of the study area.

1.2 Water resources management in Tanzania and environmental challenges

The improvement of access to safe water for drinking and other domestic purposes constitutes significant environmental challenges in Tanzania especially in urban areas. Tanzania National Environment Policy (NEP) (URT, 1997) identifies six (6) key environmental problems that need urgent attention. These are: i) Land degradation, ii) Lack of accessible good quality water for inhabitants, iii) Environmental pollution, iv) Loss of wildlife habitats and biodiversity, v) Deterioration of aquatic systems, and vi) Deforestation.

In Tanzania, just like in most of the developing countries, many of its surface water sources (rivers and lakes) have been degraded or depleted, due to exposure to pollution, increase in population, disruption of the catchment areas, over-exploitation and changes in climate. In Dar es Salaam City, where this study is focused, almost all rivers are polluted and enormous pressure is being exerted on the groundwater sources (Mato, 2002; Mjemah, 2007).

Global records show that over a billion people worldwide lack access to adequate water, and close to two billion suffer the consequences of poor sanitation; millions of people die each year from contaminated water (UNEP, 2003). Tanzania Health Policy (URT, 1990) recognizes water borne diseases are among the critical challenges in Tanzania, as they are in other developing countries.

A series of water sector crises during the 1990s, many containing environmental aspects, led Tanzania to the need of implementation of the principles of integrated water resources management (IWRM) particularly multi-sectoral management, decentralized decision making, stakeholder participation and inclusion of environmental water requirements. As a response to these crises, the National Water Policy (NAWAPO) was passed in 2002 accommodating principles of IWRM. Mtoni (2003) documented an increased emphasis on implementing water supply programmes through active community participation.

In 2004, Tanzania passed the Environmental Management Act (EMA) which is the main legislative reference for environmental management in Tanzania. EMA provided additional planning tools to tackle water-related environmental problems. It deals with the protection of environmentally sensitive areas, the control of pollution and wastes, setting environmental quality standards, and restoring environmentally degraded areas. The Act contains detailed provisions for undertaking Environmental Impact Assessments (EIAs) for development projects and introduces Strategic Environmental Assessments (SEAs) for all policies, legislation, regulations, programs and plans that may affect the environment.

In spite of the existence of several policy instruments on health, water and environment policies, significant results are not achieved and the situation is continuously deteriorating. The recent government efforts involved enactment of the Water Supply and Sanitation Act (2009) and the Water Resources Management Act (URT, 2009). The latter repeals the Water Utilization Act of 1974 and its subsequent amendments. With a view to give effect to the National Water Policy (NAWAPO) (URT, 2002), the newly formed acts focus in providing an adequate operational, institutional and legal framework, and transparent regulation of water supply and sanitation services.

NAWAPO came at a timely moment with the occurrence of the challenge set at the World summit on Sustainable Development at Johannesburg in 2002 of halving by 2015 the proportion of people who are unable to reach or afford safe drinking water. However, Tanzania is far behind from meeting this challenge when comparing the situation on the ground and the fact that 10 out of 13 years have already passed. Improper treatment and disposal of liquid wastes is among the major challenges facing water resources management in the country. Because of lack of proper sanitation practices and waste water treatment facilities, liquid and solid wastes are generally disposed into nearby waterways and public

water sources, exposing them to contamination. In Dar es Salaam City, for example, less than 10% of the population is connected to a sewerage system and the rest resorts to onsite sewage disposal systems i.e. pit latlines and septic tanks (Mato, 2002; Mjemah, 2007; Mtoni et al., 2010 and 2012a-b).

Water resources contamination in Tanzania has been the focus of research efforts over the last two decades. The shortage of good quality water from surface sources has made groundwater to be considered as an important source for water supply in various parts of the country including Dar es Salaam (Mnzava, 1986; Msindai, 1988; Nkotagu, 1989; Mato, 2002; Mtoni, 2003; Mjemah, 2007). The history of global extensive groundwater use is less than 50 years old and much of the modern increase in global water use has been contributed by groundwater (CABI, 2007). Groundwater recharge is one of the parameters considered for sustainability of groundwater supply. In Dar es Salaam coastal aquifer for example, excessive groundwater abstraction greater than replenishment rate resulted into seawater intrusion (Mtoni et al., 2011).

The focus of this research is to monitor and evaluate the hydrogeochemical characteristics of the groundwater in relation to saltwater intrusion in the coastal strip of Dar es Salaam Quaternary coastal aquifer (DQCA).

1.3 Salinization of coastal aquifers

Numerous examples of coastal aquifer salinization are known around the world. The increasing urbanization taking place along the coastlines and estuaries and the need for freshwater have produced an increase of groundwater withdrawal in sensitive areas like coastal environments, where aquifers may suffer from seawater intrusion (Custodio, 1985; Barker et al., 1998; Mato, 2002; Polemio et al., 2002; Cardoso da Silva et al., 2003; Kaushal et al., 2005; Norconsult, 2007; Mjemah, 2007; Polemio et al., 2010; Voudouris et al., 2010; Mtoni et al, 2011; Mtoni et al., 2012a-b). Coastal areas are usually densely populated as they provide a link to other ports which make accessibility to transport and trade easy. In densely populated coastal areas, the demand for freshwater is enormous. Struggle to meet this demand leads to a danger of groundwater contamination by seawater intrusion which occurs when rates of extraction of groundwater near the shoreline are raised.

The saltwater intrusion mechanism can best be defined as a dynamic equilibrium between the hydraulic gradient driving groundwater seaward and the hydraulic gradient exerted by the ocean in a landward direction (Allen and Matsuo, 2002). A zone of interface exists between freshwater and underlying seawater. Saltwater intrusion is a natural process, but excessive groundwater pumping usually results in a rise of the freshwater-saltwater interface, allowing seawater intrusion (Fig. 1.1). The relationship between the freshwater and seawater pressures is described by the Ghyben-Herzberg principle, which is based on the density differences between the two fluids. It gives an approximation to the depth to the seawater/fresh water interface and states that for every foot above sea level the fresh water head is, the depth to the seawater will be 40 times this amount below sea level. This analysis assumes hydrostatic conditions in a homogeneous, unconfined coastal aquifer. In reality we are dealing with a dynamic equilibrium.

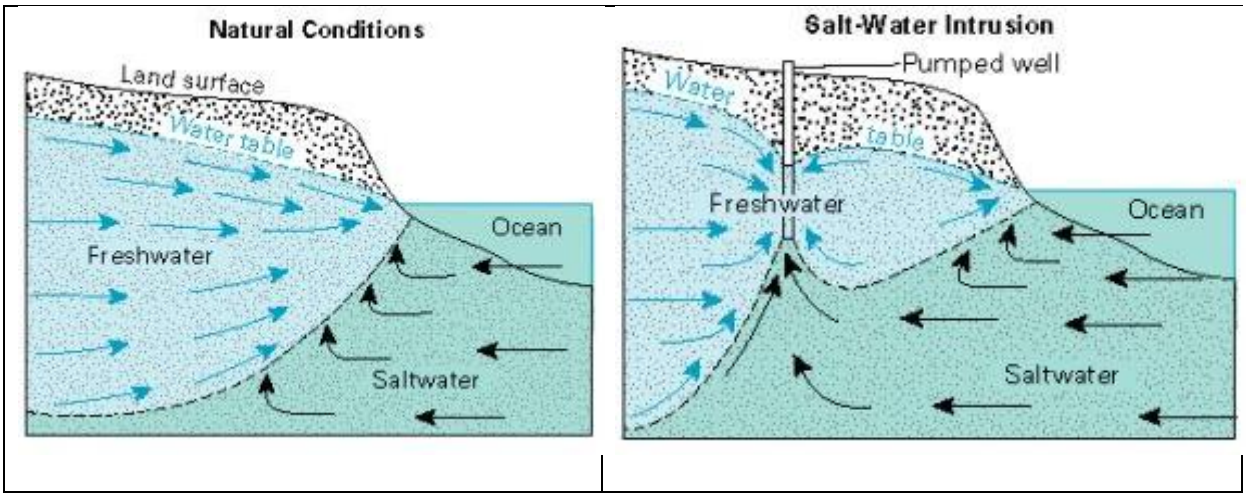

Figure 1.1: Illustration on how intensive groundwater pumping can cause saltwater intrusion in coastal aquifers (http://essea.strategies.org/contact.html).

Dar es Salaam as one of the largest coastal city in Africa identified to be at high risk to sea-level rise (UN-HABITAT, 2008): the city is vulnerable to floods, sea-level rise, coastal erosion and water scarcity. Over 80% or 3.2 million out of 4 million of Dar es Salaam's population live in unplanned areas (UN-HABITAT, 2010a). The high vulnerability is mainly attributed to poor infrastructures (i.e. poor storm water drainage systems), high population densities and the fact that the city is typically undergoing fast and unplanned growth. On December 20, 2011, the heaviest rains in 57 years occurred resulting in unprecedented flooding that devastated many areas of the city. The flooding caused over 20 casualties and left over 5,000 people homeless.

According to Kebede and Nicholls (2010), estimates of trends of sea-level change based on limited tide gauge records recorded at Dar es Salaam suggest that the coast of Tanzania has experienced a drop in sea-level (Fig. 1.2). However, their estimates are based on observations of short duration (1986-1990). Fairly long records of at least 50 years are needed to give conclusive evidence because of the influence of natural variability in the climate system (Douglas, 1992). Climate change, sea level rise and saltwater intrusion present the future challenges of water resources management in coastal areas. Climate change is expected to influence the extent of any potential or already existing environmental problems such as subsidence, coastal erosion, environmental pollution, land use pressure and degradation of ecosystems.

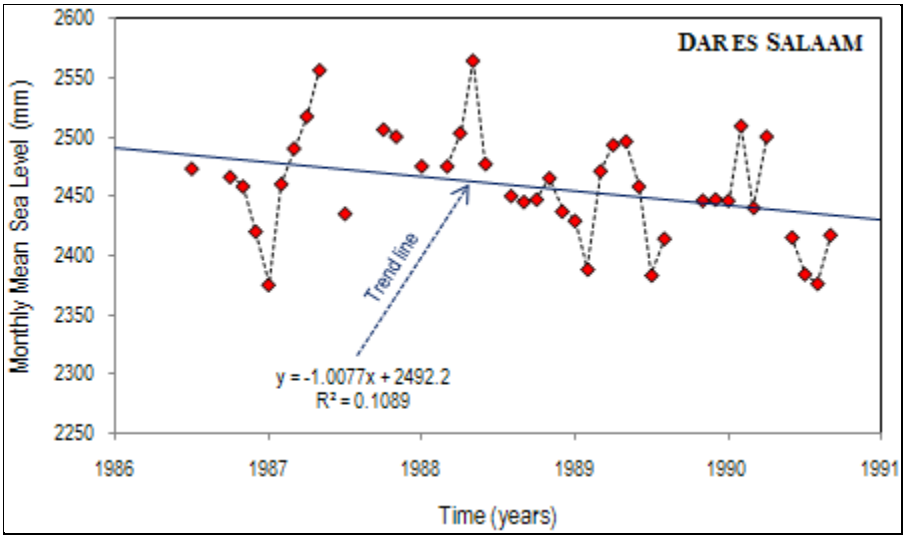

Figure 1.2: Four years of monthly mean sea level tide gauge measurements for Dar es Salaam station (06o49.2'S, 39o17.3'E), Tanzania (Source: University of Hawaii Sea Level Center, UHSLC). (Cited in Kebede and Nicholls, 2010).

Several approaches have been applied to control seawater intrusion to safeguard groundwater reserves in coastal aquifers. These include reduction of the rates of abstraction, relocation of abstraction wells, subsurface barriers, increase of natural recharge, artificial recharge, and abstraction of saline water (Todd, 1974). Features which affect coastal aquifer are summarized in Fig. 1.3.

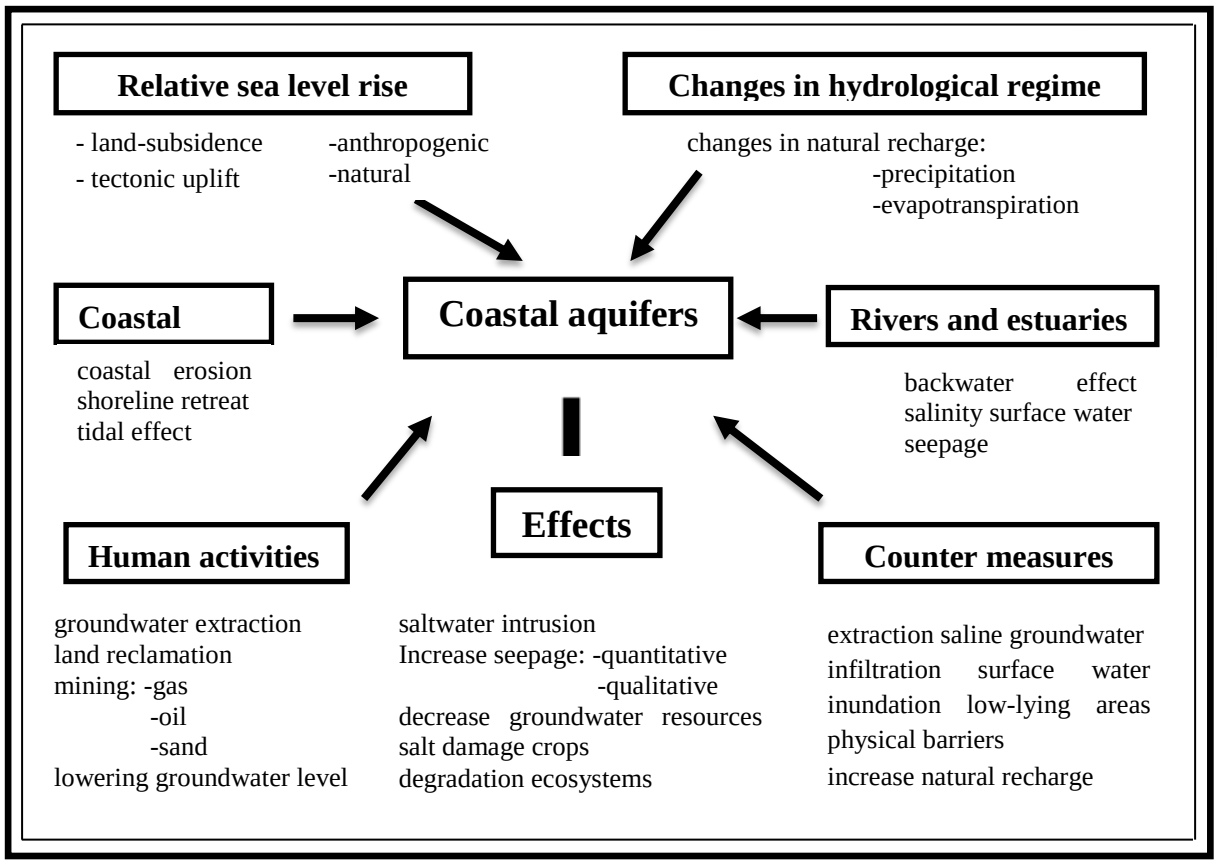

Figure 1.3: Features affecting the coastal aquifers. (Source: C.P. Kumar: http://www.angelfire.com/nh/cpkumar/publication/gwman.pdf)

1.4 Problem setting

1.4.1 High population growth

The use of groundwater in Dar es Salaam City has increased considerably following the high population growth and weakening of the surface water sources. With only 25 percent of the population receiving water supplied by Dar es Salaam Water and Sewerage Authority (DAWASA), much of the water needs must be met through private boreholes (UN-HABITAT, 2009). High dependence on groundwater use since 1997 and rapid population growth coupled with industrialization, urbanization and water-intensive lifestyles have resulted in aquifer salinization.

Dar es Salaam City located in the eastern coast of Tanzania is the largest urban centre in the country. The city receives many visitors and rural-urban migration makes it one of the fastest growing cities in the world, which in turn causes problems that are typical of a tropical mega-city. Among others, these include water scarcity, sluggish infrastructural growth and poor

sanitation. City's water demand is about 424,000m^3/day (Mato and Mujwahuzi, 2010). The population of the city is about 4 million. With the growth rate of 4.3% per year, the population can be expected to be approximately 9 million by the year 2030. This population is likely to raise water demand to over 900,000m^3/day by 2030.

1.4.2 Socio-economic development

Groundwater is the critical underlying resource for human socio-economic development. Dar es Salaam City has the highest concentration of business, industries and institutions. The city has a big habour which plays an important role in the country's economy, also because of commercial imports and exports of land-locked countries such as Uganda, Rwanda, Burundi and Congo. It attracts large number of people for business and also for its beaches and important terrestrial and marine based habitats. The city comprises about 80 per cent of the industries and over 30 per cent of the total urban dwellers in Tanzania (Mato, 2002).

The benefits of groundwater are obvious. In Dar es Salaam City, for example, residents benefited hugely from groundwater during the severe drought in 1997. Since 1997, the Tanzanian Government, Non-Government Organizations (NGOs), Community Based Organizations (CBOs) and international aid organizations have promoted the drilling of boreholes to try to meet the demand of water supply in the city. Groundwater use is in the trend of increasing and currently over 50 percent of residents in Dar es Salaam rely on groundwater. Industries, institutions and tourist hotels have sunk a number of boreholes from which large quantities of water are withdrawn using electrical and/or diesel pumps. Groundwater pumping already shows evidence of overdraft with the consequence of inducing encroachment of saltwater into the producing aquifers (Mtoni et al., 2011 and 2012a). To meet the challenges of rapid population growth, expanding industries and irrigated agriculture, proper groundwater management is necessary to tackle the problem of saltwater intrusion.

1.4.3 Deterioration of surface water

The main surface water supply to Dar es Salaam City is pumped from Ruvu River which flows some 65 km away from the city. Decrease of water level in Ruvu River is attributed to drought and disturbance on its catchments by human activities such as deforestation for the sake of cultivation, getting firewood and timber for building. In 1955 most of the area in the Ruvu basin was covered by thickets and open woodlands. However, since 1955 vegetation cover has continued to be converted to farmland (sisal estates and mixed crops) and an extensive expansion of agriculture at the expense of the natural vegetation cover occurred between 1995 and 2000 (Yanda and Munish, 2007). Over decades, land uses in Tanzania have been changing, causing a decline of agricultural area and forest and a significant increase of urban land. The spatial relationship between land use and water quality has been examined by several authors. For example, Tong and Chen (2002) showed that land use was related to many water quality parameters: increases in agricultural land has a strong positive correlation with conductivity and pH but a negative correlation with heavy metals (cadmium, lead, etc.), while growths in residential land had a positive correlation with heavy metals, BOD (Biological Oxygen Demand), and conductivity in the watersheds of Ohio State. A study by Ngoye and Machiwa (2004) assessed the influence of land-use patterns in the Ruvu river watershed on water quality in the river system. Their results showed impairment of the water quality of the river by anthropogenic activities in the catchment: forested catchments had high levels of DO (Dissolved Oxygen) and low levels of NH_4 N and NO_3 N compared to those from farmland, industrial, residential and market places.

From 1950s to late 1980s there was sufficient flow in the Ruvu River to supply water demand. From 1990 and more seriously from 1997 the river flow had gradually decreased and the supply was no longer able to meet water supply demand. Stress on surface water resources has led to a significant shift to the use of groundwater resources in many cities. In Dar es Salaam City, the water crisis can be attributed to drought, pollution of water sources and catchment disturbances. Rivers have been ill-treated by different sectors as a dumping site for effluent and other pollutants produced by the city. As a consequence of the high levels of pollution, the river's water quality is no longer safe for consumption, domestic uses, or sometimes even irrigational uses. Due to unreliability of water from Ruvu River and due to the fact that all rivers in Dar es Salaam City are polluted, this has resulted in increasing groundwater dependency.

1.4.4 Effect of climate variability

Saltwater intrusion is a major problem in coastal aquifers. Changes in climatic variables, such as precipitation and temperature can significantly alter groundwater recharge rates for aquifer systems and thus affect the availability of fresh groundwater. The great variability in precipitation can reflect higher occurrence and prolonged periods of high or low groundwater levels. Temperature increases affect the hydrologic cycle by directly increasing water evaporation and vegetation transpiration. Under such circumstances, quantification of the rate of natural groundwater recharge is a pre-requisite for effective groundwater resource management. This is particularly important in such areas like Dar es Salaam with high demands for groundwater supplies.

1.4.5 Effect of land use change and land cover

Land use and land cover changes (LULCC) may be grouped into two broad categories as conversion and modification. Conversion refers to changes from one cover or use type to another, while modification involves maintenance of the broad cover or use type in the face of changes in its attributes (Baulies and Szejwach, 1998). LULCC can have a significant impact on groundwater levels. It affects the different hydrological components like interception, infiltration and evaporation, thus influencing the soil moisture content and runoff generation (FAO, 2003).

1.4.6 Groundwater monitoring

Groundwater monitoring in Dar es Salaam is not carried out or is only carried out on a somewhat ad hoc basis. Water quality data collected by Dar es Salaam Water and Sewerage Corporation (DAWASCO) involves only surface water (Ruvu and Kizinga River) and about 10 boreholes used by the company to augment its public water supply. Measurement of groundwater level in these boreholes is not a priority and water quality measurement is limited to pH, EC, TDS, chloride, salinity, total alkalinity, total hardness, magnesium, calcium and nitrate. Generally, there has been a lack of a sustained systematic groundwater quality monitoring program. Groundwater quality data available in the Ministry of Water and Irrigation (MoWI) involve the water quality analysis conducted at the time that boreholes were drilled. Boreholes lack long term monitoring data. However, such long term monitoring data covering groundwater fluctuations and water quality are very important for management and for evaluating the implications of changes in use.

1.5 Research objectives

The main objective of the current research was to assess the current state of water quality in the coastal strip of Dar es Salaam Quaternary aquifer, especially in view of sea water intrusion. The study is focused on understanding of the patterns of movement and mixing between freshwater and saltwater, as well as the factors that influence the hydrogeochemical processes. The specific objectives of this study include:

i. Estimation of sustainable yield for the DQCA through estimation of the amount of natural groundwater recharge based on the estimation of water budget for the aquifer.

The amount of water that may be extracted from an aquifer without causing depletion is primarily dependent upon the groundwater recharge. Thus, estimation of groundwater recharge is a pre-requisite for managing groundwater resources in an optimal manner.

ii. To acquire representative samples of groundwater in order to evaluate the hydrochemical data for spatial and temporal variation.

Chemical data interpretation will help to determine the spatial distribution and the nature of occurrence of various chemical constituents found dissolved in groundwater, delineate flow regions on the basis of topography and geochemical trends, and explore potential processes that may be controlling natural groundwater evolution, in particular, salinization by saltwater intrusion.

iii. To evaluate the suitability of the groundwater for the purposes of drinking and irrigation.
iv. To acquire knowledge on the hydrological functioning of the catchment and define a conceptual model with the aim of elucidating seawater intrusion phenomenon.
v. Study groundwater chemistry by means of resistivity loggings in boreholes and by groundwater analysis.
vi. Performing pumping tests to determine hydraulic parameters to aid in providing input data.
vii. To assess the long term viability of the water supply, including water quality, and the potential to increase the yield of the aquifer.
viii. To assess how a coastal aquifer system responds to abstraction and whether the groundwater abstraction will induce seawater intrusion.

With respect to the above specific objectives, the following questions guided this research

i. How is water supply provision currently being met within the study area?
ii. What are the major factors and issues affecting groundwater quality?
iii. What is the current state of water quality near the coastline? In which areas the problem of seawater intrusion is most acute?
iv. How much groundwater (m^3/year) can be extracted sustainably?
v. How are sanitation practices related to groundwater quality?
vi. What are the main gaps in data, information or knowledge needed to promote sustainable groundwater management?

1.6 Research methodology and data generation

Research methodology and data generation involved four main stages, namely; i) review of available data, ii) collection of new data by means of fieldwork, iii) data processing, interpretation and groundwater modeling, and iv) producing final report. Fig. 1.4 depicts the research methodology of this study. The methodology is split into two parts; i) groundwater quality, and ii) groundwater quantity covering the recharge estimation and groundwater modeling. A conceptual model was prepared prior to groundwater model development. The groundwater recharge flux was determined by the soil moisture balance method.

1.6.1 Existing data

Collection of available information in relation to this research was done so as to contribute to the water quality and quantity assessment. This step involved the collection and review of all relevant available data from existing files, reports, libraries, and the databases for a wide range information related to the study area, such as: i) topographical maps, aerial photographs, satellite images, ii) geographical and geological data, iii) reports of previous geophysical studies, iv) borehole and well data files, v) water quality data, and vi) weather data. Different organizations consulted in relation to collection of existing information included government institutions, NGOs (Non-Governmental Organizations) and consulting firms working in water resources.

1.6.2 Field survey

New data were collected by means of field work. Field works were conducted in four periods between 2008 and 2012: i) December, 2008 to July, 2009, ii) January to July, 2010, iii) January to July, 2011, and iv) January, 2012. The fieldwork involved: groundwater sampling, groundwater level measurements using water level meter, monitoring of daily fluctuations of groundwater level using divers (automated water level measurements system), performing pumping tests using water pumps already installed in boreholes, vertical electrical sounding (VES) using the ABEM Terrameter SAS 1000, resistivity loggings in boreholes using Terrameter "ERDUNGS MESSER D3950" and informal interview to borehole's owners and borehole drilling companies. In order to locate the collected data on maps, recording of borehole geographical locations was done using GPS (Global Positioning System) handset. Geographical Information system (GIS) was used to analyse digital information of the groundwater samples from the boreholes/wells using ArcGIS software (GIS 9.2), which produced maps based on geodatabases. By applying the coordinates for each of the sampling sites, spatial distribution of groundwater quality and maps with the sampling points were prepared.

1.6.3 Data processing, analysis and interpretation and groundwater modeling

The majority of groundwater samples (161) were analyzed at the Laboratory for Applied Geology and Hydrogeology of Ghent University, Belgium. 16 groundwater samples were analyzed at the Southern and Eastern African Mineral Centre (SEAMIC) in Tanzania. The hydrochemical results were analyzed by means of Aquachem software (Calmbach, 1997), the Piper diagram and the Stuyfzand (1986, 1993) classification. The saturation state of minerals affecting the hydrochemistry of the study area was determined by use of the PHREEQC code (Parkhurst & Appelo, 1999) version 2.16. World Health Organization (WHO) (2004) guidelines for drinking water quality were used for the assessment of drinking water quality. Sodium Adsorption Ratio (SAR), Soluble Sodium Percent (%Na), Electrical Conductivity (EC) and other parameters such as chloride and sulphate were used for irrigation suitability assessment. Groundwater suitability was interpreted by using the US Salinity Laboratory (USSL) diagram. The field resistivity data was interpreted using the resistivity software, DCINV inversion program of Pirttijärvi (2005). Pumping and recovery test data were analysed using Infinite Extent (version 3.2) (Starpoint Softwares, 1996), aquifer test analysis

software. ArcGIS ver. 9.2 was used to generate maps from the data represented by the point features such as location of boreholes/wells, groundwater sampling sites, groundwater quality results and pumping test sites. The same software was used to process and produce maps for different parameters. MS EXCEL program was used for tables and diagrams. MODFLOW model (McDonald and Harbaugh, 1988) was used for simulation of groundwater flow.

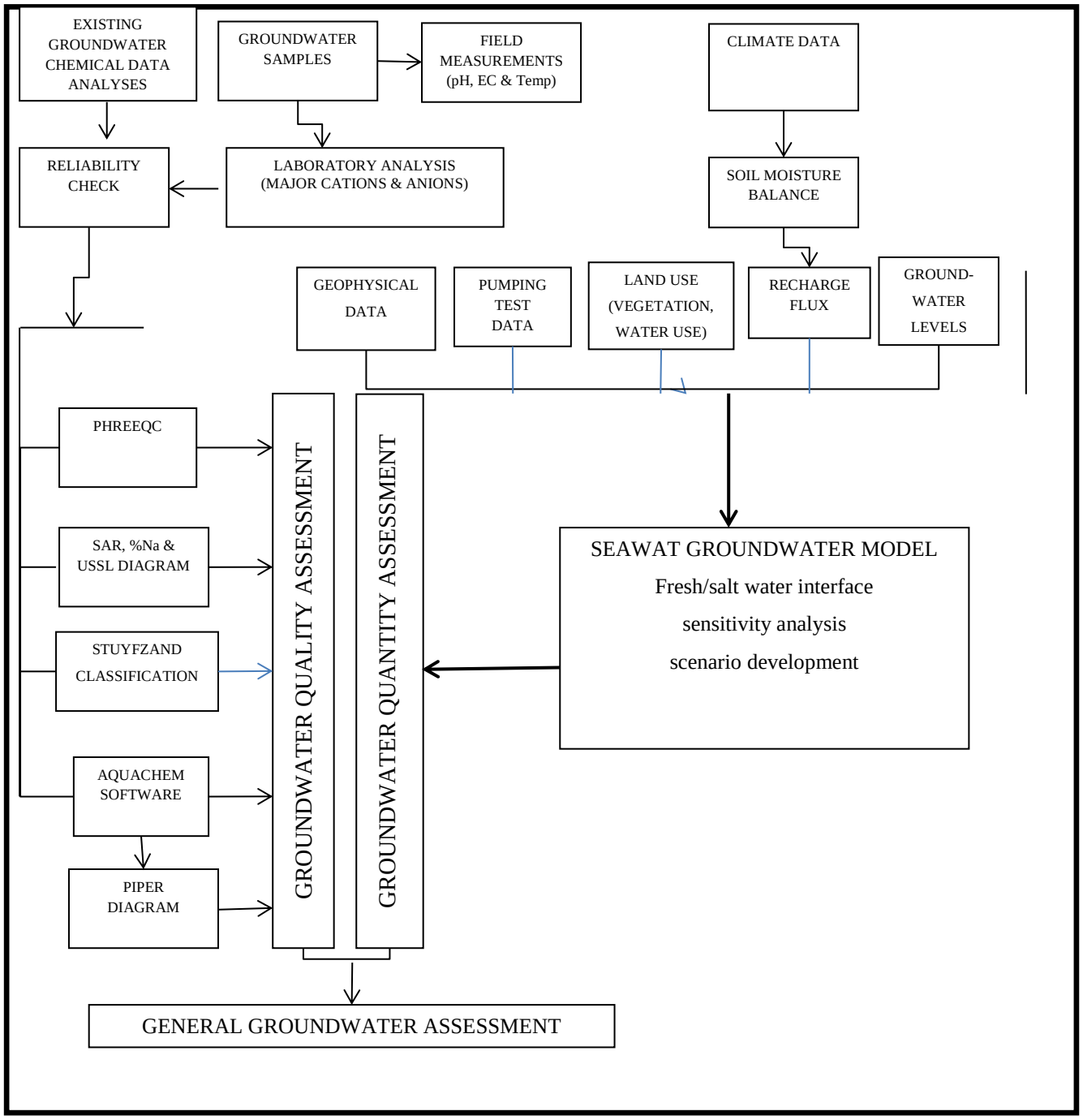

Figure 1.4: Methodology flow chart

1.7 Research motivation

In the last two decades, the use of groundwater in Dar es Salaam City has increased considerably because of the scarcity of surface water sources. With only 25 percent of the population receiving water supplied by Dar es Salaam Water and Sewerage Authority (DAWASA), much of the water needs must be met through private boreholes (UN-HABITAT, 2009). Despite the significant importance of groundwater in Dar es Salaam City, threats exist, including overabstraction that can lead to the intrusion of salt water in fresh water aquifers. Investigation of seawater intrusion in the study area has predominantly focused on Quaternary coastal aquifer due to its importance for water supply in Dar es Salaam City.

The salinization of aquifers lying in the vicinity of coastal areas is a widespread phenomenon, and is generally attributed to the sea invasion to aquifer because of over pumping of groundwater. However, it is widely known that once seawater is introduced into a fresh groundwater body it may be very difficult to restore to the original condition (Jeen et al., 2001; Papadopoulou et al., 2005). Thus the judicious use of groundwater from coastal aquifers is of great importance to protect available groundwater resources and environmental quality. It is necessary to understand the physiognomies of the aquifer system so that a water management plan can be established and it is our responsibility to ensure that water is managed and used effectively and sustainability. As millions are invested for development of future water for Dar es Salaam to meet the growing demands, information about groundwater resources is increasingly important. Thus to prevent further seawater intrusion and other contamination threats, that have already resulted in incidents of groundwater contamination (Mato, 2002; Mjemah, 2007; Mtoni et al., 2012), it is crucial to examine closely the hydrogeochemical processes in the aquifer systems. The physico-chemical parameters of groundwater play an important role in classifying and evaluating the water quality. The current study aims to define the principal hydrogeochemical processes controlling groundwater quality in the Quaternary aquifer in the coastal strip of Dar es Salaam. The hydrogeochemical and geophysical data together with assessment of groundwater recharge and saltwater intrusion modelling will help to set up strategies to aid in lessening the problem of saltwater intrusion.

1.8 Scope and thesis layout

The study covers part of the coastal strip close to the sea and is focusing on assessing seawater intrusion. Thesis layout covers three parts: A, B and C (Fig. 1.5). Part "A" comprises chapter 1 which presents the problem setting and thesis framework. It outlines research objectives, research questions, research motivation, thesis layout and description of the study area in terms of location, topography, drainage, climate and land-uses. Part "B" forms the main body of the thesis which includes six chapters (Chapters 2-7). Chapter 2 focuses on describing the geological and hydrogeological setting of the study area. Chapter three describes the water balance and groundwater recharge assessment for Dar es Salaam Quaternary coastal aquifer (DQCA). Chapter four discusses the characteristics of aquifers from pumping tests and groundwater monitoring data. Chapter five presents an in-depth analysis of seawater intrusion using the integrated application of the resistivity survey, hydrogeological investigation and hydrogeochemical parameters of groundwater to identify fresh-, brackish-, and saline-water zones in the study area. Chapter six discusses the main processes responsible for geochemical evolution of groundwater. Chapter seven deals with modelling saltwater intrusion, where the conceptual model of the hydrogeological system in the study area is defined. Part "C" comprises chapter 8 which provides the summary of main conclusions from the foregoing chapters and provides recommendations and further areas of research.

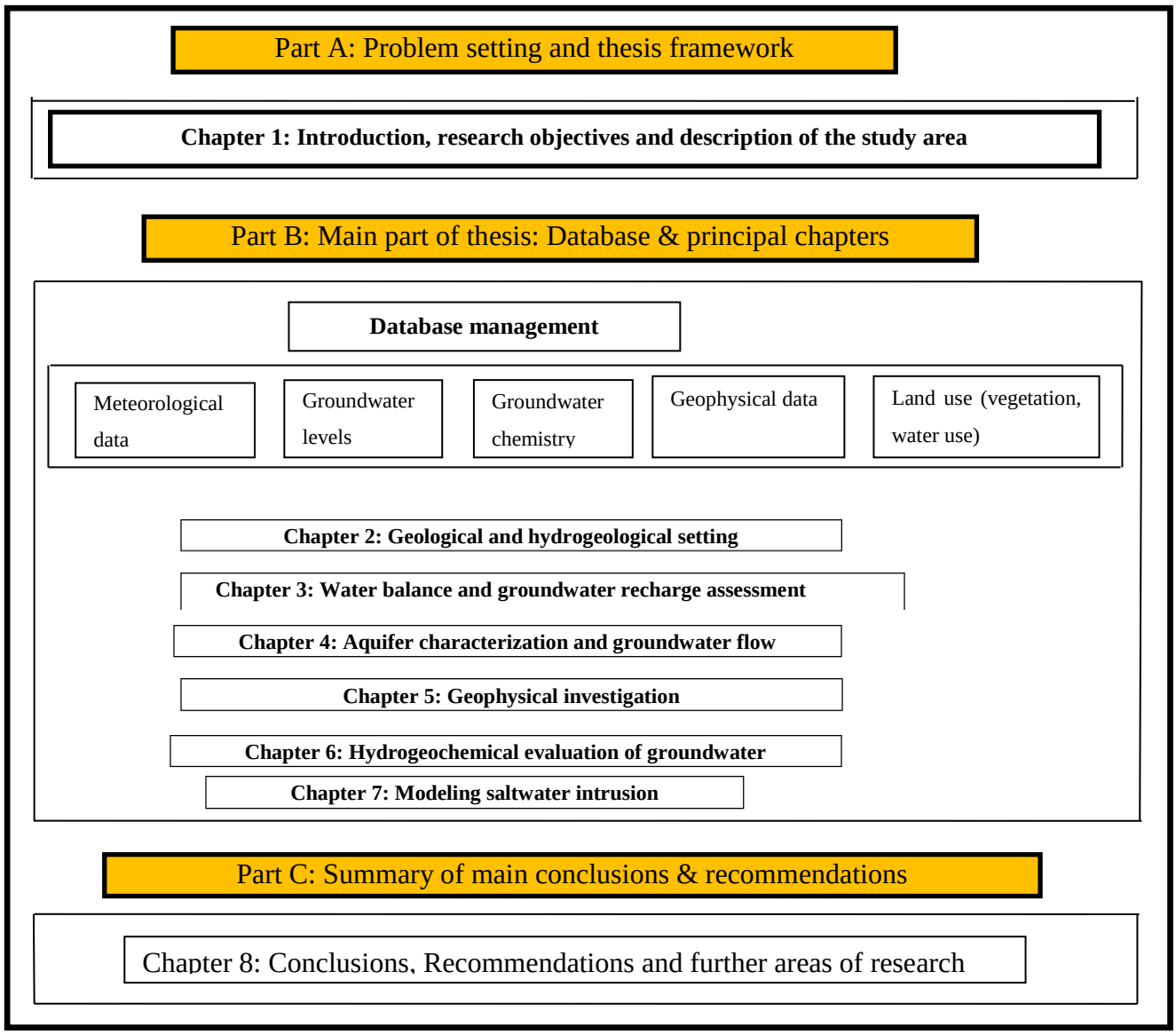

Figure 1.5: Summary of the logical flow of study approach and the operational steps

1.9 Description of the study area

1.9.1 Location

The study area is situated along the coast in Dar es Salaam City cutting across the three Municipal Districts: Ilala, Kinondoni and Temeke (Fig. 1.6(a)). It is bordering the Indian Ocean and Mzinga Creek to the east and extending from Mbezi River and Msasani Bay in the north to the area between Kizinga and Mzinga Rivers in the south (Fig. 1.6(a)). Pugu Forest Reserve and Pugu Hills located about 35 km from the coastline mark important natural features in the western part of the study area. Fig. 1.6(b) presents enlarged map of the study area showing the location of sites investigated.

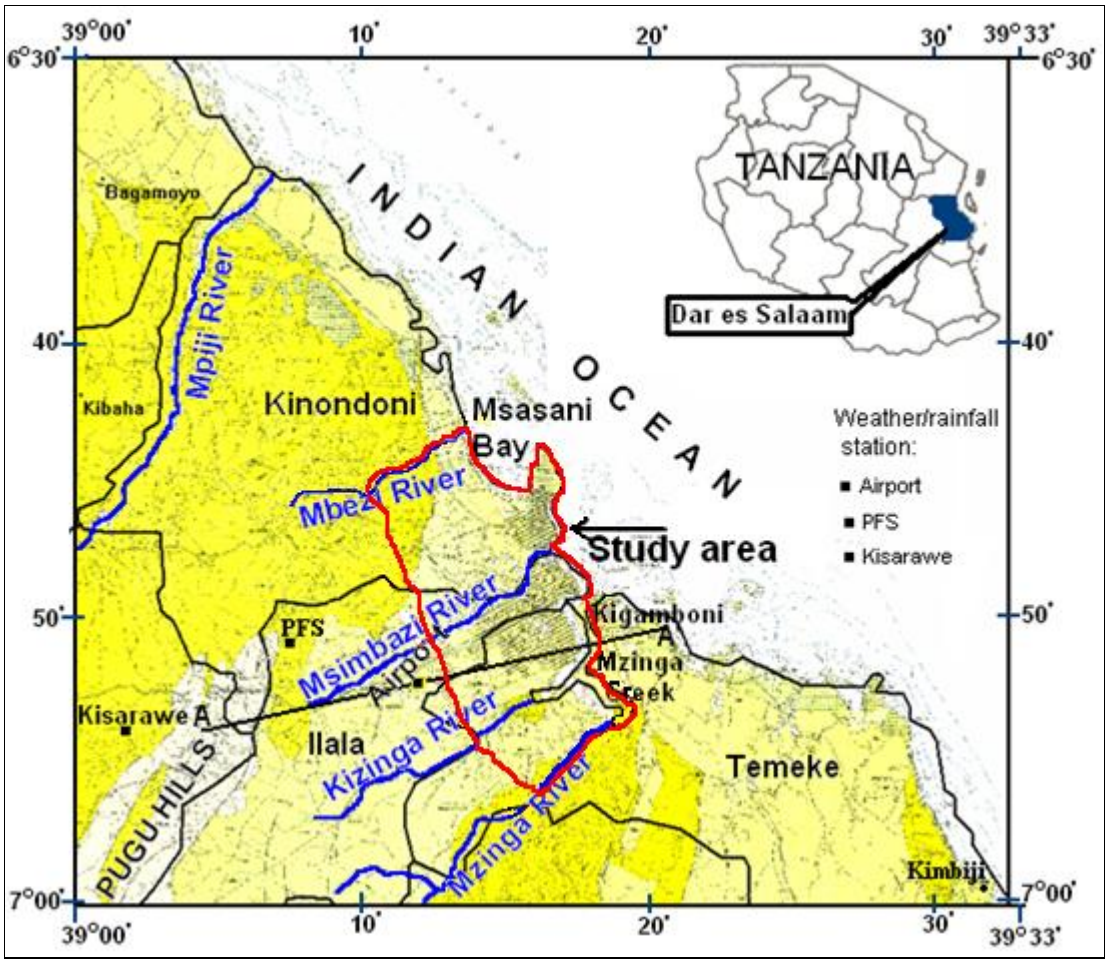

Figure 1.6(a): Location of the study area. Key: PFS = Pugu Forest Station.

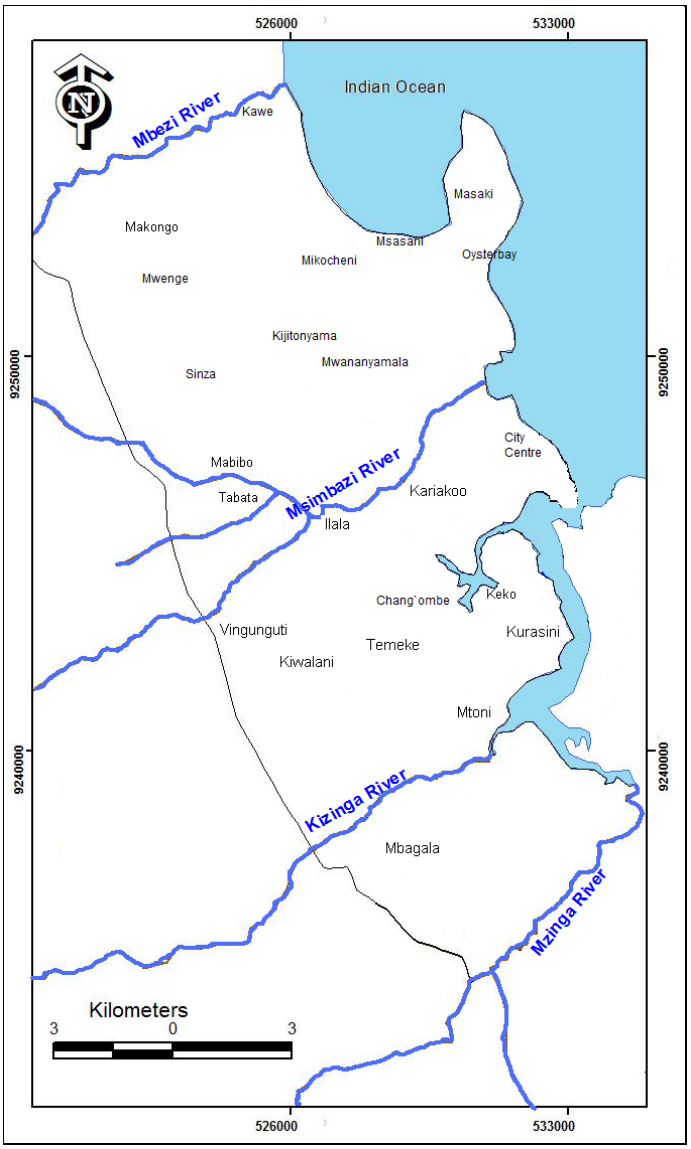

Figure 1.6(b): Enlarged map of the study area showing investigated sites

1.9.2 Topography and drainage

Dar es Salaam is situated in coastal lowland with extensive flat areas and along the entire shoreline the elevation immediately rises to 5m above sea level. The elevation rises gently from the shoreline to 15-20 m.a.s.l around the City Centre and to 50 m.a.s.l around the airport (Fig. 1.7). The upland plateau comprises dissected land and the Pugu/Kisarawe Hills to the west. Inland alluvial plains are characterised by rivers originating from Pugu Hills to the west of the study area. Pugu Hills have various elevations ranging from 100m to almost 300m masl Hills are characterised by steep weathered slopes and ranges of kaolinitic sandstones: the underlying masses of sandstone with faults and joints are the permeable layers, for the water can penetrate readily through the faults and joints which as such provide features for regional groundwater flow system. Apart from the lateral recharge from Pugu Hills, the study area

receives direct infiltration from rainfall throughout the area. The hydrographical network is such that rains/springs at Pugu Hills flow into streams which in turn flow into the main river systems (Mbezi, Msimbazi, Kizinga and Mzinga) running through the coastal plain and discharging into the Indian Ocean (Fig. 1.6(a-b)). Recharge to the local flow system is from the relatively flat land which slopes gently towards the sea (Fig. 1.7). The natural discharge is toward the sea, but surface streams are discharge areas for shallow groundwater. The lithology of the drainage basin plays a major role in river flow (Mjemah, 2007): seasonal Mbezi River is located within the clay-bound sands area, favouring runoff and reducing groundwater recharge; perennial Kizinga River and Msimbazi River are located within the coastal plain, where the sandy sediments favour infiltration, such that groundwater can continue to discharge to the river, sustaining river flow during the dry season; Mzinga River, on the border of the coastal plain and the clay-bound sands area, undergoes both influences. Groundwater discharge can also occur to Mzinga Creek. The differences in soil, brought about by the terraced nature of the undulating terrain, bring about differences in drainage. The study area is mainly covered by sandy soils, which allow a high potential infiltration. Mbezi which is a small seasonal river together with other very small rivers (i.e. Tegeta, Mlalakuwa, Sinza, Kijitonyama and Tabata) are largely forming a drainage network for Dar es Salaam City. The Msimbazi River originating from Pugu Hills about 35 km west, divides the study area into north and south parts. Groundwater seepage in the central plain supports vegetation growth along the river valley, forming a green strip. However, Msimbazi ecosystem services are highly threatened by industrial effluents and illegal sewage system. The river is seriously polluted by heavy metals from the industries and detrimental to its functional benefits which include water supply and irrigation of vegetable gardens which is commonly practiced.

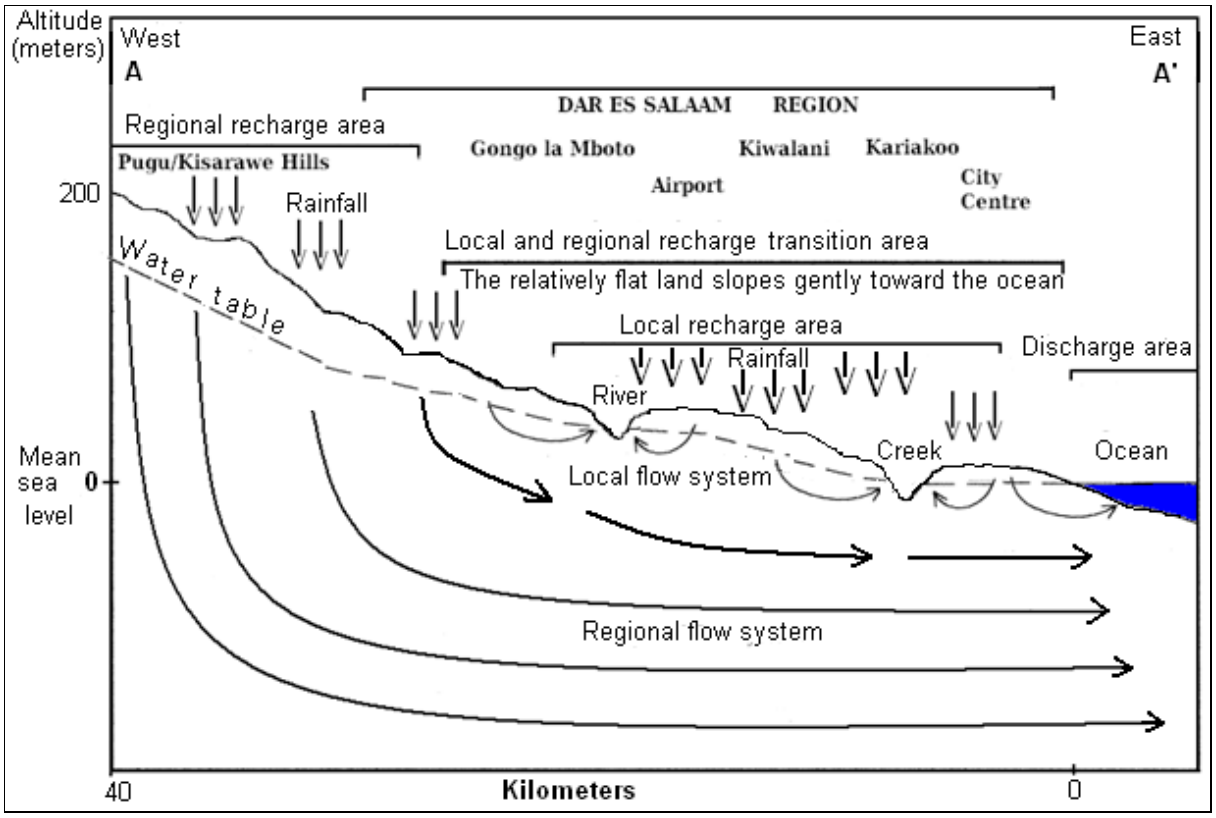

Figure 1.7: Schematic section along the groundwater flow path from Pugu/Kisarawe Hills to the ocean (diagram is not to scale). Location of the profile A-A' is shown in Fig. 1.6

1.9.3 Climate

1.9.3.1 Rainfall

An annual average rainfall of 1236 mm was recorded at Kisarawe and an average of 1090 mm of rainfall per year for 31 years (1943 – 1973) was recorded at Pugu Forest Station (PFS) rainfall station (Fig. 1.6(a)) (Clarke and Dickinson, 1995). A peak annual rainfall of 2385 mm and a minimum annual rainfall of 502 mm were recorded during this period (Clarke and Dickinson, 1995). Average annual precipitation 0f 1114 mm for 39 years (1971 – 2009) was recorded at Dar es Salaam International Airport with peak annual rainfall of 1536 mm and minimum annual rainfall of 585.4 mm (Mtoni et al., 2011). Climate in the study area has been described using available data recorded from the nearby weather station located at the airport (Fig. 1.6(a)).

The climate condition of Dar es Salaam Region is considered to be tropical, typified by hot and humid weather throughout much of the year. The two wet seasons last for six months:

long and heavy rains occurring in March to May, while short and light rains occur in October to December (Fig. 1.8). Dry seasons occur between these two periods, and are characterized by little rainfall. The long-term average annual precipitation is about 1114 mm with maximum rainfall in April. The major precipitation (78.6%) is received during the long and heavy rainfall (March to May). The long rains have a monthly average peak of 253 mm whereas the short rains give an average peak of 117 mm.

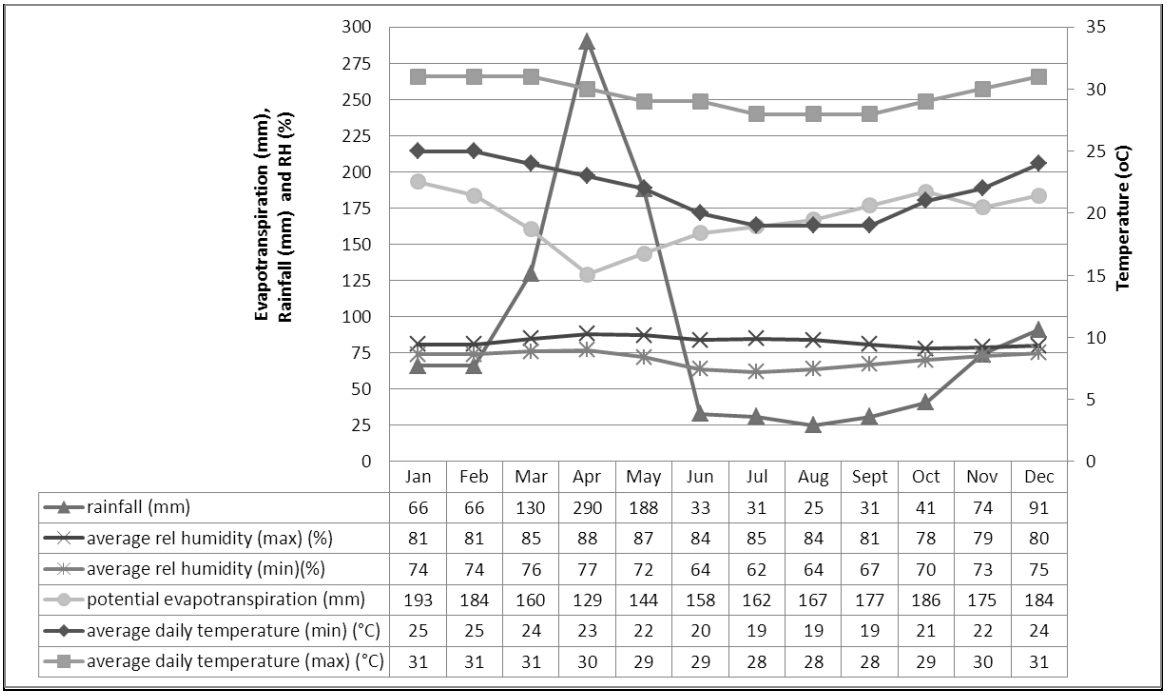

	Jan	Feb	Mar	Apr	May	Jun	Jul	Aug	Sept	Oct	Nov	Dec
rainfall (mm)	66	66	130	290	188	33	31	25	31	41	74	91
average rel humidity (max) (%)	81	81	85	88	87	84	85	84	81	78	79	80
average rel humidity (min)(%)	74	74	76	77	72	64	62	64	67	70	73	75
potential evapotranspiration (mm)	193	184	160	129	144	158	162	167	177	186	175	184
average daily temperature (min) (°C)	25	25	24	23	22	20	19	19	19	21	22	24
average daily temperature (max) (°C)	31	31	31	30	29	29	28	28	28	29	30	31

Figure 1.8: Average weather conditions for Dar es Salaam

1.9.3.2 Temperature

Temperatures are high in November through March during which the temperature can rise up to 35^{o}C. It is relatively cool between May and September with average temperature about 22°C. The average annual maximum temperature is around 32^{o}C, whereas the average annual minimum temperature is 20^{o}C.

1.9.3.3 Relative Humidity

Relative humidity in Dar es Salaam is consistently high throughout the year. The highest maximum relative humidity in the area is reached in April with 88%, whereas the lowest minimum relative humidity is achieved in June, July, August and September, and is averaged at 64%, while the average annual relative humidity is 77%.

1.9.3.4 Evapotranspiration

During the heavy rains occurring in March to May, precipitation is obviously greater than potential evapotranspiration. In dry months (January to February and June to September) including the period of short rains in October to December, monthly mean evapotranspiration is greater than monthly mean precipitation (Fig. 1.8). Because of the low precipitation, additional water used for evapotranspiration mainly comes from soil, and as a consequence soil moisture decreases in this period.

1.9.4 Population

The coastal area of Tanzania comprises 15% of the country's land area and hosts about 25% of the Tanzania mainland population that is fast growing at the rate of 4-6.5% per annum (NEMC, 2009). The population of the coastal zone and the population density continue to increase every year particularly in the urban areas. People are particularly concentrated in Dar es Salaam region where there is the highest concentration of businesses, industries and institutions (NEMC, 2009). The current population in Dar es Salaam City is estimated to be over 4 million people (Fig. 1.9). The population density of the city is about 2809 people/km^2, this is very high comparing with other coastal regions in Tanzania such as, Tanga (64 people/km^2), Pwani (29 people/km^2), Lindi (12 people/km^2) and Mtwara (69 people/km^2) (URT, 2005, quoted in NEMC, 2009). The increase in coastal population in Tanzania including Dar es Salaam is attributed to both migration of people from other parts of the country (in search of employment and/or business opportunities) (NEMC, 2009) and high natural birth rates (URT, 2003). In Dar es Salaam City, population in the municipalities varies from settlement to settlement. High population densities are found in unplanned settlements, while low population densities are found in peripheral localities. The rapid population growth in the city has proven to be a serious challenge in the provision of housing and essential services such as water, sanitation and health care (URT, 2004).

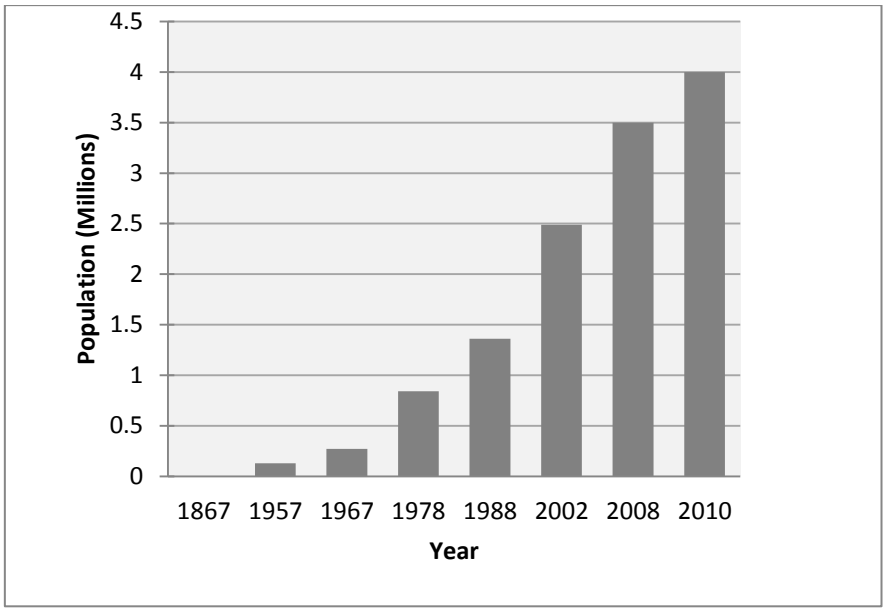

Figure 1.9: Population trend in Dar es Salaam City. Source of data; i) URT (2002) Population and Housing Census Report, ii) DCC (Dar es Salaam City Council) records, and iii) UN-HABITAT (2010a) Report.

1.9.5 Land use and land cover changes

Dar es Salaam City has both an international port (Dar es Salaam Harbour) and airport (Julius Nyerere International Airport) serving as a gateway into the region. Dar es Salaam is increasingly becoming a major sitting of industries and commercial activities and as a consequence, this has resulted in the increase of human settlement. Types of industries located in Dar es Salaam City, among others, include textiles, breweries, distilleries, beverages, cement, paints, pharmaceuticals, plastic, metal products, steel, chemicals, food products, petroleum products, dairy products, and batteries (NEMC, 2009). Most industries discharge untreated or partially treated wastewater into the neighbouring surface water bodies such as rivers and the ocean.

Extensive areas of coastal land in the study area are used for residential purposes. A number of residential properties are located adjacent to the shoreline. The recreational value of beaches is growing rapidly as more people are investing along the beaches. Accordingly, Dar es Salaam habour has undergone significant expansion and infrastructure improvements to accommodate, among others, the increased tourism related trade with other destinations including Zanzibar port.

The rapid expansion of Dar es Salaam City has required the conversion of large land areas from agricultural to urban use. The extended area covers expansion of the city in all directions with relatively high density areas along the four major roads: Morogoro, Bagamoyo, Nyerere/Pugu and Kilwa. Urban area has increased from 3081 ha in 1963 to 11331 ha in 1978 (UN-HABITAT, 2010b). Informal settlements occupied about 40% of the city's residential land in 1979 (Lupala, 2002). It was estimated that the city had a built-up area of 61,260 ha in 1999 of which 40, 315 ha (65.8%) were occupied by informal settlements (Kombe, 2005) and the population living in the informal settlements was reported to reach 70% in 2000 (URT, 2000). In 2010, over 80% or 3.2 million out of 4 million of Dar es Salaam's population lived in unplanned areas (UN-HABITAT, 2010a).

Urban development is a significant factor to land cover changes and basically consuming the agricultural land of the surrounding areas. The government reserved the un-developed areas including valleys and swampy areas, for urban agriculture and other uses such as sporting and recreation (Mwamfupe, 1994; cited in Mng'ong'o, 2004): in these valleys and swampy areas were thickets of mangrove trees along the shores of Indian Ocean and in the valleys, a mixture of shrubs and woods in the low-lying land, and forests found in the slopes of hilly areas (e.g. Kimara, Goba and Pugu hills). The Pugu Forest Reserve (PFR) located on the Pugu Hills west of Dar es Salaam, covered 22 km^2 in 1981 (Howell, 1981) but only 10 km^2 of the forest reserve had remained in 1991 (Burgess et al., 1992). The neighbouring Kazimzumbwi Forest Reserve (KFR) is located approximately 20 km south-west of Dar es Salaam on the Pugu Hills, between 120 and 280 metres altitude. The PFR and KFR were contiguous in 1956 before they were separated in 1968 (Clarke and Dickinson, 1995). The forest reserves included part of what was once a much larger forest extending to within 10 km of Dar es Salaam (Clarke and Dickinson, 1995). The two forest reserves face many threats due to high population density. PFR and KFR are very important resource to the adjacent communities. Villages (Pugu Kajiungeni, Pugu Station, Buyuni, Chanika, Kazimzumbwi, Kisanga and Kisarawe) within the area have been depending on these forests for their livelihood. Important forest products utilized includes firewood, poles for building, medicinal materials, fruits and vegetables. Streams arising from PFR and KFR used to supply all the water demand in Dar es Salaam before being replaced by water supply from Ruvu River pumping station which was established in mid-1970s.

The intense urban development in Dar es Salaam can be said to have taken place after 1978 where Dar es Salaam experienced the fastest population growth (4.8% per year between 1978 and 1988, and 4.3% per year between 1988 and 2002), mainly due to rural-urban migration (Castro and Singer, 2003). Urban expansion introduced serious changes in land cover from bushland to grassland and bare land, as vegetation and trees were cleared due to construction, fuel, sand extraction, urban farming and other developments (Mng'ong'o, 2004; Kulindwa et al., 2005; Mtoni et al., 2006; NEMC, 2009). Citywide in the period from 1982 to 2003, the quantity of green areas fell from 80% of the city's total area in 1982 to 73% in 1992 to 55% in 2003 (Mng'ong'o, 2004). Similarly, the developed areas increased from 20% in 1982 to 27% in 1992 and to about 45% in 2003. Unsustainable mangrove exploitation (logging, clearing for rice planting, and charcoal making) is taking place in various locations for urban expansion. It is highly visible in the city of Dar es Salaam, as the city's two districts (Temeke and Kinondoni) take the lead in terms of the size of the damaged mangrove areas (NEMC, 2009).

Both crop growing and livestock keeping practices exist in the built-up and in peri-urban areas of Dar es Salaam City. Zero-grazing livestock production is being practiced in some hospitals, schools and church grounds which have low-density and medium-density plots. Several large scale poultry and pig farms are also being practised in Dar es Salaam. Urban agriculture and aquaculture production are sustained by utilization of coastal resources especially wetlands, mangroves, estuaries and lagoons. Marginal lands such as road reserves, valleys and vacant lands are increasingly used for cultivation. According to the study by Dongus and Nyika (2000) concerning the extent of urban agriculture in Dar es Salaam in 1999, about 650 ha (or 4%) of Dar es Salaam was used for vegetable production, offering employment for over 4000 farmers. Of the 650 ha, 12% were privately owned land, 48% institutional and 40% publicly owned (Dongus and Nyika, 2000). Water for irrigation is mainly obtained from boreholes and shallow hand dug wells. Cultivation in low-lying areas in river valleys and depressions is much preferred, because even during the dry season cultivation is still possible since the water table is close to the surface.

Urbanisation effects on groundwater hydrology include, increase in water demand, more dependence on groundwater use, over-exploitation of groundwater, increase in run-off, reduction in infiltration and deterioration in water quality.

2 GEOLOGICAL AND HYDROGEOLOGICAL SETTING

2.1 General geology of Tanzania

The general geology of Tanzania is characterized mainly by the Precambrian and Phanerozoic formations (Fig. 2.1). The former comprises the Archaean and Proterozoic periods, whereas the latter comprises Palaeozoic, Mesozoic and Cenozoic periods. The Archaean (Tanzanian Craton) covers the central part of the territory up to south and east part of Lake Victoria. The Ubendian Belt forms, together with the Usagaran Belt, a large Palaeoproterozoic metamorphic domain that borders the Archaean Tanzanian Craton (Fig. 2.1): the Usagaran Belt bounds the craton to the south and southeast and the Ubendian Belt to the west and southwest. The belts have similar high-grade metamorphic lithologies but differ in structural parts of the trends: the Ubendian Belt strikes NW to NNW, whereas the Usagaran Belt trends NE-SW to E-W in its southern portion (Lenoir et al., 1995). Neoproterozoic Mozambique belt occurs in the East of Tanzania. Usagaran Belt and Ubendian Belt were rejuvenated during the Neoproterozoic to early Cambrian Pan-African thermo-tectonic event (Lenoir et al., 1995; Muhongo et al., 1999). Usagaran Belt and Ubendian Belt are separated from the sedimentary successions by the prominent Tanga fault striking NE-SW. This fault zone has been active with varying intensity through geological time and has to some extent controlled the sedimentation in the area. Continentally derived sediments of Mesoproterozoic and younger age cover part of the craton, especially in the east. The northern and southern highland regions are parts of the major East African Rift system which extends northwards through Kenya and Ethiopia, and which has developed through extreme crustal tension, rift faulting and volcanic activity. The Eastern Rift (Fig. 2.1) extends with a NNW trend through northern Tanzania and the Western Rift extends NW to SE along the south-western margin of Tanzania. The geology of the Rift zones comprises volcanic and intrusive rocks. Tertiary mafic to intermediate volcanics including carbonatites occur mainly in the Kilimanjaro and Eastern Rift areas (Taylor, 2009). Sedimentary rocks of various ages (Palaeozoic to Recent), including the Karroo Sandstone, extend from Tanga at the Kenyan border south-westwards to Lake Nyasa. The sediments are mixed formations, including sandstones, mudstones and limestones. The coastal plain consists of largely unconsolidated sediments (beach sands, dunes and salt marsh) together with some limestone deposits. The stratigraphic column is provided in Fig. 2.2.

2.1.1 Archean

Three divisions form the Archean system (JICA, 2008; Fig. 2.2); i) the Dodoman System: is the oldest formation in the country (confined to central Tanzania) and is in general highly metamorphosed and migmatized sediments with intrusions of volcanic rocks, ii) the Nyanzian System is confined to Lake Victoria region and consists of green schists and felsic meta-volcanics including Banded Iron Formations (BIFs) and fine-grained clastic sediments, and iii) the Kavirondian is confined to Lake Victoria region and is weakly metamorphosed, consists of quartzite and phyllite. The rocks for Dodoman system are very thick and not easily weathered: the recharge mechanism is through the fracture zone (Kashaigili, 2010). On the other hand BIF in Nyanzian System, schists and quartzite are dense and hard with possibilities for groundwater recharge through the fracture zones (Kashaigili, 2010).

2.1.2 Proterozoic

Three systems form the Proterozoic formation (JICA, 2008; Fig. 2.2); i) the Usagaran and Ubendian Systems, composed mainly of highly metamorphosed gneisses but also marbles, belong to Proterozoic and sometimes to older Archean, ii) the Karagwe-Ankolean System in North-West Tanzania consists of weakly metamorphosed schists, phyllites, argillites and quartzites, and iii) the Bukoban System which is confined to western Tanzania and has limited exposures of rocks: it consists of sandstones, conglomerates, dolomites and amygdaloidal basalts. Groundwater recharge in the Proterozoic formation is generally through faults or lineaments with high possibility for groundwater development (Kashaigili, 2010).

2.1.3 Paleozoic

Bukoban System links Proterozoic and Paleozoic formations (Figs. 2.1 and 2.2). However, Paleozoic consists of continental clastic sediments which are common in the south. Parts of the Karroo formation (Permian to Jurassic) may form the link between the Mesozoic and the Paleozoic. The Karroo sedimentation represents terrestrial sediments, consisting of sandstones, conglomerates, tillites, shales, red and grey mudstones, coal measures and occasional limestones.

2.1.4 Mesozoic (Jurassic to Cretaceous)

Shales, limestones and evaporites of this age occur near the coast (Fig. 2.2). Alkaline intrusions like carbonatites, kimberlites and similar rocks are common throughout the country.

2.1.5 Cenozoic (Quaternary)

Cenozoic deposits are in general of three types (JICA, 2008; Fig. 2.2): i) marine and continental sediments like sandy, loamy soils forming coastal plains and interior basins, as well as clays in riverbeds and on hills, ii) extrusions of alkaline and sub-alkaline rocks and intrusive gabbroid rocks in Central North and around Lake Nyasa, and iii) laterites covering nearly all types of rocks.

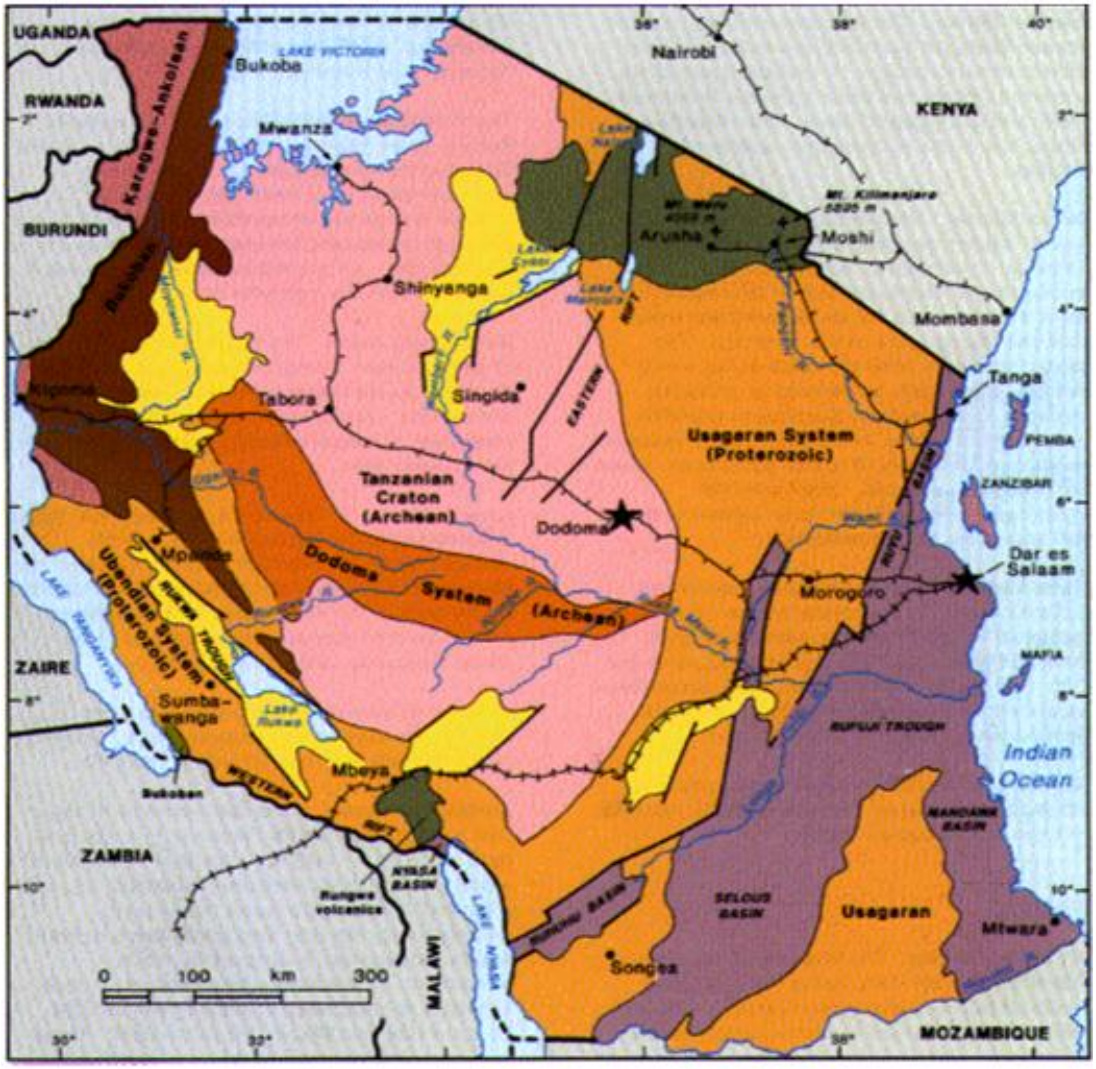

Figure 2.1: General geology of Tanzania (after Hester, 1998; cited in Taylor, 2009).

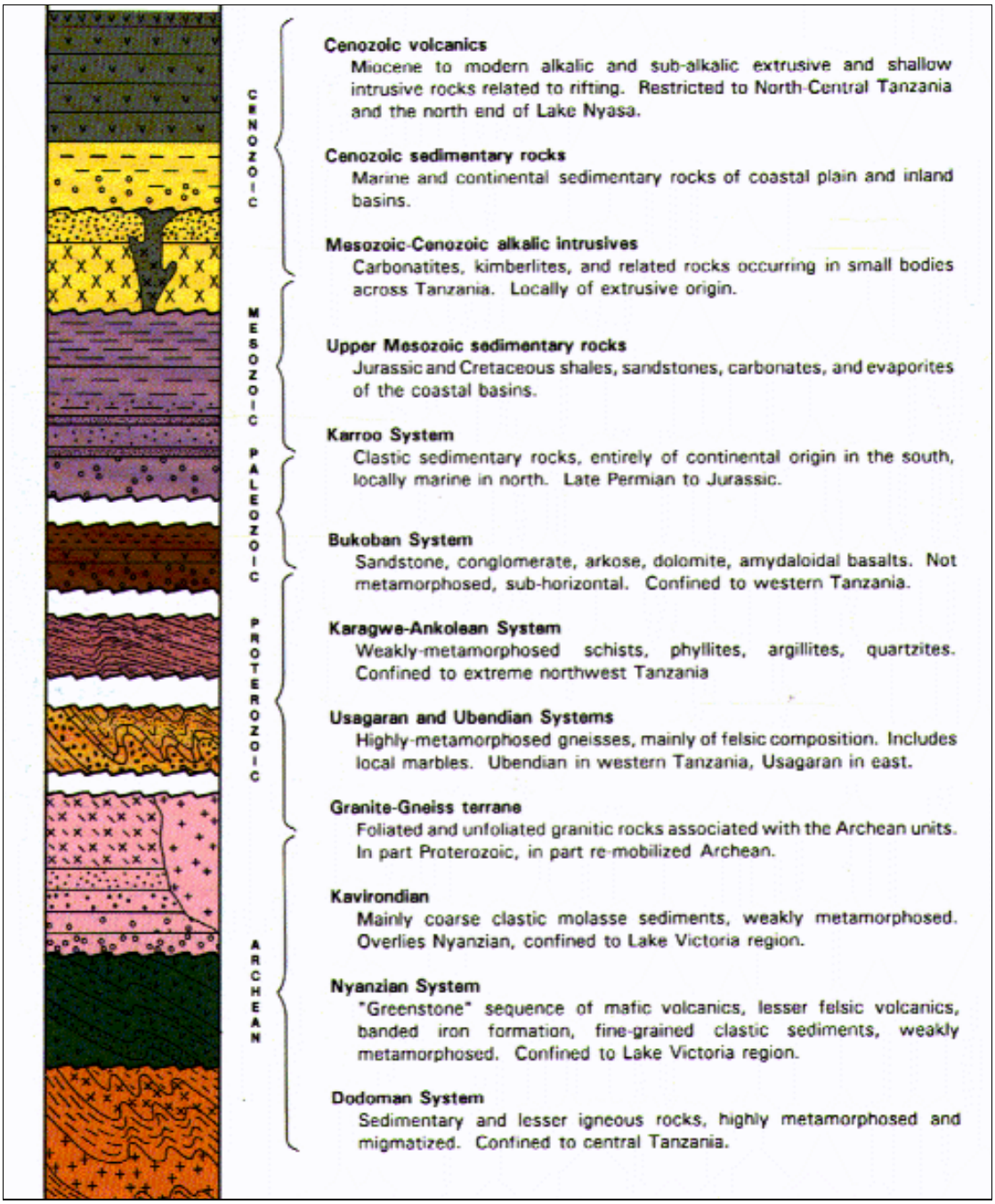

Figure 2.2: Stratigraphic column for Tanzania (after Hester, 1998; cited in Taylor, 2009).

2.2 General geology of coastal Tanzania

The coastal basin of Tanzania encompasses a narrow belt along the mainland (Fig.2.3). Several authors have studied the geology of coastal Tanzania (Alexander, 1968; Kent et al., 1971; Msindai, 1988; Mpanda, 1997; Muhongo et al., 2000; Pearson et al., 2004; Mjemah 2007). The sediments in the coastal basin of Tanzania have ages ranging from Jurassic to Recent and belong to the so-called “Somali Basin” of eastern Africa (Muhongo et al., 2000).

The western boundary of this basin is defined by a major fault zone which extends from Tanzania through Kenya and Somalia, to Ethiopia (Muhongo et al., 2000). Two major trends of the fault zone occur in the coastal basin of Tanzania: NNE-SSW and NNW-SSE trends respectively for Tanga and Lindi fault zones (Fig. 2.4). The faulting events mark the major coastal boundaries between the metamorphic crystalline rocks of the interior and the sedimentary rocks of the coastal basin (Kent et al., 1971).

The sedimentary bedrock column commences with the continental Karroo sequence, spanning from Permo-Carboniferous to Lower Jurassic (Kapilima, 2003). This Karroo unit is represented principally by fluviatile arkosic sandstones to conglomerates and shales (Ngerengere – Formation) (Fig. 2.3) characterising the Selous – Ruvu – Tanga rift sub-basin (Kapilima, 2003). In the Middle Jurassic, a continental shelf was established with deposition of shallow water oolitic to oncolitic limestones, detrital conglomeratic to coralliferous limestones and graded, detrital conglomeratic sandstones (Kapilima, 2003). These marine sediments are either overlying unconformably the metamorphic terrain in the vicinities of Msata and Lugoba or are separated from the basement complex by the continental sequence of the Karroo facies in the case of Tanga and Ngerengere (Kent et al., 1971). The marine transgression continued into the Upper Jurassic with deposition of shales, clay and marls. From the middle Jurassic to Cenozoic, several transgressions and regressions had occurred resulting into a thick accumulation of more than 4000 m and 6000 m of Mesozoic and Cenozoic sequences respectively (Kapilima, 2003).

Generalised stratigraphy of the coastal sedimentary basins of Tanzania is available in the study conducted by Mpanda (1997). Sediment types vary greatly, from the clay bound sands and gravel to the far more unconsolidated suite of recent times. The unconsolidated suites occurring adjacent to the coast include the river alluvium and terraces, lagoon sand, clays and silts, beach ridge sands, sand dunes and beach deposits, and some superficial white buff sands belonging to the Holocene. Further inland, dominant rocks date from the Miocene to Pleistocene whereas the occurrence of other outcrops includes Lower Jurassic and Cretaceous limestone and marine silts.

Coastal Tanzania has been divided into three parts (Fig. 2.5): Northern, Central and Southern Mainland, separated by the rivers Ruvu and Rufiji (Kent et al., 1971). The Northern Mainland is a narrow belt, dominated by Mesozoic rocks. The Central Mainland, in which the study

area is situated, mainly consists of the Dar es Salaam embayment. In this part Cretaceous and Neogene rocks are important. The Southern Mainland contains the Karroo salt basin of Mandawa, thick Jurassic and Cretaceous sediments and a full development of marine Tertiary beds (Kent et al., 1971). The study area is part of the Central Mainland.

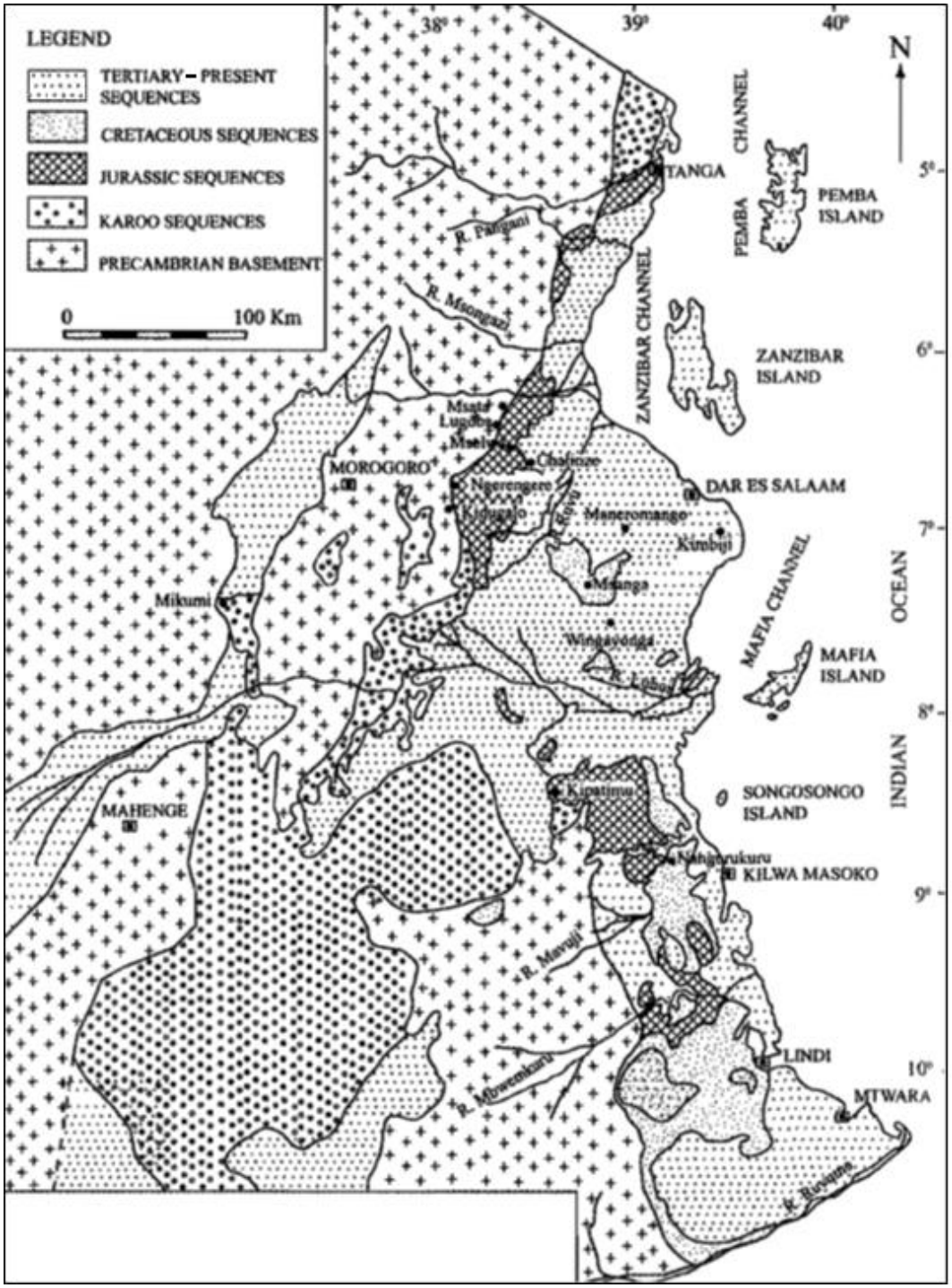

Figure 2.3: Geological map of coastal Tanzania compiled from Kent et al., 1971 (cited in Kapilima, 2002).

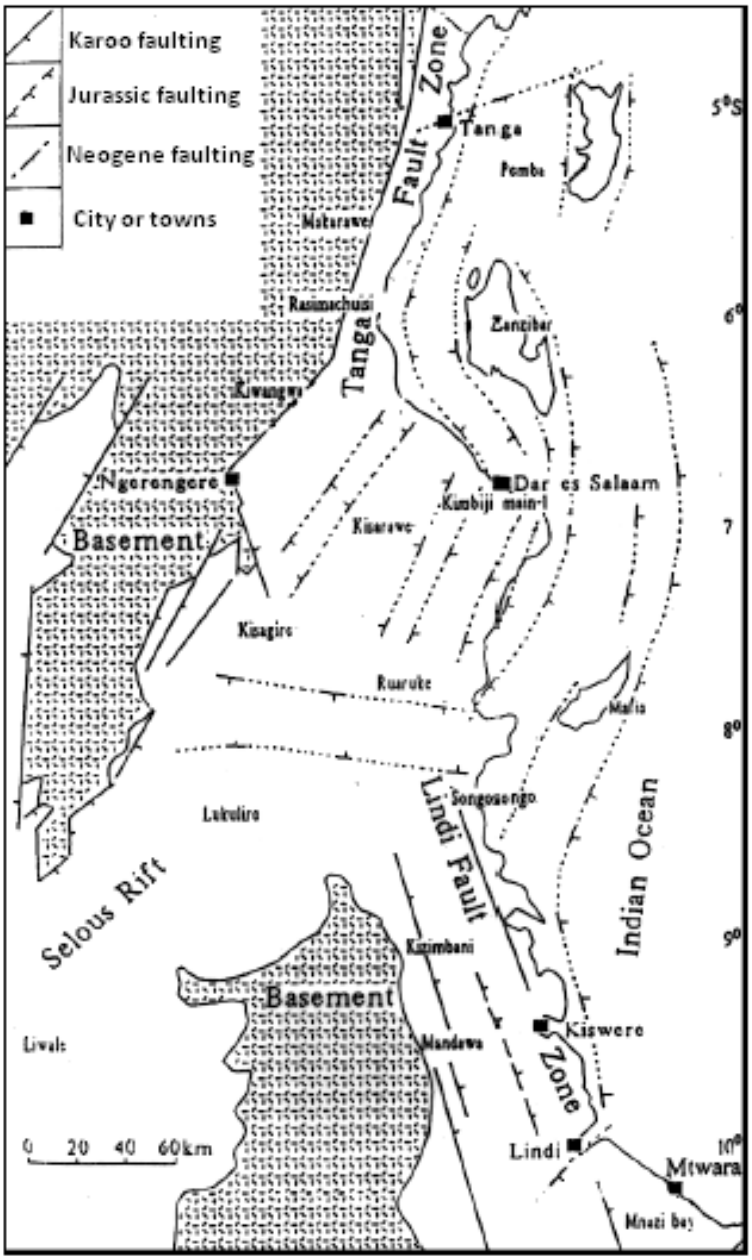

Figure 2.4: Major structural features of coastal Tanzania (Kajato, 1982; modified by Muhongo et al., 2000).

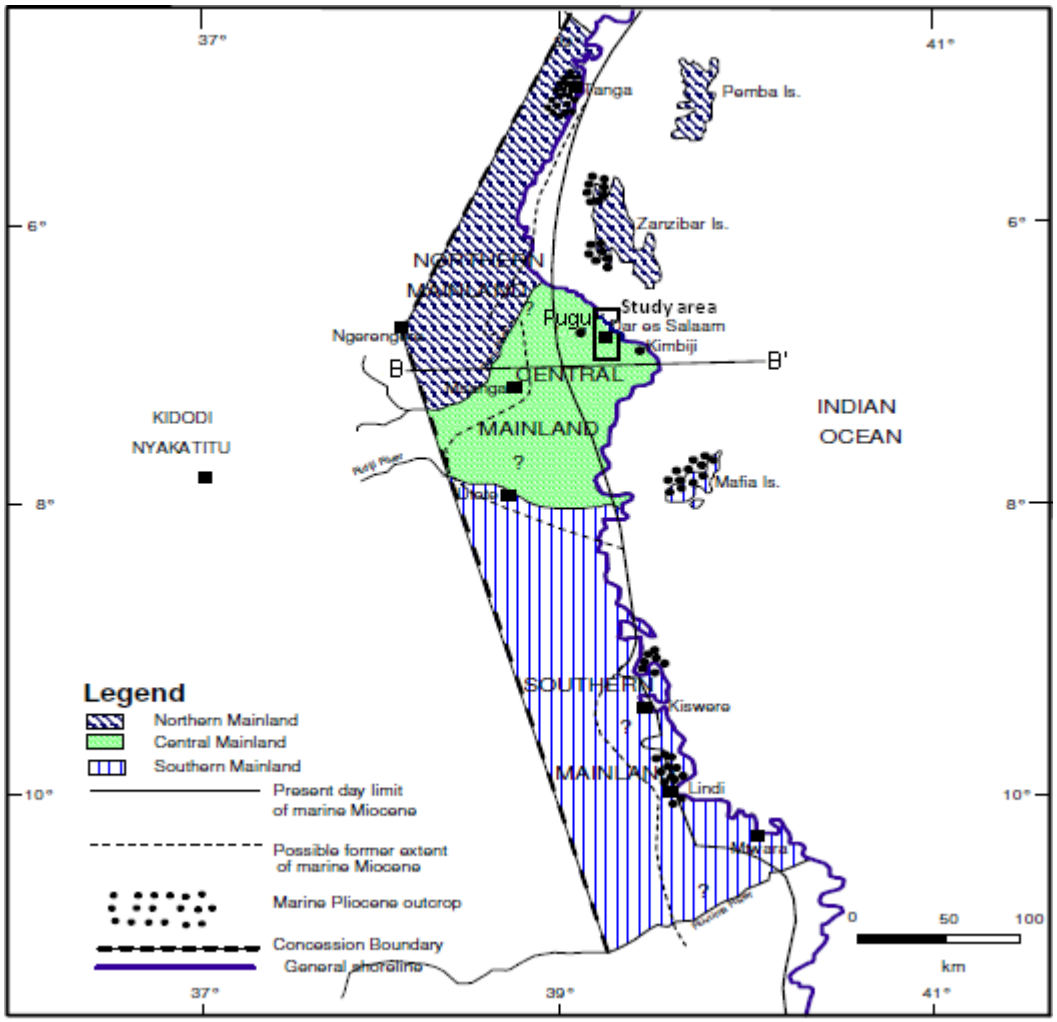

Figure 2.5: Regional divisions of coastal Tanzania (Kent et al., 1971).

2.3 Geology of Dar es Salaam Region and the study area

2.3.1 Geology of Dar es Salaam Region

The geology of Dar es Salaam Region is represented in Figs. 2.6 and 2.7. The geological formations consist mainly of Quaternary and Neogene deposits. The Quaternary deposits are subdivided into: i) alluvial deposits comprising clay, silt, sand and gravel, which are recent deposits occurring in river valleys, ii) coral reef limestone and iii) sands of Pleistocene to Recent age with Holocene white buff sands at outcrop; these sands constitute the main aquifers of Dar es Salaam Region.

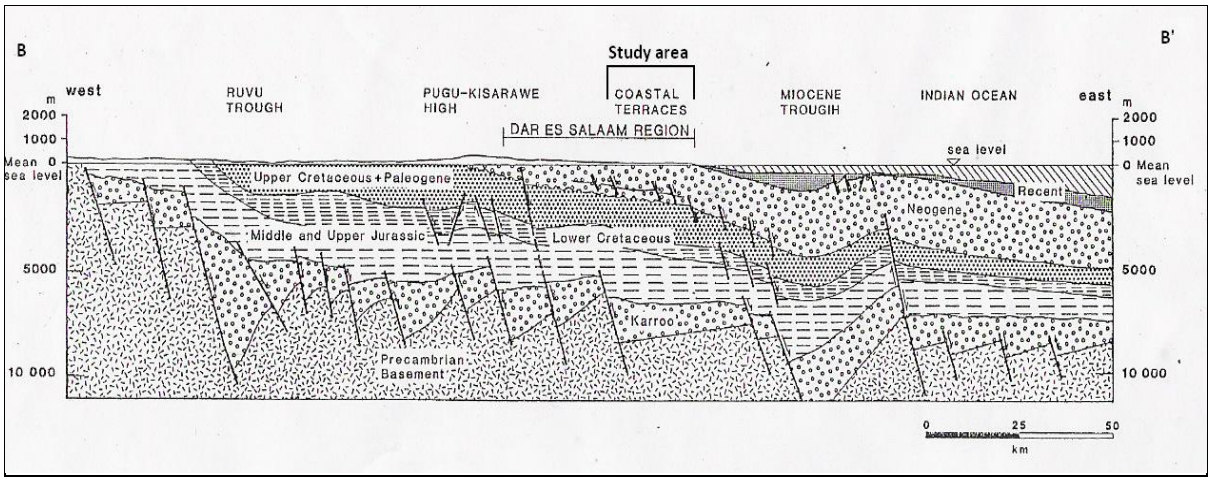

Figure 2.6: Cross-section B-B' showing the sedimentation and fault pattern (Msindai, 1988). The location of the profile is shown on Figure 2.5.

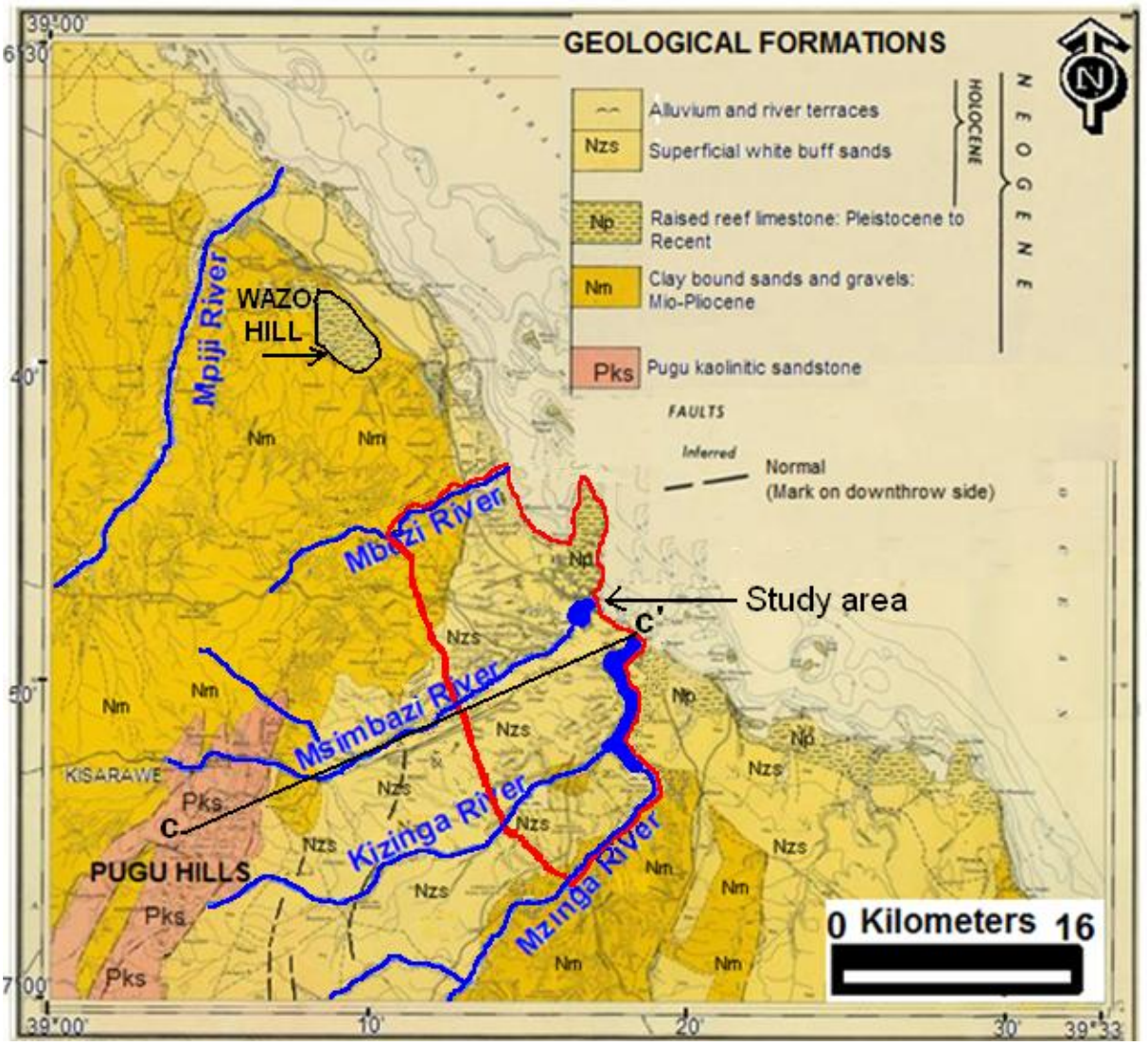

Figure 2.7: Geological map of Dar es Salaam and the study area (GST, 1963).

The Neogene deposits aref classified into two main groups: i) the Mio-Pliocene clay-bound sands and gravels formation outcropping in the northwest, south-east and to the south, and underlying the Pleistocene to Recent deposits in most of the study area. They appear to be more clayey near their top whereas in deeper parts, the clay content may decrease, leading to a deep aquifer; and ii) the Lower Miocene Pugu Kaolinitic Sandstone occurring in the west. The latter consists of reddish brown, thick-bedded sandstone inter-bedded with minor siltstone, shale, and limestone (Fig. 2.7). Sedimentary structures in the Pugu Hills sandstone suggest that they were deposited in a fluvial dominated flood plain without a significant marine influence (Mutakyahwa, 1987). The provenance of the sandstones is surmised to be the Precambrian metamorphic rocks of the Usagaran System and sediments of Permo-Carboniferous (Karroo) to Cretaceous age (Mutakyahwa, 1987).

Soil conditions are diversified and consist of two major different plains: the coastal plain soils and the river plain soils. Coastal plain soils are yellowish red, brown to dark-brown sandy loam, with a fairly thick loose sandy top with good porosity and well drained with a fairly low capacity to retain moisture. An alternation of fine and coarse grained sands occurs within the valleys, creeks, deltas and mangrove sites. The mouths of Kizinga, Mzinga and Msimbazi rivers form the main deltas.

The three main terraces in the eastern central coastal sedimentary plain are the Mtoni, Tanga and Sakura terraces (Alexander, 1968). The coastal plain is elevated at about 0-10 m.a.s.l (Mtoni terrace), 10-50 m.a.s.l (Tanga terrace) and 50-130 m.a.s.l (Sakura terrace) (Fig. 2.10). The upland plateau comprises dissected land and the Pugu/Kisarawe Hills to the west. Pugu Hills are characterised by steep weathered slopes and ranges of kaolinitic sandstones. Much of the faulting and uplifting are considered to have taken place recently and the repetition of sandstone/clay-bound sands in the Pugu Hills is best explained by block faulting (GST, 1963). The coastal area of Dar es Salaam region has tentatively been divided into three main blocks namely Wazo, Dar es Salaam and Kimbiji. Generally the blocks lie within an area traversed by a series of lineaments and faults. The lineaments are classified into regional, intermediate and local faults. Furthermore, the strike directions of the lineaments tend to form two recognizable sets NNE and NNW.

Inland alluvial plains are characterised by rivers originating from Pugu Hills to the west of the study area. In the hydrogeological cross-section in Fig. 2.10, the altitude at Pugu Hills ranges

from 175-265 masl The superficial sands of the flat low-lying coastal plain represent re-distributed outwash material from the fault blocks (GST, 1963): east of the Pugu Hills, the sands are clean and off-white in colour, but elsewhere they are buff to brown. Near the coast they grade into marine sands and silts, rich in shell fragments. Along the Msimbazi River they overlie the red sand earths and they are regarded as recent deposits.

Tertiary to Recent coral limestones occur in numerous locations along the Indian Ocean and are mined for several purposes. In Dar es Salaam, limestones show various degree of weathering and show evidence of dissolution processes. Prospecting for cement material has been carried out north of the study area at Wazo Hill (Fig. 2.7). A thick coral limestone bed and red soil are exploited for cement production by Tanzania Portland Cement Company Ltd (TPCCL). Although the history of the factory goes back into 1959, it was officially opened for production in 1967. The production of cement principally includes mining, crushing and grinding of raw materials, principally limestone and clay. Wazo Hill limestone deposit is described to have high grade limestone material, which forms the basis of the high quality cement produced. Limestone extraction comprises about 90% of raw materials for cement production and annual limestone production at Wazo Hill is estimated at 1.2 million tonnes (MTL, 2010). The typical site lithology of Wazo Hill deposit is presented in Fig. 2.8. Gypsum (around 5%), which is used for mixing with the clinker in order to help to retard the setting time of the cement is from sources elsewhere. About 80-90% of raw material for kiln feed is essentially limestone. Although the precise amount will vary, clayey raw material accounts for about 10-15%. Magnesium carbonate, which may be present in the limestone, is the main undesirable impurity: the level of Magnesia (MgO) in the clinker is supposed to be less than 5% (BGS, 2005). As the raw materials are obtained directly from limestone and clay mines, minor constituents like Magnesia (MgO), sodium, potassium, sulphur, chlorine compounds etc., may also be present in the raw materials up to a limited extent, which does not adversely affect either the manufacturing process or the quality of cement produced (Avaşar, 2006).

The process of cement production normally results in a variety of wastes, dust being the major concern compared to solid and liquid wastes. In Dar es Salaam for instance, in 1993, before the cement factory introduced mitigation measures, the factory produced 106,000 tonnes of dust in that year, accounting for 94.5% of all the suspended particulate matter in the city (URT, 2004). The deposition of limestone and clay dusts from the factory and/or dissolution of calcite from limestone deposits may have effects on the groundwater quality.

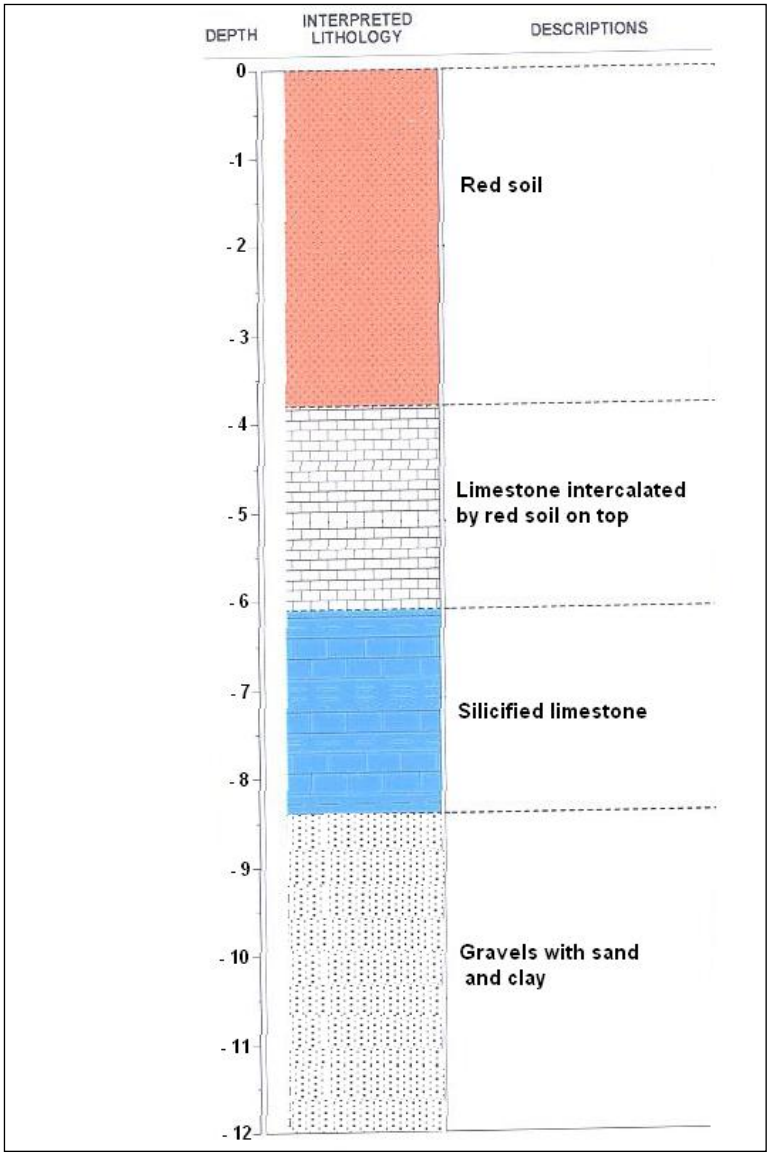

Figure 2.8: Typical site lithology (MTL, 2010) of Wazo Hill deposit.

2.3.2 Geology of the study area

Fig. 2.9 shows the geological map of the study area which is located between Mbezi River and Mzinga River. The area adjacent to the ocean is characterized by raised coral reef limestone and/or sand materials underlain by coral reef limestone of Pleistocene to Recent age. At Masaki and Oysterbay areas raised coral reef limestone is clearly observed. Recent alluvial deposits (sands, silts and clays) occur within the main river valley systems that cut across the coastal plain. Except Mio-Pliocene clay-bound sands and gravels occurring in the north-west, the rest of the study area is covered with Quaternary (Pleistocene to Recent) sand.

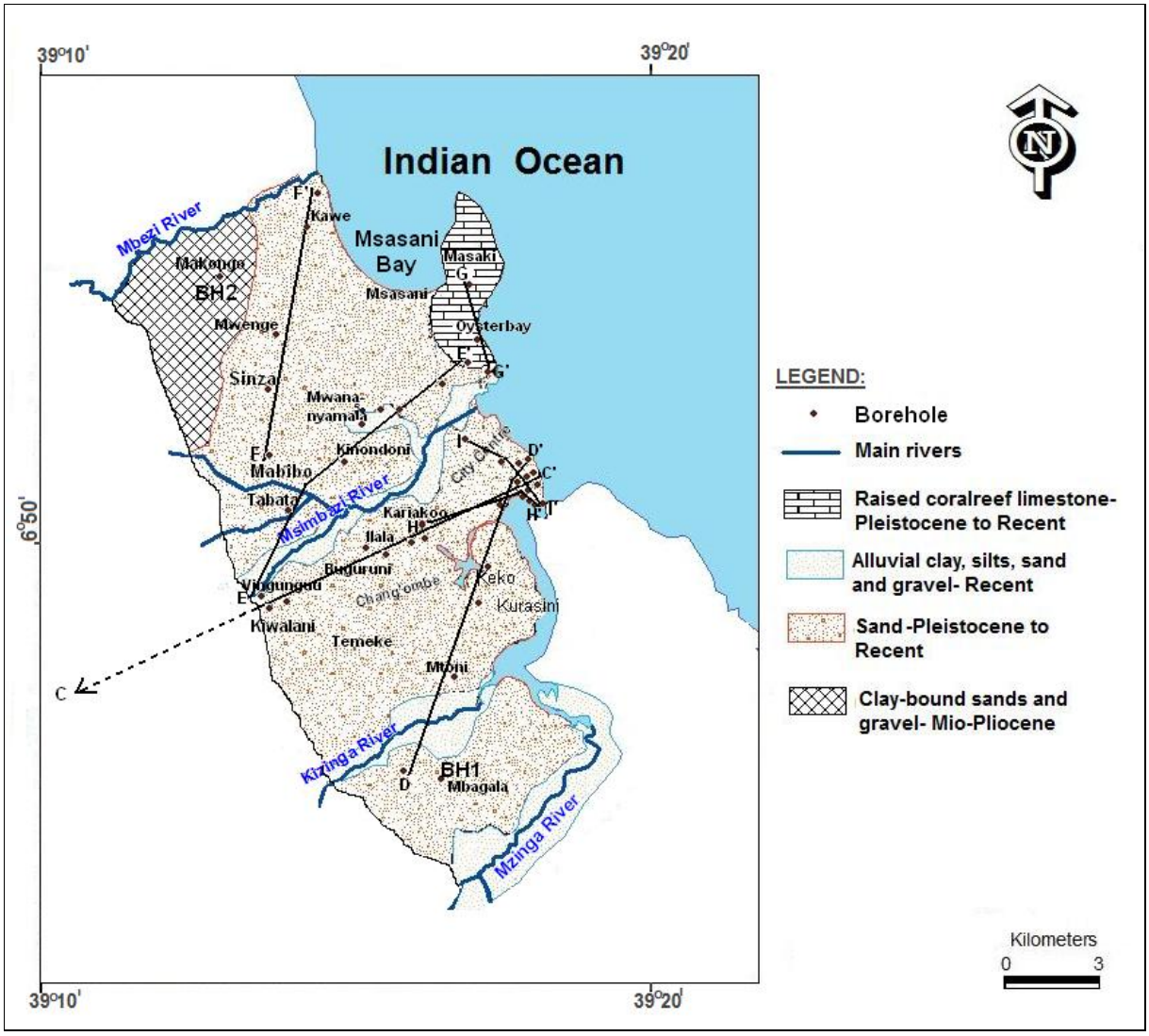

Figure 2.9: Geological map of the study area.

2.4 Hydrogeology of Dar es Salaam Region and the study area

2.4.1 Hydrogeology of Dar es Salaam Region

Dar es Salaam Quaternary coastal aquifer (DQCA) is formed by unconfined and semi-confined aquifer bands consisting of sand and/or limestone (Fig. 2.10; cfr 2.4.2). The inspection of lithological logs from the available groundwater drilling reports indicates that Dar es Salaam Region is characterized by alternating layers of sands, clays, gravel and coral limestone of various degree of weathering. Within the unconsolidated Quaternary sand deposits (Fig. 2.10) the presence of the semi-pervious unit (clay, sandy clay and silts) allows two productive aquifers both of Quaternary age to be distinguished: an upper unconfined sand aquifer and lower semi-confined sand aquifer bands, which may be separated by further semi-

pervious layers. When the upper semi-pervious layer is missing or fragmented, the unconfined aquifer can extend down directly to the second semi-pervious layer (Fig. 2.10). The lower aquifer overlies the substratum formed by Mio-Pliocene clay-bound sands. Reef limestone of Pleistocene to Recent age is prominent near the coastline and may be present both in the unconfined or in the semi-confined aquifer (Mtoni et al., 2012). However, sands are the most important in Dar es Salaam for supplying groundwater. The upper unconfined aquifer varies in thickness from 1 m near the ocean to about 25 m inland. The thickness of the semi-confined aquifer is known to vary greatly in the existing boreholes, from about 3 m to 50 m. The thickness of the semi-pervious layer separating the two aquifers also varies greatly, from about 6 m to 35 m. The lower aquifer superimposes the substratum formed by Mio-Pliocene clay-bound sands and gravels (Fig. 2.10). Based on the borehole (PW1) (Fig. 2.13) (DAWASA, 2007) drilled at Kimbiji, the thickness of the latter is more than 600 m.

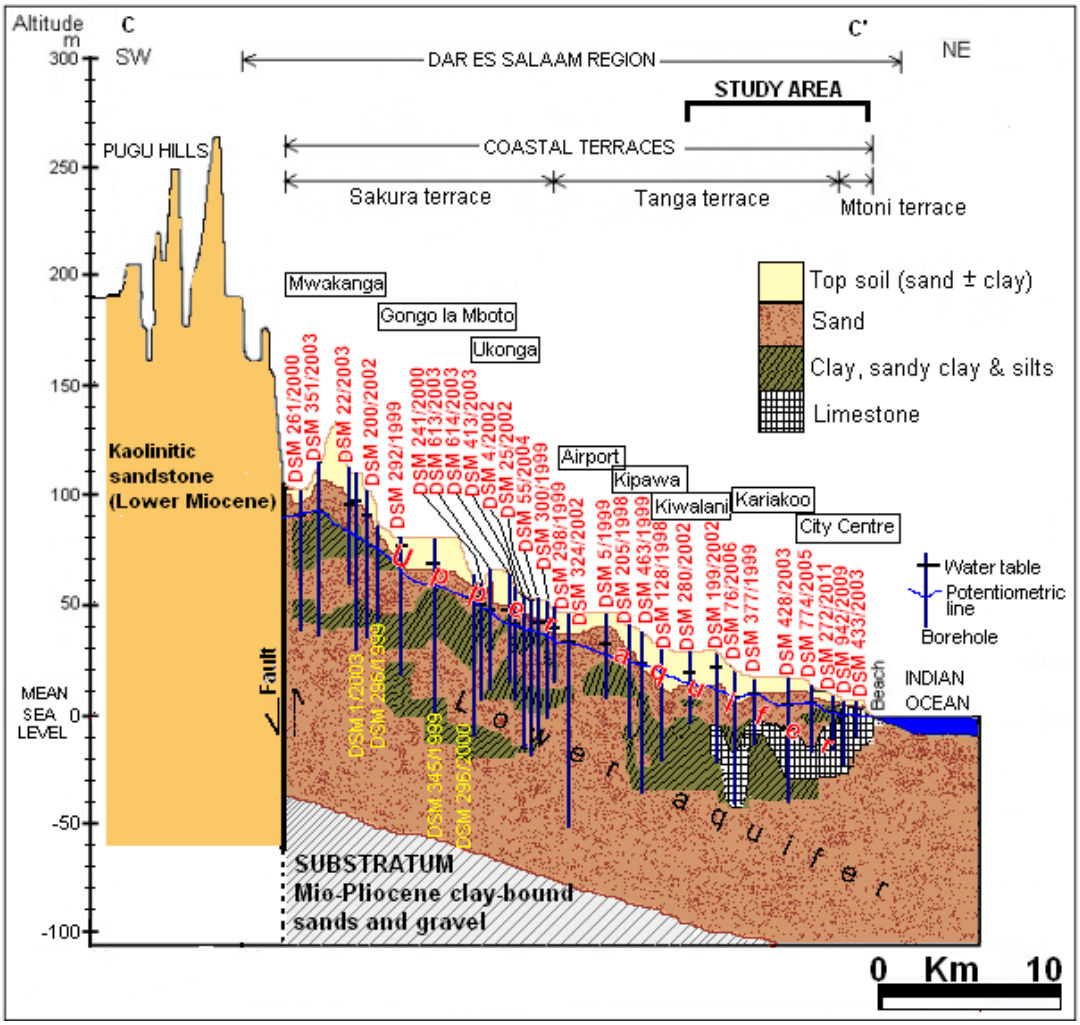

Figure 2.10: Cross-section C-C' showing hydrogeological units and coastal terraces in Dar es Salaam Region: topographic elevation in the profile was taken from Msindai (1988). Location of the cross-section is shown in Fig. 2.7.

2.4.2 Hydrogeology of the study area

Based on the lithological logs from DDCA the available groundwater drilling reports, the study area is characterized by alternating layers of sands, clays, gravel and coral limestone of various degree of weathering. Several cross-sections (Fig. 2.9) were established to describe the hydrogeology of the study area. Groundwater in the study area is abstracted from multiple layers of Quaternary age: an upper unconfined sand aquifer and semi-confined aquifer sand bands (Figs. 2.11(a-h)). The unconfined aquifer and semi-confined aquifers are separated by the presence of the semi-pervious unit (clay, sandy clay and silts); further semi-pervious layers can be found within the semi-confined aquifer. This is clearly illustrated in Fig. 2.11(a) but can as well be observed in Figs. 2.11(b-c). In some places semi-pervious units seems to be not present or fragmented: for example in borehole DSM 704/2009 (Fig. 2.11(c)). In this case, the unconfined aquifer and semi-confined aquifer can not be distinguished.

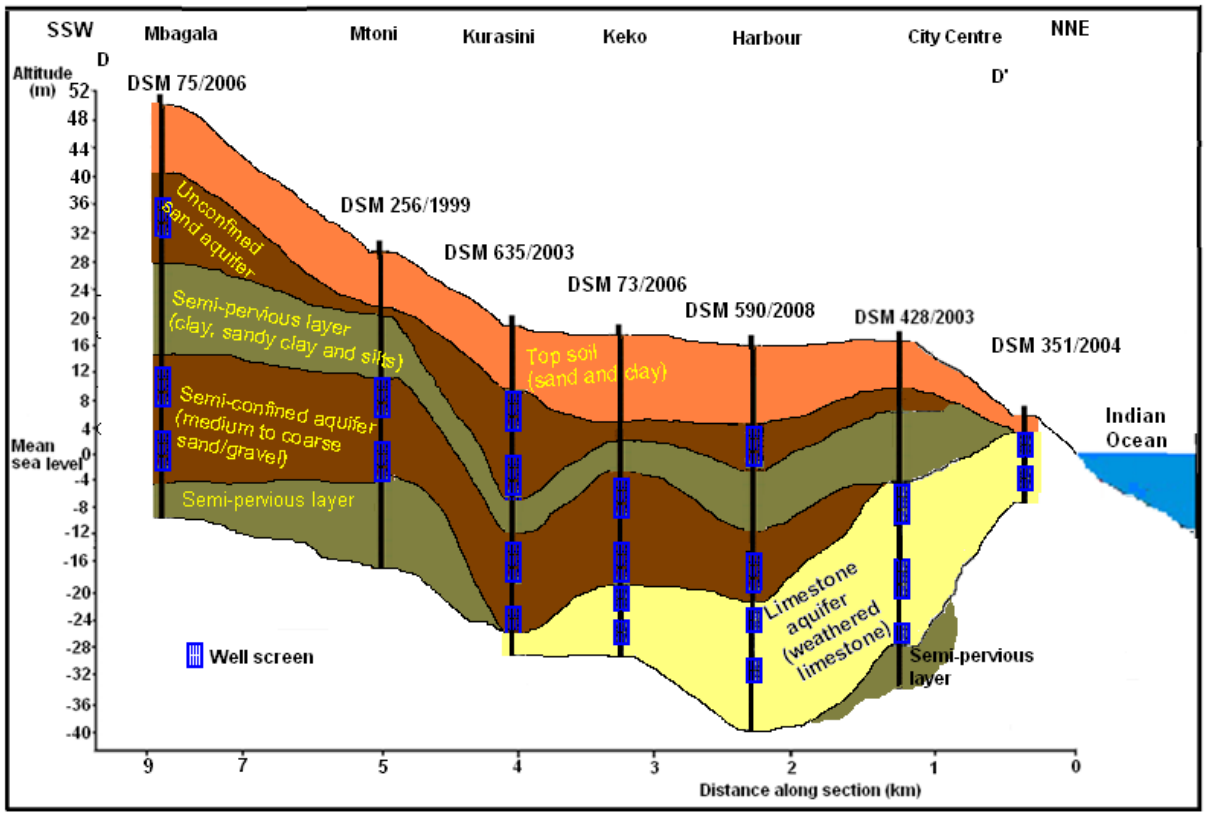

Figure 2.11(a): Cross-section D-D' showing hydrogeological units in the study area. Location of the cross-section is shown in Fig. 2.9.

Quaternary deposits also comprise coral reef limestone (Pleistocene to Recent age), especially near the ocean. To the north of Mzimbazi River this can be observed at Oysterbay (Fig. 2.11(b)), Kawe (Fig. 2.11(c)) and Msasani/Masaki (Fig. 2.11(d)). From the surface, coral reef

extends to over 32 m at borehole B8 (Fig. 2.11(d)) comprising limestone of about 20 m thick. To the south of Msimbazi River, coral reef limestone is prominent along the coast in City Centre (Figs. 2.10 and 2.11(e-f)). Significant coral limestone can be observed from the ocean at City Centre to Kariakoo area about 6 km from the coastline (Fig. 2.10). On the other hand, extensive sand deposit occurs at Kariakoo area: borehole DSM 604/2003 (Fig. 2.11(e)) indicates an extensive sand deposit of 36 m thick overlying limestone of about 3 m thick. The cross-section I-I' (Fig. 2.11(f)) constructed along the coast at City Centre indicates limestone occurring laterally connecting with or both underlying and overlying the sand aquifer. Except at Masaki peninsula where limestone is exposed and along the coastline where limestone is significant, away from the coastline to the west and south, sand deposits dominates. Fig. 2.11(g) indicates typical borehole details at Mbagala located in the south about 9 km from the coastline. Borehole DSM 395/2000 (indicated as BH1 in Fig. 2.9) was drilled to a depth of 70 m and it indicates only the alternation of sand, clay and sandy clay materials. The succession of the unconfined aquifer, semi-pervious layer and semi-confined aquifer units is visible.

Fig. 2.11(h) indicates typical details from a borehole located in the clay-bound sands in the north-west of the study area at Makongo area (Fig. 2.9). Borehole DSM 466/99 (indicated as BH2 in Fig. 2.9) was drilled to a depth of 40 m and it shows clay and sandy clay materials are dominant. However, this borehole was abandoned due to very low groundwater production possibly due the low permeability of the clay-bound sands which does not favour rainfall infiltration. Groundwater recharge mainly occurs from rainfall that falls on the sandy sediments which favour infiltration (Mjemah et al., 2011; Mtoni et al., 2013). Water also drains into the aquifer from some rivers (Msimbazi and Kizinga) within the coastal plain (Mjemah, 2007). In other reaches of the rivers, groundwater discharges into streams as base flow. Recharge through the clay-bound sands outcrops in the northeast and southeast of the study area is generally small, which is mainly favouring runoff (Mjemah, 2007). In Pugu Hills (west of the study area), the underlying masses of sandstone with faults and joints are the permeable layers, for the water can penetrate readily through the faults and joints which as such provide features for remote recharge.

In the study area, sand overlies the upper unconfined aquifer. The latter consists mostly medium to coarse sand with varying amounts of silt, clay and gravel. As already mentioned, coral reef limestone exists mainly close to the coastline (Figs. 2.11b and 2.11d). The

occurrence of a semi-pervious layer beneath unconfined aquifer allows to distinguish the lower aquifer. The latter occurs in semi-confined aquifer bands separated by semi-pervious layers. Borehole DSM 466/99 (Fig. 2.11h) indicates the presence of two semi-confined sand aquifer bands separated by semi-pervious layers. The presence of a semi-pervious layer underlying the semi-confined aquifer which is well observed in boreholes DSM 75/2006, DSM 256/1999 and DSM 428/2003 (Fig. 2.11a) and DSM 395/2000 (Fig. 2.11g) indicates the possibility of other semi-confined aquifer(s) underneath: the drill logs are not deep enough to show the whole aquifer system. Limestone in the semi-confined aquifer is well recognized to be present mainly near to the coastline (Fig. 2.11a). A situation also exists for occurrence of sand-limestone aquifer whereby sand material is mixed with highly weathered limestone as indicated in borehole DSM 301/2011 (Fig. 2.11b). The drill logs available in the study area are not deep enough to reach the lower boundary of the groundwater reservoir. However, as already indicated in Fig. 2.10, the lower aquifer superimposes the substratum formed by Mio-Pliocene clay-bound sands, which are considered as the lower boundary of the groundwater reservoir.

Surface water supply in the study area is deteriorating due to various reasons (i.e. domestic and industrial discharges). Due to the sandy nature of the subsoil in many parts of the city, sinking of boreholes/wells is easy and this has led to the increased supply of groundwater to complement the reticulated supply by surface water. Both upper unconfined and lower semi-confined aquifers undergo intense exploitation through a large number of production boreholes. The drilling depth data for a sample of 500 boreholes drilled between 1997 and 2009 in Dar es Salaam (Drilling and Dam Construction Agency, DDCA) indicate most production boreholes were drilled at depths ranging between 40 to 60 meters with an average depth of 50 m. The static water level is at a mean depth of about 12 m. Unlike the inland where boreholes exist up to 100 m deep, drilling near to the coastline ranges mostly between 10 and 20 m depth. The latter is restricted by the water quality and avoidance of seawater intrusion risk (Mtoni et al., 2012). The discharge rates for boreholes used for water supply range from 10-15 m^3/h and few of them 15-30 m^3/h.

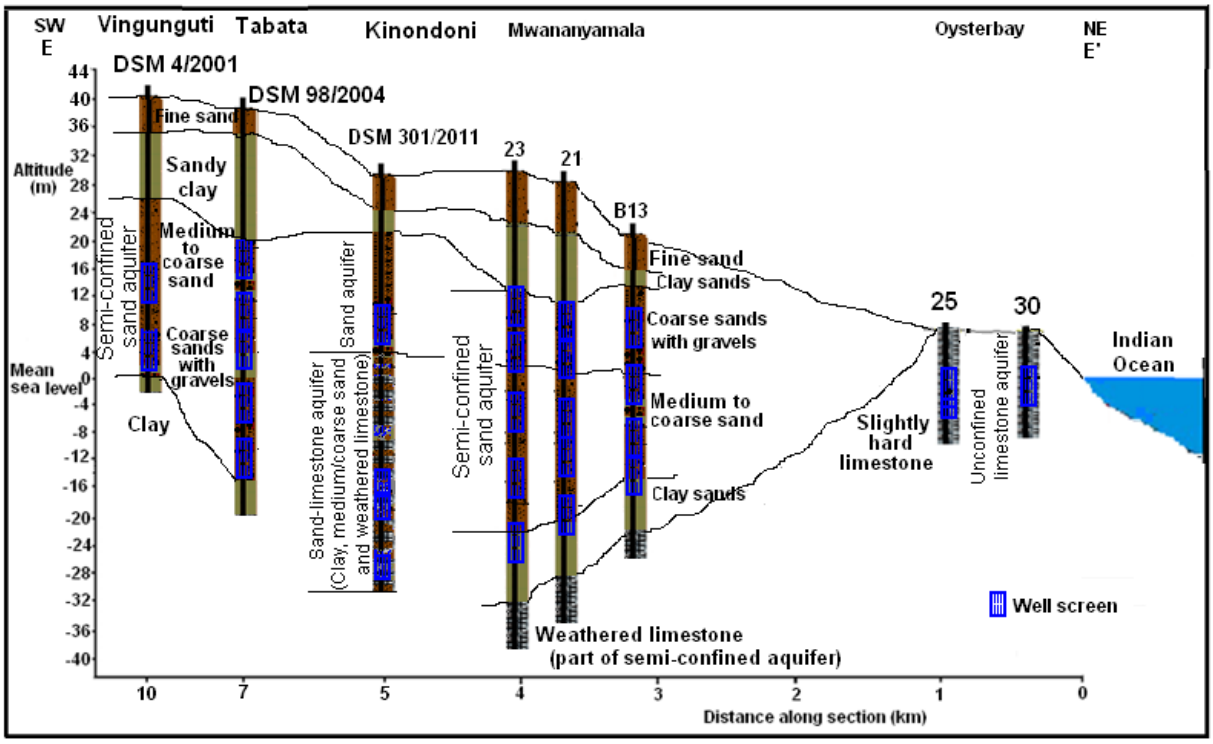

Figure 2.11(b): Cross-section E-E' showing hydrogeological units in the study area. Location of the cross-section is shown in Fig. 2.9.

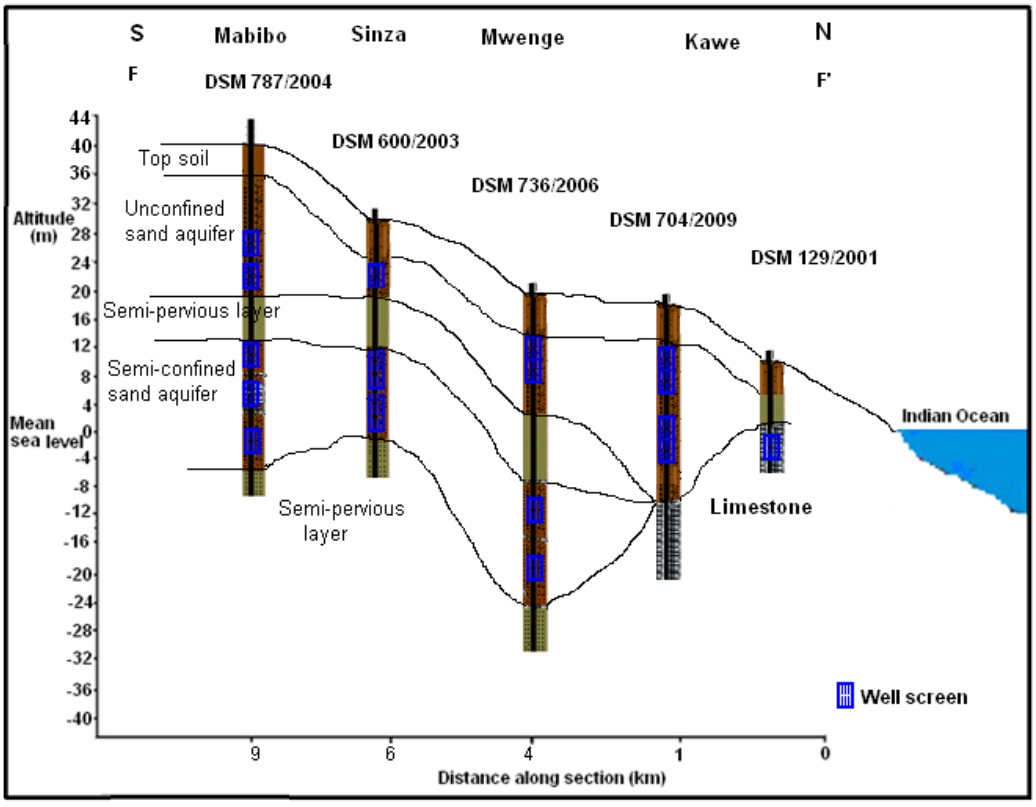

Figure 2.11(c): Cross-section F-F' showing hydrogeological units in the study area. Location of the cross-section is shown in Fig. 2.9.

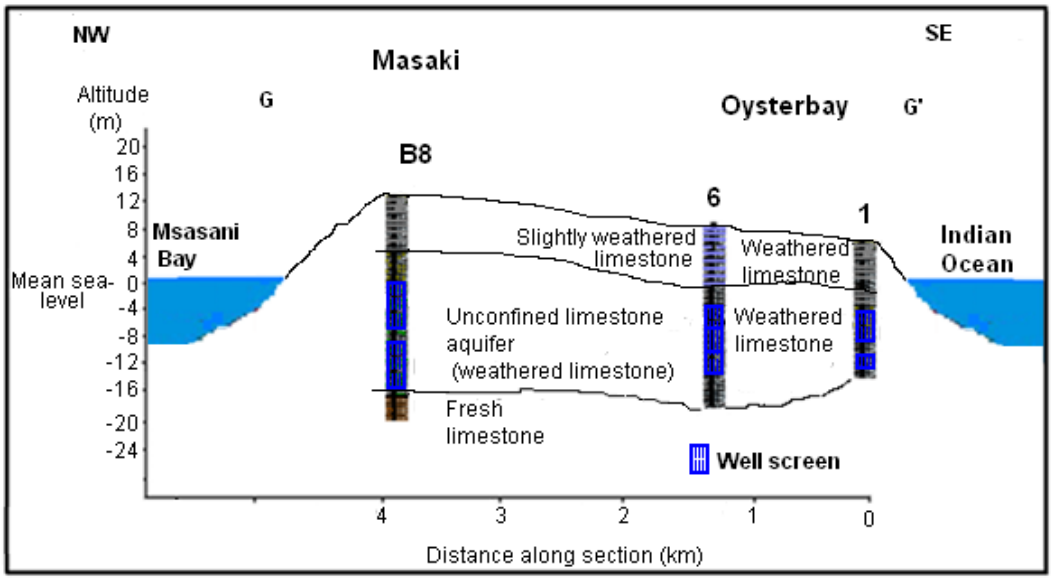

Figure 2.11(d): Cross-section G-G' showing hydrogeological units in the study area. Location of the cross-section is shown in Fig. 2.9.

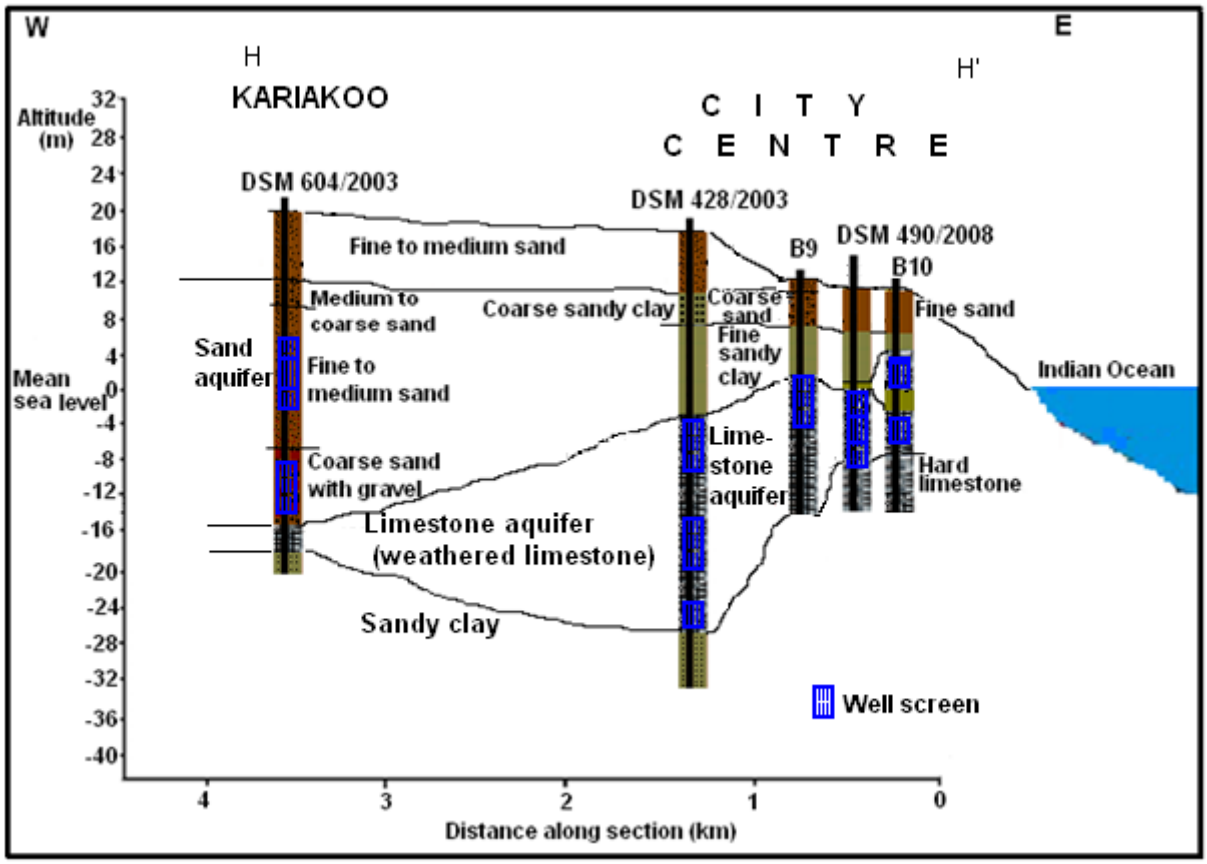

Figure 2.11(e): Cross-section H-H' showing hydrogeological units in the study area. Location of the cross-section is shown in Fig. 2.9.

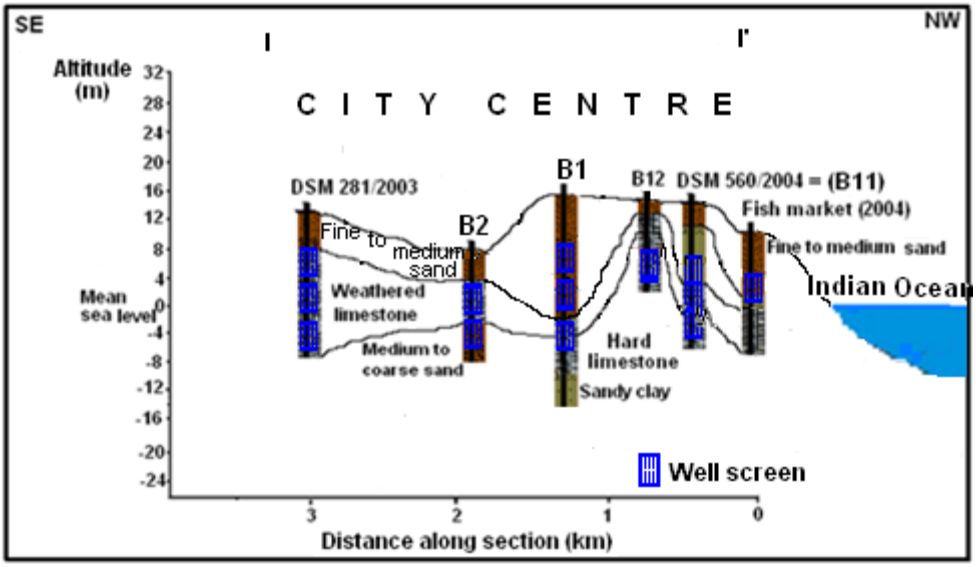

Figure 2.11(f): Cross-section I-I' showing hydrogeological units in the study area. Location of the cross-section is shown in Fig. 2.9.

present, boreholes drilling has increased tremendously and the trend can still be expected to increase in the future. It is estimated that about 1000 boreholes are drilled annually (Baumann et al., 2005). Individuals, the Community, industries, institutions and tourist hotels have sunk a number of boreholes from which large quantities of water are withdrawn using electrical and/or diesel pumps. All these put a strain on the fresh groundwater resources and increase the possibility of sea water intrusion.

Presently, water supply to Dar es Salaam City is maintained through two main sources: i) Ruvu River (Lower intake and Upper intake) which flows some 65 km away from Dar es Salaam (Fig. 2.13), and ii) Groundwater through boreholes/wells mainly exploiting Quaternary aquifer. In order to address the underlying causes of the water crisis in Dar es Salaam and to manage the growing demand for water supply for Dar es Salaam City and protect its freshwater resources from the increasing pollution loads, water management initiatives have a focus on the following areas (UN-HABITAT, 2007): i) promoting water demand management, ii) mitigating the environmental impact of urbanization on water resources (pollution control) and aquatic ecosystems with a special focus on aquifer management in Dar es Salaam, iii) conducting an environmental impact assessment of Ruvu River on the project of a dam developed that will regulate the river, and iv) public awareness campaign on water demand management, sanitation and related environmental issues.

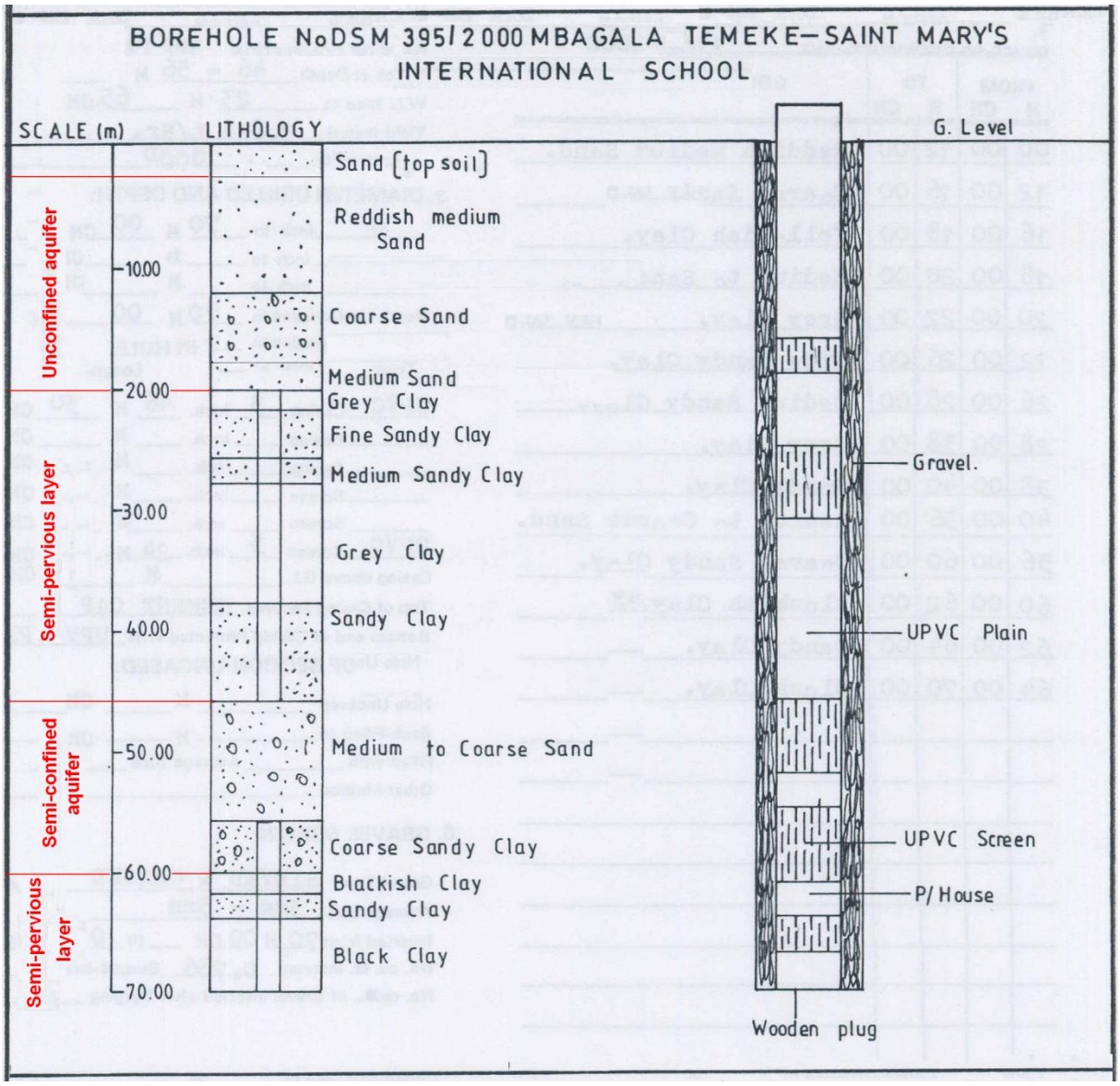

Figure 2.11(g): Typical borehole details for the study area at Mbagala (DDCA, DSM 395/2000)

Exploring other sources of water to augment the current water supply in Dar es Salaam was conducted by the Ministry of Water and Irrigation (MoWI) through DAWASA, a study which was financed by the World Bank. Several possibilities of groundwater and surface water sources were explored. Some of these included researching the possibility of improving water supply from Ruvu River and developing Kidunda dam, investigation of groundwater potentials in the Coastal Neogene Province (CNP) (Fig. 2.12) (DAWASA, 2007) and water supply from Rufiji River (Shingwela, 2009). Fig. 2.13 show relative locations of the prioritised groundwater and surface water sources. The development of Kidunda dam (Fig. 2.13) was proposed in order to augment low flows in the river system during dry periods.

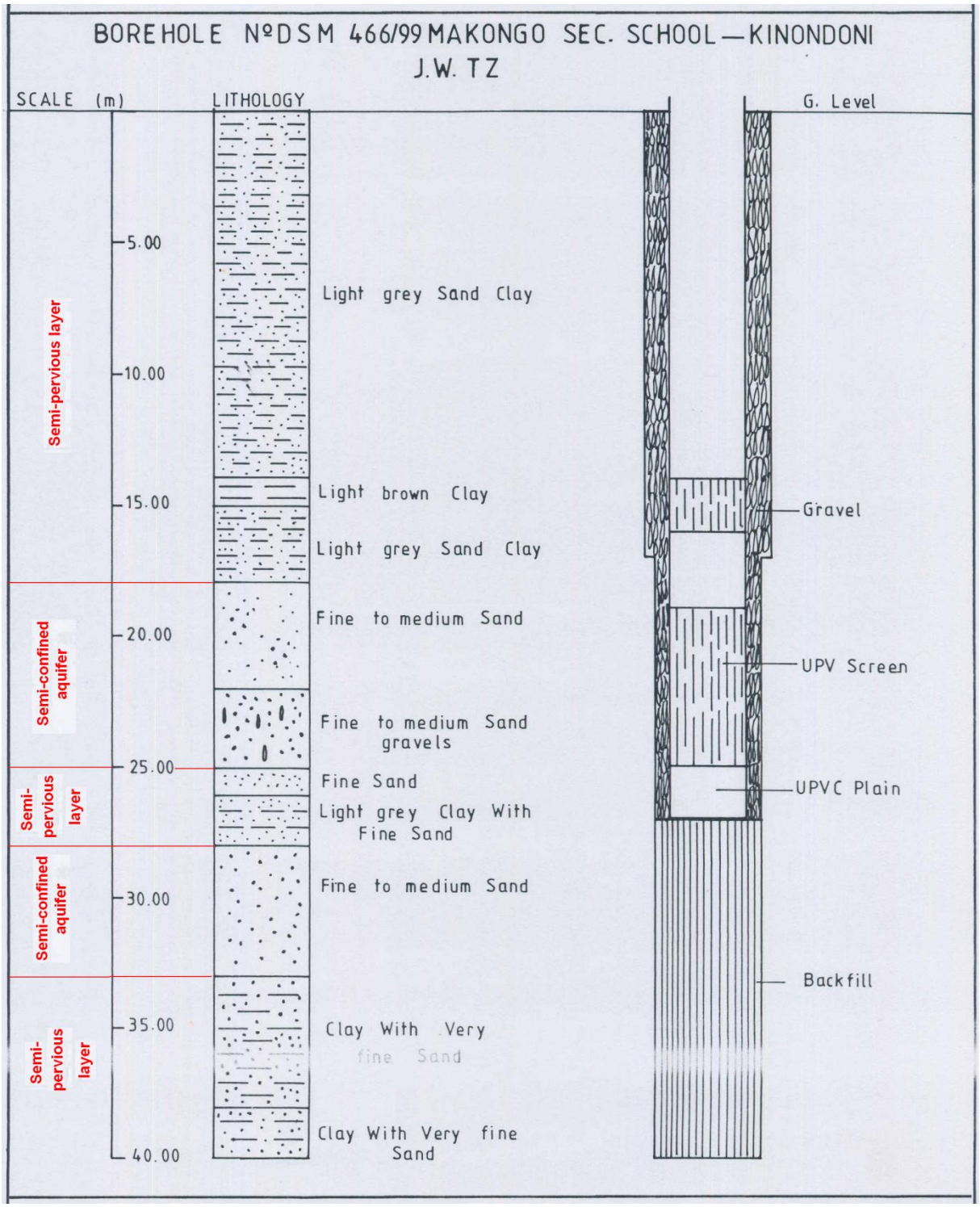

Figure 2.11(h): Typical borehole details for the study area at Makongo (DDCA, DSM 466/99)

2.5 Water resources and groundwater exploitation

The increased demand of water in Dar es Salaam City and uncontrolled groundwater abstraction poses a danger of seawater intrusion due to overpumping. From 1997 until the

A study on regional groundwater potential, aided by drilling and geophysical survey data provided by Tanzania Petroleum Development Cooperation (TPDC) revealed that an unconsolidated aquifer exists in Dar es Salaam region, south of the city. To confirm its groundwater potential, testing was conducted by drilling three 600 m deep exploration boreholes: PW1 (Kimbiji), PW2 (Mpiji) and PW3 (Mpera) (Fig. 2.13). The area north of Dar es Salaam represented by PW2 showed less favourable water quality by having elevated salinity and hardness compared to PW2 and PW3 (DAWASA, 2007). In a preliminary design needed for Master Planning purposes, safe yields of 13 million litres per day was assumed for the well fields to be established in conjunction with the two production wells at Kimbiji (PW1) and Mpera (PW3) (Fig. 2.13). Additionally, the groundwater of the Bagamoyo aquifer represented by well PW2 was considered suitable for blending with treated Ruvu River water so that both salinity and hardness are diluted to below an unpleasant level.

The assumed hydrogeological basement of the Kimbiji aquifer is represented by carbonate rocks of the Eocene Epoch (Paleogene Period). The considerable thickness of Kimbiji aquifer is part of the thick sedimentary basin that is present along most of the coastal areas of Tanzania. These sediments represent continental, deltaic and near shore marine sediments deposited during a series of transgression and regression cycles of sedimentation. Along sections of the coastline, the Neogene sediments are partly overlain by Quaternary sediments and, in some places by shallow reefal limestone of Pleistocene age.

The newly discovered Kimbiji aquifer might offer new perspectives for deep well drilling. Kimbiji Aquifer System (KAA) is considered to be a very large structure estimated to be 200 km long, 50 m wide and 1 km deep giving a bulk aquifer volume of 10,000 km^3 (DAWASA, 2007; Ruden, 2007). Area of interest for the study can be generalized to focus on the coastal region to the south of Dar es Salaam, stretching roughly from west Kisarawe to the coast in the east, and from Dar es Salaam in the north to the north of Kisiju in the south and on the coast (Fig. 2.12). However, challenges remain. Currently wells PW1 and PW3 can not necessarily reflect a true situation of groundwater conditions of the entire area. More exploration wells and pumping tests may be needed to provide necessary data for determination of actual deep aquifer gradients. Furthermore, recharge and recharge mechanisms have to be studied in detail since they are among the important factors that will determine the sustainability of development of the intended large scale groundwater production.

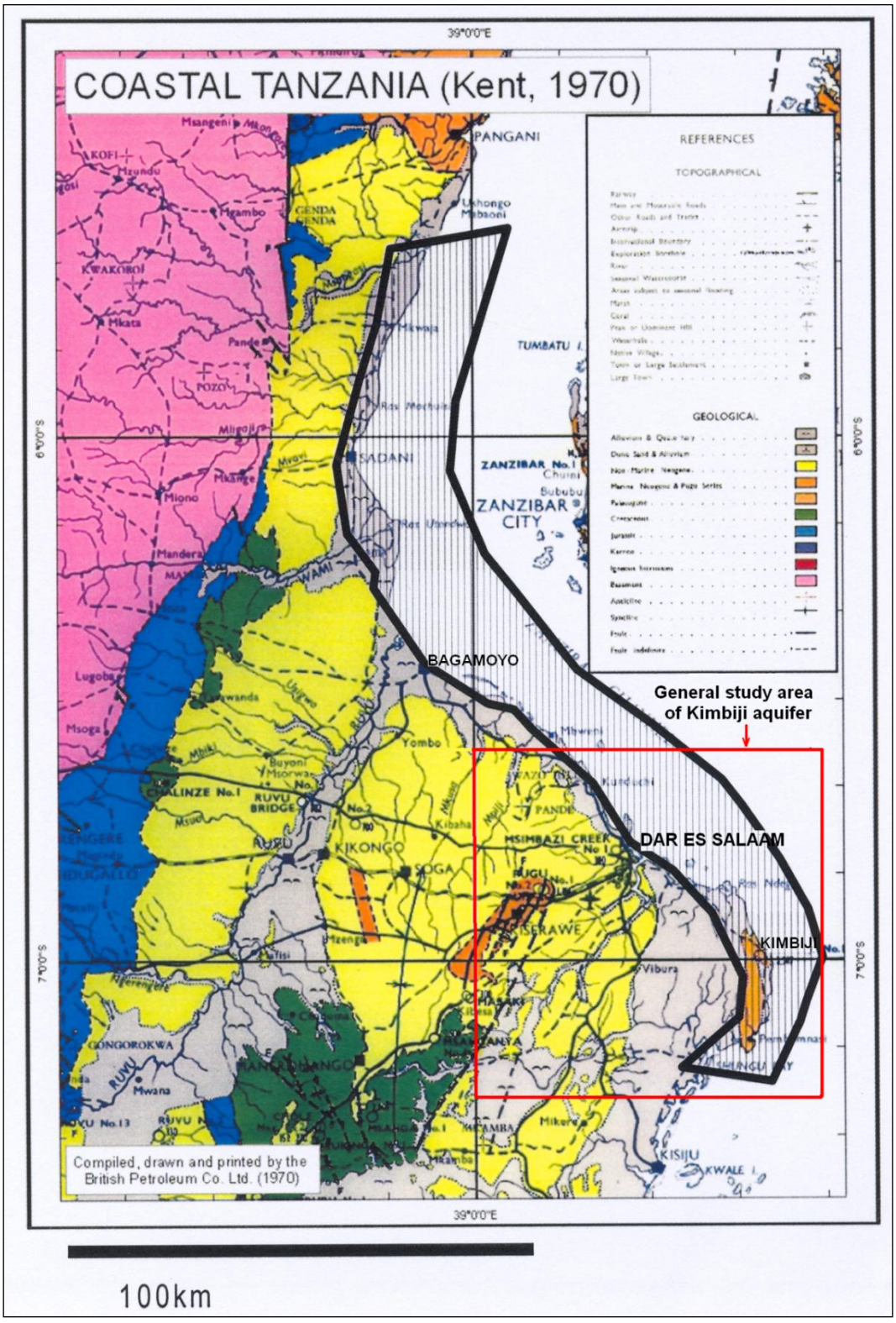

Figure 2.12: Approximate outline of the Coastal Neogene Province (CNP) denoted by black line boundary (DAWASA, 2007) (source of map: Kent 1970). The study area of interest for Kimbiji aquifer can be generalized as indicated by the red box (DAWASA, 2007).

A full resource assessment of the Kimbiji aquifer is required to draw final conclusions as to its properties and how it shall best be tapped in a sustainable and environmentally sound manner. Groundwater flow patterns, possible locations and interactions between freshwater and saltwater in coastal areas or offshore under present conditions and future scenarios have to be known as well.

Figure 2.13: Relative locations of the prioritised groundwater and surface water source features (Adapted from DAWASA, 2007).

3 WATER BALANCE AND GROUNDWATER RECHARGE ASSESSMENT

3.1 Introduction

Many areas of the world are experiencing increasingly severe water scarcity. One-third of the population of developing countries lives in regions that have insufficient water resources to meet their agricultural, domestic, industrial and environmental needs (Seckler *et al.*, 1998a, b). From a global perspective, the world's supply of water is stored mainly in oceans (97.2%), while 2.15% is frozen water (ice caps) and 0.65% is fresh water on land. Of this fresh water component, only 2.5% makes up quantities in air, soil, lakes and rivers, while the remainder is groundwater, most of which is unavailable for human use (Vander Leeden *et al.*, 1990).

Groundwater has been a vital source of urban water supply. Urbanisation has been the predominant global phenomenon of the 20th century and is predicted to continue at ever-increasing rates for the foreseeable future. As water becomes increasingly scarce as a consequence of population growth and a rise in living standards, measuring and evaluating techniques of handling water resources are essential to assist planners and decision makers to come up with control measures for groundwater development, ensuring its long-term sustainability. Knowledge of groundwater recharge rate is a key factor to determine sustainable yield of aquifers and to avoid undesirable effects, such as decline in aquifer water table and groundwater quality deterioration. This chapter presents estimation of a sustainable yield for Dar es Salaam Quaternary coastal aquifer (DQCA) through determination of the amount of groundwater recharge, based on the estimation of water budget for the aquifer.

3.1.1 Concepts of water balance

A water balance is a measure of the amount of water entering and the amount of water leaving a system. It is a way to evaluate all the sources of supply and the corresponding discharges with respect to a basin or aquifer. In hydrology, a water balance equation can be used to describe the water budget by mathematically accounting for the water budget components.
The hydrologic equation is simply the statement of the law of conservation of matter and is given by:

$$I = O + \Delta S \tag{3.1}$$

Where: I = inflow, *O* = outflow, and ΔS = change in storage. This equation states that during a given period, the total inflow into a given area must equal the total outflow from the area plus the change in storage.

The earth is composed of many interacting subsystems including the ocean, atmosphere, lithosphere and biosphere (Domenico and Schwartz, 1990, Winter et al. 1998). The interconnections between the components of the hydrologic cycle on a global scale are described by Domenico and Schwartz (1990) (Fig. 3.1a). On a global scale, the atmosphere gains moisture from the oceans, streams and land surface through evaporation (E) (Fig. 3.1) by the energy from the sun. As water condenses in clouds and falls as rain to the surface, portions are intercepted and evaporate by or are converted to runoff (R_O). The remainder infiltrates (F) into the soil (Fig. 3.1). Some of the infiltrated water that is stored in the upper regions of the soil profile transpirates (T) from vegetation, while the remainder penetrates to greater depth to recharge groundwater storage (R_N). The water contained in groundwater storage (aquifers) may receive water (Q_i) from or contribute water (Q_o) to the river and streams network. The former occurs when the groundwater table is below the stream water level whereas the latter occurs when the groundwater table in the vicinity of the stream is above the water level in the stream. Water from the streams reaches the oceans through runoff of rivers to the sea (Q_{sea}). The letter "M" in Fig. 3.1, represents the potential contribution of water of volcanic or magmatic origin to the groundwater storage, streams, ocean or atmosphere. This amount of newly formed water is very small, and can be neglected.

Fig. 3.1(b) illustrates the connection between elements of the basin scale hydrologic subsystem with the global hydrologic cycle. This connection is accomplished by accounting for precipitation (P) derived from the global system and transpiration (T), evaporation (E) and runoff to the Ocean (Q_{sea}) to the global system. The water balance of a hydrologic basin can be determined by calculating the input, output, and storage changes (ΔS) of water (Equation 3.2).

$$P - E - T - Q_{sea} = \Delta S \tag{3.2}$$

Where ΔS is the lumped change in storage in all surface and subsurface water. Each item in equation (3.2) has the units of a discharge, or volume per unit time since the balance must be applied for every time period.

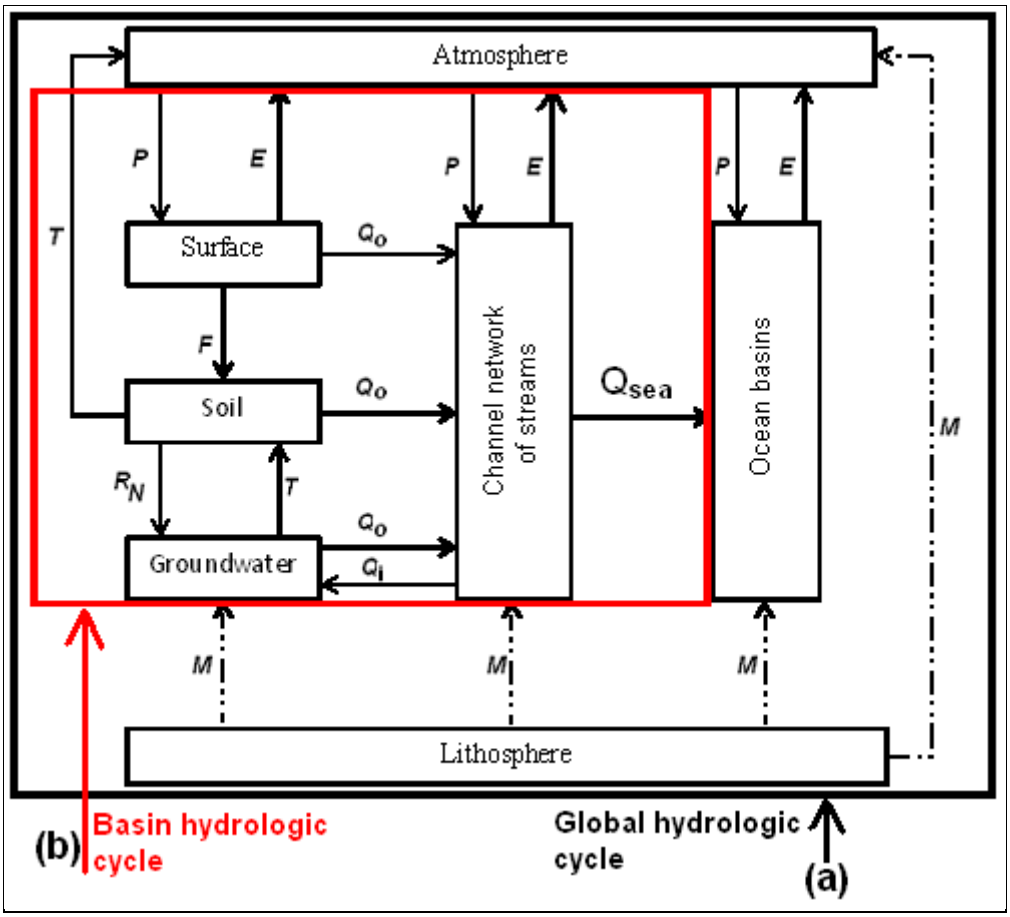

Figure 3.1: Elements of the: (a) global hydrologic cycle, and (b) basin hydrologic cycle (Domenico and Schwartz, 1990). (Key; P = precipitation, E = evaporation, F = infiltration through the soil, Qsea = runoff streams to the oceans, Qi = inflow of streams to the groundwater reservoir, Qo = outflow to the channel network of streams and atmosphere, RN = recharge to the groundwater, T = transpiration and m = water originating from volcanic or magmatic activities.

Fig. 3.1 describe the hydrological cycle, illustrating only its natural components. However, in many parts of the world the cycle is interfered with and modified by human settlement and associated activities that may alter the processes of infiltration and drainage (Lerner et al., 1990; Lerner, 1997).

Water balance computations are required for many hydrological, water management and climatic purposes. Among other purposes, this includes: i) assessment of water resources with different temporal and spatial resolution, ii) monitoring and management of water resources including their protection against exhaustion and contamination, and iii) for crop production (irrigation) and drainage. Understanding of the water balance of a hydrologic basin is very crucial to provide information on important parameters such as amount of water stored in the

soil, actual evapotranspiration, water surplus, water deficit, surface flow and underground flow.

3.1.2 Evapotranspiration

Evapotranspiration (ET) is the process that returns water to the atmosphere and therefore completes the hydrologic cycle (Fig. 3.2). ET is divided into two sub-processes: evaporation and transpiration (Allen et al., 1998) (Fig. 3.3). Evaporation occurs on the surfaces of open water (e.g. lakes, reservoirs) or from vegetation and ground surfaces. On the other hand, transpiration involves the removal of water from the soil by plant roots, transport of the water through the plant into the leaf, and evaporation of the water from the leaf‘s stomata into the atmosphere.

The ET of an area includes potential evapotranspiration (PET) and actual evapotranspiration (AET). PET is the amount of ET that would occur when there is unlimited water available whereas AET is the amount of ET that occurs when water is limited (Ward and Trimble 2004). Controlling factors of ET include: i) energy availability, ii) wind speed, iii) moisture gradient (temperature and humidity), iv) vegetation, and v) precipitation. Increasing air temperature and solar radiation increase ET whereas higher relative humidity reduces ET since the demand for water vapor by the atmosphere surrounding the leaf surface decreases with increased humidity. Reduction in relative humidity increases ET since low humidity increases the vapor pressure deficit between the vegetative surface and air, and therefore higher transpiration and evaporation need to take place to meet the evaporative demand of the air for moisture from the surface.

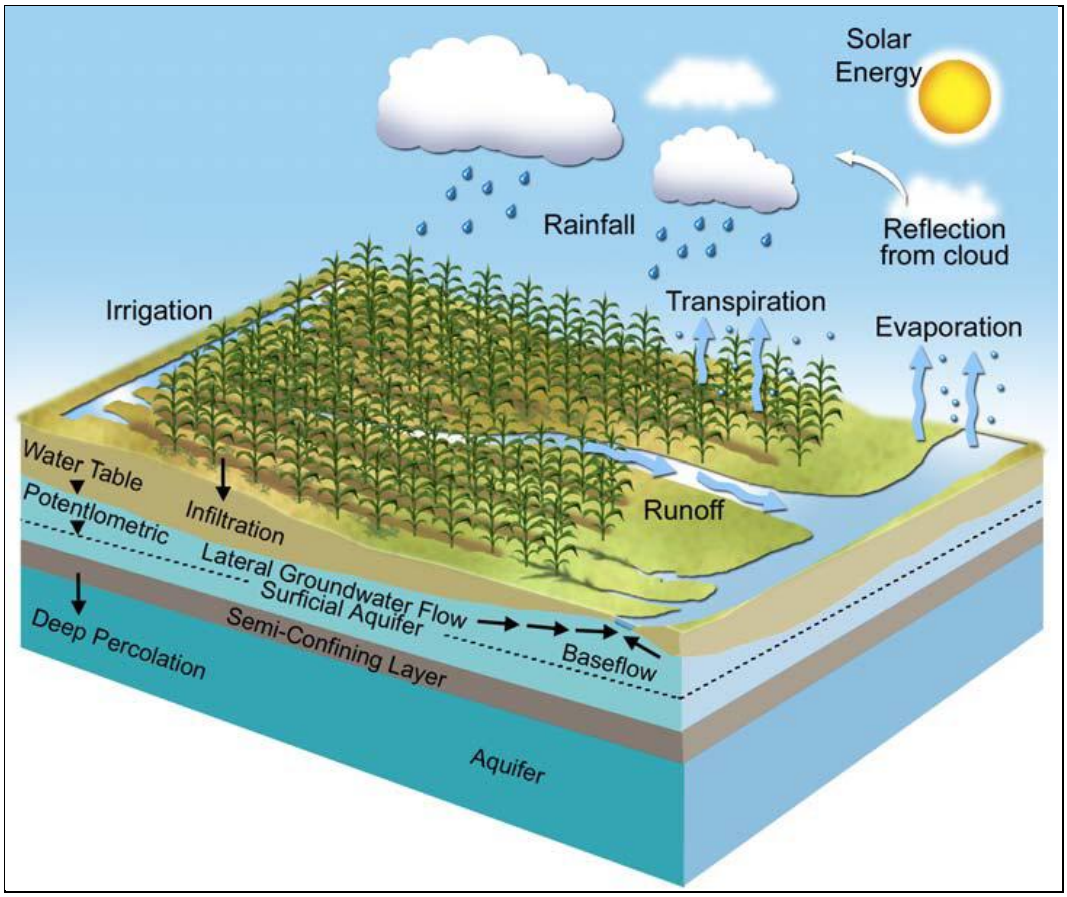

Figure 3.2: The hydrologic cycle showing different components of the hydrological process. (http://watercenter.unl.edu/downloads/ResearchInBrief/IrmakSuatET.pdf)

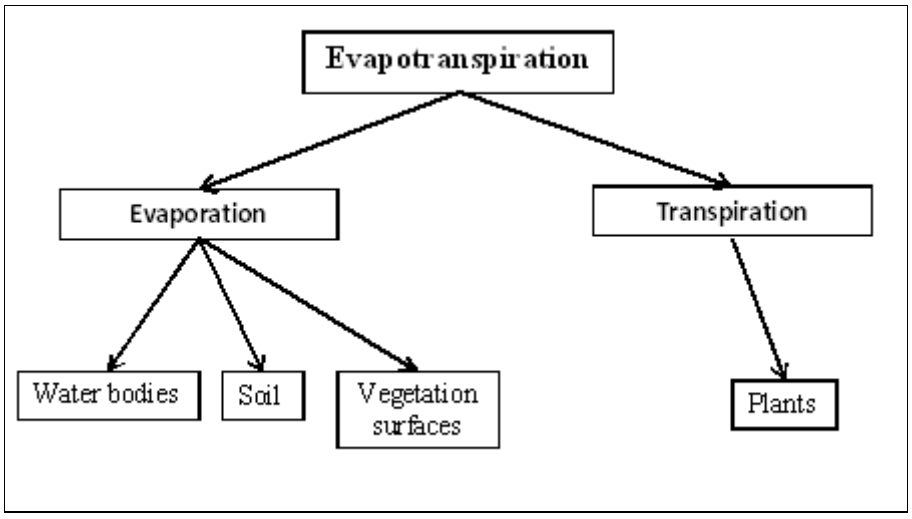

Figure 3.3: Evapotranspiration (Ward and Trimble, 2004).

3.1.3 Groundwater recharge

Groundwater recharge may be defined as the downward flow of water reaching a groundwater system, forming an addition to the groundwater reservoir (Lerner et al, 1990). If precipitation

(P) exceeds PET, the soil moisture gets recharged and when the soil moisture storage exceeds the field capacity of the soil, water surplus occurs. The water surplus either percolates downward and adds to the groundwater storage or flows laterally in the unsaturated zone: interflow, adding to streams. Also flowing groundwater adds to streams (baseflow), rivers and finally, to the oceans (Fig. 3.4). When precipitation equals or exceeds PET, evapotranspiration attains its potential rate, which implies that actual evapotranspiration (AET) and PET are equal.

Soil water balance models were developed in the 1940s by Thornthwaite (1948) and revised by Thornthwaite and Mather (1955). The method comprises a procedure which estimates the balance between the inflow and outflow of water. The soil water balance can be presented as:

$$R_N = P - AET - \Delta S_B - R_O \quad (3.3)$$

Where, R_N = groundwater recharge; P = precipitation; AET = actual evapotranspiration; ΔS_B = change in soil water storage; and Ro = run-off.

The compartments considered in the soil water balance model are indicated by the dashed line in Fig. 3.4.

Groundwater recharge may have various sources such as rainfall, percolation from streams and irrigation. According to Lloyd (1986) and Lerner et al., (1990), the principal groundwater recharge mechanisms include:

i) Direct recharge, derived from rainfall over large areas that enters the soil and, in excess of soil moisture deficits and evapotranspiration, moves downward by direct percolation through the unsaturated zone

ii) Indirect recharge, resulting from the water infiltrating through the beds of surface water courses or lakes, and

iii) Localised recharge resulting from the near-surface concentration of water in the absence of well-defined channels.

Utilization of groundwater in the study area is going on without understanding of the quantity of water generated by the aquifer. Hence, estimation of rates of groundwater recharge in the study area is crucial for sustainable utilization of the resource as well as its protection against depletion and salinization. The rate of groundwater recharge is an important factor in the analysis and management of groundwater resources.

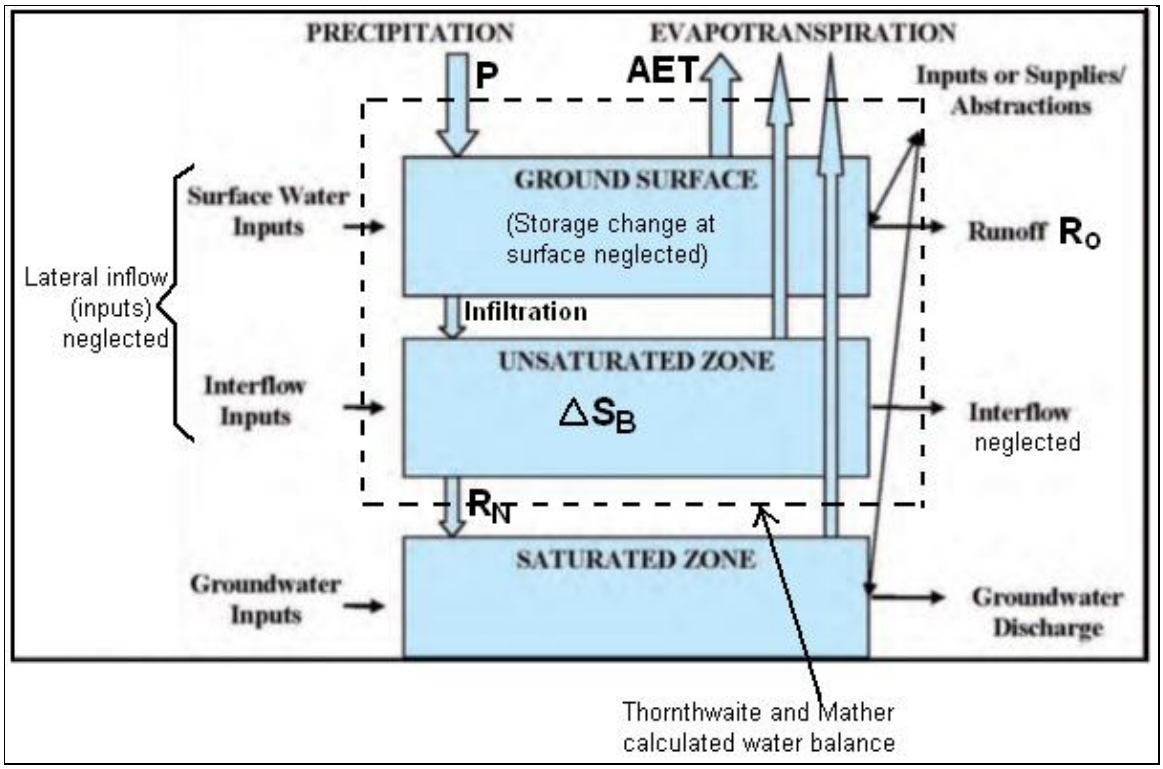

Figure 3.4: Water budget components (IWM, 2009) and overview of compartments considered in the Thornthwaite and Mather soil water balance model.

3.1.4 Sustainable yield of groundwater

In various parts of the world, groundwater exploitation has risen to the extent that numerous examples of important aquifers including coastal aquifers are known to exceed the capacity of the aquifer system to deliver (Custodio, 2002; Custodio, 1985; Walraevens et al., 1993; Barker et al., 1998; Norconsult, 2007; Mjemah, 2007; Van Camp & Walraevens, 2009). Several authors have discussed on the way in which the capacity of an aquifer to deliver water in a sustainable way should be defined and determined. The two prominent concepts developed are safe yield and later sustainable yield (Sophocleous, 2000; Hiscock et al., 2002; Ponce, 2007).

Safe yield is defined as the amount of water, which can be taken from the aquifer indefinitely without producing an undesirable result (Todd, 1959). From a hydrological point of view, the maximum safe yield is often considered equal to the long-term mean annual recharge (Stavric, 2004). Safe yield varies from season to season as rates of recharge fluctuate. Several authors suggested to abandon the use of the safe yield concept (Thomas, 1955; Kazman, 1956; Sophocleous, 1997; Sophocleous, 2000; Ponce, 2007): the problem with the safe yield concept is that it leads to the misconception that groundwater development is safe, if pumping

rate does not exceed the rate of the natural recharge. Implementation of this safe yield policy has caused many negative effects such as stream flow depletion and loss of wetlands and riparian ecosystems (Sophocleous, 2000). Important questions in regard to the safe yield concept include: how much is the annual amount of the safe yield? what defines an undesired result? However, there is neither a standard method of determining safe yield nor assessing undesired results.

On the other hand, the sustainable yield concept reserves a fraction of safe yield for the benefit of the surface waters (Ponce, 2007). However, there is a lack of compromise as to what percentage of safe yield should constitute sustainable yield. There are no general rules to define sustainable yield, since there are many factors to be taken into account such as climate and/or climate change, the hydrogeological setting, ecological impacts, the particular location of the wells, the presence of groundwater dependent ecosystems, as well as socio-economic and legal aspects (Gleick, 1993; Sophocleous, 2000; Custodio, 2002; Alley and Leake, 2004; Maimone, 2004; Seward et al., 2006; Ponce, 2007).

Ecologically, sustainable development of groundwater resources requires identification of different users and their water requirement including the environment. The amount of water that may be extracted from an aquifer without causing depletion is principally dependent upon the groundwater recharge. Rainfall is the principal means for replenishment of moisture in the soil water system and recharge to groundwater. In this study, sustainable yield is considered as a fraction of natural recharge and was calculated according to the concept proposed by Ponce (2007): average percentages estimated at approximately 40%, the least conservative approximately 70%, and reasonably conservative approximately 10%.

3.2 Materials and methods

3.2.1 Estimation of potential evapotranspiration

The potential evapotranspiration concept was first introduced in the late 1940s and 50s by Penman (1948, 1956), and defined as “the amount of water transpired in a given time by a short green crop, completely shading the ground, of uniform height and with adequate water status in the soil profile”. In the definition of potential evapotranspiration, the evapotranspiration rate is not related to a specific crop. The evapotranspiration rate from a

reference surface, not short of water, is called the reference crop evapotranspiration or reference evapotranspiration (Allen et al., 1998). The reference surface is a hypothetical grass reference crop with specific characteristics.

The evapotranspiration is determined from weather data as it difficult to measure from the field (Allen et al., 1998). The weather data (Appendix 3) for this study were obtained from Tanzania Meteorological Agency (TMA) for a period from 1971 to 2010 and are composed of precipitation (mm), relative humidity (%), maximum and minimum temperature (°C), wind speed (m/sec) and radiation (MJ $m^{-2}d^{-1}$). However, data of the relative humidity and wind speed from January to September 2010 either do not exist or are not available. Table 3.1 indicates the average of monthly means climatic data for 39 years (1971-2009). Potential evapotranspiration can be determined with different methods. Monthly potential evapotranspiration estimates were calculated for 39 years (1971–2009) of routine meteorological data using Penman-Monteith, Thornthwaite, Hargreaves and Hamon methods. Results were compared in order to show possible differences that could be attributed to the methods.

Table 3.1: Average of monthly means climatic data (Rainfall; Rs: solar radiation; Tx: maximum temperature; Tn: minimum temperature; U2: wind speed; RHx: maximum relative humidity; RHn: minimum relative humidity) for the period 1971-2009.

Month	**Rainfall**	**R_s**	**T_x**	**T_n**	**U_2**	**RH_x**	**RH_n**
	mm	**MJ $m^{-2}d^{-1}$**	**^oC**	**^oC**	**m/sec**	**%**	**%**
January	70.94	19.76	31.94	23.74	6.79	77.72	63.69
February	56.89	20.48	32.44	23.56	6.46	77.10	61.49
March	142.34	18.41	32.19	23.02	4.44	81.82	67.08
April	253.31	15.99	30.80	22.57	4.80	86.82	72.64
May	178.46	16.22	29.98	21.39	5.72	85.72	67.00
June	42.16	17.10	29.43	19.36	6.43	83.95	58.26
July	22.73	17.05	29.10	18.41	6.06	84.82	55.79
August	22.92	17.83	29.50	18.27	5.27	81.72	54.18
September	21.03	18.88	30.45	18.59	5.34	76.23	53.96
October	68.22	19.38	31.10	19.99	5.34	73.92	56.74
November	116.96	19.94	31.51	21.64	5.17	74.95	61.92
December	109.49	19.91	31.74	23.20	6.06	77.87	64.85

3.2.1.1 Penman-Monteith method

The standard Penman-Monteith method for estimating evapotranspiration can be mathematically expressed as follows (Allen et al., 1998):

$$PET = \frac{0.408\Delta\ R_n - G\ + \gamma \frac{900}{T+273} u_2 (e_s - e_a)}{\Delta + \gamma(1 + 0.34u_2)}$$

Where:

PET = reference evapotranspiration (mm day^{-1}),
R_n = net radiation at the crop surface ($MJm^{-2}day^{-1}$),
G = solar heat density ($MJm^{-2}day^{-1}$),
γ = psychrometric constant ($kPa°C^{-1}$),
T= mean air temperature (°C),
u_2 = wind speed at 2 m height (m s^{-1}),
e_s = saturation vapour pressure (kPa),
e_a = actual vapour pressure (kPa),
e_s - e_a = saturation vapour pressure deficit (kPa),
Δ= slope of the saturation vapour pressure curve ($kPa°C^{-1}$).

Wind speed data provided was measured at a height of 10 meters, a correction to a height of two meters was calculated using the following formula:

$$u_2 = u_z \frac{4.87}{ln(67.8z_w - 5.42)}$$

Where u_2 is wind speed at 2 m height (m s^{-1}) and u_z the wind speed at height z_w above the ground, in this case at 10 m height (m/s)

The disadvantage of using Penman-Monteith method is that the method needs many input data. However, the Penman-Monteith is the most reliable and more accurate method and is thus preferred if the necessary data are available. The potential evapotranspiration by Penman-Monteith in this study was calculated using excel file written by Snyder (2004).

3.2.1.2 Thornthwaite method

Thornthwaite (1948) proposed an empirical method to estimate the potential evapotranspiration from mean temperature data. The method was modified by Thornthwaite

& Mather (1955) to make it more useful over a wide range of soils and vegetations. Apart from calculating the potential evapotranspiration, the concept of water balance of the unsaturated zone (Thornthwaite and Mather, 1957) was applied to this study. This method of computing the monthly water balance was revised and summarized by Thornthwaite & Mather (1957). The required parameters to determine actual evapotranspiration using this model are mean monthly precipitation, mean monthly potential evapotranspiration, water holding capacity of the dominant soil type and monthly soil moisture storage.

The formula for the calculation of potential evapotranspiration is as follows:

$$PET = 16(10T/I)^{a}$$

Where T is the monthly temperature (^{o}C) and *I* the annual heat index:

$$I = \sum_{1}^{12} i_j$$

Where i_j is the monthly heat index of the month j;

$$i_j = (T/5)^{1.514}$$

The coefficient "a" is given by the formula:

$$a = 0.49239 + 1792\,x\,10^{-5}\ I - 771\,x\,10^{-7}\ I^2 + (665\,x\,10^{-9})I^3$$

Multiplying the PET values by one factor N, which depend on latitude, gives the corrected potential evapotranspiration.

3.2.1.3 Hargreaves method

Hargreaves method (Hargreaves and Samani, 1982) is used for evapotranspiration estimation when solar radiation data, relative humidity data and wind speed data are missing. This method estimates PET using only the maximum and minimum air temperature with the following equation:

$$PET = 0.0023 * \ T_{mean} + 17.8 \ + (T_{max} - T_{min})^{0.5} * R_a$$

where PET = reference evapotranspiration (mm day^{-1}), T_{max} and T_{min} are the maximum and minimum air temperature (^{o}C), T_{mean} = mean air temperature (^{o}C), and R_a = extraterrestrial radiation (MJ m^{-2}day^{-1}). Extraterrestrial radiation is calculated from latitude and time of year.

3.2.1.4 Hamon method

Hamon's equation for estimation of potential evapotranspiration requires only latitude, which is converted into daylength, and mean temperature, which is converted into saturated water vapor density. In this chapter, PET is calculated by using the Hamon equation (Hamon, 1961):

$$PET = 13.97 * d * D^2 * W_t$$

Where PET = potential evapotranspiration in mm per month, d = the number of days in a month, D = the mean monthly hours of daylight in units of 12 hours and W_t = saturated water vapour density (g m^{-3}), which is calculated based on temperature:

$$W_t = \frac{4.95e^{0.62T}}{100}$$

Where T = the mean monthly temperature (°C).

Calculating PET using Hamon method is simple and can automatically be solved through the computer-based TMWB model developed by McCabe and Markstrom (2007).

3.2.2 Soil moisture balance

The different terms of the soil moisture budget were computed each term separately in an excel sheet. The concept of water balance of the unsaturated zone (Thornthwaite and Mather, 1957) was applied. It consists of keeping track of the accumulated potential water loss (APWL) and the amount of water in the soil (S_B). Calculations to determine S_B and APWL were performed for each month using monthly precipitation (P) and potential evapotranspiration (PET) (Table 3.2).

Table 3.2: Annual soil-water budget calculations.

TERMS	WET SEASON $(P - R_o) - PET > 0$			DRY SEASON $P - R_o - PET < 0$
	$S_{B_{n-1}} = CAP$	$S_{B_{n-1}} < CAP$		
		$P - R_o - PET \leq CAP - S_{B_{n-1}}$	$P - R_o - PET > CAP - S_{B_{n-1}}$	
$S_{B_n}(mm)$	CAP	$S_{B_{n-1}} + (P - R_o - PET)$	CAP	$PAW.e^{-APWL_n/PAW} + WPWP$
$R_N(mm/month)$	$P - R_o - PET$	0	$P - R_o - PET - (CAP - S_{B_{n-1}})$	0
$AET(mm/month)$	PET	PET	PET	$P - R_o - \Delta S_B$
DEF (mm)	0	0	0	PET - AET
$APWL_n(mm)$	0	$-ln\ \frac{S_{B_n} - WPWP}{PAW}\ .PAW$	0	$APWL_{n-1} - (P - R_o - PET)$

Key: P = precipitation (mm), R_O = runoff (mm), PET = potential evapotranspiration (mm), APWL= accumulated potential water loss (mm) (PET – (P – R_O)) accumulated for subsequent dry months, AET = actual evapotranspiration (mm), S_B = water stored in soil, PAW = plant available water = the difference between water content at field capacity (CAP) and water content at permanent wilting point (WPWP), WPWP = average rooting depth (mm) * PWP (in volume %), CAP = soil capacity (mm): maximum water content of soil, without gravitational water (= average rooting depth (mm) * water content at field capacity (in volume %)); ΔS_B = change in S_B; DEF = deficit (PET-AET) (mm); SUR = surplus ((P- Ro)-AET) (mm); R_N = natural groundwater recharge (SUR-ΔS_B) (mm).

Water stored in the soil in a certain month *n*, S_{B_n} is calculated as:

$$S_{B_n} = PAW * e^{-\frac{APWL_n}{PAW}} + WPWP \tag{3.4}$$

Soil moisture has an upper bound that corresponds to the soils' maximum water holding capacity (CAP) and a lower bound that correspond to the soil's wilting capacity (permanent wilting point = PWP). Soil properties strongly influence water storage and availability. The maximum amount of available water that a soil can retain will vary with the soil's structure and texture (Fig. 3.5). Texture and structure have a strong influence on water storage and availability due to the size and arrangement of soil particles and pores. The soil texture determines the capacity of the soil to hold water. A soil with large particles and large pore spaces (e.g. sand) holds the least amount of water. On the other hand, a soil rich in clay has small particles and can store a large amount of water. Fine grained soils have larger field capacities than coarse grain (sandy) soils and thus have more water available for actual evapotranspiration comparing to coarse soils.

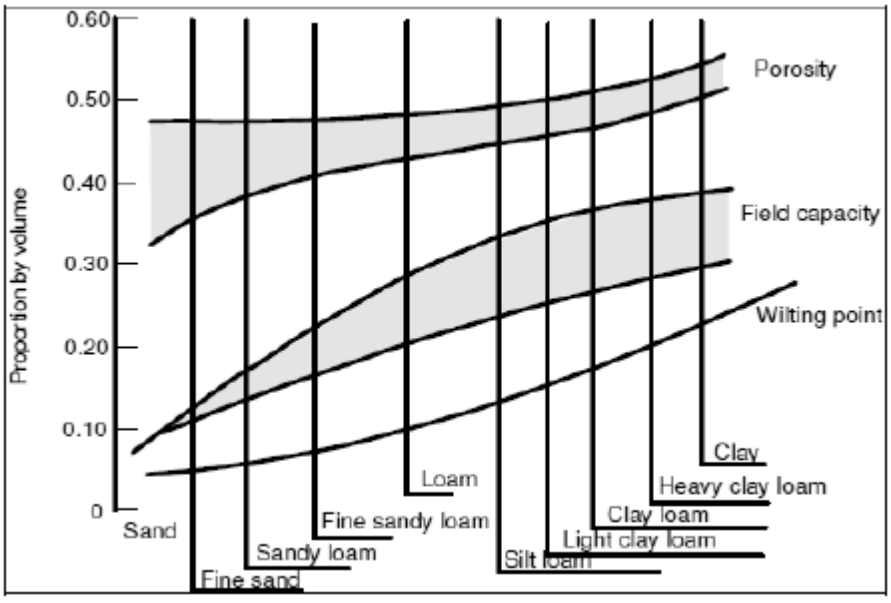

Figure 3.5: Water holding properties of various soils (Dunne et al., 1975).

The study area is characterized by vegetation cover (grass) with shallow roots (0.5 m) and a lithology of fine sand (vadose zone), which, according to Thornthwaite and Mather (1957), assumes a plant available water capacity of 10% over the entire root zone (Table 3.3). This gives a plant available water content of the root zone of 50 mm. This refers to the plant available water (PAW) calculated as the difference between CAP and PWP (PAW = 50 mm).

Excess soil moisture to the CAP is drained to the groundwater reservoir in the form of groundwater recharge. Soil water content at PWP for sand is assumed to be 6% by volume (Raes et al., 2010) (Table 3.4). This gives 30 mm available water content of the root zone at PWP. Thus CAP is 80 mm.

In order to quantify R_N, calculations to determine S_B and APWL were performed for each month using monthly mean precipitation (P) and PET. Direct runoff (R_O) is subtracted from P to compute the amount of remaining precipitation (P- R_O). The hydrological year has been considered from the beginning of June (the beginning of the dry season) to the end of May of the next year (i.e. the end of rain season). The initial soil storage S_B at the start of June 1971 is assumed to be equal to CAP. Surface runoff is subtracted from the precipitation to compute the amount of remaining precipitation which participates into the further steps of the soil water balance process. The runoff factor for this study was taken as 8% of the precipitation, as suggested by previous studies (Mjemah 2007; Mjemah et al. 2011).

The soil moisture storage fluctuates between the WPWP and the CAP. In order to track changes in soil moisture, intermediary values are determined, including P-PET, APWL, AET, SUR and DEF. Groundwater recharge occurs only during the wet season when there is a surplus of rainfall, when (P - R_0) - PET is greater than zero. Negative value of (P-R_o)-PET represents a potential deficiency of water whereas positive value of (P-R_o)-PET represents a potential surplus of water. APWL is calculated as sum of (P-R_o)-PET values during periods when (P-R_o)-PET is negative. This sum represents the total amount of unsatisfied potential evapotranspiration to which the soil has been subjected (Westenbroek et al., 2010). Soils yield water more easily during the first days in which (P-R_o)-PET is negative, whereas on subsequent days, as APWL grows, soil moisture is less readily given up. Potential recharge occurs when infiltration brings the soil moisture deficit to a negative value, that is, the soil water content becomes greater than CAP. At this point, soil is assumed to be free draining hence all excess water drains through the bottom of the soil zone.

The different parameters associated with soil moisture storage are computed, depending on the time scale used, as the difference between the current soil moisture and the previous one (Bakundukize, 2012). When (P-R_o)-PET is positive, the new soil-moisture value is found by adding this (P-R_o)-PET term to the preceding soil moisture value (Westenbroek et al., 2010).

If the new soil moisture value is still below the maximum water holding capacity, a new reduced APWL value is calculated (Westenbroek et al., 2010). Water is added to the soil moisture storage during the wet months (PET< $P-R_o$) until the water content is at field capacity (CAP). If the soil moisture value exceeds the maximum water holding capacity, the soil moisture value is capped at the value of the maximum water holding capacity CAP, the excess moisture is converted to recharge, and the APWL is reset to zero: when $(P-R_o)$-PET is negative, the new soil moisture term is found by calculating the soil moisture value associated with the current APWL value (Westenbroek et al., 2010).

The amount by which AET differs from PET is referred to as soil moisture deficit (DEF) (Ritter, 2006; Westenbroek et al., 2010). DEF is a quantitive expression of the amount of water, which is not available either by precipitation or irrigation to compensate the water need (Ritter, 2006). DEF occurs when PET exceeds AET (Ritter, 2006). In wet season, when there is enough rain, i.e. when $(P-R_o)$-PET is positive, AET is at its maximum value and is equal to PET. When $(P-R_o)$-PET is negative, the AET is equal to $P-R_o$, supplemented by the amount of water that can be extracted from the soil ($-\Delta S_B$). During the wet season, if the soil moisture reaches the maximum soil moisture capacity CAP, any excess precipitation is added to groundwater recharge.

Table 3.3: Plant available water (PAW) with different combinations of soil and vegetation types (Thornthwaite and Mather 1957)

Vegetation	Soil texture	Available water capacity (% volume)	Rooting depth (m)	Plant-available water in root- zone (mm) = (PAW)
Shallow rooted crops (spinach, peas, beans, beets carrots etc.)	Fine sand	10	0.50	50
	Fine sandy loam	15	0.50	75
	Silt loam	20	0.62	125
	Clay loam	25	0.40	100
	Clay	30	0.25	75
Moderately rooted crops (corn, cereals, cotton, tobacco)	Fine sand	10	0.75	75
	Fine sandy loam	15	1.00	150
	Silt loam	20	1.00	200
	Clay loam	25	0.80	200
	Clay	30	0.50	150
Deep rooted crops (alfalfa, pasture grass, shrubs)	Fine sand	10	1.00	100
	Fine sandy loam	15	1.00	150
	Silt loam	20	1.25	250
	Clay loam	25	1.00	250
	Clay	30	0.67	200
Orchards	Fine sand	10	1.50	150
	Fine sandy loam	15	1.67	250
	Silt loam	20	1.50	300
	Clay loam	25	1.00	250
	Clay	30	0.67	200
Mature forest	Fine sand	10	2.50	250
	Fine sandy loam	15	2.00	300
	Silt loam	20	2.00	400
	Clay loam	25	1.60	400
	Clay	30	1.17	350

Table 3.4: Soil physical characteristics for various soil types (Raes et al., 2010)

Soil type	Soil water content			Saturated hydraulic conductivity
	Saturation	Field Capacity	Permanent wilting point	
	% vol	% vol	% vol	mm/day
Sand	36	13	6	1500
Loamy sand	38	16	8	800
Sandy loam	41	22	10	500
Loam	46	31	15	250
Silt loam	46	33	13	150
Silt	43	33	9	50
Sand clay loam	47	32	20	125
Clay loam	50	39	23	100
Silty clay loam	52	44	23	120
Sandy clay	50	39	27	75
Silt clay	54	50	32	15
Clay	55	54	39	2

3.3 Results and discussion

3.3.1 Potential evapotranspiration

Fig. 3.6 shows the comparison between the average values of monthly potential evapotranspiration calculated using the four methods; Hargreaves and Penman methods show a comparable trend, as opposed to Thornthwaite and Hamon methods. Mostly, Thornthwaite and Hamon show lower values, except in April where all methods show more or less the same value. Table 3.5 shows values of annual PET whereas Tables App. 3.2-3.5 (appendix 3) represent values of monthly PET.

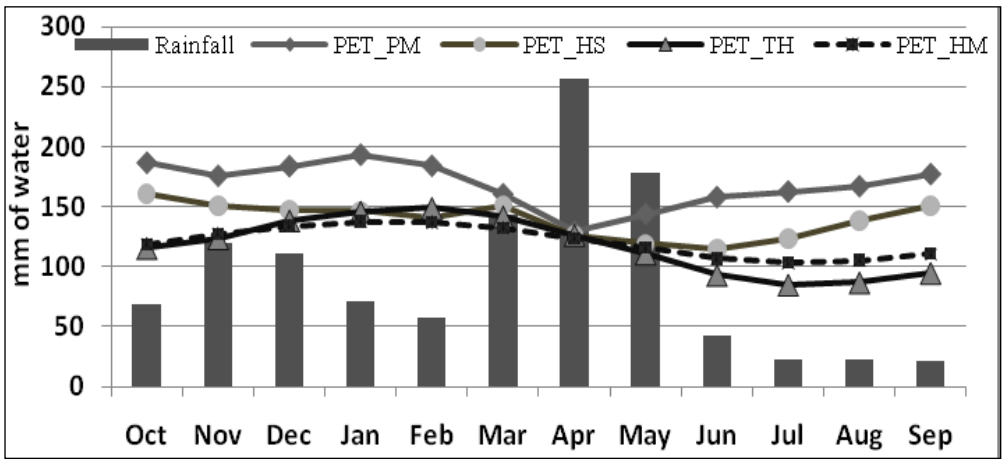

Figure 3.6: Comparison of average monthly potential evapotranspiration (PET) computed using different methods (PM: Penman-Monteith; HS: Hargreaves; TH: Thornthwaite; HM: Hamon) for the period 1971/1972-2008/2009.

Table 3.5: Potential evapotranspiration (PET) computed by different methods (PM: Penman-Monteith; TH: Thornthwaite; HS: Hargreaves and HM: Hamon) for the period 1971/72-2008/09.

Year	PET_PM	PET_TH	PET_HS	PET_HM
1971/72	1917.40	1461	1631.18	1451.18
1972/73	1900.69	1401	1637.73	1461.56
1973/74	1963.30	1433	1670.44	1424.08
1974/75	2129.57	1423	1680.90	1414.88
1975/76	2092.71	1452	1657.63	1406.59
1976/77	2166.05	1428	1689.67	1434.22
1977/78	2124.58	1434	1742.77	1420.61
1978/79	1921.25	1442	1691.54	1411.19
1979/80	2162.30	1441	1763.62	1426.5
1980/81	1972.92	1451	1747.84	1406.85
1981/82	2075.02	1447	1786.62	1410.9
1982/83	2013.89	1398	1686.28	1461.17
1983/84	2171.45	1419	1719.67	1438.44
1984/85	1781.77	1460	1636.68	1404.27
1985/86	1946.75	1429	1713.18	1433.35
1986/87	2018.63	1400	1734.06	1469.47
1987/88	2129.82	1378	1738.00	1484.03
1988/89	1860.76	1411	1604.63	1438.39
1989/90	2125.52	1436	1641.04	1427.68
1990/91	1952.32	1417	1668.56	1447.23
1991/92	1740.79	1414	1625.92	1447.04
1992/93	1641.05	1425	1630.72	1432.69
1993/94	1822.45	1423	1653.91	1447.63
1994/95	1758.45	1405	1595.63	1453.29
1995/96	1789.26	1414	1641.54	1446.75
1996/97	1990.71	1428	1624.56	1437.43
1997/98	1774.51	1390	1604.64	1471.81
1998/99	2032.91	1399	1653.23	1466.71
1999/00	1979.02	1407	1663.72	1437.72
2000/01	2088.38	1399	1653.41	1461.56
2001/02	2313.72	1394	1625.50	1466.54
2002/03	2277.44	1356	1680.12	1511.22
2003/04	2344.11	1353	1669.66	1515.96
2004/05	2336.47	1369	1629.47	1502.58
2005/06	2073.81	1371	1677.90	1497.84
2006/07	2047.98	1360	1623.71	1502.89
2007/08	2106.72	1366	1663.47	1492.89
2008/09	2082.11	1357	1675.94	1510.65
Average	2016	1410	1669	1452

3.3.2 Groundwater recharge

Table 3.6 gives an example of the scheme used for the calculation of groundwater recharge in excel sheet. The average annual recharge computed on a monthly basis using the evapotranspiration calculated respectively by Penman-Monteith (PM_PET), Hargreaves (HS_PET), Thornthwaite (TH_PET) and Hamon (HN_PET), gave the values of 166.1 mm/year, 180.8 mm/year, 198 mm/year and 200 mm/year respectively. The four methods gave a mean of 186 mm/year.

The variation of natural groundwater recharge rate calculated for each year, as the average of groundwater recharge values based on different PET methods is presented in Fig. 3.7. Table 3.7 gives the variation of annual groundwater recharge for the four PET calculation methods. The highest groundwater recharge rate is 512 mm/year (average value), which occurred in 1994/95. In 1979/80, 1984/85, 1999/2000 2002/2003 and 2008/2009, very little or no groundwater recharge occurred. Years with no recharge are not always relatively dry years: when rainfall is spread over all the months of the year, recharge will be smaller than in the case of great amounts of rainfall during a few months of the year (Dejager, 2011). For instance in 2001/02, the recharge occurred only in April: 569.4 mm precipitation out of a total of 1231 mm/year rain occurred in April, causing the yearly recharge of 403.3 mm (average of PET method). The year 1984/85, with a comparable total amount of rainfall (1138 mm/year) to the year 2001/02, showed almost no recharge. In a year with rainfall concentrated during a few months, the soil is first brought to field capacity, after which all the precipitation surplus will recharge the groundwater system (Dejager, 2011). In the case of spread precipitation the soil is dewatered during each dry period: thus the soil has to be brought to field capacity after each dry period leading to less water remaining for the groundwater recharge (Dejager, 2011). Low groundwater recharge between 2002/2003 and 2008/2009, and high dependence on groundwater use since 1997 induced by high population growth, rapid urbanization, and deficient water sector services, highlight the vulnerability of groundwater resources in the area.

Table App. 3.1 in appendix 3 presents the distribution of the monthly rainfall for the period 1970/71-2008/09. Fig. 3.8 and App. 3.6-3.9 (Appendix 3) show the distribution of monthly recharge calculated using the PET estimated by different methods for the same period. The distribution pattern of monthly recharge indicates a bimodal pattern similar to that of rainfall

(Fig. 3.8). In the study area, rainfall falls primarily during two distinct seasons: the first season or 'light rains' occurs between October and December, and the second season or 'heavy rains' falls between March and May. Following the significant rainfall occurring during the second rainy season, the soil moisture storage exceeds the field capacity of the soil and water surplus occurs. The peak recharge occurs in April, with an average of 89 mm/month. Significant recharge is also recorded in the month of May with average of 60 mm/month. Low recharge occurs in November, December and March with average of 12 mm/month, 10 mm/month and 10 mm/month respectively. Dry seasons (with little rainfall) occur from January to mid-March and June to September. There is no recharge in February and July to September reflecting the dry seasons. Little recharge ($\leq$ 3 mm/month) occurs during the months of January, June and October depending on the amount of precipitation in these months and also the amount of precipitation during and after the rainy seasons. The soil moisture must be brought to its field capacity, before recharge can occur. During months in which precipitation exceeds PET, the soil moisture gets recharged and when the soil moisture exceeds the field capacity of the soil, groundwater recharge occurs.

Table 3.6: Example of the scheme used for the calculation of recharge in excel sheet for the hydrologic year 1971/1972 (Penman-Monteith used for PET)

Month/Year	P	Ro	P-R0	PET	(P-Ro)-PET	PET-(P-Ro)	APWL	APWL/PAW	S_B	ΔS_B	AET	DEF	SUR	R_N	Annual R_N
Jun_1971	53	4.24	48.76	162.55	-113.79	113.79	113.79	2.28	35.14	0.00	48.76	113.79	0.00	0.00	
Jul_1971	19.9	1.59	18.31	153.73	-135.42	135.42	249.21	4.98	30.34	4.79	23.10	130.63	0.00	0.00	
Aug_1971	27.8	2.22	25.58	166.42	-140.84	140.84	390.05	7.80	30.02	0.32	25.90	140.52	0.00	0.00	
Sep_1972	3.9	0.31	3.59	172.95	-169.37	169.37	559.42	11.19	30.00	0.02	3.61	169.35	0.00	0.00	
Oct_1972	50.2	4.02	46.18	183.79	-137.60	137.60	697.02	13.94	30.00	0.00	46.18	137.60	0.00	0.00	
Nov_1972	7.6	0.61	6.99	189.62	-182.63	182.63	879.65	17.59	30.00	0.00	6.99	182.63	0.00	0.00	
Dec_1972	93.6	7.49	86.11	184.39	-98.28	98.28	977.93	19.56	30.00	0.00	86.11	98.28	0.00	0.00	
Jan_1972	65	5.20	59.80	185.77	-125.97	125.97	1103.90	22.08	30.00	0.00	59.80	125.97	0.00	0.00	
Feb_1972	74.1	5.93	68.17	150.00	-81.83	81.83	1185.73	23.71	30.00	0.00	68.17	81.83	0.00	0.00	
Mar_1972	150.1	12.01	138.09	139.85	-1.76	1.76	1187.49	23.75	30.00	0.00	138.09	1.76	0.00	0.00	
Apr_1972	351.3	28.10	323.20	107.40	215.80	-215.80	0.00	0.00	80.00	-50.00	107.40	0.00	215.80	165.80	
May_1972	263.4	21.07	242.33	120.93	121.40	-121.40	0.00	0.00	80.00	0.00	120.93	0.00	121.40	121.40	287.20

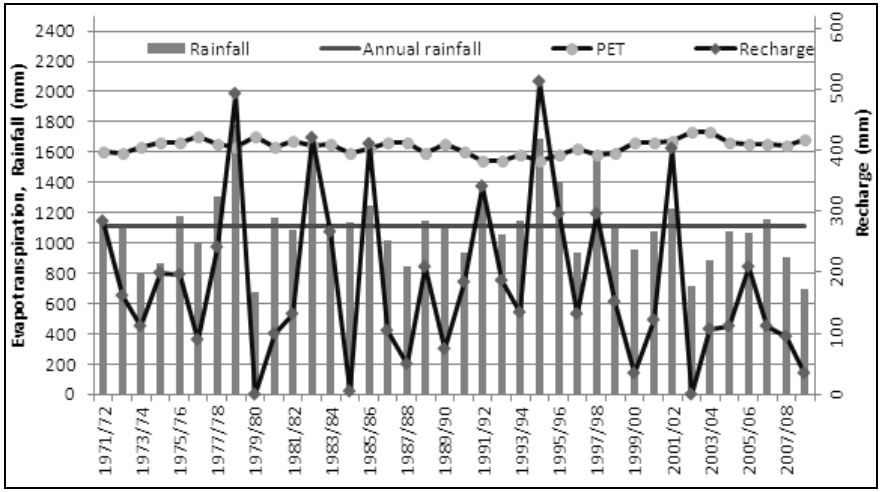

Figure 3.7: Variation of annual rainfall, potential evapotranspiration (average of different methods) and groundwater recharge (average of groundwater recharge calculated with different PET methods).

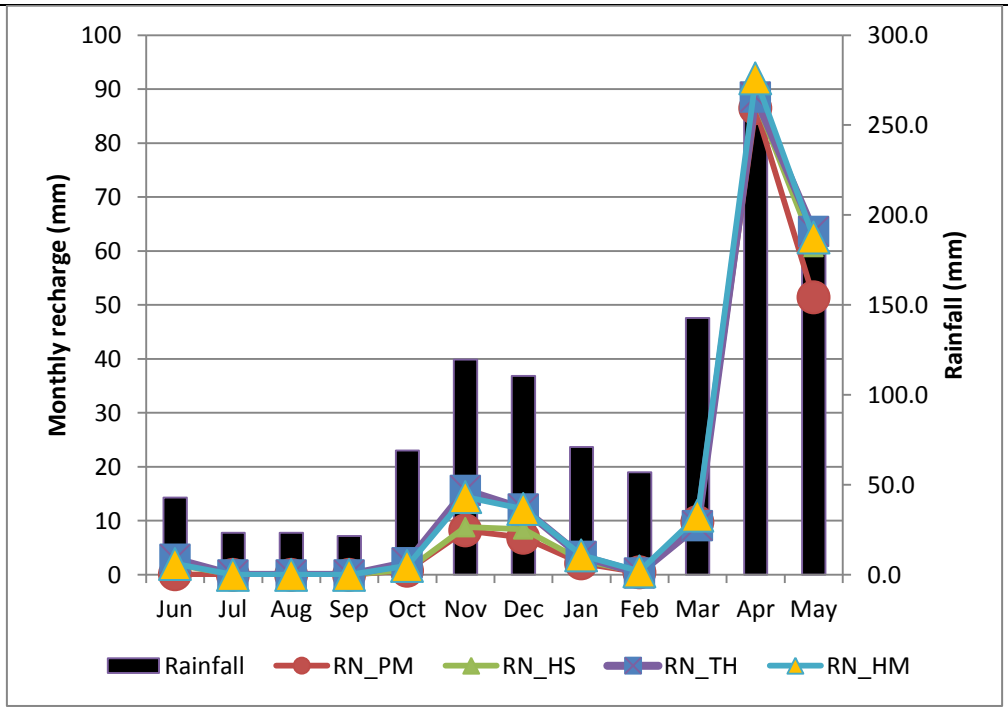

Month	Rainfall	R_N_PM	R_N_HS	R_N_TH	R_N_HM	Avrg R_N
Jun	43.0	0	2	3	2	2
Jul	23.3	0	0	0	0	0
Aug	23.4	0	0	0	0	0
Sep	21.5	0	0	0	0	0
Oct	69.0	1	1	2	2	1
Nov	119.6	8	9	16	14	12
Dec	110.5	7	8	12	12	10
Jan	71.1	2	3	3	4	3
Feb	57.0	0	0	0	1	0
Mar	142.7	10	9	9	11	10
Apr	256.5	86	88	89	92	89
May	178.3	51	61	64	62	60

Figure 3.8: Mean monthly recharge for the period 1971/72-2008/2009 (PM: Penman-Monteith; TH: Thornthwaite; HS: Hargreaves and HM: Hamon).

Table 3.7: Groundwater recharge (RN) computed by different methods (PM: Penman-Monteith; TH: Thornthwaite; HS: Hargreaves and HM: Hamon) for the period 1971/72-2008/09

Year	Rainfall	R_N_PM	R_N_HS	R_N_TH	R_N_HM	Average/year
1971/72	1160.00	287.20	283.91	258.06	289.44	279.7
1972/73	1075.70	169.38	157.03	160.99	156.66	161.0
1973/74	855.50	120.98	112.09	102.84	110.01	111.5
1974/75	825.00	194.32	198.74	203.39	199.75	199.1
1975/76	1110.50	166.65	206.76	188.64	227.15	197.3
1976/77	1054.20	68.96	87.50	91.71	102.42	87.7
1977/78	1331.90	211.45	213.52	262.41	276.12	240.9
1978/79	1749.40	433.51	475.18	525.85	567.27	500.5
1979/80	759.20	0.00	0.00	0.00	0.00	0.0
1980/81	1128.90	79.72	61.17	113.97	147.78	100.7
1981/82	960.00	81.59	96.32	125.78	144.71	112.1
1982/83	1718.00	318.27	412.80	527.94	501.89	440.2
1983/84	1119.20	253.61	268.22	278.61	280.20	270.2
1984/85	1159.60	0.00	0.69	0.00	15.46	4.0
1985/86	1236.00	434.47	386.55	404.22	416.87	410.5
1986/87	1011.80	64.04	86.55	129.51	121.73	100.5
1987/88	767.30	44.23	43.65	54.34	50.55	48.2
1988/89	1221.90	197.86	218.80	229.89	222.03	217.1
1989/90	1109.10	71.60	75.78	64.83	85.09	74.3
1990/91	961.20	161.18	179.60	201.12	194.66	184.1
1991/92	1288.50	349.77	319.83	345.43	342.08	339.3
1992/93	1103.20	186.14	193.63	181.33	191.27	188.1
1993/94	1123.70	116.54	135.55	141.16	138.47	132.9
1994/95	1641.50	460.35	510.38	542.45	541.05	513.6
1995/96	1490.20	294.59	297.99	292.67	310.41	298.9
1996/97	810.50	86.46	109.05	92.84	110.88	99.8
1997/98	1673.40	240.88	307.27	382.85	349.31	320.1
1998/99	1032.90	150.40	143.85	135.66	156.60	146.6
1999/00	936.70	4.65	34.23	48.21	57.15	36.1
2000/01	1224.30	69.66	136.06	141.82	142.80	122.6
2001/02	1109.00	396.74	404.15	405.86	402.29	402.3
2002/03	737.10	0.00	0.00	0.00	0.00	0.0
2003/04	955.10	84.15	113.11	131.35	103.64	108.1
2004/05	1111.80	96.27	111.46	124.98	111.69	111.1
2005/06	917.30	163.02	174.69	213.72	184.00	183.9
2006/07	1292.80	88.33	154.59	229.62	180.45	163.2
2007/08	922.80	126.59	114.44	139.10	123.27	125.9
2008/09	716.10	37.25	46.62	51.89	43.04	44.7
Average for each method		166.07	180.84	198.03	199.95	
Average for all methods					186.22	

3.3.3 Water balance and sustainable yield

The total surface area of the alluvial aquifer is about 388 km² (Mjemah, 2007; Mjemah et al., 2011). Determination of groundwater recharge rates gave a mean value of 186 mm/year being equivalent to 72.17 x 10^6 m^3 /year, an amount which represents 16.7% of the long term average annual precipitation of 1114 mm. This amount refers to the water recharging the Quaternary aquifer regulating the amount of water that can be pumped annually from this aquifer.

Sustainable yield is considered as a fraction of natural recharge and was calculated according to the concept proposed by Ponce (2007): average percentages estimated at approximately 40%, the least conservative approximately 70%, and reasonably conservative approximately 10%. These estimates are presented in Table 3.8.

Table 3.8: Estimates of sustainable yield according to the concept of Ponce (2007)

Estimated recharge	**40% of recharge**	**10% of recharge**	**70% of recharge**
72.17 x 10^6 m^3 /year	28.67 x 10^6 m^3 /year	7.22 x 10^6 m^3 /year	50.52 x 10^6 m^3 /year

3.3.4 Estimation of water budget

Groundwater provides over 50 percent of the present water supply for Dar es Salaam City. Since 1997, industries (e.g. beverage, pharmaceutical, chemical, etc), big hotels, institutes, colleges and urban farming are increasingly depending on groundwater. Groundwater survey in the study area was conducted in different periods between 2009 and 2010. The information obtained was used as a guide to estimate the amount of groundwater use in the Dar es Salaam area. 500 boreholes were visited in the study area. Dar es Salaam is situated largely on a sand aquifer and most boreholes are drilled between 20-60 m. The aquifer shows high yield of more than 6 m^3/h in median value. Most of the visited boreholes used for water supply have yields ranging between 10-15 m^3/h and few of them have yields between 15-30 m^3/h.

Mjemah et al. (2011) estimated boreholes yield from Dar es Salaam Quaternary aquifer at 8.56 x 10^6 m^3/year using data collected in 2005. This estimation was based on investigation of 1300 registered boreholes. While registered boreholes in 2005 was 1300 (Mjemah et al., 2010), Baumann et al. (2005) in the same year estimated over 4000 boreholes exists in Dar es

Salaam and about 1000 boreholes are drilled annually. Many unregistered boreholes exist and most of them were drilled illegally. A study by Danert et al. (2008) reports that about 9000 boreholes exists in Dar es Salaam. Using the estimation of Baumann et al. (2005) of about 1000 borehole drilled annually, over 10000 boreholes is expected to have been drilled in Dar es Salaam by the end of the year 2010: i.e. over 4000 boreholes estimated in 2005 plus 6000 boreholes estimation of six years (2006-2010).

On the other hand, Mato and Mjwahuzi (2010) report the existence of over 3500 registered boreholes in the city. Out of 500 boreholes randomly visited during this study, about two third of them are not found in the database and about 30 percent are not operating. Based on the record of 3500 boreholes registered by the year 2010, it is likely that there will be about 7000 unregistered boreholes. This makes a total of about 10,500 boreholes drilled in Dar es Salaam by 2010. The estimation of Baumann et al. (2005) of about 1000 borehole drilled annually is considered to be reasonable. A total of 10500 boreholes are very likely to exist in Dar es Salaam by the end of the year 2010. Using the experience of the field survey, we can assume that only about 70 percent of these boreholes are actively operating and the rest are abandoned due to either high salinity in water, drying up or low yield of boreholes and/or pump problems.

According to Mjemah et al. (2011) boreholes/wells used for domestic purposes are assumed to be pumping for 1 h/day, at every day of the year, while wells used for public water supply are assumed to pump for 6 h/day, during 365 days/year. The industrial wells are assumed to pump for 6 h/day, during 260 days/year. The yearly totals per well were then summed whereby the yield of 1300 boreholes/wells was estimated to be 8.56×10^6 m^3/year (Mjemah et al., 2011). Based on more or less the same approach and different use of water, for 10500 boreholes/wells one will expect a yield of about 69.3×10^6 m^3 /year (Table 3.9). 70 percent of 500 boreholes/wells (which is equivalent to 350 boreholes/wells) were considered in calculation as productive boreholes. The estimated value of 3.3×10^6 m^3/y (Table 3.9a) calculated for 350 productive borehole represent a total yield for 500 boreholes/wells visited during fieldwork. This total was divided by 500 and then multiplied by the total number of boreholes/wells in Dar es Salaam (i.e.10500) to obtain the total abstraction of groundwater (Table 3.9b).

Table 3.9: Estimation of yearly yields in the 7350 productive boreholes/wells

a) Yearly yields in the 350 productive boreholes/wells visited				
Groundwater purpose	**Number of boreholes/wells**	**Yield (m^3/h)**	**Pumping duration considered**	**Yield (m^3/year)**
Domestic	213	1944	1-hour x 365 days	14900760
Water supply	71	710	6-hour x 365 days	32652900
Industrial	31	315	6-hour x 260 days	10319400
Irrigation	35	349.8	6-hour x 260 days	11459448
Total	*350*	*3318.8*		*3301548*
b) Yearly yields in the 7350 productive boreholes/wells				
Groundwater purpose	**Number of boreholes/wells**	**Yield (m^3/year) in borehole/wells visited**	**Multiplication factor**	**Yield (m^3/year) in Dar es Salaam**
Domestic	213	14900760	x 10500/500	14900760
Water supply	71	32652900	x 10500/500	32652900
Industrial	31	10319400	x 10500/500	10319400
Irrigation	35	11459448	x 10500/500	11459448
Total	*350*			*69332508*

The water balance of the catchment suggests an average sustainable yield of 28.67 x 10^6 m^3 $year^{-1}$ (calculated as 40% of natural groundwater recharge) which leaves a shortfall of 40.63 x $10^6 m^3$ $year^{-1}$. The current abstraction is nearly equal to the amount of the groundwater recharge and is far greater than the estimated sustainable yield of the aquifer.

Aquifer overexploitation leads to decrease of groundwater level. One of the consequences of the decreasing groundwater level is the disturbance of the freshwater/saltwater equilibrium leading to the deterioration of groundwater quality. DQCA is frequently used for drinking water, irrigation and for industry purposes. Due to groundwater overexploitation, this aquifer has become very susceptible to potential saltwater contamination. In some cases, the demand for groundwater supply may upset the natural balance in a watershed. This can lead to reduced groundwater levels, changes in the surface water system (i.e. reduced base flow), and environmental impacts.

3.4 Conclusion and recommendations

Increase of population in recent decades and the resultant higher demands for water have led to many attempts aimed at optimal exploitation of DQCA. A study of the water balance has

been found to be very relevant and useful. The seasonal and annual distributions of important water balance parameters such as rainfall, potential evapotranspiration, actual evapotranspiration, water surplus, water deficit, have been calculated and discussed to provide a better understanding of the hydro-climatic background of the study area.

The water balance of the catchment suggests an average sustainable yield of 28.67 x 10^6 m^3 $year^{-1}$ (calculated as 40% of natural groundwater recharge) which leaves a shortfall of 40.63 x 10^6 m^3 $year^{-1}$. In conclusion, so far the study on water balance for DQCA has provided an increased understanding of a number of important factors including the need for further research. Conclusive factors were that: i) the estimated water balance shows that the coastal aquifer in Dar es Salaam is clearly overexploited: as a result of immense industrialization and high population growth, groundwater is heavily relied on in Dar es Salaam City to serve as alternative to surface water which is seriously deteriorating; ii) increase of borehole drilling that goes unchecked affects the protection of the groundwater resource; iii) minimizing the adverse effects of scarcity requires optimal as well as sustainable groundwater management; and iv) developing a systematic groundwater model to control seawater intrusion will provide more insight in understanding the hydrological behaviour of the system in relation to the current imposed stress on the recharge flux.

4 AQUIFER CHARACTERIZATION AND GROUNDWATER FLOW

4.1 Introduction

The flow of water from an aquifer into a well is related to the aquifer characteristics. Recharge to and discharge from the aquifer system can be measured or estimated. When working on problems of groundwater flow, the geologist or engineer has to find reliable values for the hydraulic characteristics of the geological formations through which the groundwater is moving. Pumping tests have proven to be one of the most effective ways of obtaining such values (Kruseman and Ridder, 1994). During a pumping test, water is discharged from a well at a known rate, and the drawdown or change in water level over time within the well is recorded. Water levels may also be measured concurrently within nearby wells or surface water bodies to evaluate the response of the aquifer at a distance from the discharging point. Prediction of the quantitative and qualitative response of aquifers to abstraction and recharge, which requires a good knowledge of aquifer parameters, is critically important for sustainable management of groundwater resources. This chapter refers to characterization and hydrodynamics of Dar es Salaam Quaternary coastal aquifer (DQCA). It presents: i) the aquifer parameters (i.e. transmissivity and hydraulic conductivity) obtained through interpretation of pumping tests, ii) piezometric maps made from static water level (SWL) measurements, and iii) monitoring data of daily fluctuation of the groundwater level.

4.2 Materials and methods

4.2.1 Aquifer properties

Most important aquifer properties essential for the determination of natural water flow through an aquifer comprise the hydraulic conductivity (K), transmissivity (T) and specific well capacity (S_c).

4.2.1.1 Hydraulic conductivity

Hydraulic conductivity is defined as the volume of water that will move through a porous medium in unit time under a unit hydraulic gradient through a unit area measured at right angles to the direction of flow (Kruseman and Ridder, 1994). It is an important hydrogeologic

parameter as it describes the ease in which a fluid can flow through the porous media. Hydraulic conductivity affects the flow paths and local groundwater velocities. Table 4.1 shows variation of hydraulic conductivities depending on the geological formations.

Table 4.1: Typical hydraulic conductivity values for unconsolidated sediments and rock types (Freeze and Cherry, 1979).

Sediment or Rock Type	**Hydraulic conductivity (m/s)**
Sandstone	1×10^{-12} to 1×10^{-8}
Clay	1×10^{-11} to 1×10^{-9}
Limestone	1×10^{-11} to 1×10^{-8}
Silt	1×10^{-9} to 2×10^{-7}
Silty Sand	1×10^{-7} to 6×10^{-5}
Sand	1×10^{-5} to 6×10^{-3}
Gravel	1×10^{-3} to 2×10^{-1}

4.2.1.2 Transmissivity

Transmissivity measures the amount of water transmitted through a unit width of the saturated thickness of an aquifer under a unit hydraulic gradient. It is defined by the product of the hydraulic conductivity and the saturated thickness of the aquifer (Bear, 2007; Fetter 2001) as expressed in the equation below.

$$T = bK \tag{4.1}$$

T is the transmissivity [L^2T^{-1}], b is the saturated thickness of the aquifer [L] and K is the hydraulic conductivity [LT^{-1}]. The saturated thickness of the aquifer is equal to the thickness of the aquifer in the case of a fully saturated, confined aquifer, or equal to the distance between the aquifer base and the water table in the case of an unconfined aquifer.

4.2.1.3 Specific well capacity

The specific capacity (S_c) of a well is a measure for the performance of a well and is determined from a test that involves pumping a well at a constant rate and measuring the resulting drawdown in a water level (Mace, 1997). In short, is defined as the discharge of the well divide by the drawdown (Fetter, 2001). The higher the value of Sc, the better the yield capacity of the well will be. In mathematical terms, the specific capacity is expressed as:

$$S_c = \frac{Q}{s} \tag{4.2}$$

Where S_c is the specific well capacity [L^2/T], Q is the pumping rate [L^3/T], and s is the drawdown in the pumping well [L].

4.2.2 Deduction of transmissivity from specific well capacity

Transmissivity is often estimated by using specific capacity data when standard pumping test data are not available or drawdown is stabilized early (Hamm et al., 2005). The deduction of the transmissivity derived from specific capacity is not as precise as the one obtained using the standard methods such as pumping tests. However, it helps obtain a fairly acceptable estimate of this parameter because the specific capacity itself is controlled by the hydraulic parameters, especially the transmissivity. The specific capacity is empirically expressed as:

$$T = c.\ \frac{Q}{s} \tag{4.3}$$

Where T is the transmissivity [L^2/T], Q/s = the specific well capacity [L^2/T], and c is a constant which depends on hydrogeological and hydrodynamic conditions. c was estimated by Driscoll (1986) at 1.385 for confined aquifers and at 1.042 for unconfined aquifers. The value between 0.9-1.5 for alluvial sediments was estimated by Thomasson et al. (1960). Other estimations of the constant involve the work of Theis et al. (1963) and Johnson et al. (1966) whereby a value between 0.5 and 1 for transient conditions and a value of 1.1 for wells in confined alluvial aquifer were estimated respectively.

The study area is characterized by alternating layers of sands, clays, gravel and coral limestone of various degree of weathering. Based on this variation of lithology, for estimation of the transmissivity from the specific capacity, a constant value of c = 1 was used for both unconfined and semi-confined aquifer, which seems to be a good average value.

4.2.3 Analytical methods to determine hydraulic properties

Aquifer types are identified as confined, leaky (semi-confined), or water table (unconfined) (Kruseman and Ridder, 1994). Thiem developed an analytical method for a confined aquifer in steady state. Another method used to determine the aquifer parameters relies on analytical solutions which are used as the basis of curve-fitting methods as described by several authors (Ferris et al., 1962; Kruseman and Ridder, 1970 and 1994; Lohman, 1972). In 1935, Theis presented a formula derived from considerations of the analogy between groundwater flow and heat flow. His formula accounts for the effect of time, and the storage characteristics and the transmissivity of the aquifer (section 4.2.3.2). This method was the first method developed for transient flow, meaning that water levels have not reached steady state. Thereafter several pumping test solutions were developed as discussed below.

4.2.3.1 Dupuit/Thiems's method

For steady radial flow in a confined aquifer, the Thiem's equation (4.4) (Dupuit 1863; Kruseman and de Ridder 1994) applies. In this method, transmissivity is determined for each possible combination of two wells (two observation wells, or pumping well and observation well).

$$T = \frac{Q}{2\pi(h2-h1)} ln\frac{r2}{r1} \quad (4.4)$$

Where: h1 is the hydraulic head (m) in the nearest observation well or the pumped well, h2 is the hydraulic head (m) in the furthest observation well, r1 is the distance from the pumped well to the nearest observation well (or the radius of the pumping well) and r2 is the distance from the pumping well to the furthest observation well.

Dupuit's method (equation 4.5), for an unconfined aquifer, has a similar formula to Thiem's formula for confined aquifer.

$$T = \frac{Q}{\pi(h_2^2-h_1^2)} ln\frac{r2}{r1} \quad (4.5)$$

4.2.3.2 Theis (1935)/Hantush (1961)

The Theis (1935) method is a famous method that can be applied to a number of hydrogeologic settings. The original Theis method is limited to fully penetrating wells, but

Hantush (1961) made it possible for this method to be applied to partially penetrating wells. In its original form, the Theis (1935) method is only applicable to confined aquifers. However, the method can be applied to unconfined aquifers by adjusting the drawdown data (Jacob, 1944). Theis equation can be written as follows:

$$s = \frac{Q}{4\pi T} W\ u \tag{4.6}$$

Where $u = r^2 S/4Tt$

$$S = \frac{4\pi T}{Q}\ s$$

$$\mathrm{t} = Tt/r^2 S$$

Where Q is pumping rate [L^3/T], T is transmissivity [L^2/T], S is storativity [dimensionless], s is drawdown [L], r is radial distance [L], and t is time [T]. The exponential integral in the drawdown equation is known as the Theis well function and is abbreviated as W(u). In the curve-fitting method based on the Theis solution, the type curve W(u) against the values of u is plotted to determine S and T graphically.

Hantush (1961a, b) derived equations for effects of partial penetration in a confined aquifer. For a pumping well, the partial penetration correction is as follows (cited in Duffield, 2007):

$$S = \frac{Q}{4\pi T}\left(W\ u\ + \frac{2b}{\pi\ l-d}\ \sum_{n-1}^{\infty}\frac{1}{n}\left[\sin\ \frac{n\pi l}{b}\ - \sin\ \frac{n\pi d}{b}\ \right].\cos\ \frac{n\pi z}{b}\ .W\left(u,\ \overline{\frac{K_z}{K_r}}\overline{\frac{n\pi r}{b}}\right)\right) \tag{4. 7}$$

For an observation well, the following partial penetration correction applies:

$$S = \frac{Q}{4\pi T}\left(W\ u\ + \frac{2b^2}{\pi^2\ l-d\ \ l'd'}\ \sum_{n-1}^{\infty}\frac{1}{n^2}\left[\sin\ \frac{n\pi l}{b}\ - \sin\ \frac{n\pi d}{b}\ \right].\left[\sin\ \frac{n\pi l'}{b}\ .\sin\left(\frac{n\pi d'}{b}\right)\right]\right. \tag{4.8}$$

Where b is aquifer thickness [L], n is flow dimension [dimensionless], d is depth to top of pumping well screen [L], d' is depth to top of observation well screen [L], l is depth to bottom of pumping well screen [L], l' is depth to bottom of observation well screen [L], Kz/Kr is vertical to horizontal hydraulic conductivity (anisotropy) [dimensionless], w(u,β) is the Hantush-Jacob well function for leaky confined aquifers, z is depth to piezometer opening [L].

At large distances, the effect of partial penetration becomes negligible when

$$r > 1.5b/\ \overline{\frac{K_z}{K_r}}$$

4.2.3.3 Cooper-Jacob straight-line method

Cooper-Jacob method (1946) is the straight-line method with roots based on the Theis (1935) method. The Cooper-Jacob method can be useful when matching a Theis type curve to data poses a challenge, such as in case of discharge fluctuations, irregularities in the early-time data or the presence of inflection points caused by boundaries. The Cooper-Jacob equation to estimate transmissivity is given as follows:

$$T = 2.30\ \frac{Q}{4\pi\Delta s} \qquad (4.9)$$

Where Δs = the slope of the semi-logarithmic time-drawdown plot.

4.2.3.4 Walton method

Walton's method is applied for semi-confined aquifers (Kruseman and De Ridder, 1994). A semi-confined (leaky) aquifer is an aquifer whose upper and lower boundaries are aquitards, or one boundary is an aquitard and the other is an aquiclude. By considering the effects of aquitard storage negligible, the drawdown due to pumping in a leaky aquifer is described by the following formula (Hantush and Jacob, 1955):

$$s = \frac{Q}{4\pi KD} \int_u^\infty \frac{1}{y} exp\ \left(-y - \frac{r^2}{4L^2 y}\right)\ dy \qquad (4.10)$$

or

$$s = \frac{Q}{4\pi KD} W\ u, r/L$$

Where:

$$\mathrm{u} = \frac{\mathrm{r}^2\mathrm{S}}{4\mathrm{KDt}}$$

and L is leakage factor $(m) = \overline{k_h D c_r}$, c_r is resultant hydraulic resistance of the aquitard in d, $\frac{1}{c_r} = \frac{1}{c_1} + \frac{1}{c_2}$ with c_1 and c_2 the hydraulic resistance of the overlying and underlying aquitard respectively.

Walton's method can be applied if the following assumptions and conditions are satisfied:

- The aquifer is leaky
- The aquitard is incompressible (i.e. the changes in aquitard storage are negligible)
- The flow to the well is in unsteady state.

4.2.3.5 Hantush curve-fitting method

Hantush (1960) curve-fitting method for leaky (semi-confined) aquifers takes into account the storage changes into the aquitard. For small values of pumping time, the drawdown equation for unsteady flow can be defined as:

$$s = \frac{Q}{4\pi T} W\ u, \beta \qquad (4.11)$$

Where: $u = r^2 S / 4Tt$

$$\beta = \frac{r}{4} \overline{\frac{K'/D'}{T} \cdot \frac{S'}{S}}$$

Where β is the leakage factor [L], K' is the vertical hydraulic conductivity of the leaky aquitard (L/T), D' is the saturated thickness of the leaky aquitard [L], S' and S are the storativities of the aquitard and aquifer respectively [dimensionless].

$$W\ u, \beta = \int_u^\infty \frac{e^{-y}}{y} erfc \frac{\beta \sqrt{u}}{\sqrt{y(y-u)}} dy$$

4.2.3.6 Neuman curve –fitting method

The Neuman (1974) method is a transient flow solution similar to the Theis (1935) method. However, the Neuman method accounts for fully or partially penetrating wells in

homogeneous, anisotropic unconfined aquifers with delayed gravity response. The Neuman model assumes instantaneous drainage at the water table. The solution also assumes a line source for the pumped well: it neglects wellbore storage. The presence of vertical flow is taken into account (Kruseman & De Ridder, 1994).

$$s = \frac{Q}{4\pi T} W\ u_A, u_B, \beta \qquad (4.12)$$

The first, early-time, segment is described by:

$$s = \frac{Q}{4\pi T} W\ u_A, \beta$$

Where $u_A = r^2 S/4Tt$

S is the elastic storage coefficient, the volume of water immediately released from the storage, per unit surface area and per unit decline in head [dimensionless].
The late-time conditions are described by:

$$s = \frac{Q}{4\pi T} W\ u_B, \beta$$

Where $u_B = r^2 S_O/4Tt$

S_o is the specific yield, the volume of water released from the storage per unit surface area and per unit decline of the water table [dimensionless].

Neuman's parameter β is defined as:

$$\beta = r^2 K_z/b^2 K_r$$

Where b is aquifer thickness [L], r is radial distance [L], K_r is radial hydraulic conductivity [L/T], and Kz is vertical hydraulic conductivity [L/T].

4.2.4 Pumping tests in the study area

Pumping test is the elementary and commonly used method for the determination of aquifer hydraulic parameters. It is a means of determining the aquifer properties indirectly and it consists of pumping groundwater from a well, usually at a constant rate, and measuring water levels in the pumped well and nearby wells (observation wells) during and after pumping. The sketch in Fig. 4.1 shows the pumping phase of a constant rate pumping test and the recovery phase.

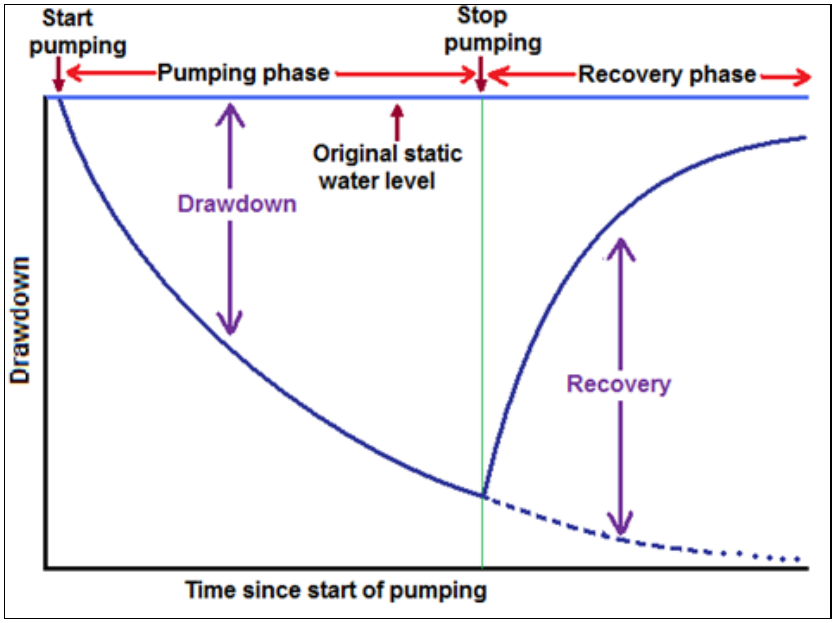

Figure 4.1: Sketch showing the pumping phase of a constant rate pumping test and the recovery phase.

The data collection methodology applied employed a review of existing pumping test data and the collection of new data obtained through execution of new pumping tests.

4.2.4.1 Available pumping tests

Collection of available information in relation to this research was done so as to contribute to the aquifer characterization and groundwater flow. Data collected include borehole lithological logs and raw pumping test data. Borehole lithological logs included in borehole drilling reports drilled between 1997 and 2011 facilitated to understand the variation of lithologic layers and the differentiation of unconfined and semi-confined aquifers. Pumping test data were analysed to determine T and K from pumping and recovery data. 5 raw single well pumping test data (P1-P5) were collected from Drilling and Dam Construction Agency (DDCA) (Fig. 4.2). This study also utilized 3 raw pumping test data (P6-P8) obtained from

the previous work in the study area by Mjemah (2007) (Fig. 4.2). Mjemah's study involved 39 pumping tests scattered in a large area extending over a distance of about 35 km from the coastline to Pugu Hills. Raw pumping test data collected from his study are situated near the coastline where this study is concerned. Pumping tests P6 and P7 were carried out with observation wells. In the following subsections the location and brief lithology is provided for each well indicating the depth at which different lithologies are intersected.

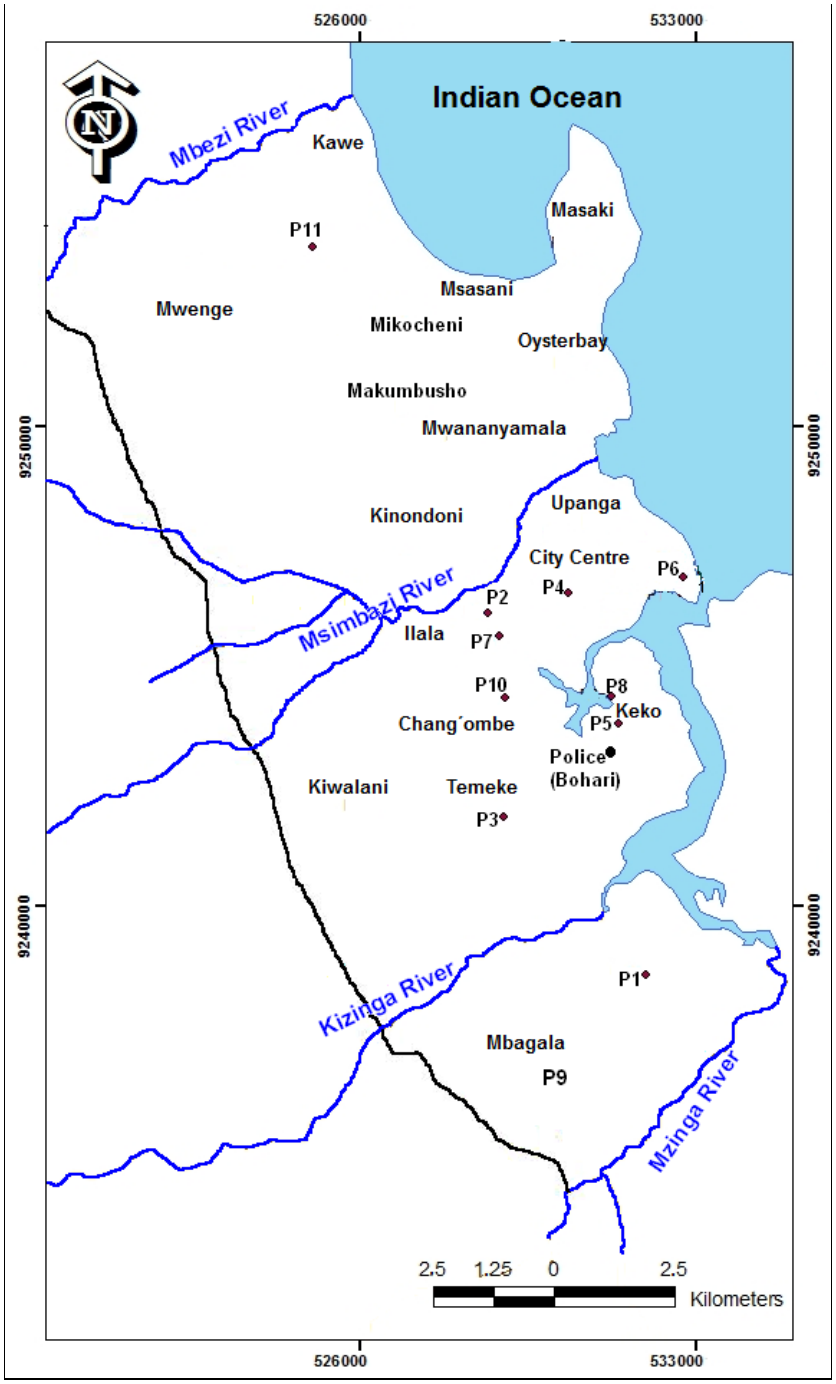

Figure 4.2: Location of pumping tests.

4.2.4.1.1 Pumping test on well P1

P1 is located at Mbagala (Fig. 4.2) and was drilled to a total depth of 60 m. It intersects medium to coarse sand (0-10 m), clay with minor sand (10-22 m), sand with minor clay (22-36 m), greyish medium to coarse sand (36-55 m), and clay (55-60 m) (drilling report DSM 1126/2011). The screens are positioned at the depth between 20 m and 55 m (not continuous), tapping water from the lower semi-confined aquifer (Fig. 4.5).

4.2.4.1.2 Pumping test on well P2

P2 is located at Ilala (Fig. 4.2) and was drilled to a total depth of 52 m. It intersects fine to medium sand (0-10 m), medium to coarse sand with minor clay (10-16 m), clay with sand (16-36 m), coarse grained sand with weathered limestone (36-40 m) and fresh limestone (40-52 m) (DDCA drilling report DSM 76/2006). The screens are positioned at the depth between 10 m and 42.5 m (Fig. 4.6) (different sections). However, according to the lithological description, the depth of 40 – 52 m should be considered as aquitard since the limestone is described as fresh. P2 is considered to be pumping the unconfined aquifer with a thickness of 30 m (Fig. 4.6).

4.2.4.1.3 Pumping test on well P3

P3 is located at Temeke (Fig. 4.2) and was drilled to a total depth of 80 m. P3 intersects fine to medium sand (0-12 m), coarse sand (12-15 m), fine sand with clay (15-22 m), medium to coarse sand (22-42 m), sand with clay (42-52 m), coarse sand (52-54 m), fine sandy clay (54-62 m), coarse sand with minor limestone (62-70 m), sandy clay with limestone (70-74 m), medium sand with limestone (74-76 m) and sandy clay with limestone (76-80 m) (DDCA drilling report DSM 1089/2011). The screen is positioned at the depth between 18 m and 78 m (different sections). According to the lithological description, P3 is considered to be pumping semi-confined aquifer with a thickness of 58 m (depth between 22 m and 80 m) (Fig. 4.7).

4.2.4.1.4 Pumping test on well P4

P4 is located at City Centre (Fig. 4.2). It intersects sand, sandy clay and medium to coarse sand and weathered limestone. P4 is considered to be pumping the semi-confined aquifer with screen sections located between a depth of 20 m and 63 m (not continuous) (Fig. 4.8). No full

lithological information could be accessed during the moment of writing this thesis. However, more information should be available in DDCA drilling report "DSM 490/2011".

4.2.4.1.5 Pumping test on well P5

P5 is located at Keko (Fig. 4.2) and was drilled to a total depth of 60 m. It intersects medium sand soil (0-10 m), sandy clay (10-14 m), clay (14-24 m), medium sand (24-34m), sandy clay (34-40 m), medium sand (40-42 m), weathered limestone with minor clay and medium sand (42-50 m), medium sand with limestone (50-56 m) and fresh limestone (56-60 m) (drilling report DSM 453/2011). P5 is considered to be pumping semi-confined aquifer with screens positioned at depth between 24 m and 56 m(different sections) (Fig. 4.9).

4.2.4.1.6 Pumping test on well "P6"

P6 is located at City Centre (Fig. 4.2) and was drilled to a total depth of 30 m. It intersects sand, sandy clay and medium sand at the depth between 0 and 12 m. From the depth between 12 m to 30 m, P6 comprises coarse sand and weathered limestone. P6 is considered to be pumping the unconfined aquifer with screens sections located at a depth between 12 m and 29 m (Fig. 4.10). The Pumping test was carried out with one observation well located at 9 m from the pumping well.

4.2.4.1.7 Pumping test on well P7

P7 is located at Ilala (Fig. 4.2) and was drilled to a total depth of 42 m. It intersects sand, sandy clay and medium sand at the depth between 0 and 10 m. From the depth between 10 m to 42 m, P7 comprises medium to coarse sand and yellowish weathered limestone. P7 is considered to be pumping the unconfined aquifer with screen sections located at a depth between 10 m and 42 m (Fig. 4.11) (DDCA drilling report DSM 199/2002). The pumping test was carried out with one observation well located at 100 m distance from the pumping well.

4.2.4.1.8 Pumping test on well P8

P8 is located at Keko (Fig. 4.2) and was drilled to a total depth of 51 m. It intersects sand, fine to medium sand at the depth between 0 and 15 m. From the depth between 15 m to 48 m, P7 comprises medium to coarse sand and weathered limestone. From the depth of 48 m to 51 m, P7 consists of fresh limestone. P7 is considered to be pumping the semi-confined aquifer with

screen sections located at a depth between 18 m and 48 m (Fig. 4.12) (DDCA drilling report (DSM 199/2002).

4.2.4.2 New pumping tests

The field work was conducted which involved checking up the borehole/well locations (presented in drilling reports/literature), carrying out pumping tests and collection of other pertinent data (i.e. water level, rainfall and temperature measurements).

Due to budget limitations, no boreholes were drilled and constructed for this study. On the other hand, few well owners would allow restriction of water use during the pump tests, which made finding appropriate test wells very difficult and challenging. Three pumping tests, at three wells with boreholes around that could be used as observation points, were planned for execution. However, only two pumping tests were successful (Fig. 4.2) which involved wells P9 and P10 belonging to DAWASCO (Dar es Salaam Water and Sewerage Corporation), constructed in the lithology dominated by sand materials. The third pumping test at well P11 located at Coca-Cola Company constructed in limestone lithology was not successful due to pump failure. Well P9 taps water from the semi-confined aquifer and well P10 is constructed in the upper unconfined aquifer. These boreholes had pumps equipped with a flow meter for discharge measurement. The flow rate was determined by dividing the volume of water discharged by the time used for discharge. The flow rate was calculated every half hour during the first two hours of the test and thereafter, the flow rate was calculated after every hour.

Groundwater level measurements were made prior to pumping test (using water-level meter), during pumping test and water recovery using divers. Immediately after the pumping period, water level was taken using a water-level meter. A pressure transducer ("Diver") takes measurement by recording water level and temperature automatically. Divers were programmed to take reading every ten seconds. Divers used in this study have ranges of 10 or 50 m. A diver of 50 m (J02701) range that can accommodate a larger drawdown range was used in the test well. Divers of 10 m (J0496 and H0507) ranges were used in the observation wells. Divers were lowered to a depth deeper than the greatest possible drawdown, but shallower than the maximum range of the Diver. Barometric pressure measurements were

taken using the barometric pressure sensor (Baro-Diver G5943) for compensating any barometric fluctuations during the tests. Each test consisted of pumping and recovery phases.

4.2.4.2.1 Pumping test on well P9

P9 is located at Mbagala (Fig. 4.2) and was drilled to a total depth of 80 m. It intersects fine sand, sandy clay and medium sand (0-10 m), medium to coarse sand with minor clay (10-25 m), sticky clay with minor sand (25-30 m), greyish medium to coarse sand (30-55 m), fine to medium sand with clay (55-60 m), medium sand and coarse sandy clay (60-80 m) (drilling report DSM 226/1199). The screen is positioned at the depth between 30 m and 80 m (different sections), tapping water from the lower semi-confined aquifer (Fig. 4.13).

4.2.4.2.2 Pumping test on well P10

P10 is located at Chang'ombe (Fig. 4.2) and was drilled to a total depth of 45 m. It intersects fine sand, medium to coarse sand (0-10 m), sandy clay (22-24m), medium to coarse sand (24-34), and coarse sand with minor clay (34-45 m) (DDCA drilling report DSM 248/2002). The screen is positioned at the depth between 10 m and 45 m (different sections), tapping water from unconfined aquifer (Fig. 4.19).

4.2.4.3 Processing and analysis of pumping test data

Different types of methods were used to analyse the pumping test data. These include: i) specific well capacity (SWC) calculated based on the pumping rate and measured maximum drawdown for pumping tests, ii) Dupuit/Thiem for unconfined and confined aquifer under steady-state flow, iii) Neuman type curve fitting for the unconfined aquifer, Walton and Hantush leaky aquifer type curve fitting for the semi-confined aquifer, and Theis type curve fitting for confined aquifer under unsteady state (or transient) flow. For recovery data is possible to be re-arranged and then processed by curve fitting methods just like pumping data.

The above used methods are included in the software Infinite Extent, a Windows-based pump test analysis package (Starpoint Software, 1996). The software enables analysis of aquifer test data which involve a constant rate of water discharge from a well.

The data are categorized based on the initial analysis using borehole log data, curve type of the pumping test raw data and general knowledge of the hydrogeologic settings of the study area before selection of methods of analysis. The analytical methods are governed by basic assumptions for steady and unsteady state flows. These can be generalized as (Kruseman & De Ridder, 1994; Fetter, 2001): i) the aquifer has infinite areal extent and horizontal layering, ii) the aquifer is bounded on the bottom by a confining layer, iii) the aquifer is homogeneous and isotropic, iv) the pumped well penetrates the entire thickness of the aquifer and thus receives water by horizontal flow, v) the aquifer is pumped at a constant discharge rate, vi) the pumped well has an infinitesimal diameter so that the storage in the well is negligible.

Infinite Extent Software allows plotting the data against type curve for the various methods. The type curve yielding the best fit apparently reflects the hydrologic condition prevailing for the material tested and provides the best representative result. However, the results are evaluated in view of field experience of the hydrogeology of the area.

4.2.5 Groundwater level measurements

4.2.5.1 Acquisition of groundwater level data

Groundwater level measurements were collected to provide information on regional head distribution and hydraulic gradients within the upper unconfined aquifer and lower semi-confined aquifer. The water level meter with a probe attached to a tape, fitted on a reel (Fig. 4.3), was used to measure the total depth and static water level (SWL) within the boreholes. The probe detects the presence of a conductive liquid between its two electrodes and is powered by a battery. When contact is made with water, the circuit is closed, sending a signal back to the reel. This activates a buzzer and a light. The water level is then determined by taking a reading directly from the tape, at the top of the borehole casing. A total of 183 measurements of static water level (SWL) were conducted during the fieldwork in Tanzania. A total of 88 (60 in the unconfined and 28 in the semi-confined aquifer) and 95 (53 in the unconfined and 42 in the semi-confined aquifer) measurements of the static water level (SWL) were conducted in July 2010 and July 2011 respectively. Total borehole depths were measured by lowering the water level meter until the probe reaches the bottom of the borehole. When the probe reaches the bottom the tape becomes slack; lifting and dropping the tape several times helps to feel the bottom of the borehole.

Automatic (semi-)continuous groundwater level measurement provides information on the temporal trends in groundwater levels due to the effects such as drought, high rainfall events and groundwater pumping. Fig. 4.4 and Table 4.2 indicate monitoring locations and data available during the time of writing this thesis. The study used "Divers" (automated water level measurement systems) for monitoring groundwater fluctuations. The Diver combines a pressure transducer and a data logger, and is designed to measure the pressure exerted by the weight of the above-standing water column. Divers use battery power and are designed for long-term underwater deployment. They can be installed and left in-situ for a period dependent on the monitoring frequency for collecting water level data at user-defined intervals. Using Divers for monitoring facilitates monitoring of multiple locations at the same time. To measure variations in atmospheric pressure, which need to be taken into account to obtain the correct water level, a Baro-Diver has to be used as well. Depending on terrain and other conditions one Baro-Diver suffices for an area with radius of 15 km. The atmospheric pressure was subtracted from the Diver measurement using the barometric compensation wizard in Diver-Office.

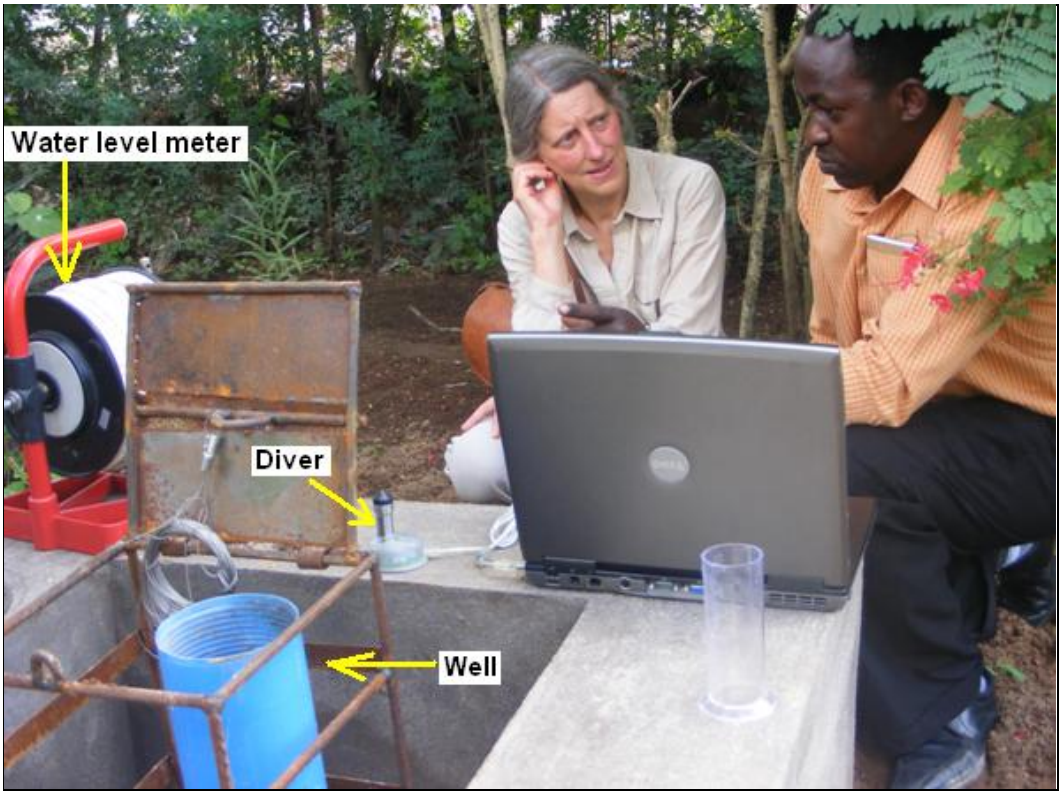

Figure 4.3: Long-term groundwater level measurement is conducted by using divers (automated water level measurement systems). Data downloading from the diver is conducted in the field. Manual water level measurement is executed using water level meter before returning diver into the well.

Divers were installed in the study area in order to have continuous time-series of water level measurements. They were installed in different areas depending on the anticipated cause of groundwater fluctuation was targeted to be monitored. Divers were programmed to take reading every 15 minutes. Selection of boreholes for monitoring groundwater fluctuations was also somehow influenced by two main factors: i) securing a place where Divers and other monitoring equipment (i.e. rain gauge and thermometer) will be safe, ii) available boreholes which were not in use (e.g. new boreholes which pumps were not yet installed to exploit water, abandoned boreholes due to high salinity or boreholes temporarily not in use due to pump failure). Institutions and companies with well protected areas were targeted. The following institutions were qualified and accepted the request of conducting groundwater monitoring in their areas: Mnazi Mmoja primary school (MNAZ_1) which had a borehole not in use due to a pump failure, Zanaki secondary school (95) and Temeke Municipal Garden (179) had new boreholes which were not started using them, Dar es Salaam Bunge offices (B11) and Coca-Cola Company (B3) with boreholes abandoned due to high salinity, Gymkhana Golf Club provided access to two boreholes (B1 & B2) that are not in use since they were drilled. Boreholes ID in brackets correspond with the boreholes identification indicated in Fig. 4.4. Currently boreholes with Divers include B1, B2, B3 & B11. Monitoring in boreholes 95, MNAZI_1, and 179 stopped because the access provided to these boreholes was just for the short time (1-3 months) before pump installation for water production.

Table 4.2: Continuous monitoring locations and data available

S/N	Monitoring location	Monitoring equipment	Measurements	Periods of measurements	Monitoring Borehole	Last time data download/access
1	Mnazi Mmoja Primary School	Mini-Diver (10m) H**0461**	Pressure & water temperature	7-18 July 2010; 22-01 August 2010. Diver failed to record after 1 June 2011	**MNAZI_1**	1 June 2011
		Baro-Diver G5943	Atmospheric pressure	7-31 July 2010; 27 February - 2 August 2011.		Baro-Diver relocated to Gymkhana Golf Club at 2 August 2011
		Rain Gauge	Rainfall	1-31 July 2010; 27 February 2011 to 30 April 2012		April 2012
		Six Thermometer	Minimum and maximum temperature	1-31 July 2010; 27 February 2011 to 30 April 2012		April 2012
2	Zanaki Secondary School	Mini-Diver (10m) J0496	Pressure & water temperature	7-19 July 2010; 22-01August 2010.	**95**	31 July 2010
		Rain Gauge	Rainfall	1-31 July 2010		Stopped on 1st August 2010
		Six Thermometer	Minimum and maximum temperature	1-31 July 2010		Stopped on 1st August 2010
3	Temeke Municipality Garden	Mini-Diver (10m) H**0507**	Pressure & Temperature	22 April - 9 June 2011 Diver failed to record after 9 June 2011	**179**	9 June 2011
		Rain Gauge	Rainfall	27 February 2011 to 30 April 2012		April 2012
		Six Thermometer	Minimum and maximum temperature	27 February 2011 to 30 April 2012		April 2012
4	Gymkana Golf Club	Mini-Diver (10m) H0461	Pressure & Temperature	27 February - 7 July 2011	**B1(Baro-Diver)**	7 July 2011
		Baro-Diver G5943	Atmospheric pressure	2 August 2011 to 24 June 2012	**B2**	June 2012
		Mini-Diver (50m) J02701	Pressure & Temperature	22 June 2011 to 6 December 2011 and 10 January 2011 to 24 June 2012		
		CTD-Diver K2697 (replaced Mini-Diver H0461in B1)	Pressure, temperature & Conductivity	8 July 2011 to24 June 2012	**B2**	
5	Coca-Cola Company	Mini-Diver (10m) K2697	Pressure & Temperature	8 July 2011 to 13 January 2012	**B3**	
6	Dar es Salaam Bunge Offices	Mini-Diver (10m) K7351	Pressure & Temperature	13 January 2012 to 19 April 2012	**B11**	9 April 2012

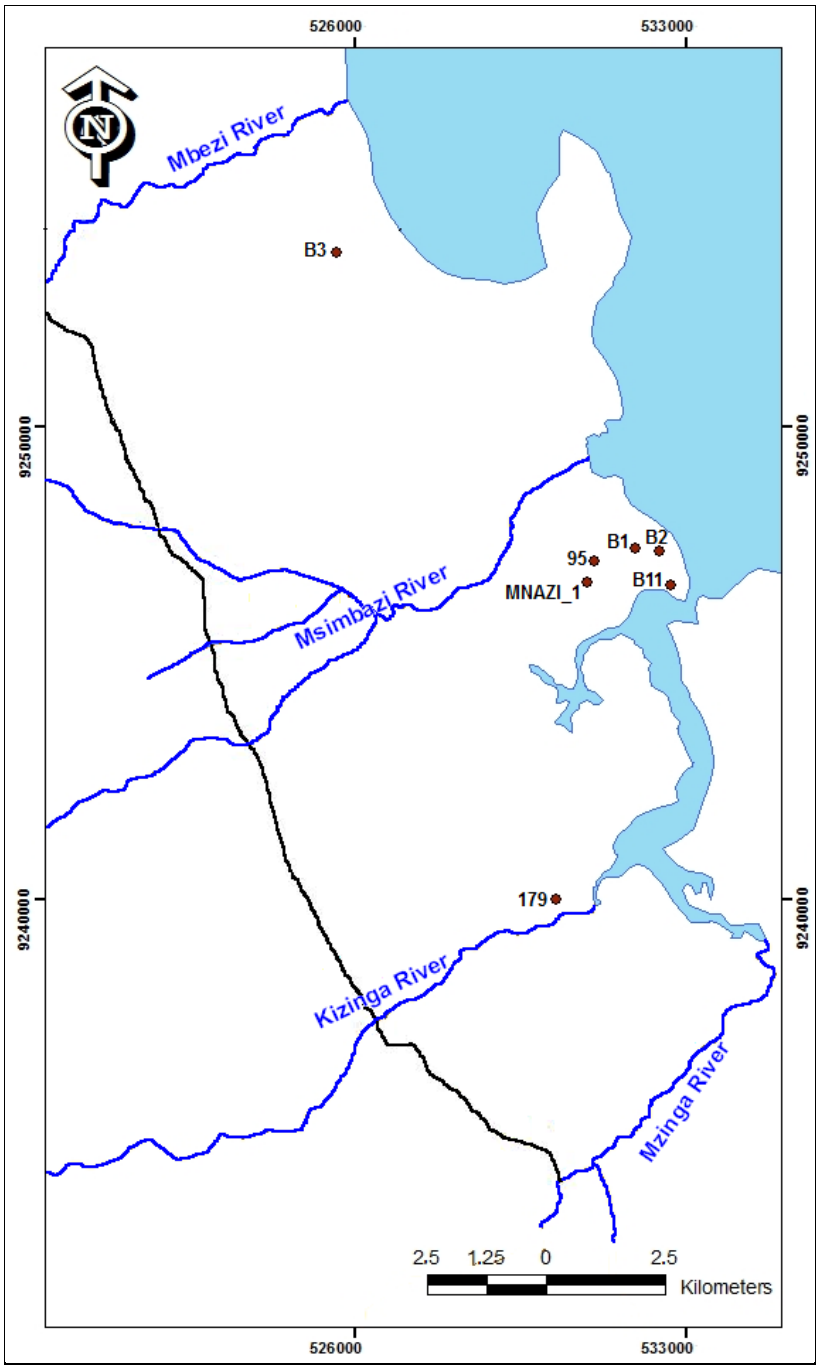

Figure 4.4: Locations of groundwater monitoring using divers.

4.2.5.2 Processing and analysis of groundwater level data

4.2.5.2.1 Static water level measurements

Static water level measurements were used to develop water table contour maps for both unconfined and semi-confined aquifers. Water table contour maps show the elevation and configuration of the water table at the time the measurements were taken. In order to construct a water table map, first the water level measurements are converted from the form of depth

below the ground or meters below ground (mbg) to the form of water table elevation (e.g. meters above mean sea level "mamsl"). The map is prepared by plotting the water levels of observation points on a topographical map and drawing lines connecting points of equal water table elevation (equipotential lines). A proper contour interval is chosen depending on the topography and slope of the water table. A water table contour map is an important tool in groundwater investigations as it is possible to derive from it the gradient of the water table, and the direction of the groundwater flow. The direction of the groundwater flow is perpendicular to the equipotential lines and can be directly deduced from a water table contour map.

4.2.5.2.2 Daily fluctuation of groundwater level measurements

In order to get net results of "Diver" measurements of groundwater level fluctuation, Diver Office Software which incorporates Barometer Wizard was used to subtract the Baro-Diver atmospheric air pressure data from the total pressure data (atmospheric + water level) collected by separately installed Divers. The software enables numerous possibilities to connect these final compensated data sets with fixed levels as sea water level or installation heights of the Divers (water column above Diver).

4.3 Results and discussion

4.3.1 Pumping tests and hydraulic parameter estimation

4.3.1.1 Available pumping tests

4.3.1.1.1 Specific capacity

Specific capacity Q/s is a function of the hydraulic properties of an aquifer. The data used for the calculation of specific well capacity were obtained from the constant discharge rate Q used in the constant rate test and the steady state drawdown s obtained at the end of constant rate test.

The specific capacity was calculated for the 8 pumping tests and varies between a minimum of 13.1 m^2/d (well P2) and a maximum of 107.4 m^2/d (well P1). In view of the classification of transmissivity and specific capacity magnitude according to Krasny (1993), the specific

capacity is divided into 4 classes, namely low (< 8.64m^2/d), intermediate (8.64 to 86.4 m^2/d), high (86.4 to 864 m^2/d) and very high (> 864 m^2/d) (Table 4.3). Except well P1 which shows a value categorized as high specific capacity, all other values fall within the intermediate class. Table 4.4 represents hydraulic parameters deduced from the specific well capacity method.

Table 4.3: Classification of specific capacity values according to Krasny (1993).

Well	**Low (< 8.64m^2/d)**	**Well**	**Intermediate (8.64 - 86.4 m^2/d)**	**Well**	**High (86.4-864 m^2/d)**	**Well**	**Very high (> 864 m^2/d)**
		P2	41.58	P1	107.4		
		P3	26.6				
		P4	61.3				
		P5	13.1				
		P6	64.3				
		P7	20.5				
		P8	59.6				

Table 4.4: Hydraulic parameters deduced from specific well capacity method (UC = unconfined aquifer, SC = semi-confined aquifer, Q= discharge rate, s= drawdown, T = transmissivity, and K = hydraulic conductivity).

Well	**Location**	**Aquifer type**	**Aquifer lithology**	**Q (m^3/d)**	**s (m)**	**Q/s = T(m^2/d)**	**Aquifer thickness (m)**	**K (m/d)**
P1	Mbagala	SC	Sand	380	3.54	107.4	35	3.07
P2	Ilala	UC	Sand/limestone	250	6.05	41.58	30	1.38
P3	Temeke	SC	Sand	470.4	17.7	26.6	58	0.46
P4	City Centre	SC	Sand/limestone	528	8.62	61.3	50	1.23
P5	Keko	SC	Sand/limestone	172.8	13.18	13.1	32	0.41
P6	City Centre	UC	Sand/limestone	135.77	2.11	64.3	17	3.79
P7	Ilala	UC	Sand/limestone	116.26	5.66	20.5	32	0.64
P8	Keko (R.C.C)	SC	Sand/limestone	172.8	2.9	59.6	30	1.99

4.3.1.1.2 Dupuit/Thiem's method

Through the Infinite Extent software it was possible to calculate transmissivity for each possible combination of two wells (pumping well and observation well). Data required as inputs to the steady state calculator in the Infinite Extent include well discharge rate, pumping well radius, aquifer thickness, distance to the observation well, drawdown data for both pumping well and observation well. Before pressing a button to allow calculation to be executed, one has to indicate the aquifer type (confined or unconfined) in the option box. Pumping tests in wells P6 and P7 were carried out along with observation wells and thus it was possible to calculate transmissivity values using Dupuit/Theim's method. Both wells tap water from the unconfined aquifer. The transmissivity values of 59.08 m^2/d and 25.30 m^2/d were obtained for well P6 and well P7 respectively. Table 4.5 represents the results of hydraulic parameters deduced from pumping test analysis by Dupuit/Thiem's method for steady-state flow.

Table 4.5: Hydraulic parameters deduced from pumping test analysis by Dupuit/Thiem's method for steady-state flow.

Well	Location	Aquifer type	T (m^2/d)	Aquifer thickness (m)	K (m/d)
P6	City Centre (Ramani)	unconfined	59.08	17	3.48
P7	Ilala (Boma)	unconfined	25.30	32	0.79

4.3.1.1.3 Analytical curve fitting methods

Classifying the aquifer type correctly was one of the significant steps before selecting the solution methods. Classifying the aquifer type was mainly conducted by using the lithological logs. The presence of the semi-pervious unit (clay, sandy clay and silts) within the Quaternary deposit allows distinguishing the type of aquifer in which the pumping test was carried out. The clay bands are responsible for the local confining of groundwater in most of the boreholes/wells. Aquifer thickness at the well site was determined through examining the lithology of the well and assessing the thickness of the productive aquifer formation and any aquitards or confining layers. Pumping test period for data analysed in the study area range from 3 hours and 45 minutes conducted at well P6 to 48 hours conducted at well P4. The recovery phase data for the former and the latter were recorded for 15 minutes and 24 hours respectively.

The scheme used for pump test data analysis includes showing well construction sketches indicating the type and thickness of aquifer, water level before pumping and water level during pumping. Figures produced indicate the pumping periods and recovery phase conducted.

PUMPING TEST AT MBAGALA (SEMI-CONFINED AQUIFER): MEASUREMENTS IN PUMPING WELL (P1)

Well P1 taps water from the semi-confined aquifer. Fig. 4.5(i-ii) provides results of the analysis. The pumping test at P1 was analysed by the Walton Leaky Type Curve technique (for a leaky aquifer) which provided a good fitting comparing to other methods. The analysis of pumping data yielded a T value of 74.28 m^2/d and K value of 2.12 m/d (Fig. 4.5iia). On the other hand, the analysis of the recovery data shows similar hydraulic response with T value of 71.17 m^2/d and K value of 2.03 m/d (Fig. 4.5iib).

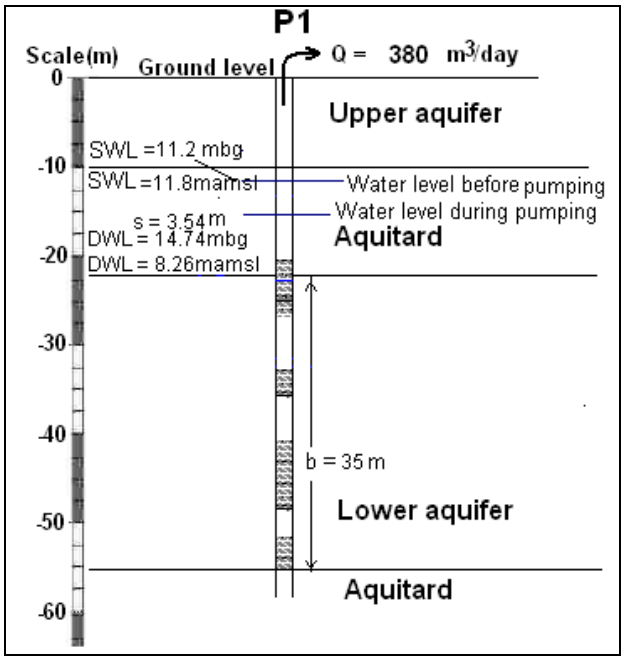

(a)Well construction sketch: SWL = Static Water Level; DWL = Dynamic Water level; s = drawdown; mbg = meter below ground; mamsl = meter above mean sea level; b = aquifer thickness

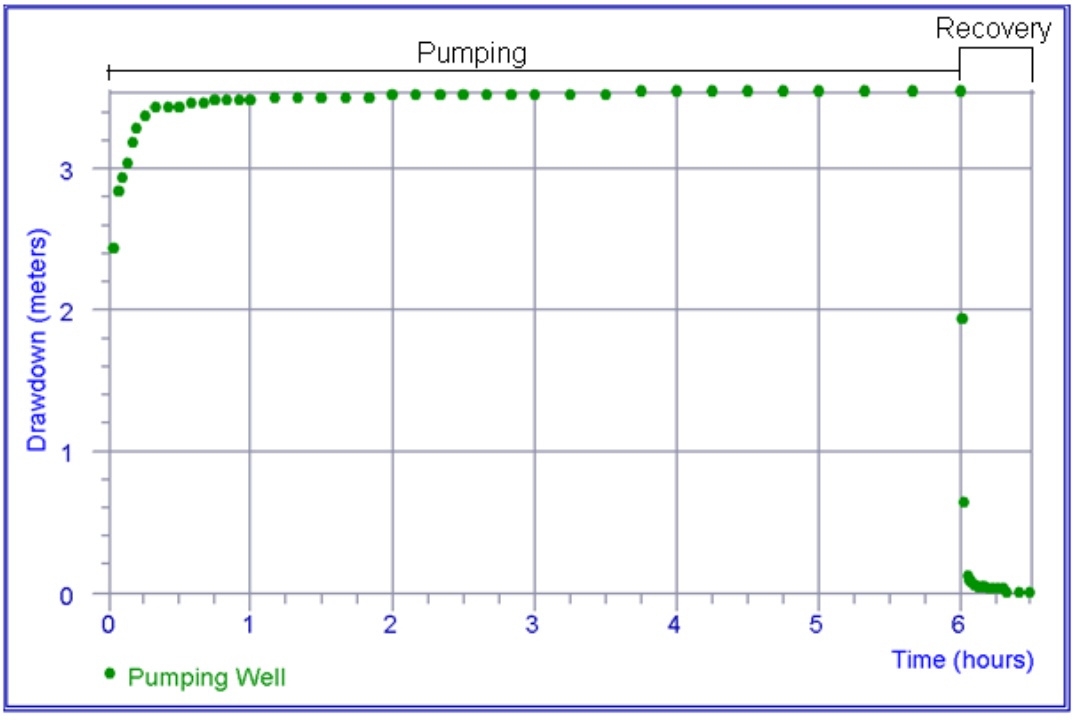

(b)Pumping period and recovery phase

Figure 4.5(i): Pumping test at P1: (a) well construction sketch, and (b) arithmetic graph for pumping well.

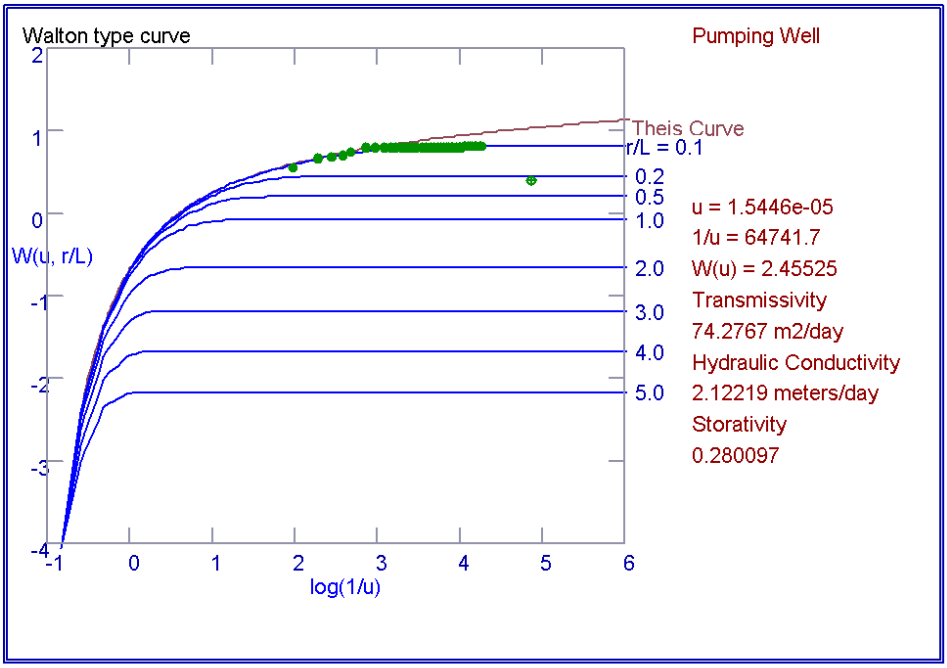

(a)Pumping

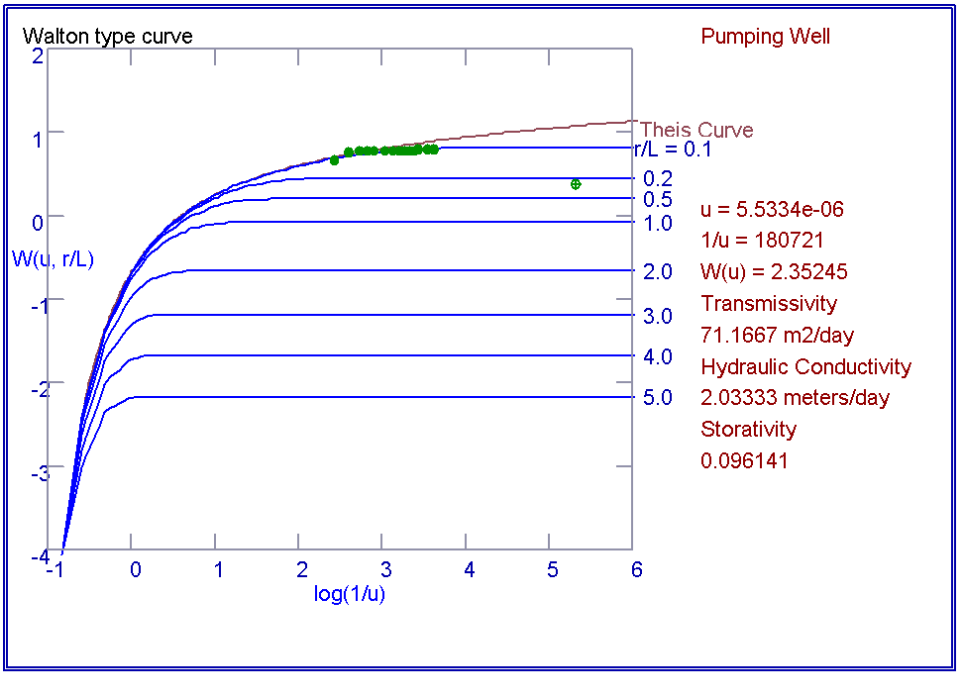

(b)Recovery

Figure 4.5(ii): Pumping test at P1 (semi-confined aquifer; measurements in pumping well).

PUMPING TEST AT GYMKHANA (UNCONFINED AQUIFER): MEASUREMENTS IN PUMPING WELL (P2)

Well P2 taps water from the unconfined aquifer (Fig. 4.6(i)-a). Examining the pumping period phase, the curve misses crucial data on the very early drawdowns (starting from 0 minutes). This is because the measurements were done manually and using heavy pump involving high rate of discharge. It was not easy to record the early time part of the curve, as the water was reaching almost to the steady state condition within a few seconds.

Pumping test data for P2 were analysed by the Neuman method which provided a T value of 16.79 m^2/d and K value of 0.56 m/d (Fig. 4.6(ii)-a). On the other hand, the analysis of the recovery data yielded a T value of 31.3 m^2/d and K value of 1.04 m/d (Fig. 4.6(ii)-b). The results of recovery data are more reliable than those of drawdown, and show very clearly that measurement in a pumping well leads to too low value for transmissivity. The recovery results are comparable to the transmissivity value (41.58 m^2/d) deduced from the specific well capacity (Table 4.4).

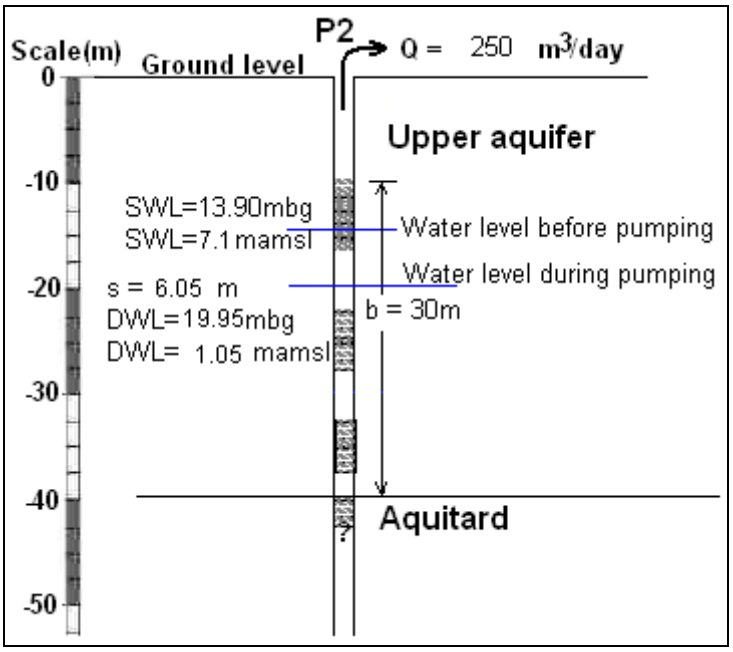

(a)Well construction sketch: SWL = Static Water Level; DWL = Dynamic Water level; s = drawdown; mbg = meter below ground; mamsl = meter above mean sea level; b = aquifer thickness

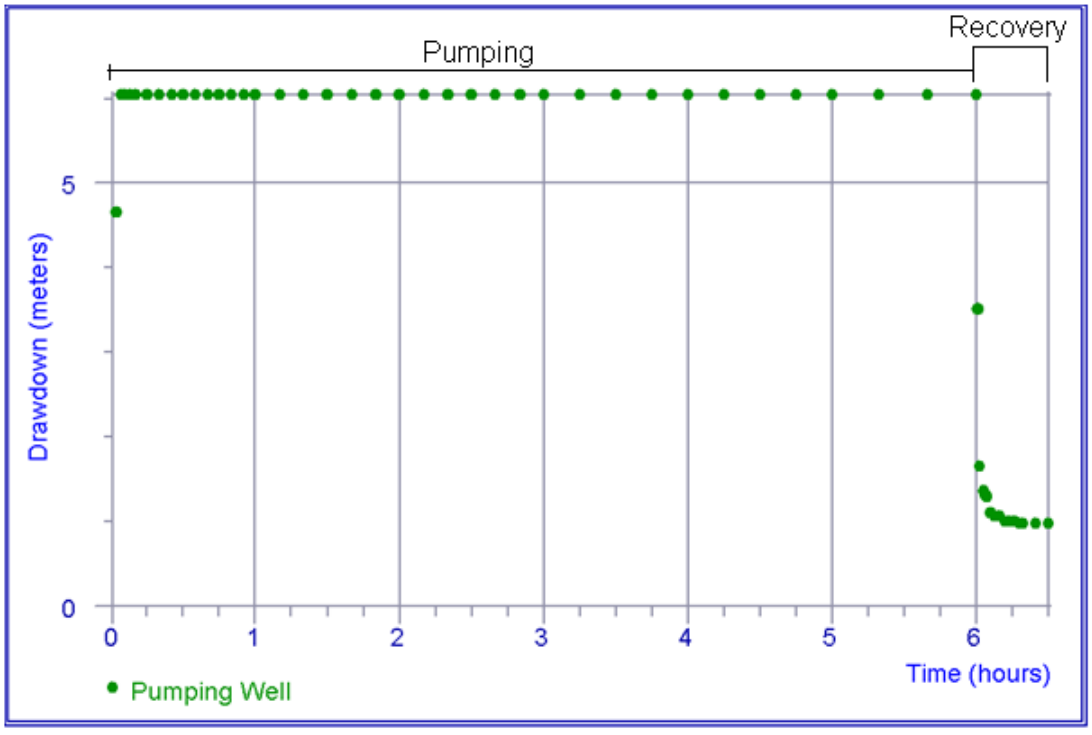

(b)Pumping period and recovery phase

Figure 4.6(i): Pumping test at P2: (a) well construction sketch, and (b) arithmetic graph for pumping well.

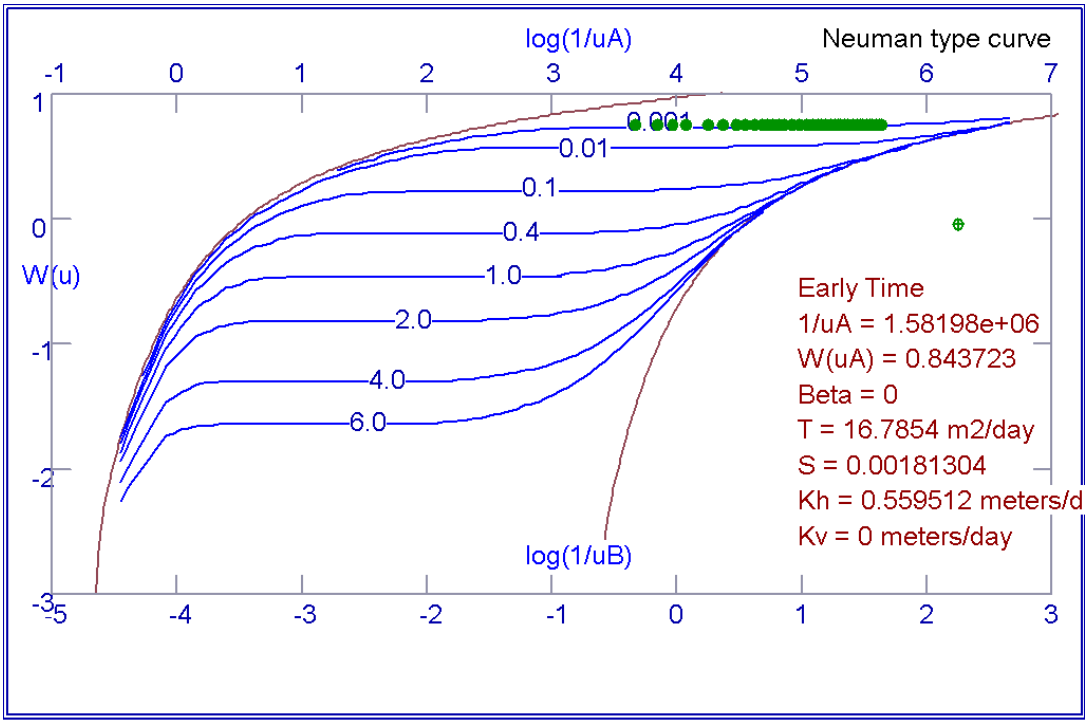

(a) Pumping

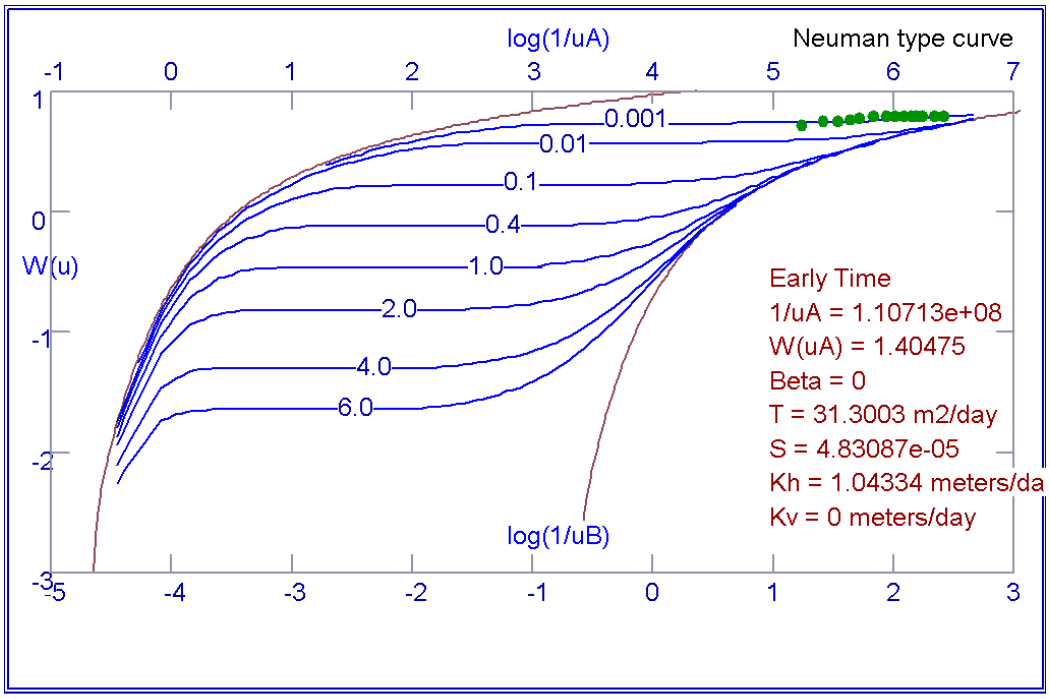

(b) Recovery

Figure 4.6(ii): Pumping test at P2 (semi-confined aquifer; measurements in pumping well).

PUMPING TEST AT TEMEKE (SEMI-CONFINED AQUIFER): MEASUREMENTS IN PUMPING WELL (P3)

Well P3 taps water from the semi-confined aquifer. Fig. 4.7(i-ii) provides results of the analysis. P3 was analysed by the Walton Leaky Type Curve technique (for a leaky aquifer) which provided a good fitting. The analysis of pumping data yielded a T value of 26.59 m^2/d and K value of 0.46 m/d (Fig. 4.7(ii)-a). On the other hand, the analysis of the recovery data shows identical hydraulic responses with T value of 26.59 m^2/d and K value of 0.46 m/d (Fig. 4.7(ii)-b). The transmissivity value obtained from both pumping and recovery data at pumping test at well P3 seems to be reliable. This value matches with the transmissivity value deduced from specific well capacity (Table 4.4).

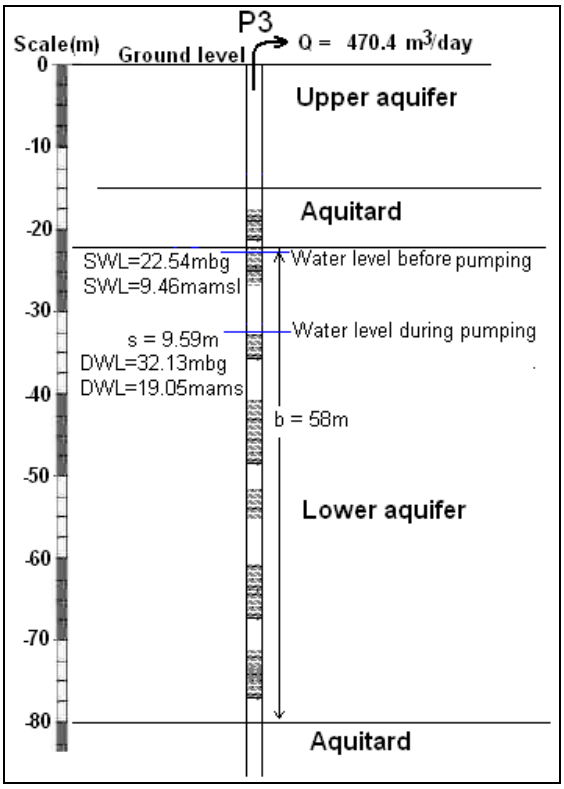

(a)Well construction sketch: SWL = Static Water Level; DWL = Dynamic Water level; s = drawdown; mbg = meter below ground; mamsl = meter above mean sea level; b = aquifer thickness

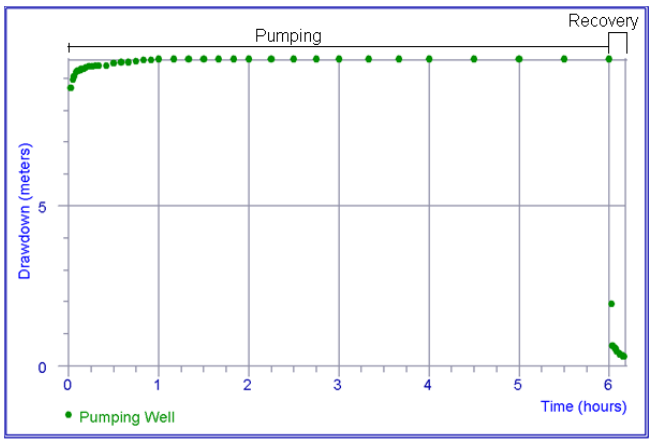

(b)Pumping period and recovery phase

Figure 4.7(i): Pumping test at P3: (a) well construction sketch, and (b) arithmetic graph for pumping well.

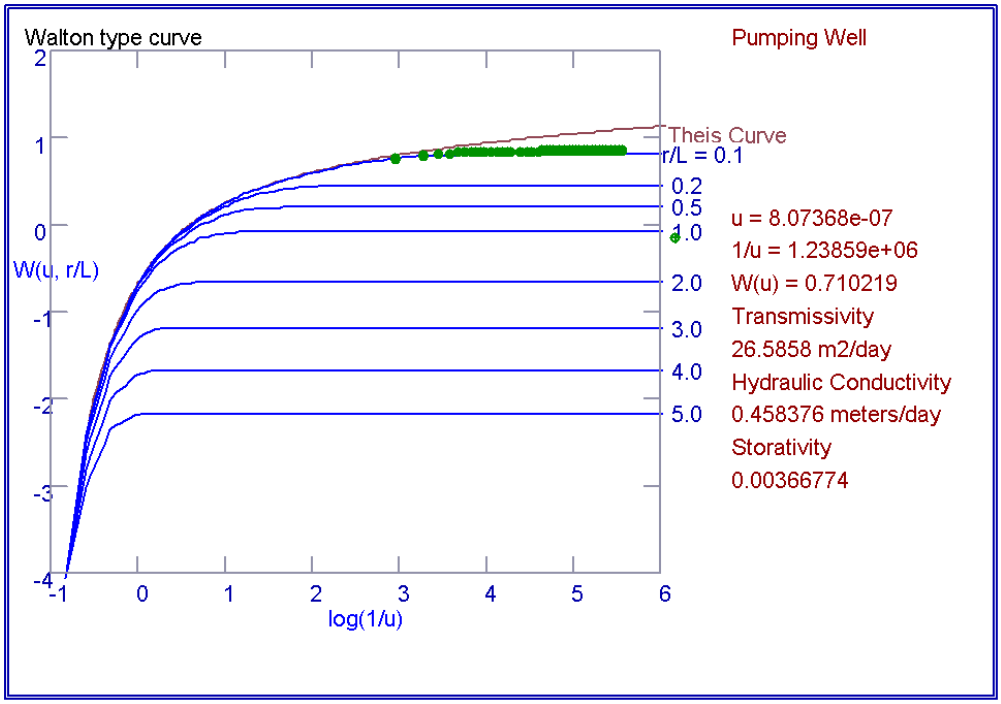

(a)Pumping

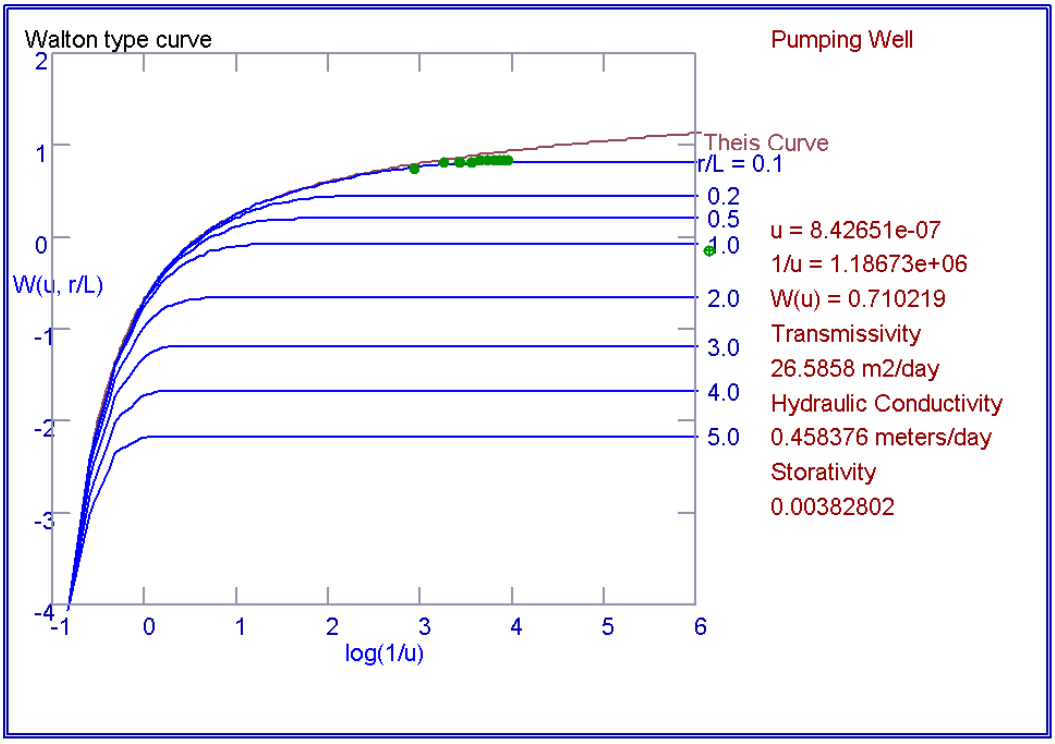

(b) Recovery

Figure 4.7(ii): Pumping test at P3 (semi-confined aquifer; measurements in pumping well).

PUMPING TEST AT CITY CENTRE (SEMI-CONFINED AQUIFER): MEASUREMENTS IN PUMPING WELL (P4)

Well P4 taps water from the semi-confined aquifer. Fig. 4.8(i-ii) provides results of the analysis. Pumping data at well P4 do not show a smooth curve (Fig. 4.8(i)-b) especially at the beginning which leads to irregular curve fitting (Fig. 4.8(ii)-a). P4 was analysed by the Walton Leaky Type Curve technique (for a leaky aquifer). The analysis of pumping data yielded a T value of 17.11 m^2/d and K value of 0.34 m/d (Fig. 4.8(ii)-a). these values are not considered as realistic, as they are very low compared to specific well capacity. However, recovery data show a good curve whereby the transmissivity value obtained (56.18 m^2/d) provides a good comparison with the transmissivity value (61.3 m^2/d) deduced from specific well capacity method (Table 4.4).

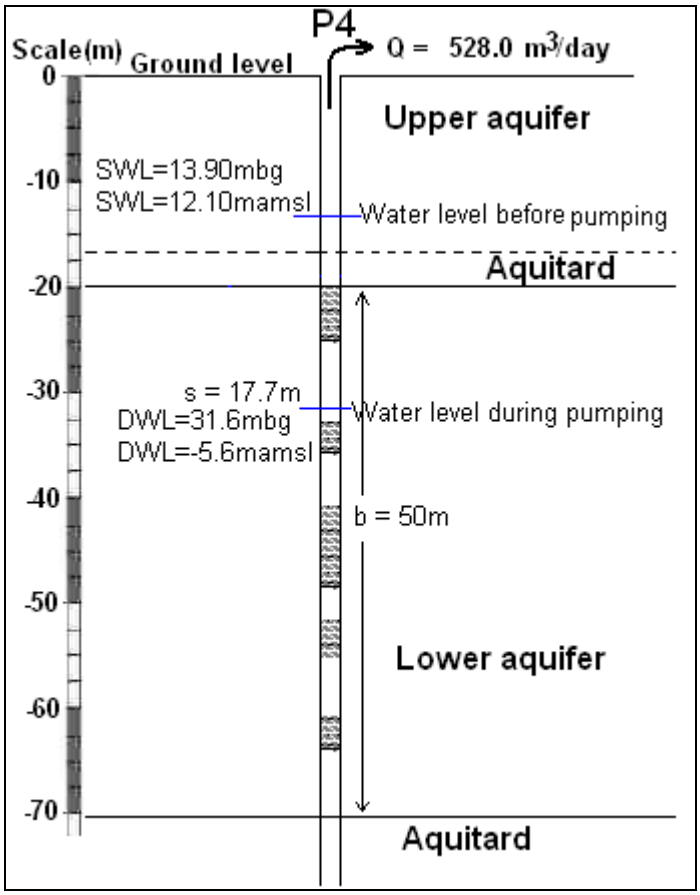

(a)Well construction sketch: SWL = Static Water Level; DWL = Dynamic Water level; s = drawdown; mbg = meter below ground; mamsl = meter above mean sea level; b = aquifer thickness

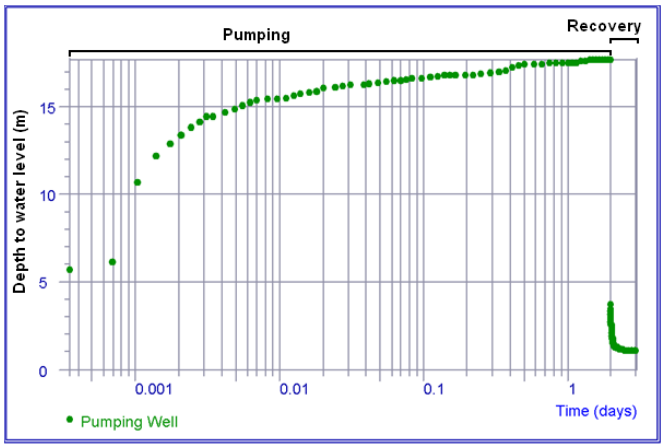

(b)Pumping period and recovery phase

Figure 4.8(i): Pumping test at P4: (a) well construction sketch, and (b) arithmetic graph for pumping well.

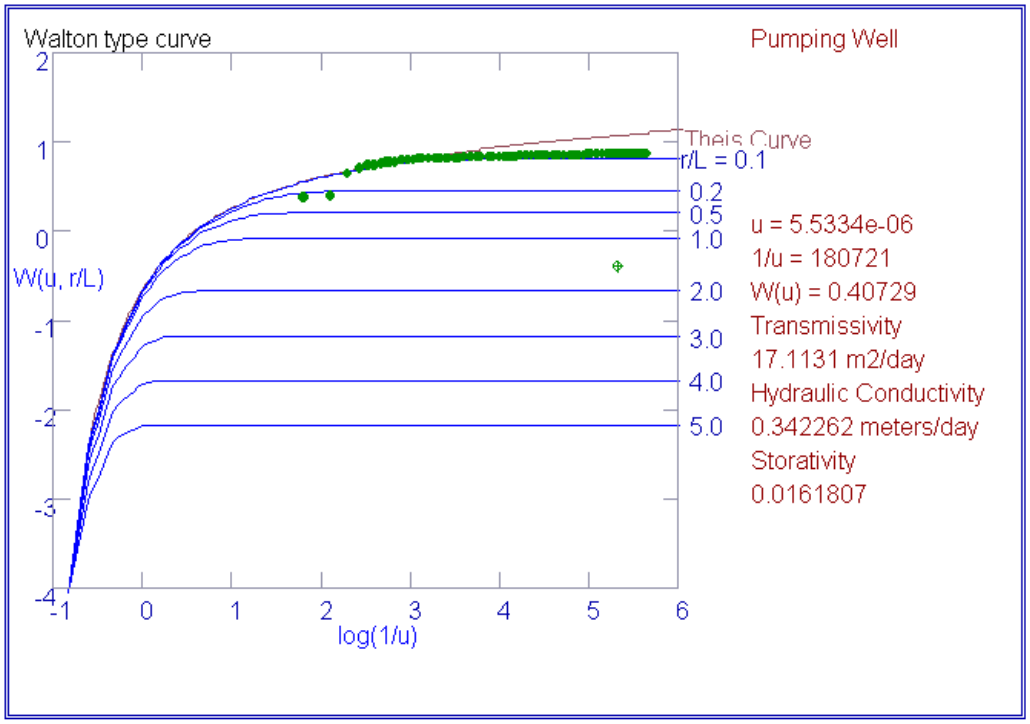

(a)Pumping

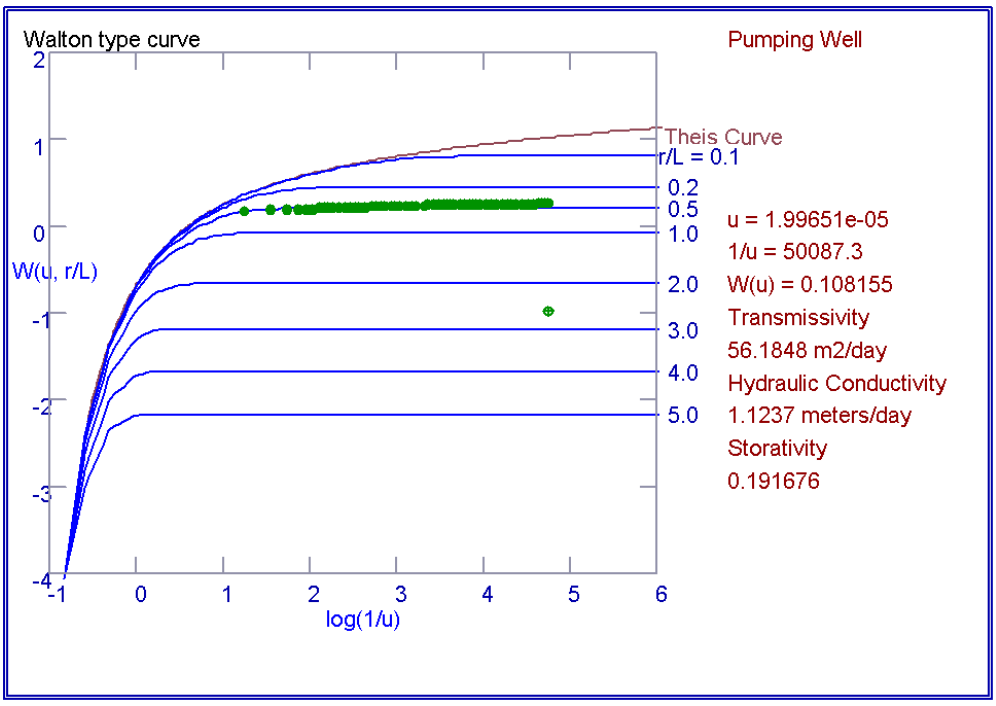

(b)Results of pump test data analysis

Figure 4.8(ii): Pumping test at P4 (semi-confined aquifer; measurements in pumping well).

PUMPING TEST AT KEKO (SEMI-CONFINED AQUIFER): MEASUREMENTS IN PUMPING WELL (P5)

Well P5 taps water from the semi-confined aquifer (Fig. 4.9(i)-a). Pumping data for P5 were analysed by the Walton method which provided a T value of 6.1 m^2/d and K value of 0.19 m/d (Fig. 4.9(ii)-a). On the other hand, the analysis of the recovery data yielded a T value of 13.75 m^2/d and K value of 0.43 m/d (Fig. 4.9(ii)-b). The results of recovery data are considered to be more reliable than for drawdown and show very clearly that measurement in a pumping well leads to too low value for transmissivity. The transmissivity value (13.75 m^2/d) (Fig. 4.9(ii)-b) obtained from recovery data is similar to the value deduced by SWC method (Table 4.4).

.

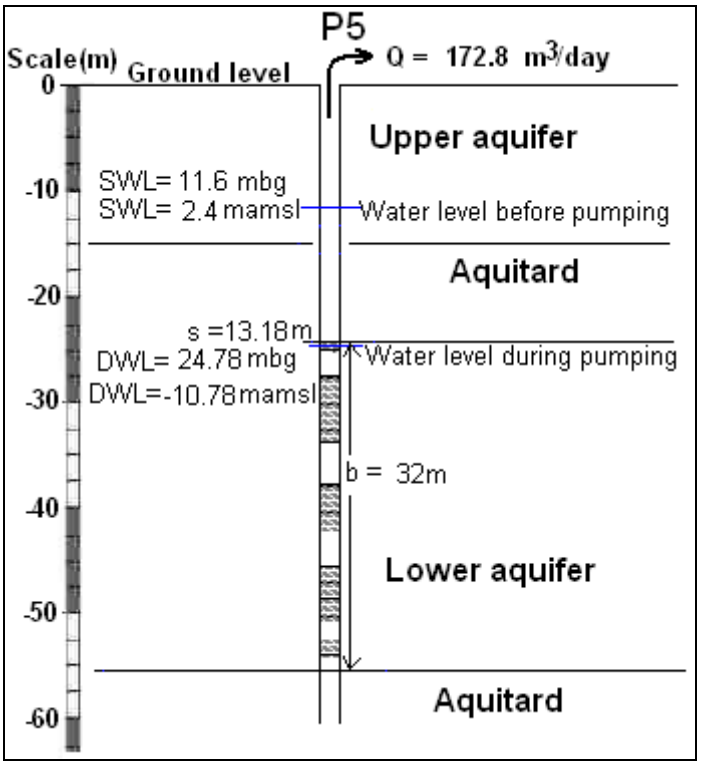

(a)Well construction sketch: SWL = Static Water Level; DWL = Dynamic Water level; s = drawdown; mbg = meter below ground; mamsl = meter above mean sea level; b = aquifer thickness

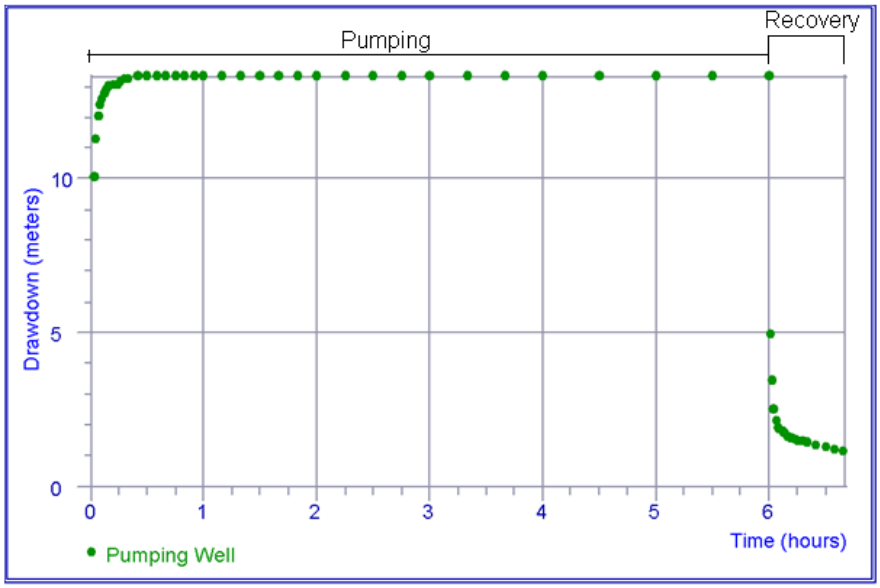

(b)Pumping period and recovery phase

Figure 4.9(i): Pumping test at P5: (a) well construction sketch, and (b) arithmetic graph for pumping well.

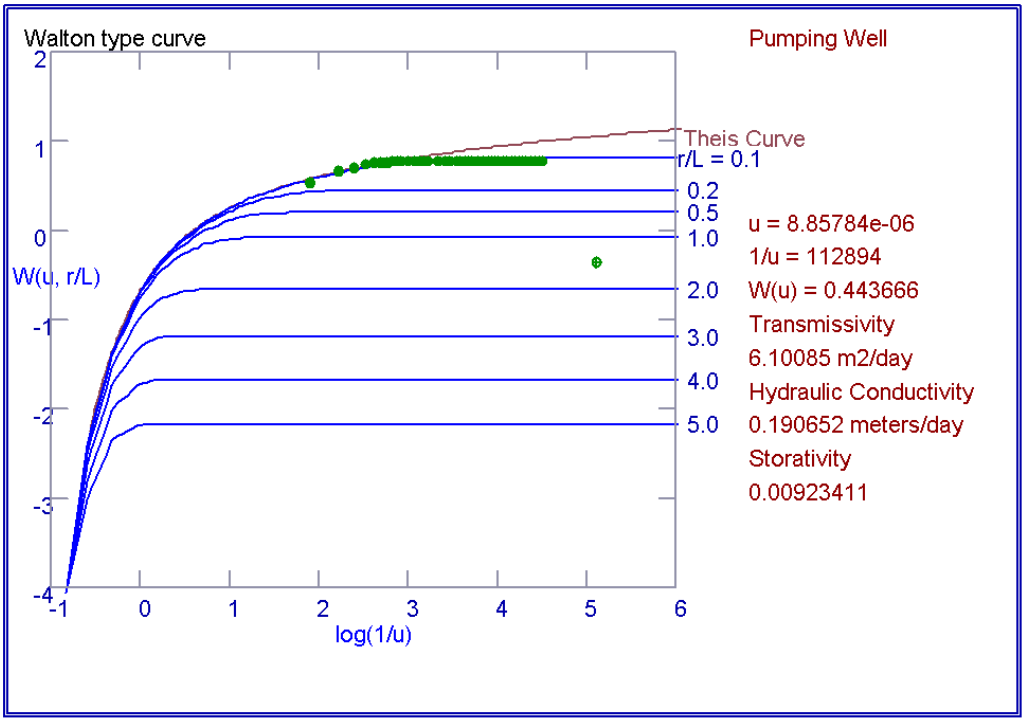

(a)Pumping

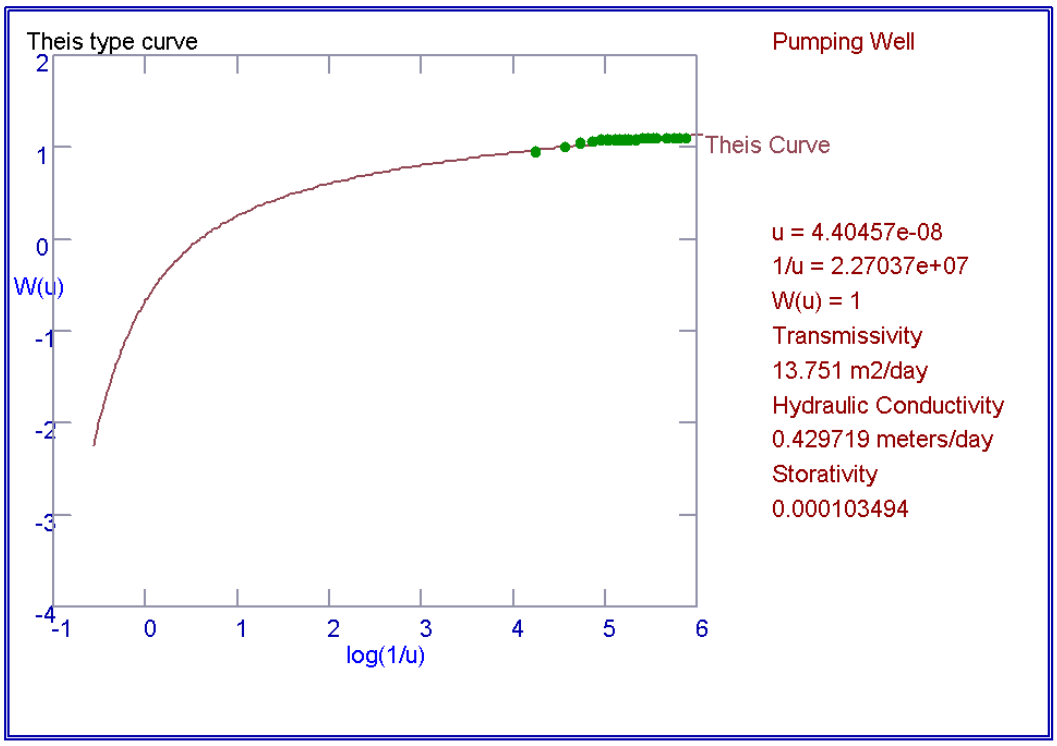

(b)Recovery

Figure 4.9(ii): Pumping test at P5 (semi-confined aquifer; measurements in pumping well).

PUMPING TEST AT CITY CENTRE- RAMANI (SEMI-CONFINED AQUIFER): MEASUREMENTS IN PUMPING WELL (P6)

Well P6 taps water from the unconfined aquifer and the pumping test was carried out with one observation well located at 9 m from the pumping well (Fig. 4.10(i)-a). However, observation data did not show curve fitting which could be interpreted. Only pumping data were analysed. Analysis of pumping data at well P6 does not show a smooth curve (Fig. 4.10(ii)-b). Pumping data for P6 were analysed by the Neuman method which provided a T value of 25.19 m^2/d and K value of 0.49 m/d (Fig. 4.9(ii)-a). On the other hand, the analysis of the recovery data yielded a T value of 63.26 m^2/d and K value of 3.72 m/d (Fig. 4.10(ii)-b). The results of recovery data are considered to be more reliable than drawdown and show very clearly that measurement in a pumping well leads to too low value of transmissivity. The transmisivity value obtained from recovery data analysis is similar to the transmissivity values of 64.3 m^2/d (Table 4.4) and 59.08 m^2/d (Table 4.5) deduced by SWC and Dupuit/Thiem's methods respectively.

.

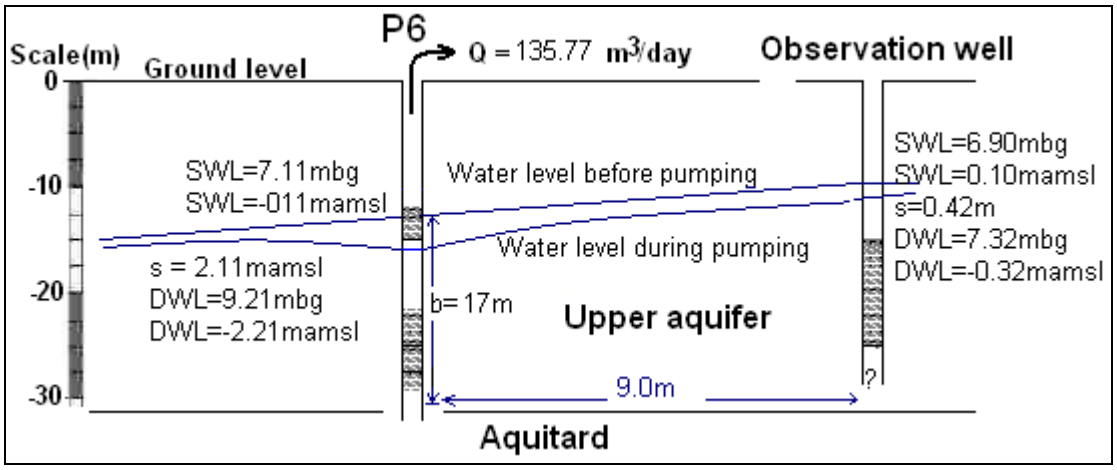

(a)Well construction sketch: SWL = Static Water Level; DWL = Dynamic Water level; s = drawdown; mbg = meter below ground; mamsl = meter above mean sea level; b = aquifer thickness

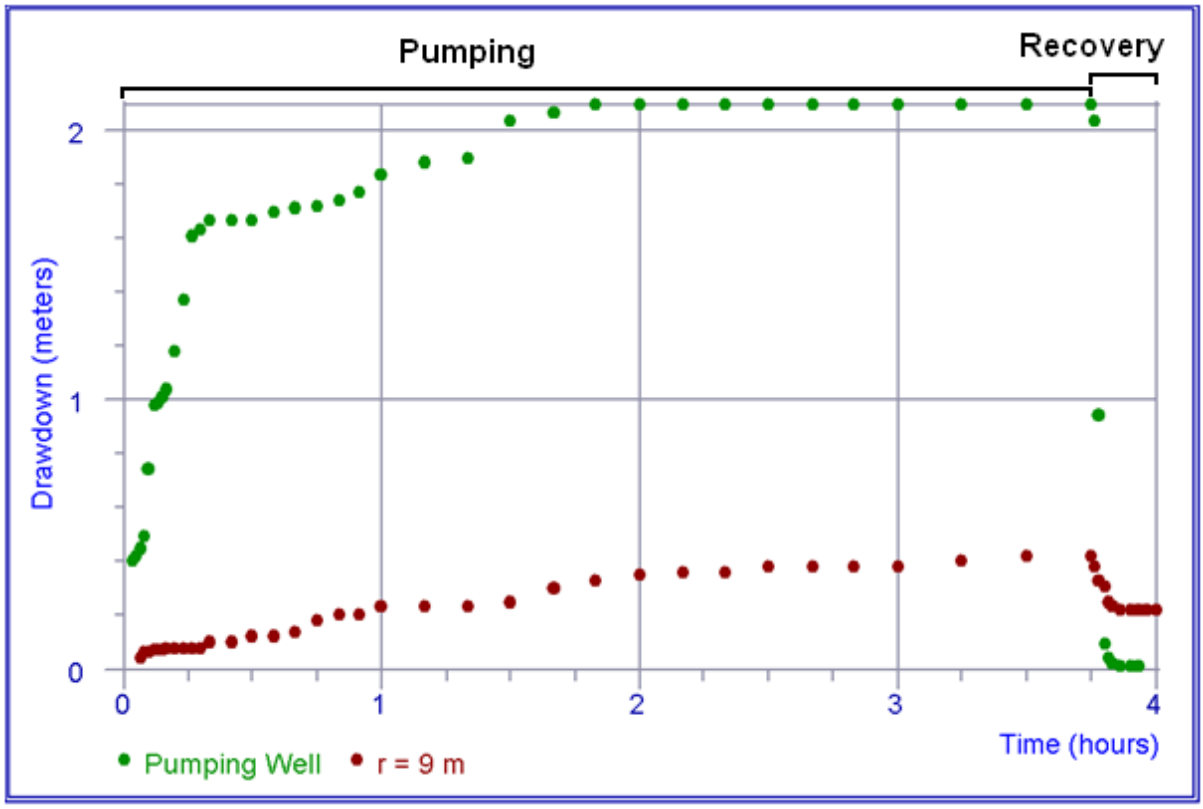

(b)Pumping period and recovery phase

Figure 4.10(i): Pumping test at P6: (a) well construction sketch, and (b) arithmetic graph for pumping well and observation well.

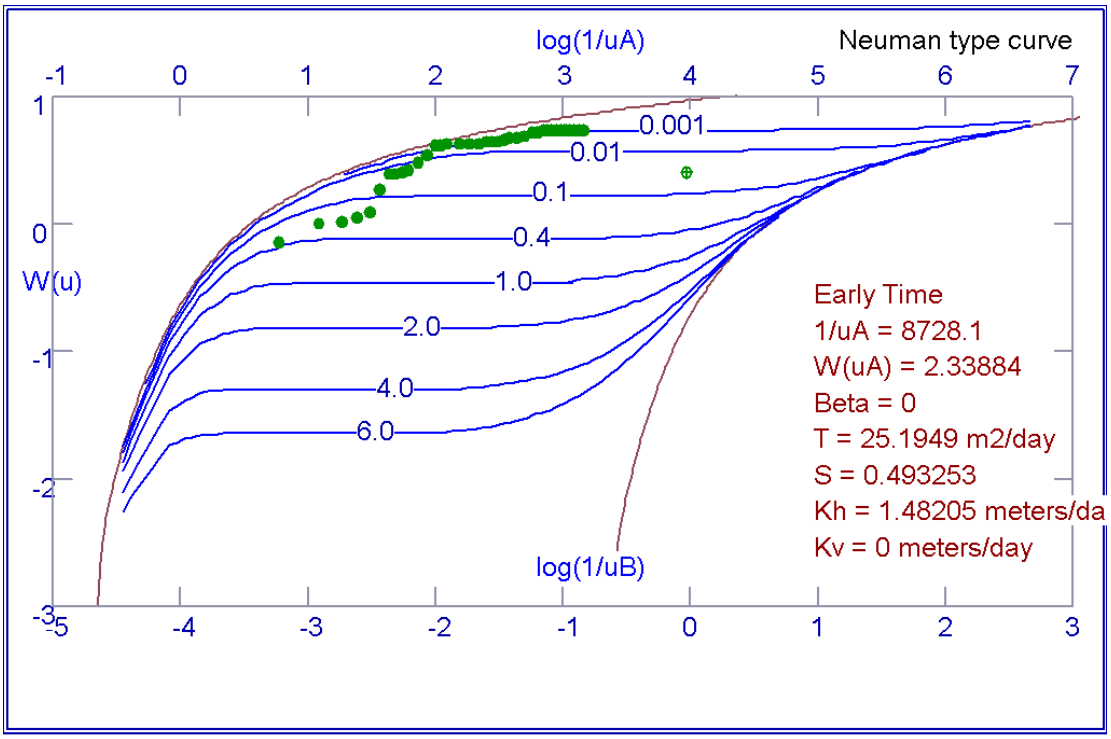

(a)Pumping

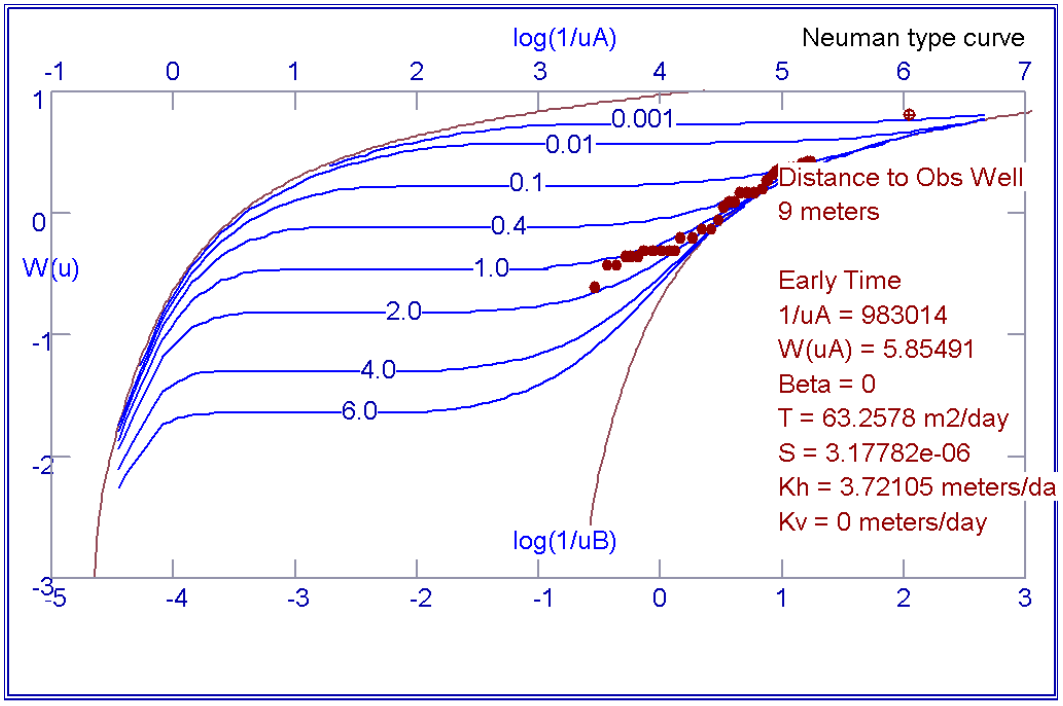

(b) Recovery

Figure 4.10(ii): Pumping test results of pump test data analysis at P6: (a) pumping well, and (b) observation well.

PUMPING TEST AT ILALA BOMA (SEMI-CONFINED AQUIFER): MEASUREMENTS IN PUMPING WELL (P7)

Well P7 taps water from the unconfined aquifer and the pumping test was carried out with one observation well located at 100 m from the pumping well (Fig. 4.11(i)-a). However, observation data did not show curve fitting which could be interpreted. Data analysis involved only measurements in pumping well. Analysis of pumping data at well P7 does not show a smooth curve (Fig. 4.11(ii)-b). Pumping data for P7 were analysed by the Neuman method which provided a T value of 8.52 m^2/d and K value of 0.27 m/d (Fig. 4.11(ii)-a). On the other hand, the analysis of the recovery data does not show a good curve either. Recovery analysis yielded a T value of 24.45 m^2/d and K value of 0.76 m/d (Fig. 4.11(ii)-b). Although the curve fitting provided by recovery data is not good, the results obtained still might be considered to be more reliable than for drawdown. The transmissivity value obtained from recovery data analysis is comparable to the transmissivity values of 20.5 m^2/d (Table 4.4) and 25.30 m^2/d (Table 4.5) deduced by SWC and Dupuit/Thiem's methods respectively.

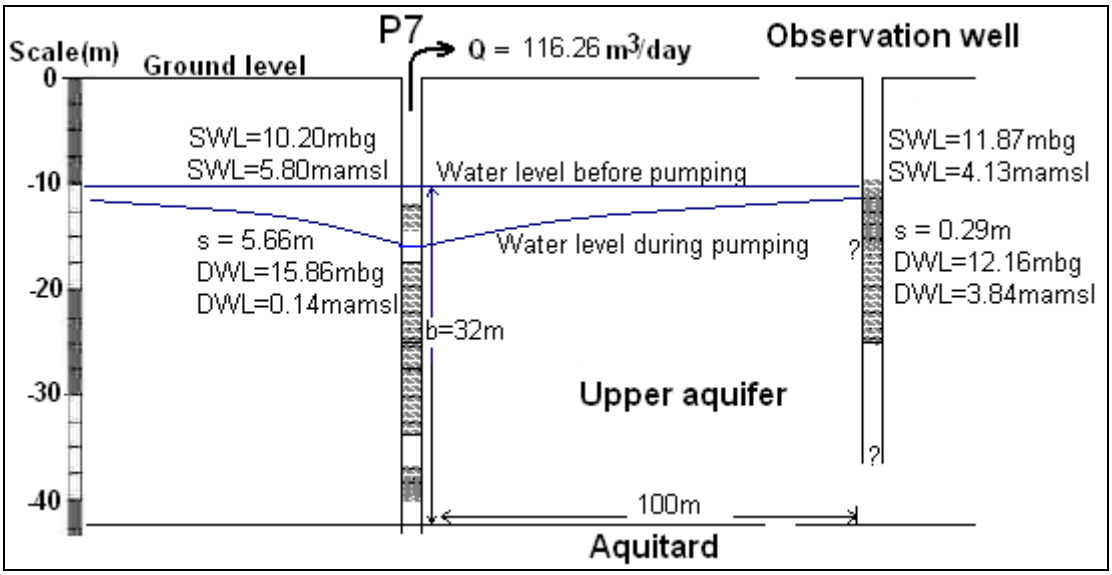

(a)Well construction sketch: SWL = Static Water Level; DWL = Dynamic Water Level; s = drawdown; mbg = meter below ground; mamsl = meter above mean sea level; b = aquifer thickness

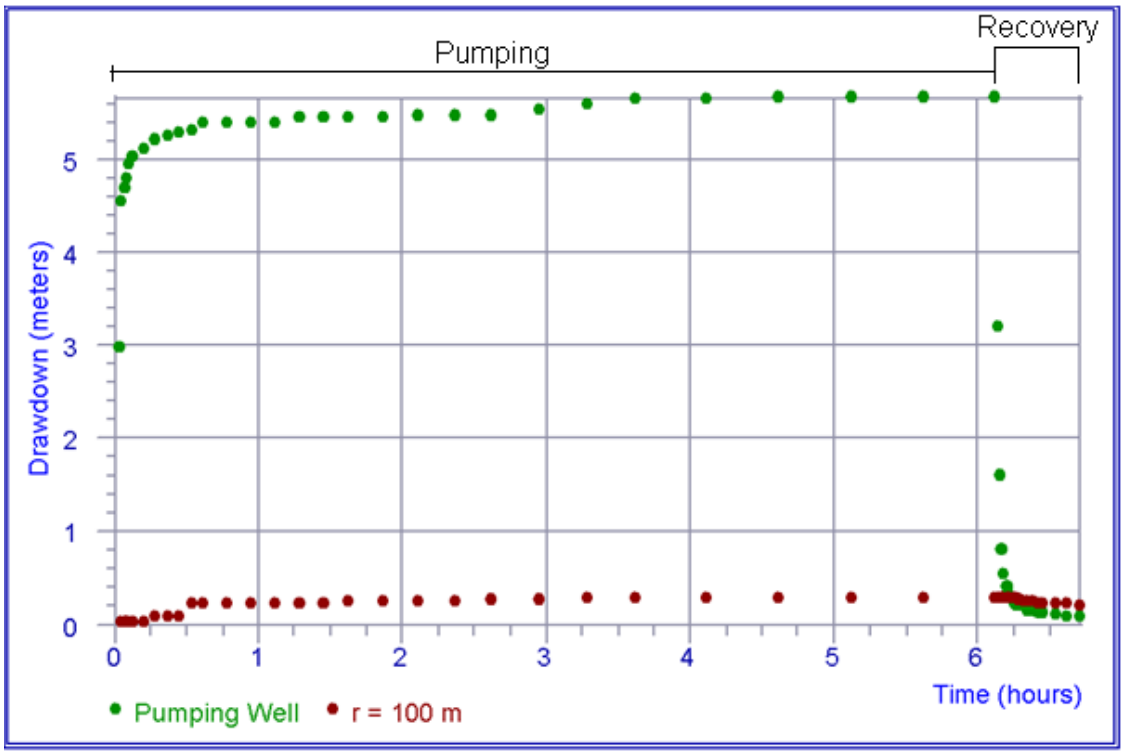

(b)Pumping period and recovery phase

Figure 4.11(i): Pumping test at P7: (a) well construction sketch, and (b) arithmetic graph for pumping well and observation well.

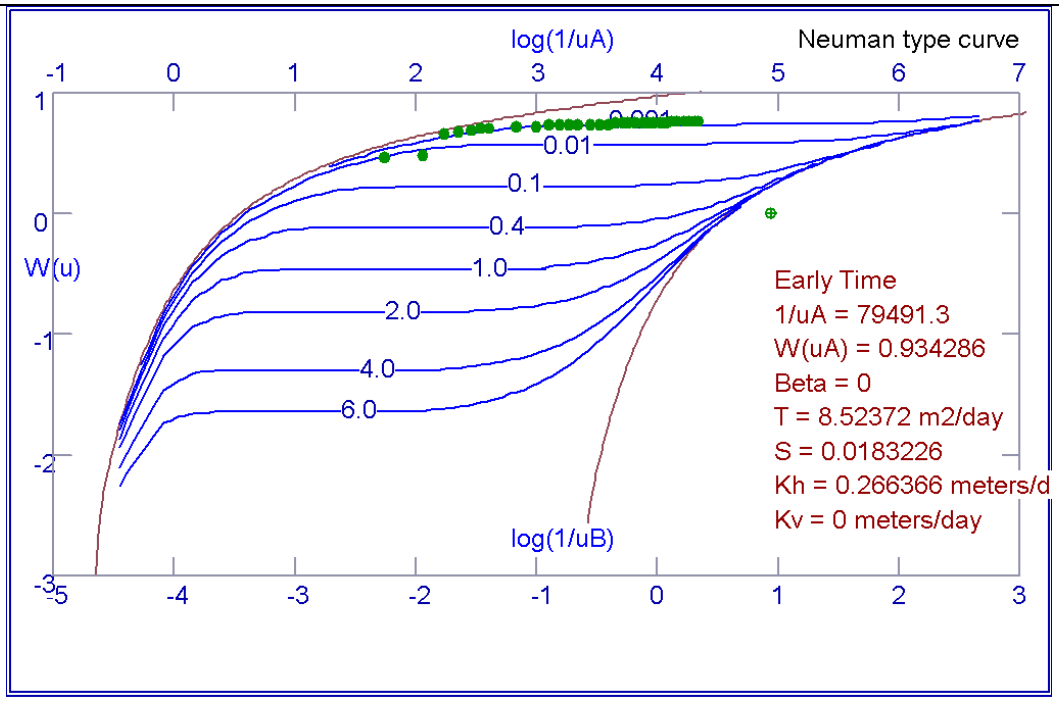

(a) Pumping

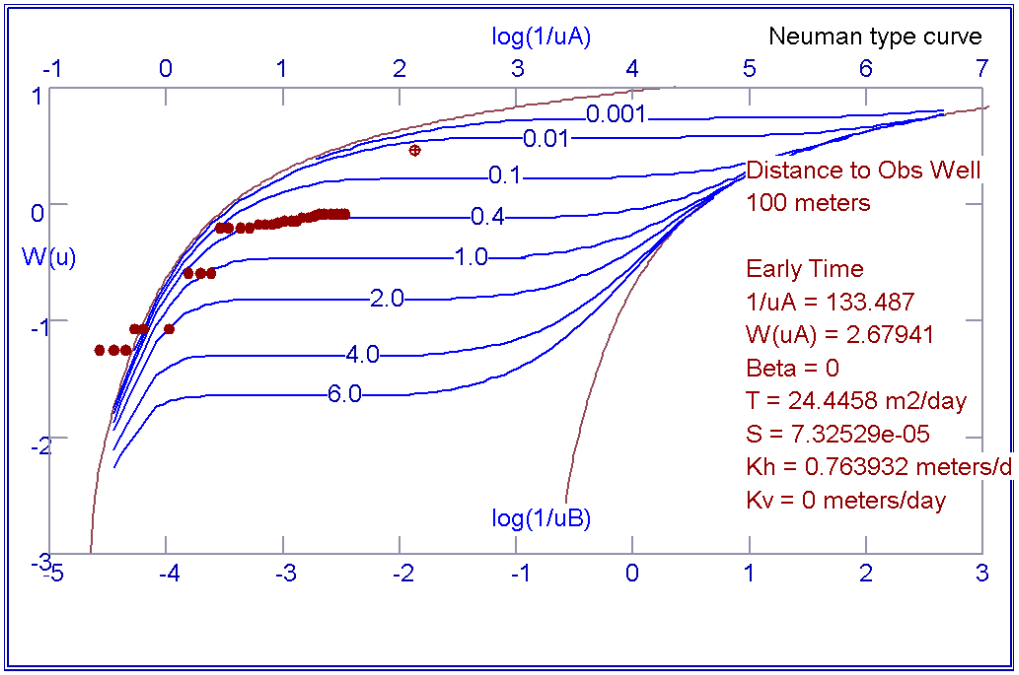

(b) Recovery

Figure 4.11(ii): Pumping test results of pump test data analysis at P7.

PUMPING TEST AT KEKO (SEMI-CONFINED AQUIFER): MEASUREMENTS IN PUMPING WELL (P8)

Well P8 taps water from the semi-confined aquifer (Fig. 4.12(a)). Only data during the pumping phase were analysed. Observation data did not produce curve fitting which could be interpreted. Pumping data indicate a good fit of the curve with Theis method (Fig. 4.12(c)): a T value of 58.79 m^2/d and K value of 1.96 m/d were obtained (Fig. 4.12(c)). This result is considered to be reliable. The transmissivity value obtained is very similar to the transmissivity value (59.64 m^2/d) obtained from the specific well capacity method (Table 4.4).

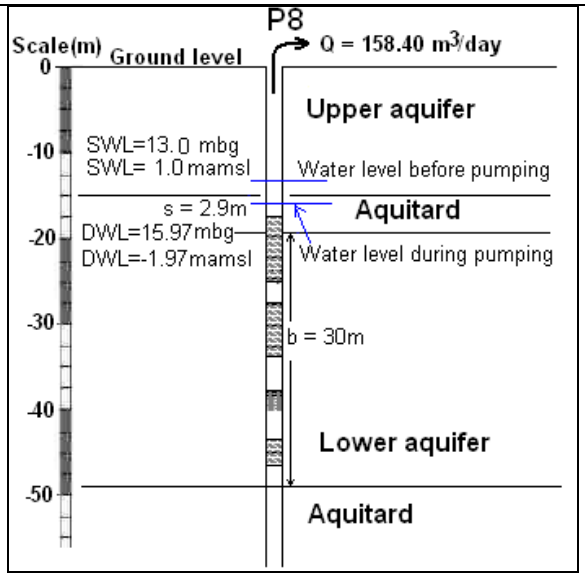

(a)Well construction sketch: SWL = Static Water Level; DWL = Dynamic Water level; s = drawdown; mbg = meter below ground; mamsl = meter above mean sea level; b = aquifer thickness

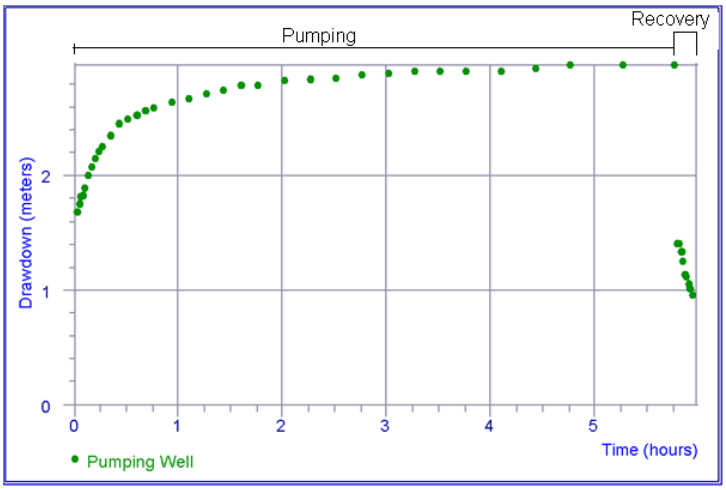

(b)Pumping period and recovery phase

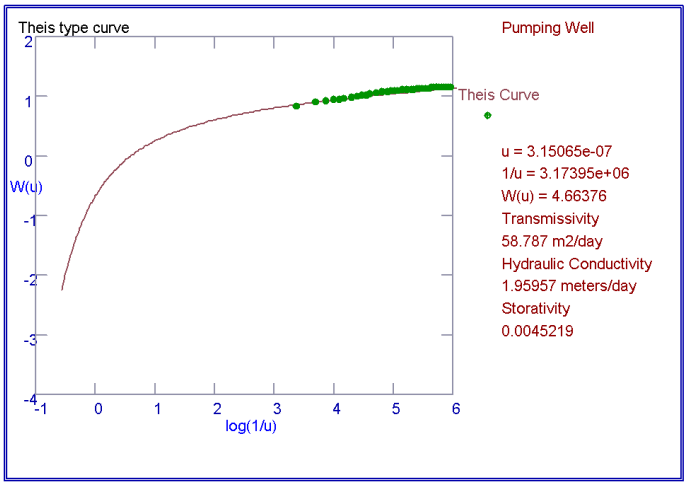

(c)Results of pump test data analysis

Figure 4.12: Pumping test at P8: (a) well construction sketch, and (b) arithmetic graph for pumping well and (c) Results of pump test data analysis.

4.3.1.2 New pumping tests

4.3.1.2.1 Pumping test at Mbagala (semi-confined aquifer): measurements in pumping well (P9) and 2 observation wells

EXECUTION OF PUMPING TEST

Fig. 4.13 indicates a well construction sketch and the pumping phase and recovery phase of the constant rate pumping test which was conducted at the well belonging to DAWASCO (Dar es Salaam Water and Sewerage Corporation), located at Mbagala area. Table 4.6 indicates the flow rate during the pumping period. The pumping test was conducted for 6 hours followed by measuring the recovery for 1 hour. The pumping test conducted involved pumping groundwater from the borehole (P9) at a constant rate, and measuring water levels in the pumped well and two nearby boreholes, which were used as observation wells. Observation wells (O1 and O2) were at a distance of about 80 m south and 200 m north of the pumping well (P9) respectively.

A clear response is indicated during the 6 hours of pumping and 1 hour recovery both for the pumping well (P9) and observation well O1 located at a distance of 80 m from the pumping well. This was not observed for the observation well O2 located at 200 m from the pumping well because of the big distance (200 m). Data for observation well O2 were not useful for analysis and interpretation and thus have been discarded from a further discussion.

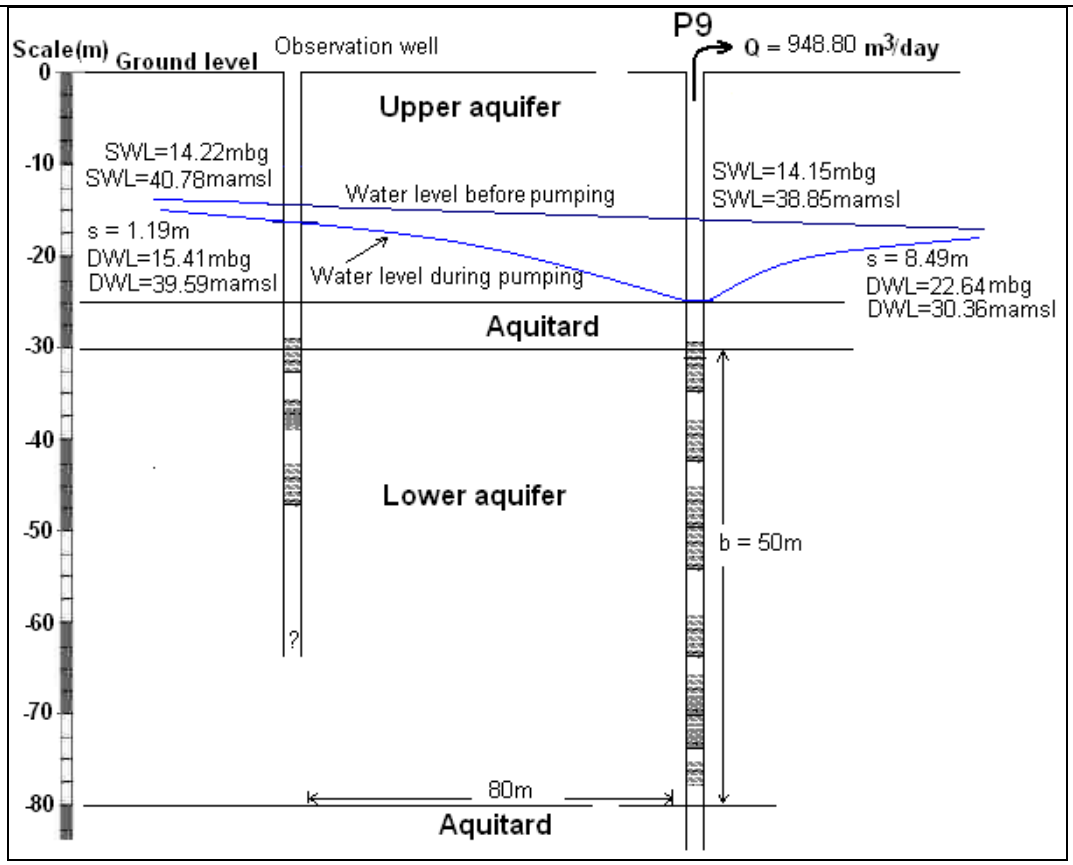

(a)Well construction sketch: SWL = Static Water Level; DWL = Dynamic Water level; s = drawdown; mbg = meter below ground; mamsl = meter above mean sea level; b = aquifer thickness

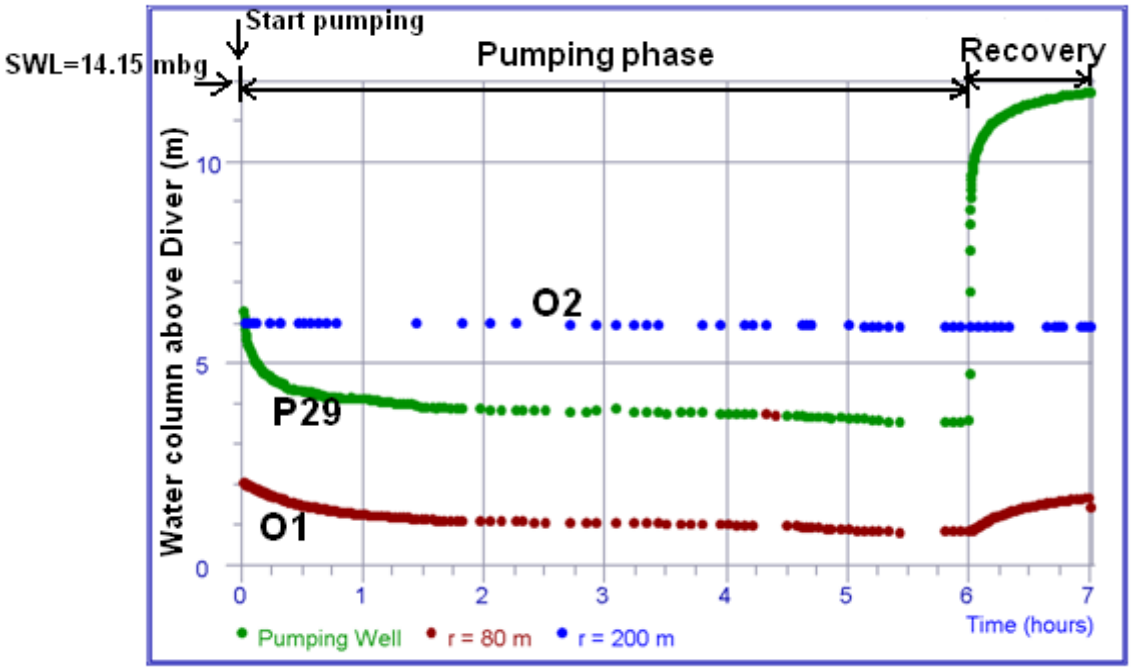

(b)Pumping period and recovery phase

Figure 4.13: Pumping test conducted at Mbagala showing: a) well construction sketch, and b) pumping period and recovery phase for pumping well (P9) and two observation wells (O1 and O2).

Table 4.6: Flow rate during 6 hours of pumping test.

Time (h)	**Discharge meter (m^3)**	**m^3 of water pumped per time step**	**Flow rate per time step (m^3/h)**
0	29160.0		
0.5	29181.7	21.7	43.4
1	29200.7	19	38
1.5	29220.5	19.8	39.6
2	29240.3	19.8	39.6
3	29279.4	39.1	39.1
4	29318.5	39.1	39.1
5	29357.6	39.1	39.1
6	29397.2	39.1	39.1
			Average = $39.45m^3/h$ = $946.8m^3/d$

After a preliminary assessment of the pumping period and recovery phase, a further discussion is carried on for the drawdown curves both for the pumping well P9 and observation well O1 (Fig. 4.14). The pumping well shows a rapid drop of water column above the Diver (ca. 8 m) attained during the first hour of pumping (Fig. 4.14a). In the next 5 hours of pumping, the water level decrease was smooth till the pumping stopped. A drawdown of 849 cm (8.49 m) was attained. Water level recovery was almost complete after one hour since the stop of pumping. On the other hand, observation well O1 indicates a relatively slow rate of water level decrease (Fig. 4.14b) comparing to the pumping well. A significant decrease of water column (ca. 80 cmH_2O) above the diver occurred during the first hour of pumping. Thereafter the decrease continued gradually till a water column of 81.4 cm above the diver. A drawdown of 119.1cm was attained. 70% of water level recovery was attained after one hour since pumping stopped.

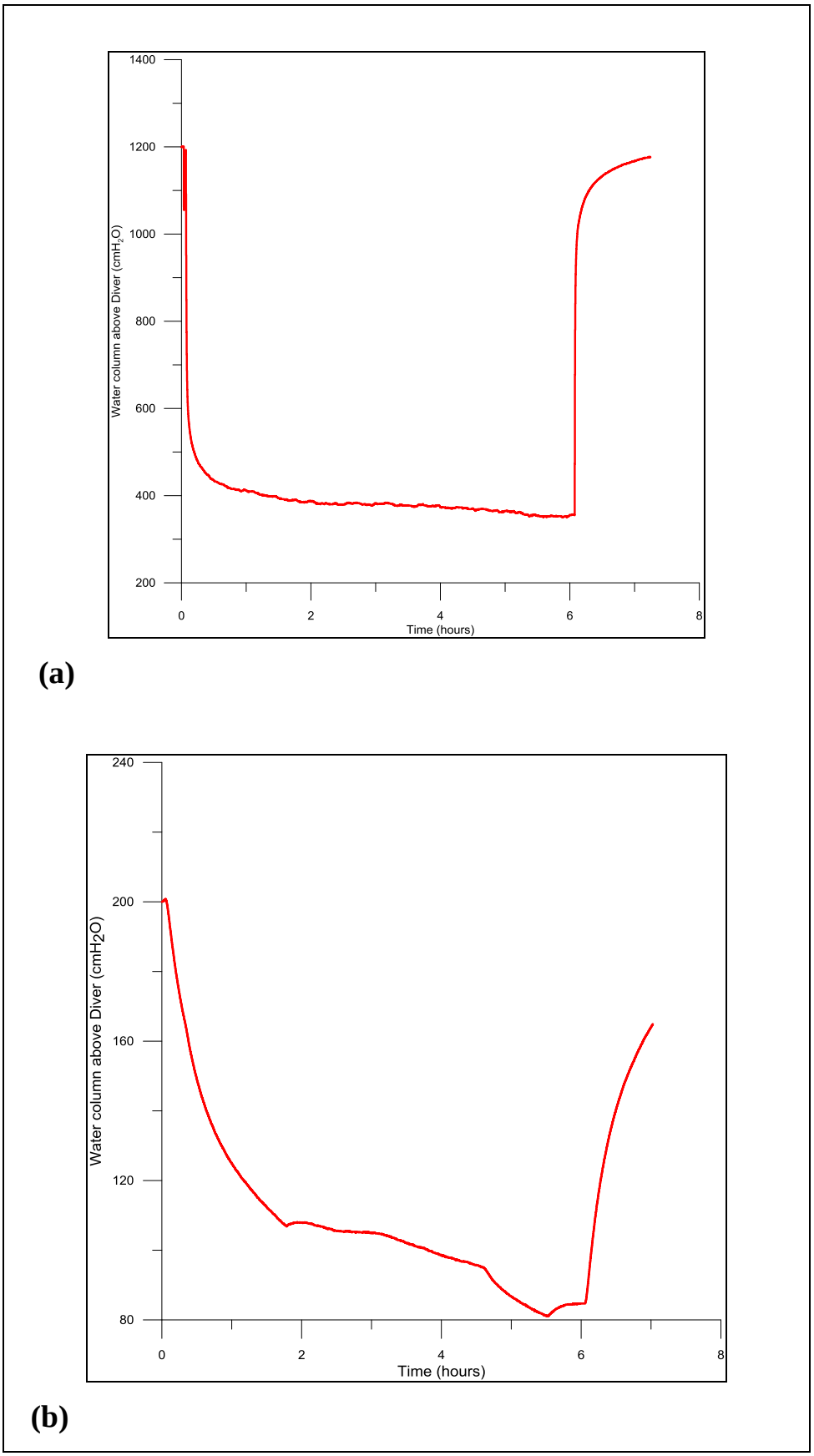

Figure 4.14: Water column above Diver for pumping test at Mbagala: a) pumping well (P29), and b) observation well (O1).

INTERPRETATION

Specific well capacity

The specific capacity was calculated using the flow rate of 946.8 m^3/d and the drawdown of 8.49 m giving the value of 111.51 m^2/d. In view of the classification of specific capacity magnitude according to Krasny (1993), well P9 falls within the high specific capacity class (Table 4.7). Table 4.8 represents the hydraulic parameters deduced from the specific well capacity method.

Table 4.7: Classification of specific capacity values according to Krasny (1993).

Well	**Low (< 8.64m^2/d)**	**Well**	**Intermediate (8.64 - 86.4 m^2/d)**	**Well**	**High (86.4-864 m^2/d)**	**Well**	**Very high (> 864 m^2/d)**
				P9	111.51		

Table 4.8: Hydraulic parameters deduced from specific well capacity method.

Well	**Location**	**Q (m^3/d)**	**s (m)**	**T(m^2/d)**	**Aquifer thickness (m)**	**K (m/d)**
P9	Mbagala	948.8	8.49	111.8	50	2.24

Dupuit/Thiem's method

Through the Infinite Extent software it was possible to calculate transmissivity for a combination of the pumping well P9 and observation well O1. Table 4.9 represents the hydraulic parameters deduced from Dupuit/Thiem's method.

Table 4.9: Hydraulic parameters deduced from pumping test analysis by Thiem-Dupuit/Thiem's method for steady-state flow.

Well	**Location**	**Aquifer type**	**T (m^2/d)**	**Aquifer thickness (m)**	**K (m/d)**
P9	Mbagala	Semi-confined	128.49	50	2.57

Curve fitting

Pump test data recorded in the pumping well and observation well were analysed using Infinite Extent software whereby the hydraulic parameters were determined. The analysis of pumping test data was done by several methods which include Theis (Fig. 4.15a), Walton (Fig. 4.16a) and Hantush (Fig. 4.17a). Theis method (Fig. 4.15a) showed a good curve fitting

for pumping well data analysis comparing to other methods. On the other hand, Hantush method (Fig. 4.17b) showed a good curve fitting for analysis of observation well comparing to Theis (Figs. 4.15b) and Walton (Fig. 4.16b) methods. The transmissivity value of 109.93m^2/d obtained by Theis method from the pumping well measurements is considered to be reasonable and comparable to the transmissivity values deduced from the specific well capacity (111.8 m^2/d) (Table 4.8) and from Dupuit/Theim's method (128.49 m^2/d) (Table 4.9). The transmissivity value of 130.44 m^2/d deduced from the observation well data by Hantush method shows a very close match with the transmissivity value deduced by Theim method. Furthermore, Theis and Hantush methods showed a good curve fitting with reasonable results for recovery data both for pumping and observation wells (Fig. 4.18): the two methods showed the transmissivity values of 119.74 m^2/d and 129.16 m^2/d respectively.

The transmissivity value of 217.93 m^2/d obtained by Theis method from the observation well measurements is higher than the values obtained by other methods. This value is considered not reasonable as the graph did not show a very good fitting, and was thus rejected. Likewise the transmissivity value of 81.48 m^2/d represented by Hantush method in the pumping well measurements is also rejected for a similar reason.

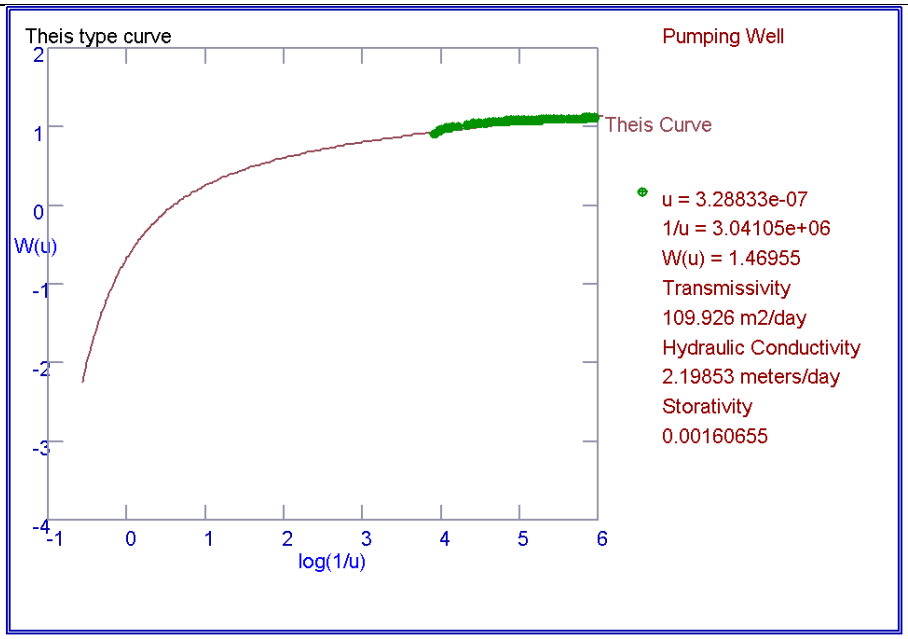

(a)Pumping well

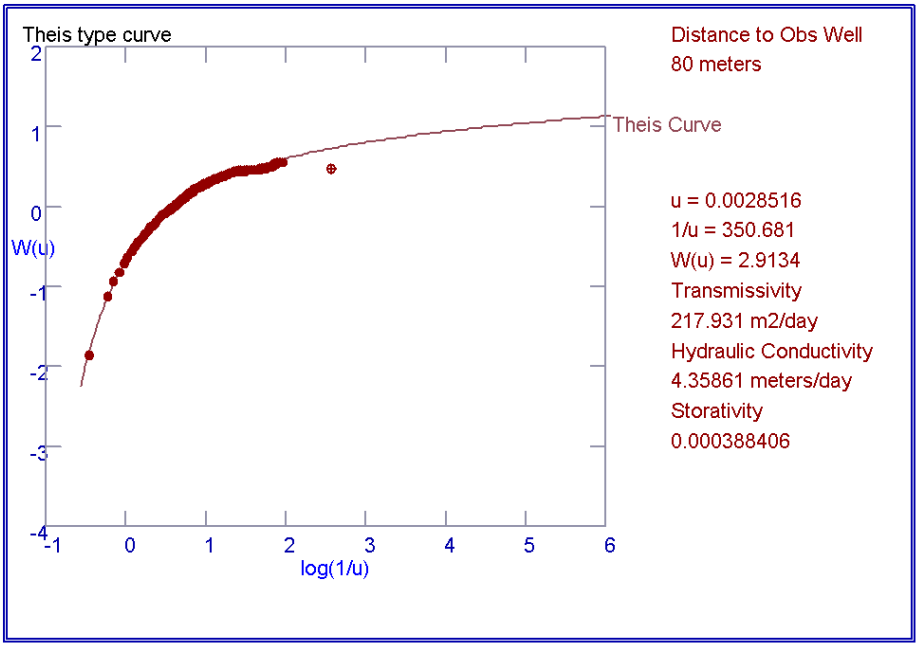

(b)Observation well

Figure 4.15: Results of Theis method for pumping test at P9: pumping phase.

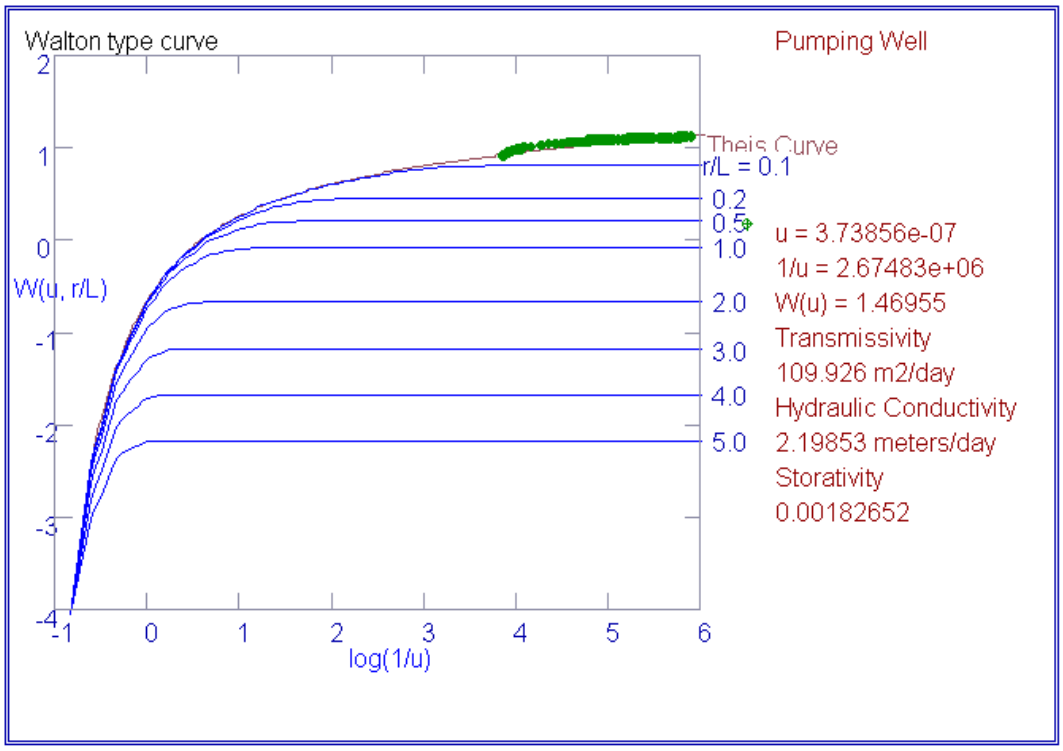

(a)Pumping well

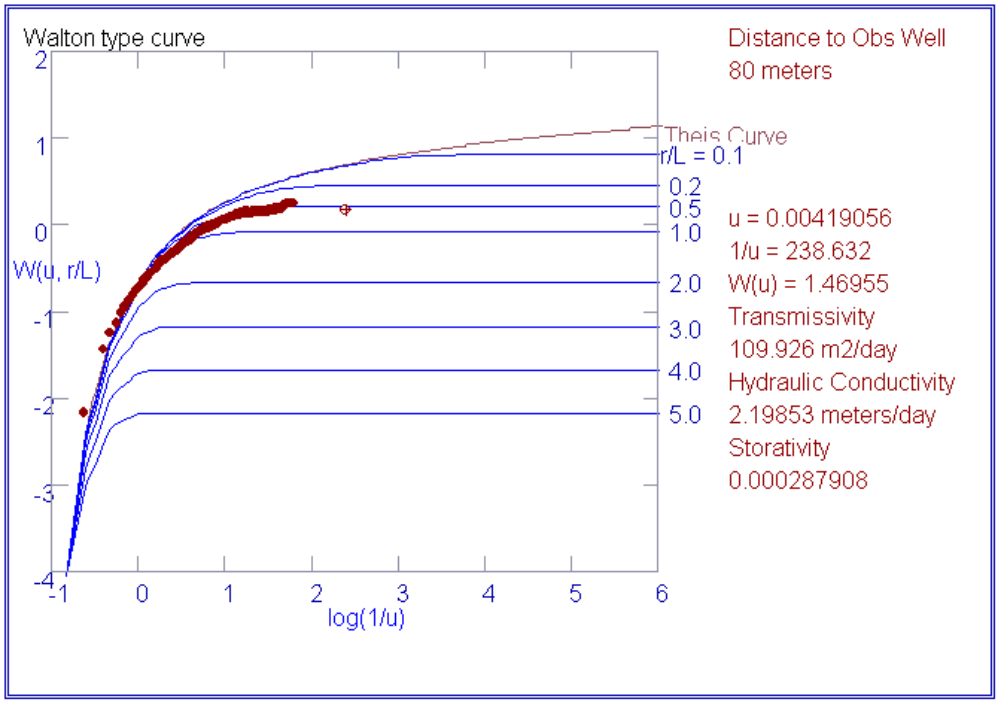

(b)Observation well

Figure 4.16: Results of Walton method for pumping test at P9: pumping phase.

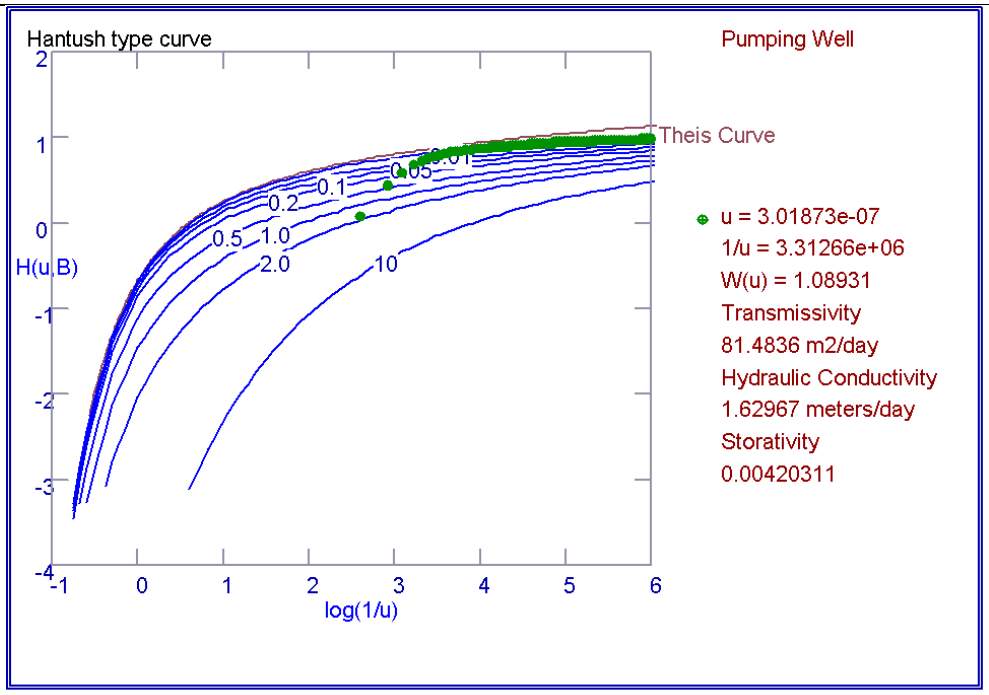

(a)Pumping well

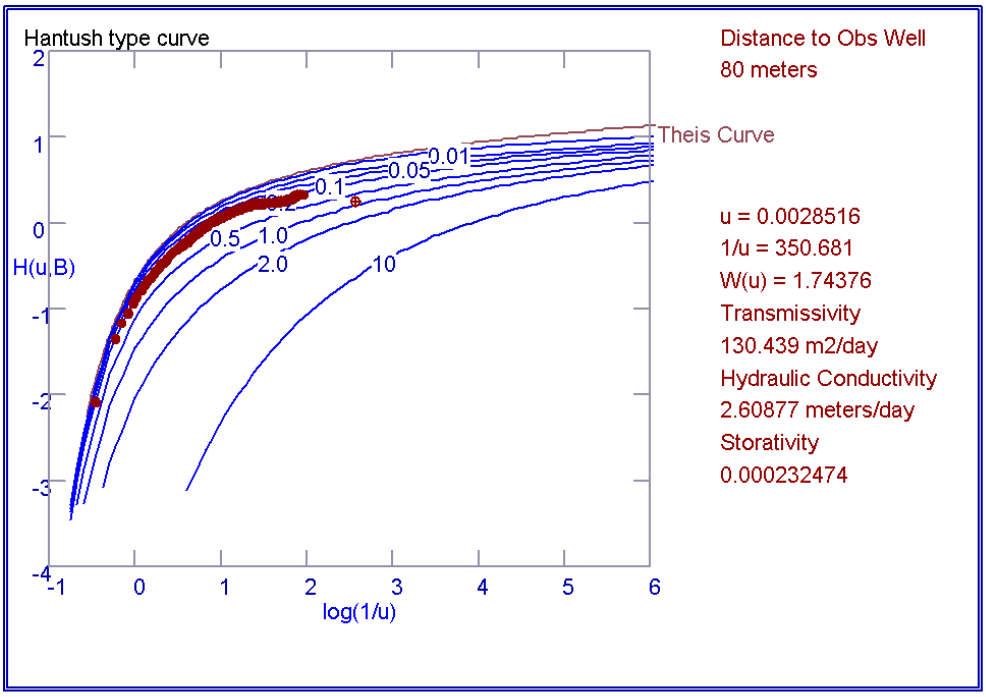

(b)Observation well

Figure 4.17: Results of Hantush method for pumping test at P9: pumping phase.

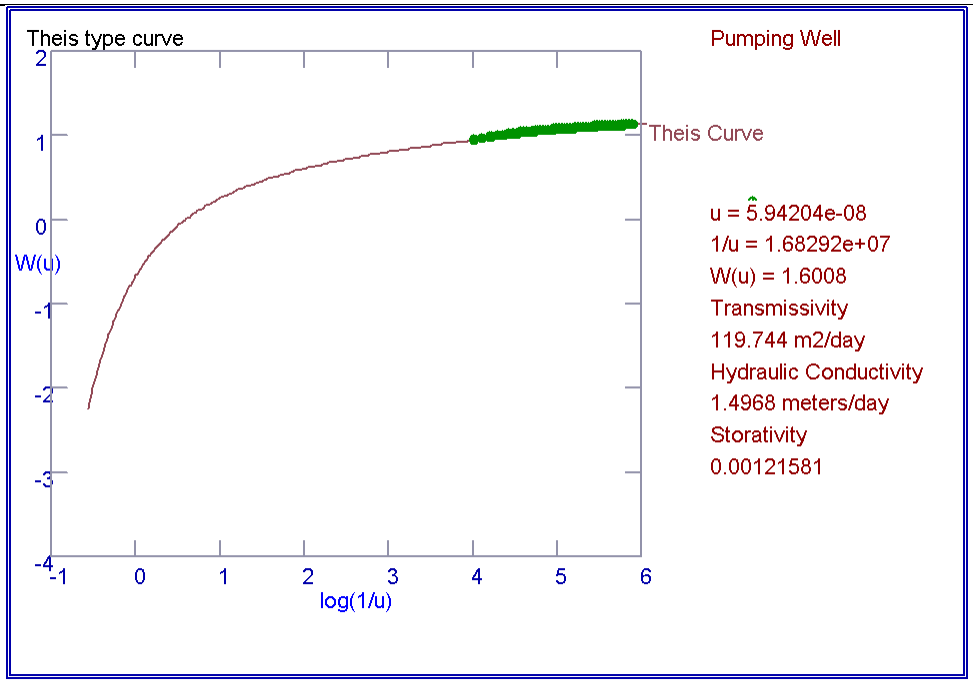

(a)Pumping well

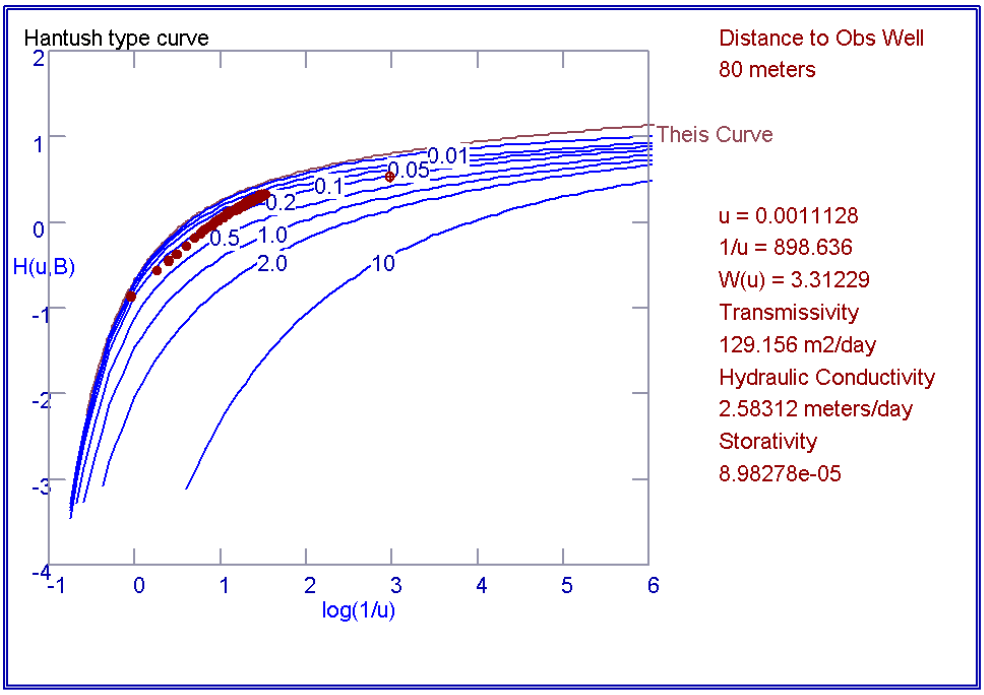

(b)Observation well

Figure 4.18: Results of Theis and Hantush methods for recovery data for pumping test at P9.

4.3.1.2.2 Pumping test at Chang'ombe (P10): unconfined aquifer; measurements in pumping well and 1 observation well

EXECUTION OF PUMPING TEST

Fig. 4.19 indicates a well construction sketch and the pumping phase and recovery phase of the constant rate pumping test which was conducted at the well belonging to DAWASCO, located at Chang'ombe area near to the Dar es Salaam University College of Education (DUCE). Table 4.10 indicates the flow rate during the pumping period. Pumping test was conducted for 6 hours followed by the recovery for 1 hour. Pumping test conducted involved pumping groundwater from the borehole P10 at a constant rate, and measuring water levels in the pumped well and one nearby borehole that was used as observation well. The Observation well O1 was at a distance of 60 m.

Table 4.10: Flow rate during 6 hours of pumping test at P10.

Time (h)	Discharge meter (m^3)	m^3 of water pumped per time step	Flow rate per time step (m^3/h)
0	10382.9		
0.5	10391.1	8.2	16.4
1	10400.4	9.3	18.6
1.5	10409.6	9.2	18.4
2	10419.9	10.3	20.6
3	10437.5	17.6	17.6
4	10455.7	18.2	18.2
5	10474.1	18.4	18.4
6	10492.4	18.3	18.3
			Average = 18.25m^3/h = 438m^3/d

The pumping well shows a rapid drop of water column above the diver (ca. 137 cmH_2O) attained within 2 minutes (Fig. 4.20a). In the next 5 hours of pumping period, the water level decreased gradually till the pumping stopped. A maximum drawdown of 163 cm (1.63 m) was attained. Water level recovery was almost completely attained after one hour since the stop of pumping. For the observation well (Fig. 4.20b) a drawdown of 18.2 cmH_2O was reached 1 hour after pumping began. At the end of the pumping test the water level reached a drawdown of 24.5 cmH_2O.

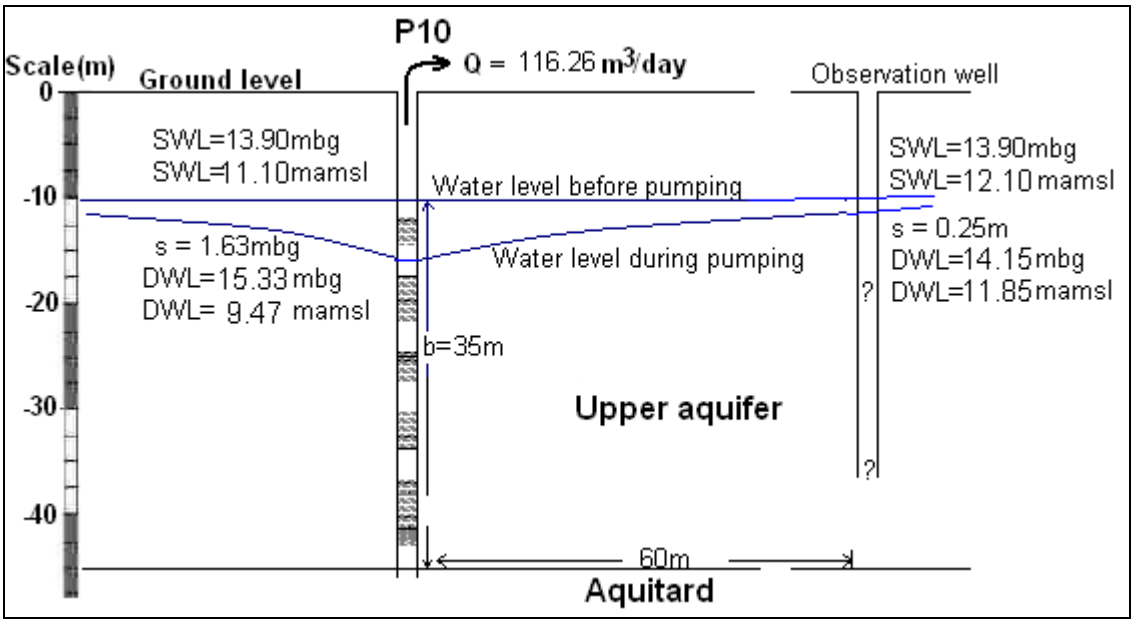

(a)Well construction sketch: SWL = Static Water Level; DWL = Dynamic Water level; s = drawdown; mbg = meter below ground; mamsl = meter above mean sea level; b = aquifer thickness

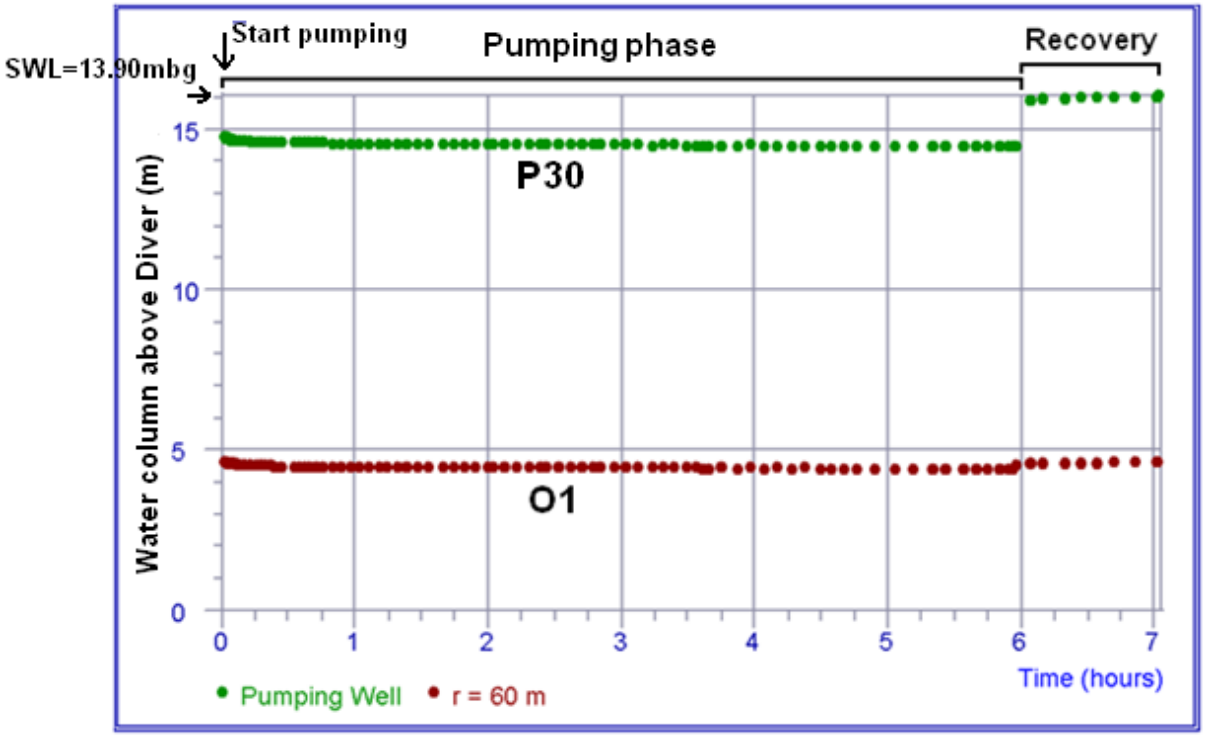

(b)Pumping period and recovery phase

Figure 4.19: Pumping test conducted at Chang'ombe area showing: a) well construction sketch, and b) pumping period and recovery phase for pumping well (P10) and observation well (O1).

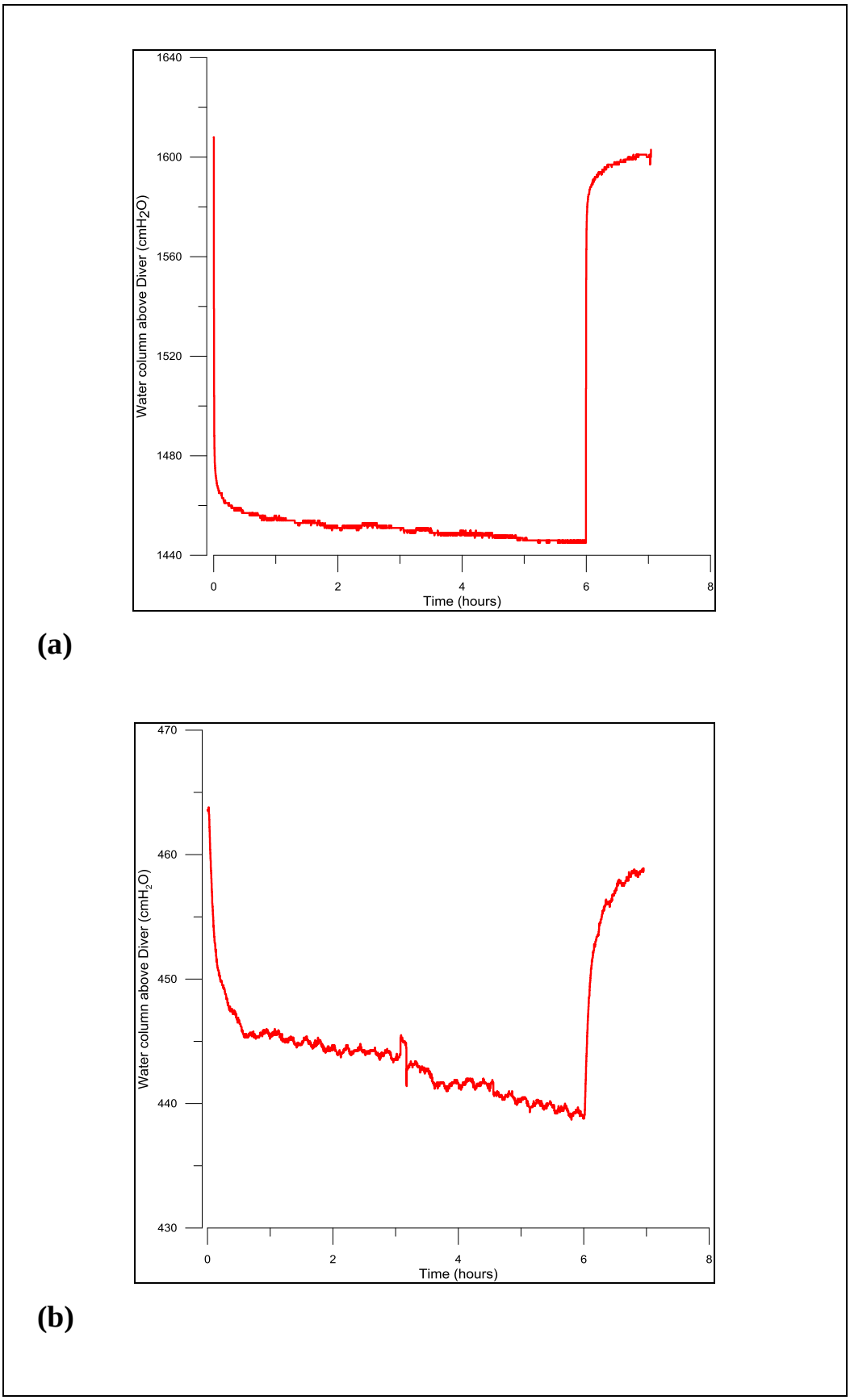

Figure 4.20: Water column above Diver for pumping test at Chang'ombe: a) pumping well (P10), and b) observation well (O1).

INTERPRETATION

Specific well capacity

The specific capacity was calculated using the flow rate of 438 m^3/d and the drawdown of 1.63 m giving the value of 268.71 m^2/d. In view of the classification of specific capacity magnitude according to Krasny (1993), well P10 falls within the high specific capacity class (Table 4.11). Table 4.12 represents the hydraulic parameters deduced from the specific well capacity method.

Table 4.11: Classification of specific capacity values according to Krasny (1993).

Well	Low (< 8.64m^2/d)	Well	Intermediate (8.64 - 86.4 m^2/d)	Well	High (86.4-864 m^2/d)	Well	Very high (> 864 m^2/d)
				P10	268.71		

Table 4.12: Hydraulic parameters deduced from Specific well capacity method.

Well	**Location**	**Q (m^3/d)**	**s (m)**	**T(m^2/d)**	**Aquifer thickness (m)**	**K (m/d)**
P10	Chang'ombe	438	1.63	268.7	35	7.68

Dupuit/Thiem's method

Through the Infinite Extent software it was possible to calculate transmissivity for a combination of the pumping well P10 and observation well O1. Table 4.13 represents the hydraulic parameters deduced from the Dupuit/Thiem's method.

Table 4.13: Hydraulic parameters deduced from pumping test analysis by Thiem-Dupuit/Thiem's method for steady-state flow

Well	**Location**	**Aquifer type**	**T (m^2/d)**	**Aquifer thickness (m)**	**K (m/d)**
P10	Chang'ombe	unconfined	320.57	35	9.16

Curve fitting

Pump test data recorded in the pumping well and observation well were analysed using Infinite Extent software whereby the hydraulic parameters were determined. Fig. 4.21 (a) indicates the results obtained using Neuman method: the transmissivity of 106.99 m2/d and hydraulic conductivity of 3.06 m/d were obtained from the pumping well measurements. On the other hand, the values of 277.09 m2/d and 7.92 m/d (Fig. 4.21b) respectively for transmissivity and hydraulic conductivity were obtained from the observation well measurements which are higher than those obtained in the pumping well. Furthermore, Neuman method showed higher transmissivity values 296.58 m^2/d for recovery data for the

observation well (Fig. 4.22b), comparing to the transmissivity value of 118.47 m^2/d indicated by the same method for recovery data from the pumping well (Fig. 4.22a). Transmissivity values obtained for observation well during pumping and recovery phases are considered to be reliable when comparing to the transmissivity values of 268.7 m^2/d and 320.57 m^2/d obtained by SWC and Dupuit/Theim's methods respectively. These values clearly show that measurements in the pumping well lead to too low values for transmissivity.

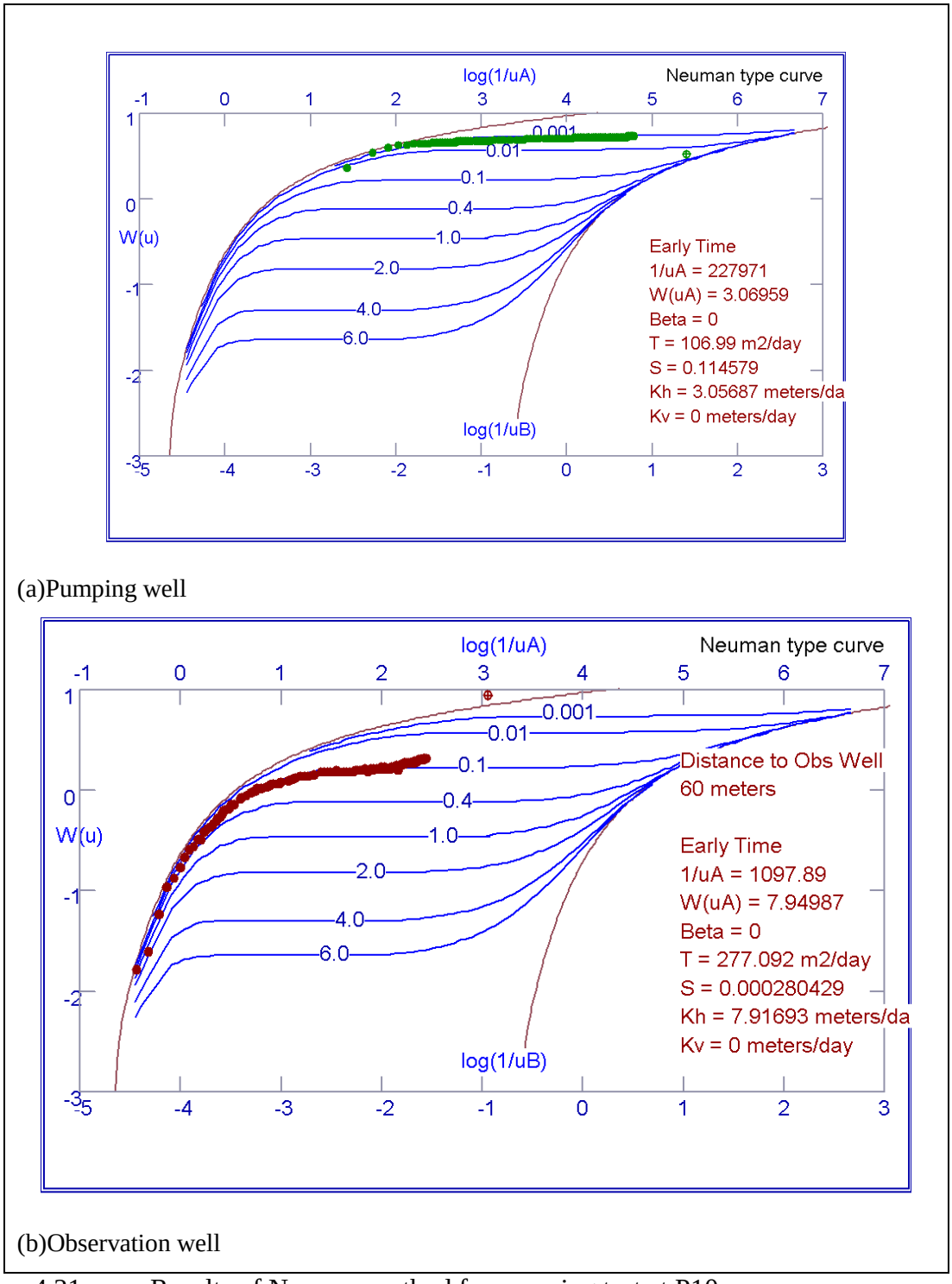

Figure 4.21: Results of Neuman method for pumping test at P10.

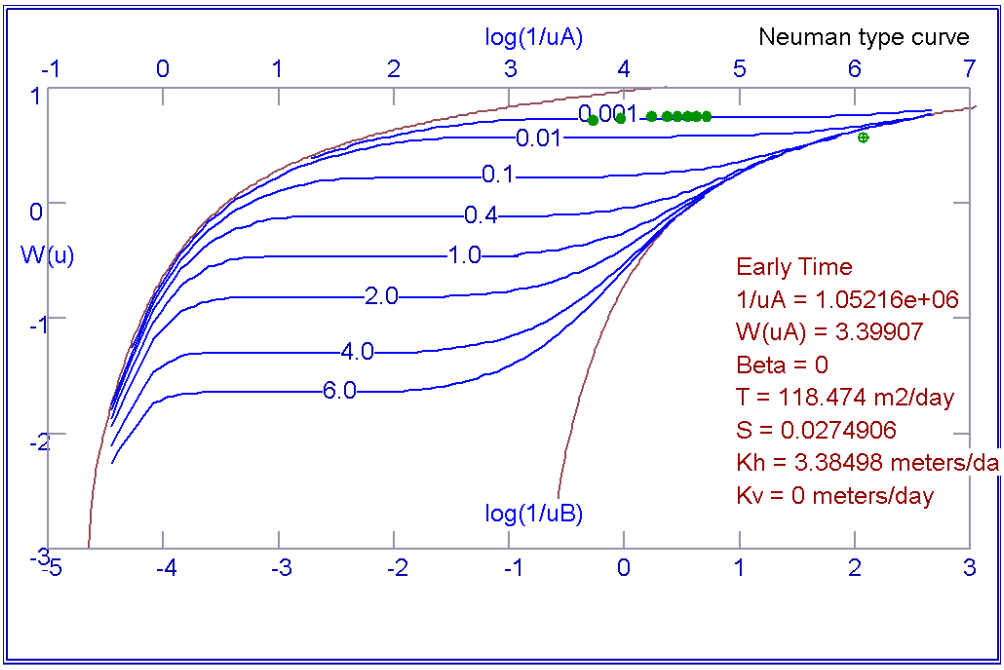

(a)Pumping well

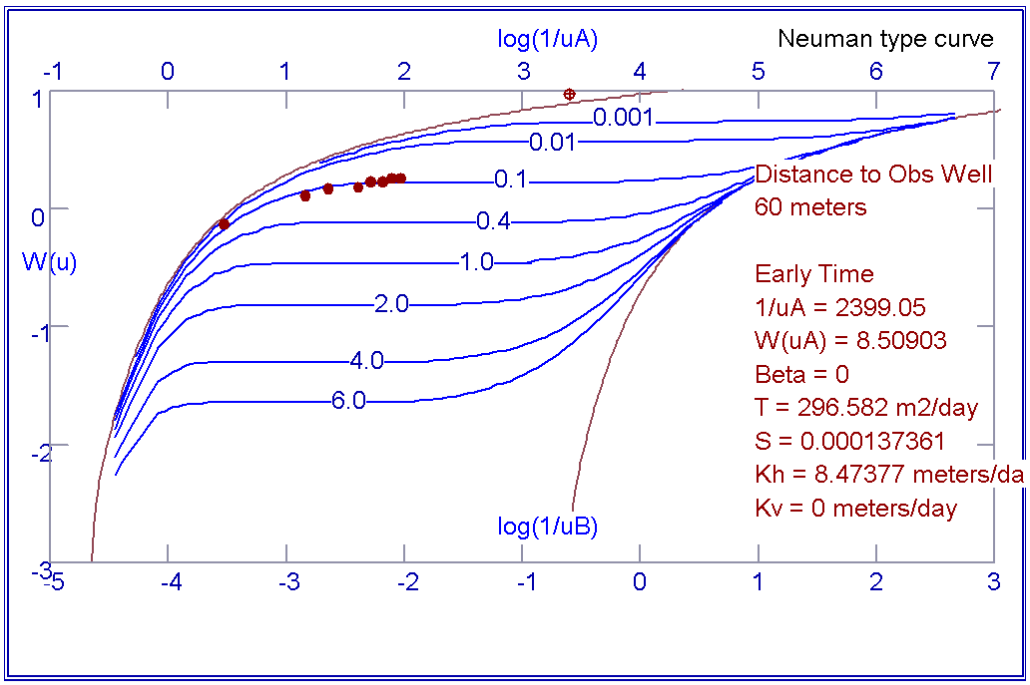

(b)Observation well

Figure 4.22: Results of Neuman method for recovery data for pumping test at P10.

4.3.1.2.3 Summary of pumping test interpretation

Different types of methods were used to analyse the pumping test data (Table 4.14). These include: i) specific well capacity (SWC) calculated based on the pumping rate and measured maximum drawdown for pumping tests, ii) Dupuit/Thiem for unconfined and confined aquifer under steady-state flow, iii) Neuman type curve fitting for the unconfined aquifer, Walton and Hantush leaky aquifer type curve fitting for the semi-confined aquifer, and Theis type curve fitting for the confined aquifer under unsteady state (or transient) flow. The overall results indicate that average transmissivity, and hydraulic conductivity values of 138.52 m^2/d and 4.27 m/d respectively were obtained for the upper unconfined aquifer (Table 4.17(a)). The semi-confined aquifer showed average values of 79.0 m^2/d and 1.7 m/d for transmissivity and hydraulic conductivity respectively (Table 4.15(a)). Transmissivity and hydraulic conductivity values for the unconfined aquifer range from 24.45 m^2/d to 296.58 m^2/d and from 0.76 m/d (8.80 x 10^{-6} m/s) to 8.47 m/d (9.8 x 10^{-5} m/s) respectively (Table 4.15(a)). Transmissivity and hydraulic conductivity values for the semi-confined aquifer range from 13.75 m^2/d to 130.44 m^2/d and from 0.43 m/d (4.97 x 10^{-6} m/s) to 2.61 m/d (3.02 x 10^{-5} m/s) respectively (Table 4.15(a)). Well P10 represents a pumping test which was conducted in the unconfined aquifer and in sand dominated lithology. This well indicates the highest hydraulic conductivity of 8.47 m/d (9.80 x 10^{-5} m/s) among the pumping test data analysed. P1, P3 and P9 wells represent the semi-confined aquifer dominated by sand lithology. Hydraulic values in these wells range from 0.46 m/d (5.32 x 10^{-6} m/s) at well P3 to 2.61 m/d (3.02 x 10^{-5} m/s) at well P9. Conductivity values in sand/limestone dominated lithology in the unconfined aquifer range from 0.76 m/d (8.8 x 10^{-6} m/s) at well P7 to 3.18 m/d (3.68 x 10^{-5} m/s) at well P6 (Table 4.14). Conductivity values in sand/limestone dominated lithology in the semi-confined aquifer range from 0.43 m/d (4.98 x 10^{-6} m/s) at well P5 to 1.96 m/d (2.27 x 10^{-5} m/s) at well P8 (Table 4.14). The conductivity values vary reflecting the type of lithology in which the well is constructed. Referring to Table 4.1, the hydraulic parameters deduced from the pumping tests correspond to sediments comprising silty sand and sand. However, lithological logs from the available groundwater drilling reports indicate that in the study area the aquifer lithology also comprises gravel and coral limestone of various degree of weathering. One of the earliest studies in the Dar es Salaam coastal aquifer was performed by Mjemah (2007), which involved mapping the hydrogeologic units, and determining aquifer parameters and recharge rates. The results obtained by Mjemah (2007) (Table 4.15b), who evaluated 39 wells in a larger area in regard to pumping tests, reflect the aquifer heterogeneity from clay to sand. The study by Mjemah (2007) and the current results of hydraulic

parameters deduced from pumping tests, and variation of specific capacity values ranging from intermediate to high (Table 4.16) suggest that the hydraulic parameters of the Dar es Salaam Quarternary coastal aquifer (DQCA) vary widely from very low to high reflecting their lithological compositions. Compaared to the results obtained by Mjemah (2007), the current results is more or less the same values for semi-confined aquifer. But the average values for unconfined aquifer are over 2 times larger comaring to that obtained by Mjemah (2007). This could be due to the sediments near to the ocean are coarser compared to inland part that was also included in Mjemah's study.

Table 4.14: Summary of pumping test results (UC = unconfined aquifer, SC = semi-confined aquifer, O1 = Observation well, T = transmissivity, and K = hydraulic conductivity)

Well	**Aquifer type**	**Aquifer lithology**	**HYDRAULIC PROPERTIES: CURVE FITTING METHODS**								**HYDRAULIC PROPERTIES: Dupuit/Thiem & SWC**			
			METHODS	**PUMPING**				**RECOVERY**						
				Pumping well		**Observation well**		**Pumping well**		**Observation well**		**Dupuit/Thiem**		**SWC**	
				T (m^2/d)	**K (m/d)**	**T (m^2/d)**	**K (m/d)**	**T (m^2/d)**	**K (m/d)**	**T (m^2/d)**	**K (m/d)**	**T (m^2/d)**	**K (m/d)**	**T (m^2/d)**	**K (m/d)**
P1	SC	Sand	Walton	74.28	2.12			71.17	2.03					107.4	3.07
P2	UC	Sand/limestone	Neuman	X	X			31.30	1.04					41.32	1.38
P3	SC	Sand	Walton	26.59	0.46			26.59	0.46					26.6	0.46
P4	SC	Sand/limestone	Walton	X	X			56.18	1.12					61.3	1.23
P5	SC	Sand/limestone	Theis	X	X			13.75	0.43					13.1	0.41
P6	UC	Sand/limestone	Neuman	X	X	63.26	3.18							64.3	3.79
P7	UC	Sand/limestone	Neuman	X	X	24.45	0.76							20.5	0.64
P8	SC	Sand/limestone	Theis	58.79	1.96									59.6	1.99
P9	SC	Sand	Theis	109.93	2.20	X	X	119.74	1.50			128.49	2.57	111.51	2.24
			Hantush	X	X	130.44	2.61			129.16	2.58				
			Walton	X	X	X	X								
P10	UC	Sand	Neuman	X	X	277.01	7.92			296.58	8.47	320.57	9.16	268.71	7.68

x: results rejected due to bad curve fitting and/or results deviating with very high degree from other methods or SWC.

Table 4.15(a): Average of hydraulic parameters obtained by curve fitting methods.

Aquifer	Parameter	Minimum	Average	Maximum
Unconfined aquifer	T (m^2/d)	24.45	138.52	296.58
	K (m/d)	0.76	4.27	8.47
	K (m/s)	8.80×10^{-6}	4.94×10^{-5}	9.8×10^{-5}
Semi-confined aquifer	T (m^2/d)	13.75	79.0	130.44
	K (m/d)	0.43	1.7	2.61
	K (m/s)	4.97×10^{-6}	1.97×10^{-5}	3.02×10^{-5}

Table 4.15(b): Hydraulic parameters obtained by Mjemah (2007).

Aquifer	Parameter	Minimum	Average	Maximum
Unconfined aquifer	T (m^2/d)	0.1	33.95	155.18
	K (m/d)	0.003	1.58	6.05
	K (m/s)	3.47×10^{-8}	1.83×10^{-5}	7×10^{-5}
Semi-confined aquifer	T (m^2/d)	11.57	63.25	190.34
	K (m/d)	0.39	2.14	5.44
	K (m/s)	4.53×10^{-6}	2.50×10^{-5}	6.30×10^{-5}

Table 4.16: Classification of specific capacity values according to Krasny (1993).

Well	Low (< 8.64m^2/d)	Well	Intermediate (8.64 - 86.4 m^2/d)	Well	High (86.4-864 m^2/d)	Well	Very high (> 864 m^2/d)
		P2	9.8	P1	107.4		
		P3	26.6	P9	111.51		
		P4	61.3	P10	268.71		
		P5	13.1				
		P6	64.3				
		P7	20.5				
		P8	59.6				

4.3.1.3 Challenges associated with the execution of pumping tests and data reliability

The trustworthiness of hydrologic test data depends on the consistency of the stress applied during testing and the reliable operation of test equipment. The rate of water discharge during the test must not vary significantly. The pump used must withdraw water at a fairly constant rate. Data reliability also depends on the precise working of all the equipment involved in measurements, including water-level probes and flow meters. Existing pump tests in the study area have been mostly carried out by drilling companies. Frequently, water pumps used are of high capacity which causes for some well, especially those located in an area with low transmissivity, their upper screens to become dry with very large drawdown (Mjemah, 2007). This often causes unstable discharge rate instead of the constant discharge rate required. On

the other hand, lack of information about the exact location of the screens in the wells can also lead to inaccuracies and problems during the interpretation of the tests (Dejager, 2011). If a screen does not comprise the entire thickness of the aquifer, vertical flows will occur, distorting the results.

Most of pumping tests available in the study area were carried out as single well tests. This kind of test is generally used to describe well performance opposed to aquifer tests with observation wells which best describe aquifer response to pumping. Drilling companies in the study area perform a single well performance test since it is quick, relatively simple and inexpensive to conduct. However, a well performance test, generally, does not describe aquifer parameters in detail and is of only limited use in determining the effects of groundwater abstraction consent.

The results of pumping tests conducted by using Divers gave smooth curves comparing to the existing information where the manual method was used to measure the dynamic water level. Water level measured manually hinders measurements at very small time intervals like seconds, which is actually required in the beginning of the test. Analysis of the recovery data was more reliable than drawdown in pumping wells.

4.3.2 Static water level measurements

Piezometric measurements, borehole location, borehole coordinates, elevation, depth and type of aquifer are available in Appendix 4. Piezometric maps have been presented in Figs. 4.23(a-d). In the piezometric maps of the unconfined aquifer (Fig. 4.23 a and c), the influence of the rivers which drain the unconfined aquifer were taken into account assuming a lowering of the groundwater level near to the rivers. The direction of groundwater flow is similar in both unconfined and semi-confined aquifers (Figs. 4.23 (a-d)). The groundwater flows toward northeast and east, where the ocean represents the natural discharge area.

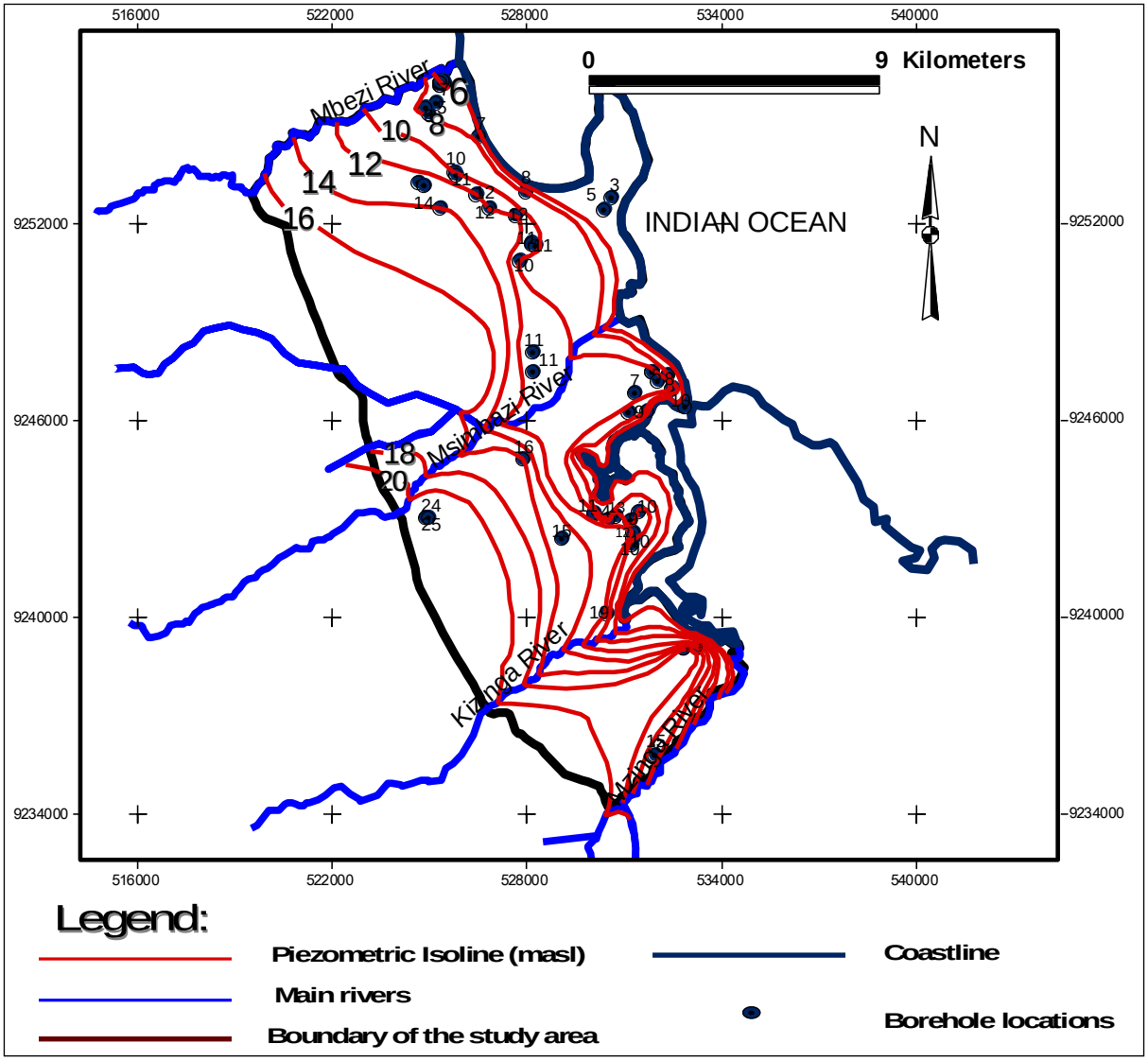

Figure 4.23(a): Groundwater level (masl) map of the upper DQCA, July 2010. (Equidistance: 2 m).

The values for the water elevation for July of the years 2010 and 2011 for the unconfined aquifer vary from 3 masl to 37.0 masl and from 1.56 masl to 20.5 masl respectively. The values for the water elevation for the year 2010 and 2011 for the lower semi-confined aquifer vary from -1.0 masl to 40.8 masl and from 1.0 masl to 21.65 masl respectively. Piezometric measurements taken in July 2010 can not be directly compared with piezometric measurements taken in July 2011 since most measurements were not taken in the same location. Water level measurements depend on the access which has to be provided by the borehole/well owners and this lead to the measurements to be conducted where permission was given. However, the general trend is that the area near the coastline constitutes the lowest piezometric levels. The lowest values are situated along the coast at areas such as Kawe

(1.5 masl), City Centre (1.56 masl) and Msasani (3 masl). The highest water levels are found in the west and southwest of the study area. Highest water elevation of 40.8 masl was recorded at Mbagala area. However, negative value (-1.0 masl) was measured at Police (Bohari) which is likely that this water level has been disturbed by pumping as it is surrounded by values of 5.8 masl to 12.2 masl. The location of Police is indicated in Fig. 4.2. Furthermore, well P5 (Fig. 4.9) located at Keko near to Police (Bohari) (Fig. 4.2) indicate dynamic water levels, during pumping becoming lower than sea level (-10.78 mamsl with Q=172.8 m^3/day).

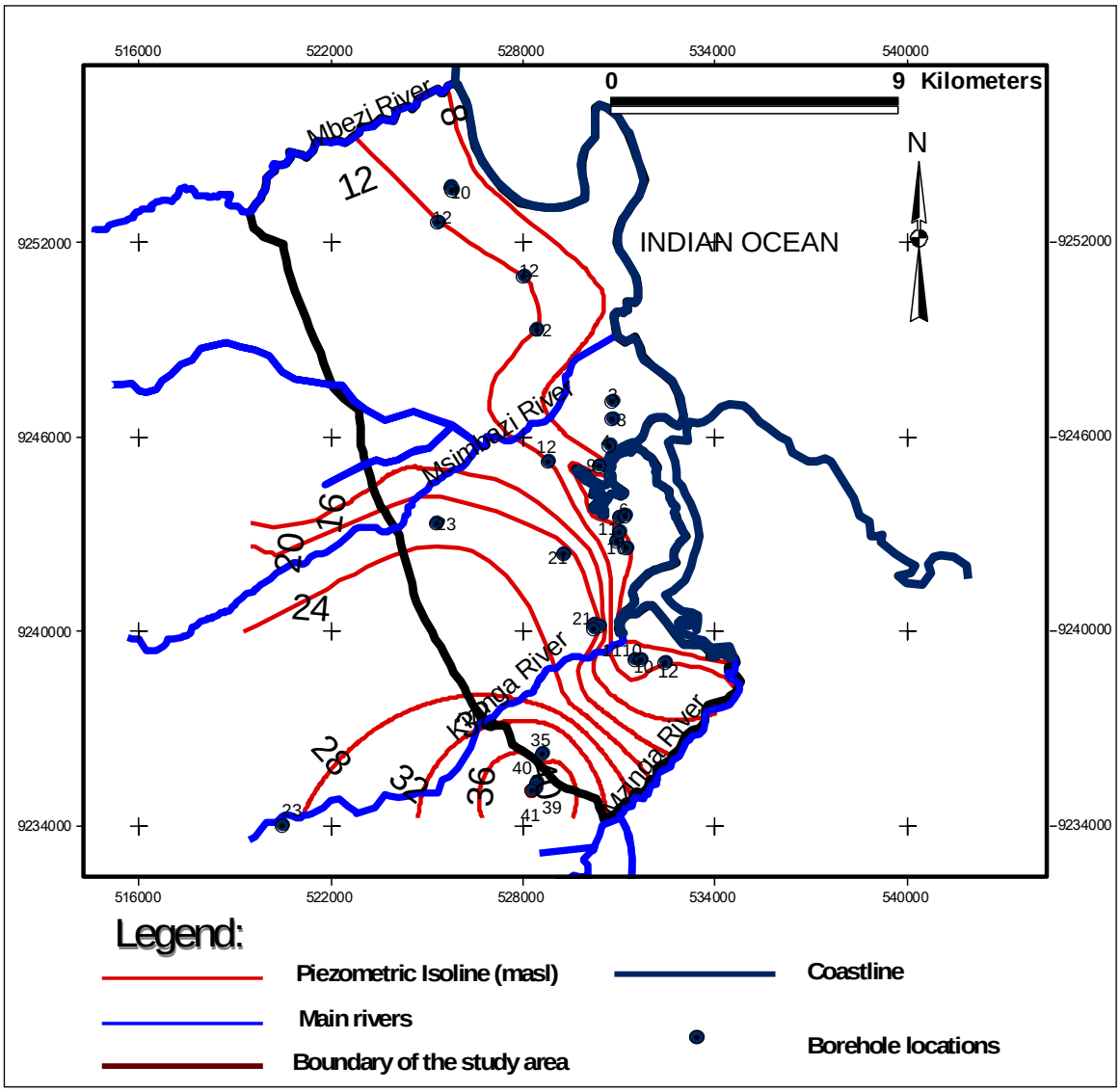

Figure 4.23(b): Groundwater level (masl) map of the lower DQCA, July 2010. (Equidistance: 4 m).

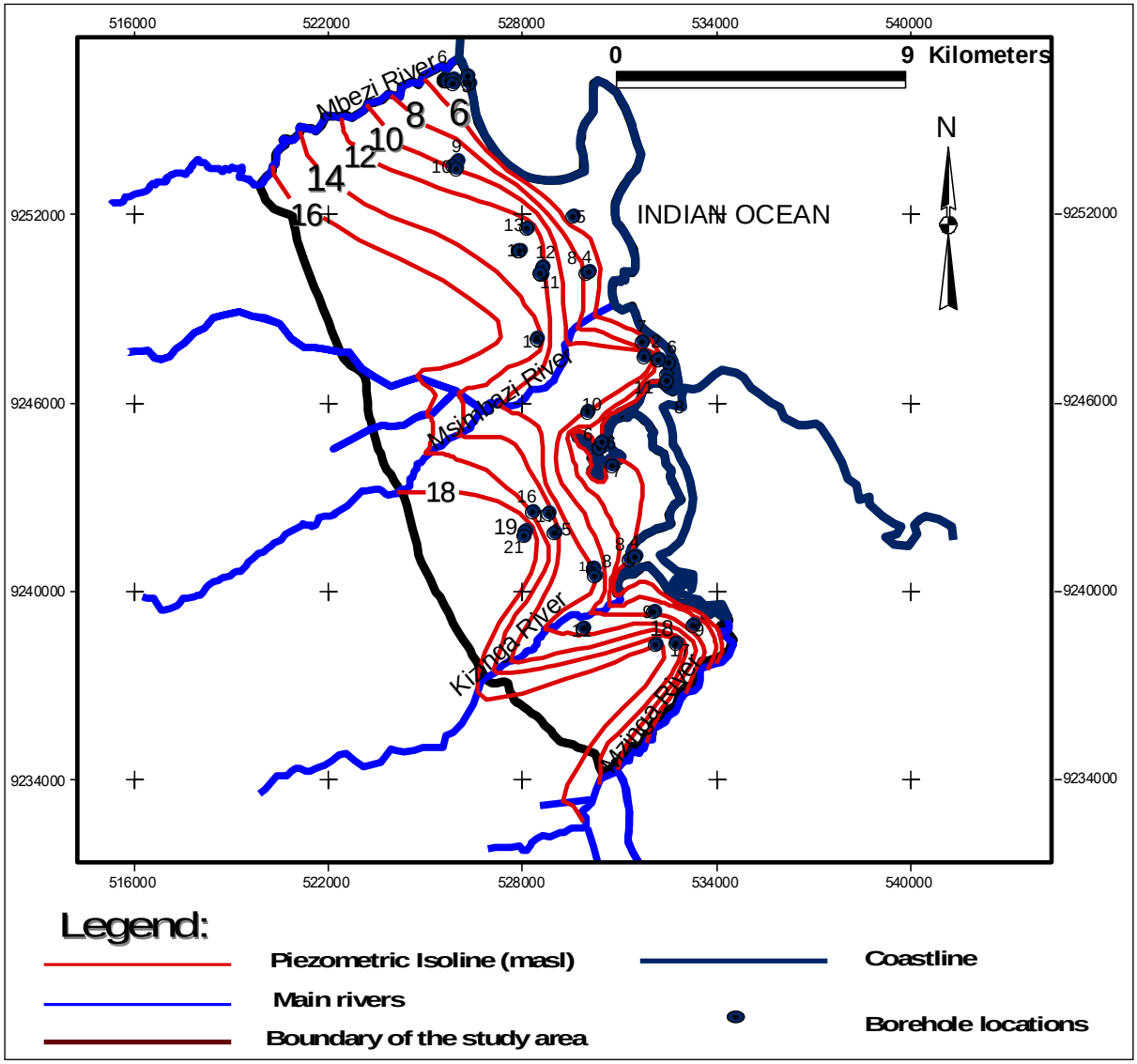

Figure 4.23(c): Groundwater level (masl) map of the upper DQCA, July 2011 (Equidistance: 2 m).

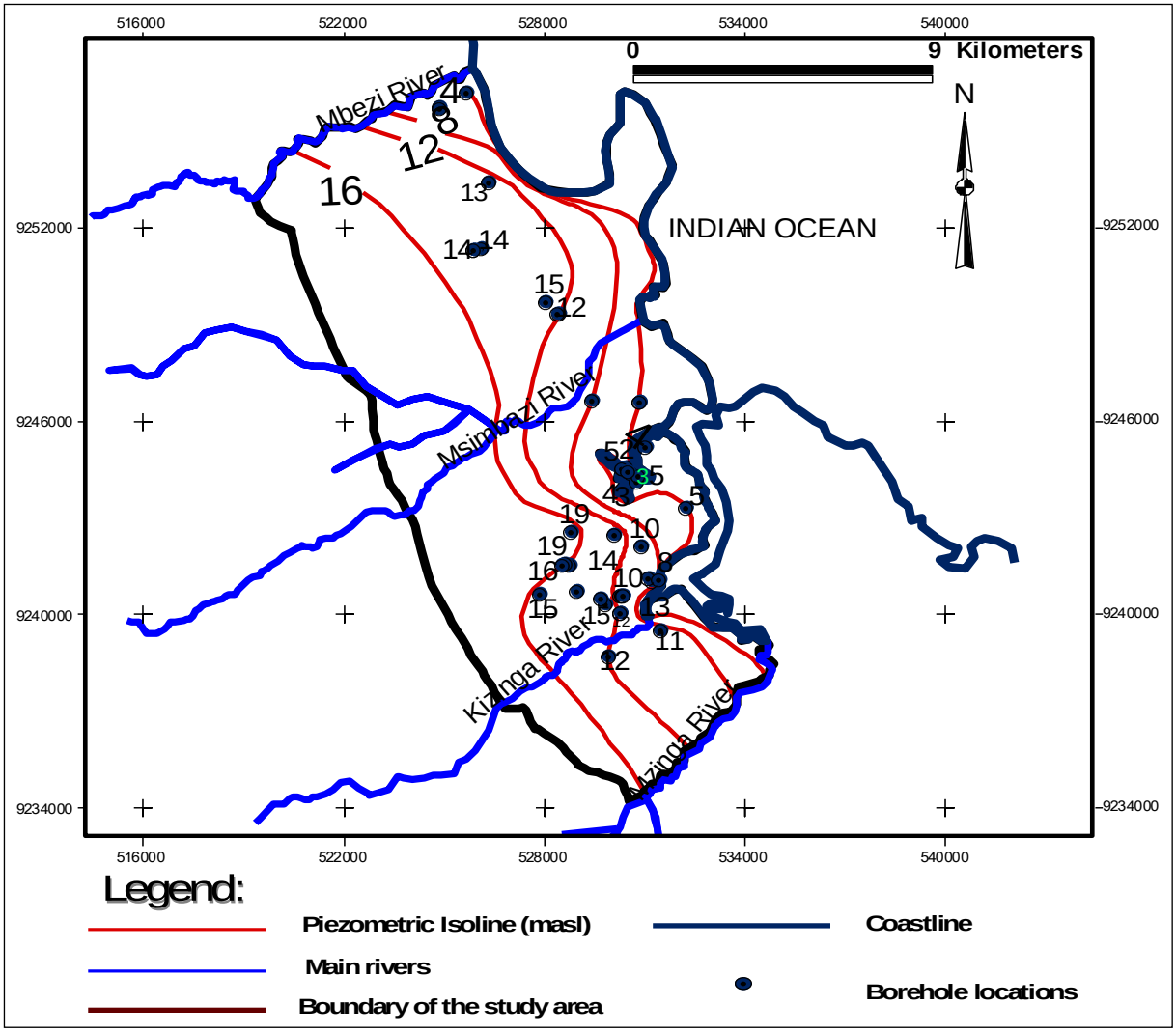

Figure 4.23(d): Groundwater level (masl) map of the lower DQCA, July 2011 (Equidistance: 4 m).

4.3.3 Continuous groundwater level monitoring

4.3.3.1 Observations

4.3.3.1.1 Continuous barometric pressure monitored by Baro-Diver G5943

Fig. 4.24 presents atmospheric pressure measurements recorded between the year 2010 and 2012: i) 07/07/2010 – 01/08/2010, ii) 27/02/2011 – 21/10/2011, and (iii) 21/10/2011 – 24/06/2012. The three figures give the atmospheric conditions throughout the year. Increase and decrease of the atmospheric pressure are related to the different seasons in the year such as rainfall and dry periods. During the rainy period, which occurs in March to May and in October to December, the atmospheric pressure during these periods is low. The high atmospheric pressure is documented in the dry period which occurs mainly from June to September. Fig. 4.25 is a close-up of Fig. 4.24(i) indicating a detail of the time sequence of

the atmospheric variation. The atmospheric pressure fluctuates between 1029.3 and 1037.2 cmH_2O. The recorded atmospheric pressure in Fig. 4.24(i) indicates a semidiurnal cycle with higher maxima peaks occurring around 08:30 hrs and lower maxima peaks occurring around 20:33 hrs (Fig. 4.25). The former has an amplitude of about 4 cmH_2O whereas the latter has an amplitude of about 2 cmH_2O.

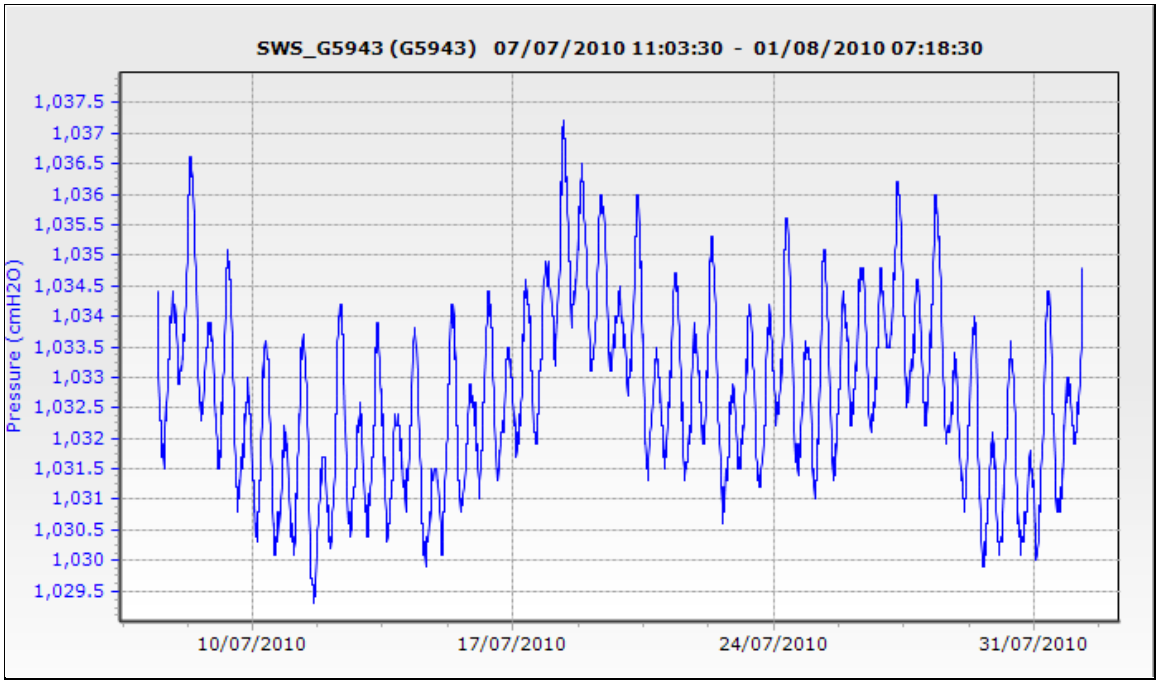

Figure 4.24(i): Atmospheric pressure measurements recorded by the Baro-Diver for the period between 07/07/2010 and 01/08/2010.

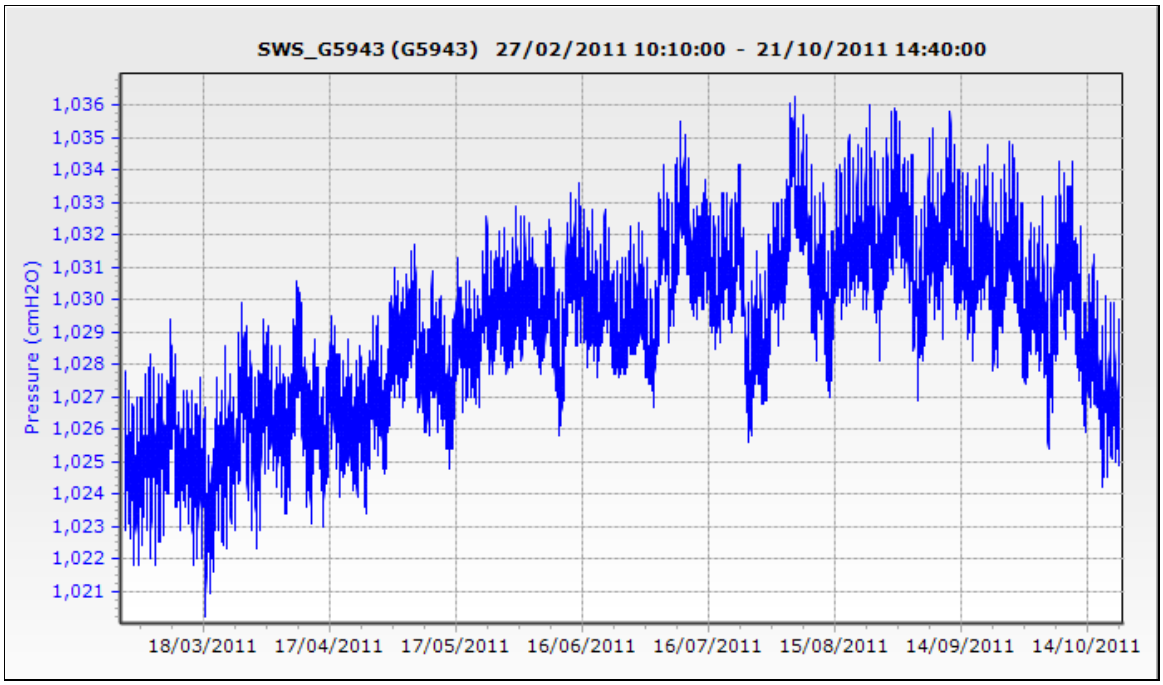

Figure 4.24(ii): Atmospheric pressure measurements recorded by the Baro-Diver for the period between 27/02/2011 and 21/10/2011.

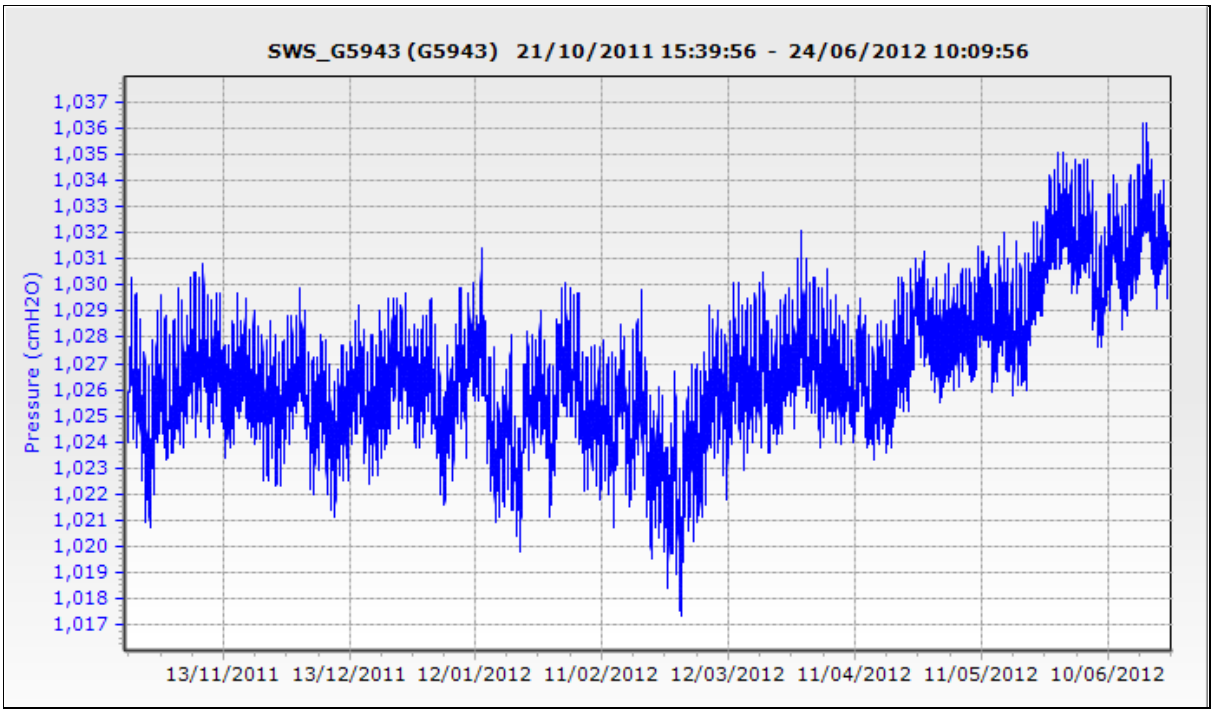

Figure 4.24(iii): Atmospheric pressure measurements recorded by the Baro-Diver for the period between 21/10/2011 and 24/06/2012.

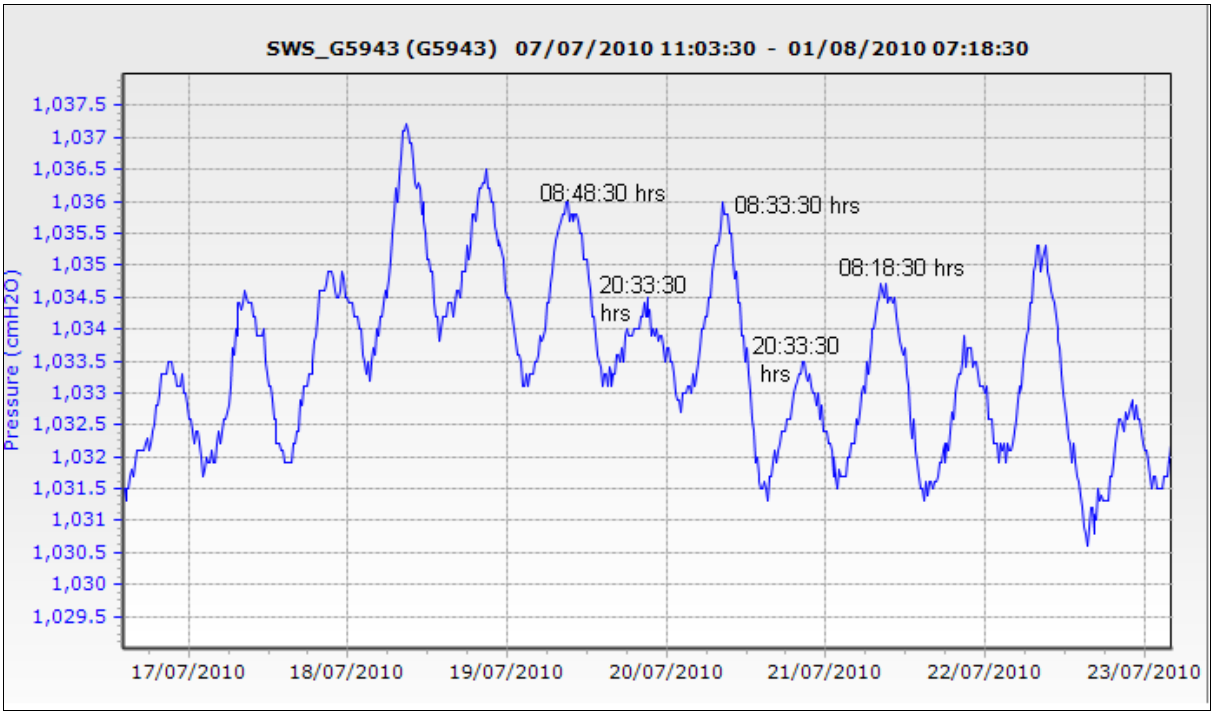

Figure 4.25: Close-up of Fig. 4.24 (i) indicating detail of time sequence of the atmospheric variation.

Atmospheric pressure is caused by the Earth's gravitational attraction of air in the atmosphere: the largest difference in pressure occurs near the equator which experiences the largest amplitude of atmospheric tides, generated by the periodic heating of the atmosphere by

the sun (Ahrens, 2007). This causes the clear detection of both the higher maxima peaks and the second lower maxima peaks in tropical zones, compared to the situation in the polar areas (Ahrens, 2007). Fig. 4.26 shows the amplitude of the solar semidiurnal oscillation over the globe.

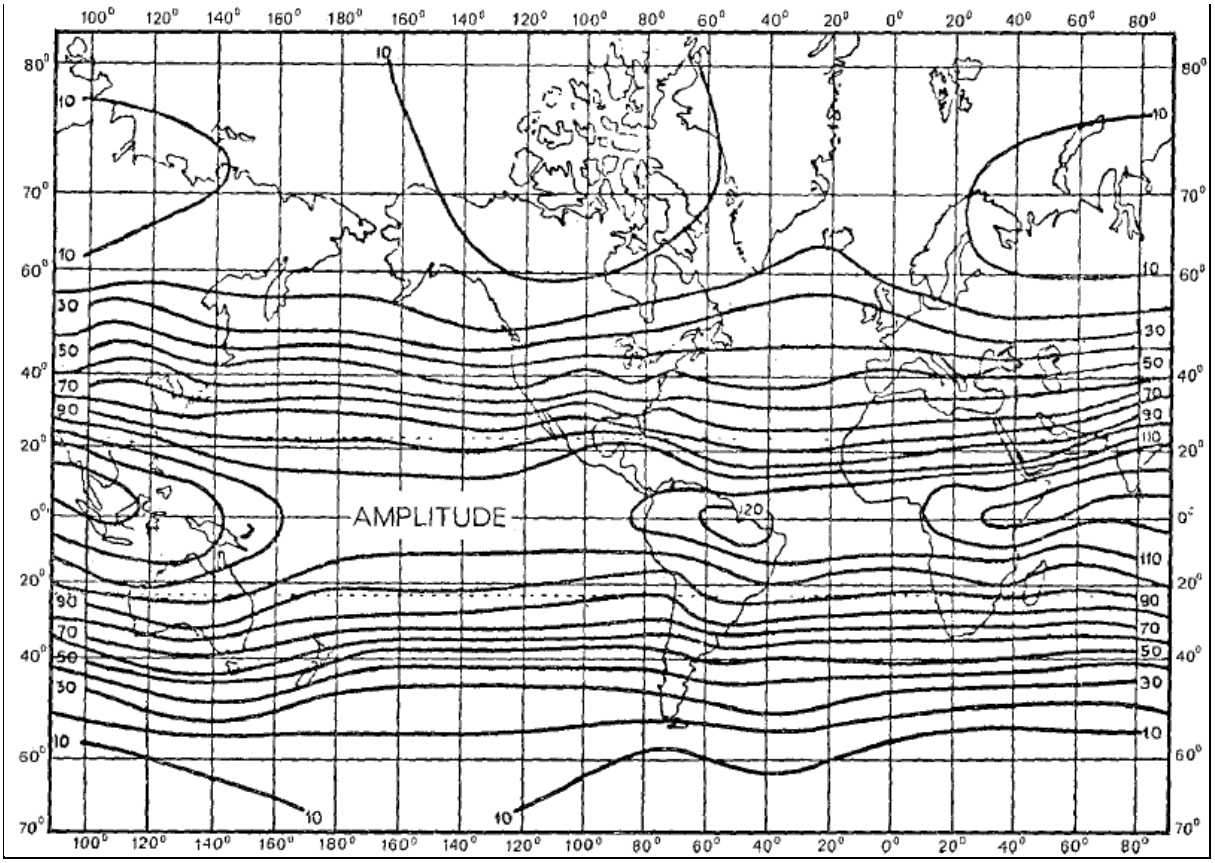

Figure 4.26: World maps showing equilines of amplitude (After Haurwitz, 1956 cited in Lindzen and Chapman, 1969).

4.3.3.1.2 *Continuous groundwater level monitoring at Mnazi Mmoja Primary School by Mini-Diver (10m) H0461*

Fig. 4.27(a, b) presents groundwater level fluctuation measurements recorded by the Mini-Diver J0461 in monitoring borehole "MNAZI_1" at Mnazi Mmoja Primary School, 1.85 km from the ocean. The measurements cover two periods: a) 07-18 July 2010, and b) 22 July – 01 August 2010, which coincide with the dry period (June to September). The recorded measurements indicate a semidiurnal cycle with higher maxima peaks occurring constantly at 03:45 hrs and the lower maxima peaks which occur at varying times but with a dominant trend of shifting one hour every day (Fig.4.27(a)). The former has an amplitude of 6.5 to 10.6 cmH_2O whereas the latter has an amplitude of 2.2 to 6 cmH_2O.

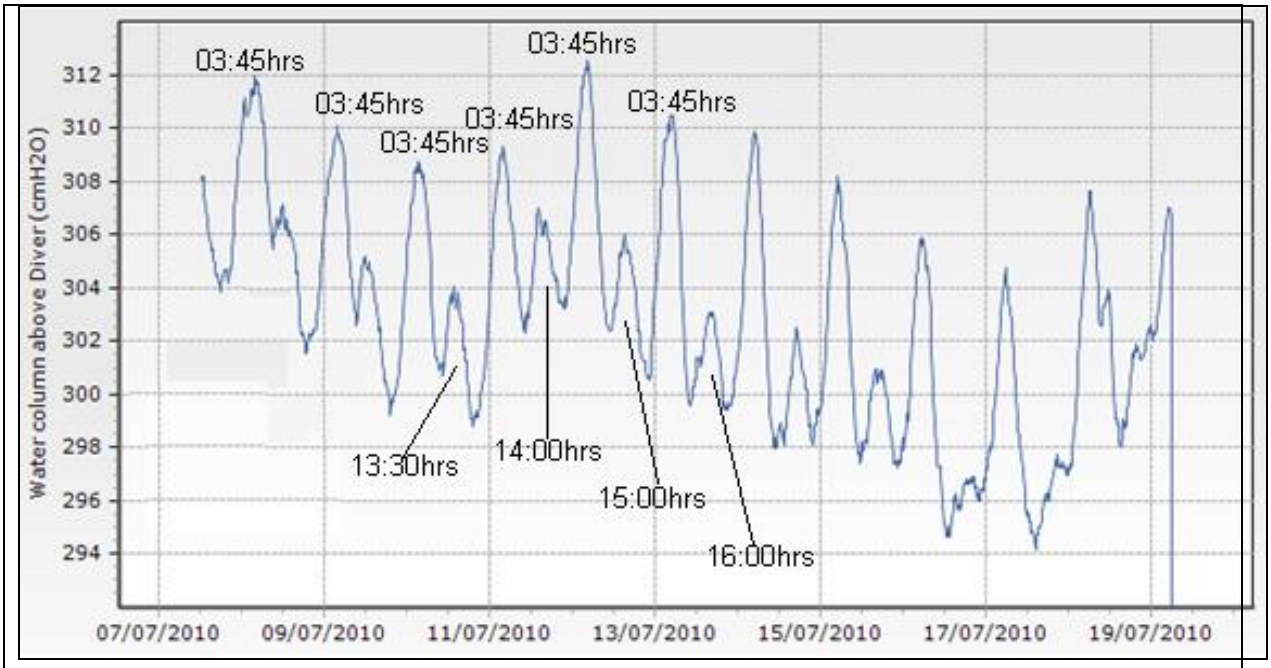

(a)

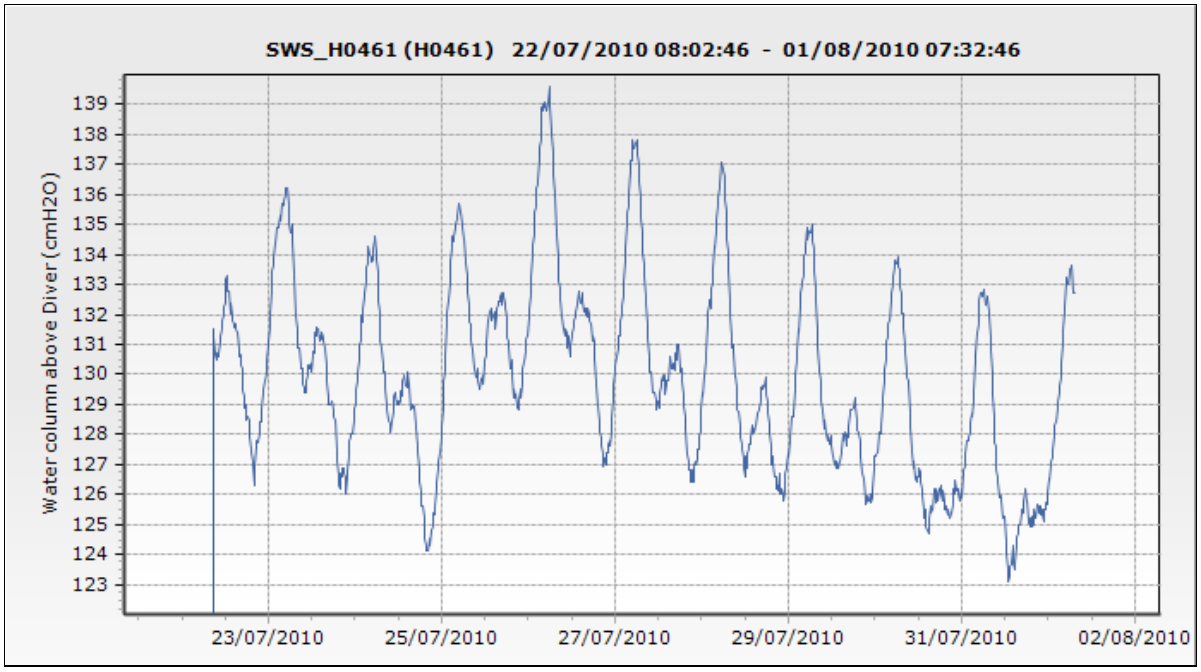

(b)

Figure 4.27: Monitored groundwater elevation at Mnazi Mmoja Primary School for the period: a) 07/07 – 19/07/2010, and b) 22/07 – 01/08/2010.

4.3.3.1.3 Continuous groundwater level monitoring at Zanaki Secondary School by Mini-Diver (10m) J0496

Fig. 4.28 presents groundwater level fluctuation measurements recorded by the Mini-Diver J0496 in monitoring borehole "95" at Zanaki Secondary School, 1.5 km from the ocean. The measurements cover the period: a) 07-19 July 2010, and b) 22 July – 01 August 2010 conducted during the dry period (June to September). The recorded measurements indicate a semidiurnal cycle with higher maxima peaks and lower maxima peaks, both of them occurring at varying times (Fig. 4.28(a)). For a period of 8 days (8-15 July), the large peak has occurred at a time varying between 03:15 to 5:00hrs whereas the small peak has occurred at a time varying between 13:00hrs to 16:00hrs (Fig. 4.28a). The large peak has an amplitude ranging from 13.6 to 25.2 cmH_2O whereas the small peak has an amplitude varying from 4 to 8 cmH_2O.

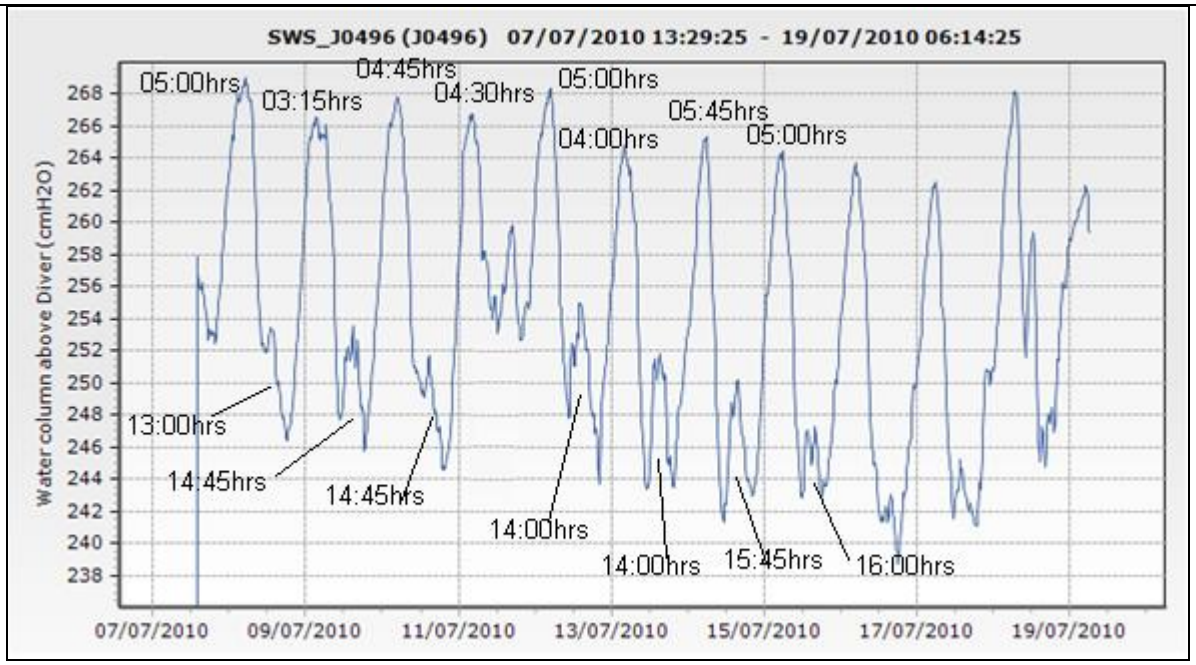

(a)

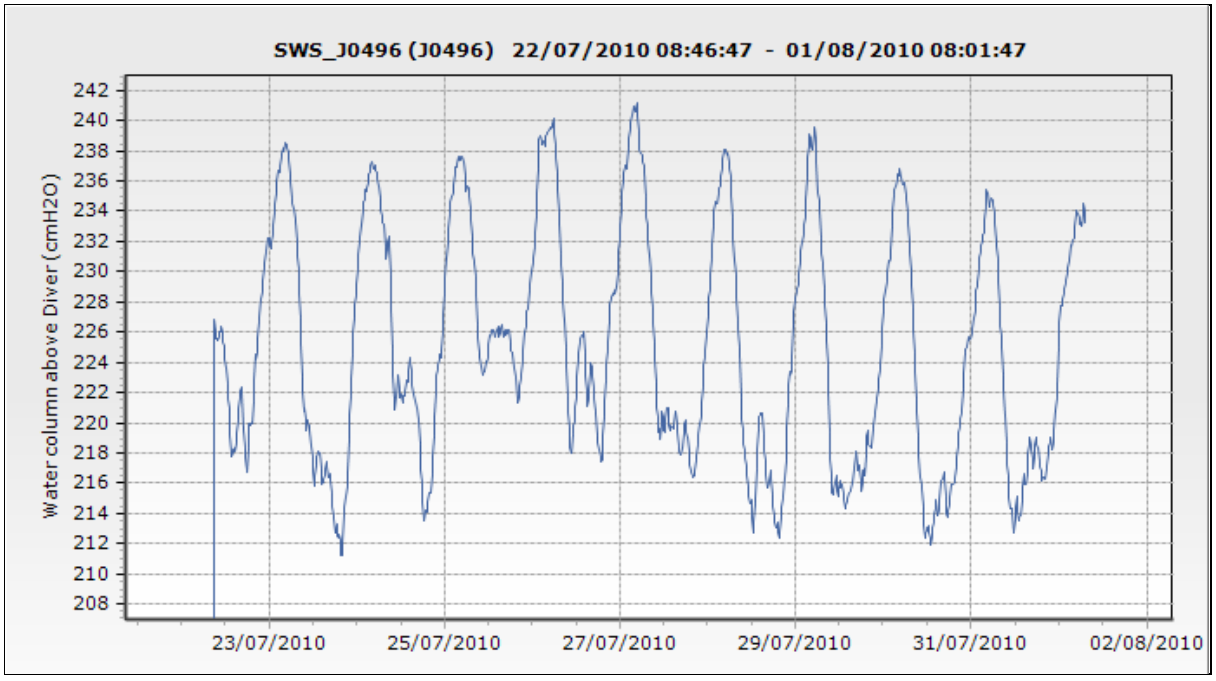

(b)

Figure 4.28: Groundwater elevation recorded by Mini-Diver J0496 for the period: a) 07/07 to 19/07/2010, and b) 22/07 to 01/08/2010).

4.3.3.1.4 Continuous groundwater level monitoring at Temeke Municipality Garden by Mini-Diver (10m) H0507

Fig. 4.29 presents groundwater level fluctuation measurements recorded by the Mini-Diver H0507 in monitoring borehole "179" at Temeke Municipality Garden, 0.5 km from Mzinga Creek and 7 km from the ocean (measuring from the mouth of Mzinga Creek). The measurements cover the period of about two months: 22 April to 9 June 2011. Fig. 4.30 is a close-up of Fig. 4.29. Two kinds of peaks with more or less the same height can be recognized clearly: a peak occurring at 04:00 hours, followed by a peak occurring at 14:30 hours. These peaks have an amplitude ranging from 2.5 to 5 cmH_2O. Next to this, there is another cycle of peaks low in size occurring irregularly.

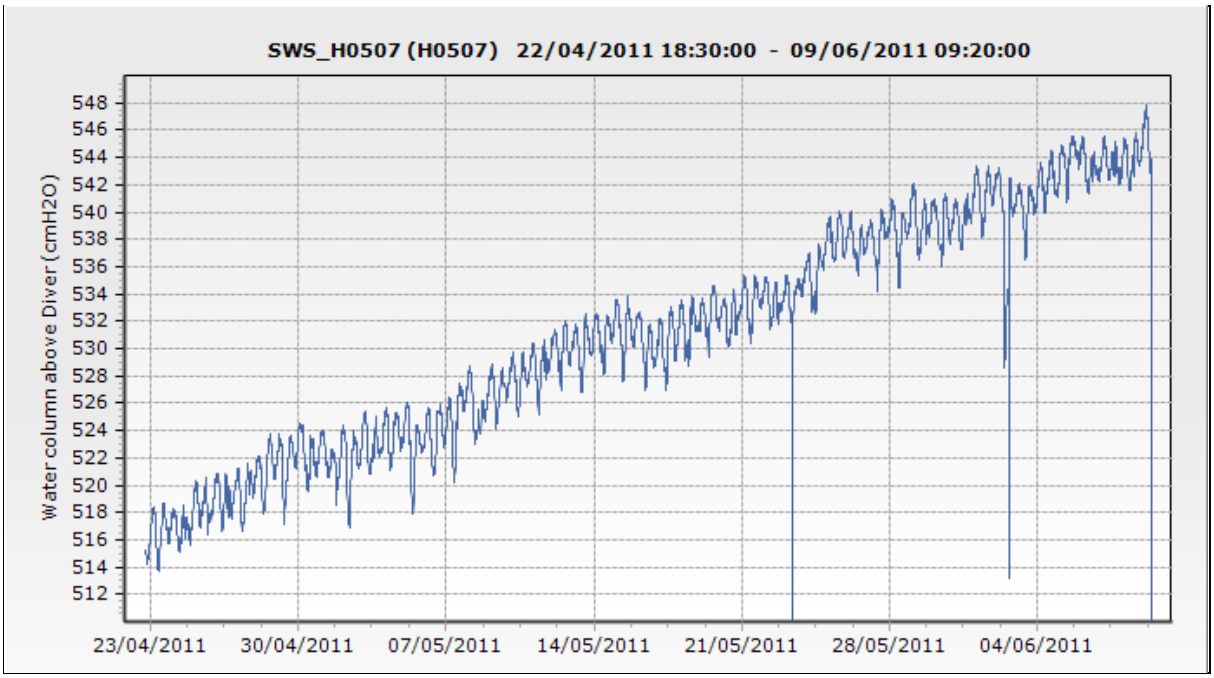

Figure 4.29: Groundwater elevation recorded by Mini-Diver H0507 for a period from 22/04 to 9/06/2011.

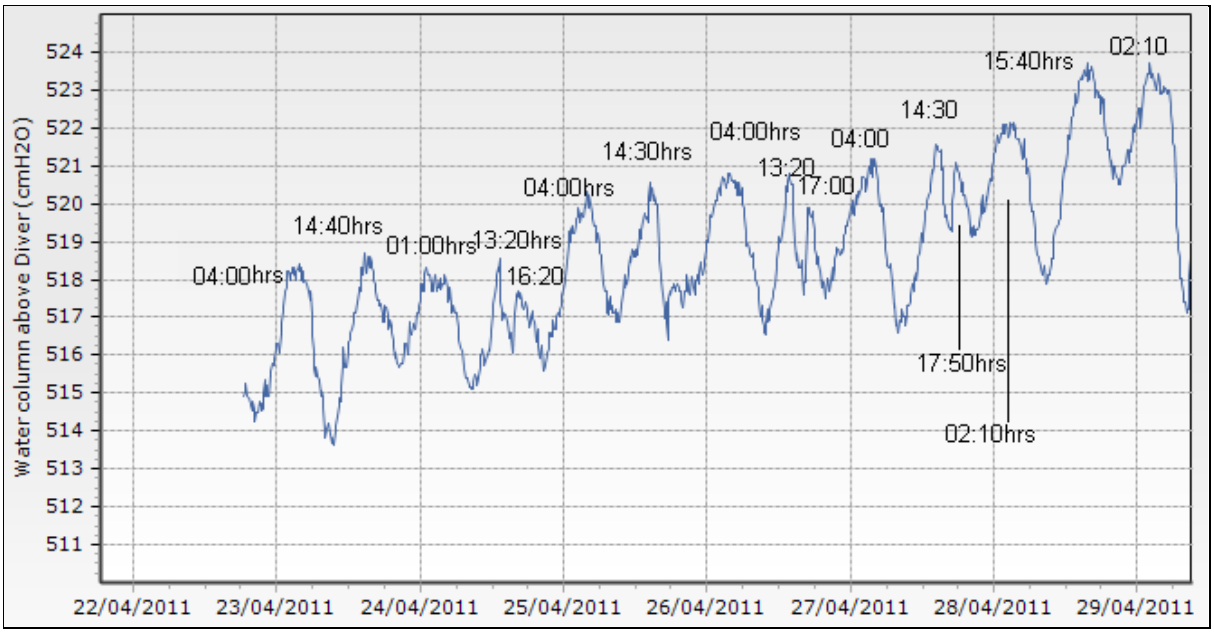

Figure 4.30: A close-up view of Fig. 4.29.

4.3.3.1.5 Continuous groundwater level monitoring in borehole B1 at Gymkhana Golf Club by Mini-Diver (10m) H0461/CTD-Diver K2697 and Mini-Diver (50 m) J02701

Borehole "B1" (Fig. 4.22) located at about 0.22 km from the ocean, was first equipped with Mini-Diver (10m) H0461, which afterwards was replaced by CTD-Diver K2697. Additional to the pressure and temperature measurements, the CTD-Diver is designed to monitor conductivity and is suitable for use in semi-saline water and/or seawater. CTD-Diver is made of ceramic materials that are able to withstand semi-saline water and/or seawater: the Mini-Diver is made of 316L stainless steel which is not suited for semi-saline and/or seawater because it is subject to corrosion/split corrosion (www.eijkelkamp.com).

Figure 4.31: Borehole B1 located at about 0.22 km from the ocean, since 27 February 2011 was equipped with Mini-Diver H0461 for monitoring water level and temperature. The Mini-Diver was replaced by CTD-Diver K6627) on the 7 July 2011.

4.3.3.1.6 Mini-Diver (10m) H0461 in borehole B1 at Gymkhana Golf Club (27/02/2011 - 07/07/2011)

Figs. 4.32 present groundwater elevation measurements by the Mini-Diver H0461 for the period from 27/02/2011 to 07/07/2011. Fig. 4.33(a) is a close-up of Fig. 4.32 showing detail of time sequence for the measurements taken in April/May 2011. Groundwater fluctuates corresponding to the low and high sea tides. During the sea level rise, the pressure from sea level rise pushes the groundwater level up. Two peaks are recognizable per day (Fig. 4.33a): the main, largest peak and a smaller peak. The water elevation varies between 15 and 20 cmH_2O corresponding to the small peaks and the large peaks respectively. Both the large and small peaks occur at varying times (Fig. 4.33b). It is observed that on 30th April/1st May the large peak and small peak occurred at 15:25 hours/03:25hrs whereas in 4th May/5th May the large peak and small peak occurred at 18:10hrs/6:10 hours which makes a total change of 2.45 hours.

The sea tides are not the only factor that affects groundwater level fluctuation. The spring-neap cycle is clearly observed in the close-up figure (Fig. 4.33b). Spring-neap tide cycles are differentiated from the daily tides by their longer cycles which are associated with the

movement of the sun and moon relative to each other. Depending on the position of the moon and/or new/full moon, this leads to either larger than average tides (spring tides) or smaller than average tides (neap tides). During the spring tide and neap tide, the groundwater level is at the highest and minimum respectively and the largest variation occurs between high and low tides (Fig. 4.33b). The variation between high and low tide accounts for a minimum of about 5 cmH_2O and a maximum of about 25 cmH_2O. The alternation of the spring and neap tides is very clear during the month of March (where the rainfall is moderate) comparing to the month of April whereby this alternation is masked due to high rainfall (Fig. 4.33c).

Rainfall is one of the weather factors also affecting groundwater levels. An increase of groundwater level by 1 meter is observed in the month of April (Fig. 4.33(c)-i). Major rainfall occurs between March and May (Fig. 4.33(c)-ii). April corresponds with the peak of rain season with the highest amount of rainfall of 75.18 mm occurring on 20th April 2011. The beginning of June is the start of the dry period and water level starts to decline. However, there is an unusually high rise in groundwater elevation of 2.7 m occurring between 4th and 14th June, 2011, during the time when rainfall is zero. This is likely to be caused by the sewage pond which is located nearby. During the monitoring period, it was observed that a sewage pond is located at about 0.065 km from borehole "B1". The sewage pond at Gymkhana indicates that the aquifer can be artificially recharged. However, the wastewater for aquifer recharge needs to be treated first to ensure the water does not result in health effects, and to prevent polluting the aquifer.

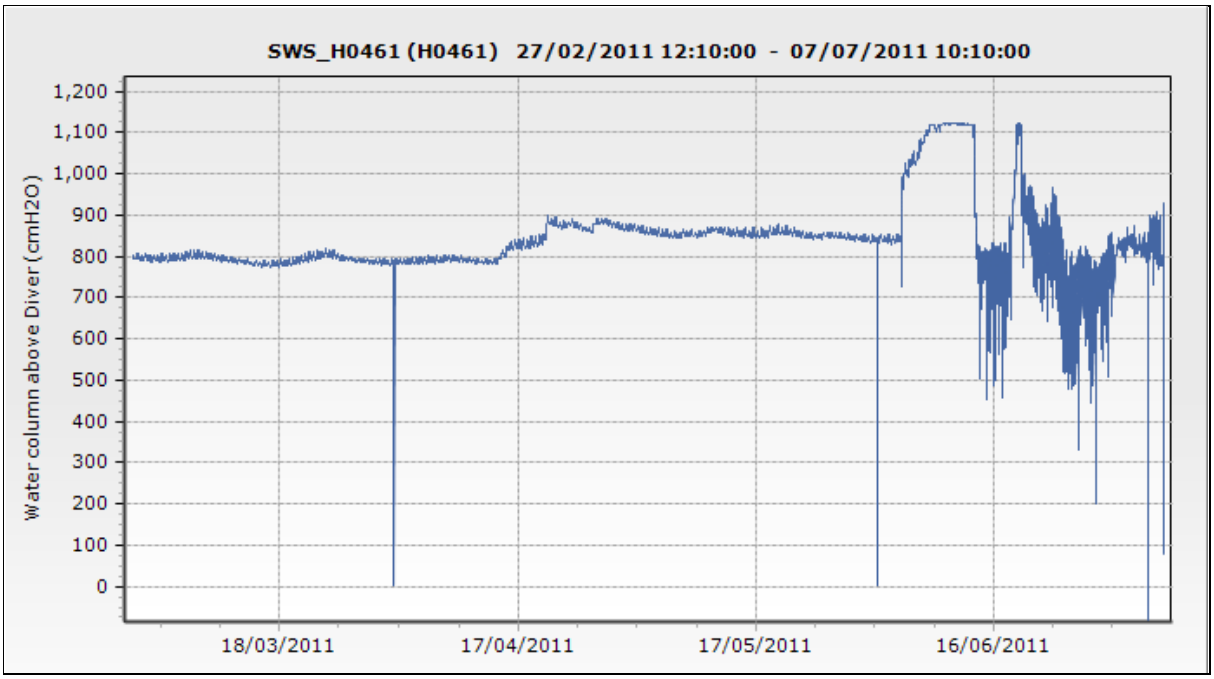

Figure 4.32: Measured groundwater elevation by Mini-Diver H0461 for a period of 27/02/2011 to 07/07/2011.

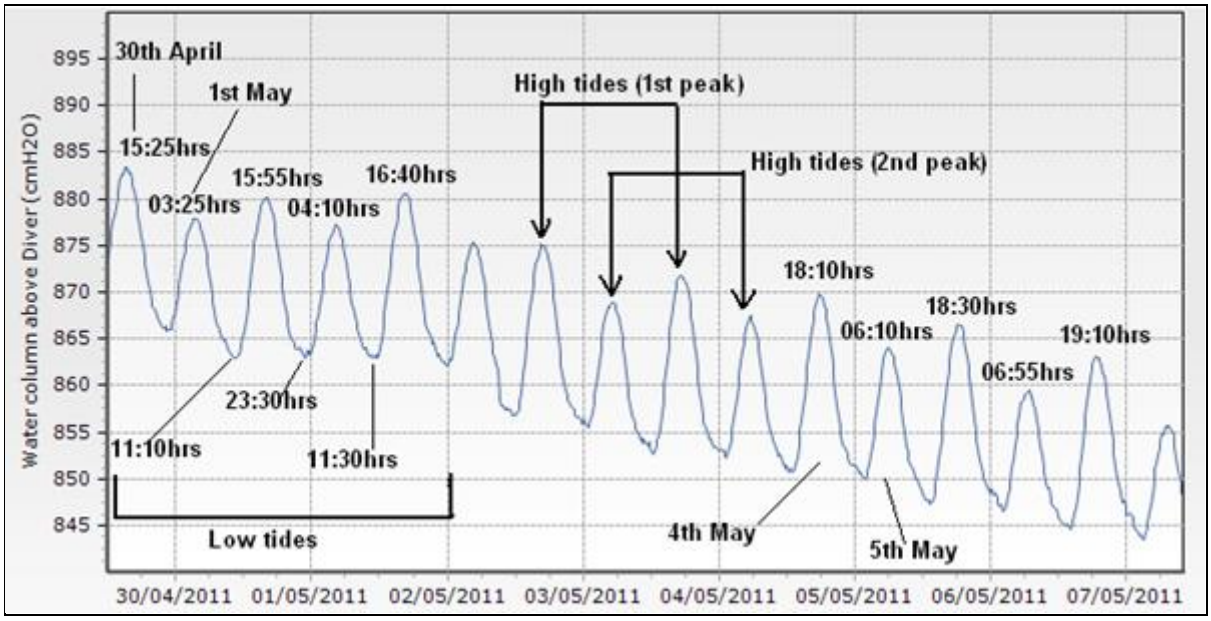

Figure 4.33(a): Close-up view of Fig. 4.32 showing detail of time sequence of Mini-Diver H0461.

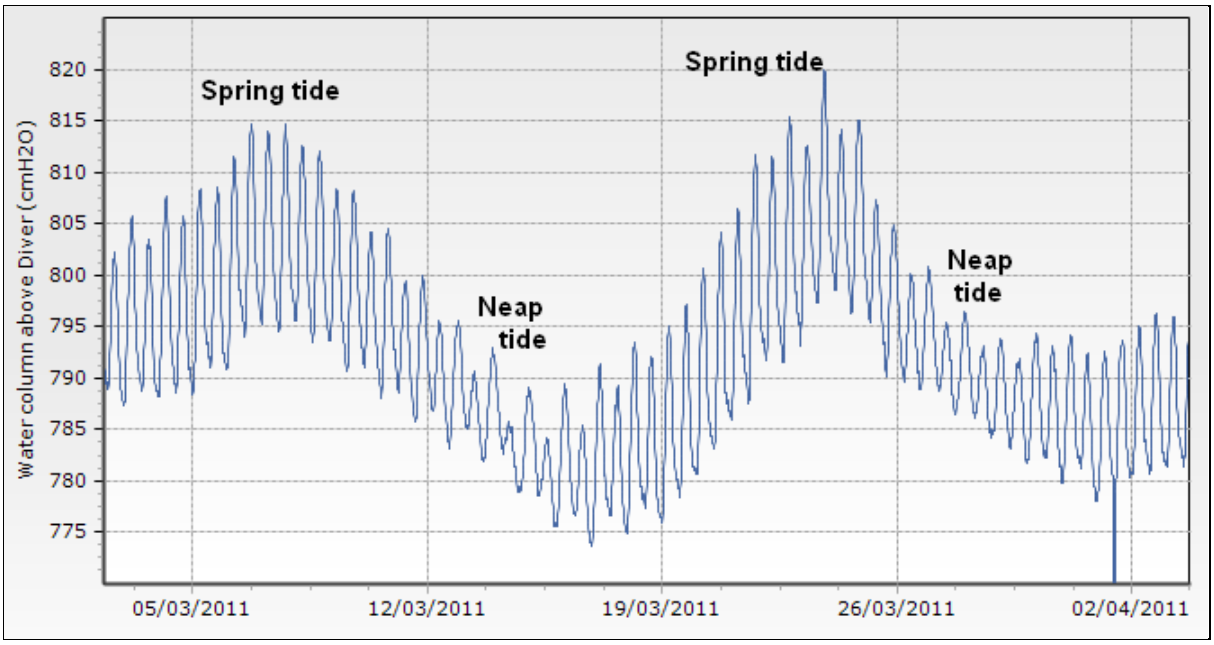

Figure 4.33(b): Close-up view of Fig. 4.23.

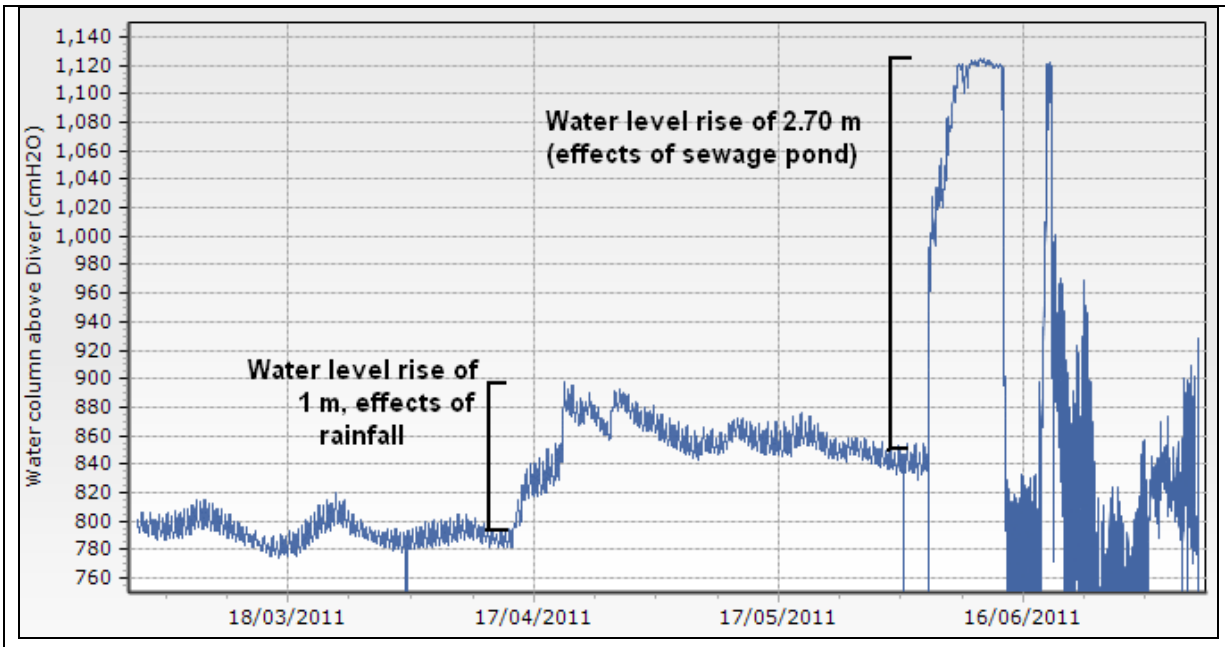

(i)

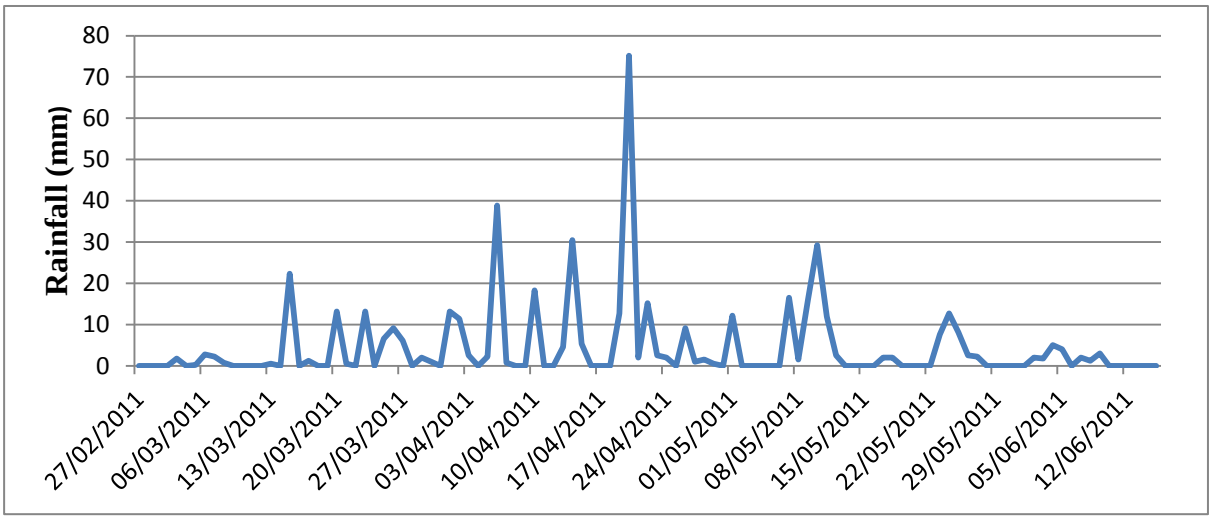

(ii)

Figure 4.33(c): (i) Close-up of Fig. 4.23 showing detail of time sequence of Mini-Diver H0461, (ii) Rainfall data monitored at Mnazi Mmoja primary school with a focus for a wet period of rainfall (March – May).

4.3.3.1.7 CTD-Diver K6627 in borehole B1 at Gymkhana Golf Club (07/07/2011 – 24/06/2012

Fig. 4.34 presents groundwater elevation measurements by the CTD-Diver K6627. This is the continuation of the measurement by Mini-Diver H0461 (discussed above) which starts from 07/07/2011 to 24/06/2012. Daily tides and the spring-neap tides cycles can clearly be observed in Fig. 4.34(a) which is a close-up of Fig. 4.34. On the other hand, the tidal effect in borehole "B1" seems to create conductivity variation: for ocean storm surges, high tides result in higher sea-levels, and the conductivity in the well increases. These elevated conductivity levels fluctuate in correspondence with the tidal phases (Fig. 4.34b). Conductivity fluctuated between 2.151 mS/cm and 2.35 mS/cm (Fig. 4.34b). When water of low conductivity is recharged into the aquifer, this causes the conductivity to go down (Fig. 4.34b). However, according to Levanon et al. (2012) in a research conducted at the coastal aquifer of Israel, the amplitude of electrical conductivity (EC) fluctuations is determined by the length of screens. Long screens (contrary to short screens) cause high distortion in EC measurements due to vertical flow in the boreholes as a result of high sea tides: in direct measurements in the aquifer through buried EC sensors, almost no fluctuations were found (Levanon et al., 2012).

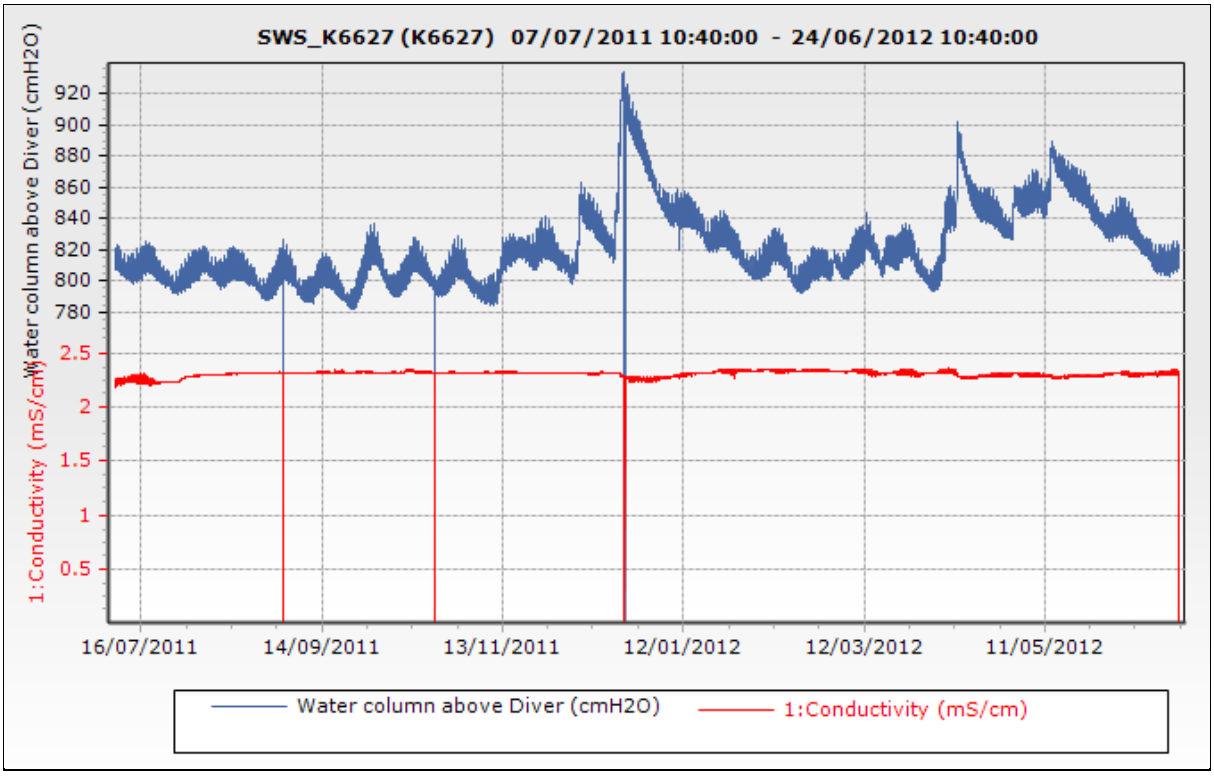

Figure 4.34: Groundwater elevation recorded by CTD-Diver K6627 for a period from 07/07/2011 to 24/06/2012.

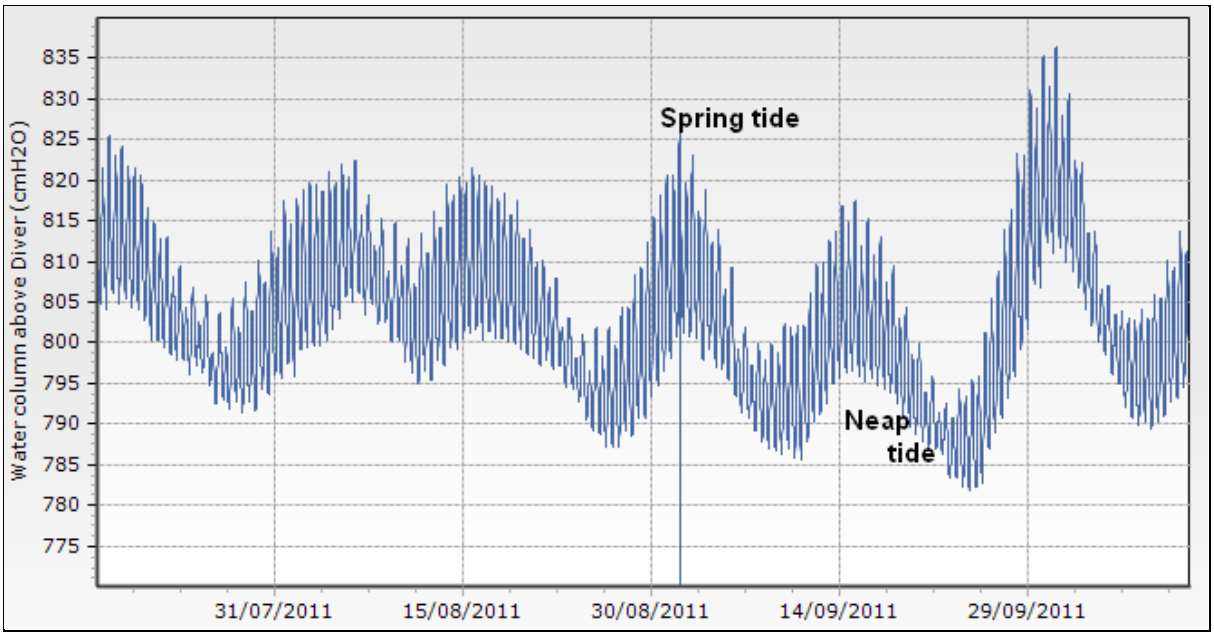

Figure 4.34(a): Close-up view of Fig. 4.34.

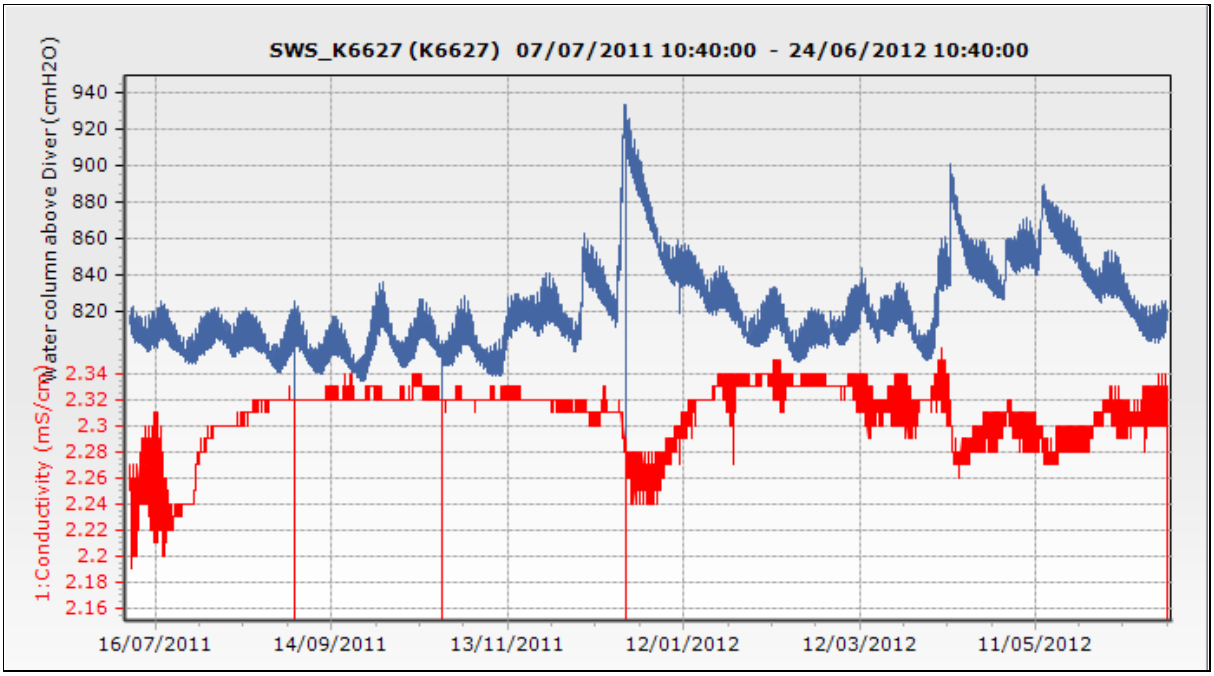

Figure 4.34(b): Electrical conductivity (mS/cm) and groundwater elevation (cmH2O) recorded by CTD-Diver K6627 in monitoring borehole B1.

Groundwater recharge in the study area is associated with the short rainy season (November-December) and the long rainy season (March-May) (Fig.4.34(c)-ii). However, the water level rise of about 1.14 m in December 2011 (Fig. 4.34(c)-i) was not caused by a normal rain, instead by the effect of flood which occurred on 20-22 December, 2011, the heaviest rains in

57 years record, which devastated many areas of the city. The flooding caused over 20 casualties and left over 5,000 people homeless.

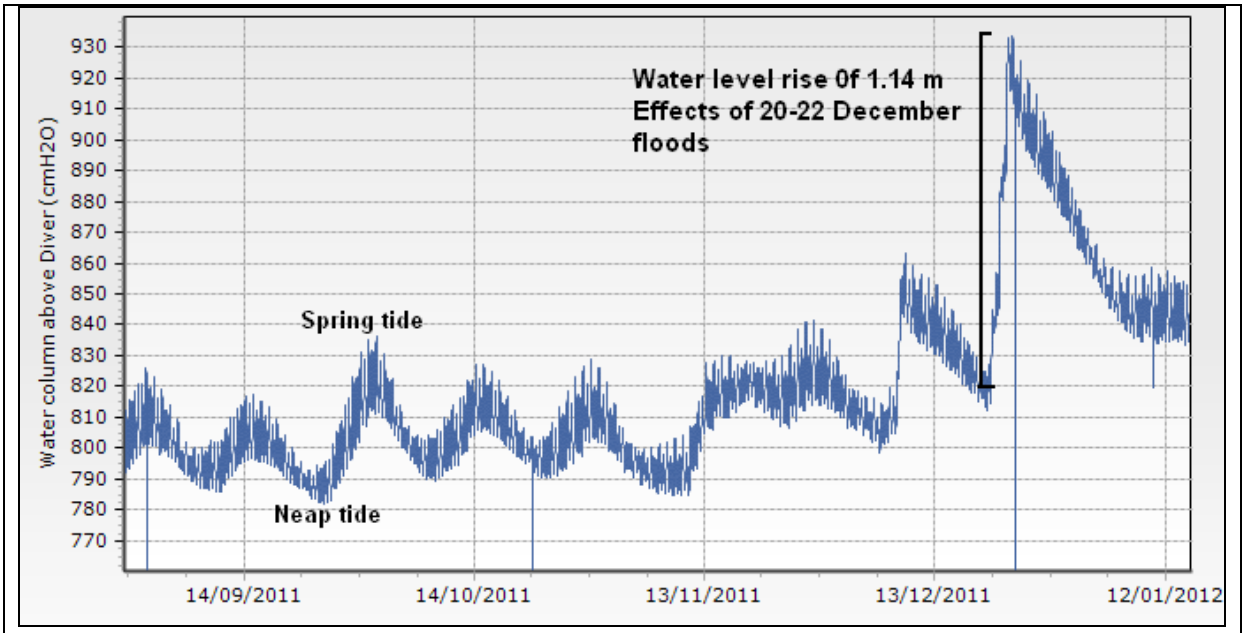

(i)

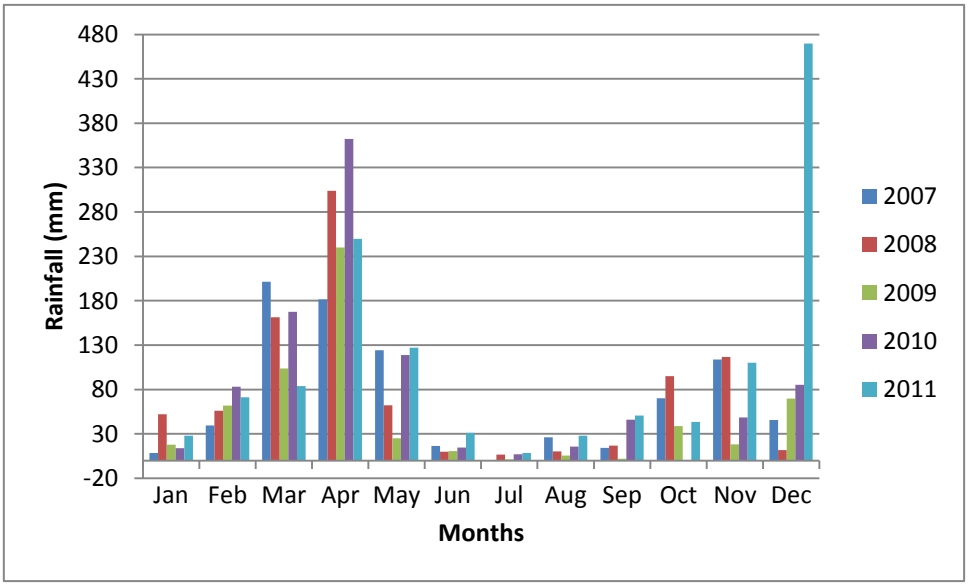

(ii)

Figure 4.34(c): (i) Close-up of Fig. 4.25 showing detail of time sequence of CTD-Diver K6627, (ii) Monthly rainfall average data for the last 5 years showing the effect of flood in Dec 2011.

4.3.3.1.8 Continuous groundwater level monitoring in borehole B2 at Gymkhana Golf Club by Mini-Diver (50 m) J02701

Fig. 4.35 shows production borehole and groundwater monitoring borehole (B2) at Gymkhana Golf Club (GGC). GGC depends on groundwater for irrigation, washing and cleaning. Fig. 4.35(a) presents the hydrograph of groundwater table daily fluctuations due to the effect of pumping. Measurements recorded by Mini-Diver J2701 for a period of one year between: i) 22 June to 6 December 2011, and ii) 10 January to 24 June 2012. Fig. 4.35(b) is a close-up view of Fig. 4.35(a)-i indicating groundwater drawdown occurring during pumping and water recovery when pumping stops. Monitoring borehole "B2" which is also close to the ocean (0.48 km) does not show clear tidal effects comparing to borehole B1 (0.22 km from ocean). Curve characteristic for the former is mostly affected by pumping (Fig. 4.35(b).

Figure 4.35: Gymkhana Golf Club production borehole covered by a concrete slab (a fellow researcher standing right on top of it) and monitoring borehole B2 (installed with Mini-Diver (50m) J02701).

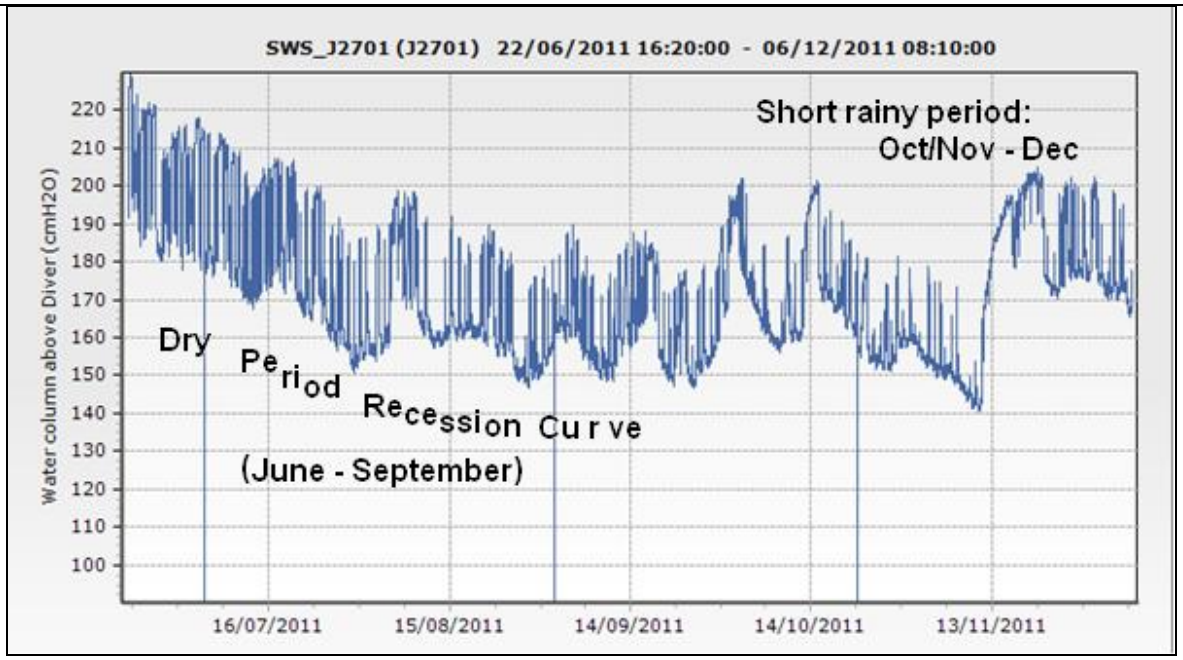

(i)

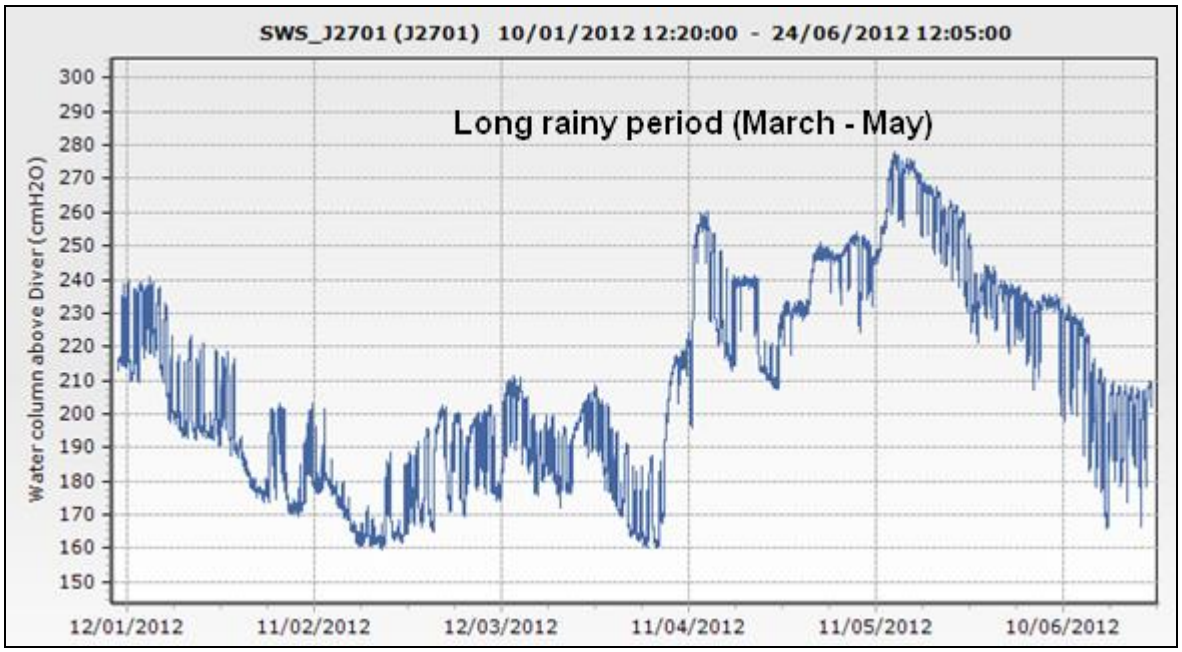

(ii)

Figure 4.35(a): Groundwater monitoring at Gymkhana Golf Club showing hydrograph of groundwater table daily fluctuations due to the effect of pumping. Measurements recorded by Mini-Diver J2701 for a period of one year between: i) 22 June to 6 December 2011, and ii) 10 January to 24 June 2012.

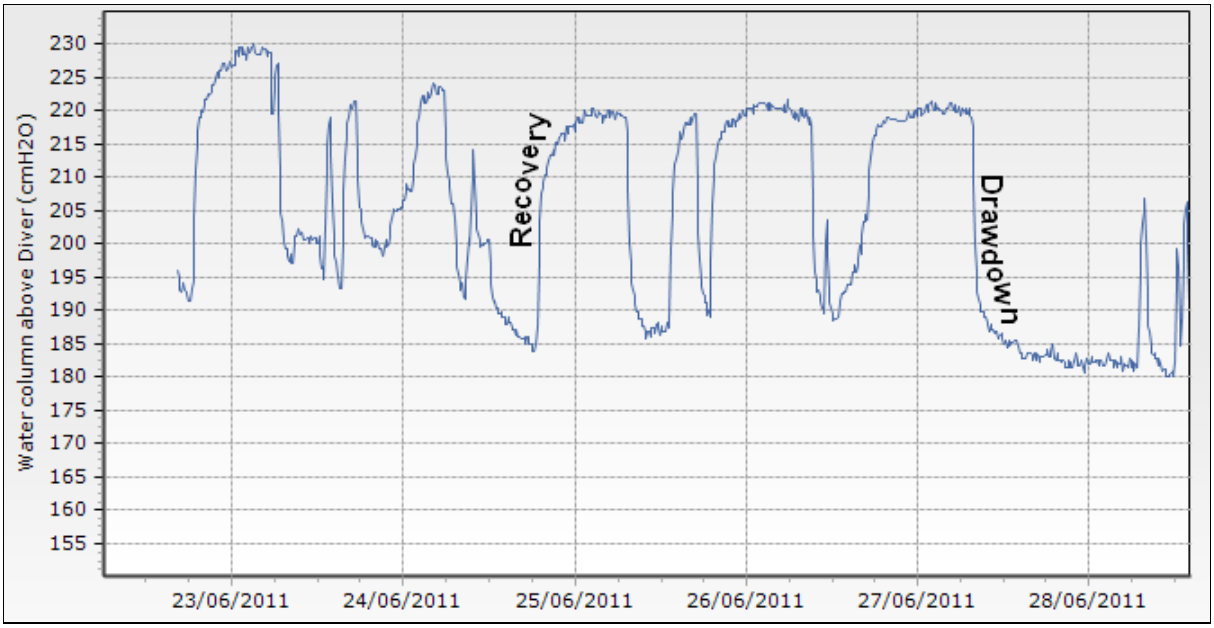

Figure 4.35(b): Close-up view of Fig. 4.35(a)-i indicating groundwater table daily fluctuations due to the effect of pumping (groundwater discharge) and recovery (groundwater recharge). The location of borehole "B2" is indicated on Fig. 4.4.

4.3.3.1.9 Continuous groundwater level monitoring in borehole B3 at Coca-Cola Company by Mini-Diver (10m) K2697

Fig. 4.36 presents groundwater level fluctuation measurements recorded (by the Mini-Diver K2697) in monitoring borehole "B3" at Coca-Cola Cmpany, 1.5 km from the ocean. The measurements cover the period from 08 July 2011 to 13 January 2012 which coincide with the dry period (June to September) and the short rainy period (October/November to December). Groundwater level fluctuations reflect very well the dry time (recession curve) and rainy period concomitant with increase of water level. On the other hand, the semi-diurnal tidal signal and spring-neap tidal cycle are clearly observed in the close-up view figures (Fig. 4.36a and Fig.4.36b). Just like it was seen in other monitoring boreholes, the former are the daily tides whereas the latter are longer cycles which coincide with the movement of the sun and moon relative to each other. Depending on the position of the moon and/or new/full moon, this leads to either larger than average tides (spring tides) or smaller than average tides (neap tides). The maximum amplitude between high and low tide is 17.5 cmH_2O with the minimum amplitude of 2 cmH_2O.

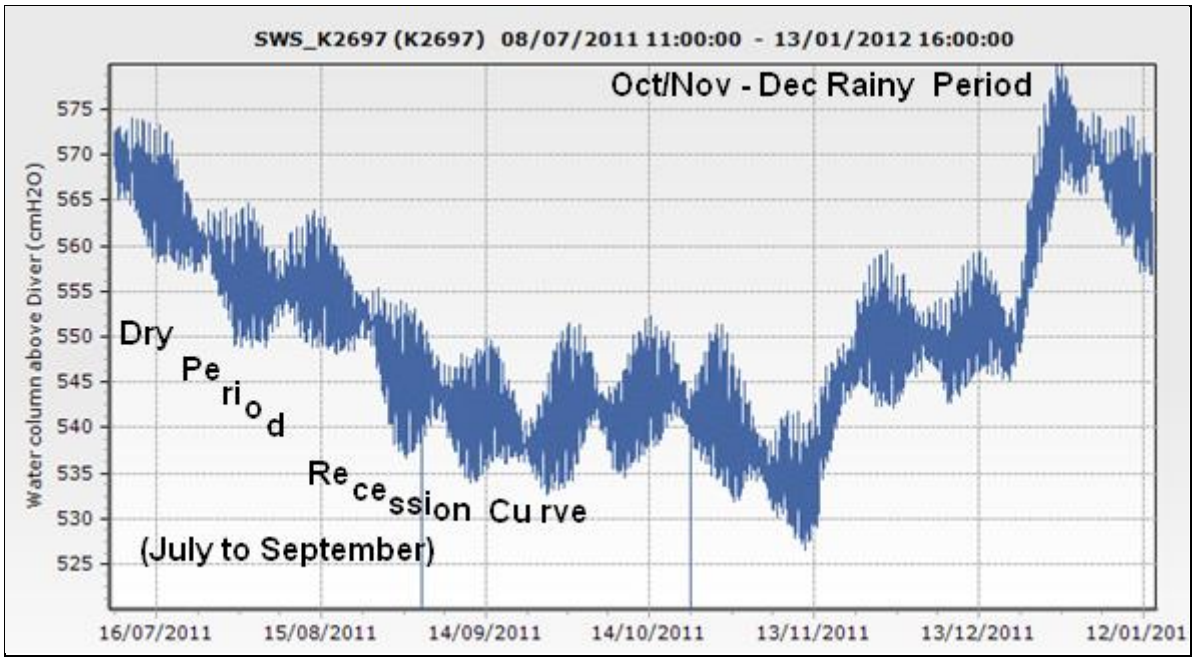

Figure 4.36: Groundwater level fluctuation recorded at Coca-Cola Company by the Mini-Diver K2697 in monitoring borehole "B3" for a period from 08/07/2011 to 13/01/2012.

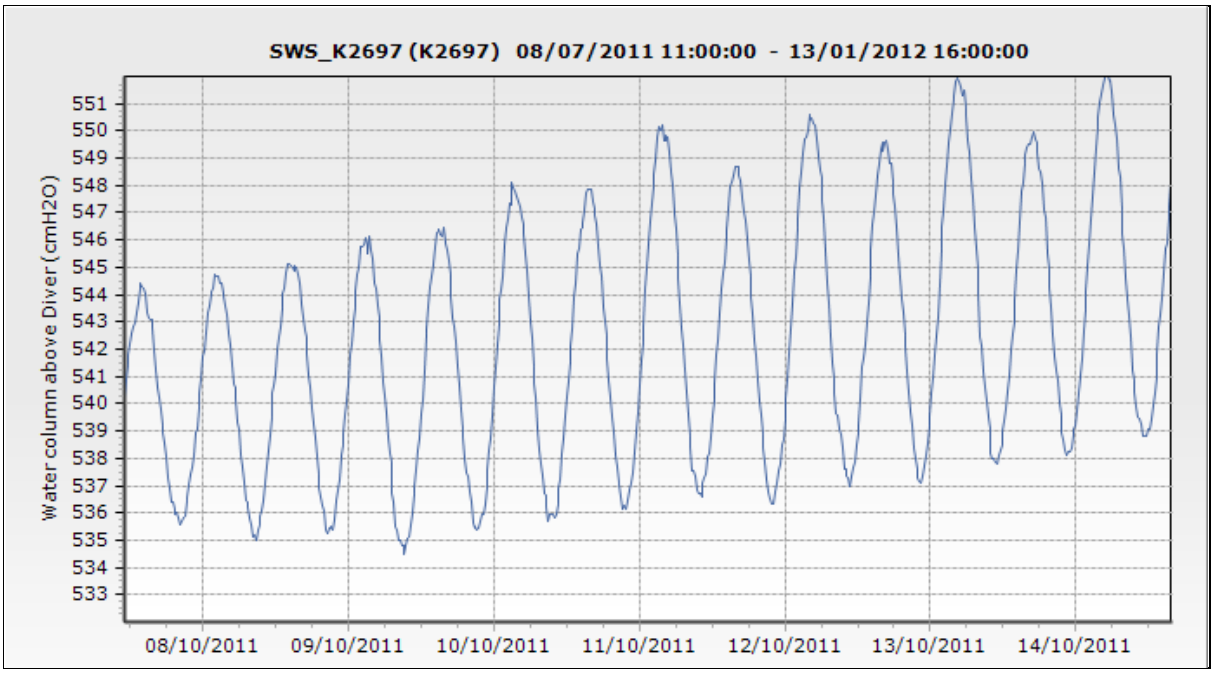

Figure 4.36(a): Close-up view of Fig. 4.36 indicating the semi-diurnal tidal signal.

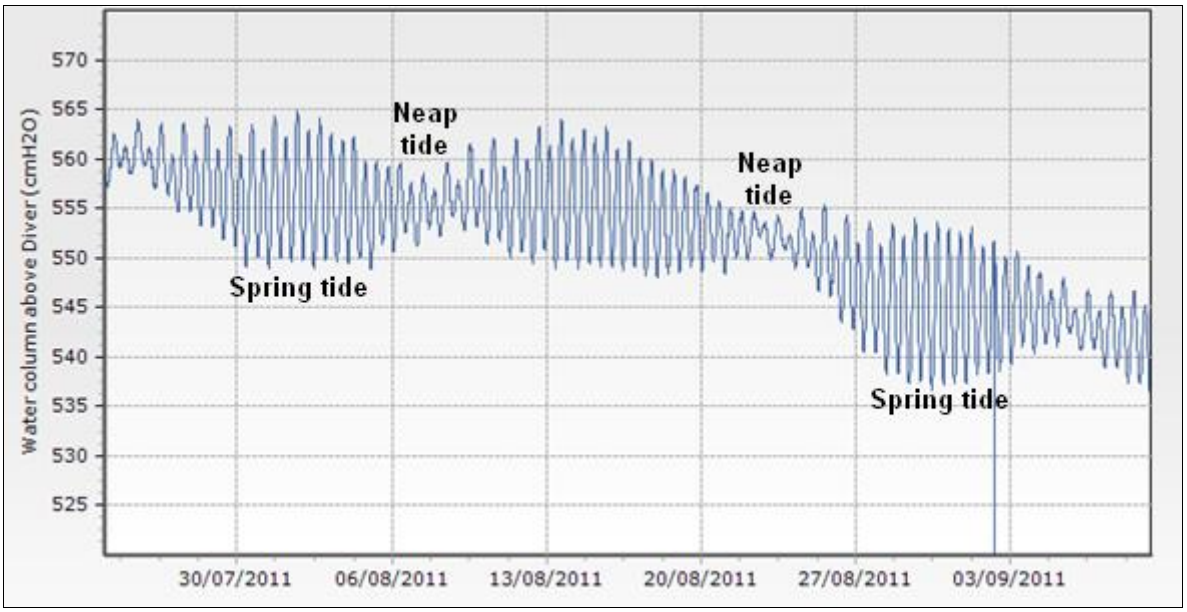

Figure 4.36(b): Close-up view of Fig. 4.36 indicating the spring-neap tidal cycle.

4.3.3.1.10 Continuous groundwater level monitoring in borehole B11 at Dar es Salaam Bunge Offices by Mini-Diver (10m) K7351

Fig. 4.37 presents groundwater level fluctuation measurements recorded (by the Mini-Diver K7351) in monitoring borehole "B11" at Dar es Salaam Bunge Offices. The measurements cover the period from 13 January to 19 April 2012 which coincide with the short dry period (January and February) and long rainy period (March to May). Groundwater level fluctuations reflect the short dry period (recession curve) occurring in the months of January and February and the long rainy period from March to May.

The semi-diurnal tidal signal and spring-neap tidal cycle can still be identified but are not clear like at the monitoring point at Coca-Cola Company. Fig. 4.37(a) and Fig. 4.37(b) are the close-up view of Fig. 4.37 indicating the spring-neap tidal cycle and semi-diurnal tidal signal respectively. The maximum amplitude between high and low tide is 42.5 cmH_2O with the minimum amplitude of 2.5 cmH_2O.

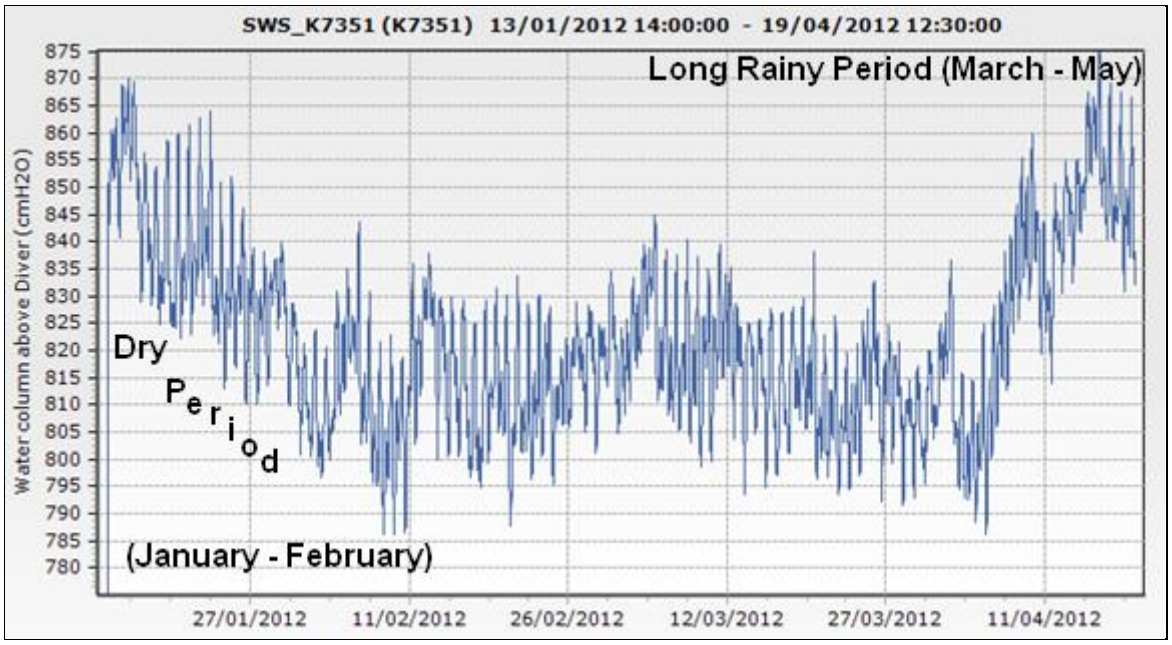

Figure 4.37: Groundwater level fluctuation recorded at Dar es Salaam Bunge Offices by the Mini-Diver K7351 in monitoring borehole "B11" for a period from 13 January to 19 April 2012.

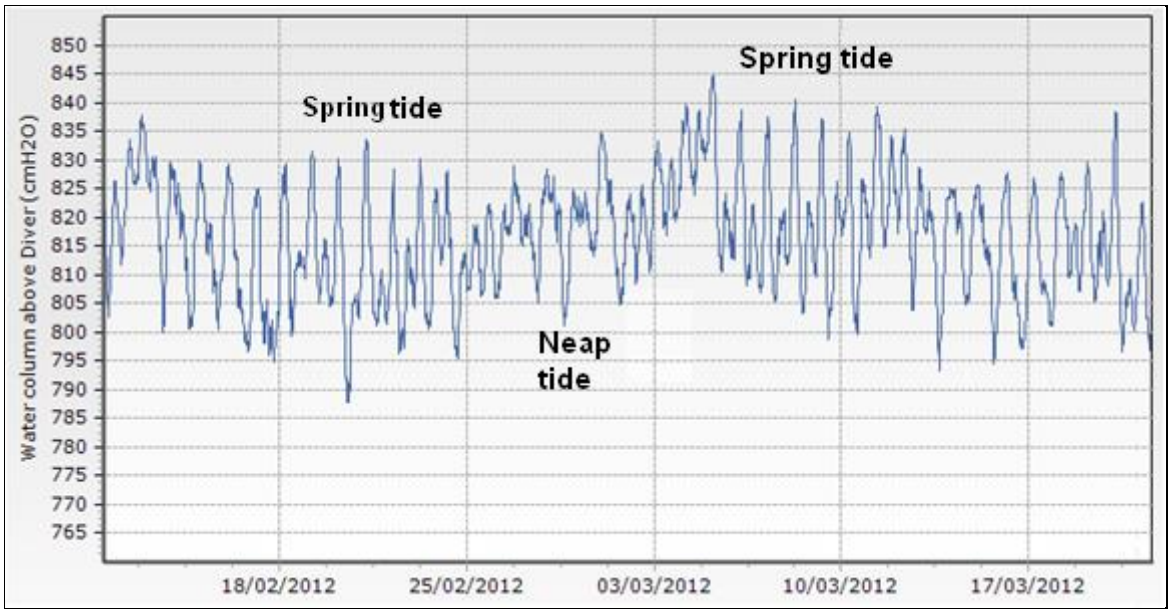

Figure 4.37(a): Close-up view of Fig. 4.37 indicating the spring-neap tidal cycle.

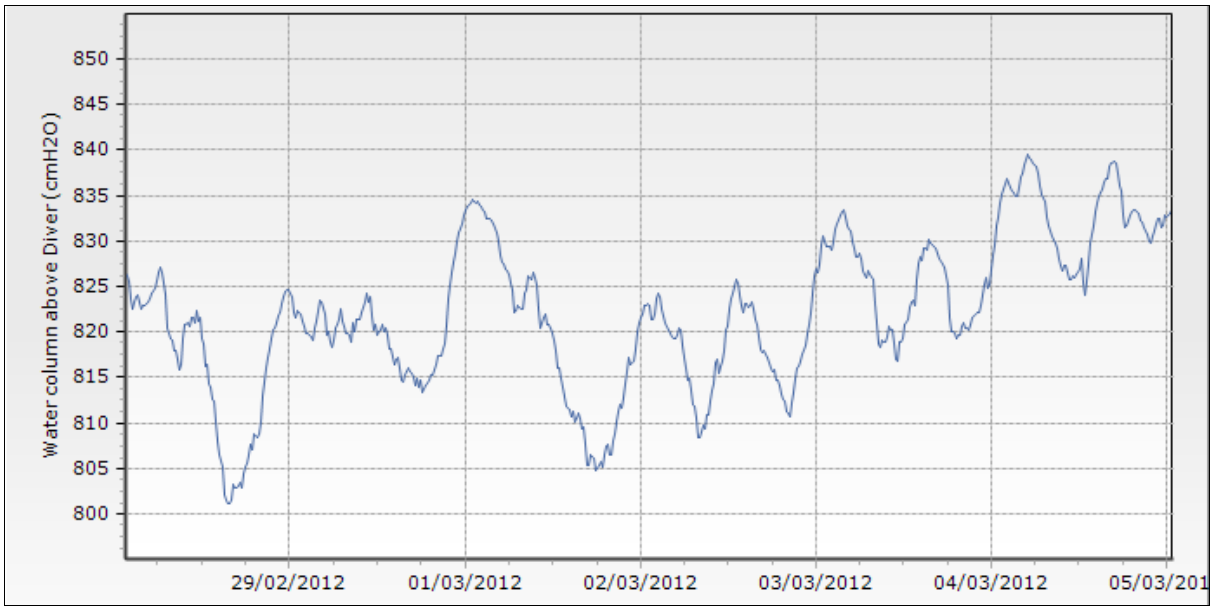

Figure 4.37(b): Close-up view of Fig. 4.37 indicating the semi-diurnal tidal signal.

4.3.3.2 Discussion and interpretation

From the observations above, the aquifer water levels are constantly changing in response to both natural (rainfall/floods, tides due to gravitational forces of the earth and the moon, and evapotranspiration cycle) and human (i.e. pumping) influences.

4.3.3.2.1 Natural influences

RAINFALL EFFECTS

Rainfall is one of the weather factors that can affect groundwater levels. Groundwater recharge occurs naturally where the earth materials are permeable enough to allow water to move downward through them. The study area is dominated mainly by sand materials which allow water provided by rainfall to move downward from the land surface to the water table. Direct inputs of recharge water due to rainfall cause obvious rises of groundwater levels as it was observed in most of the monitoring wells. The most significant water level changes due to recharge occur during the main rainy season (March to May) where precipitation is generally greatest and evapotranspiration is low. For example, groundwater level at Gymkhana borehole B1 (Fig. 4.33(c)-i) in a week's time rose by 1 meter during the month of April which corresponds with the peak of the rain season. The unusual groundwater level rise by 1.14 meter in December 2011 during the short rainy season, as indicated by CTD-Diver K6627 (Fig. 4.34(c)-i) installed in borehole B1, is interpreted to be due to heavy rainfall occurring in three days (20^{th} – 22^{nd} December) consecutively, which caused floods in Dar es Salaam City.

TIDAL AND EVAPOTRANSPIRATION EFFECTS

Precipitation is not only the weather aspect that affects groundwater levels. Groundwater fluctuation can also be caused by the atmospheric pressure changes as the result of earth's gravitational attraction of air in the atmosphere. Besides, coastal aquifers are affected to varying degrees by the rise and fall in sea level as the tide changes every six hours (Fig. 4.33a). In addition to daily tides, groundwater level monitoring data display other cycles, which are interpreted to be related with the movement of the sun and the moon relative to each other causing spring and neap tides (e.g. Fig.4.36b).

Clear tidal effects may be observed when wells are not influenced by factors such as nearby heavy pumping and high groundwater recharge. Where these mentioned factors are applicable, the smooth sine-wave curve characteristic of tidal effect is lost or camouflaged. Monitoring data indicate that boreholes located at larger distance from the ocean display more clearly spring tides and neap tides than boreholes close to the ocean. This can be well seen for monitoring point at B3 (eg. Fig. 4.36b) which is located at 1.5 km from the sea, indicating very clearly the spring-neap tidal cycle comparing to the boreholes B1, B2 and B11 located at less than 0.5 km from the sea. Unlike the spring-neap tidal cycle, the amplitudes of both the high and low tides decrease away from the ocean. This is due to the difference in frequency of cycles: lower frequency signals will penetrate further as they are not muffled as much as high frequency signals (De Witte, 2012).

The recorded measurements at point "179" located about 0.5 km from Mzinga Creek and 7 km away from the main ocean, indicate irregular peaks occurring at varying times, except for the peaks which occur repeatedly at 04:00 hrs and 14:30hrs. The monitoring well is located at Temeke Municipal Garden. This garden has dense vegetation which includes some grass and lots of ornamental plants such as hibiscus, bougainvillea, roses, etc, as well as nursery sites for fruit trees such as oranges, mango, papaya, coconut etc. The erratic trend of groundwater measurements observed has been influenced by evapotranspiration (because of vegetation) and daily water irrigation whereby part of water is recharging back the aquifer: the source of irrigation water is a wide (ca. 9 m^2) shallow well located within the garden draining water from unconfined aquifer. On the other hand, interpretation of the measurements at point "95" located at Zanaki Secondary School which showed the shift in time of both high maxima and lower maxima peaks should take account on the factor of tidal effect and a little bit the effect might be caused by car washing which was observed taking

place near the well during the end of monitoring period. Moreover, the influence of the tidal effect is a strong factor to be taken into account as this well is located at the same distance (1.5 km) from the ocean just as the well "B3", which has shown a very clear sine-wave curve characteristic of tidal effect. However, the location of these wells is located at different lithologies. Monitoring point "B3" is situated in the lithology dominated by limestone whereas monitoring borehole at "95" is constructed in the lithology dominated by sand materials. Porous nature of limestone seems to communicate better the effect of tides comparing to sand.

At monitoring point "MNAZ_1" the situation was somehow different as the first maxima peaks indicate constant occurrence at 03:45 hrs but with the lower maxima peaks occurring at varying times though with a clear trend of shifting in time. Due to the constant occurrence of the first maxima peaks, the influence of evapotranspiration is considered to be an important factor, additional to the tidal effect which is likely to be associated to the cause of the shifting of lower maxima peaks. "MNAZ_1" is located about 350 m behind "95" (at Zanaki Sec School) in the direction away from the ocean. Since evapotranspiration is high in the day time and little at night, one needs to know the declining trend of groundwater level during the day time, and recovery at night. According to Gribovszki (2010) early morning maximum and afternoon minimum of the groundwater level are distinctive for a diurnal variation of the groundwater level induced by evapotranspiration. A study by Dejager (2011) in Dar es Salaam indicates the possibility of tidal peaks being superimposed by the evapotranspiration especially for the tidal peaks occurring in the morning. A simulation of the possibility of superposition of the evapotranspiration peak and tidal peaks at "MNAZ_1" was proven by Van Camp (Fig. 4.38).

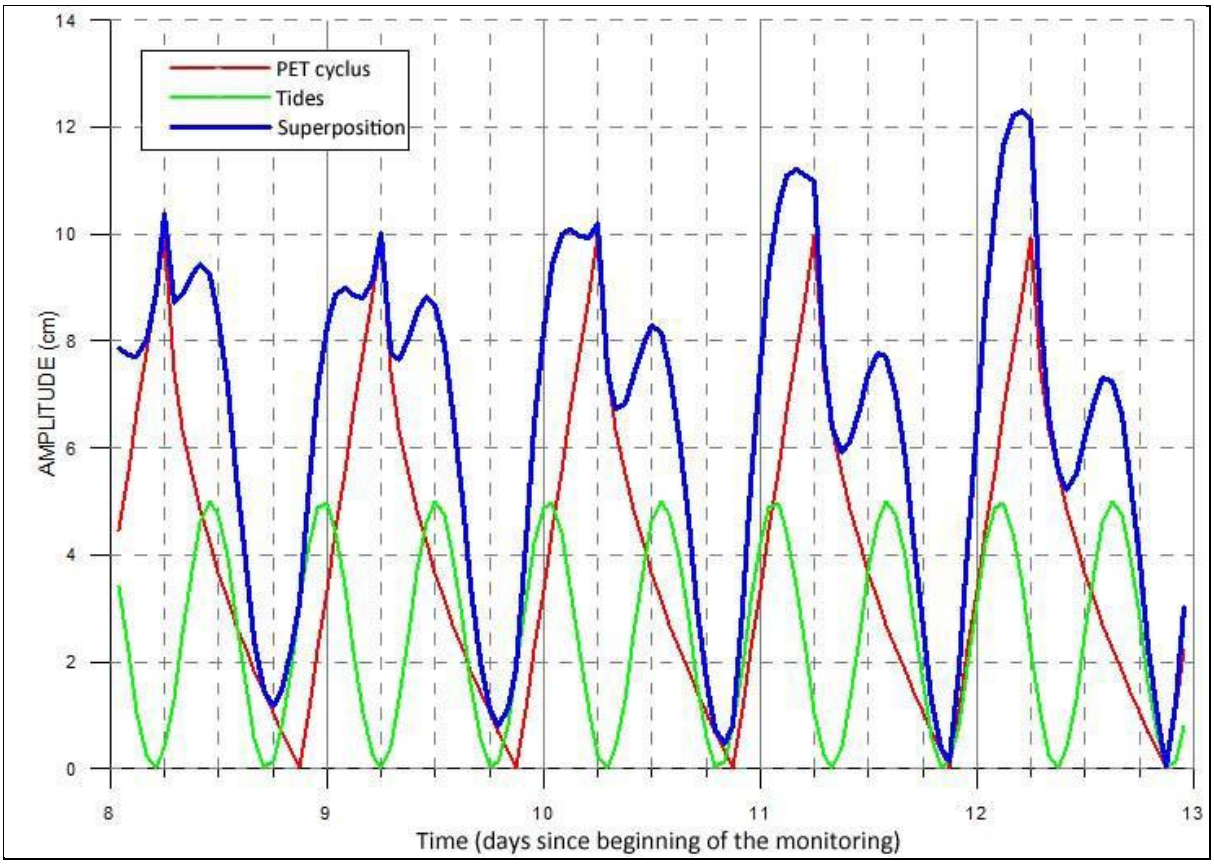

Figure 4.38: Simulation of the superposition of the influence by the evapotranspiration and tides in the monitoring series at Mnazi Mmoja Primary School (by Marc Van Camp cited by Dejager, 2011).

4.3.3.2.2 Human influences

The human factor is one of the most dramatic effects on groundwater level changes associated with pumping. When groundwater is pumped as it is the case in the study area (Fig. 4.35a), groundwater is drawn out of the aquifer causing decline of water level. Human influence to groundwater changes was also seen in Diver data for monitoring borehole B1. A sharp rise of groundwater water level of 2.7 m (Fig. 4.33(c)-i) is associated with improper sewage disposal near borehole "B1", leading to recharging the aquifer.

4.4 Conclusions and recommendations

4.4.1 Conclusions

The findings of this study are a significant step in the understanding of Dar es Salaam Quaternary coastal aquifer (DQCA). The study quantified the variability of transmissivity and hydraulic conductivity. Analysis results of ten (10) pumping test data show the average

transmissivity and hydraulic conductivity values of 138.52 m^2/d and 4.27 m/d respectively for the upper unconfined aquifer. The semi-confined aquifer showed average value of 79.0 m^2/d and 1.7 m/d for transmissivity and hydraulic conductivity respectively. The transmissivity and conductivity values vary reflecting the type of lithology in which the well is constructed. Transmissivity and hydraulic conductivity values for the unconfined aquifer range from 24.45 m^2/d to 296.58 m^2/d and from 0.76 m/d to 8.47 m/d respectively. Transmissivity and hydraulic conductivity values for the semi-confined aquifer range from 13.75 m^2/d to 130.44 m^2/d and from 0.43 m/d to 2.61 m/d respectively.

The water table contour maps show the elevation and configuration of the water table at the time the measurements were taken. The highest water levels are found in the west and southwest of the study area. The groundwater flows toward northeast and east, where the ocean represents the natural discharge area. The direction of groundwater flow is similar in both unconfined and semi-confined aquifers. Piezometric data indicate a general lowering of the piezometric level especially in areas close to the coastline.

In the study area groundwater levels change for many reasons. Some changes are due to natural phenomena and others are caused by human activities. The influence of evapotranspiration is more important in the wells located at Mnazi Mmoja Primary School and Temeke Municipal Garden. Fluctuations of the groundwater level for boreholes located near to the coastline indicate that variations of sea level affect the groundwater level directly. The effect of the tides is strong near the coastline and becomes weak inland. Apart from the influence of evapotranspiration and tides, groundwater resources are mostly at great risk from the results of human activities, and an increase in population which leads to high demand of fresh water. Improper disposal of sewage was observed in the study area to recharge the groundwater, and is a potential source of groundwater contamination.

Monitoring data show a strong relationship between the rainfall amount and groundwater level. At the onset of the major rainy season, the groundwater level is low and as the season sets in, the groundwater level rapidly increases. The use of Divers in this research for groundwater level monitoring has proven to be extremely valuable. Interpretation of data for daily fluctuation of groundwater level identified changes in water levels caused by major rainfall events, tides, evapotranspiration, and human activities. The provision of continuous time-series water level measurements is a significant improvement and has enhanced

understanding of groundwater resources in the study area. Monitoring data show a strong relationship between the rainfall amount and groundwater level. At the onset of the major rainy season, the groundwater level is low and as the season sets in, the groundwater level rapidly increases. The fluctuations of the groundwater level for boreholes located near to the coastline indicate that variations of sea level affect the groundwater level.

4.4.2 Recommendations

This study recommends further investigation of water level measurements in the area by installation of piezometers and regular measurements. This will help to control the groundwater exploitation. Currently, groundwater monitoring is considered inadequate to provide data needed to support groundwater management. Sustainable abstraction from the aquifer system will require monitoring boreholes to appropriately monitor potential saltwater intrusion, particularly near the coastline. More pumping tests are needed to have a better understanding of aquifer properties.

5 GEOPHYSICAL INVESTIGATION

5.1 Introduction

The geoelectrical technique is widely used in groundwater studies to correlate between the electrical properties of the geologic formations and their fluid content (Zohdy et al., 1974). The resistivity of materials depends on many factors such as groundwater salinity, saturation, aquifer lithology and porosity (Lashkarippour et al., 2005). Many researchers in different parts of the world have reported on the effectiveness of the electrical resistivity method in the investigation of groundwater related issues (Walraevens et al., 1993; Walraevens et al., 1994; Kumar et al., 2006; Vandenbohede et al., 2010; Bakundukize, 2012; Obikoya and Bennell, 2012). This chapter reports on the application of a resistivity survey in identifying fresh-, brackish-, and saline-water zones in Dar es Salaam Quaternary coastal aquifer (DQCA).

For the effective management of groundwater resources in the study area, the dynamic nature of the saltwater interface needs to be investigated to properly assess seawater intrusion under different management approaches. To achieve this, an in-depth analysis of seawater intrusion was carried out using the integrated application of the resistivity survey, hydrogeological investigation and hydrogeochemical parameters of groundwater to identify fresh-, brackish-, and saline-water zones in the study area. This chapter addresses as well the lack of any scientific groundwater resources management of the study area by the local water authorities. The results of this study contribute knowledge and information to the wider-ranging implementation of the Millennium Development Goals (MDGs) of sustainable clean water for all.

5.2 Materials and methods

5.2.1 Background on geophysical resistivity method

The resistivity method generally allows mapping subsurface zones and makes it possible to determine the depths and thicknesses of different formations. The field technique for collecting resistivity data involves measuring the potentials between one electrode pair while transmitting direct current (DC) between another electrode pair. The depth of penetration is proportional to the separation between the electrodes in homogeneous ground; varying the electrode separation provides information about the stratification of the ground (Reynold,

1997; Kirsch 2009). Fig. 5.1 is a schematic diagram showing the basic principle of DC resistivity measurements. The resistivity of the ground is measured by sending current into the ground at the current electrodes (A and B) and the corresponding potential difference is measured between the potential electrodes (M and N), which is then converted to apparent resistivity value.

Resistivity surveys typically involve vertical sounding or horizontal profiling. The former is used to obtain variations in resistivity with depth at a particular location whereas the latter is used to identify lateral variations in resistivity at a given depth of investigation. In performing vertical sounding, the center of the electrode array remains fixed and measurements are taken in sequence as the electrodes are moved to increasingly greater distances apart to enable greater depth of investigation. For the profiling technique, the spacing between the electrodes remains constant and for each new measurement all four electrodes are shifted laterally over the same distance.

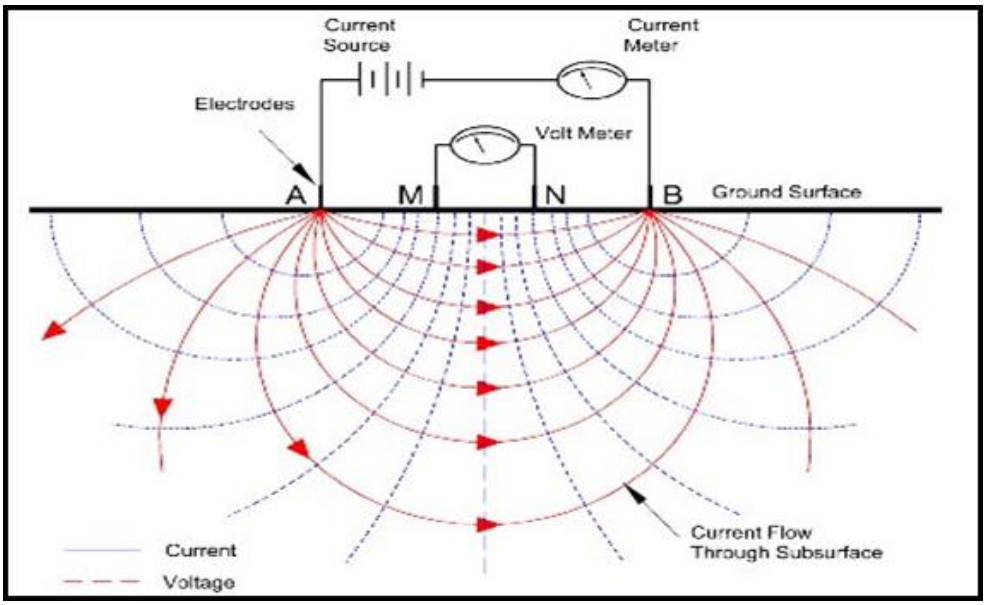

Figure 5.1: Electrodes A and B are the current electrodes, and electrodes m and N are the potential electrodes. A current is injected into the subsurface via current electrode A and travels in the subsurface (solid lines) normal to the equipotential lines (dotted lines) to current electrode B. The potential difference is measured between electrodes m and N. (http://www.nga.com/Geo_ser_DC_tech.htm).

Data from resistivity surveys collected by either sounding or profiling techniques are displayed in different ways. Sounding data are plotted on a log-log scale where the apparent resistivity is plotted versus the electrode spacing. The plot is called an "apparent resistivity sounding curve" which can be interpreted numerically or by manual curve fitting. When these data are reduced or processed by numerical means, a best fit solution is generally computed for two to four subsurface layers. Values for the thickness and electrical resistivity of each layer can be deduced from the best fit solution generated. On the other hand, data collected by resistivity profiling are plotted on linear (or semi-log) axes with apparent resistivity versus traverse distance. Profiling data can easily be interpreted by visual inspection.

5.2.2 Research methodology and data analysis

The data collection methodology carried out employed a review of existing data sources and the collection of new data obtained through vertical electric soundings (VES), resistivity profiling and resistivity logging.

5.2.2.1 Existing information

Collection of available information in relation to this research was done so as to contribute to the water quality assessment. Data collected include borehole lithological logs and geophysical data from Drilling and Dam Construction Agency (DDCA). Borehole lithological logs collected from borehole drilling reports drilled between 1997 and 2011 were studied in order to understand the variation of lithologic layers and to facilitate the interpretation of resistivity data. A total of 107 of VES curves/data were collected from groundwater survey reports (of 2000-2008) available at DDCA. In the study area, VES is carried out before borehole drilling in order to have an overview of subsurface conditions. The drilling depth is recommended based on the interpretation of the VES curves. Existing VES data collected from DDCA were carried out using the Schlumberger array (Fig. 5.2). In the Schlumberger array, the pairs of current and potential electrodes have a common mid-point, but the distances between adjacent electrodes differ. The potential electrodes have an internal spacing of (*l)* and the current electrodes are spaced an increasing distance of ($\frac{L-l}{2}$) from the potential electrodes, where the maximal L varies dependent upon target size and depth (Fig. 5.2). The distance between potential electrodes is usually kept small and fixed, while only the ($\frac{L-l}{2}$) spacing is changed.

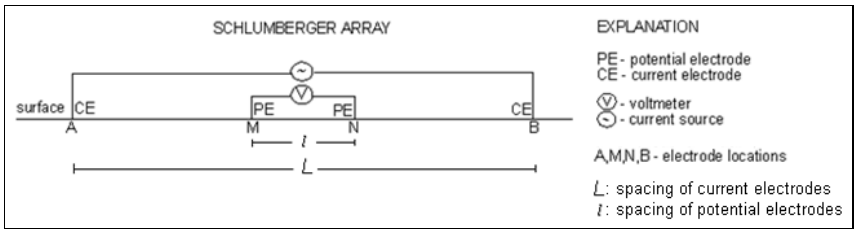

Figure 5.2: Schlumberger array (http://www.state.nj.us/dep/njgs/geophys/elec.htm).

From the current (I) injected into the ground and the resulting voltage difference (ΔV) values, an apparent resistivity (ρ_a) value can be calculated by the following relation:

$$\rho_a = K\frac{\Delta V}{I} \tag{5.1}$$

Where K is a geometric factor which can be calculated from the electrode spacing by (Kirsch, 2009):

$$K = 2\pi\left[\frac{1}{AM} - \frac{1}{MB} - \frac{1}{AN} - \frac{1}{BN}\right]^{-1} \tag{5.2}$$

The substitution of equation 5.2 into equation 5.1 gives:

$$\rho_a = 2\pi\frac{\Delta V}{I}\left[\frac{1}{AM} - \frac{1}{MB} - \frac{1}{AN} - \frac{1}{BN}\right]^{-1} \tag{5.3}$$

For Schlumberger configuration: $AM = NB = (L-l)/2 \; and \; AN = MB = (L+l)/2$

The substitution of these values into equation 5.3 gives:

$$\rho_a = \frac{\pi}{4}\frac{\Delta V}{I}\frac{L^2 - l^2}{l} \tag{5.4}$$

If the separation of the current electrodes is much larger than that of the potential electrodes (L >> l), equation 5.4 becomes:

$$\rho_a = \frac{\pi}{4}\frac{\Delta V}{I}\frac{L^2}{l} = K\frac{\Delta V}{I} \tag{5.5}$$

The geometrical factor K (for L>>l) is deduced to be:

$$K = \frac{\pi}{l} * \frac{L}{2}^{2} \tag{5.6}$$

5.2.2.2 New data collection

New data in the study area were collected in January 2012 to aid a better understanding of the seawater intrusion phenomenon and estimation of the depth to the saltwater interface. A total of 8 VES (S1-S8) and 6 electrical resistivity profiles (P1-P6) with Wenner array configuration were carried out using the ABEM Terrameter SAS 1000 (Fig. 5.3).

Figure 5.3: Setting ABEM Terrameter SAS 1000 before starting measurements at Gymkhana Golf Club (January 2012).

In a Wenner configuration VES, all four electrodes have to be moved on increasing the spread. The electrode spacing is equal (AM = MN = NB= a) with the same lateral spacing *(a)* between adjacent electrodes: this makes each electrode to be separated from the adjacent electrode by a distance that is one-third of the distance between current electrodes (Fig. 5.4). Potential electrodes are nested within the current electrodes. The electrodes are expanded about a center point in subsequent measurements. The current therefore progressively passes into deeper layers. This procedure provides apparent resistivity values that are dependent upon vertical conductivity variations of the subsurface. To estimate the maximum depth mapped, the maximum spacing *(a)* is multiplied by the depth factor (0.519) (Loke, 1999): for example, if the maximum spacing *(a)* used is 100 m, then the maximum depth mapped is about 52 m.

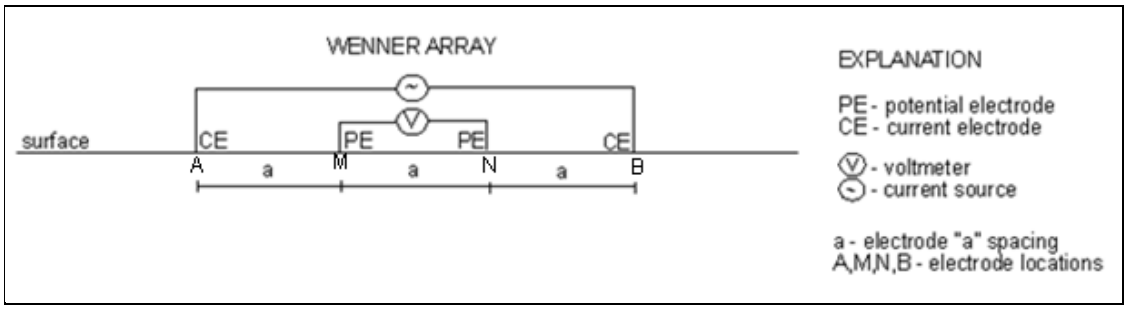

Figure 5.4: Wenner array (http://www.state.nj.us/dep/njgs/geophys/elec.htm).

In the Wenner array the current and potential electrode pairs have a common mid-point and the distances between adjacent electrodes are equal (AM = MN = NB = a), thus:

$$AM = NB = a \; and \; AN = \; MB = 2a$$

The substitution of these values into equation 5.3 gives:

$$\rho_a = 2\pi a \frac{\Delta V}{I} \tag{5.7}$$

The geometrical factor is thus computed to be

$$K = 2\pi a \tag{5.8}$$

Profiling resistivity survey using Wenner array was employed in the study area to detect lateral variations in resistivity. This type of survey is conducted by keeping the spacing constant and moving the entire array laterally between subsequent measurements. It provides estimates of the spatial variation in resistivity at some fixed electrode spacing (Zohdy et al., 1974). The value of a = 30 m was used for all profiles except profile P5, where both 30 m and 40 m were used.

5.2.2.3 Resistivity logging

The distribution of saline groundwater inside the borehole/well, caused by the different resistivities of fresh- and salt water, was investigated by resistivity logging using the resistivity meter "Gossen Geohm" (Fig. 5.5). Thirteen resistivity logs were measured in January 2012. The instrument was used to directly measure the resistance of water in every 0.5 m depth interval, starting from the static water level to the bottom of the borehole. The measured resistances were multiplied by a constant factor of 0.0114 m to obtain the resistivity values. Using MS EXCEL program, the resistivity values (ρ_w) were plotted in graphs against the depth. The resistivity logging helped to gain more information about the three-dimensional distribution of the salt content dissolved in water.

Figure 5.5: Resistivity logging (Borehole B10) at Civil Servant Service Offices, Dar es Salaam.

5.2.2.4 Data analysis

The main purpose of interpretation of VES is to determine the true resistivity and the thickness of different layers. The field resistivity data were interpreted using the resistivity software DCINV inversion program of Pirttijärvi (2005). The degree of uncertainty of the computed model parameters in the curve fitting algorithm are expressed in terms of residual error (RMS). The resistivity of the different layers and the corresponding thicknesses are reproduced by a number of iterations until the model parameters of the VES curve are resolved with minimum residual error. More than one iteration was tried to reach the best fit between the field curve and the calculated one. This ensures the final subsurface 1-D resistivity image that best explains the data is obtained. ArcGIS ver. 9.2 was used to generate maps from the data represented by the point features.

5.3 Results and discussion

According to Walraevens et al. (1994), formation resistivities of < 1.56 Ωm, 1.56 – 3.12 Ωm, 3.12 - 6.25 Ωm and 6.25 – 12.5 Ωm correspond to Salt (S), Moderately Salt (MS), Very Brackish (VB) and Brackish (B) groundwater quality classes according to De Moor and De Breuck (1969) (Table 5.1): these are water types whose TDS concentration is above 3200 mg/l. As regards to the water classification according to Stuyfzand (1986), Brackish salt

(Bs) and Salt (S) signify water whose chloride concentration is greater than 1000 mg/l. In this study area, for elaborating the freshwater/saltwater interface map (Fig. 5.13a-h), the interface is interpreted to be at the depth where formation resistivity decreases below 12.5 Ωm, corresponding to TDS greater than 3200 mg/l, and chloride concentration approximately greater than 1000 mg/l. Thus Brackish (B) up to Salt (S) groundwater classes (Table 5.1) are below the interface.

For somewhat more detailed schematic subdivision, in which the "brackish layer" is to be identified separately as well, the transition fresh-brackish is put at $\rho_t = 25$ Ωm, corresponding to $\rho_w = 6.25$ Ωm and to TDS = 1600 mg/l (boundary between "weakly fresh" and "moderately brackish" water), while the transition brackish-salt is put at $\rho_t = 6.25$ Ωm, corresponding to $\rho_w = 1.56$ Ωm and TDS = 6400 mg/l (boundary between "brackish" and "very brackish").

Table 5.1: Relation of formation resistivity (ρ_t) and water resistivity (ρw) to groundwater quality and the groundwater classification of De Moor and De Breuck (1969) (Walraevens et al., 1994).

Schematic subdivision		**ρ_t (Ωm, 11 °C)**	**ρ_w (Ωm, 11 °C) ($\rho_w = \rho_t/4$)**	**TDS (mg/l)**	**Groundwater quality class**
Fresh	Fresh	>200	>50	<200	very fresh (VF)
		200-100	50-25	200-400	fresh (F)
		100-50	25-12.5	400-800	moderately fresh (MF)
		50-25	12.5-6.25	800-1600	weakly fresh (WF)
	Brackish	25-12.5	6.25-3.13	1600-3200	moderately brackish (MB)
Salt		12.5-6.25	3.13-1.56	3200-6400	brackish (B)
	Salt	6.25-3.12	1.56-0.78	6400-12800	very brackish (VB)
		3.12-1.56	0.78-0.39	12800-25600	moderately salt (MS)
		<1.56	<0.39	>25600	salt (S)

5.3.1 Geophysical survey

5.3.1.1 Existing information

A total of 107 Vertical Electrical Sounding (VES) curves/data from groundwater survey reports (of 2000-2008) from Drilling and Dam Construction Agency (DDCA) were studied. Their location is shown in Fig. 5.6. Appendix 5.1(a) presents the VES curves, whereas

appendix 5.1 (b) presents in table format the reported formation resistivities and depths of horizons, according to DDCA. However, the former does not include curves for some VES points (i.e. 30, 36, 55, 57, 58, 59, 80, 82, 84, 86-88, 91-94, 99, 101-104) since in some existing reports only the table of results was presented (i.e. ρ1, h1; ρ2, h2; ρ3, …). In cases where there were no curves but sounding results presented the raw measurement data (i.e. VES 75, 76, 77, 78, 79, 105, 106 and 107), these data were re-interpreted using DCINV1-D software, and the curves shown in Appendix 5.1(a) are our own interpretation.

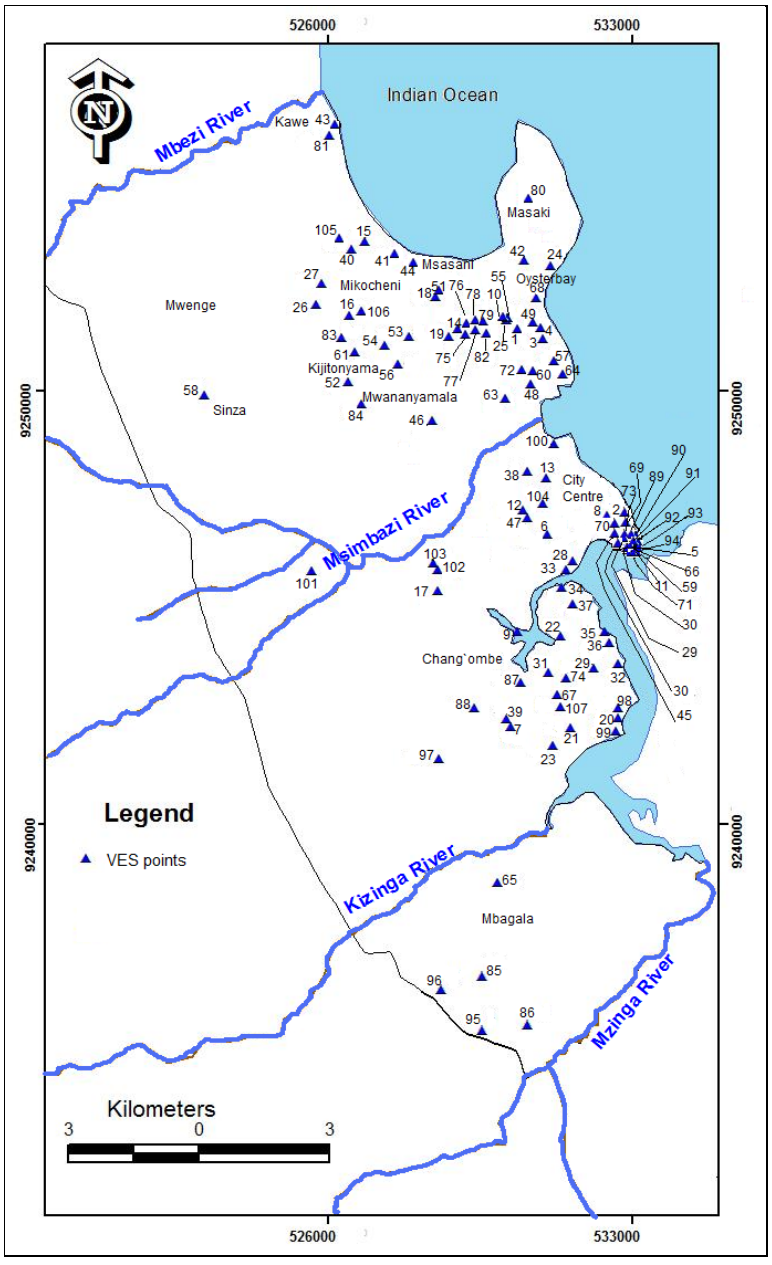

Figure 5.6: Map showing location of available VES points.

5.3.1.2 New resistivity information

5.3.1.2.1 Introduction

New information in the study area (Fig. 5.7) was collected in January 2012 to aid a better understanding of the seawater intrusion phenomenon and estimation of the depth to the saltwater interface. A total of 6 electrical resistivity profiles (P1-P6) (Appendix 5.2a) and 8 VES (S1-S8) (Appendix 5.2b) and 13 resistivity logs (B1-B13) were conducted.

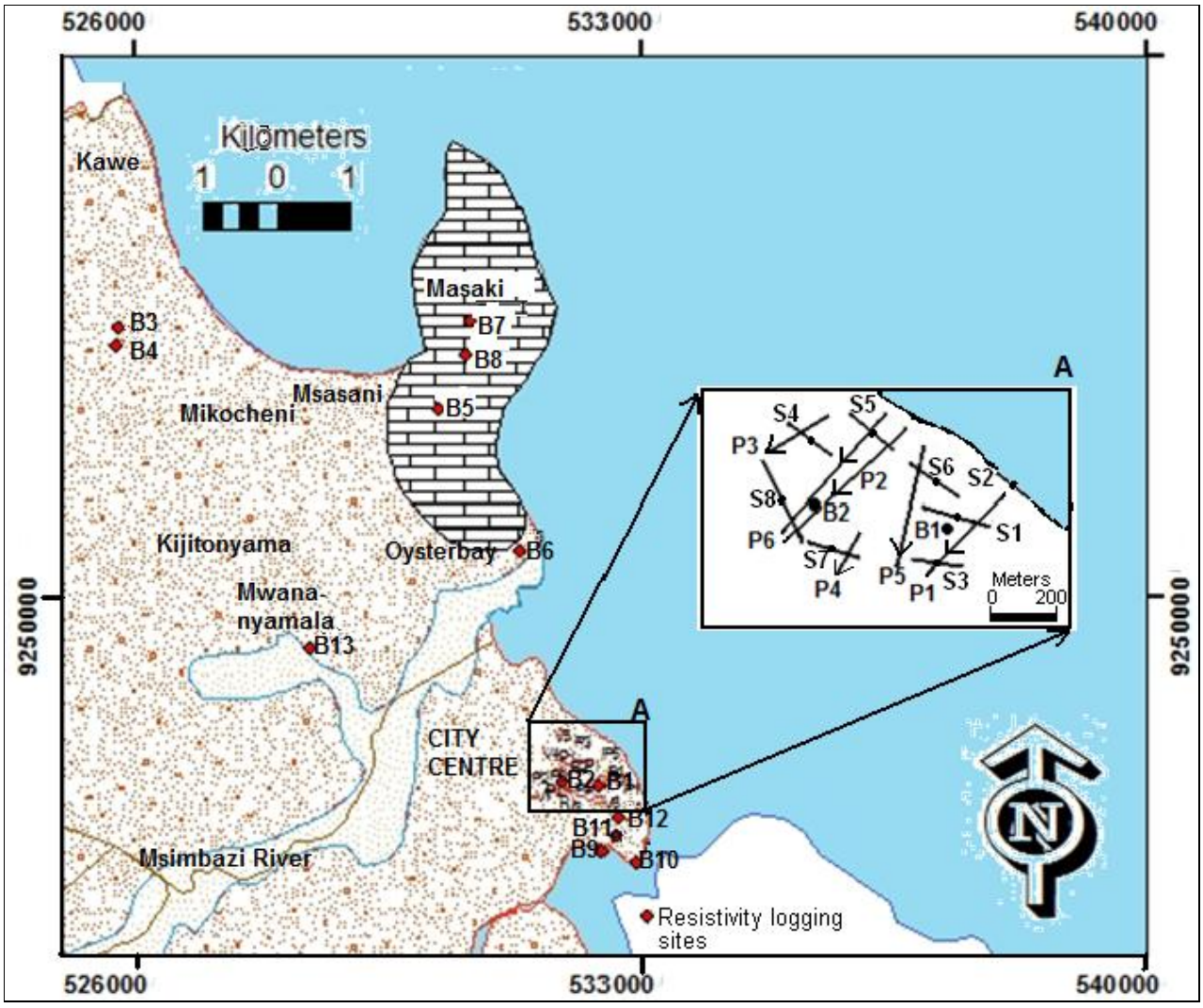

Figure 5.7: Map showing the locations of the test sites of resistivity logging (B1-B13), resistivity profiles (P1-P6) and vertical electrical soundings (S1-S8) (the latter in area "A" on the map).

5.3.1.2.2 Resistivity profiles

PROFILE 1

Profile P1 is orientated in NE to SW direction (Fig. 5.7), and was carried out over a length of 345 m, perpendicular to the coastline, starting at a distance of 20 m away from the coast. Profile P1 (Fig. 5.8a) generally indicates a conductive zone (0.5 to 5 Ωm) for the distance between 0 to about 165 m (in a direction away from the coast) (Fig. 5.7). The low resistivity in this area is interpreted to be due to saline groundwater. The distance between 165 m and 275 m was skipped due to error readings caused by the presence of a ditch. Beyond 275 m distance, for most of the survey points, resistivity fluctuates above 10 Ωm .

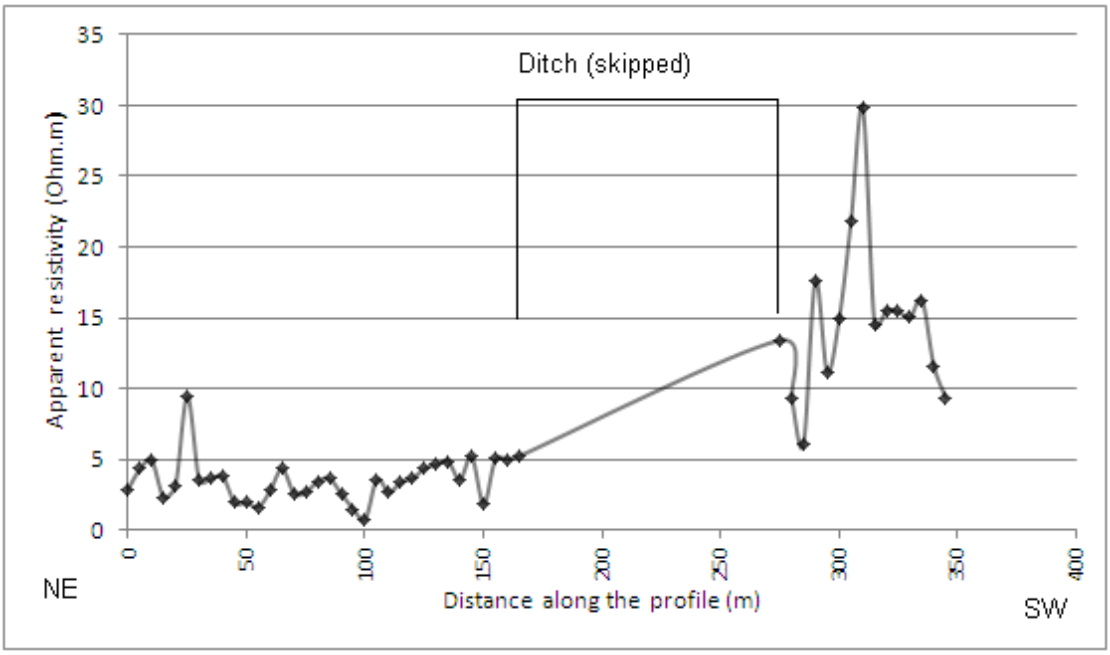

Figure 5.8(a): Resistivity profile P1with electrode spacing a of 30 m.

PROFILE 2

Profile P2 is orientated in NE to SW direction (Fig. 5.7), and was carried out over a length of 510 m, perpendicular to the coastline, starting at a distance of 20 m away from the coast. Apart from three high resistivity values at a distance of 0 m (67 Ωm), 15 m (228 Ωm) and 75 m (37 Ωm), which could be due to error (probably caused by underlying pipes), profile P2 (Fig. 5.8b) for the most points indicates a conductive zone between 3Ωm to 6 Ωm for the distance between 0 to about 150 m (in a direction away from the coast) (Fig. 5.7). The low resistivity in this area is interpreted to be due to saline groundwater. For the next 165 m distance (between 150 m to 315 m), resistivity fluctuates mainly between 7 Ωm and 10 Ωm, signifying less effect of saline water compared to the previous first 150 m of the profile, but

still influenced by brackish water. Beyond 315 m, the relatively high resistivity values greater than 10 Ωm indicate slightly fresh water.

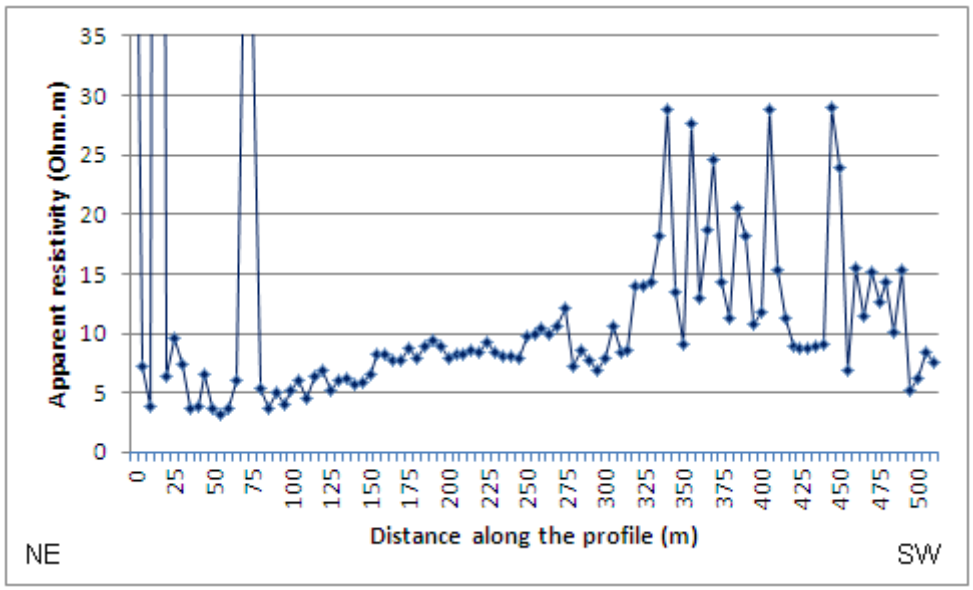

Figure 5.8(b): Resistivity profile P2 with electrode spacing a of 30 m.

PROFILE 3

Profile P3 is orientated in the NE and SW direction (Fig. 5.7), and was carried out over a length of 195 m, perpendicular to the coastline, starting at a distance of 170 m away from the coast. Resistivity in profile P3 fluctuates around 10 Ωm, mainly between 7 Ωm and 14 Ωm (Fig. 5.8(c)). Peak resistivity (26.55 Ωm) measured at a distance of 75 m can be associated with error due to crossing water pipe. The beginning of resistivity survey of P3 is located at a relatively greater distance from the sea compared to the previous profiles (P1 and P2) which makes it to have relatively high values of resistivity showing less effect of saline groundwater.

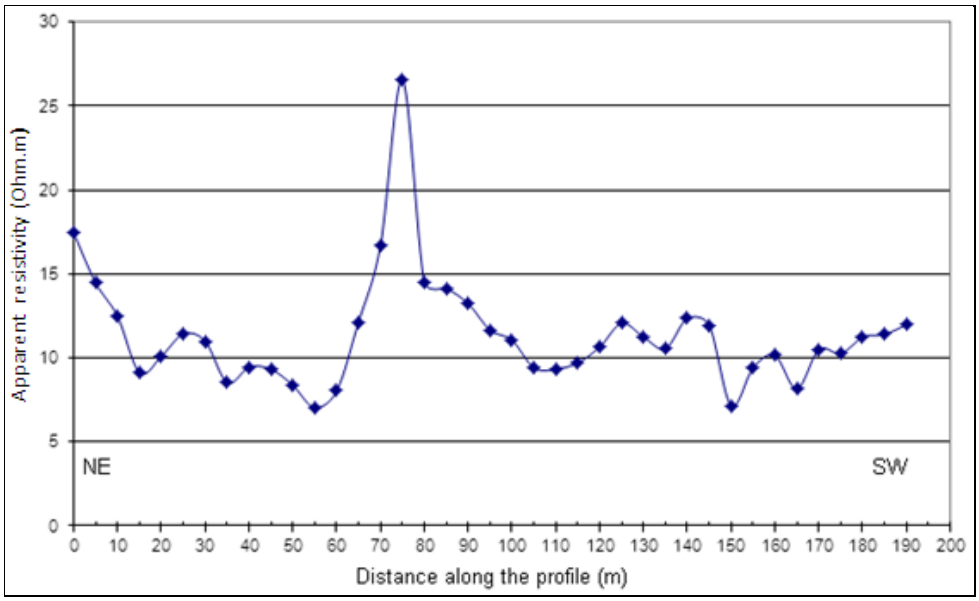

Figure 5.8(c): Resistivity profile P3 with electrode spacing a of 30 m.

PROFILE 4

Profile P4 is orientated in NNE to SSW direction (Fig. 5.7), and was carried out over a length of 135 m, perpendicular to the coastline, starting at a distance of 417 m away from the coast. Profile P4, with its beginning and location far from the coastline compared to the other profiles, shows resistivities around 10 Ωm, comparable to profiles P2 and P5 at the same distance from the sea (Fig. 5.8(d)).

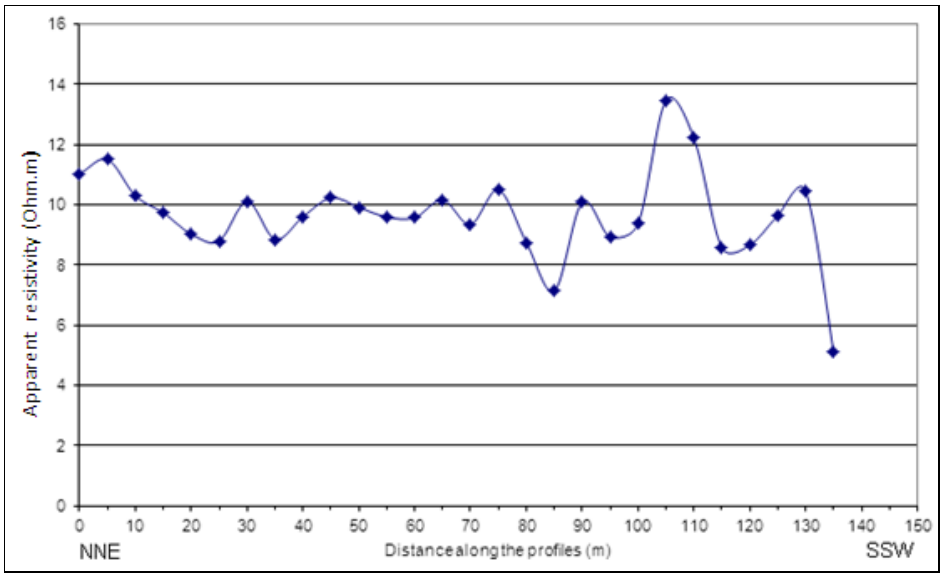

Figure 5.8(d): Resistivity profile P4 with electrode spacing a of 30 m.

PROFILE 5

Profile P5 is orientated in N to S direction (Fig. 5.7), and was carried out over a length of 350 m, perpendicular to the coastline, starting at a distance of 30 m away from the coast. Profile P5 (Fig. 5.8e) with electrode spacing "a" of 30 m and 40 m indicates a conductive zone (0.5 to 4 Ωm) for the distance between 0 to about 120 m (in a direction away from the coast), which is interpreted to be due to saline groundwater. Beyond 120 m distance, resistivity fluctuates above 4 Ωm. The trend of increasing resistivity away from the coast is comparable mostly to profiles P1, P2 and P6.

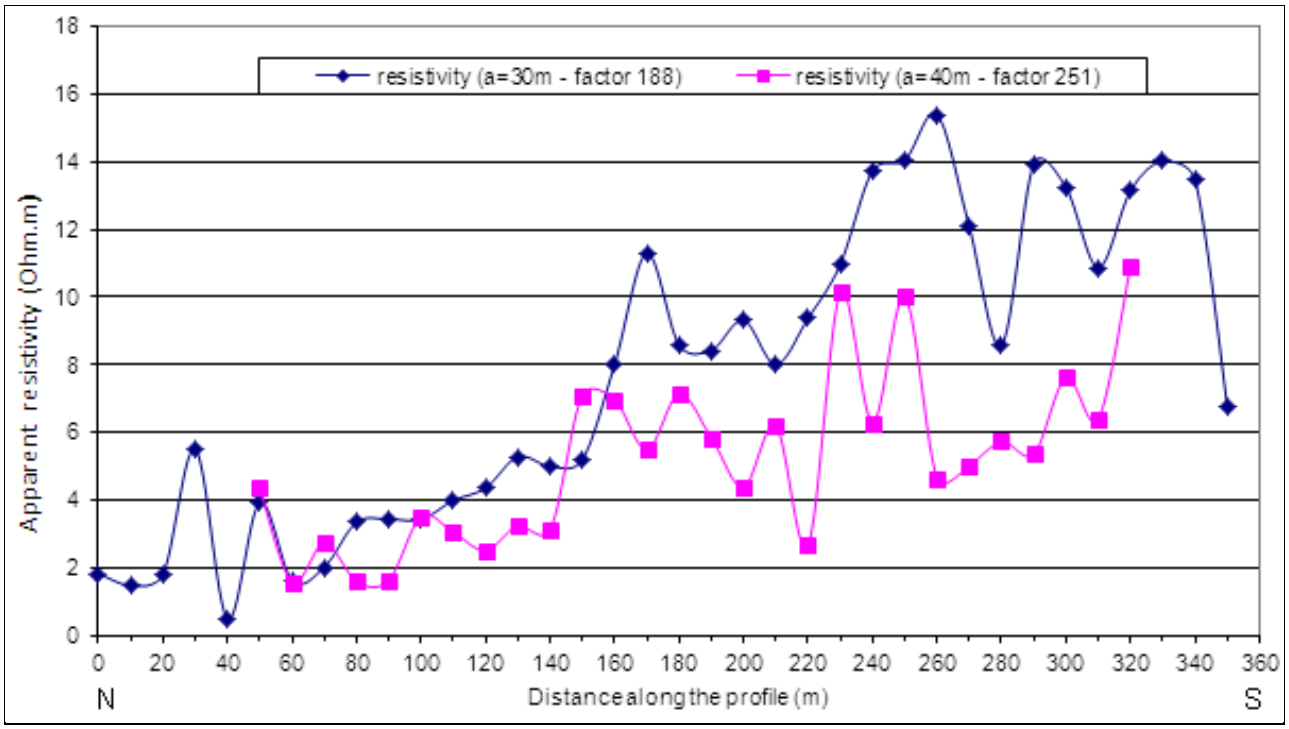

Figure 5.8(e): Resistivity profile P5 with electrode spacings a of 30 m and 40 m.

PROFILE 6

Profile P6 is orientated in NE to SW direction (Fig. 5.7), and was carried out over a length of 470 m, perpendicular to the coastline, starting at a distance of 20 m away from the coast. Profile P6 (Fig. 5.8f) shows the trend of increasing resistivity away from the coast from a minimum of 3 Ωm to a maximum of 21 Ωm. Except the first reading, all other readings have values above 4 Ωm. At around 370 m, a drastic increase of resistivity above 10 Ωm is observed.

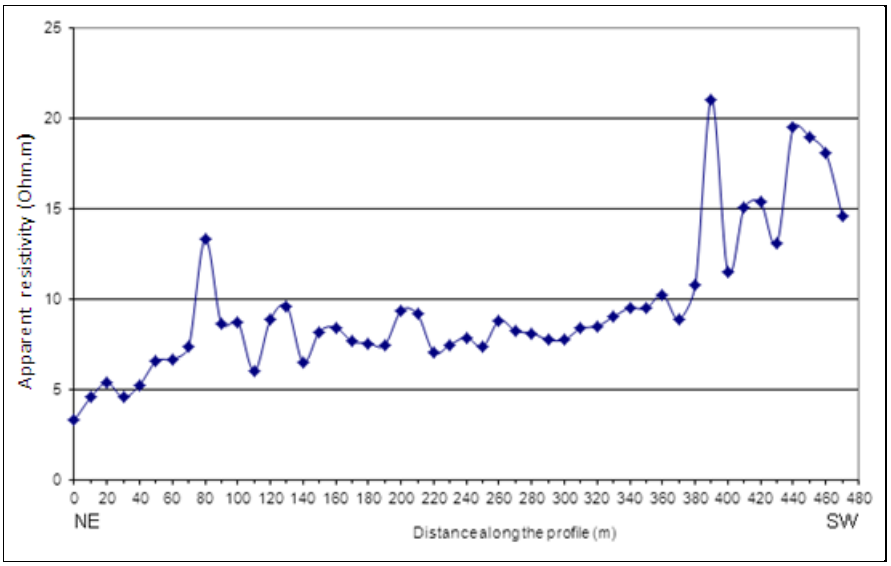

Figure 5.8(f): Resistivity profile P6 with electrode spacing a of 30 m.

5.3.1.2.3 *VES*

Both the Terrameter readings (Ω) and calculated apparent resistivity (Ωm) are found in appendix 5.2(b). The apparent resistivity is plotted against the electrode spacing "a" on a double logarithmic scale. Data for all 8 VESs (Fig 5.9a-h) were interpreted with the resistivity software DCINV inversion program. The interpretation of data indicates 4-layered VES curves except for two curves, S2 and S6, which are 3- layered (Fig. 5.9(b and f)). Table 5.2 presents interpreted model results which include true resistivity and depth of horizons. VES resistivity curves indicate a general trend of decreasing resistivity with depth and towards the coastline. This is interpreted to be due to the effect of saline groundwater as was also observed in the resistivity profiles. S2 was performed at the coastline and indicates resistivity lowering from 1.92 Ωm to 1.45 Ωm. At this point the resistivity is much lower comparing to the resistivity (2.91 Ωm) observed at the beginning of profile P1 which is perpendicular to S2: profile P1 starts at 20 m from S2 and the coastline. S1 and S3 are also performed perpendicular to profile P1 but further away from the coastline compared to S2; they show relatively higher resistivity values compared to S2. The effect of resistivity increase with increasing distance from the sea is also well observed in S6, located closer to the coastline compared to S7. Likewise S5 and S4 performed relatively close to the sea show low resistivity at depth compared to S8, which is located further away from the sea.

Table 5.2: True resistivity and depth of horizons for VES conducted at Gymkhana Golf Club.

VES	Distance (m) to coastline	ρ1 (Ωm)	h1 (m)	ρ2 (Ωm)	h2 (m)	ρ3 (Ωm)	h3 (m)	ρ4 (Ωm)	Depth of fresh/saline interface (ρt=25 Ωm) (Key: f/s = fresh/saline; s/f = saline/fresh)
S1	220	80	0.71	3.5	1	27	7.6	2	f/s:0.71; s/f:1.71 and f/s:/9.31
S2	0	1.92	0.69	1.68	5.94	1.45			0
S3	350	1000	1	16.6	4.71	150	5	0.5	10.71
S4	250	780	0.81	13.8	8.48	66	10.26	0.32	19.55
S5	110	100	0.61	2.77	7.60	25.41	6.43	0.085	f/s:0.61; s/f:/8.21 and f/s:14.64
S6	160	19	0.5	2.69	2.68	1.92			0.5
S7	500	585	0.61	2.33	0.63	15	13.06	4.26	f/s:0.61; s/f:1.24 and f/s:14.30
S8	480	150	0.5	1.5	1.03	15	17.09	11.79	f/s:0.5; s/f:1.53 and f/s:18.62

Salt water has resistivity below 1.56 Ωm (Walraevens et al., 1994; Table 5.1) and in particular seawater has an average resistivity of 0.2 Ωm (Nowroozi et al., 1999). All VES (S1-S8) indicate formation resistivity decreases below 12.5 Ωm (Table 5.2), and are interpreted to have reached the freshwater/saltwater interface (Table 5.1). However, the interface between brackish and saltwater (6.25 Ωm taken as a limit between brackish and salt water (Table 5.1)) was reached for all VES except S8. Vertical electrical sounding did not continue for sufficiently large spacing "a" to reach the interface in S8. S2 was taken at the coastline, and the whole curve reflects saltwater. From Table 5.2, VES S1, S5, S7 and S8 indicate an alternation of fresh/salt/fresh/salt water types. A shallow salt zone at water table is linked to daily sprinkler irrigation conducted at Gymkhana Golf Club. It is estimated over 160 m^3/day of groundwater is pumped from boreholes located within Gymkhana premises mainly for irrigation purpose. This irrigation water contains some salts. After irrigation the water added to the soil is used by grass or evaporate directly and salt is left in the soil. During the rainy season, the salt can be dissolved by the infiltrating water and are washed to the groundwater. However, on vegetated land, transpiration typically far exceeds evaporation: capillary forces can draw water up from the water table to depths from which it supplies the process of evapotranspiration (Nimmo, 2009). When the capillary rise attains the depth of reach of the evaporation, the evaporation process takes place to the uplifted groundwater. Thus, groundwater with high salinity can result from the upward movement of shallow groundwater through concentration salts during the evaporation process which follows the capillary rise.

The above explanation gives the reason of salt zone observed at water table in some VES points. In elaborating depth map of interface the lower fresh/salt interface will be used and not those regarded to be caused by capillary rise. At points S1, S3, S6 (Fig. 5.7), located in the eastern part of the survey zone, saltwater was found at less depth (between 3.18 and 10.71 m) compared to points S4 (19.55 m) and S5 (14.64 m), located in the cental part of the survey zone (Fig. 5.7). Likewise, S7, located in the eastern part of the survey zone and far from the coastline indicates the interface between brackish and salt water was reached at 14.30 m which is comparable to the depth (14.64 m) of which the interface was reached at S5 located in the western part of the survey zone and close to the coastline. However, VES S6 is influenced by sewage drainage ditch along which VES was carried: only saline water is observed, the low resistivity value starts very near to the surface making a continuous salt layer. Further insight into the fresh- salt water interface as deduced from VES S1-S8 is gained through cross-sections (Figs. 5.13(d-f) in section 5.3.1.3).

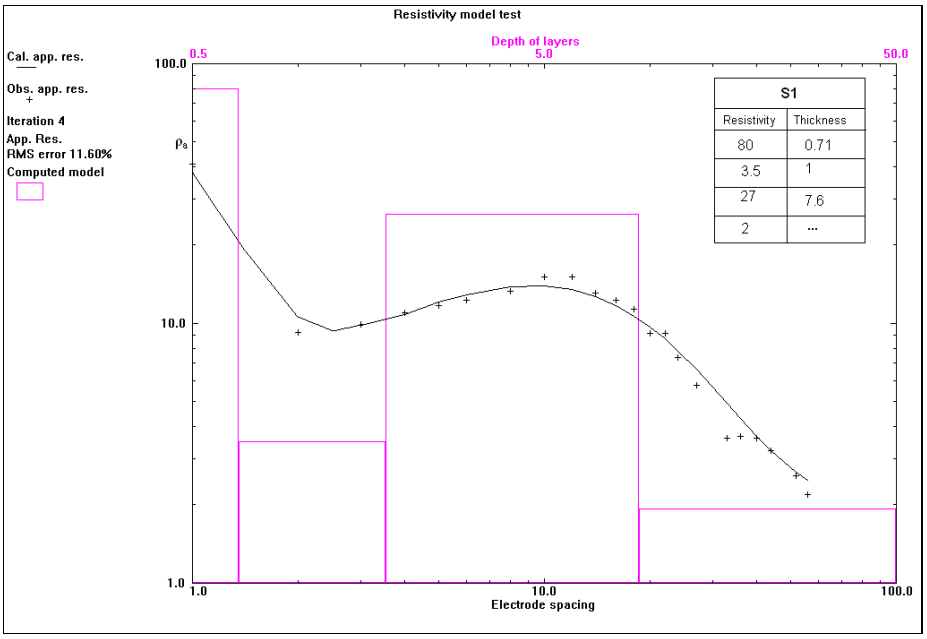

Figure 5.9(a): S1 image and interpretation with the DCINV-software with electrode spacing a (primary x-axis, in m) and layer thickness (secondary x-axis in m) against apparent resistivity (y-axis, Ωm).

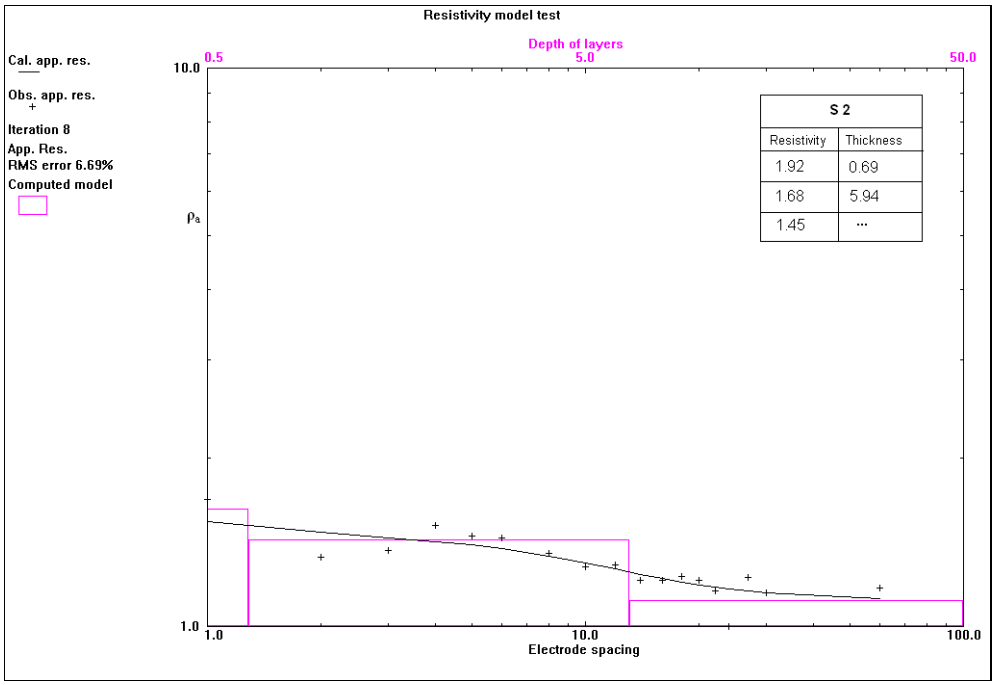

Figure 5.9(b): S2 image and interpretation with the DCINV -software with electrode spacing a (primary x-axis, in m) and layer thickness (secondary x-axis in m) against apparent resistivity (y-axis, Ωm).

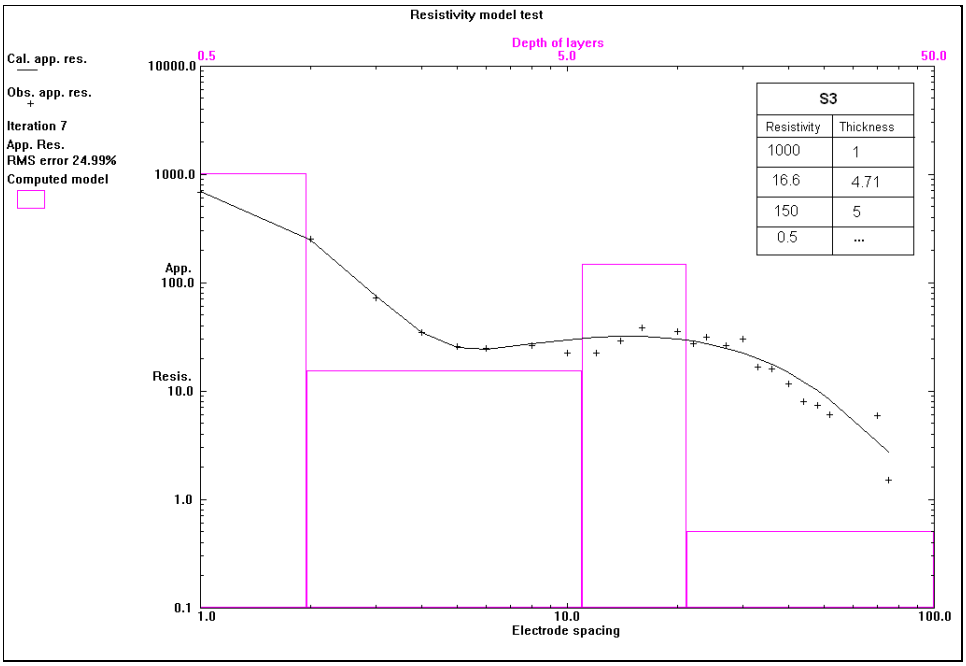

Figure 5.9(c): S3 image and interpretation with the DCINV -software with electrode spacing a (primary x-axis, in m) and layer thickness (secondary x-axis in m) against apparent resistivity (y-axis, Ωm).

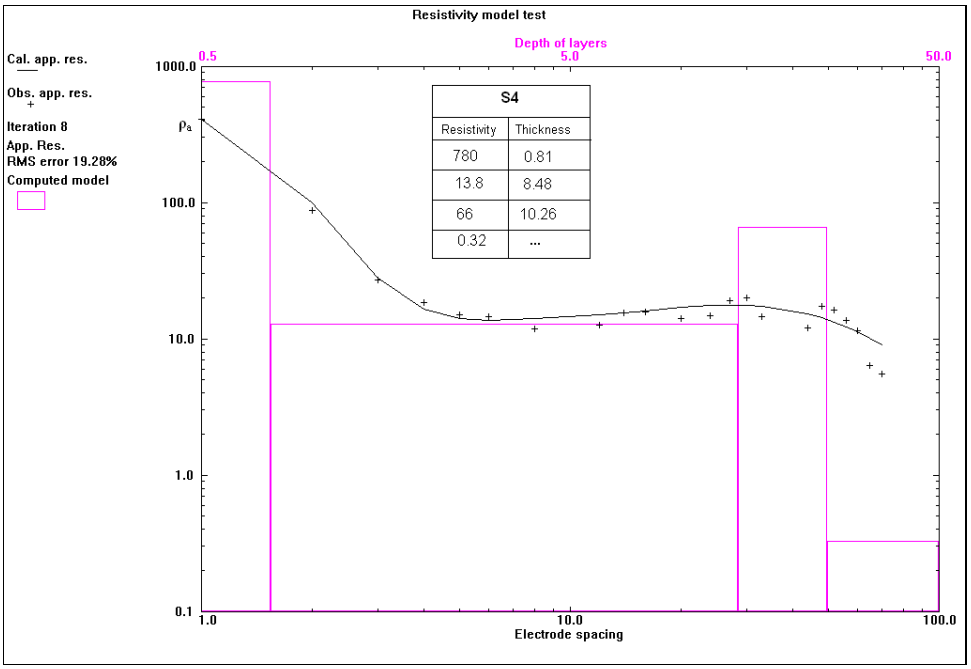

Figure 5.9(d): S4 image and interpretation with the DCINV -software with electrode spacing a (primary x-axis, in m) and layer thickness (secondary x-axis in m) against apparent resistivity (y-axis, Ωm).

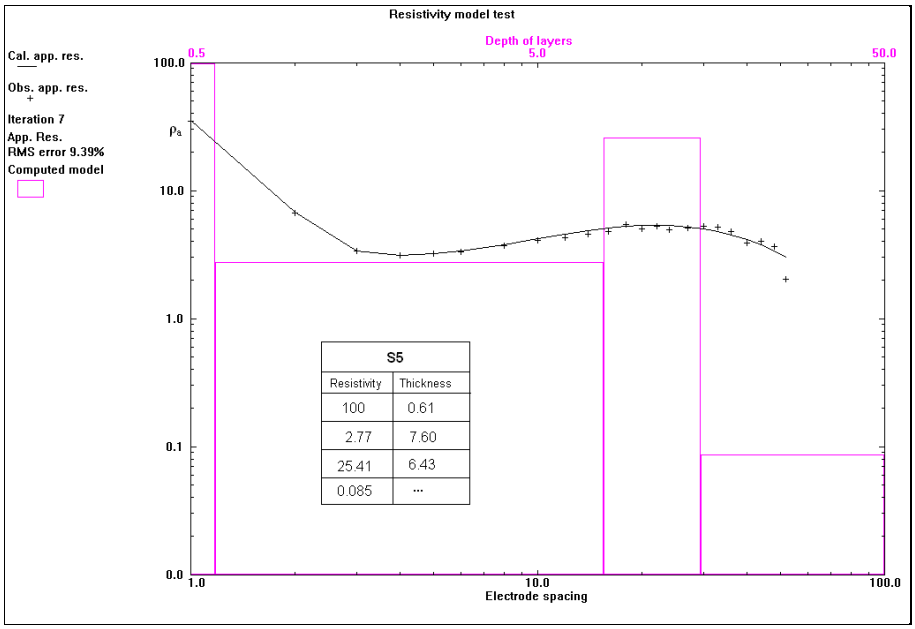

Figure 5.9(e): S5 image and interpretation with the DCINV -software with electrode spacing a (primary x-axis, in m) and layer thickness (secondary x-axis in m) against apparent resistivity (y-axis, Ωm).

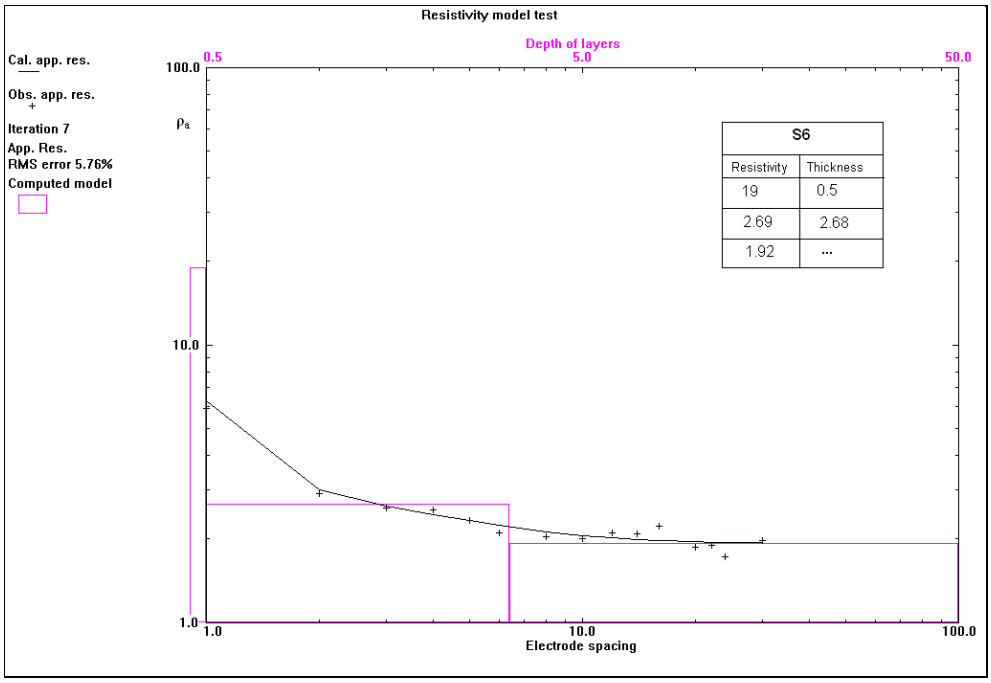

Figure 5.9(f): S6 image and interpretation with the DCINV -software with electrode spacing a (primary x-axis, in m) and layer thickness (secondary x-axis in m) against apparent resistivity (y-axis, Ωm).

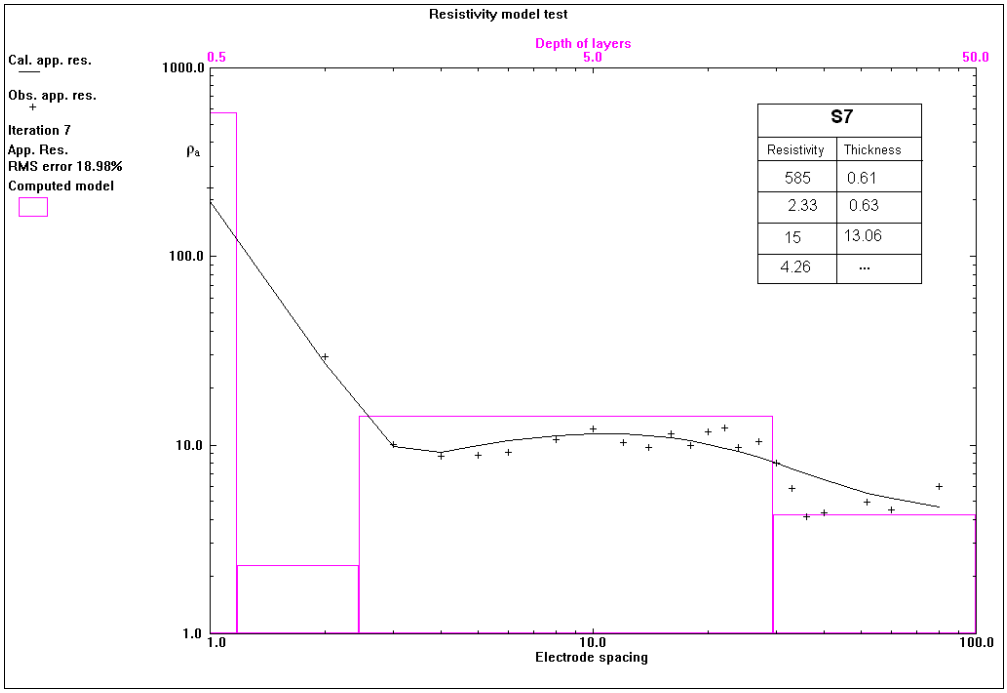

Figure 5.9(g): S7 image and interpretation with the DCINV -software with electrode spacing a (primary x-axis, in m) and layer thickness (secondary x-axis in m) against apparent resistivity (y-axis, Ωm).

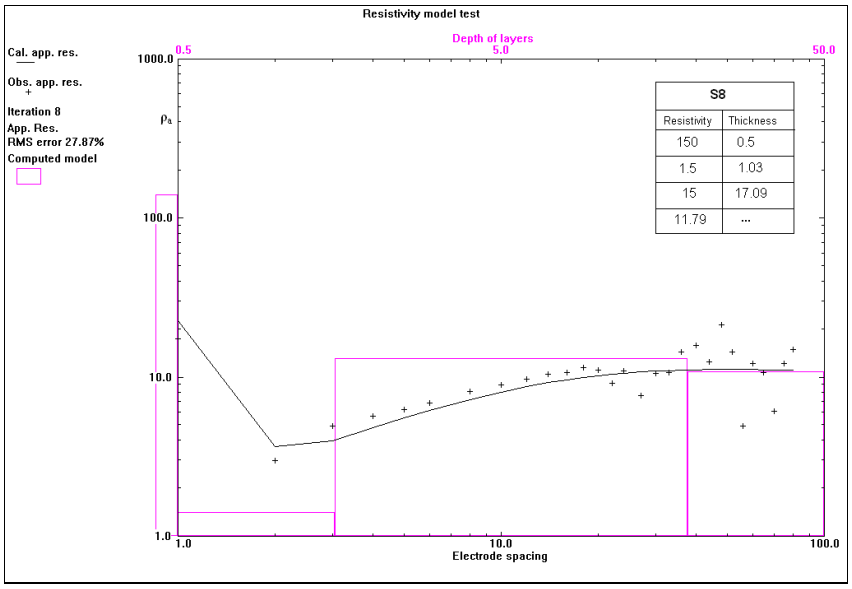

Figure 5.9(h): S8 image and interpretation with the DCINV -software with electrode spacing a (primary x-axis, in m) and layer thickness (secondary x-axis in m) against apparent resistivity (y-axis, Ωm).

5.3.1.2.4 Resistivity logging

Resistivity logs demonstrate the decrease of resistivity with depth from freshwater to saline or very brackish water. The freshwater/saltwater interface or brackish-water/saltwater interface for all 13 resistivity loggings (B1-B13) has been presented in Fig. 5.10(a-m). Where lithological logs (from the available groundwater drilling reports) exist in boreholes where resistivity log measurements were taken, they have been indicated in Fig. 5.10(a-b and h-m). Additionally, resistivity logging measurements were interpreted in terms of groundwater quality according to Table 5.1.

RESISTIVITY LOGGING AT POINT B1

Resistivity logging at point B1 (Fig. 5.7) is located about 0.22 km from the ocean and is located near VES S1. The static water level (SWL) of 0.5 m below the ground was measured at borehole B1. Resistivity curve at point B1 (Fig. 5.10a) shows drastic decrease of resistivity in two steps: decease from 6.3 Ωm to 4 Ωm at 10 m depth, and from 3.5 Ωm to 1.0 Ωm at 17-19 m depth. Based on the water resistivity (ρ_w) classification in Table 5.2, the borehole indicates water quality variation from weakly fresh (WF) to very brackish (VB). A very clear brackish- salt water interface can be observed at a depth of around 17.5 m. The transition fresh brackish at a depth of 10 m in B1, associated with the decrease in water resistivity from 6.3 Ωm to 4 Ωm, seems to correspond with the lower fresh/salt water interface indicated by

VES S1 whereby the formation resistivity changes from 27 Ωm to 2 Ωm (Table 5.2) at a depth of 9.31 m.

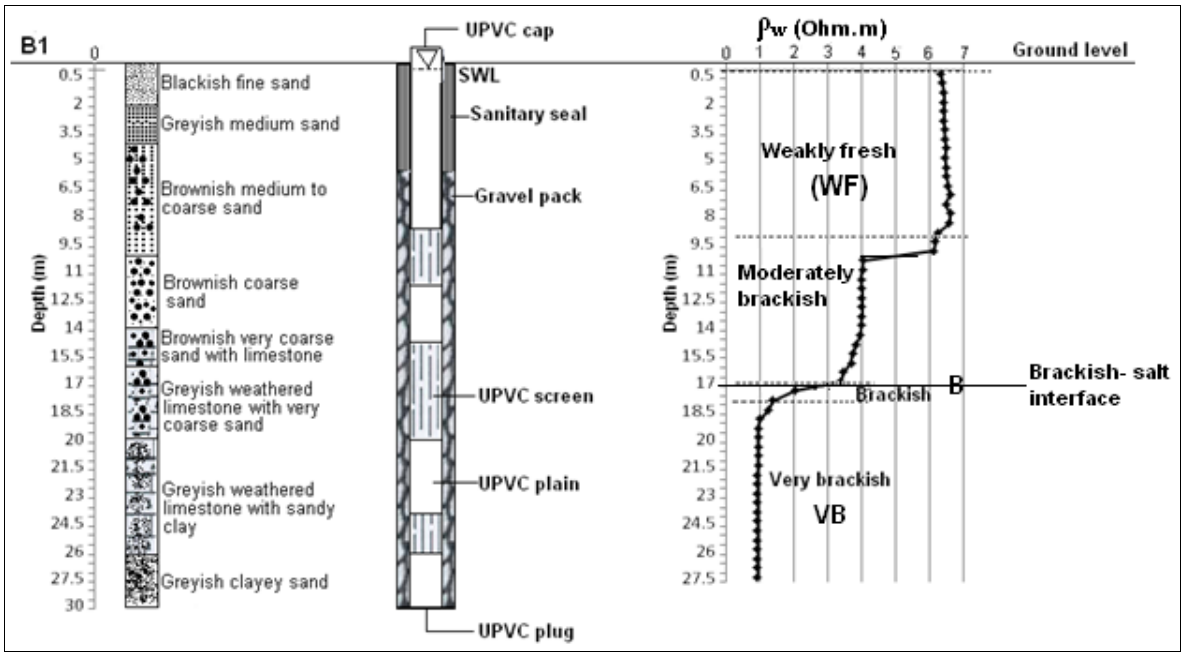

Figure 5.10(a): Resistivity log at observation borehole B1 (location of the borehole is indicated in Fig. 5.7).

RESISTIVITY LOGGING AT POINT B2

The resistivity logging at point B2 (Fig. 5.7) is located about 0.48 km from the ocean. The static water level of 3.5 m below the ground was measured at borehole B2. Based on the water resistivity (ρ_w) classification in Table 5.1, the borehole indicates water quality variation from weakly fresh (WF) to brackish (B) (Fig. 5.10b). Resistivity values show a decrease of resistivity from 10 Ωm at 4 m depth to about 3 Ωm at 6.5 m depth. The fresh-brackish interface occurs at 5.25 m depth (limit between WF and MB water type) (Fig. 5.10). Point B2 is located in the vicinity of VES S7 and S8. The second fresh/salt water interface is reached at a depth of 14.30 m and 18.62 at VES S7 and VES S8 respectively (Table 5.2) (Fig. 5.13(e-f)). The borehole was drilled up to a depth of 20 m, and backfilled starting from 12.5 m, probably because salinity was detected at depth during drilling (Fig. 5.10(b)). It is a common practice in the study area for boreholes where salinity is detected, to reduce their depth through backfilling. Possibly, the interface occurred at 12.5 m depth or more at the time of drilling, but has now risen to 5.5 m in response to pumping.

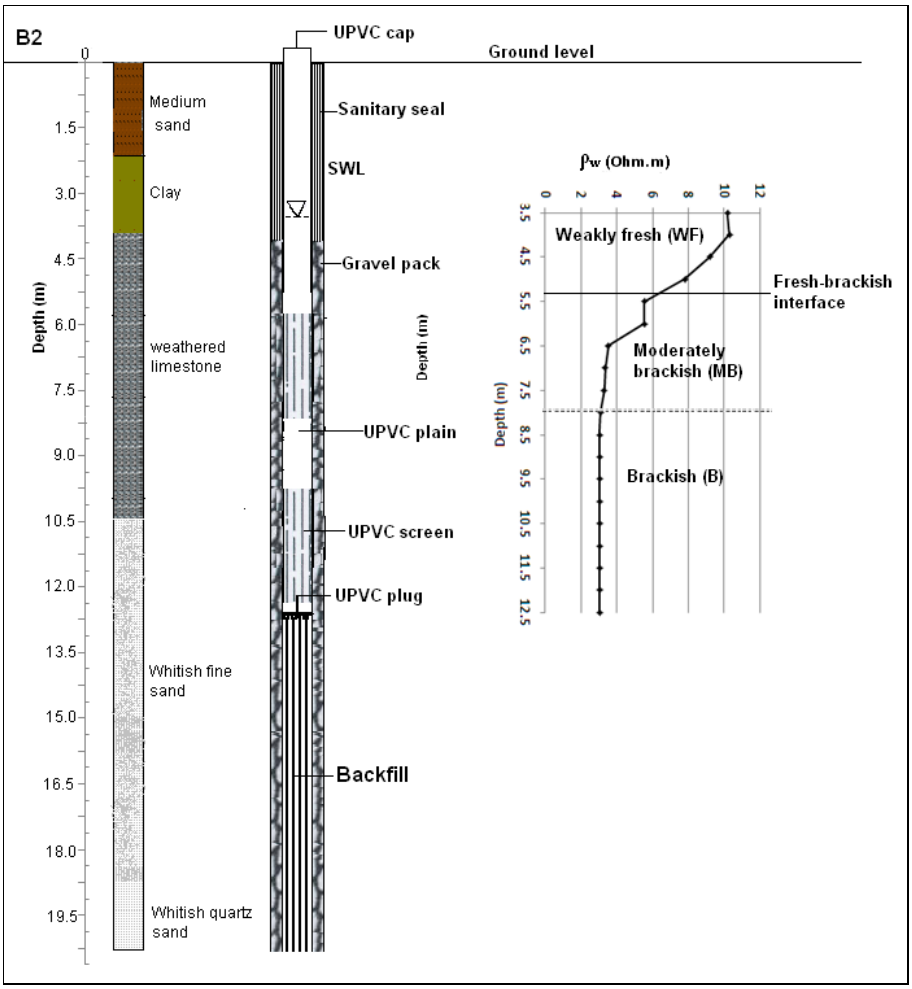

Figure 5.10(b): Resistivity log at observation borehole B2 (location of the borehole is indicated in Fig. 5.7).

RESISTIVITY LOGGING AT POINT B3

The resistivity logging at point B3 (Fig. 5.7) is located about 1.5 km from the ocean. The water table at borehole B3 is relatively at large depth. The static water level of 10.5 m below the ground was measured at B3. The resistivity curve at point B3 (Fig. 5.10c) shows a decrease of resistivity from 2.9 Ωm at about 16 m depth to 2.62 Ωm at 23 m depth. Thereafter the resistivity of water remains stable at about 2.6 Ωm. Based on the water resistivity (ρ_w) classification in Table 5.1, the borehole indicates brackish (B) water quality. No interface could be determined at point B3 since the curve shows only brackish water: there is neither freshwater on top nor very brackish/salt water at the bottom.

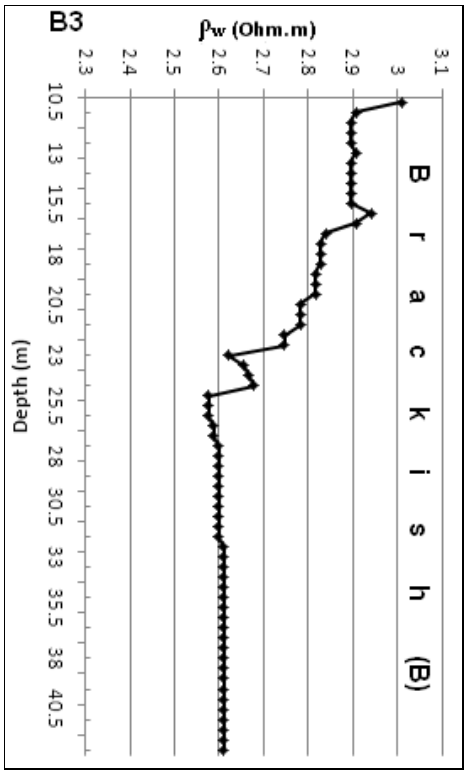

Figure 5.10(c): Resistivity log at observation borehole B3 (location of the borehole is indicated in Fig. 5.7).

RESISTIVITY LOGGING AT POINT B4

The resistivity logging at point B4 (Fig. 5.7) is located about 200 m south of point B3 and about 1.54 km from the ocean. The static water level of 8.5 m below the ground was measured at B4. Resistivity curve at point B4 (Fig. 5.10d) shows slight fluctuation (at the beginning) between 20.5 Ωm and 20 Ωm from the depth of 9 m to 15.5 m. This was followed by a drastic decrease of resistivity from 20 Ωm to 9.8 Ωm at 18 m depth. Thereafter the resistivity of water fluctuates between 8 to 9 Ωm till end of the borehole depth. Based on the water resistivity (ρ_w) classification in Table 5.1, the borehole indicates moderately fresh (MF) to weakly fresh (WF) water quality. No interface as defined before could be determined at point B4 since the curve shows only fresh water: there is no brackish/salt water at the bottom. Yet, the transition from MF water with $\rho_w = 20$ Ωm to water with $\rho_w = 10$ Ωm occurs abruptly. Borehole B4 shows good water quality comparing to borehole B3. The two boreholes belong to Coca-Cola Company and were drilled for sake of pumping water for production. However, water for production was only pumped from borehole B3 until the increase of water salinity was detected, and the company shifted to water supplied by DAWASCO. Thus brackish water in borehole B3 is the result of pumping which pulled in saline water, whereas borehole B4 was never pumped since its construction.

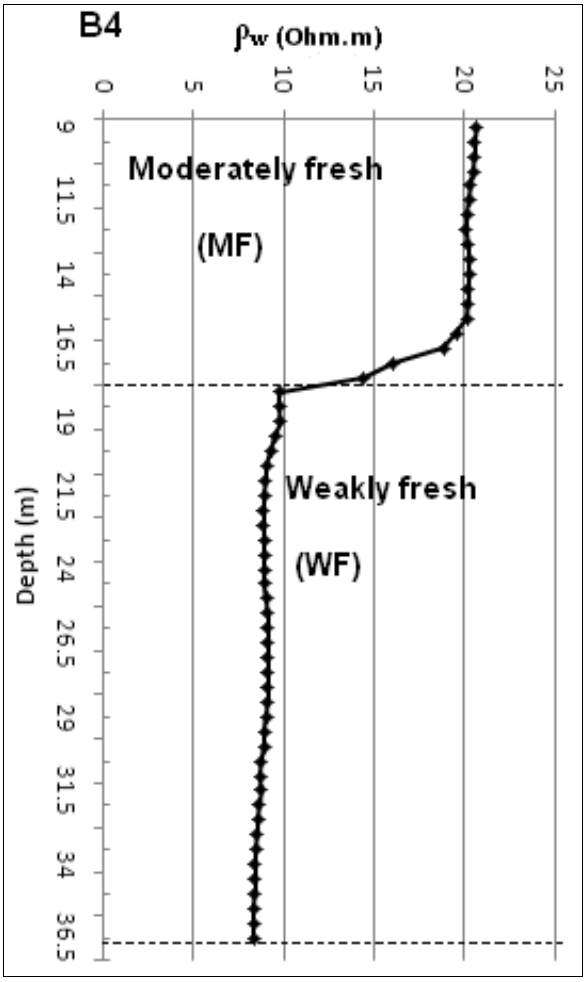

Figure 5.10(d): Resistivity log at observation borehole B4 (location of the borehole is indicated in Fig. 5.7).

RESISTIVITY LOGGING AT POINT B5

The resistivity logging at point B5 (Fig. 5.7) is located at the reefal limestone at Masaki peninsular about 0.669 km from the ocean. Raised reefal limestone at Masaki forms a high relief locally. Water table at borehole B5 occurs at large depth. The static water level of 12 m below the ground was measured at B5. Resistivity curve at point B5 (Fig. 5.10e) shows that for a depth interval of 1 meter (12 m to 13 m depth), resistivity decreases from 4.2 Ωm to 3.2 Ωm. Thereafter the resistivity of water remains stable at around 3.1 Ωm till the depth of 15 m. Decrease of resistivity continues till 0.79 Ωm at the bottom of the borehole. Based on the water resistivity (ρ_w) classification in Table 5.1, the borehole indicates moderately brackish (MB) to very brackish (VB) water quality. Brackish-salt water interface seem to occur at a depth of about 18.25 m.

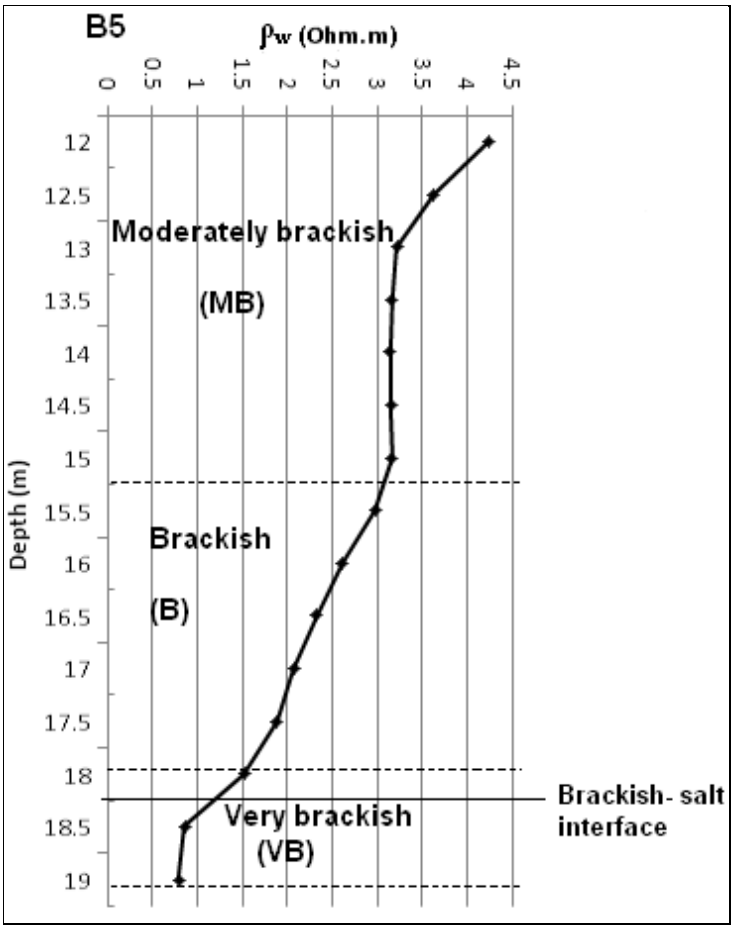

Figure 5.10(e): Resistivity log at observation borehole B5 (location of the borehole is indicated in Fig. 5.7).

RESISTIVITY LOGGING AT POINT B6

The resistivity logging at point B6 (Fig. 5.7) is located at Oysterbay, 3 km south-east of borehole B5 at about 0.266 km from the ocean. The static water level of 11 m below the ground was measured at B6. Resistivity curve at point B6 (Fig. 5.10f) shows a gradual decrease in resistivity from 2.3 Ωm at 11 m depth to 0.68 Ωm at 16.5 m depth. Based on the water resistivity (ρ_w) classification in Table 5.1, the borehole indicates brackish (B) to moderately salt (MS) water quality. The brackish-salt water interface occurs at a depth of about 14.25 m. B5 and B6 show comparable pattern. Brackish-salt water interface in the latter which is located closer to the sea occurs at a relatively low depth comparing to the former.

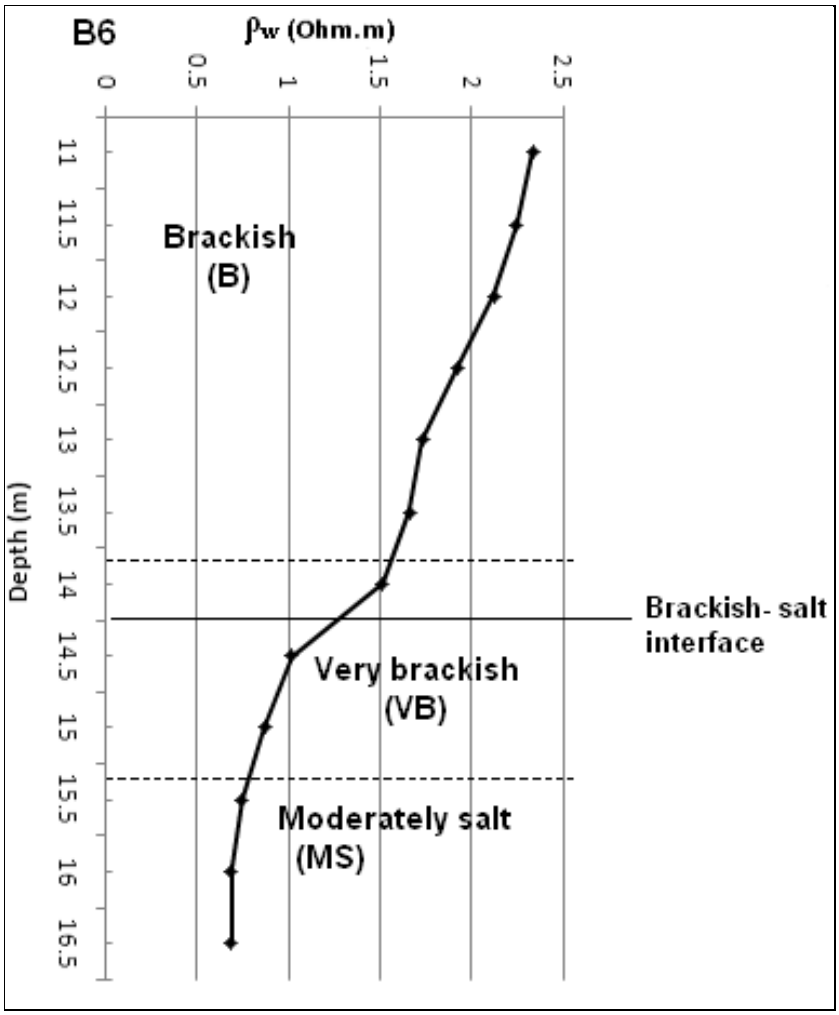

Figure 5.10(f): Resistivity log at observation borehole B6 (location of the borehole is indicated in Fig. 5.7).

RESISTIVITY LOGGING AT POINT B7

The resistivity logging at point B7 (Fig. 5.7) is located at the reefal limestone at Masaki peninsular, about 0.661 km from the ocean (measured from Msasani side). The static water level of 12.5 m below the ground was measured at B7. Resistivity curve at point B7 (Fig. 5.10g) shows a sharp drop in resistivity from 1.72 Ωm at a depth of 12.5 m to 1.04 Ωm at a depth of 13 m. Thereafter a further drop in resistivity continues to 0.52 Ωm at a depth of 16 m; the resistivity of water remains stable fluctuating around 0.4 Ωm till the end of the borehole depth. Based on the water resistivity (ρ_w) classification in Table 5.1, the borehole indicates brackish (B) to moderately salt (MS) and salt (S) water quality. The brackish-salt water interface is observed at a depth of about 12.75 m (Fig. 5.10g).

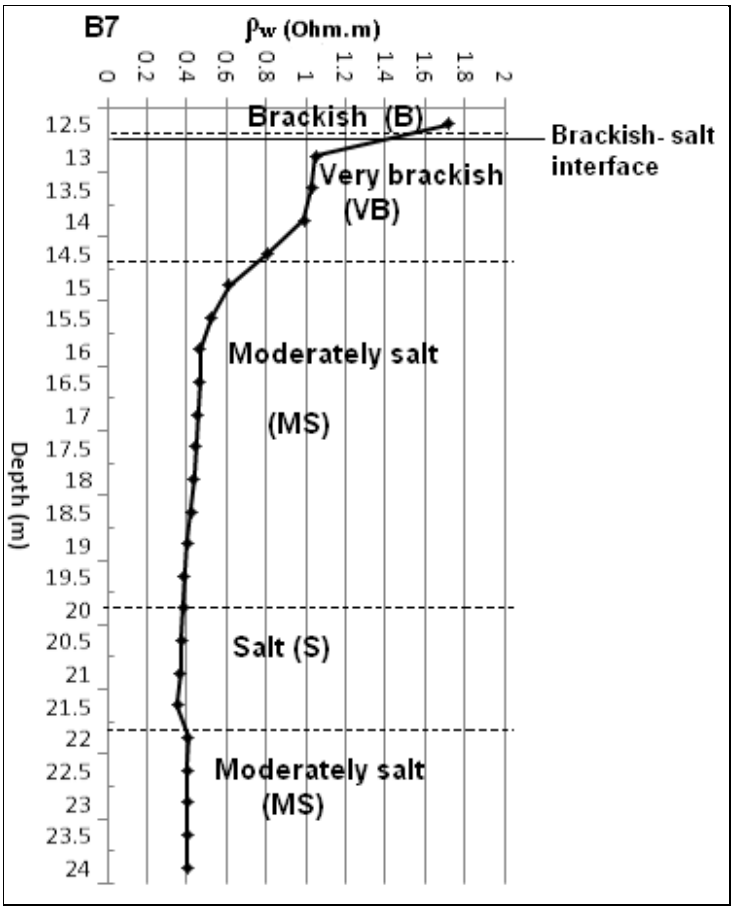

Figure 5.10(g): Resistivity log at observation borehole B7 (location of the borehole is indicated in Fig. 5.7).

RESISTIVITY LOGGING AT POINT B8

The resistivity logging at point B8 (Fig. 5.7) is located at the reefal limestone at Masaki peninsular, about 0.650 km from the ocean (measured from Msasani side), 0.47 k m south of borehole B7. It is about 1.3 km away from point B5. The static water level of 12.5 m below the ground was measured at B7. Resistivity curve at point B8 (Fig. 5.10h) shows a drop of resistivity observed to occur from 1.16 Ωm at a depth of 12.5 m to 0.48 Ωm at a depth of 15.5 m. Thereafter resistivity of water decreases until it reaches a value of 0.35 Ωm at the end of the borehole depth (23.5 m). Based on the water resistivity (ρ_w) classification in Table 5.1, borehole B8 (Fig. 5.12c) indicates water quality variation from very brackish (VB) to salt (S). The brackish-salt water interface occurs at a depth of about 12.75 m. B8 is comparable to B7: interface is at water table, and all measured water resistivity values are strikingly low in both boreholes.

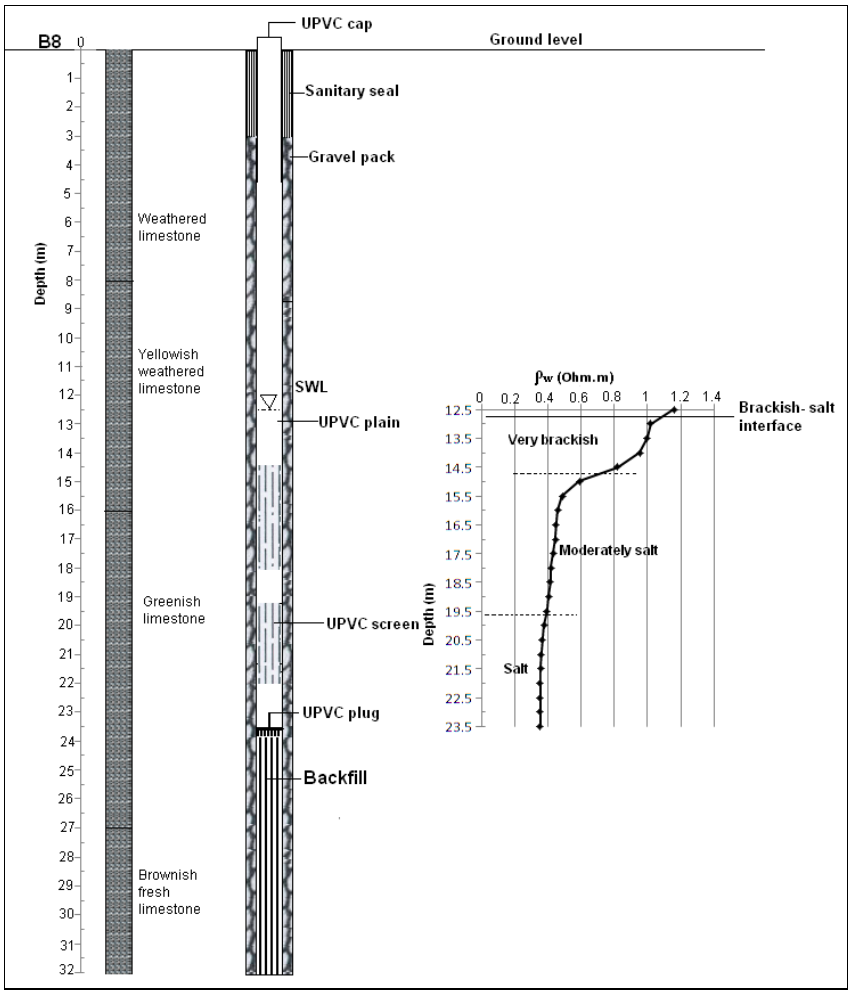

Figure 5.10(h): Resistivity log at observation borehole B8 (location of the borehole is indicated in Fig. 5.7).

RESISTIVITY LOGGING AT POINT B9

The resistivity logging at point B9 (Fig. 5.7) is located on the northern shore of Mzinga estuary at 0.060 km distance from the shore. The static water level of 7 m below the ground was measured at B9. The resistivity curve at point B9 (Fig. 5.10i) indicates a constant resistivity of 5 Ωm from the depth of 7 m to 12 m. Thereafter a sharp drop of resistivity from 4.8 Ωm to 1.39 Ωm occurs in the depth interval between 12.5 m to 13 m. A gradual decrease of resistivity continues till the value of 0.97 Ωm at the bottom of the borehole (15 m). Based on the water resistivity (ρ_w) classification in Table 5.1, this borehole indicates water quality variation from moderately brackish (MB) to very brackish (VB). A clear brackish- salt water interface occurs at a depth of around 13 m.

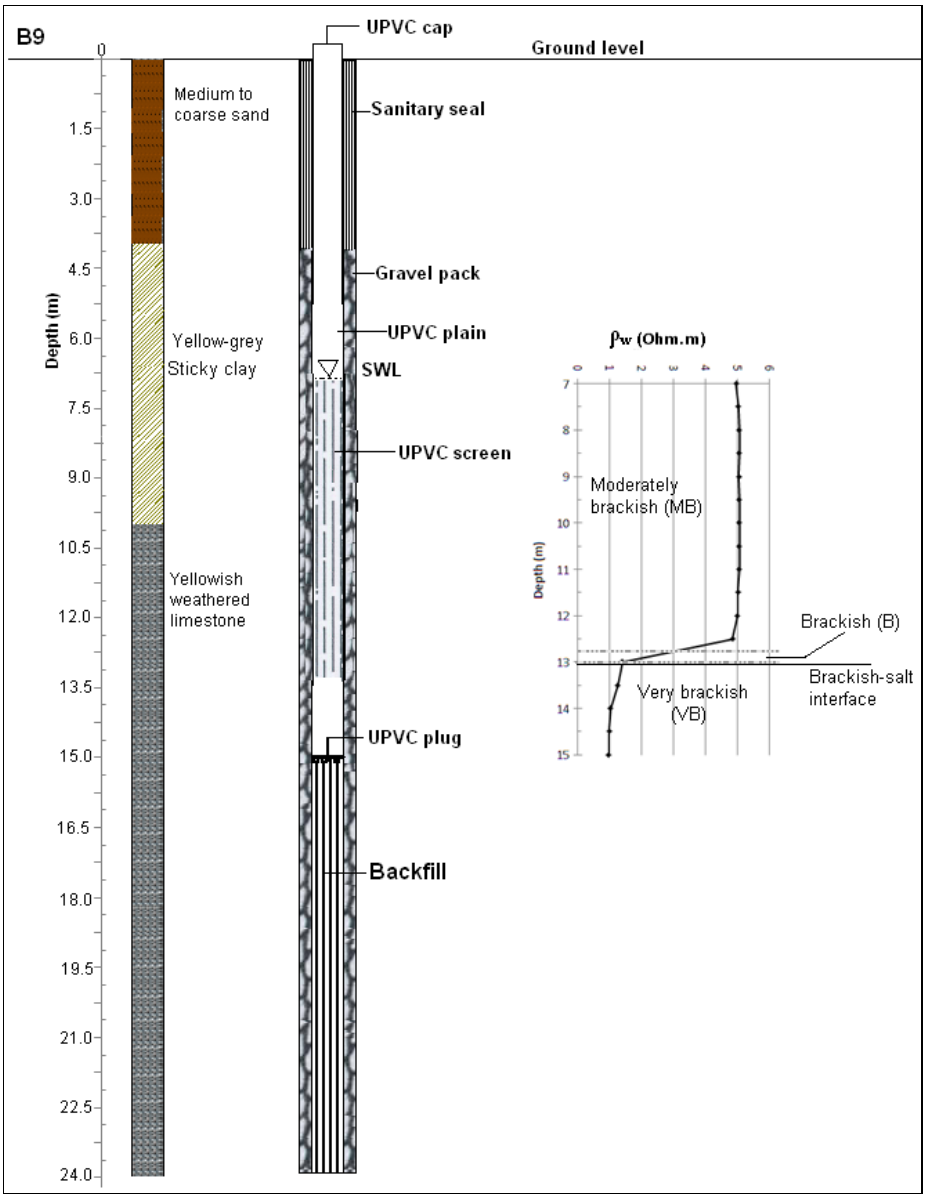

Figure 5.10(i): Resistivity log at observation borehole B9 (location of the borehole is indicated in Fig. 5.7).

RESISTIVITY LOGGING AT POINT B10

The resistivity logging at point B10 (Fig. 5.7) is located at the outlet of Mzinga estuary, at 0.150 km from the ocean. The static water level of 9 m below the ground was measured at B10. The resistivity curve at point B10 (Fig. 5.10j) indicates a gradual decrease of resistivity from 2.05 Ωm to 1.65 Ωm over the depth interval from 9 m to 12.5 m. A sharp drop with a gradual decrease of resistivity is observed between a depth of 12.5 m and 13 m whereby the resistivity drops from 1.65 Ωm to 1.05 Ωm. This is followed by a constant resistivity of 1 Ωm to the depth of 18 m. Thereafter the resistivity slightly decreases till it reaches the value of 0.95 Ωm at the bottom of the borehole (20 m deep). Based on the water resistivity (ρ_w)

classification in Table 5.1, this borehole indicates water quality variation from brackish (B) to very brackish (VB). A clear brackish- salt water interface occurs at a depth of around 12.75 m.

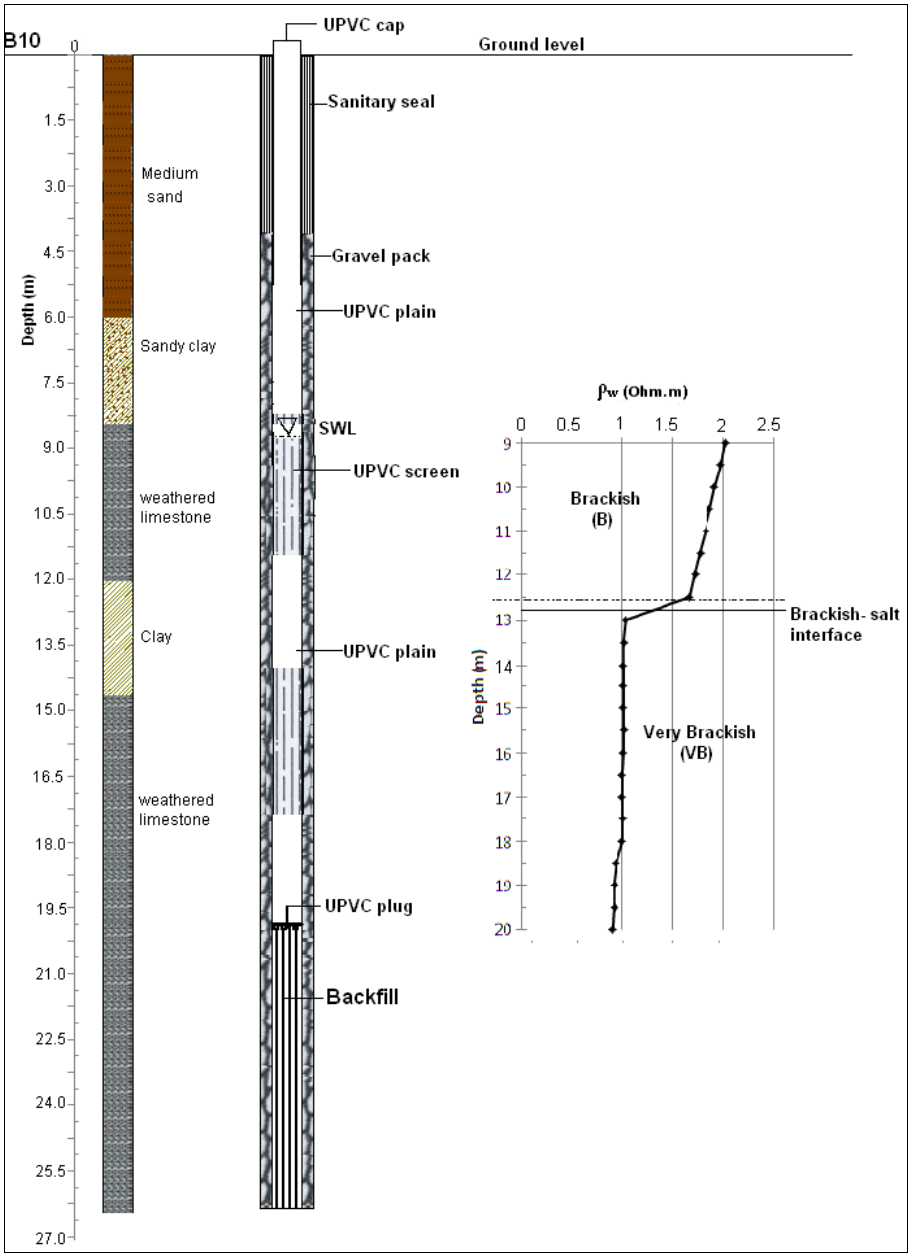

Figure 5.10(j): Resistivity log at observation borehole B10 located near the coastline (location of the borehole is indicated in Figs. 5.7).

RESISTIVITY LOGGING AT POINT B11

The resistivity logging at point B11 (Fig. 5.7) is located on the northern shore of Mzinga estuary, at 0.563 km distance from the shore. It is 0.4 km north of borehole B9. The static water level of 6 m below the ground was measured at B7. The resistivity curve at point B11

(Fig. 5.10k) indicates no significant change of resistivity. In the first 1 m depth interval between 6 m to 7 m depth, resistivity drops from 3.07 Ωm to 2.94 Ωm. Thereafter resistivity fluctuates between 2.90 Ωm and 2.95 Ωm. Based on the water resistivity (ρ_w) classification in Table 5.1, this borehole indicates brackish (B) water quality. No interface could be determined at point B11 since the curve shows only brackish water: there is neither freshwater on top nor very brackish/salt water at the bottom. Most probably, the brackish-salt water interface occurs somewhere in the backfilled bottom part of the borehole (backfill from 15 m to 19.5 m depth).

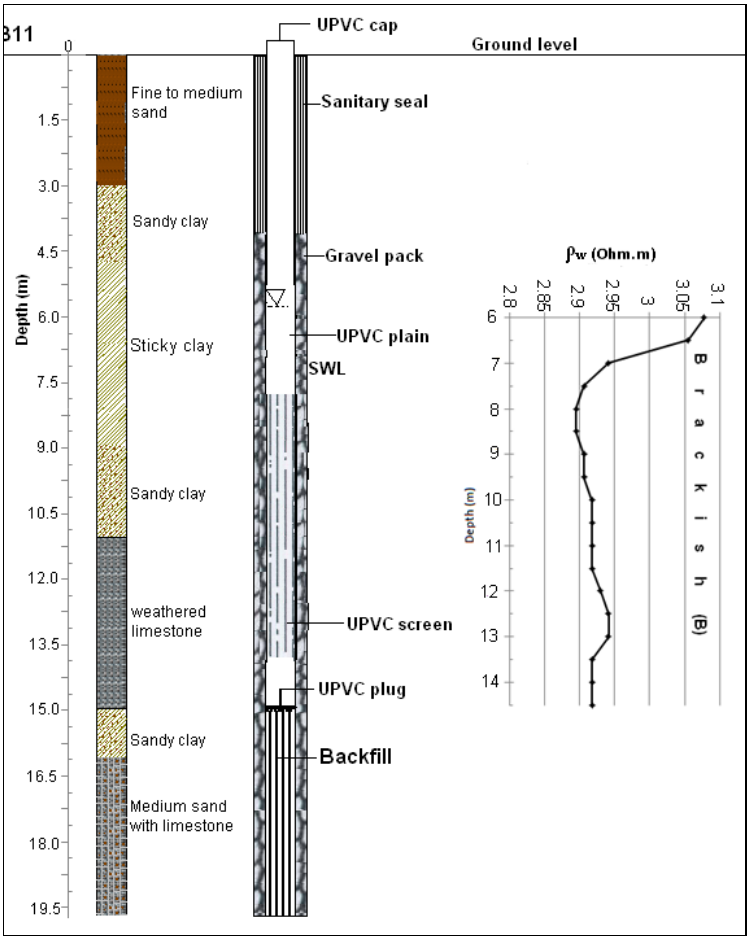

Figure 5.10(k): Resistivity log at observation borehole B11 located near the coastline (location of the borehole is indicated in Figs. 5.7 and 5.6e).

RESISTIVITY LOGGING AT POINT B12

The resistivity logging at point B12 (Fig. 5.7) is located at 0.611 km from the ocean. It is 0.33 km north of B11. The static water level of 5 m below the ground was measured at B7. The water resistivity curve at point B12 (Fig. 5.10) indicates a gradual decrease of resistivity from 29.18 Ωm at 5.0 m depth to 26.75 Ωm at a depth of 6.5 m. A sharp drop of resistivity is observed between the depths of 6.5 m and 7.5 m whereby the resistivity drops from 26.79 Ωm to 1.60 Ωm. This is followed by a constant resistivity of 1.3 Ωm to the bottom of the borehole at 10 m. Based on the water resistivity (ρ_w) classification in Table 5.2, this borehole indicates water quality variation from fresh (F) to very brackish (VB). A clear brackish- salt water interface occurs at a depth of around 7.5 m.

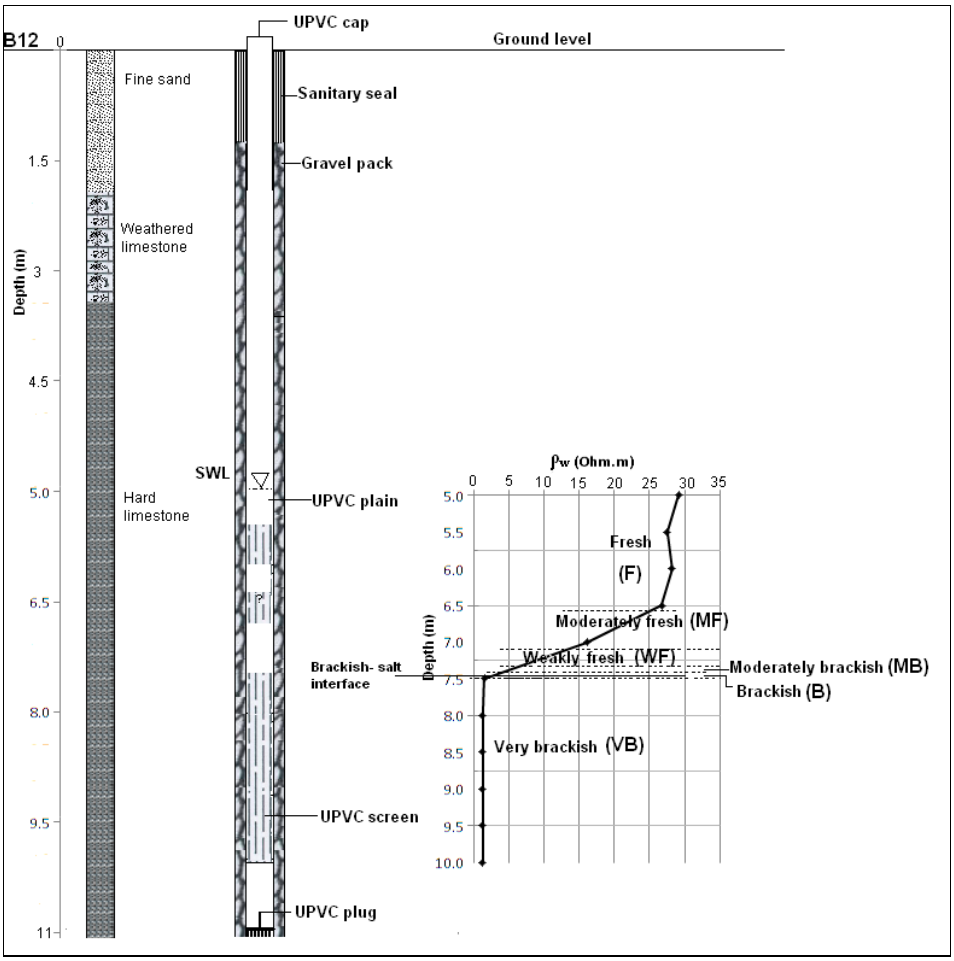

Figure 5.10(l): Resistivity log at observation borehole B12 (location of the borehole is indicated in Figs. 5.7).

RESISTIVITY LOGGING AT POINT B13

The resistivity logging at B13 (Fig. 5.7) is located about 2.7 km from the ocean. It is the most inland borehole where a resistivity logging was performed. The static water level of 8.5 m below ground was measured at B13. The resistivity curve at point B13 (Fig. 5.11d) was conducted up to the depth of 37 m but the saltwater interface was not reached. A quick drop of resistivity is observed between a depth of 8.5 m and 14 m whereby the resistivity drops from 17.77 Ωm to 10.83 Ωm. For the depth between 14 m and 37 m, resistivity fluctuates around 10 Ωm. Based on the water resistivity (ρ_w) classification in Table 5.2, water quality in this borehole varies from moderately fresh (MF) to weakly fresh (WF).

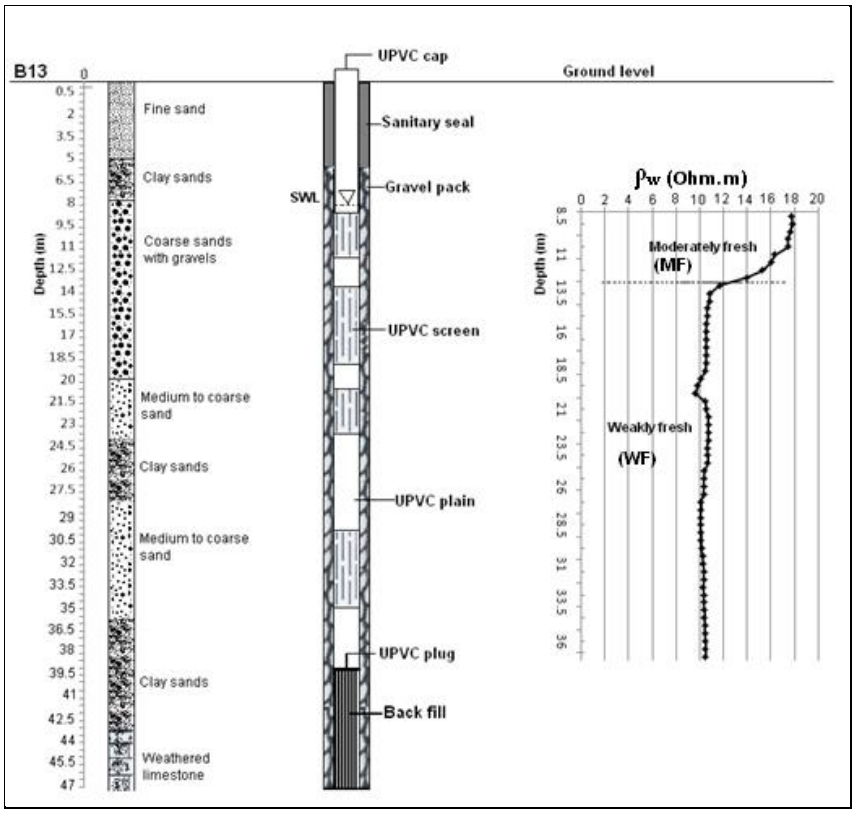

Figure 5.10(m): Resistivity log at observation borehole B13 (location of the borehole is indicated in Figs. 5.7).

5.3.1.3 Seawater intrusion zones

Geophysical data supported by groundwater hydrogeochemical data (Fig. 5.11) and groundwater hydrochemical/lithological sections (Fig. 5.12a-e), have enabled to draw a map showing the depth of the freshwater/saltwater interface (Fig. 5.13).

Fig. 5.11 indicates the zone where seawater intrusion has taken place, and the fresh water zone. Electrical conductivity (EC) of groundwater shows a general increase down gradient to the east towards the coastline (Fig. 5.11). EC values in groundwater between 2000-10000 μS/cm have been recorded in several points and a value higher than 10000 μS/cm has been measured in six points. Hydrochemical/lithological cross-sections in Figs. 5.12 (b-c) indicate the trend of EC and chloride concentration decreasing from the ocean to inland. The findings that salinity decreases with increasing distance from the coast and that salinity increases with increasing depth, indicate that seawater intrusion causes the salinization. Some boreholes close to the coastline, such as 30 (EC: 7490 μS/cm) in cross-section A-A' (Fig. 5.12b); B10 (17600 μS/cm) in cross-section B-B' (Fig. 5.12c); Fish Market (19310 μS/cm) in cross-section C-C' (Fig. 5.12d) & 1 (15400 μS/cm) in cross-section D-D' (Fig. 5.12e), show high values of EC, which is consistent with the high salinity values ($Cl^- \geq 2500$ mg/l) of these boreholes. The Fish Market borehole (cross-section C-C') indicates that, at the time the borehole was drilled in 2004, values for EC and Cl^- concentration were 1542 μS/cm and 226.9 mg/l respectively. Groundwater analysis conducted in 2010 in this study shows EC and Cl^- concentration values have changed tremendously to 19310 μS/cm and 4906.3 mg/l respectively. This has been caused by excessive pumping to meet the water demand needed for several activities taking place at the fish market, especially washing, cleaning and cooking.

Boreholes 25 and 30 in Fig. 5.12(b), boreholes B9, DSM 490/2008 and B10 in Fig. 5.12c, boreholes B12, DSM 560/2004 and Fish Market in Fig. 5.12d, and all boreholes (B8, 6 & 1) in Fig. 5.12(e) are located mainly in the limestone formation and close to the coastline with elevation less than 15 m above sea level: these boreholes tap water from weathered/fractured calcareous limestone and are within the relatively flat land; EC values in these boreholes are above the acceptable limit (1500 μS/cm) of WHO (2004) for drinking water. On the other hand, boreholes B13, 21 and 23 in Fig. 5.12(b) and borehole DSM 604/2003 in Fig. 5.12(c), located more inland, at elevation greater than 15 m above sea level are characterized by EC values within the acceptable limit for drinking water. These boreholes penetrate the medium to coarse sand formations. Borehole DSM 428/2003 (Fig. 5.12c) located near Mzinga estuary at a distance of 0.1 km, in the intermediate area between the boreholes close to the coastline and those located away from the coastline, taps water from weathered limestone which shows

good water quality as regard to chloride concentration (113.6 mg/l) and EC (840 µS/cm). The low chloride concentration in this borehole is associated with the large distance from ocean.

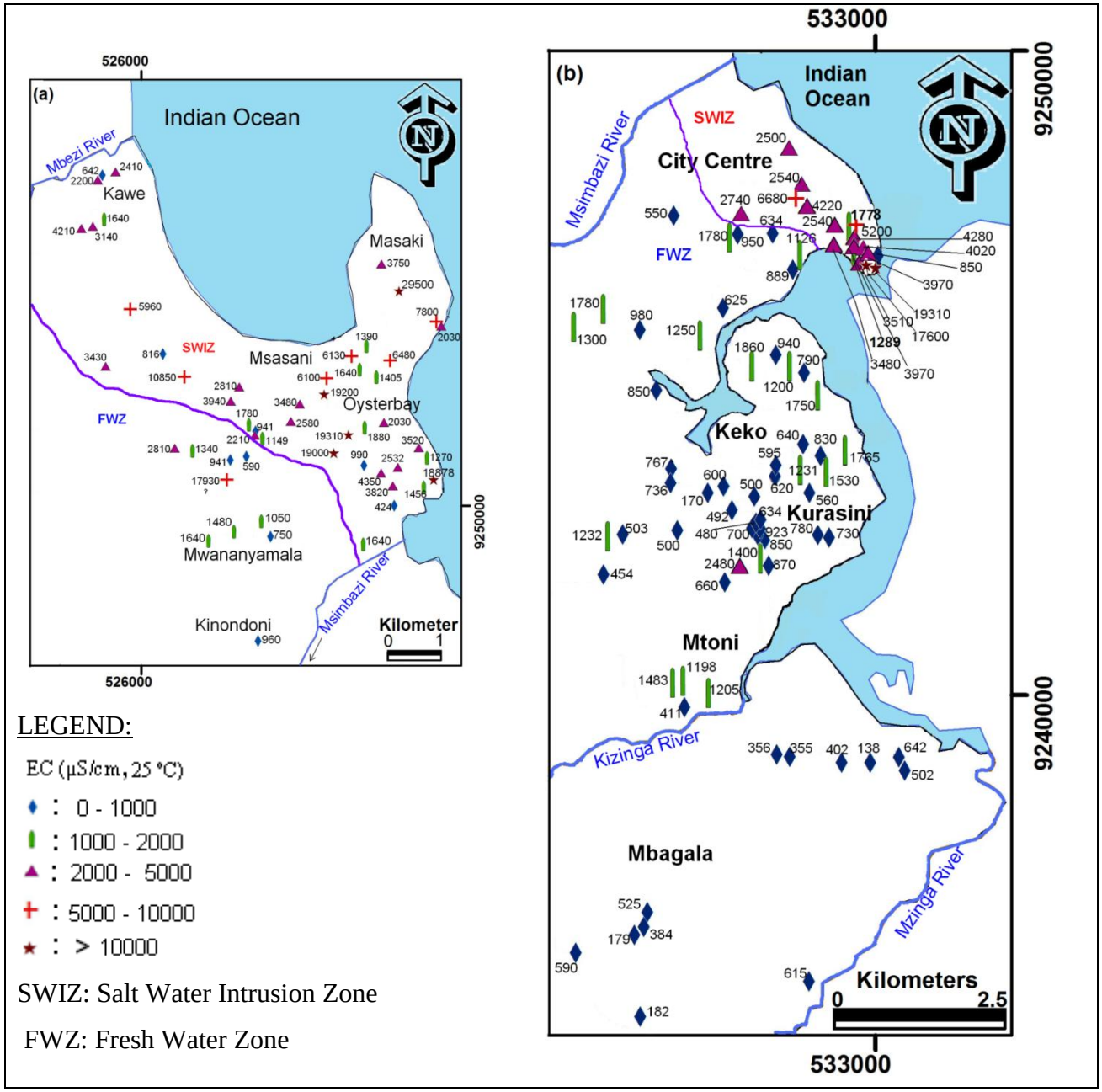

Figure 5.11: Electrical conductivity (EC) values for selected groundwater samples and estimated limit of seawater intrusion zone.

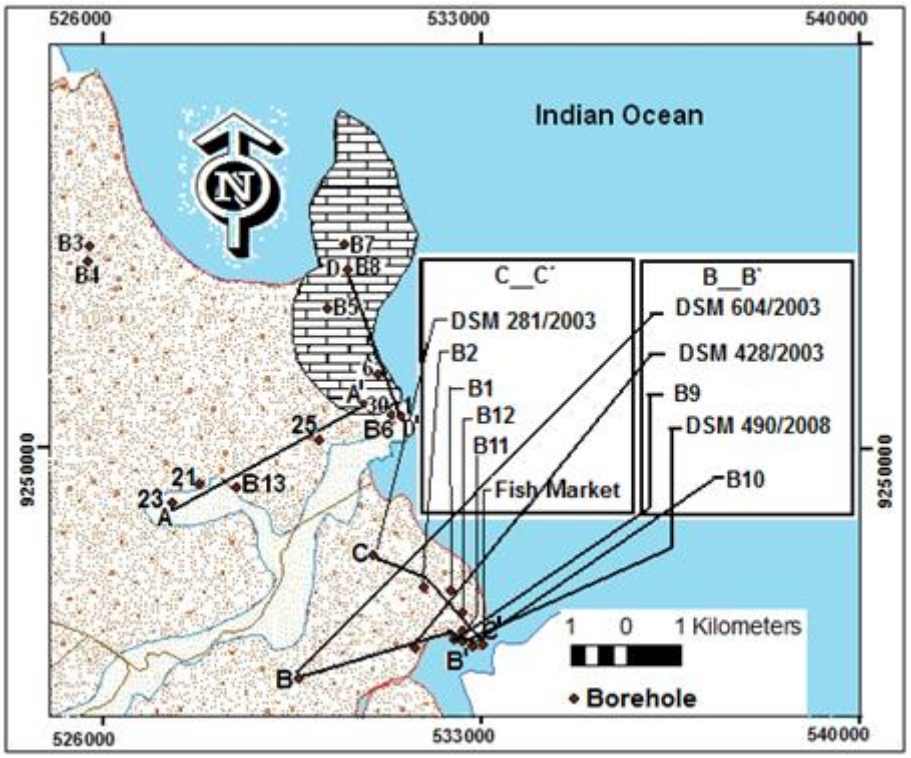

Figure 5.12(a): Location map of hydrochemical/lithological profiles in the study area.

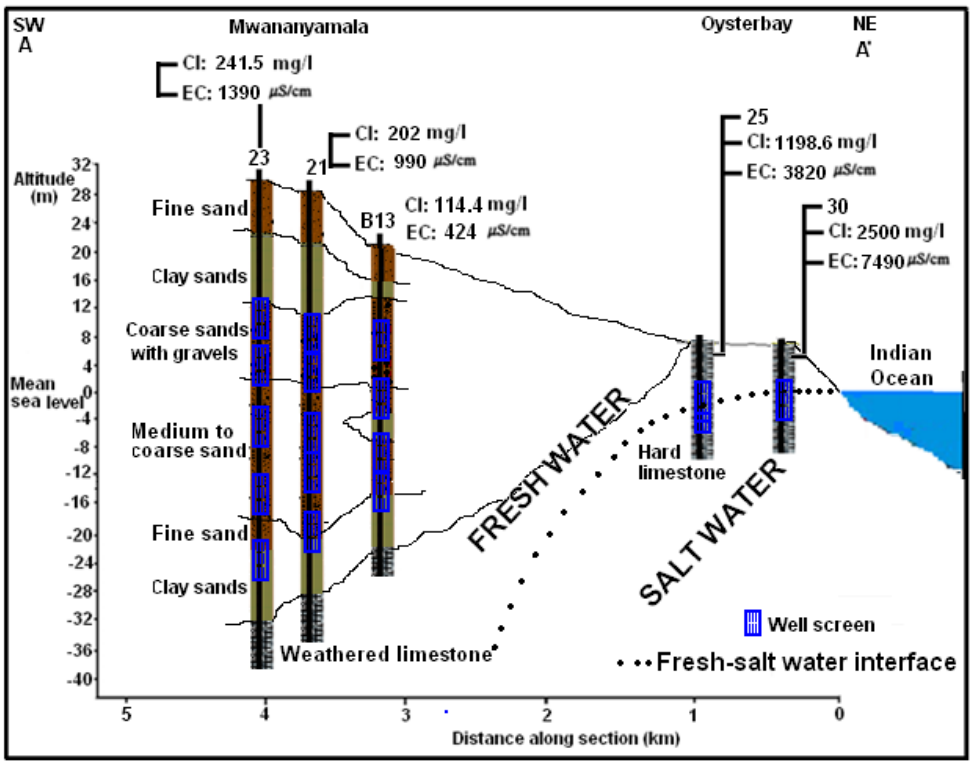

Figure 5.12(b): Hydrochemical/lithological cross-section A-A' showing electrical conductivity and chloride concentration values decreasing from the coastline to inland. Location of the profile is shown in Fig. 5.12(a).

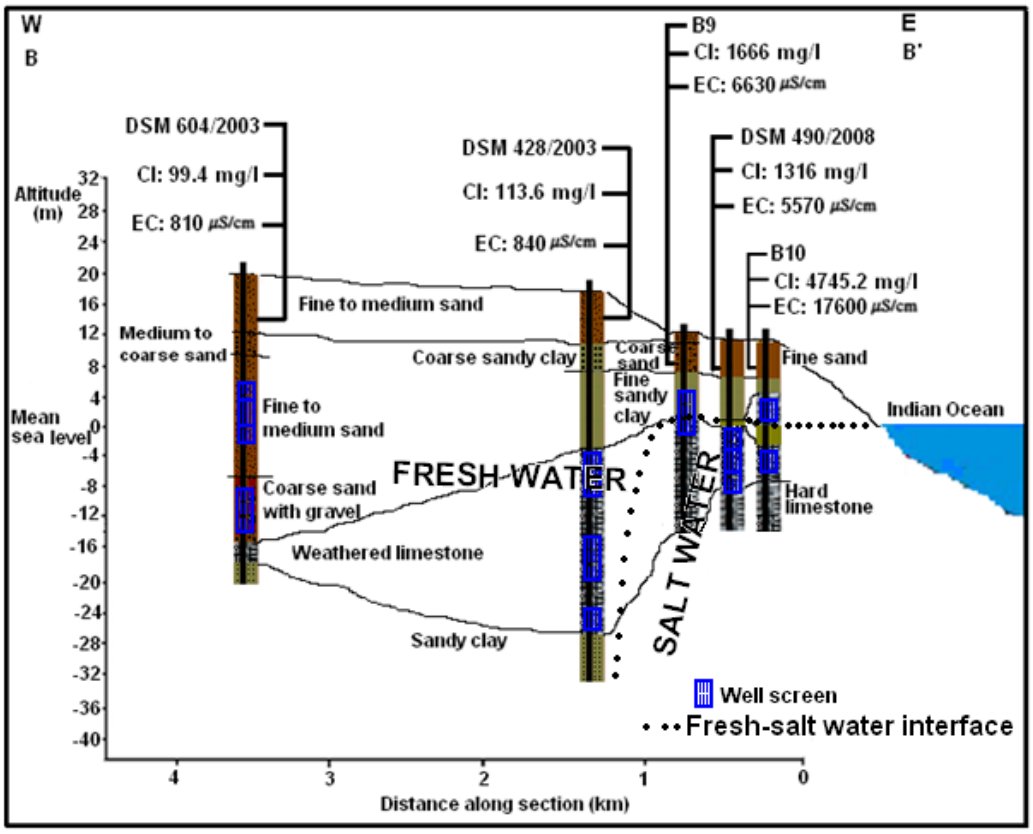

Figure 5.12(c): Hydrochemical/lithological cross-section B-B' showing electrical conductivity and chloride concentration values decreasing from the coastline to inland. Location of the profile is shown in Fig. 5.12(a).

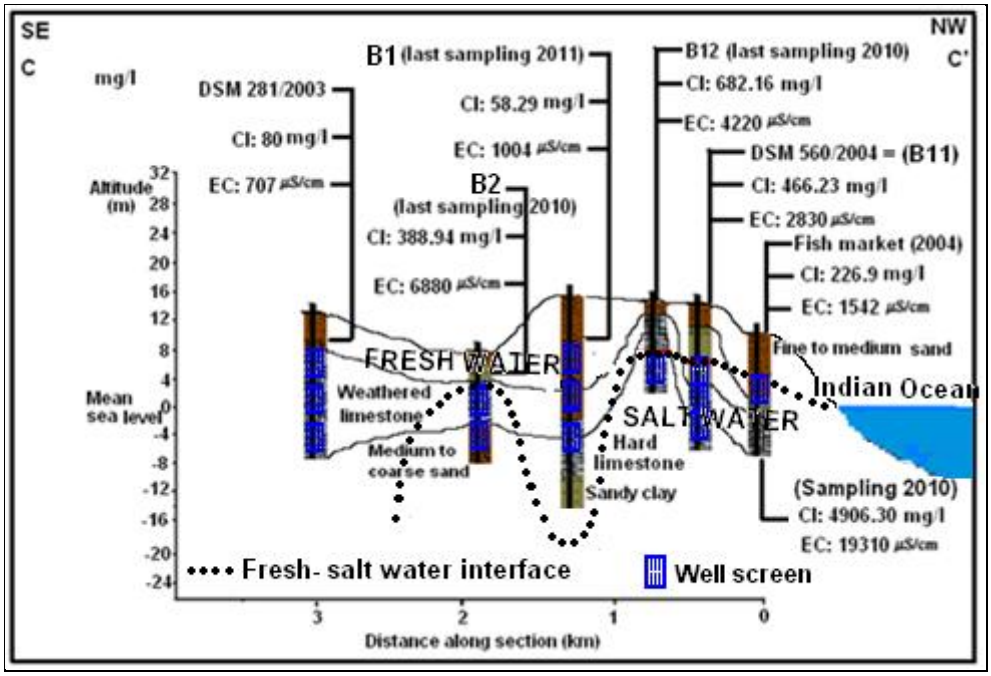

Figure 5.12(d): Hydrochemical/lithological cross-section C-C' showing electrical conductivity and chloride concentration values decreasing from the coastline to inland. Location of the profile is shown in Fig. 5.12(a).

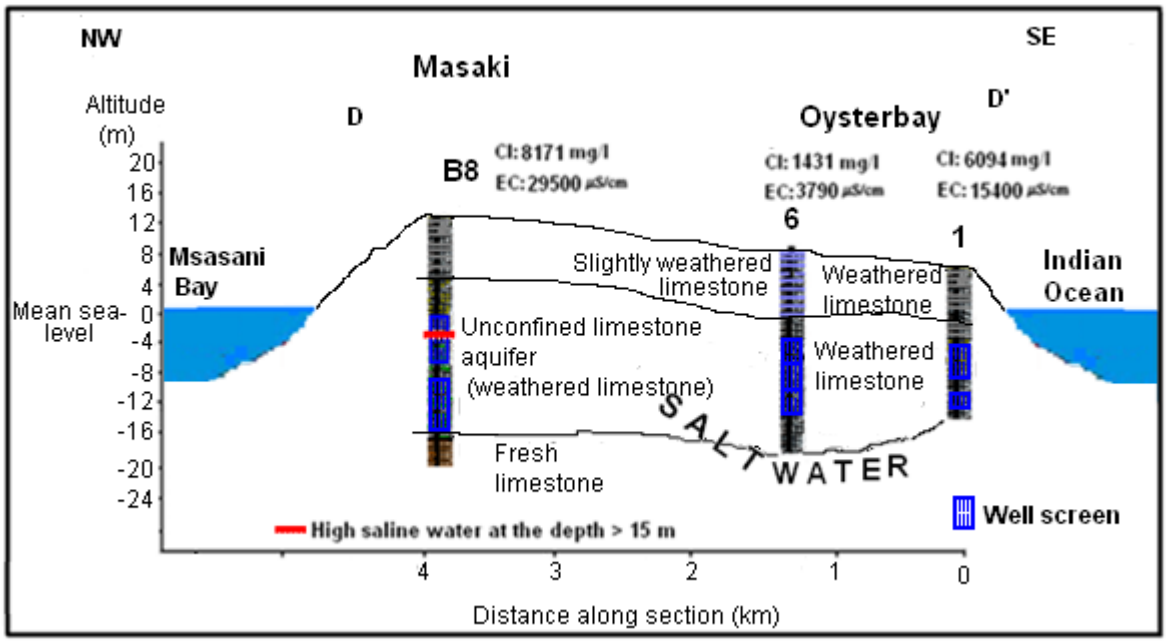

Figure 5.12(e): Hydrochemical/lithological cross-section D-D' showing high electrical conductivity and chloride concentration values near the coastline in limestone formation. Location of the profile is shown in Fig. 5.12(a).

The interpretation of the VES resistivity data indicates that there are three to four layers in the study area (Table 5.2; Figs. 5.9a-h and Appendix 5.1a-b). The inspection of lithological logs from the available groundwater drilling reports indicates that the study area is characterized by alternating layers of sands, clays, gravel and coral limestone of various degree of weathering. VES data for points located near monitoring boreholes, together with the water salinity data of these boreholes, allowed to identify the unsaturated zone and zones of water bearing formation.

Most of VES carried out near the coastline in the study area indicate: the top layer consists of the unsaturated zone, the intermediate layer consists of fresh-water saturated limestone or sands and the bottom layer is saltwater saturated. Unlike the inland where boreholes exist up to 80 m deep, drilling near to the coastline ranges mostly between 10 and 20 m depth, restricted by the water quality and avoidance of seawater intrusion risk. In the study area, several points especially near the coastline have indicated low resistivity less than 10 Ωm. The majority (68%) of VES have shown resistivity values as low as 12.5 Ωm. Six cross sections (Fig. 5.13c-h) were drawn showing the presence of salt water near the coastline. The cross-sections through S2, S1 and S3 (cross-section II-II'; Fig. 5.13(d)) and through S6 and S7 (cross-section III-III'; Fig. 5.13(e)) located in the eastern and central parts of the survey zone (Fig. 5.7 section 5.3.1.2.3) indicate saltwater was found at less depth compared to the

cross-section through S5, S4 and S8 (IV-IV'; Fig. 5.13(f)) located in the western part of survey zone (Fig. 5.7 section 5.3.1.2.3). Vertical electrical sounding did not continue for larger spacing "a" to reach brackish-saltwater interface for S8 (Fig. 5.13(f)). The boundary between fresh and saline waters is marked. Borehole B13 (Fig. 5.13g) indicates the presence of fresh water away from the coastline. 32% of VES did not reach resistivity values as low as 12.5 Ωm and the interface was assumed not to be reached (and possibly salt water is absent in these points). The fresh/saline water interface deepens to the west and southward of the study area, giving rise to a large fresh water body in these directions. Salt water was found mostly in the area within 2 km of the coastline, and the depth to the interface is ranging from 1.3 m to 20 m. Away from the coastline, the interface (if present) is at greater depth that could not be reached by the instrument/lower-power equipment used. However, toward the south of the study area, the VES (67: Appendix 5.1b; Fig 5.13a) executed at Kurasini (located 4 km from the sea at the mouth of Mzinga Creek to the sea), showed the freshwater/saltwater interface at a greater depth (43 m).

Resistivity logging measurements were as well interpreted in terms of groundwater quality according to Table 5.1 whereby a constant formation factor = 4 is assumed. The subdivision of water quality of resistivity logging measurement is already given in section 5.3.1.2.4. The fresh- salt water interface defined based on VES (ρ_t = 12.5 Ωm) is divided by 4 and thus the interface for resistivity logging measurement is defined by ρ_w = 3.13 Ωm (Figs. 5.13(a) and 5.14(a-c)). Eleven (11) out of thirteen (13) boreholes have shown resistivity values as low as 3.13 Ωm. The depth to the fresh- salt water interface ranges from 6 m to 17 m. If measurements in the boreholes remained greater than 3.13 Ωm, again the interface was assumed not to be reached (and possibly salt water is absent in these points). Borehole B11 (Fig. 5.14b) and B7 and B8 (Fig. 5.14c) located very close to the coastline and which tap water from the weathered/fractured limestone are highly affected by salt water due to groundwater exploitation and also related to the highly transmissive limestone zone that underlies the unsaturated zone.

The results of VES and resistivity logging indicate areas affected by saltwater intrusion include City Centre, Oysterbay, Masaki, Msasani, Kawe, some parts of Mikocheni and Kurasini (Fig. 5.13a).

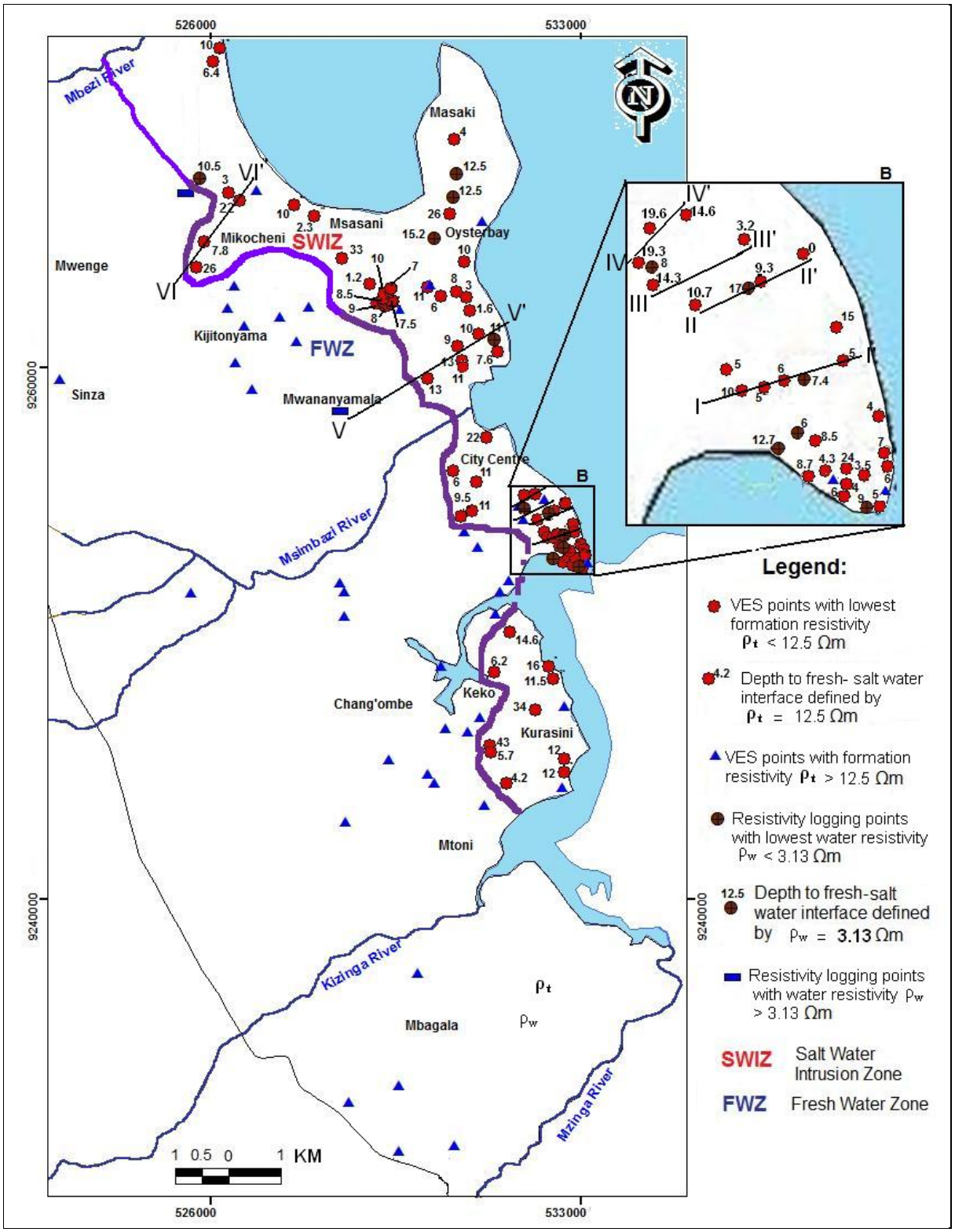

Figure 5.13(a): Map showing depth to fresh- salt water interface based on VES (defined by ρ_t = 12.5 Ωm) and resistivity logging (defined by ρ_w = 3.13 Ωm) data. Fresh water and brackish/salt water are found above and below the interface respectively.

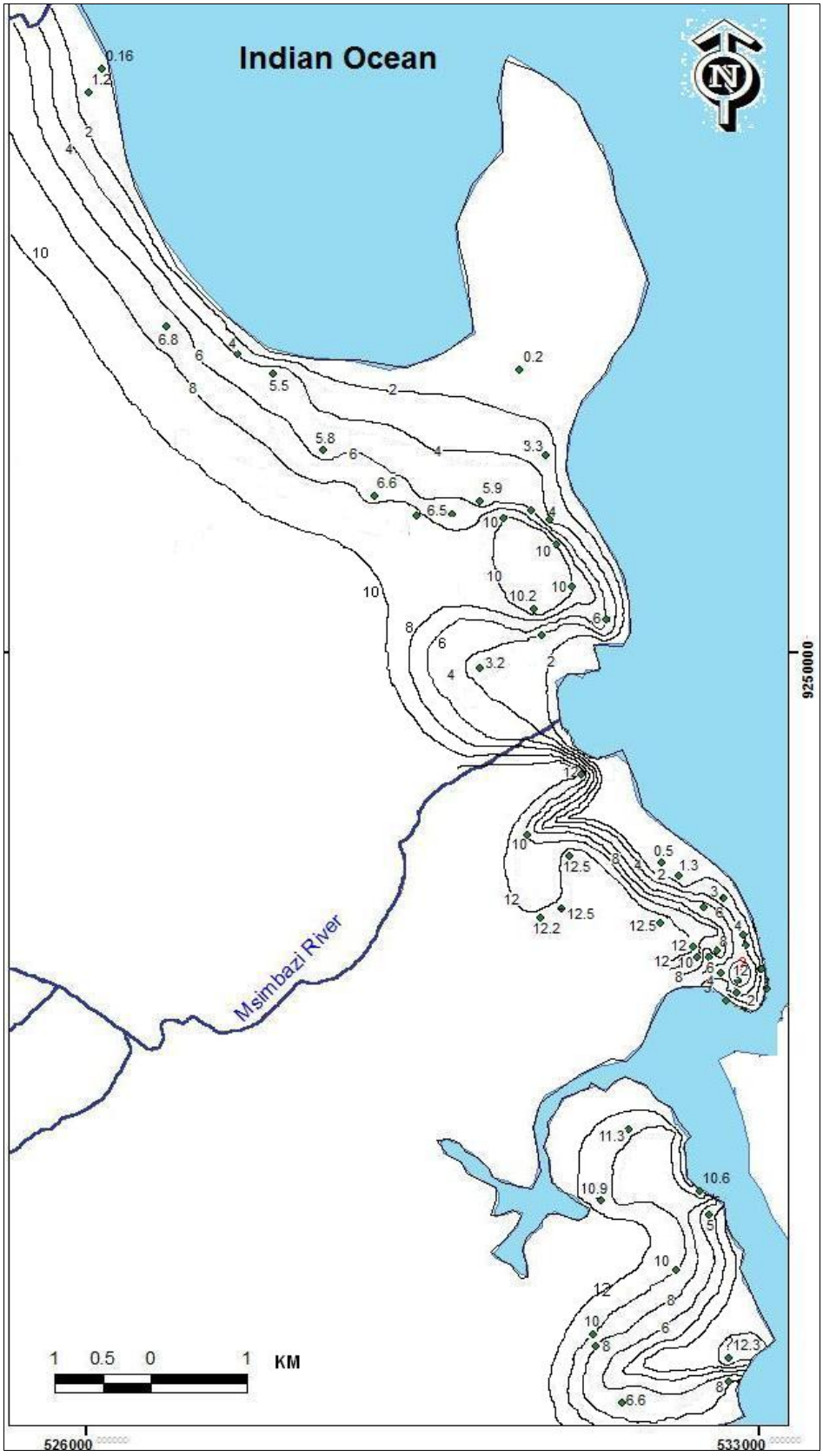

Figure 5.13(b): Resistivity isoline (Ωm) map of aquifer in the saline zone.

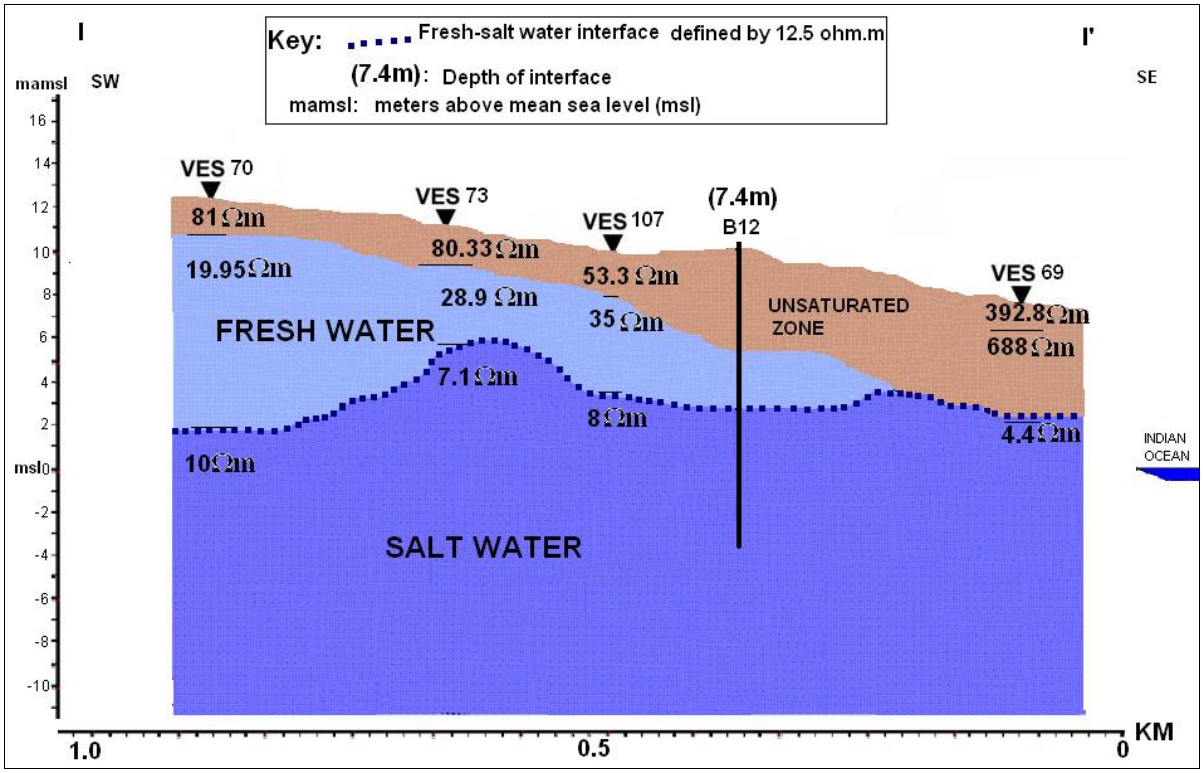

Figure 5.13(c): Fresh- salt water interface based on VES (defined by $\rho_t = 12.5\ \Omega m$) (Location of resistivity profile I-I' is indicated in Fig. 5.13a).

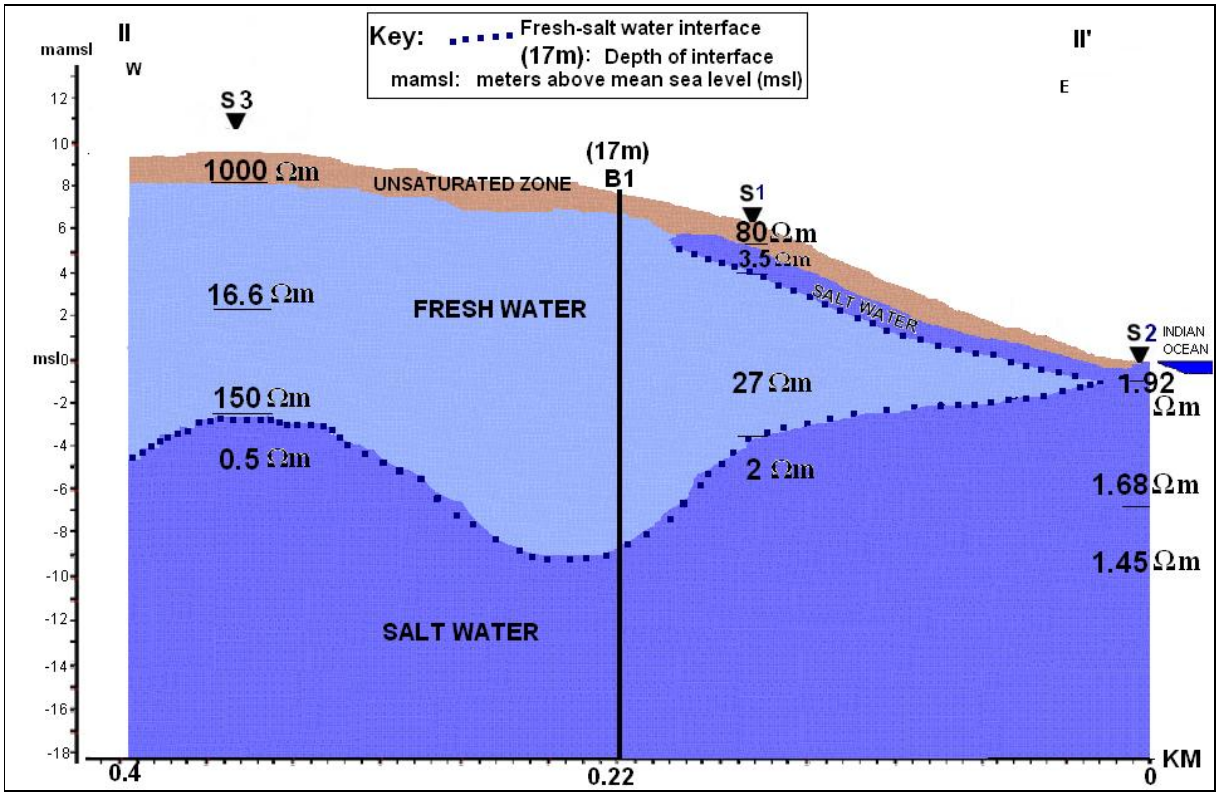

Figure 5.13(d): Fresh- salt water interface (defined by $\rho_t = 12.5\ \Omega m$) based on VES (location of resistivity profile II-II' is indicated in Fig. 5.13a).

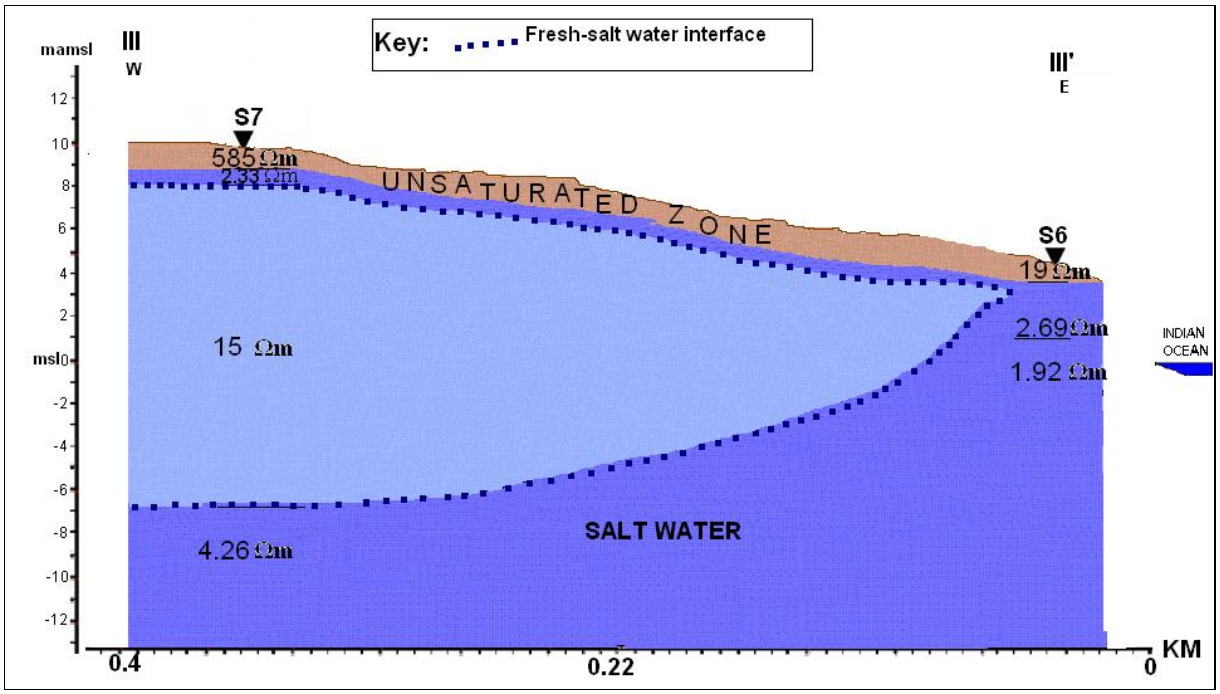

Figure 5.13(e): Fresh- salt water interface based on VES (defined by $\rho_t = 12.5\ \Omega m$) (Location of resistivity profile III-III' is indicated in Fig. 5.13a).

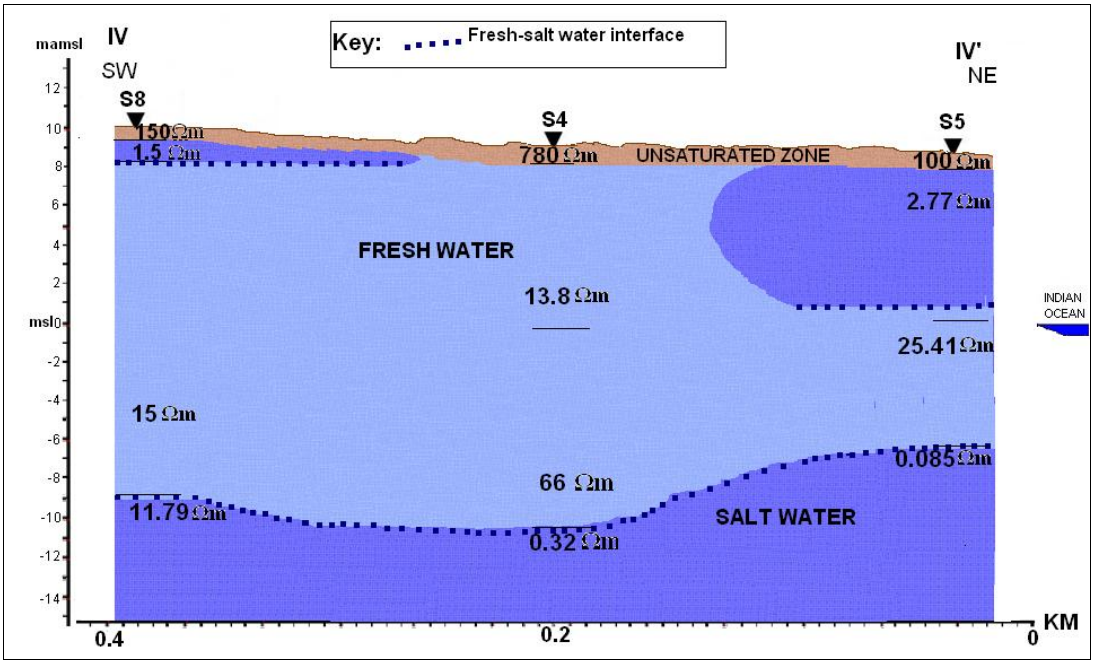

Figure 5.13(f): Fresh- salt water interface based on VES (defined by $\rho_t = 12.5\ \Omega m$) (Location of resistivity profile IV-IV' is indicated in Fig. 5.13a).

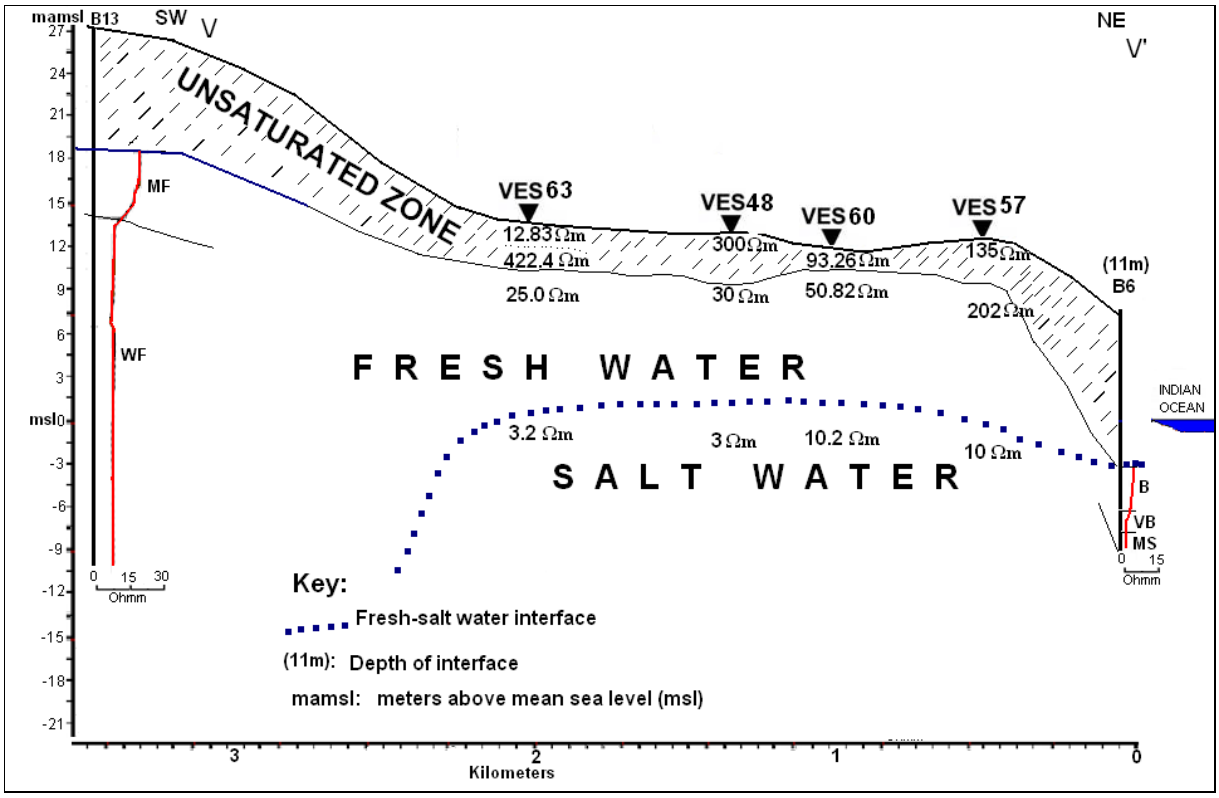

Figure 5.13(g): Fresh- salt water interface based on VES (defined by $\rho_t = 12.5\ \Omega m$) and resistivity logging (defined by $\rho_w = 3.13\ \Omega m$) (location of resistivity profile V-V' is indicated in Fig. 5.13a).

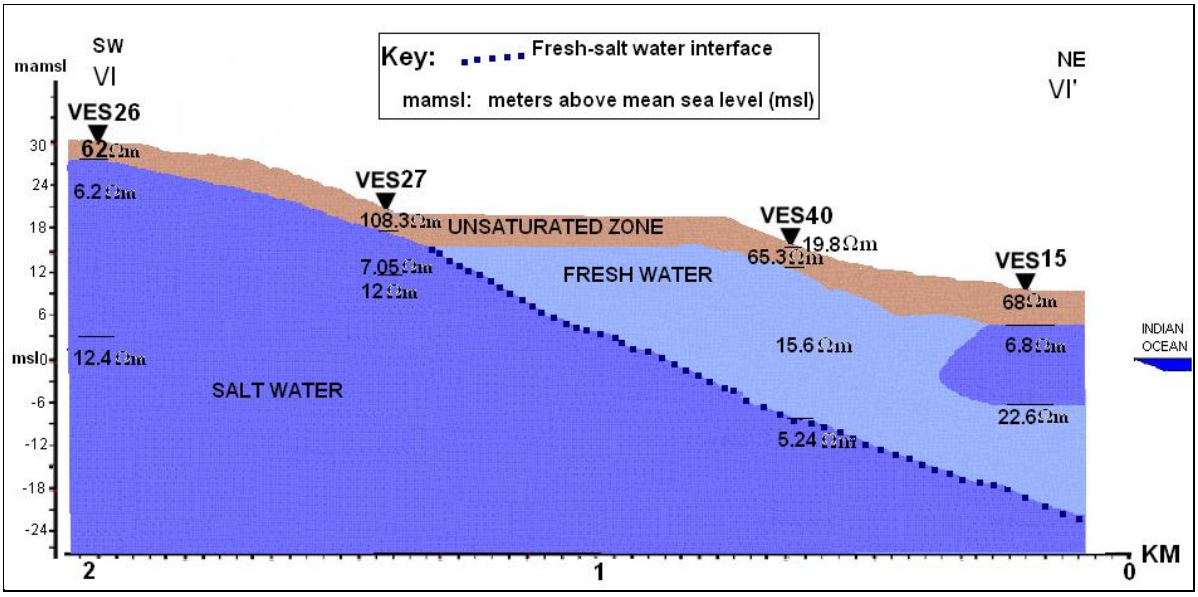

Figure 5.13(h): Fresh- salt water interface based on VES (defined by $\rho_t = 12.5\ \Omega m$) (location of resistivity profile VI-VI' is indicated in Fig. 5.13a).

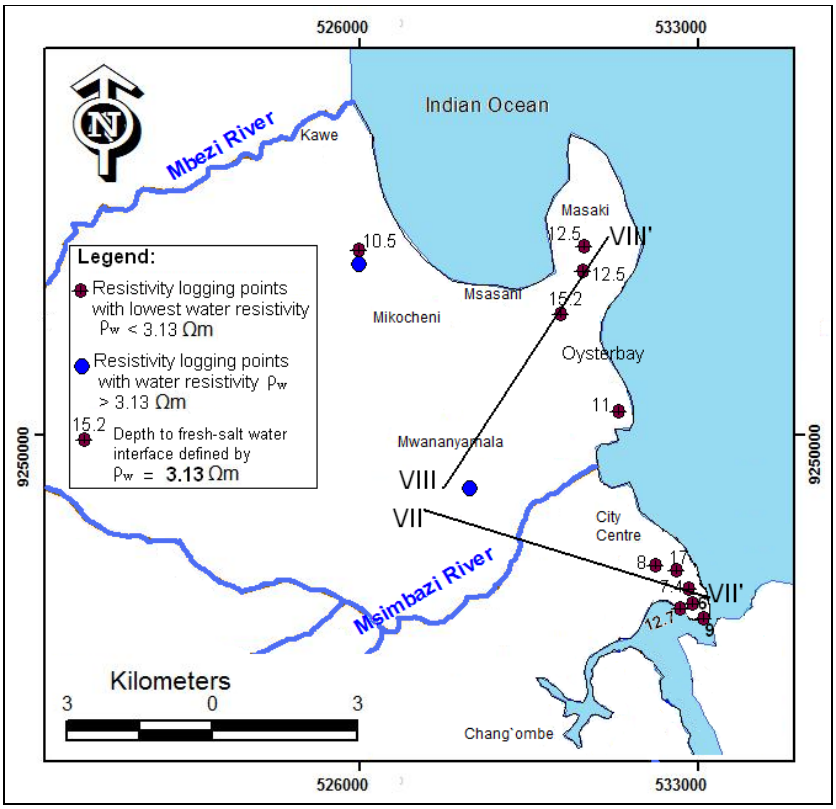

Figure 5.14(a): Map showing depth to fresh- salt water interface based on water resistivity logging data (defined by ρ_w = 3.13 Ωm).

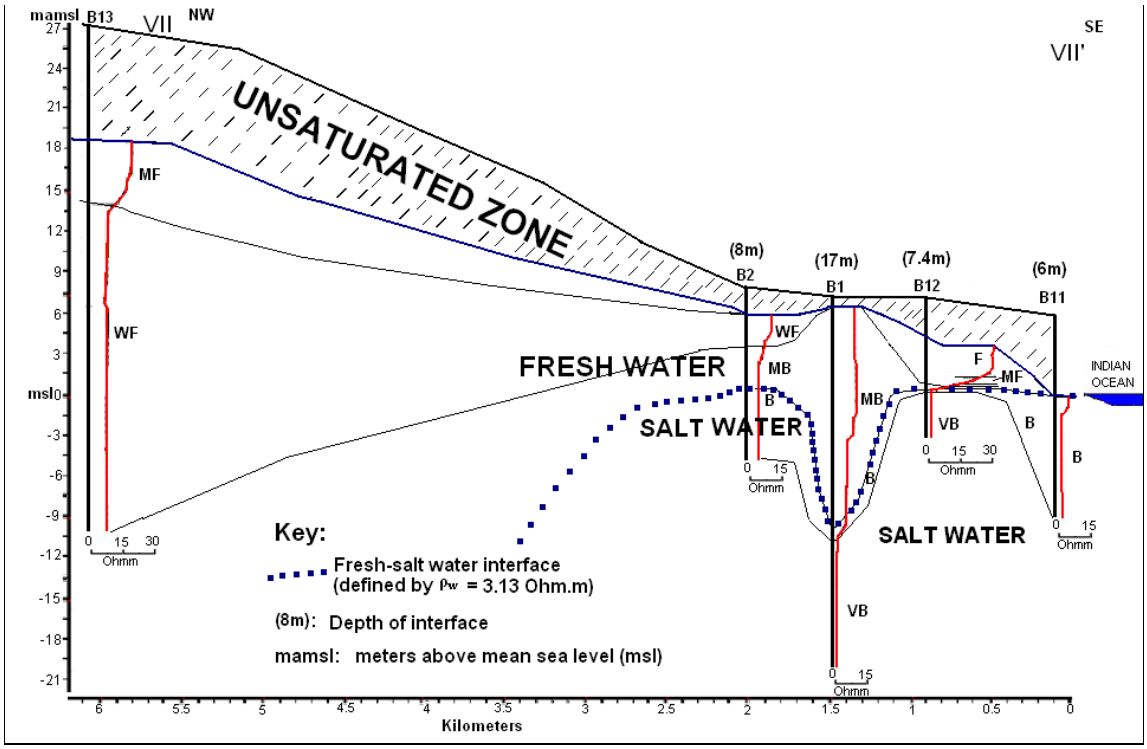

Figure 5.14(b): Fresh- salt water interface based on water resistivity logging data (defined by ρ_w = 3.13 Ωm). (Location of resistivity profile VII-VII' is indicated in Fig. 5.14a).

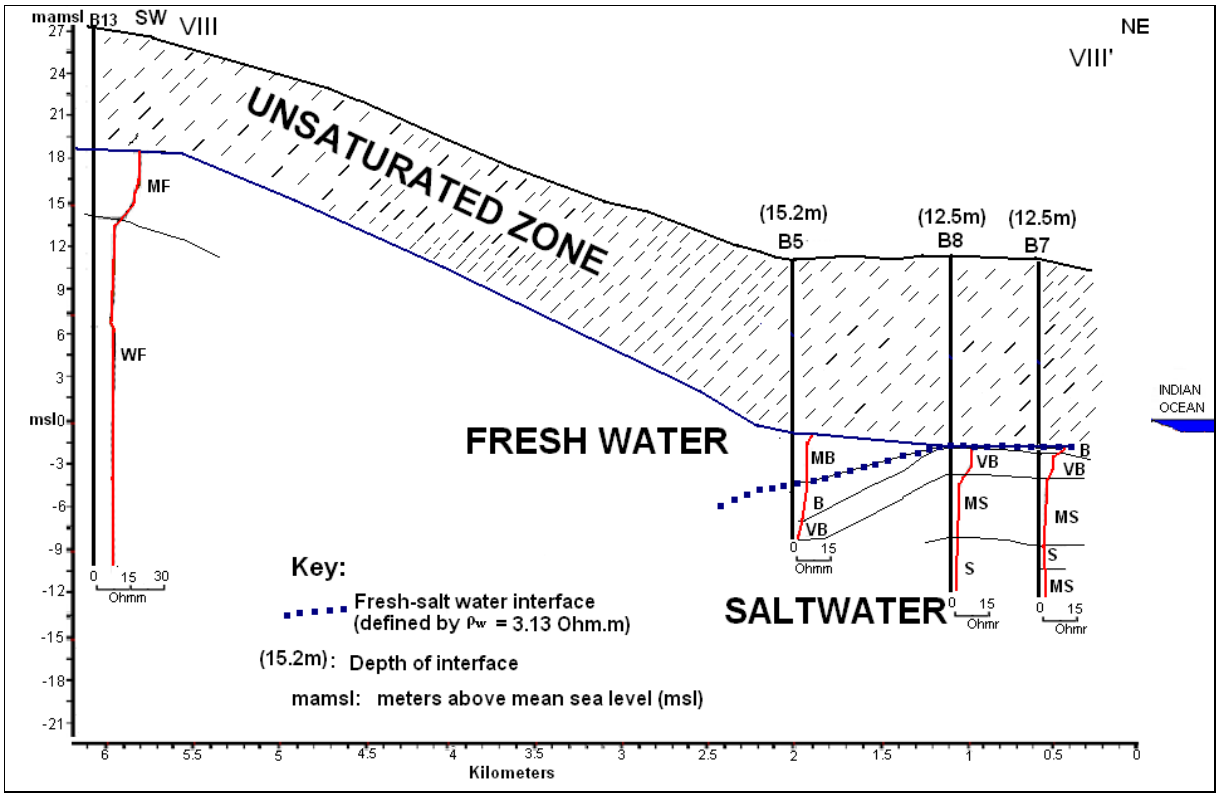

Figure 5.14(c): Fresh- salt water interface based on water resistivity logging data (defined by ρ_w = 3.13 Ωm). (Location of resistivity profile VIII-VIII' is indicated in Fig. 5.14a).

5.3.2 Applied geophysics for groundwater studies and borehole drilling

The use of geophysics for groundwater studies has been stimulated in part by a desire to reduce the risk of drilling dry holes and also to offset the costs associated with poor groundwater production. Despite the success of resistivity survey for both groundwater resource mapping and groundwater quality evaluation, the use of geophysics in Tanzania is still often not adequate. Partly this is because of poor publicity of the potential use of geophysics, practical implementation difficulties and financial limitations. Regrettably it is occasionally because geologists/hydrogeologists/hydrogeophysicists and engineers may have experienced an in-appropriate use of geophysics, ending by getting misleading and/or wrong results.

In the typical situation of the study area near to the coastline, most existing VES show a 3-layer geoelectric section. From the apparent resistivity model and information from a borehole log, their equivalent geologic units are: top soil, sands and/or limestone with variable degree of weathering occupying the intermediate and bottom layers: the top layer

consists of the unsaturated zone, the intermediate layer consists of fresh-water saturated limestone or sands and the bottom layer is saltwater saturated. The intermediate layer is the one of interest/target because it contains freshwater.

VES in the study area is carried out before borehole drilling in order to have an overview of subsurface conditions. The drilling depth is recommended based on the interpretation of the VES curves. However, this study observed that, in Dar es Salaam, there are fundamental knowledge gaps that persist in the field of seawater intrusion investigation, including wrong interpretation (i.e using apparent resistivity instead of true resistivity) and giving false recommendations from VES data in relation to determining the drilling depth. There are a number of cases the suggested drilling depth is actually in the saltwater layer. Few examples are given below for elaboration of this situation.

In Box 1 (Fig. 5.15a), the intermediate unit, with a thickness of 10 m and resistivity of 105 Ωm, is overlain by top soil that is characterized by resistivity and depth of 56.3 Ωm and 0.48 m respectively. The third layer, which underlies the intermediate unit, has an infinite thickness and resistivity value of 1.5 Ωm. The three layers can thus be interpreted as follows: top soil of 0.48 m thick, followed by 10 m of freshwater saturated limestone, on top of the saltwater zone at 10.48 m depth. The recommendation of drilling 40m deep borehole is definitely wrong: the well will tap water from the saltwater layer, starting at 10.48m. Probably the interpretation is based on reading the depth from the apparent resistivity curve, which is not correct. The true formation resistivity, found by interpretation of the curve, should be considered.

In Box 2 (Fig. 5.15b), the intermediate unit, with a thickness of 7.05 m and resistivity of 271 Ωm, is overlain by top soil that is characterized by resistivity and depth of 1134 Ωm and 1.1 m respectively. The third layer, which underlies the intermediate unit, has an infinite thickness and resistivity value of 3.28 Ωm. The three layers can thus be interpreted as follows: unsaturated sand on top (1.1m thick), followed by 7.05m of freshwater saturated sand and limestone, on top of the saltwater zone at 8.15 m depth. The recommendation of drilling 20 m deep borehole is definitely wrong: the borehole will end up in the saltwater layer. Probably the interpretation is based on reading the depth from the apparent resistivity curve, which is not correct.

In Box 3 (Fig. 5.15c), the second and the third layer (with possibility of some freshwater bearing units), with thicknesses of 0.07 m and 0.53 m and resistivities of 24.08 Ωm and 55.97 Ωm respectively, are overlain by top soil that is characterized by resistivity and depth of 194.1 Ωm and 2.89 m respectively. The fourth layer has an infinite thickness and resistivity value of 0.21 Ωm. The four layers can be interpreted as follows: 2.89 m of unsaturated zone on top, followed by (only) 0.60 m of freshwater saturated sand and limestone (layers 2+3), on top of the saltwater zone at 3.49 m depth. The recommendation of drilling a 12 m deep borehole corresponds to well installation in the saltwater layer.

In Box 4 (Fig. 5.15d), the second and the third layer, with thicknesses of 0.75 m and 12.11 m and resistivities of 422.4 Ωm and 25.07 Ωm respectively, are overlain by top soil that is characterized by resistivity and depth of 12.83 Ωm and 0.29 m respectively. The fourth layer has an infinite thickness and resistivity value of 3.20 Ωm. The four layers can be interpreted as follows: both upper layers probably 1.04 m thick unsaturated zone (including 0.29 m wet top soil on top), followed by 12.11 m of freshwater saturated sand and limestone on top of the saltwater zone at 13.15 m depth. The recommendation of drilling 30 m deep borehole is definitely wrong: the borehole will end up in the saltwater layer. A borehole (DSM. 68/2006 drilled 20th January 2006) corresponds to this geophysical survey (of 3rd February 2005), which was drilled 20 m instead of 30 m. However, 20 m according to VES is still much deeper than it was supposed to be (< 13 m). According to the water analysis results accompanying the borehole report, chloride concentration is 788 mg/l, which is brackish water.

In Box 5 (Fig. 5.15e), the intermediate unit, with a thickness of 5.98 m and resistivity of 85 Ωm, is overlain by top soil that is characterized by resistivity and depth of 256.4 Ωm and 1.1 m respectively. The third layer, which underlies the intermediate unit, has an infinite thickness and resistivity value of 0.21 Ωm. The three layers can be interpreted as follows: unsaturated sand on top (1.1 m thick), followed by 5.98 m of freshwater saturated sand with limestone, on top of the saltwater zone at 7.08 m depth. The recommendation of drilling 12 m deep borehole is definitely too deep: the borehole will end up in the saltwater layer.

In Box 6 (Fig. 5.15f), no VES curve (surveyed on 14th May 2007) appears in the groundwater survey report. However, according to the VES results presented, the intermediate unit, with a thickness of 6 m and resistivity of 202.5 Ωm, is overlain by top soil that is characterized by

resistivity and depth of 135 Ωm and 2 m respectively. The third layer, which underlies the intermediate unit, has an infinite thickness and resistivity value of < 100 Ωm. The recommendation of drilling 25 m deep borehole seems to be justifiable based on the apparent resistivity of the bottom layer. Because the area is within the limestone formation, this could be thought of as fresh water saturated limestone. However, based on the outcome of the borehole drilled (in July 2007) about 2 months later, doubt rises on the inaccurate value of apparent resistivity (<100 Ωm) obtained in the bottom layer during the geophysical survey. The borehole was drilled to 20 m and afterward the last 6 m was backfilled and the screen was installed from 7 m to 14 m. The recommendation from the laboratory analysis (of 18 July 2007) was that the water is not suitable for domestic use because of its high salinity content. The value of chloride concentration in these results is 1431 mg/l signifying Brackish-saltwater according to Stuyfzand (1986) water classification. This borehole represents a number of boreholes that were drilled into the brackish salt/salt water and afterwards the depth was decreased by backfilling. However, for this particular borehole even at the depth of 14 m, water is brackish-saline, as shown by chemical analysis.

BOX 1

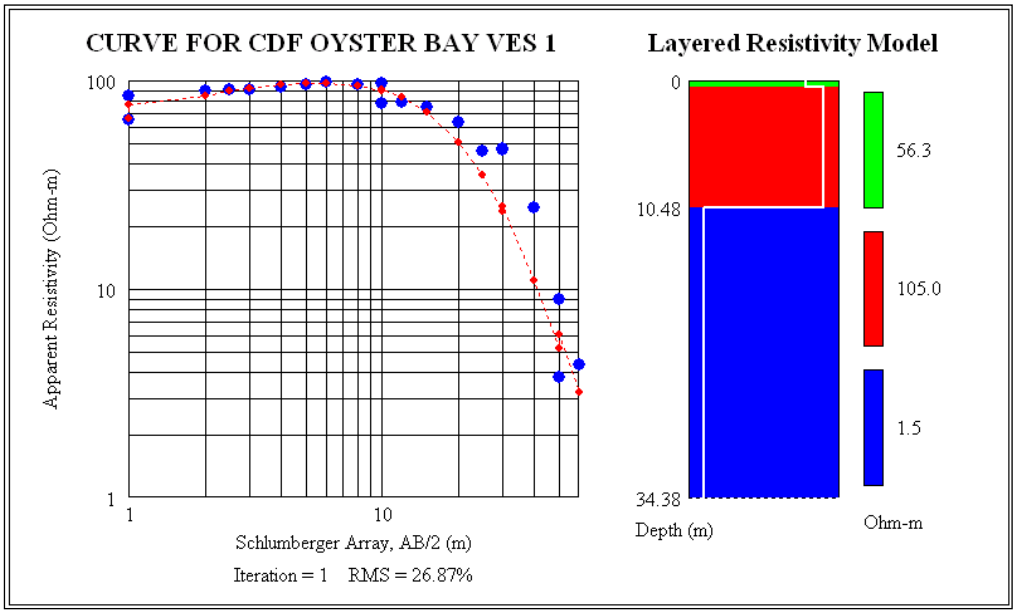

VES No.	Type of Layers	Resistivity model (Ohm.m)	Thickness (m)	Coordinates	Remarks
1	1	56.29	0.48	0530656E 9250508N Elev: 01a.m.s.l	**Drilling to 40m deep**
	2	105.0	10.0		
	3	1.5	+++		

DISCUSSION OF RESULTS

The VES point, predict essentially a three layers Hydrogeological model of the subsurface within the surveyed area. This usually suggests a sequence of interbeded sedimentary formations. The interpreted VES field curve shows that, the first (top) layer characterized by relatively medium values of the apparent Resistivity, which considered being dry sand. The second layer characterized by high value of apparent resistivity, this indicates a presence of limestone with shallow to deep water bearing bodies of varying the degree of water saturation and water quality. The third layer characterized by medium values of apparent resistivity, this suggests the presence of coastal formation with saline water. The thickness of the bottom/last layer was not determined by this survey separation.

CONCLUSIONS AND RECOMMENDATIONS:

Detailed geological, hydrogeological, topographical and geophysical analysis has been taken into consideration to select the suitable drilling site. Based on the results of the geophysical investigation, a **40m** deep borehole is recommended for drilling at **VES № 1.** However, saline water is highly anticipated within the surveyed area. The actual quantity and quality of water will be known after drilling. The drilling exercise must be supervised by hydro geologist or Tech. Hydrogeology who will closely monitoring the insitu cuttings, the drilling penetration rates, water strikes, water quality changes and provide the borehole designing for casing installation. The water central laboratory, before any use, should analyze the water obtained.

Figure 5.15(a): Example of wrong VES data interpretation/recommendation by DDCA (Source: DDCA groundwater survey report).

BOX 2

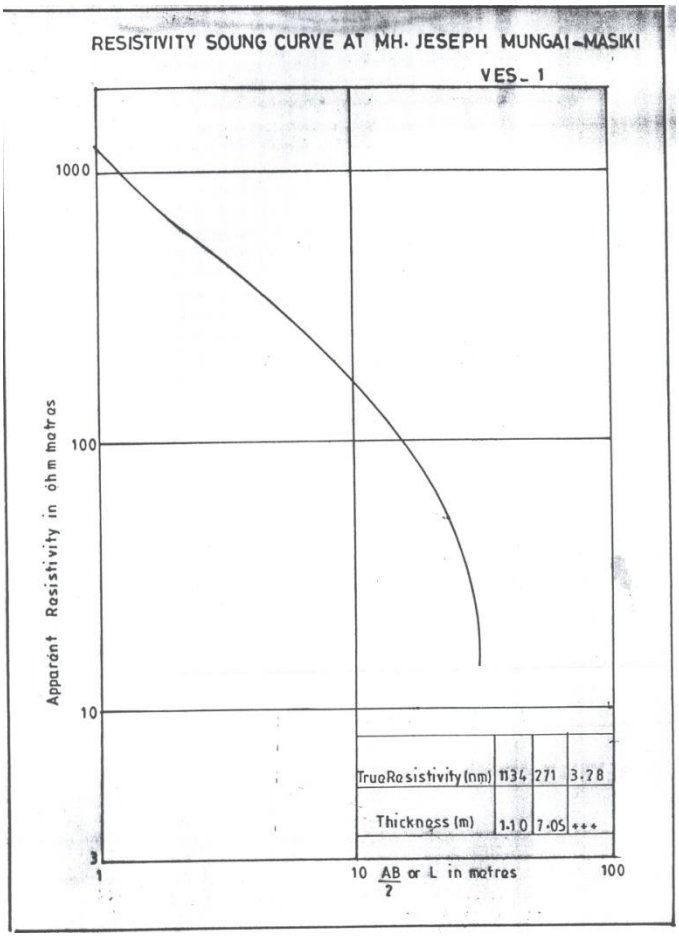

VES No.	Type of Layers	Resistivity model (Ohm.m)	Thickness (m)	Coordinates	Remarks
1	1	1134	1.10	530783E 9252105N	**Drilling to 20m deep**
	2	271	7.05		
	3	3.28	+++		

DISCUSSION AND RECOMMENDATIONS:

The curve obtained is characterized by medium resistivity value which indicates dry sand formation. The underlying formation consists of sand formations intercalated with limestone formations of varying moisture content. From the analysis of the above results, the survey team recommends to drill borehole of **20 m** deep in the surveyed area at VES no 1. This is due to the salinity content present in the surveyed area. Strictly cable and tool machine is recommended. The drilling must be supervised by hydrogeologist or Tech. hydrogeologist and the water obtained should be analyzed by the Maji Central Water Laboratory before it is put into use.

NOTE: Percussion drilling is highly recommended due to the anticipation of salinity.

Figure 5.15(b): Example of wrong VES data interpretation/recommendation by DDCA (Source: DDCA groundwater survey report).

BOX 3

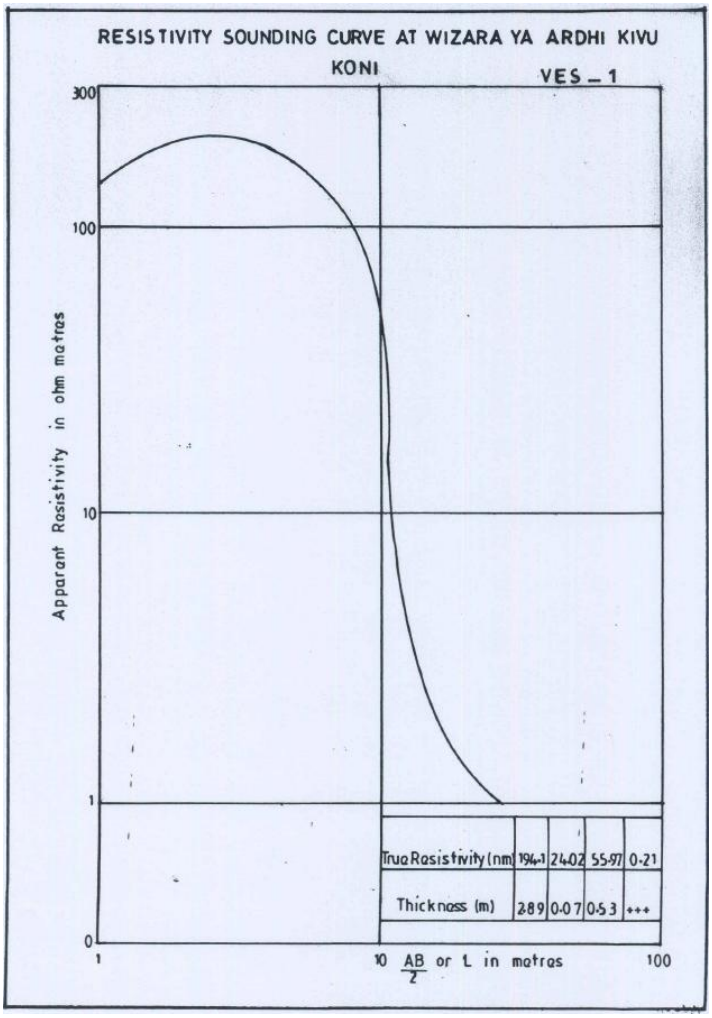

VES No.	Type of Layers	Resistivity model (Ohm.m)	Thickness (m)	Coordinates	Remarks
1	**1**	**194.1**	**2.89**	**532961E 9246488N**	**Drilling to 12m deep**
	2	**24.08**	**0.07**		
	3	**55.97**	**0.53**		
	4	**0.21**	**+++**		

DISCUSSION AND RECOMMENDATIONS:

The curve obtained is characterized by medium resistivity value which indicates dry sand formation. The underlying formation consists of sand formations intercalated with limestone formations of varying moisture content. From the analysis of the above results, the survey team recommends to drill borehole of **12 m** deep at VES no 1. The geophysical results indicate the strike underground water although their quantity and quality will be known after drilling. However, the pilcon machine is strictly recommended due to the suspect of striking the saline water. The drilling must be supervised by hydrogeologist or Tech. hydrogeologist and the water obtained should be analyzed by the Maji Central Water Laboratory before it is put into use.

Figure 5.15(c): Example of wrong VES data interpretation/recommendation by DDCA (Source: DDCA groundwater survey report).

BOX 4

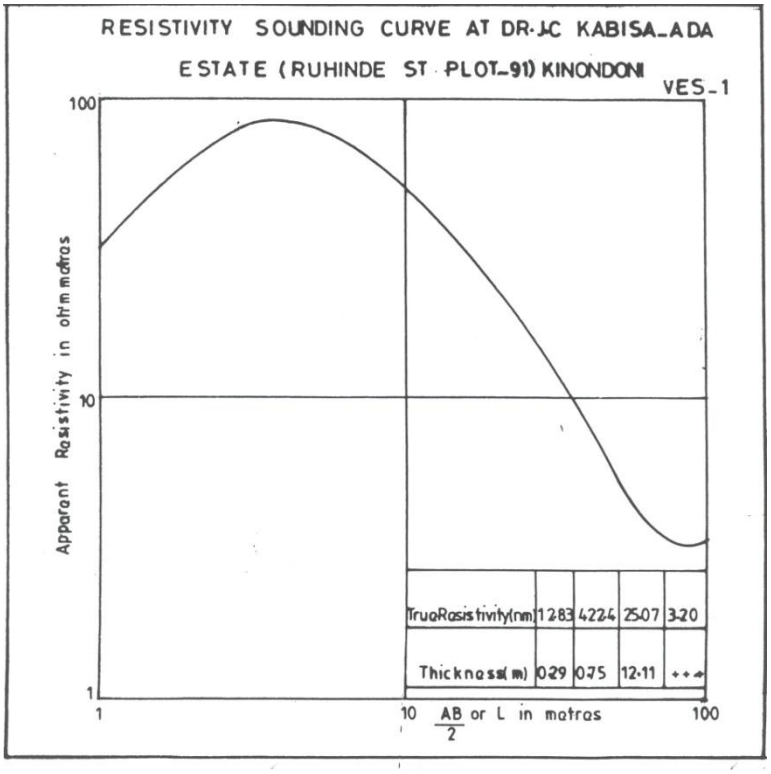

VES No.	Type of Layers	Resistivity model (Ohm.m)	Thickness (m)	Coordinates	Remarks
1	**1**	**12.83**	**0.29**	**530104E 924988N**	**Drilling to 30m deep**
	2	**422.4**	**0.75**		
	3	**25.07**	**12.11**		
	4	**3.20**	**+++**		

DISCUSSION AND RECOMMENDATIONS:

The curve obtained is characterized by high resistivity value which indicates dry sand formation. The underlying formation consists of sand formations intercalated with limestone formations of varying moisture content. From the analysis of the above results, the survey team recommends to drill borehole of **30 m** deep at VES no 1. The geophysical results indicate the strike underground although saline water is anticipated. However, the the quantity and quality of water will be known after drilling. Percussion machine is recommended for striking saline water. The drilling must be supervised by hydrogeologist or Tech. hydrogeologist and the water obtained should be analyzed by the Maji Central Water Laboratory before it is put into use.

Figure 5.15(d): Example of wrong VES data interpretation/recommendation by DDCA (Source: DDCA groundwater survey report).

BOX 5

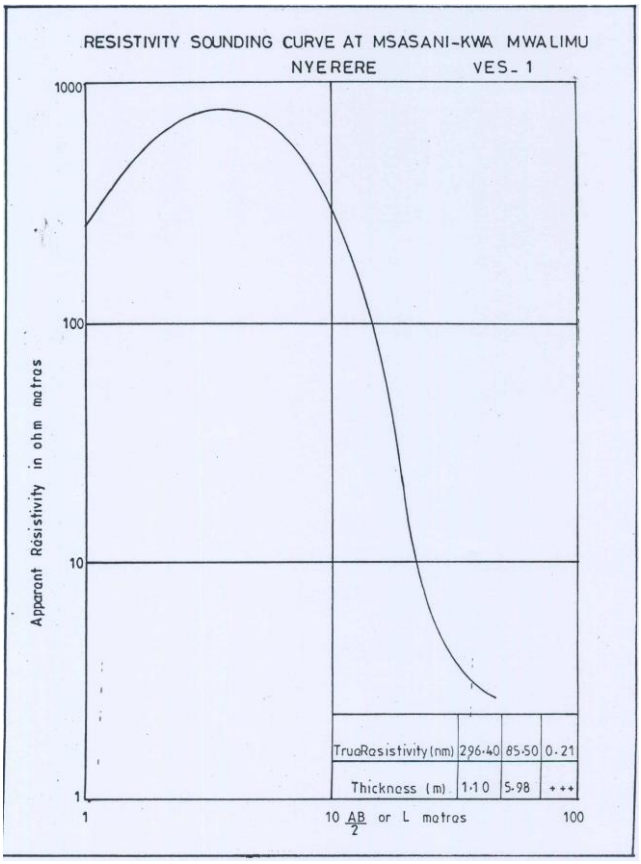

VES No.	Type of Layers	Resistivity model (Ohm.m)	Thickness (m)	Coordinates	Remarks
1	**1**	**256.4**	**1.1**		**Drilling to 12m deep**
	2	**85**	**5.98**		
	3	**0.21**	**+++**		

DISCUSSION AND RECOMMENDATIONS:

The curve obtained is characterized by medium resistivity value which indicates dry sand formation. The underlying formation consists of sand formations intercalated with limestone formations of varying moisture content. From the analysis of the above results, the survey team recommends to drill borehole of **12 m** deep at VES no 1. This is due to the salinity content present in the surveyed area. The geophysical results indicate the strike underground water although their quantity and quality will be known after drilling. Strictly cable and tool machine is recommended. The drilling must be supervised by hydrogeologist or Tech. hydrogeologist and the water obtained should be analyzed by the Maji Central Water Laboratory before it is put into use.

Figure 5.15(e): Example of wrong VES data interpretation/recommendation by DDCA (Source: DDCA groundwater survey report).

BOX 6: Geophysical investigation conducted on 14 May, 2007

VES No.	Type of Layers	Resistivity model (Ohm.m)	Thickness (m)	Depth to Layer (m)	Remarks
1	1	135	2		**Drilling to 25m deep**
	2	202.5	6	2	
	3	<100		8	

DISCUSSION OF RESULTS

The VES point, predict essentially a three layers Hydrogeological model of the subsurface within the surveyed area. This usually suggests a sequence of interbeded sedimentary formations. The interpreted VES field curve shows that, the first (top) and third layer characterized by relatively medium values of the apparent Resistivity, which considered being dry sand clay. The second layer characterized by high value of apparent resistivity, this indicates a presence of limestone with shallow to deep water bearing bodies of varying the degree of water saturation and water quality.

CONCLUSIONS AND RECOMMENDATIONS:

Detailed geological, hydrogeological, topographical and geophysical analysis has been taken into consideration to select the suitable drilling site. Based on the results of the geophysical investigation, a **25m** deep borehole is recommended for drilling at a surveyed point (VES № 1). However, saline water is highly anticipated within the surveyed area. The actual quantity and quality of water will be known after drilling. The drilling exercise must be supervised by hydro geologist or Tech. Hydrogeology who will closely monitoring the insitu cuttings, the drilling penetration rates, water strikes, water quality changes and provide the borehole designing for casing installation. The water central laboratory, before any use, should analyze the water obtained.

Note: Percussion Drilling is highly recommended in order to monitor the water quality changes.

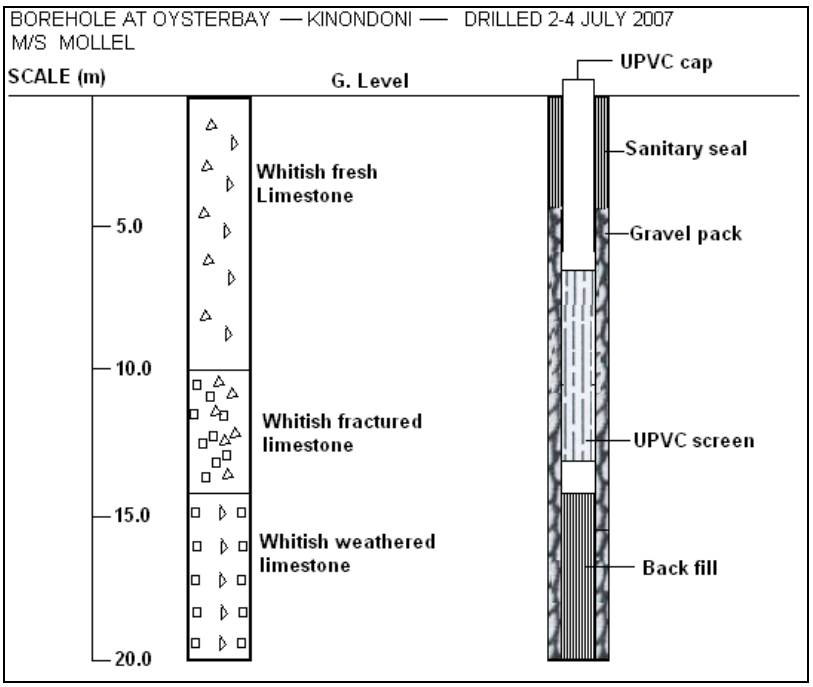

Figure 5.15(f): Example of wrong VES data interpretation/recommendation by DDCA (Source: DDCA groundwater survey report).

5.4 Conclusions and recommendations

5.4.1 Conclusions

The study used the application of the resistivity survey supported by hydrogeological investigation and hydrogeochemical parameters of groundwater to identify fresh-, brackish-, and saline-water zones in the study area. VES curves and resistivity profiles have shown a decrease of resistivity by going deeper and towards the coastline respectively. This therefore substantiates that there is saltwater intrusion in the area close to the coastline. Cross-sections have shown the presence of salt water near the coastline and the boundary between fresh and saline waters is marked. The depth of fresh- salt water interface was estimated which is an important information in regard to coastal water resources management (Goes et al., 2009; Obikoya and Bennell, 2012) and especially is a vital document for hydrogeologists (Vandenbohede, 2010). Salt water was found mostly in the area within 2 km of the coastline, and the depth to the interface is ranging from 1.3 m to 20 m. Away from the coastline, the interface (if present) is at greater depth that could not be reached by the instrument/lower-power equipment used. However, toward the south of the study area, the VES executed at Kurasini (located 4 km from the sea/mouth of Mzinga Creek to the sea), showed the freshwater/interface at a greater depth (43 m). Towards the west of the study area (about 2.7 km from the coastline) the resistivity logging at point B13 was conducted up to the depth of 37 m but the saltwater interface (if present) was not reached.

5.4.2 Recommendations

In the past decades, the application of geophysical surveys has proven to be a valuable tool in studying issues related to groundwater resources. Although borehole contractors cannot guarantee to find water with no salt, the application of geophysical survey is very suitable in this respect, provided that data interpretation is done accurately.

Over-exploitation of groundwater should be avoided especially near the coast to prevent seawater intrusion. Sustainable groundwater management is needed and will require restriction of well development and appropriate monitoring of potential saltwater intrusion, particularly near the coastline. Given the highly specialized nature of the field of seawater intrusion expertise, there is great need for the training of hydrogeologists/hydrogeophysicists for effective monitoring, evaluation and management of coastal aquifers.

6 HYDROGEOCHEMICAL EVOLUTION OF GROUNDWATER

6.1 Introduction

Despite the significant importance of groundwater in Dar es Salaam City, threats exist, which include: i) groundwater over-abstraction that leads to the intrusion of seawater in fresh water aquifers (Mjemah, 2007; Mtoni et al., 2011; Mtoni et al., 2012a), ii) poor sewerage system and industrial disposal (Mato, 2002; Mjemah, 2007; Napacho and Manyele, 2010; Mtoni et al., 2010; Mtoni et al., 2012a-b). The major focus of this study is on the seawater intrusion problem. A thorough study of the saltwater intrusion phenomenon was conducted in the study area so as to put in place measures that will stem the trend of this problem.

Over 7500 active boreholes/wells extracting water from the Quaternary aquifer exist in different localities of the study area. In the coastal plain, scarcity of surface water, increase in population and rapid urbanization have resulted in high dependency on groundwater; if groundwater is overexploited, seawater moves into the aquifer and quality of groundwater starts to deteriorate. It is widely known that once seawater is introduced into a fresh groundwater body it may be very difficult to restore to the original condition (Jeen et al., 2001; Papadopoulou et al., 2005). Seawater intrusion causes many ecological, environmental, real problems for the social and economic development in affected coastal areas (Polemio et al., 2002; Rygaard et al., 2011). Successful management of coastal groundwater resources in the study area will not only depend on planning and regulation but also on the accurate prediction of the behavior of the saltwater intrusion to both natural and man's developmental activities (Polemio et al., 2010; Voudouris et al., 2010). It is against this background, that this study was conceived, among other things, to study the hydrochemical characteristics of groundwater in the Dar es Salaam Quaternary coastal aquifer (DQCA), based on the hydrochemical data.

The assessment of groundwater quality status is important for socio-economic development of any region of the world. The chemical composition of groundwater determines its suitability for different uses including domestic, agricultural or industrial purposes. Major chemical parameters dissolved in groundwater include Ca^{2+}, Mg^{2+}, Na^{+}, K^{+}, Cl^{-}, HCO_3^{-} and SO_4^{2-}**.** The chemical parameters of groundwater play an important role in classifying and assessing water

quality. This chapter presents the principal hydrogeochemical processes controlling groundwater quality in the study area. It provides a detailed profile of the dominant hydrogeochemical facies distribution and processes in groundwater. A number of techniques and methods have been used in this study to interpret the chemical data. Water classification according to Stuyfzand (1986) and Piper (1944), graphical methods (Durov diagram, scatter diagrams, ionic ratios), maps showing the spatial distribution of water quality parameters, Aquachem (Calmbach, 1997) computer software for plotting diagrams and PHREEQC (Parkhurst & Appelo, 1999) for saturation indices calculation, USSL guidelines (US Salinity Laboratory, 1954) for irrigation water classification have been used to study critically the hydrochemical characteristics of groundwater of Dar es Salaam Quaternary coastal aquifer (DQCA) .

6.2 Groundwater in a coastal environment: Overview

6.2.1 Composition of groundwater

The chemical composition of groundwater is controlled by many factors that include the composition of precipitation, mineralogy of the watershed and aquifer, topography and climate (Chenini and Khemiri, 2009). The interaction of all factors leads to various water facies. Usually, major ions studies are used to define hydrochemical facies of waters where the spatial variability can provide insight into aquifer heterogeneity and connectivity (Murray, 1996; Rosen and Jones, 1998). Groundwater quality depends, to a large extent, on its chemical composition (Wadie and Abduljalil, 2010) which may be modified by natural and anthropogenic sources. Assessment of both the existing and potential sources of contamination and the spatial extent of the existing groundwater contamination is needed before considering methods to monitor and prevent future groundwater quality problems.

6.2.1.1 The impact of TDS on groundwater uses

The amount of total dissolved solids (TDS) is a general indicator of groundwater suitability for different purposes (drinking, agriculture and industrial use). For example, the palatability of water with TDS level of less than about 600 mg/l is generally considered to be good; drinking-water becomes significantly and increasingly unpalatable at TDS levels greater than about 1000 mg/l (WHO international standards, 2004). When dissolved solids are high, water

can also be useless for irrigation and industrial purposes and it could be corrosive to steel materials.

6.2.1.2 Human impact on groundwater quality

Fig. 6.1 summarises different kinds of contamination sources. In additional to natural processes, practically every installed facility or structure and every human physical activity may eventually cause groundwater contamination. Groundwater pollution in major cities is a growing environmental problem. Vulnerable groundwater is in many cases located below major cities, where the poor knowledge of aquifer characteristics, indiscriminate disposal of municipal wastes, industrial effluents, and urban agriculture contribute to groundwater resources degradation (Foster et al., 1993; Foster et al., 1999; Morris et al., 2003; Whitehead et al., 1999; Mato, 2002; Vâzquez-suné, 2003; Mjemah, 2007). In low-income countries (like Tanzania), the situation is aggravated by rapid urbanization, which is characterized by inadequate provision of water supply, sanitation, solid waste management and drainage infrastructure (Mato, 2002).

Groundwater contamination occurs when materials seep through the soil and reach the water, which can happen when rainfall washes contaminants into the ground, or when polluted surface water comes into contact with groundwater. Groundwater pollution can also occur when underground storage tanks or waste disposal sites start to leak. The issue of groundwater contamination by wastewater disposal is a major problem in cities of developing countries where, generally, there are many densely populated and unsewered areas created by high rates of migration into cities. Dar es Salaam City, which is the major seat of government institutions, is the largest urban centre in Tanzania and a major financial, commercial, manufacturing and transport hub. The city currently with a population of about 4 million people receives many visitors, and rural-urban migration makes it one of the fastest growing cities in the world, which in turn causes problems that are typical of a tropical mega-city. Among others, these include sluggish infrastructural growth and poor sanitation. The high demographic growth and economic development activities taking place in Dar es Salaam occur along with environmental destruction that includes also deterioration of groundwater quality. Pit latrines and septic tanks form the major ways to dispose of sewage in the city.

Groundwater quality degradation in coastal areas is most often affected by saltwater intrusion caused by excessive exploitation of coastal aquifers. Furthermore, human activities in urbanized areas threaten the groundwater both due to diffuse contaminant loading from urban agriculture and point contaminant loading from landfill leakage, industrial sites, uncontrolled waste disposal sites and residential areas involving pit latrines/septic tanks. In some parts of the city (especially in informal settlements), the use of pit latrines can be considered as diffuse source of pollution due to the fact that pit latrines are many, located close to each other and spread over large area. The occurrence of contaminants in groundwater depends both on the characteristics of contaminant loading and the inherent attenuation capacity of the intervening strata between contaminant source and water table (Mato, 2002; Morris et al., 2003). This inherent attenuation capacity of the intervening strata depends on its geological, hydrological and hydrogeological condition.

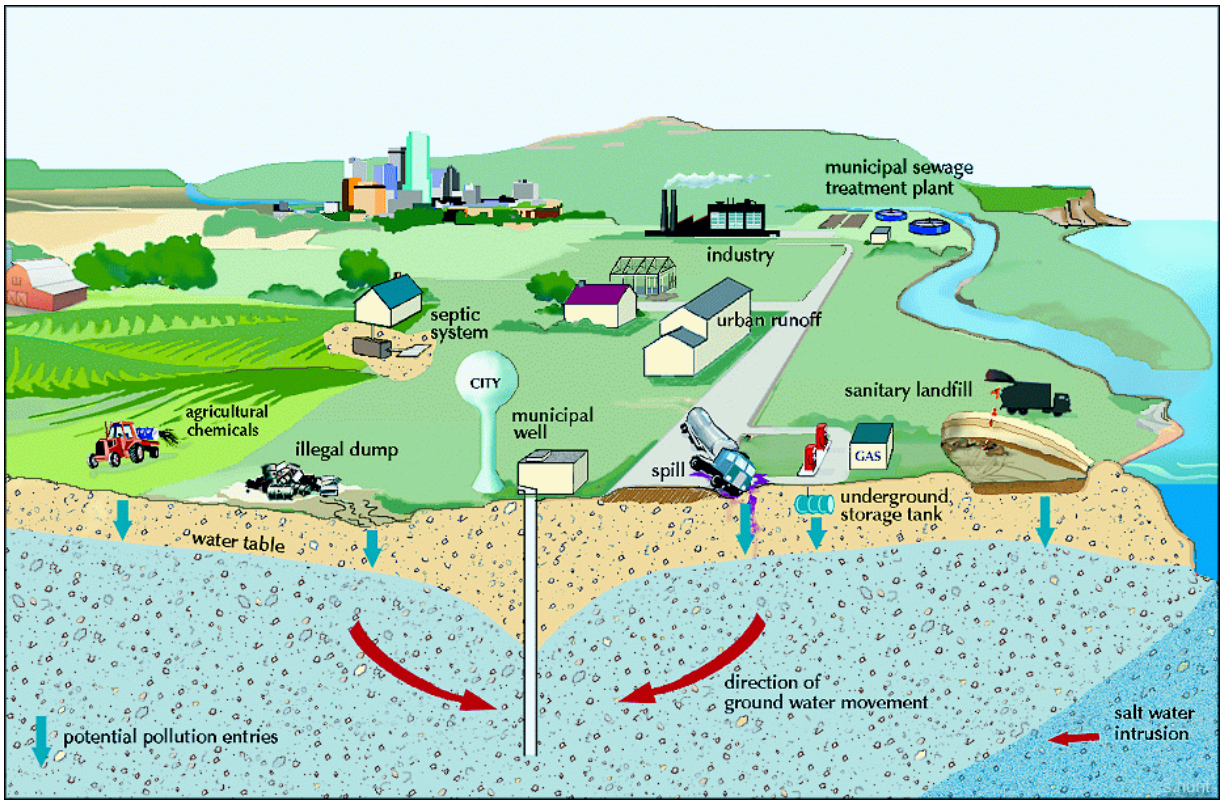

Figure 6.1: Sources of groundwater contamination are numerous and are as diverse as human activities (source: Zaporozec and Miller, 2000 cited in Zaporozec, 2004).

6.2.2 Hydrogeochemical processes

The composition of groundwater in coastal aquifers can be quite variable comparing to the composition of seawater which is relatively stable. This is mainly due to the chemical reactions between the host material and groundwater that occur when deposits are intruded by seawater. The geochemical properties of the rocks determine the dominant chemical processes. Due to the distinct difference in the chemical composition of fresh groundwater and seawater, various hydrochemical processes can accompany saltwater intrusion, which can lead to changes in water quality. This section describes dissolution and precipitation of mineral phases, important chemical reactions in coastal groundwater systems and the effects of seawater and freshwater mixing.

6.2.2.1 Dissolution and precipitation of mineral phases

Groundwater is always in interaction with the aquifer material. This is called rock-water interaction. This interaction is important and the dissolution of minerals can increase the concentration of related elements. Mineral phases can be formed by precipitation if concentrations in the groundwater are higher than the solubility of the mineral. It is postulated that mineral phases that are clearly undersaturated ($SI \leq -0.1$) will tend to dissolve, and mineral phases that are clearly oversaturated ($SI \geq +0.1$) will precipitate out of solution (Adams et al., 2001); equilibrium is taken to be between SI= -0.1 to +0.1.

Examples of studies on the effect of seawater and freshwater mixing in carbonate aquifers include the work of Plummer (1975) and Wigley and Plummer (1976). These studies show carbonate dissolution can be an important process in the mixing zone. Furthermore, these studies show the dissolution process occurring even when both the seawater and freshwater end members in the mixture are at chemical equilibrium with the carbonate mineral. This is due to the redistribution of carbonate species and the non-linear dependence of activity coefficients on ionic strength whereby the resultant mixture has the capacity to dissolve carbonate.

6.2.3.2 Cation exchange

Cation exchange is one of the most important geochemical processes taking place in aquifers, which is determined by the differences in cation dominance in seawater and fresh groundwater (section 6.2.3.3). Cations may be attracted to the region close to a negatively

charged clay mineral surface and held by electrostatic forces. When saltwater enters into fresh aquifers, an exchange of cations occurs and Na^+ is taken by the exchanger (X), resulting in deficit of Na^+ and surplus of Ca^{2+} in water (Reaction 6.1): this leads to the development of the Ca–Cl water type, which is typical for salinization (Walraevens & Van Camp, 2005).

$$2Na^+ + CaX_2 \leftrightarrow Na - X + Ca^{2+} \qquad (6.1)$$

Upon the inflow of freshwater in a salt water aquifer a reverse process takes place whereby Ca^{2+} is taken by the exchanger (X) and at the same time the release of Na^+. This is normally reflected in the increase of the Na^+/Cl^- ratio, and formation of the $NaHCO_3$ water type, which is typical for freshening (section 6.2.3.3, Fig. 6.2). The amount of cations that can be exchanged is determined by the cation exchange capacity (CEC), quantifying the number of moles of adsorbed ion charge that can be desorbed per unit mass of sediment. The CEC value of an aquifer will depend on the clay content of the sediments.

6.2.3.3 Freshening and salinization

Groundwater quality in the aquifer systems bordering the sea is largely influenced by the interaction with the sea. This interaction can result in either of the two: freshening of saline aquifers or salinization of fresh water bodies. However, both situations can happen in the same aquifer system. The main reaction operating during salinization or freshening events in coastal aquifers is cation exchange. Sediments in general have a natural ion exchange capacity. Intruding seawater (normally with high concentrations of Cl^-, Na^+, K^+ and Mg^{2+}) is displacing fresh water with high Ca^{2+} and HCO_3^- concentrations or vice versa: Na^+ is adsorbed during salinization, and Ca^{2+} during freshening of the aquifer system (Walraevens & Van Camp, 2005).

For clear understanding of the natural groundwater quality and the controlling processes in a coastal aquifer, first and foremost it is important to know both the hydrodynamical and hydrochemical behaviour and the way these are linked together. Fig. 6.2 gives detailed illustration on the processes of freshening and salinization of coastal aquifers with the end members seawater and freshwater. Factors determining groundwater composition under freshening or salinization conditions include: i) the composition and mixing ratio of end members, ii) hydrodynamics (mass transport processes): advection due to groundwater flow

and hydrodynamic dispersion (mixing), and iii) chemical reactions within the water phase and with the aquifer matrix Walraevens and Van Camp, 2005).

The end members as expressed in Fig. 6.2 include recharge water (infiltrating rain dissolving calcite) and seawater. The former and the latter water types are F-$CaHCO_3Ø$ and S-NaClØ respectively. The water types are according to Stuyfzand classification (1986, 1993) as explained in section 6.3.4.3. Besides the major ions, the classification name expresses the chloride content and the cation exchange code. The latter indicates either a surplus (+) of marine cations ($(Na^+ + K^+ + Mg^{2+})_{corrected} > \sqrt{(½Cl^-)}$), or a cation exchange equilibrium (Ø) ($-\sqrt{(½Cl^-)} \leq (Na^+ + K^+ + Mg^{2+})_{corrected} \leq \sqrt{(½Cl^-)}$), or a deficit (-) of marine cations ($(Na^+ + K^+ + Mg^{2+})_{corrected} < -\sqrt{(½Cl^-)}$). All concentrations are expressed in meq/l. The parameter $(Na^+ + K^+ + Mg^{2+})_{corrected}$ represents the marine cations in the sample that are not due to admixture of the seawater end member, and is calculated as the sum of measured marine cations, from which 1.061Cl is subtracted (section 6.3.4.2, Equation 6.6), the latter representing the marine cations in the end member fraction with $(Na^+ + K^+ + Mg^{2+})/Cl^- = 1.061$ for mean ocean water). A surplus of marine cations (+) points to cation exchange resulting from freshening, whereas a deficit (-) indicates cation exchange caused by salinization. The end members by definition show cation exchange equilibrium (Ø).

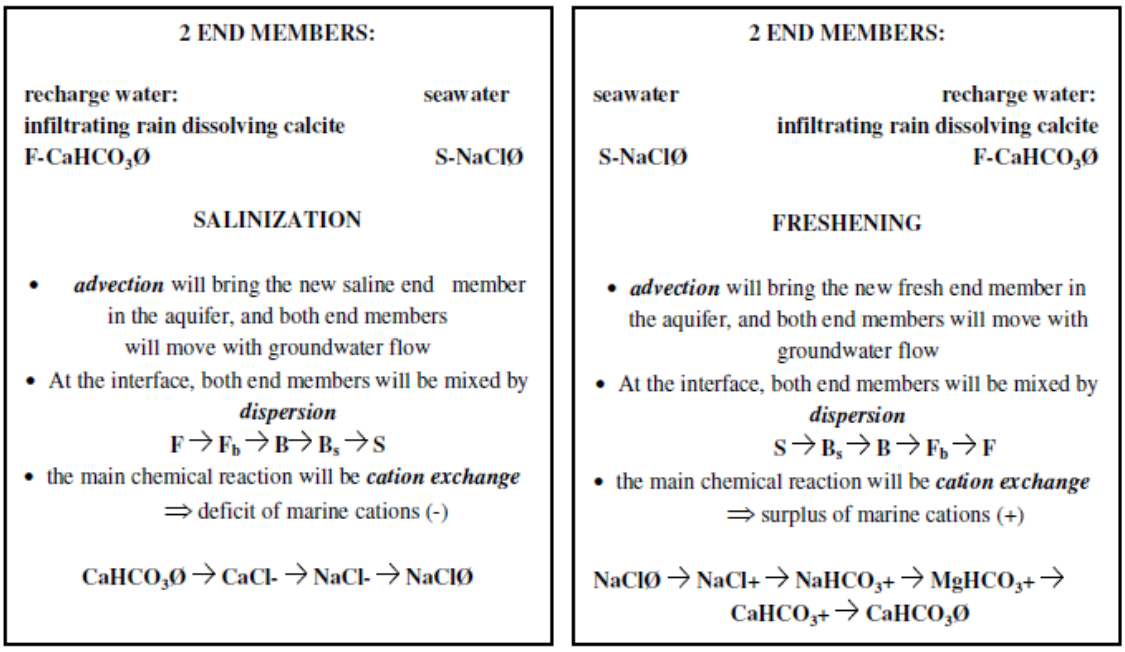

Figure 6.2: Factors changing groundwater quality as a result of freshening or salinization (Walraevens and Van Camp, 2005).

6.2.3 Seawater intrusion indicators

6.2.3.1 Chloride

Unusually high or steadily increasing chloride concentrations are one of the most commonly used indicators of seawater intrusion (HydroMetrics, 2008; Craig, 2008). Seawater intrusion involves mixing of saline and fresh water. Chloride concentrations significantly greater than historical average concentrations (HydroMetrics, 2008), or concentrations ranging from higher than background values to slightly less than seawater concentrations (~19,000 mg/l) indicate seawater intrusion (Craig, 2008). This is indicated by a clear trend of increasing chloride concentrations. However, while chloride concentrations are strongly indicative of seawater intrusion, it often takes time for the increasing chloride trend to be recognizable due to the long-term and relatively slow increase in chlorides during seawater intrusion (HydroMetrics, 2008).

6.2.3.2 Bivariate scatter plots and Na+/Cl- ratio

A bivariate scatter plot represents the variation of two ion concentrations in X and Y-axes. In the plots the positions of freshwater and saltwater indicate their mixing line. Table 6.1 provides the compositions of freshwater and seawater. Chemical composition of groundwater in many coastal aquifers subjected to seawater intrusion deviates from simple conservative seawater-freshwater mixing (El Moujabber et al., 2006). The Na^+/Cl^- ratios of coastal aquifers exposed to seawater intrusion are commonly lower than marine values, since when saltwater enters into fresh aquifers, Na^+ in saltwater is exchanged with Ca^{2+} adsorbed by the clay (section 6.2.3.2). This process removes sodium from the water, and Na^+/Cl^- molar ratios decrease. This results in a deviation from the mixing line on the scatter plot. A rapid decline in the molar ratio of sodium to chloride may indicate seawater intrusion (HydroMetrics, 2008). Na^+/Cl^- molar ratio in groundwater can be used to differentiate between seawater intrusion and other sources of salinity. Thus Na^+/Cl^- molar ratio can sometimes be used as an indicator of seawater intrusion.

Table 6.1: Composition of fresh and saltwater, concentrations in mmol/l (Appelo and Postma, 1993).

	Seawater	**Freshwater**
Na^+	455	0.30
K^+	10.6	0.00
Ca^{2+}	10.7	0.18
Mg^{2+}	55.1	0.19
Cl^-	566	0.25
SO_4^{2-}	29.3	0.21
HCO_3^-	2.4	0.10

6.2.3.3 Piper diagram

Seawater intrusion is often indicated by graphically analyzing shifts in groundwater quality. Example of one of the common graphical techniques for these analyses is the Piper diagram. Piper diagrams plot the relative abundances of individual cations and anions on two triangles (the left one for the cations and the right one for the anions), and their combined distribution is plotted on a central diamond shaped field (Fig. 6.3). The concentrations of the major ions are plotted in the triangles as percentages expressed in milli-equivalents (meq/l). Waters from similar or related sources will generally plot together (Appelo and Postma, 2005; HydroMetrics, 2008). The Piper diagram not only shows graphically the nature of a given water sample, but also dictates the relationship to other samples. For example, by classifying samples on the Piper diagram, geologic units with chemically similar water can be identified, and define the evolution in water chemistry along the flow path (Back and Hanshaw, 1965). The water type is based on the names of the main cation and anion (Fig. 6.3).

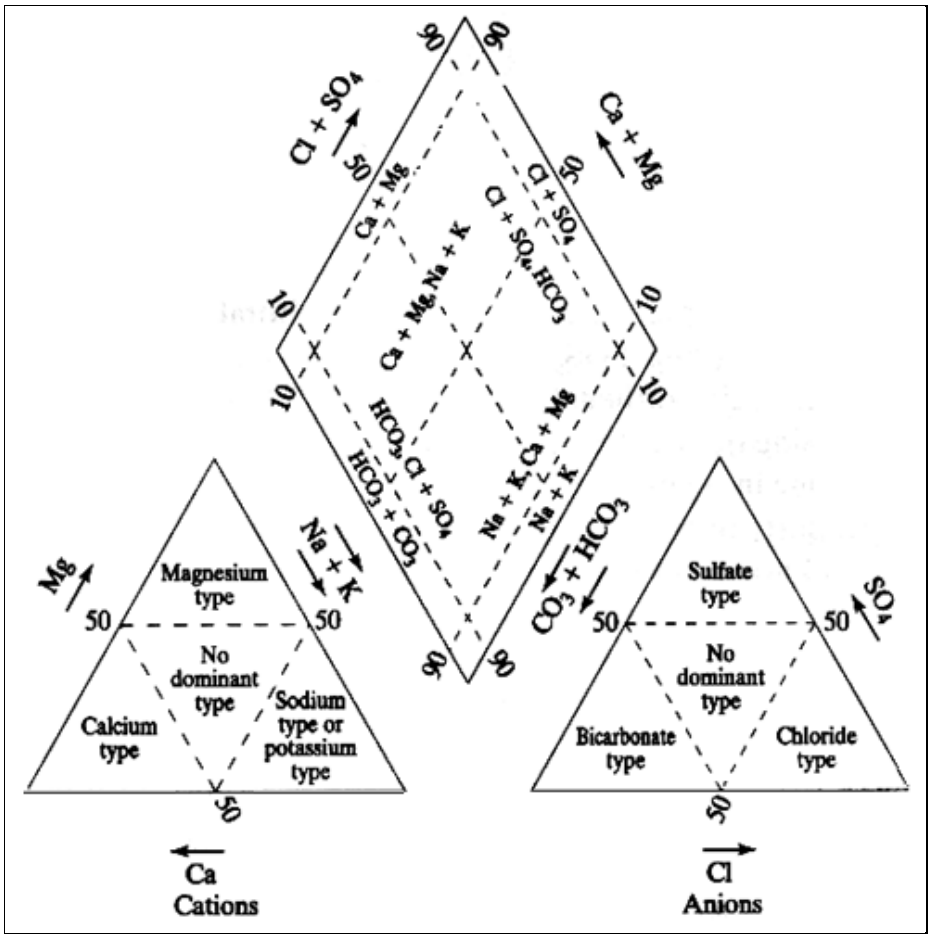

Figure 6.3: Piper diagram (Kehew, 2001).

Within the central diamond field, freshwater end member ($CaHCO_3$) and saltwater end member (NaCl) can be represented (Fig. 6.4). The mixture of two waters without chemical reactions will plot along a straight line between the two end-member types. However, in most cases, hydrochemical reactions and cation exchange occur. In the case of salinization, mixing of fresh and saline end members occurs by hydrodynamic dispersion and as admixture of the saline end member increases, the chloride concentration in the water is raised proportionally and the main chemical reaction is cation exchange resulting in a surplus of the fresh-water cation Ca^{2+} (Walraevens and Van Camp, 2005) (Reaction 6.1). The trend towards seawater intrusion plots along a curved path (red arrow) above the mixing line tracking the evolution of water from freshwater ($CaHCO_3$) to seawater (NaCl) (Fig. 6.4). Cation exchange which leads to the development of the Ca–Cl water type is represented by a straight blue arrow above the mixing line. On the other hand, for the case of freshening, the admixture of the fresh end member increases over the saline end member and as a result the chloride concentration in the water is reduced proportionally (Walraevens and Van Camp, 2005). Likewise, the main chemical reaction is cation exchange (represented by a straight blue line below mixing line),

resulting in a surplus of marine cations and a deficit of the fresh-water cation Ca^{2+} (Fig. 6.4). The freshening trend plots along a curved path (red arrow) below the mixing line.

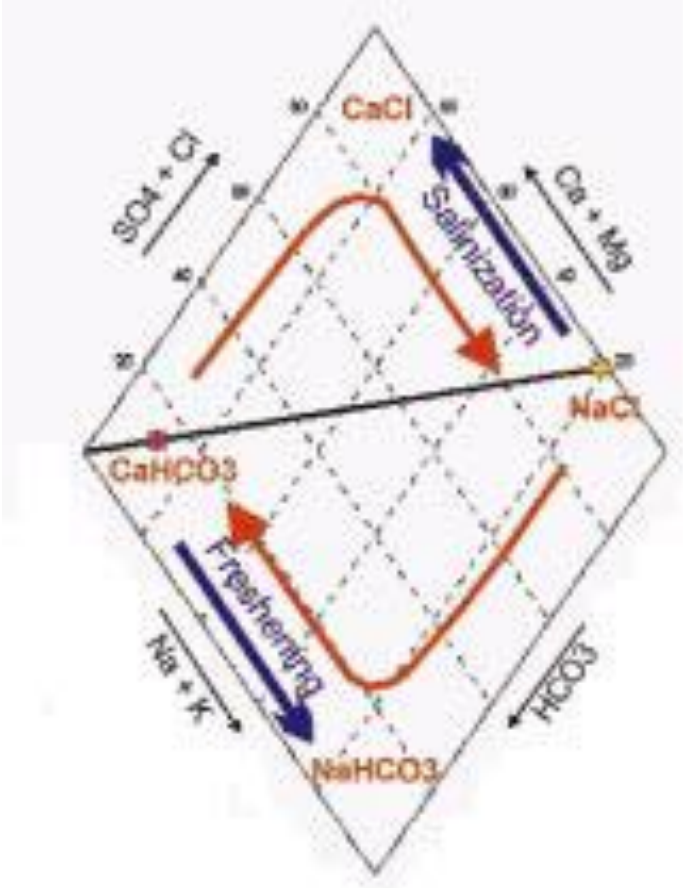

Figure 6.4: Piper diagram showing the shift in ion distribution due to salinization and freshening (Walraevens and Van Camp, 2005).

Cation exchange is an important factor modifying groundwater quality and is one of the most important geochemical processes taking place in aquifers affected by salinization or freshening. In coastal aquifers, where the relationship between seawater and fresh water is complex, cation exchange contributes significantly to the final composition of the groundwater (Walraevens & Van Camp, 2005): the ion exchange reaction (Reaction 6.1) of Na^+ and Ca^{2+} occurs when seawater intrudes fresh groundwater. When seawater intrudes a fresh groundwater aquifer, Na^+ is adsorbed and Ca^{2+} is released into the water. This process leads to the change of NaCl water type to the CaCl water type. The opposite process takes place with refreshening of groundwater (Reaction 6.1 in the direction to the left). It is quite well known that the displacement of seawater by freshwater in an aquifer is shown by a

$NaHCO_3$ type water (Stuyfzand, 1993; Walraevens, 1990; Walraevens & Van Camp, 2005). Ca^{2+} from fresh $CaHCO_3$ water type exchanges with adsorbed Na^{+}.

6.3 Methodology

Fig. 6.5 depicts the research methodology of this study. The data collection methodology carried out employed a review of existing data sources, and the collection of new data. The latter were generated through a field survey and groundwater quality testing. In order to present a clear view of spatial distribution of groundwater quality data, the study area is divided into two parts located between: i) Mbezi River and Msimbazi River, and ii) Msimbazi River and Mzinga River. Fig. 6.6 (a-b) indicates the location for groundwater sampling points both with existing chemical analyses (1-18') and groundwater sampling conducted during this research (19-195). The chemical and physical quality of groundwater resources depends on boreholes/wells depth, permeability of sediments and chemical composition of sediments through which the groundwater flows, climatic variations and anthropogenic activities. The depth of groundwater has therefore important implications on water quality. Appendix 6.1 gives characteristics of sampled boreholes/wells which include coordinates, altitude, borehole/well depth and whether a borehole/well taps the unconfined or semi-confined aquifer.

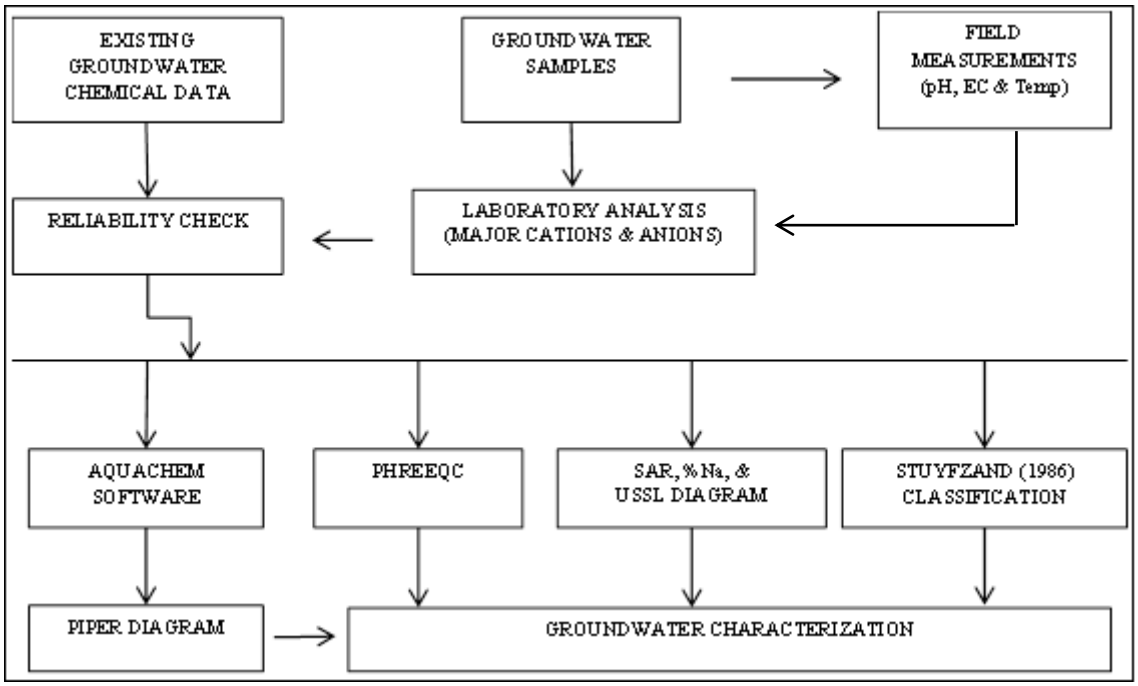

Figure 6.5: Methodology flow chart.

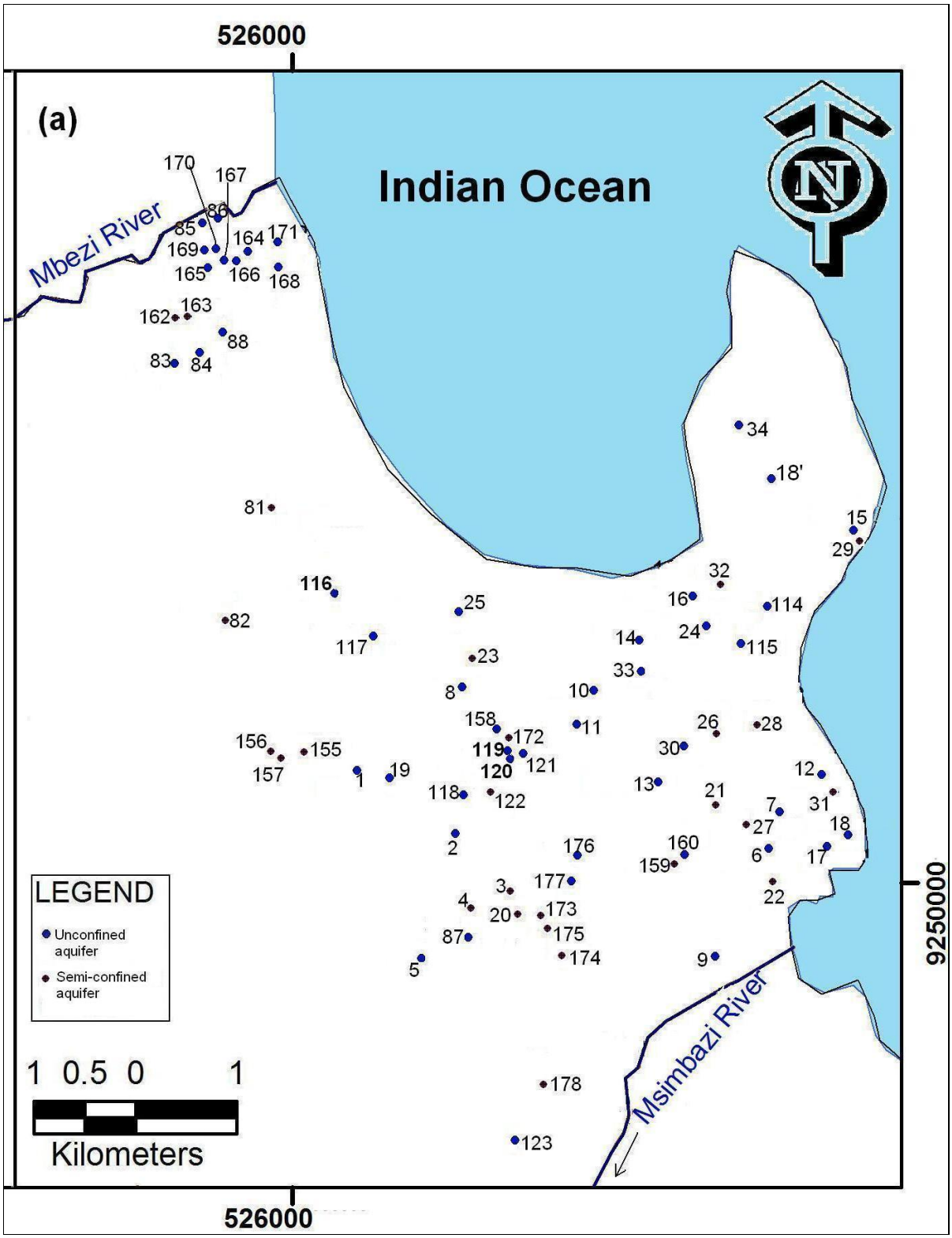

Figure 6.6(a): Map showing groundwater sampling points between Mbezi River and Msimbazi River.

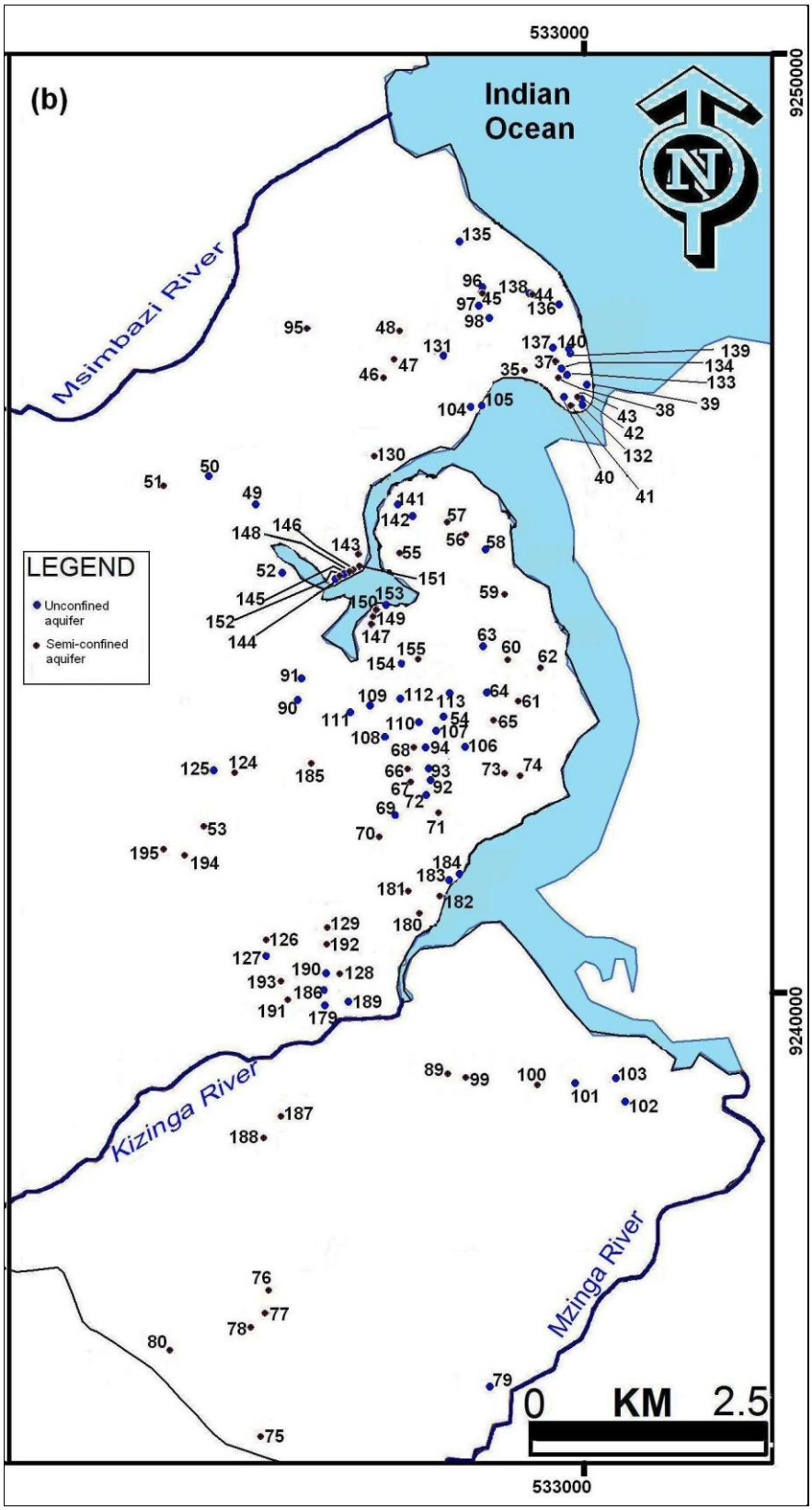

Figure 6.6(b): Map showing groundwater sampling points between Msimbazi River and Mzinga River.

6.3.1 Existing groundwater chemical data

Hydrogeochemical data for 19 boreholes (number 1-18') (Appendix 6.2a; Fig. 6.6a) in the study area were collected from well drilling reports from Drilling and Dam Construction Agency (DDCA). Groundwater analyses involve mainly pH, EC and the major chemical parameters (Na^+, K^+, Ca^{2+}, Mg^{2+}, Cl^-, SO_4^{2-}, NO_3^-).

6.3.2 Groundwater sampling and field measurements

Groundwater samples were collected during the fieldwork conducted between 2009 and 2012. The depths of the sampled boreholes/wells range from a shallow well with a depth of 1.66 m (located close to the coastline) to a borehole with a depth of 100 m constructed near Mzinga River in the south. The groundwater samples in the study area were taken after pumping the boreholes. As all boreholes were regularly being used, it was not necessary to include a long pre-pumping period. A total of 177 groundwater samples (numbers 19-195: Fig. 6.6a-b) from boreholes and hand dug wells were collected in plastic containers of 250 ml capacity for detailed chemical analysis. Two samples were taken from each borehole in polyethylene bottles of 250 ml. Samples for cation analysis were acidified with nitric acid to around pH=1.5, while those for anion analysis were stored without preservation. The containers were numbered serially along with a proper record of borehole/well sample location, date and static water level. The groundwater samples in the study area were taken after pumping the boreholes. Field measurements such as pH, temperature, and electrical conductivity were made at the time of collection using multimeter electrode equipment. Samples (i.e. numbers 35-195) were kept in refrigeration at 4°C until the time of shipping to the Laboratory for Applied Geology and Hydrogeology, Ghent University, Belgium.

6.3.3 Laboratory analysis

6.3.3.1 Southern and Eastern African Mineral Centre in Tanzania

Groundwater analysis of 16 samples (Sampling points 19-34) (Appendix 6.2b) collected on 22 July 2009 was carried out at the Southern and Eastern African Mineral Centre (SEAMIC) in Tanzania for selected major cations (Ca^{2+}, Mg^{2+}, K^+, and Na^+) and anions (Cl^-, SO_4^{2-}, NO_3^-, CO_3^{2-} and HCO_3^-). The concentrations of major cations (Ca^{2+}, Mg^{2+}, K^+, and Na^+) and anions (Cl^-, $NO_3^-$and SO_4^{2-}) were determined by ion chromatography technique. The concentration of CO_3^{2-} and HCO_3^- was determined by titration with HCl.

6.3.3.2 Laboratory for Applied Geology and Hydrogeology of Ghent University, Belgium

Complete groundwater analysis for a total of 161 samples (sampling points 35-195) collected during the field work in Tanzania was conducted in the Laboratory for Applied Geology and Hydrogeology of Ghent University, Belgium. Chemical analyses of major ions (Ca^{2+}, Mg^{2+}, Na^{+}, K^{+}, Fe^{2+}, Mn^{2+}, NH_4^{+}, Cl^{-}, SO_4^{2-}, HCO_3^{-}, CO_3^{2-}, NO_3^{-}, NO_2^{-} and PO_4^{3-}) were carried out. Quantification of the cations Na^{+}, K^{+}, Ca^{2+}, Mg^{2+}, Fe^{2+} and Mn^{2+} was done by Flame Atomic Absorption Spectrometry (FAAS). Molecular absorption spectrophotometry (colorimetry) was used to determine the concentrations of Cl^{-}, NH_4^{+}, NO_3^{-}, NO_2^{-} and PO_4^{3-}. The concentration of HCO_3^{-} and CO_3^{2-} was determined by titration with HCl. SO_4^{2-} was measured with a turbidimetric method.

Detailed descriptions of the different analytical methods for major ions and trace elements are extensively explained in the Laboratory Manual and in Standard Methods for Examination of Water and Waste water (APHA, 1992).

6.3.4 Error on ionic balance

Before interpreting chemical analysis data, the reliability check of the quality of the laboratory analysis was done by the following formula:

$$Error\ on\ ionic\ balance\ \ \% \ = 100 * \frac{cation - \ anion}{cation + \ anion} \qquad (6.2)$$

The error on ionic balance is based on the principle that all aqueous solutions must be electrically neutral, meaning that the sum of equivalents of the positively charged cations must be equal to the sum of equivalents of the negatively charged anions. The analysis is considered as reliable if the error on the ionic balance is smaller than 10%, and preferably smaller than 5%. If an error larger than 10% occurs, among other things it is an indication of a serious systematic error that has occurred during the analysis (e.g. poor standardization or failure to correct the results for laboratory dilutions), or the list of constituents which have been analysed is incomplete (Weight, 2008).

As a general rule, error on ionic balance (%) calculated using the above equation should be within the limits ± 5% although in most of the cases the charge balance will be less than 2% if correct procedures during sampling and laboratory analysis were followed (Freeze & Cherry,

1979). If groundwater has a very low mineralisation, a charge balance error greater than 5% can be acceptable.

The reliability check of the chemical analysis data was done for all 196 groundwater samples (Appendix 6.2). Majority of groundwater samples (190 samples, ca. 97%) showed acceptable charge balance error, whereas 6 samples have shown high error greater than 10%. The latter include the following sampling points on which error is indicated in brackets: 3 (12.07%), 4 (11.69%), 19 (11.08), 20 (36.51%), 33 (20.64%) and 34 (33.09%). All analysis based on these samples were interpreted with care, including comparing their results with chemical data of groundwater samples collected from the same location. Samples with unacceptable error were found still useful especially for general indication of possible areas which might be affected by saltwater intrusion, and for that purpose chloride and conductivity parameters were retained.

6.3.5 Data analysis

The hydrochemical results were analyzed by means of Aquachem software (Calmbach, 1997), the Piper diagram and the Stuyfzand (1986) classification. In order to study the chemical equilibrium existing in groundwater from the study area, the concept of speciation modeling was used. Important results of speciation calculations are saturation indices (SI) with respect to minerals, which indicate whether a mineral should dissolve or precipitate. SI relative to some common minerals were calculated using the program PHREEQC (Parkhurst and Appelo, 1999).

The seawater fraction in the groundwater was estimated using the chloride concentration in the sample (Appelo and Postma, 1993): chloride is assumed to be a conservative parameter. Referring to Appelo and Postma (1993), the chemical reactions during fresh saltwater displacement can be deduced by calculating a composition based on the conservative mixing of salt and freshwater, and comparing the conservative concentrations with those observed in the sample. Based on the conservative mixing of seawater and freshwater, the concentration of an ion i (m_i) in the mixture was calculated using the mass fraction of seawater and the concentrations of the ion in both end members (seawater and freshwater), as follows (Appelo and Postma, 1993):

$$m_{i,mix} = f_{sea}.m_{i,sea} + \ 1 - f_{sea} \ .m_{i,fresh} \qquad (6.3a)$$

Where m_i is concentration of an ion i in mmol/l and subscripts $_{mix}$, $_{sea}$, and $_{fresh}$ indicate the conservative mixture, and end members seawater and freshwater respectively.

Any change in concentration mi_{react} as result of reactions (not mixing) then becomes:

$$m_{i,reaction} = m_{i,sample} - m_{i,mix} \qquad (6.3b)$$

Where $m_{i,\ samples\ =}$ the actually observed concentration in the sample.
The seawater fraction of a conservative mixture is calculated based on the Cl^- concentration in the sample (Appelo and Postma, 1993):

$$f_{sea} = \frac{m_{Cl^-,sample} - m_{Cl^-,fresh}}{m_{Cl^-,sea} - m_{Cl^-,fresh}} \qquad (6.3c)$$

Where:

$f_{sea} =$ the fraction of seawater

$m_{Cl,^-sample} =$ the concentration of Cl^- in the sample expressed in mmol/l

$m_{Cl,^-fresh} =$ the concentration of Cl^- in the freshwater expressed in mmol/l

$m_{Cl,^-sea} =$ Cl^- concentration in the seawater end member in mmol/l (Cl^- = 566 mmol/l).
Ions in freshwater near the coast are often derived from sea spray, and only Ca^{2+} and HCO_3^- are added due to calcite dissolution (Appelo and Postma, 1993). In this case m_i fresh= 0 for all components except Ca^{2+} and HCO_3^-. If there is no other source for Cl^- and all of it considered to be derived from seawater, f_{sea} can be written as:

$$f_{sea} = \frac{m_{Cl^-,sample}}{566} \qquad (6.3d)$$

Where Cl^- concentration is expressed in mmol/l, and the Cl^- concentration of 35% seawater is set at 566 mmol/l.

World Health Organization (WHO) (2004) guidelines for drinking water quality were used for the assessment of drinking water quality.

In terms of evaluating water quality for agricultural purposes, Sodium Adsorption Ratio (SAR) is the most useful parameter. The United States Department of Agriculture (USDA) (1954) classifies irrigation water with respect to SAR. SAR is calculated from the following formula, all concentrations expressed in milli-equivalents per litre:

$$SAR = \frac{Na^+}{\frac{Ca^{2+} + Mg^{2+}}{2}} \qquad (6.4)$$

The waters having SAR values less than 10 are considered as excellent, 10 to 18 as good, 18 to 26 as fair, and above 26 are unsuitable for irrigation use (USDA, 1954). The USDA (1954) has also classified irrigation waters on the basis of electrical conductivity (EC) as: low salinity water (100 – 250 μS/cm), medium salinity water (250 - 750 μS/cm), high salinity water (750 – 2250 μS/cm), and very high salinity water (> 2250 μS/cm). According to USSL's diagram (US Salinity Laboratory Staff, 1954), which is widely used for rating irrigation waters, water can be grouped into 16 classes. It uses SAR (vertical axis) and EC (horizontal axis). The conductivity (horizontal axis) is classified into low (C1), medium (C2), high (C3) and very high (C4) salinity zones. These zones (C1 to C4) have the value of EC less than 250 μS/cm, 250 to 750 μS/cm, 750 to 2,250 μS/cm and more than 2,250 μS/cm, respectively. The SAR (vertical axis) is subdivided into four classes, with decreasing limiting values as EC increases: low (S1), medium (S2), high (S3) and very high (S4) sodium hazard.

Soluble Sodium Percentage (%Na), defined as the ratio of sodium to the total of cations, is also used to evaluate sodium hazard (Khodapanah et al. 2009). Water with %Na greater than 60% may result in sodium accumulations that will cause a breakdown in the soil's physical properties (Khodapanah et al. 2009). The %Na determines the ratio of sodium to total cations including sodium, potassium, calcium and magnesium. The %Na is calculated as follows:

$$\%Na = \frac{Na}{Na+K+Ca+Mg} X\ 100 \qquad (6.5)$$

All concentration values are expressed in milli-equivalents/l.

Other parameters such as chloride and sulphate have been also used for assessment of suitability of water for irrigation (Sagnak, 1991). Chloride and sulphate are essential elements

for plants and were used an important criterion for irrigation water. Chloride and sulphate greater than 710 mg/l and 960 mg/l respectively, are considered unsuitable (Sagnak, 1991).

Field data such as location of boreholes/wells and sampling sites were compiled using ArcGIS 9.2. The same software was used for processing and producing groundwater quality maps.

6.3.5.1 Piper diagram

The concentrations of major ionic constituents of water samples were plotted in the Piper trilinear diagram (Piper, 1953) to determine the water type. Piper diagram provides a convenient method to classify and compare water types based on the ionic composition of different water samples. Cation and anion concentrations (in meq/l) for each groundwater sample are converted to cation and anion totals respectively, and plotted as percentages of their respective totals in two triangles. The cation and anion relative percentages in each triangle are then projected into a quadrilateral polygon that describes the water type. The classification by Piper diagram helps to understand the different geochemical processes occurring along the flow path of the groundwater (cfr 6.2.2.3). Thus the data can be used to illustrate evolution of water quality as it migrates through the ground (classically from bicarbonate rich water to chloride rich water) or as it mixes with water of different composition.

6.3.5.2 Durov diagram

The Durov diagram designed by Durov (1948) is one of the useful forms of trilinear graphical representation for hydrochemical data. The diagram plotting is based on the milli-equivalent percentage of the total major cations and the total major anions in the water samples. It is an alternative form of the Piper tri-linear diagram. Durov plots the major ions as percentage of meq/l in two base triangles and total cations and total anions are set equal to 100%. The data points in the two base triangles are projected into the square of the main field which lies perpendicular to the third axis in each triangle. The plot shows clustering of water quality data points and finally displays some possible geochemical processes that could affect the water genesis.

6.3.5.3 Stuyfzand water classification (1986, 1993)

Water classification by Stuyfzand (Stuyfzand, 1986, 1993) method involves subdividing the most important chemical water characteristics at 4 levels: the primary type, type, subtype, and class. The primary type is determined based on the chloride content (F = fresh: Cl^- < 150 mg/l; Fb = fresh-brackish: 150-300 mg/l; B = brackish: 300-1000 mg/l; Bs = brackish-salt: 1000-10000 mg/l & S = salt: 10000-20000 mg/l) (Table 6.2). The type (code) is determined on the basis of total hardness (Very soft (*): Ca + mg < 0.5 mmol/l; Soft (0): 0.5-1 mmol/l; Moderately hard (1): 1-2 mmol/l; Hard (2): 2-4 mmol/l; Very hard (3): 4-8 mmol/l; Extremely hard (4-7): > 8 mmol/l) (Table 6.2). The classification into subtypes is determined based on the dominant cation and anion. Fig. 6.7 is showing the subdivision of types into subtypes. The main cation and anion are derived from the two triangles. In each corner of the triangle, a hydrochemical family is represented. The location of the sample in the triangle determines the cation and anion group of the water type. If the water sample plots into a section that represents more than one ion, the one with the highest concentration will be selected. For anions, if all hydrochemical families represent less than 50 percent of the total sum anions, the anion will be represented by the name Mix. Finally, the class is determined on the basis of the sum of Na^+, K^+ and Mg^{2+} (meq/l), corrected for a seawater contribution, determined from the Cl^- content (Equation 6.6) (Table 6.2).

$$(Na + K + Mg)_{corrected} = (Na + K + Mg)_{measured} - 1.061\ Cl \quad \frac{meq}{l} \quad \ldots\ldots\ldots\ldots\ldots (6.6)$$

This parameter is further tested against $\overline{0.5}Cl$, as a margin of error in order to conclude to a meaningfully positive (marine cations surplus; positive cation exchange code), negative (marine cations deficit; negative cation exchange code) or equilibrium value (cation exchange code Ø). This classification enables to recognize if cation exchange has occurred in a water sample.

Table 6.2: Classification of water based on chloride concentration, hardness and correction for a seawater contribution: Stuyfzand (1986) classification.

Classification	Critical parameter	Description criterion	Code
Primary type	Cl^- (mg/l)	<150	Fresh (F)
		150-300	Fresh-Brackish (Fb)
		300-1000	Brackish (B)
		1000-10000	Brackish salt (Bs)
		>10000	Salt (S)
Type	Total hardness (mmol/l)	0-0.5	Very soft (*)
		0.5-1	Soft (0)
		1-2	Moderately hard(1)
		2-4	Hard (2)
		4-8	Very hard (3)
		8-16	Extremely hard (4)
		16-32	Extremely hard (5)
		32-64	Extremely hard (6)
		64-128	Extremely hard (7)
Class	$[Na^+ + K^+ + Mg^{2+}]$ (meq/l) corrected for seawater contribution	$(Na^+ + K^+ + Mg^{2+})_{corrected} > \sqrt{(½Cl^-)}$,	+
		$(-\sqrt{(½Cl^-)} \leq (Na^+ + K^+ + Mg^{2+})_{corrected} \leq \sqrt{(½Cl^-)})$,	Ø
		$(Na^+ + K^+ + Mg^{2+})_{corrected} < -\sqrt{(½Cl^-)})$	-

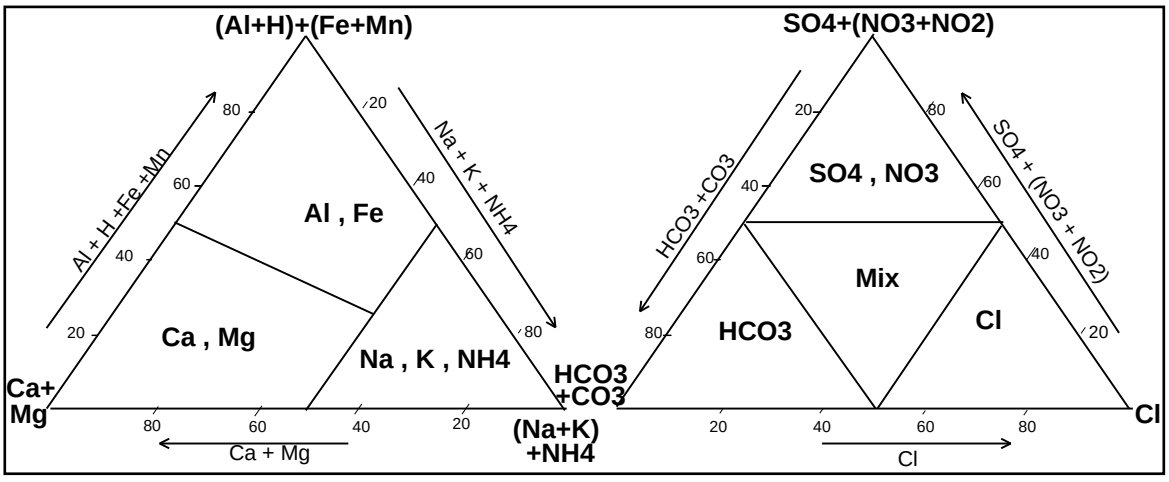

Figure 6.7: A ternary diagram showing the subdivision of types into subtypes (Stuyfzand, 1986).

6.4 Results and discussion

6.4.1 Composition of major ions

The results of laboratory analysis are presented in Appendix 6.2. Statistical analysis of various chemical constituents is presented in Table 6.3. This section presents the results and discussion of all main parameters as presented in Table 6.3.

6.4.1.1 pH, acidity and alkalinity

The pH is an important variable in water quality evaluation as it influences many biological and chemical processes within a water body. The pH value of water is a measurement of acidity or alkalinity: a pH of 7 represents a neutral solution in which hydrogen and hydroxide ions have the same concentration. The dissolution of carbonates leads to an increase of the pH. High values of pH in water are most often caused by presence of carbonate minerals such as calcite and dolomite. Absence of the latter in the aquifer may lead to low pH. However, some pollution sources such as landfills may also cause lower pH (Mato, 2002). Seawater is considered to have a pH value of about 8.2.

Fig. 6.8 shows the spatial distribution of pH in the study area. pH ranges from 6.2–8.55 and 5.7 – 8.66 in unconfined and semi-confined aquifers respectively (Table 6.3). 3 samples from the unconfined aquifer and 5 of the semi-confined aquifer are more acid than permissible (min. 6.5).

Table 6.3: Statistical summary of hydrochemical parameters of groundwater (n=196: 105 samples from the unconfined aquifer and 91 samples from the semi-confined aquifer).

Parameter	**PL**	**EPA**	**Unconfined aquifer water samples**						**Semi-confined aquifer water samples**					
			Min	**Max**	**Mean**	**Median**	**SD**	**> PL**	**Min**	**Max**	**Mean**	**Median**	**SD**	**> PL**
Ca^{2+}	200		4.6	503	89.39	66	79.5	10	3.7	186.9	51.9	44.68	34.4	0
Mg^{2+}	150		2.3	916.9	65.2	24.1	124.2	7	2.8	265	25.1	15.53	32.6	1
Na^{+}	200		2.1	10000	773.3	173	1550.9	41	14.6	2492.5	185.6	98.15	293.7	21
K^{+}	-	12	2.5	165	22.8	15.5	24.56	59	1.0	116	18.3	12	17.9	46
SO_4^{2-}	250		2.1	1063.9	123.5	86	141.8	15	0.66	703.1	84.2	61.66	91.3	4
HCO_3^{-}	240		7.9	797.9	265.1	248.88	170.5	52	5.5	584.9	177.0	163.79	122.9	26
Cl^{-}	250		6.4	15478	955.2	188.69	2672.1	47	14.1	4745.2	260.2	89.96	547.7	25
NO_3^{-}	50		0.0	435.4	73.7	24	98.3	50	0.0	423.9	64.1	24.61	89.3	32
EC	1500		8.6	29500	3003.4	1640	3881.9	57	170.2	17600	1532.2	990	2011.9	30
pH	6.5-9.2		6.2	8.55	7.55	7.48	0.55	3	5.7	8.66	7.6	7.59	0.73	5
TDS	1000		114.5	16225	1564.54	931	1919.9	49	89.48	8778.58	871.85	618	998.12	25

Key: i) PL = WHO (2004) permissible limit; EPA = EPA (2004) permissible limit; ii) all values are in mg/l except pH and EC (µS/cm –25 ^{o}C); iii) SD = Standard Deviation; and iv) > PL = number of samples beyond permissible limit of WHO (2004)/EPA (2004).

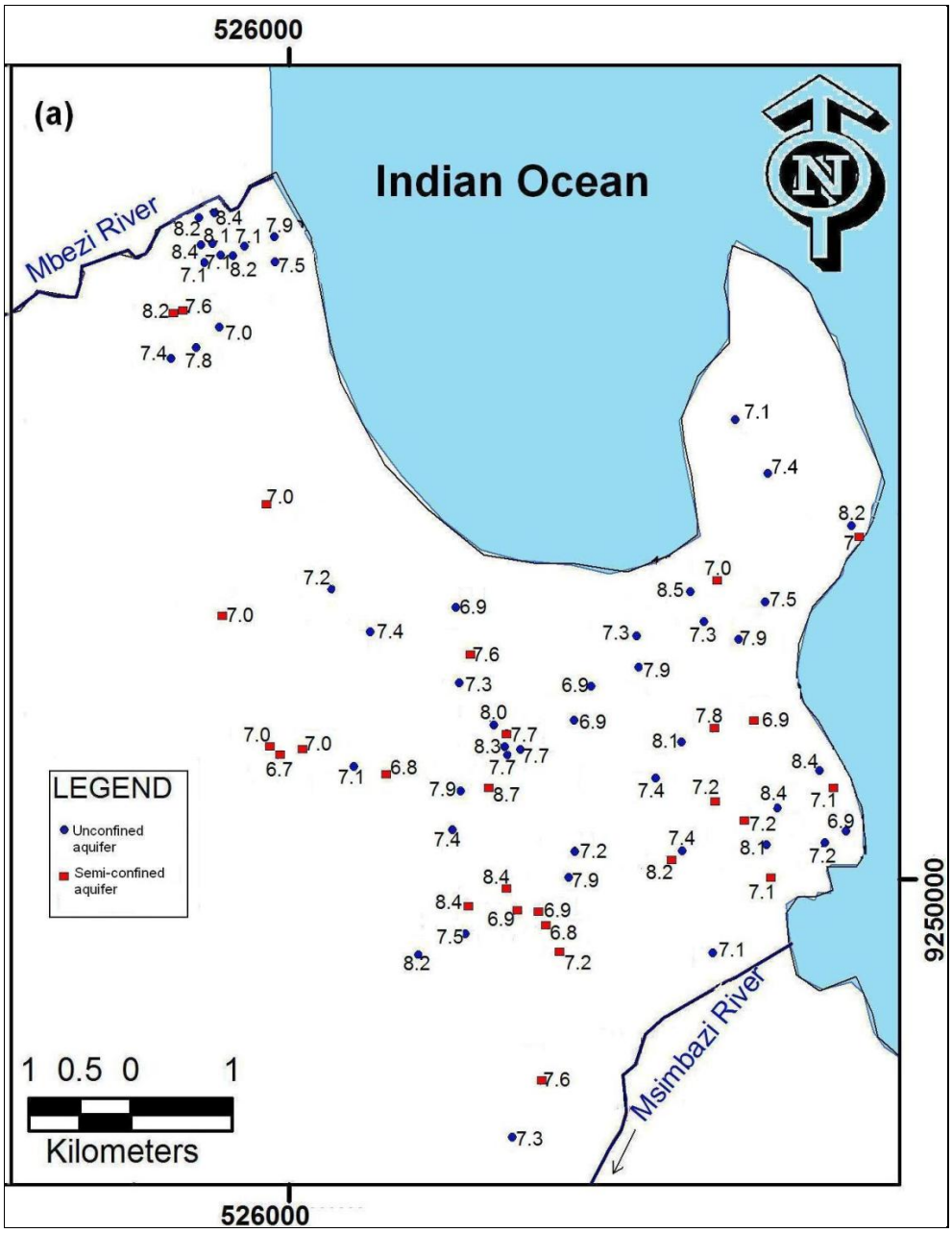

Figure 6.8(a): Spatial distribution of pH (for both unconfined aquifer and semi-confined aquifer) in the area between Mbezi River and Msimbazi River.

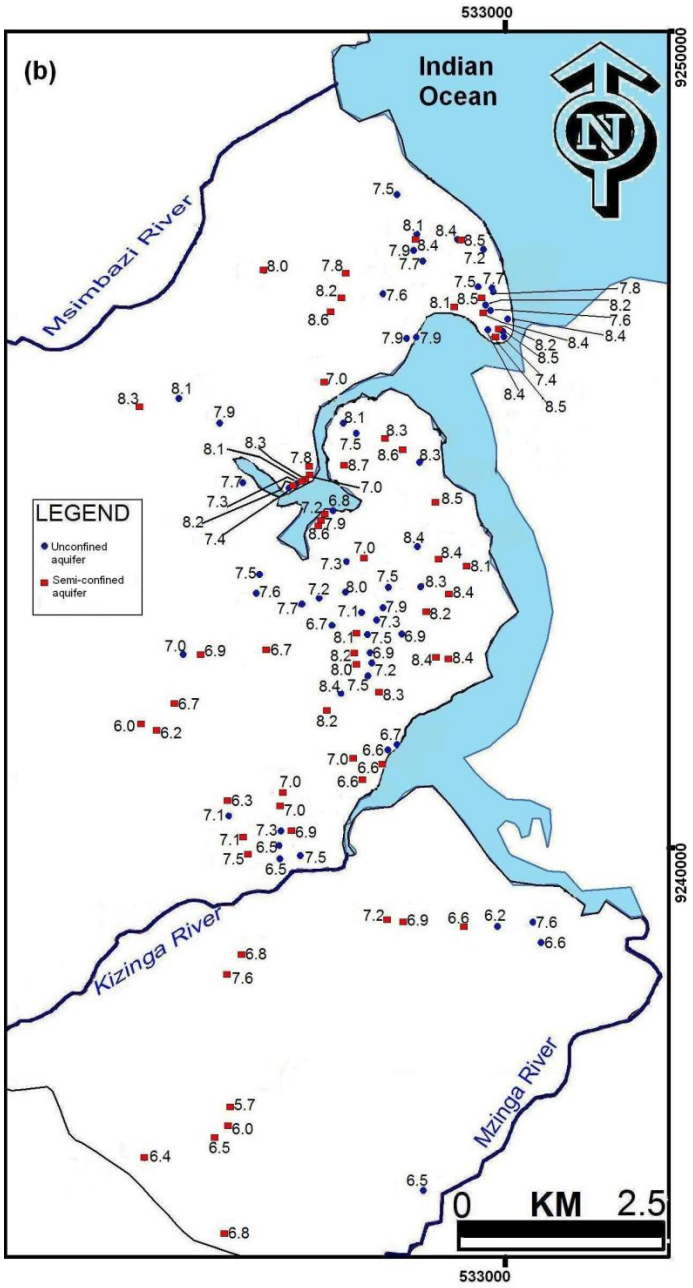

Figure 6.8(b): Spatial distribution of pH (for both unconfined aquifer and semi-confined aquifer) in the area between Msimbazi River and Mzinga River.

6.4.1.2 Electrical conductivity

Electrical Conductivity (EC) is a measure of the ability of water to conduct an electrical current. It is related to the concentrations of ions, the more dissolved ions in the water the greater the conductivity. EC is the simplest indicator of seawater intrusion or salinization (El Moujabber et al., 2006). Seawater EC is around 35000 µS/cm.

The spatial distribution of EC from analysed groundwater samples in the studied area is presented in Fig. 6.9. EC ranges from 8.6–29500 μS/cm and 170.2–17600 μS/cm in unconfined and semi-confined aquifers respectively. 54.28% of samples from the unconfined aquifer and 32.97% of the semi-confined aquifer exceed the permissible limit for EC.

Along the coastline, high values of EC are usually attributed to salinization by seawater intrusion (Stamatis & Voudouris, 2003). Samples (with water types in brackets) located near to the coastline which shows high values greater than 10,000 μS/cm include: 13 (Na-Cl), 18 (Na-Mg-Cl), 18' (Na-Cl), 33(Na-Cl), 41 (Na-Cl), 117 (Na-Ca-Cl) and 132 (Na-Cl). Several samples with EC values between 5000-10000 μS/cm, also located towards the coastline, have been documented. These include samples: 14 (Na-Ca-Cl-HCO_3), 16 (Na-Cl), 30 (Na-Cl), 81 (Na-Cl), 97 (Na-HCO_3-Cl), l15 (Na-Cl), 114 (Na-Cl) and 137 (Na-Cl). High EC values decrease and water types change away from the coastline. In Fig. 6.9b, the City Centre which is close to the sea is the area which is most affected by saltwater intrusion. Moving away from the City Centre to the south, areas such as Kurasini, Mtoni and Mbagala indicate several samples with EC values less than 1000 μS/cm. The lowest EC value is 138 μS/cm for sample number 101 with Ca-Mg-HCO_3 type. Fresh groundwater that is not affected by seawater intrusion is characterized by low values of EC and Ca-Mg-HCO_3 or Ca-HCO_3 water type. Examples of these include samples (with water types in brackets) number 95 (Ca-Mg-HCO_3) and 64 (Ca-HCO_3) with EC values of 549 μS/cm and 700 μS/cm respectively.

Due to the seaward-sloping nature of coastal plain strata, aquifers are recharged from inland sources, with fresh water flowing down-gradient and discharging to the sea (Fig. 1.7 in section 1.8.2). According to the above description related to EC values in the study area, the following characteristics can be drawn: The electrical conductivity shows a trend of increase from the inland recharge areas towards the lowlands and discharge area in the sea. High values of electrical conductivity (E.C.) along the coastline are attributed to seawater intrusion, as a result of the intensive groundwater exploitation. The groundwater EC values range from 138.4–2,200 μS/cm at distances greater than 2 km away from the coastline, to about 760–29500 μS/cm at a distance of less than 2 km from the coastline, respectively. The former are related to areas such as Mbagala, Temeke, Mtoni, Kurasini, Ilala and Mwananyamala, whereas the latter are related mainly to the areas close to the coastline such as City Centre, Oysterbay, Masaki, Msasani, Mikocheni and Kawe.

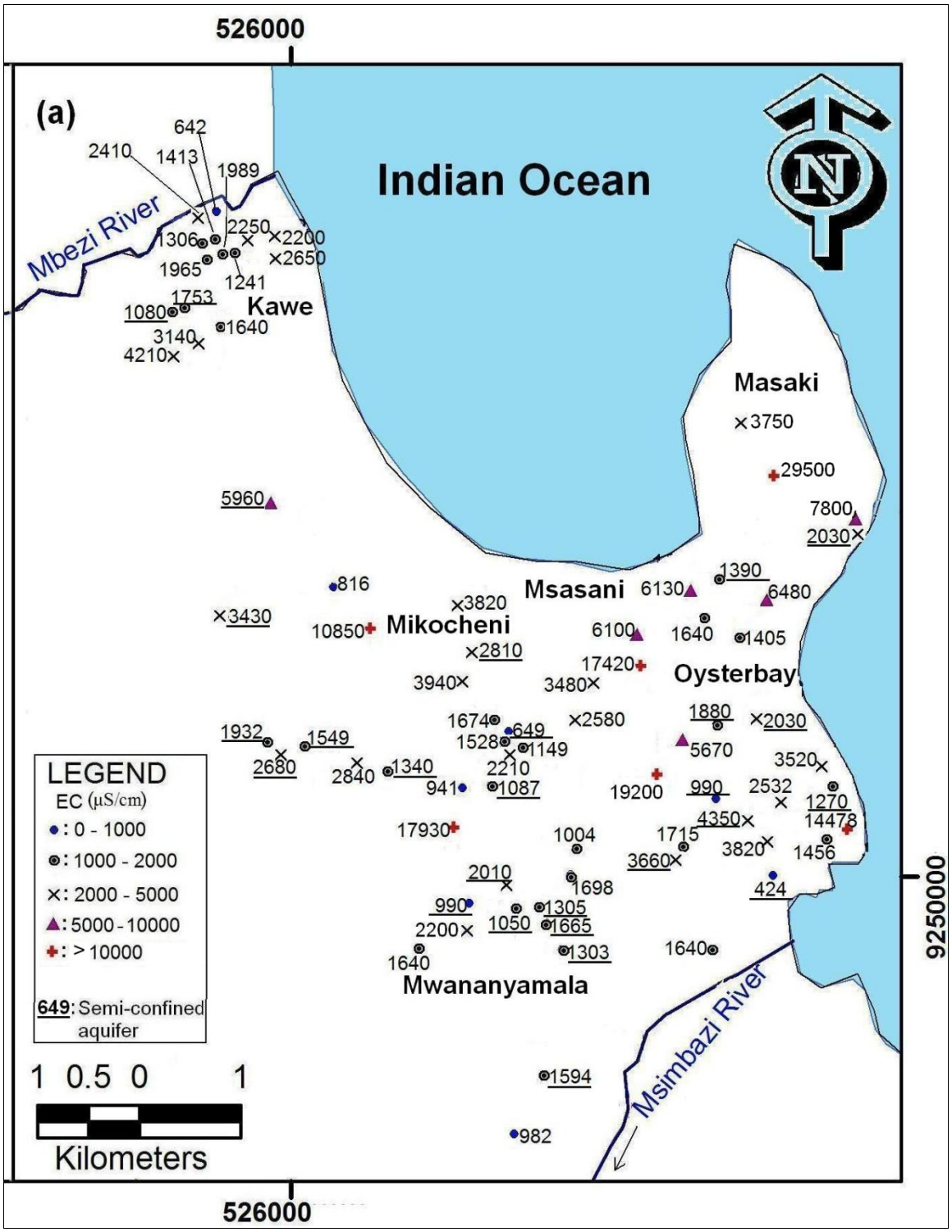

Figure 6.9(a): Spatial distribution of electrical conductivity (EC) (µS/cm) in the area between Mbezi River and Msimbazi River. Plain numbers and underlined numbers signify unconfined aquifer and semi-confined aquifer respectively.

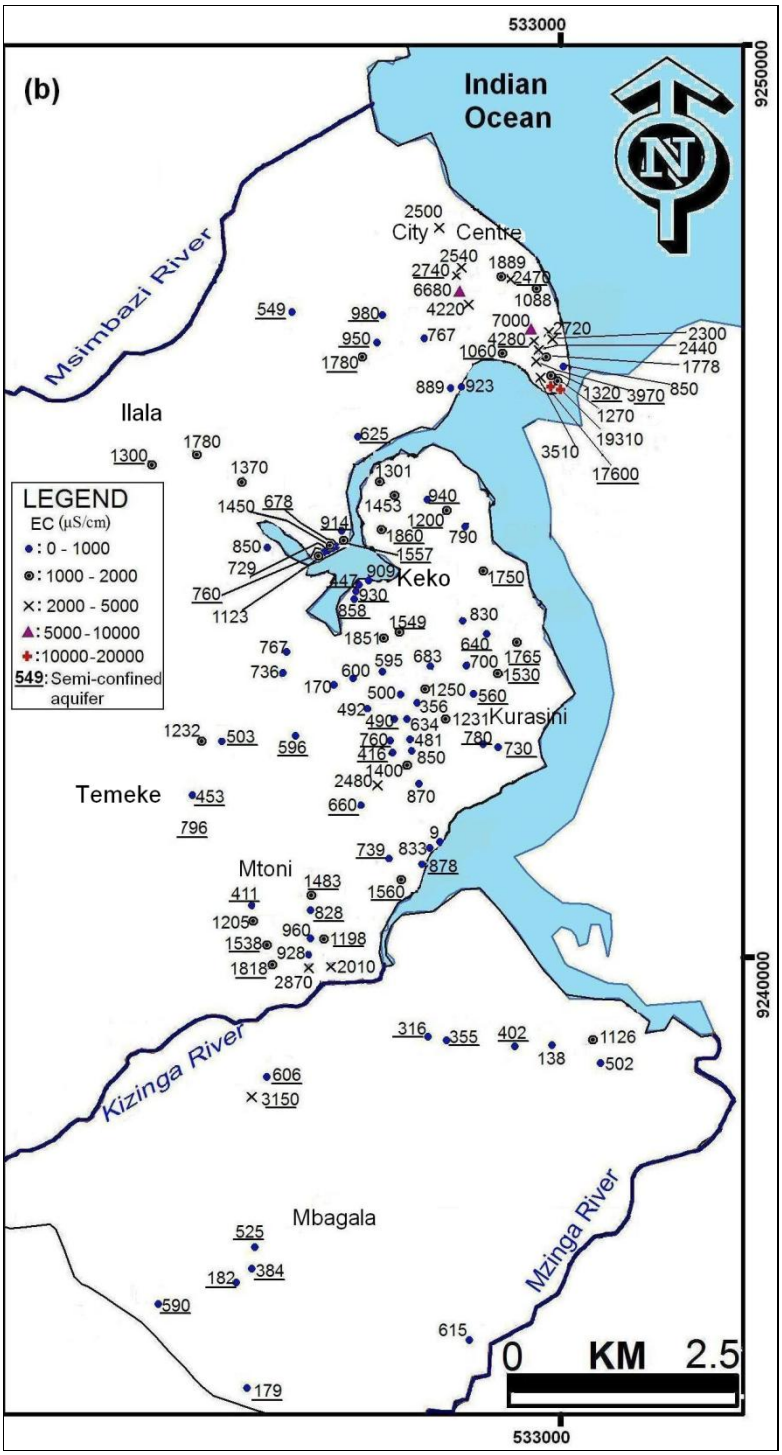

Figure 6.9(b): Spatial distribution of electrical conductivity (EC) (µS/cm) in the area between Msimbazi River and Mzinga River. Plain numbers and underlined numbers signify unconfined aquifer and semi-confined aquifer respectively.

6.4.1.3 Total dissolved solids

Total dissolved solids (TDS) is considered as an indicator of water salinity, which for natural groundwater comprises mainly the major ions (i.e. Ca^{2+}, Mg^{2+}, Cl^{-}, Na^{+}, HCO_3^{-} and SO_4^{2-}) and minor ions (i.e. K^{+}) and NO_3^{-}. It is a summation of all constituents dissolved in water (in mg/l). TDS was obtained in this study by summing up all analytical concentrations for the sample. TDS may also be deduced from measurement of EC from the relationship between both. Fig. 6.10 indicates an obvious positive correlation of total dissolved solids (TDS) and electrical conductivity (EC) of groundwater samples in the studied area. From the graph, a polynomial equation (6.7) with a correlation coefficient of $R^2 = 0.97$, defines the relationship of TDS and EC in the study area.

$$TDS = 2\,x\,10^{-6}\,x\,EC^2 + 0.4811\,x\,EC + 142.12 \qquad (6.7)$$

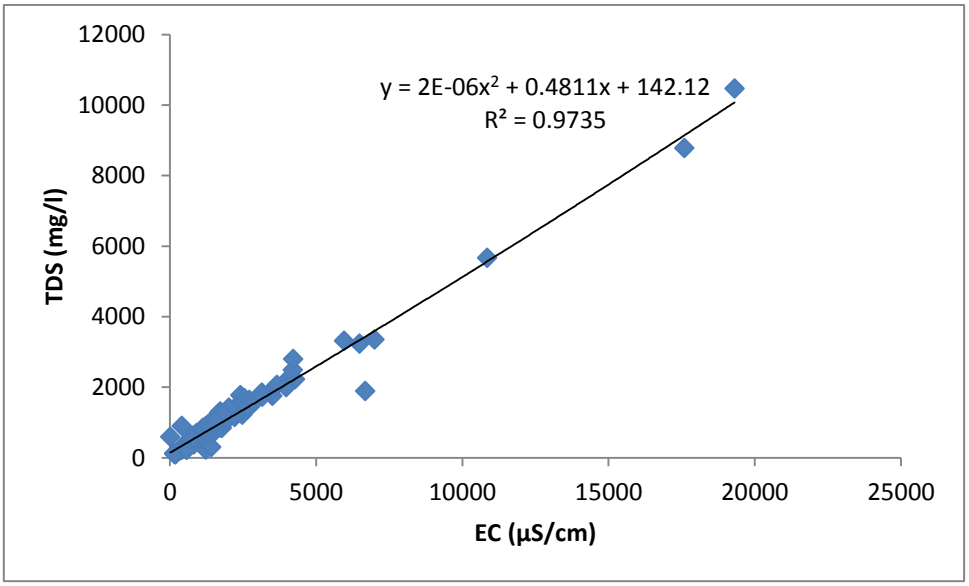

Figure 6.10: Correlation of total dissolved solids (TDS) and electrical conductivity (EC) of groundwater samples in the studied area.

Dissolved ions in water can originate from a number of sources, both natural and as a result of human activities. For example, seawater intrusion, waste water discharges, agricultural and urban runoff can carry excess minerals into water sources. Mineral constituents dissolved in water usually are less than 5000 mg /l, but some brines contain as much as 300,000 mg l/l (Todd, 1980). Seawater with TDS of 35,000 mg/l is considered standard seawater

(http://www.filmtec.com). The actual TDS content may, however, vary within wide limits from one sea to another.

The spatial distribution of TDS from analysed groundwater samples in the study area is presented in Fig. 6.11(a-b). TDS ranges from 114.5–16225 mg/l and 89.5–8779 mg/l in unconfined and semi-confined aquifers respectively. 46.67% of samples from the unconfined aquifer and 27.47% of semi-confined water samples exceed the permissible limit for TDS. Water with TDS value less than 1000 mg/l is regarded to be fresh water (De Moor and De Breuck, 1969) and considered as potable water (WHO, 2004). In the study area samples belonging to this group are mostly located to the south of Msimbazi River and away from the City Centre (Fig. 6.11b). Water samples collected from the City Centre show TDS values ranging from 579 mg/l (sampling point 35) to 10470 mg/l (sampling point 132). Using the groundwater classification of De Moor and De Breuck (1969) this indicates groundwater quality classes ranging from moderately fresh (MF) to very brackish (VB).

Groundwater salinization is the result from the high local pumping rate, which leads to the lateral attraction of seawater or the upconing of deep saline water. Furthermore, to the north of Msimbazi River, over 60% of samples indicate TDS values greater than 1000 mg/l: majority of samples (45) fall in the intermediate TDS values (1000 < TDS < 5000 mg/l) and six samples within 3-4 km from the coastline have shown TDS values greater than 5000 mg/l. The high pumping rate along the coastline leads to a greater drawdown at the extraction points causing vertical rise of saltwater below the pumping wells.

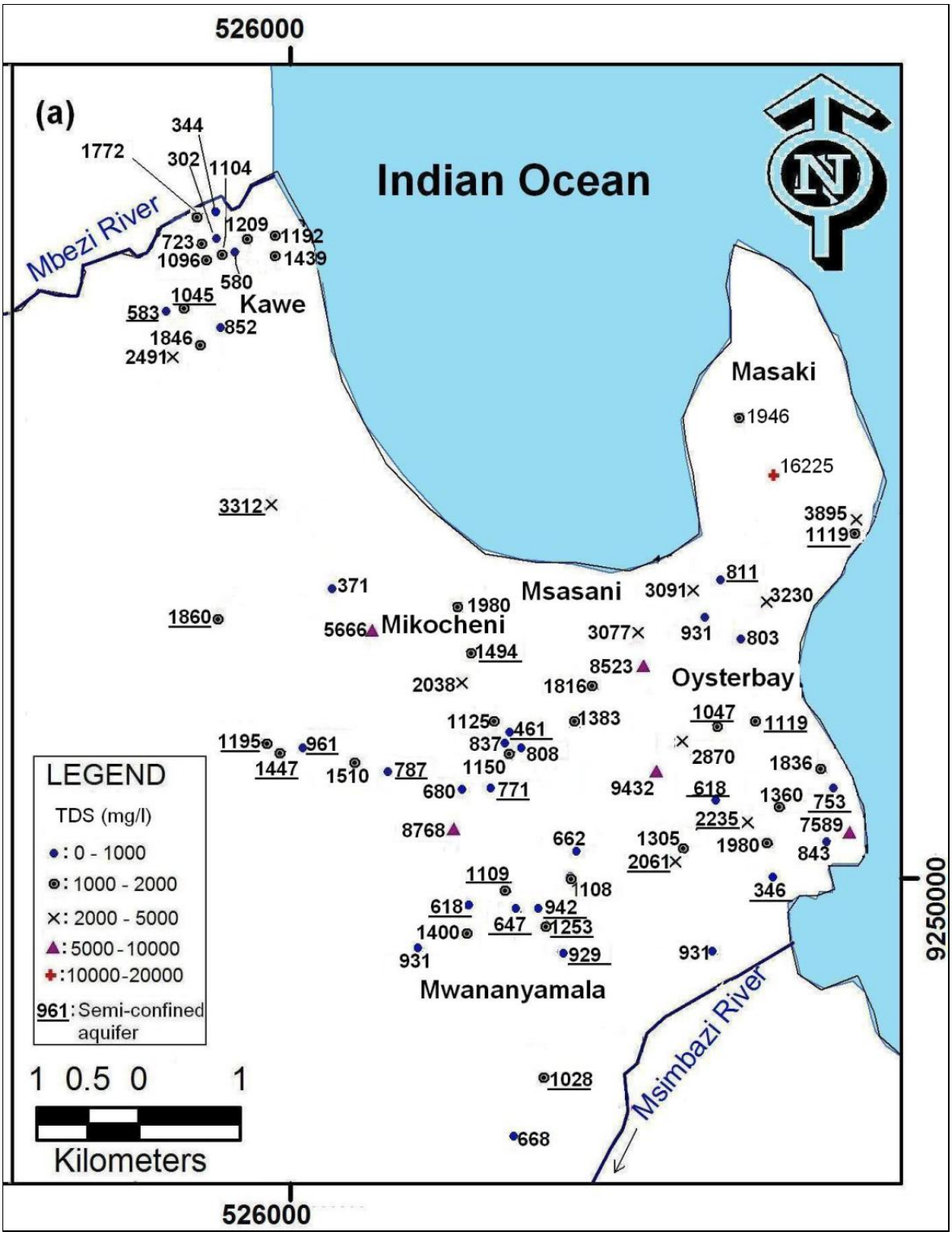

Figure 6.11(a): Spatial distribution of total dissolved solids (TDS) (mg/l) in the area between Mbezi River and Msimbazi River. Plain numbers and underlined numbers signify unconfined aquifer and semi-confined aquifer respectively.

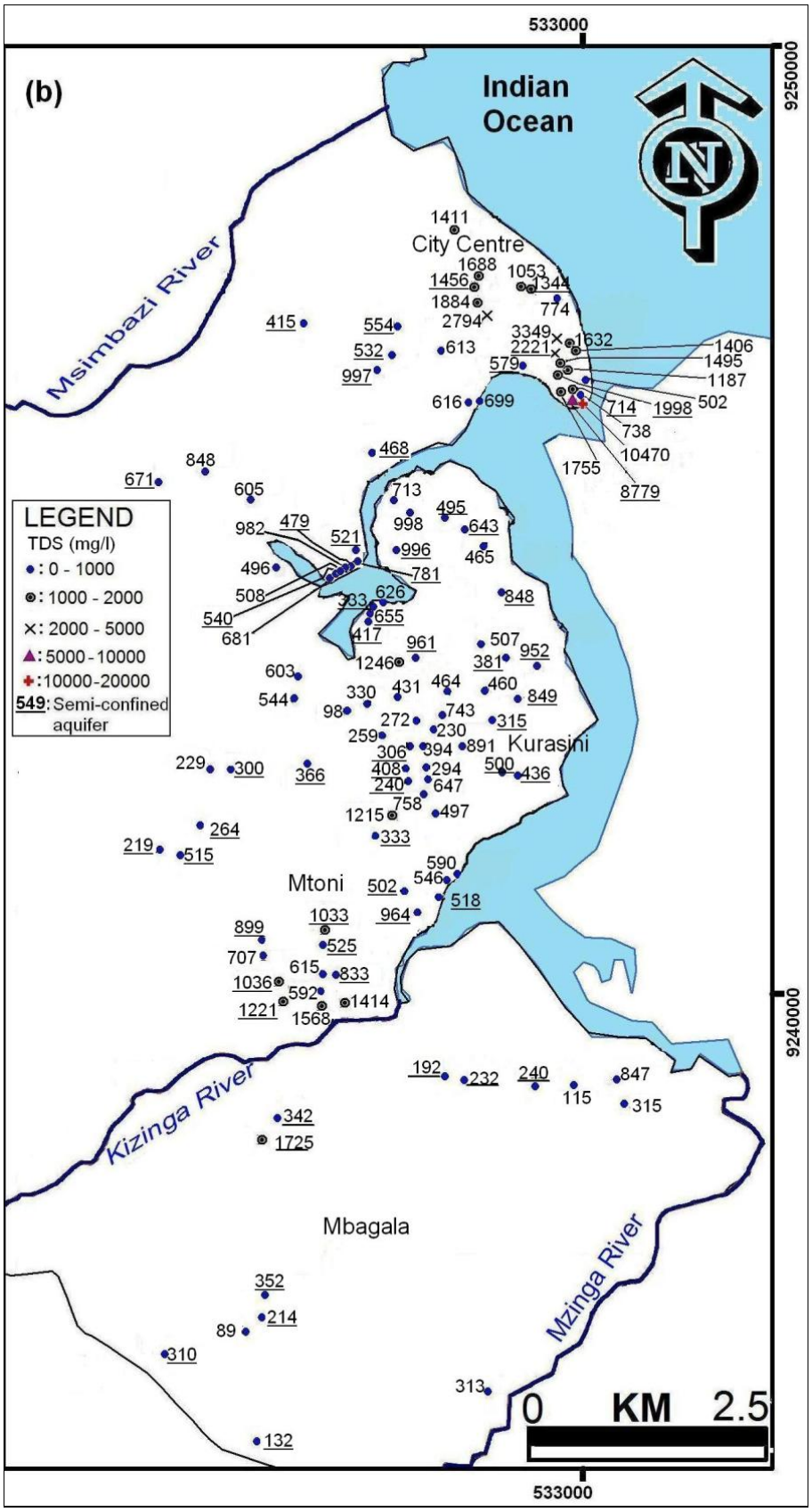

Figure 6.11(b): Spatial distribution of total dissolved solids (TDS) (mg/l) in the area between Msimbazi River and Mzinga River. Plain numbers and underlined numbers signify unconfined aquifer and semi-confined aquifer respectively.

6.4.1.4 Calcium

Rocks rich in calcium minerals, mainly carbonates and sulphates, especially limestone, dolomite and gypsum are the sources of calcium (Ca^{2+}) which is found present in all waters. Ca^{2+} together with Mg^{2+} are responsible for the hardness of water (Appelo and Postma, 1993). The spatial distribution of Ca^{2+} from analysed groundwater samples in the study area is presented in Fig. 6.12 (a-b). Ca^{2+} ranges from 4.6 – 503 mg/l and 3.7 – 186.9 mg/l in unconfined and semi-confined aquifers respectively. Ca^{2+} and Mg^{2+} are of secondary importance in both unconfined and semi-confined aquifers. In the upper aquifer, Ca^{2+} and Mg^{2+} represent an average of 11.91% and 8.68% of all cations respectively, whereas in the lower aquifer these cations represent respectively an average of 18.42% and 8.94% of all cations.

Natural water has calcium concentration less than 100 mg/l whereas concentration of calcium up to several hundred milligrams per liter or more can be associated with salt waters (Todd, 1980). According to Appelo and Postma (1993) (Table 6.1), the calcium ion concentration in seawater is 10.7 mmol/l (ca. 428 mg/l). In the study area several water samples especially from boreholes located close to the coastline show elevated values of calcium concentrations. Examples of samples showing much higher values (> 200 mg/l) include numbers 41 and 132 (in City Centre) (Fig. 6.12b), and nine wells (sampling points 1, 2, 9, 15, 18, 18', 30, 83 and 117) located in the area north of Msimbazi River (Fig. 6.12a). The possible source of this escalation in Ca^{2+} is mixing with the seawater, whereby cation exchange occurs when saltwater intrudes the freshwater aquifer, leading to excess of Ca^{2+} and therefore increasing its concentration in groundwater.

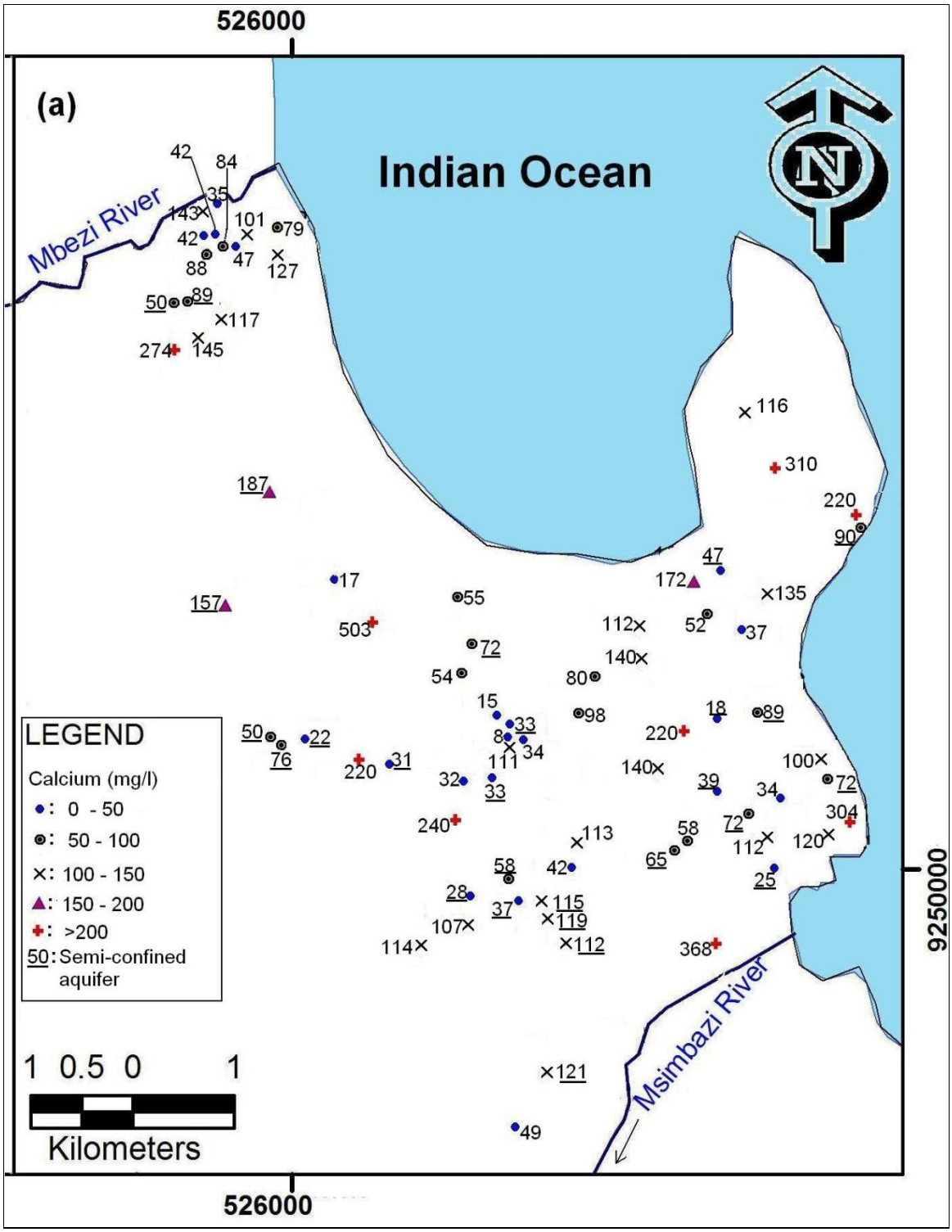

Figure 6.12(a): Spatial distribution of Ca^{2+} concentrations (mg/l) in the area between Mbezi River and Msimbazi River. Plain numbers and underlined numbers signify unconfined aquifer and semi-confined aquifer respectively.

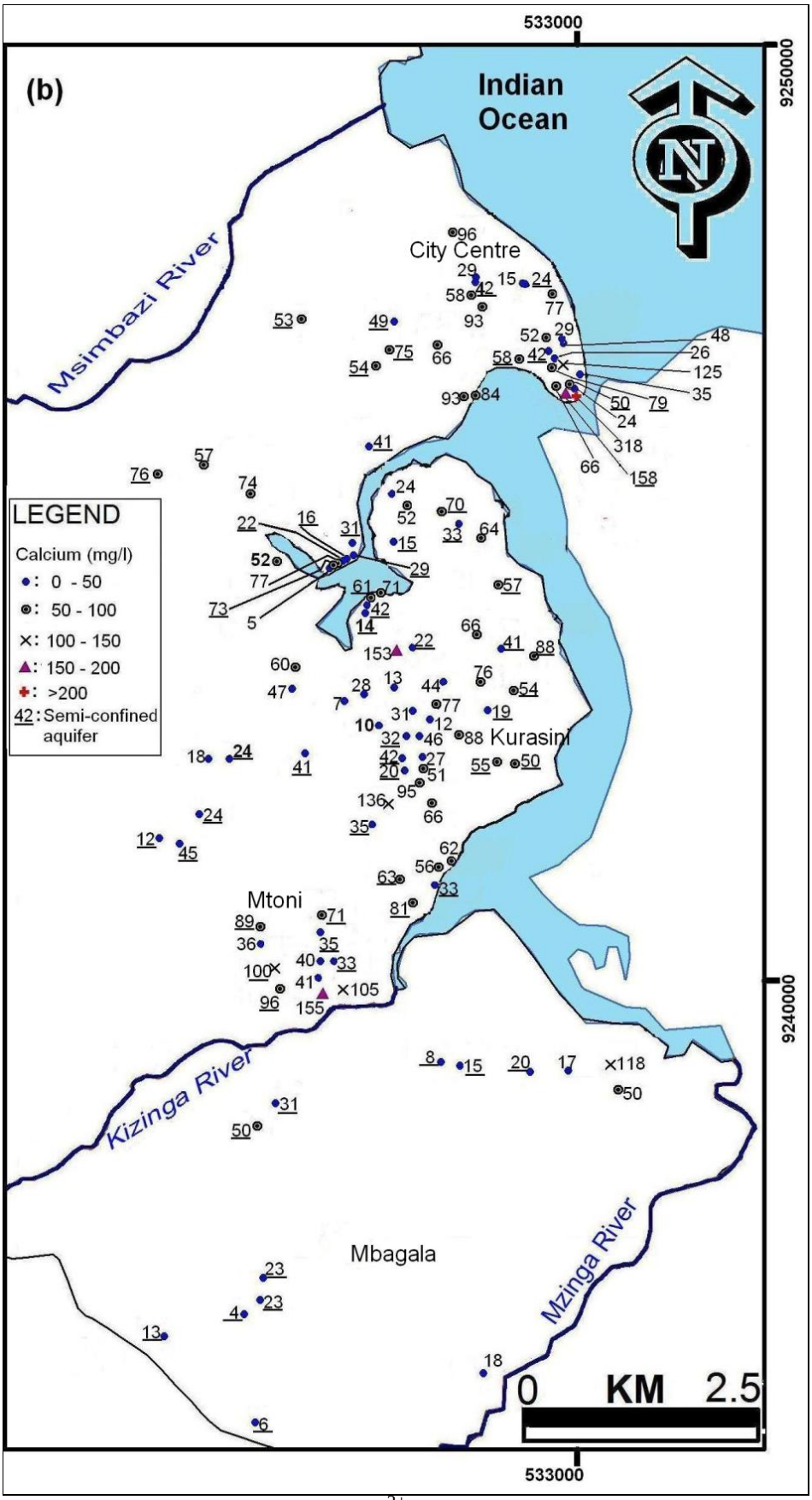

Figure 6.12(b): Spatial distribution of Ca^{2+} concentrations (mg/l) in the area between Msimbazi River and Kizinga River. Plain numbers and underlined numbers signify unconfined aquifer and semi-confined aquifer respectively.

6.4.1.5 Magnesium

Magnesium arises principally from the weathering of rocks containing ferromagnesium minerals, dolomite and clay minerals (Todd, 1980). Natural concentration of magnesium in natural water is usually less than 50 mg/l and about 1000 mg/l in seawater (Todd, 1980).

Fig. 6.13(a-b) shows the spatial distribution of Mg^{2+} in the study area Mg^{2+} ranges from 2.3–917 mg/l and 3.7–187 mg/l in unconfined and semi-confined aquifers respectively. Spatial distribution of Mg^{2+} concentration (Fig. 6.13a-b) follows more or less the same pattern as the spatial distribution of Ca^{2+} concentration map (Fig. 6.12a-b). Just like Ca^{2+} the same explanation can be given to the possible sources of this escalation in mg^{2+}. Increase in Mg^{2+} is observed in samples collected towards the coastline and this suggest possible admixture of freshwater with seawater. The dissolution of dolomite and/or Mg^{2+} bearing calcite forms another source of Mg^{2+} in the study area.

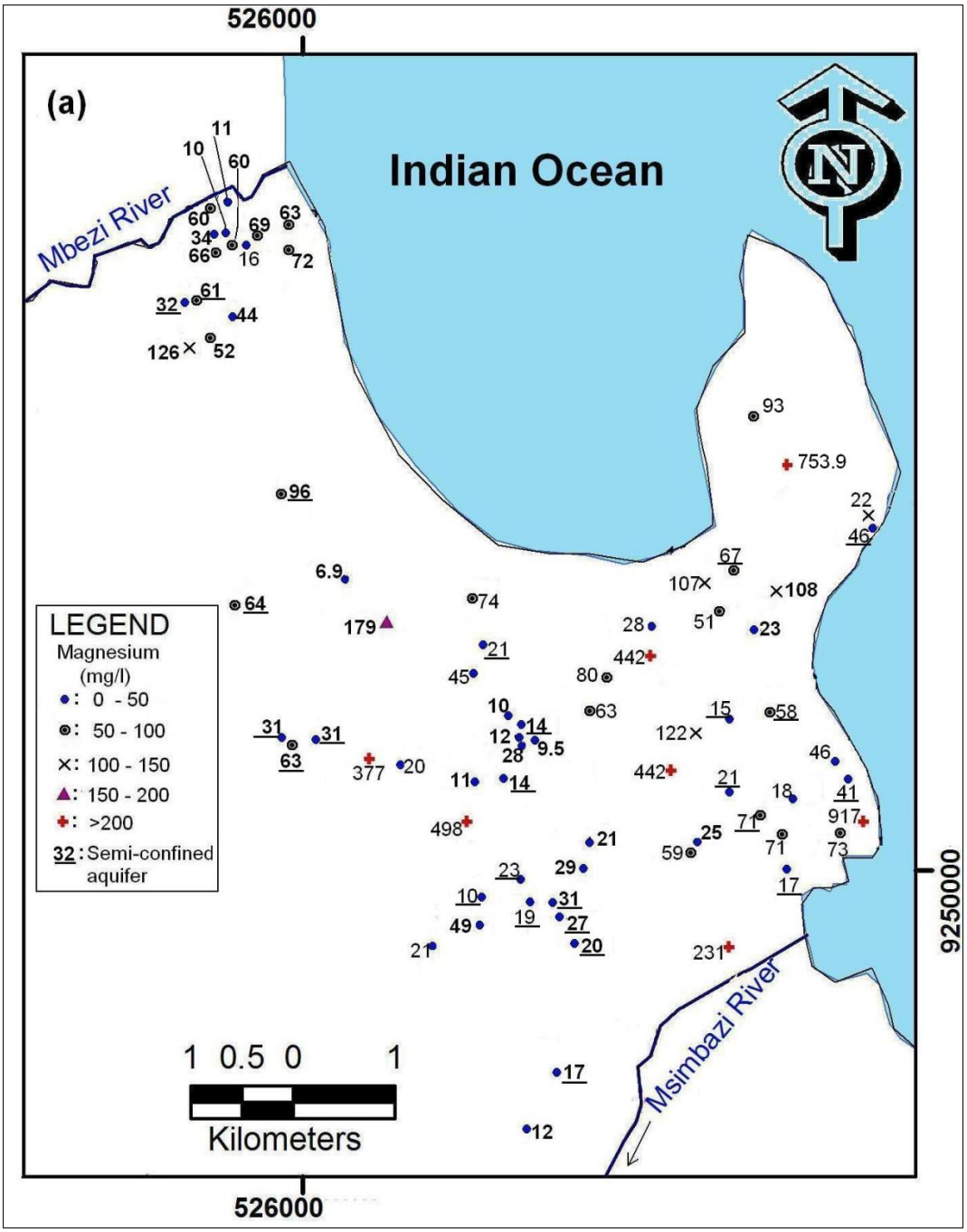

Figure 6.13(a): Spatial distribution of Mg^{2+} concentrations (mg/l) in the area between Mbezi River and Msimbazi River. Plain numbers and underlined numbers signify unconfined aquifer and semi-confined aquifer respectively.

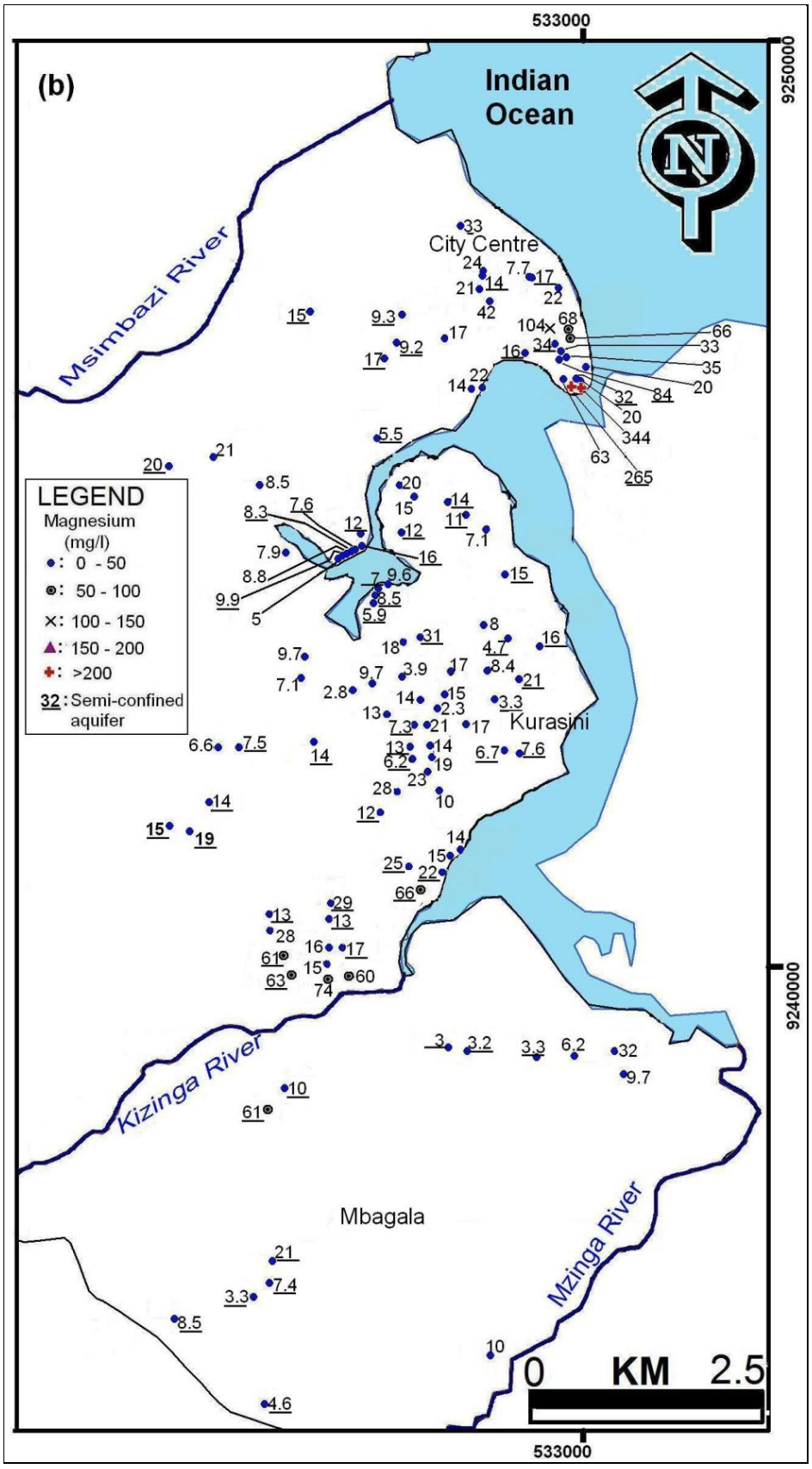

Figure 6.13(b): Spatial distribution of Mg^{2+} concentrations (mg/l) in the area between Msimbazi River and Mzinga River. Plain numbers and underlined numbers signify unconfined aquifer and semi-confined aquifer respectively.

6.4.1.6 Sodium

Feldspars (albite), clay minerals, evaporites such as halite, industrial wastes are sources of sodium (Na^+) (Todd, 1980). Concentration of sodium in natural water is generally < 200 mg/l, about 10,000 mg/l in seawater, and about 25,000 mg/l in brines (Todd, 1980). Sodium is released in groundwater through the weathering of silicate minerals and especially silicates containing Na^+, for example albite (Matthess, 1982; Appelo and Postma, 1993; Appelo & Postma, 2005). High concentration of Na^+ in groundwater may result from contamination by sewage, industrial effluents and saltwater intrusion in coastal aquifers (Chapman and Kimstach, 1996; Walraevens and Van Camp, 2005).

The spatial distribution of Na^+ from analysed groundwater samples in the study area is presented in Fig. 6.14 (a-b). Na^+ is dominant among the major cations in both unconfined and semi-confined aquifers. In unconfined aquifer water samples, it ranges from 2.1 – 10,000 mg/l and represents on average 76.37% of all cations. In the semi-confined aquifer, Na^+ ranges from 14.6 – 2493 mg/l representing on average 66.04% of all cations. 39.05% of samples from the unconfined aquifer and 23.08% of the semi-confined water samples are beyond the permissible limit of WHO (2004) for Na^+ (Table 6.3).

WHO permissible limit for sodium in drinking water is 200 mg/l. In the study area samples belonging to this group are located mainly to the south of Msimbazi River and away from the City Centre (Fig. 6.14b). Some samples collected to the north of the Msimbazi River also show sodium concentration less than 200 mg/l, especially for the boreholes/wells located relatively far away from the coastline. Majority of samples collected from boreholes/wells located towards the coastline within the City Centre (Fig. 6.14b) and to the north of Msimbazi River (Fig. 6.14a) show elevated sodium concentration ranging from above 200 mg/l to 10000 mg/l. Very close to the shoreline sodium is the dominant cation with very high concentrations. This high increase is an indicator of the strong influence of seawater intrusion along the coast.

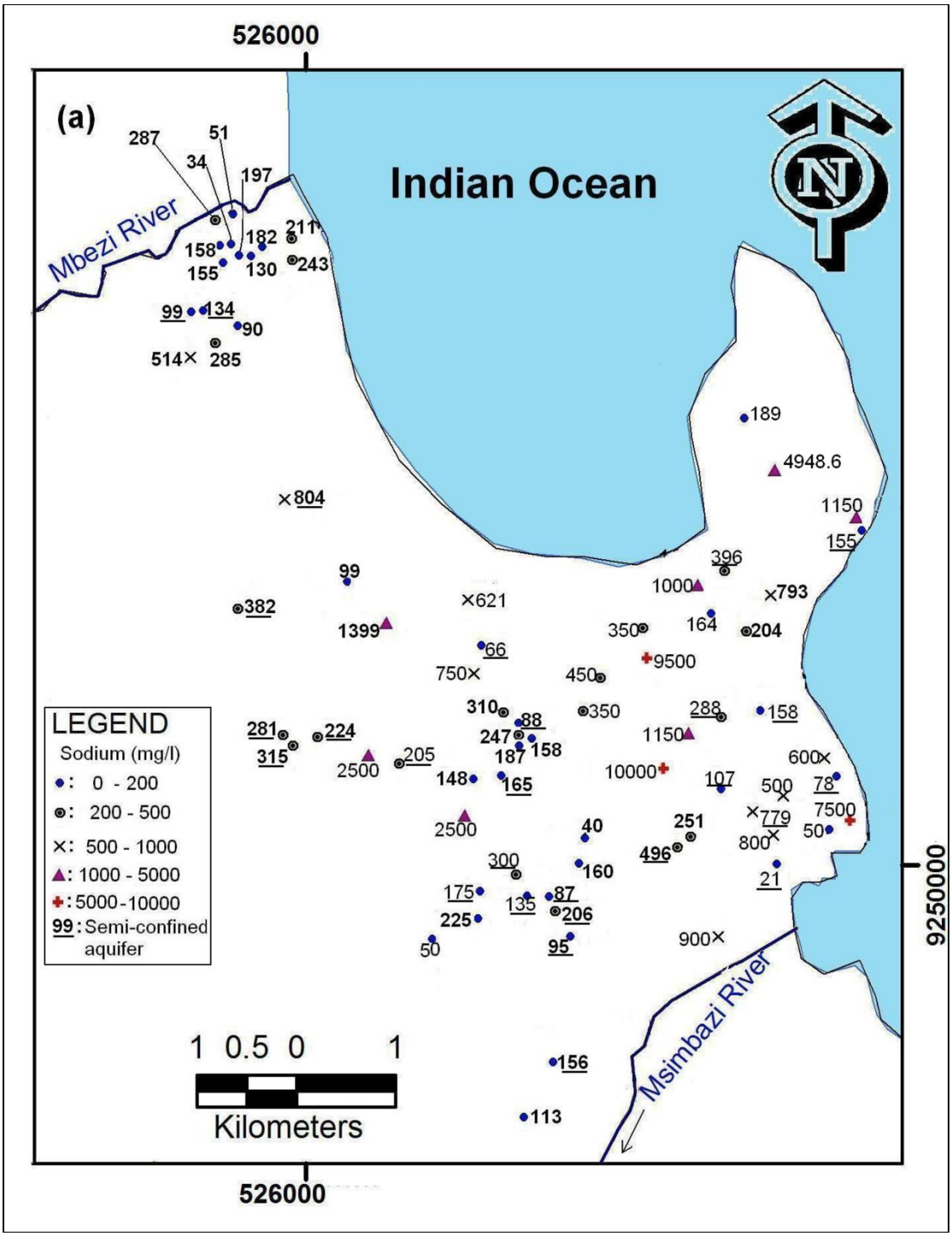

Figure 6.14(a): Spatial distribution of Na^+ concentrations (mg/l) in the area between Mbezi River and Msimbazi River. Plain numbers and underlined numbers signify unconfined aquifer and semi-confined aquifer respectively.

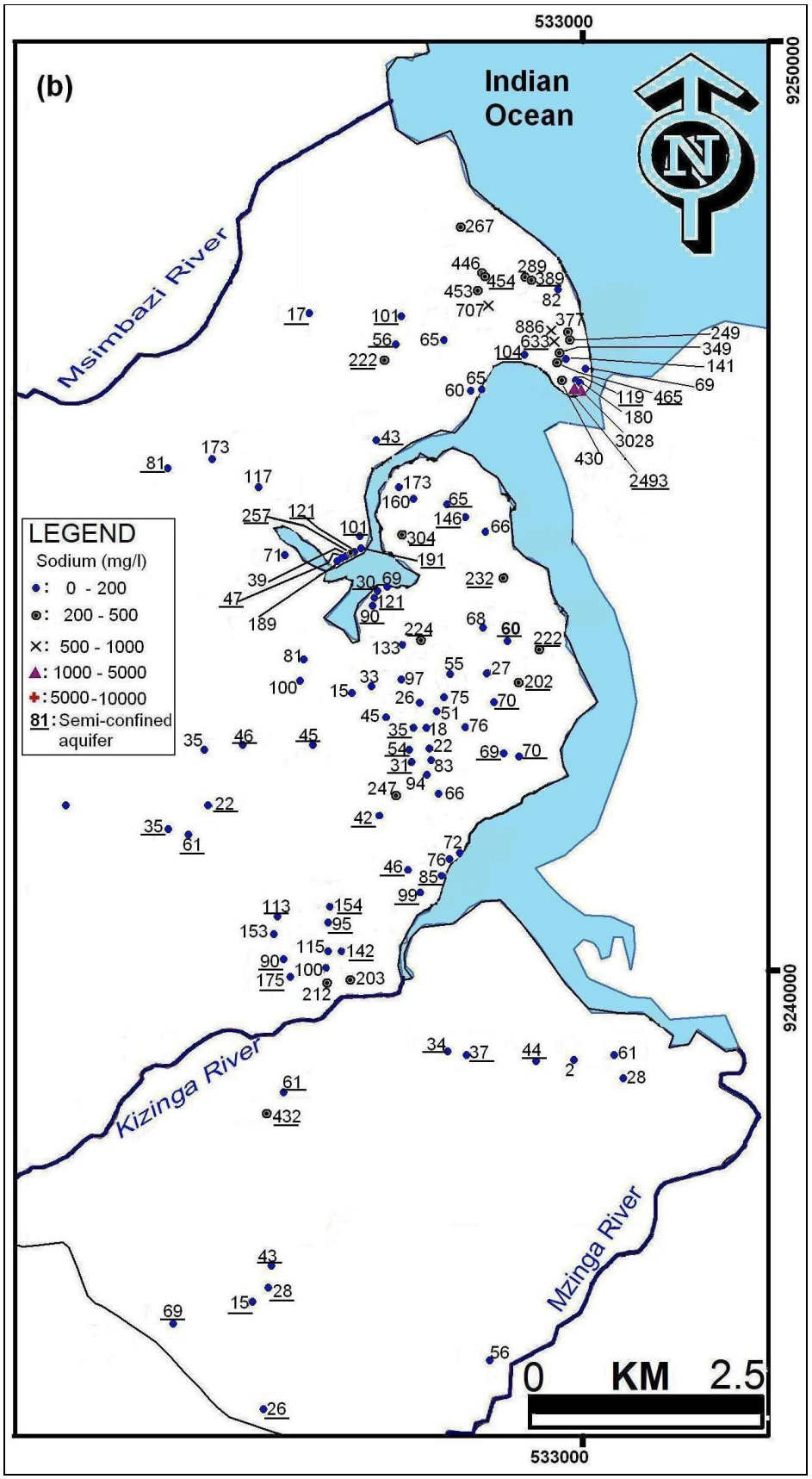

Figure 6.14(b): Spatial distribution of Na^+ concentrations (mg/l) in the area between Msimbazi River and Mzinga River. Plain numbers and underlined numbers signify unconfined aquifer and semi-confined aquifer respectively.

6.4.1.6 Potassium

Feldspars (orthoclase, microcline), feldspathoids, some micas, clay minerals are natural sources of potassium (K^+) (Todd, 1980). Concentration of potassium in natural water is usually less than 10 mg/l (Davis et al., 1966; Todd, 1980), but can occur up to 100 mg/l in hot springs and 25,000 mg/l in brines (Todd, 1980). According to Appelo and Postma (1993) (Table 6.1), the potassium ion concentration in seawater is 10.6 mmol/l (ca. 414 mg/l).

K^+ is minor representing on average 3.04% of all cations in the upper aquifer and 6.60% in the semi-confined aquifer. The spatial distribution of K^+ from analysed groundwater samples in the study area is presented in Fig. 6.15 and Fig. 5.16. K^+ ranges from 2.5–165 mg/l and 1–17.9 mg/l in unconfined and semi-confined aquifers respectively. There is no clear indication of maximum permissible limit of K^+ in drinking water in WHO guideline (WHO, 2004). European Union recommends a maximum of 12 mg/l (EPA, 2004). 55.77% of samples from the unconfined aquifer and 50.55% of semi-confined water samples exceed the permissible limit for K^+.

In the study area, K^+ concentration is observed to occur up to over 100 mg/l in samples number 84 and 177 (Fig. 6.15) and samples number 41 and 132 (Fig. 6.16). These higher concentrations values are nothing else but associated to seawater intrusion as a result of intensive groundwater exploitation.

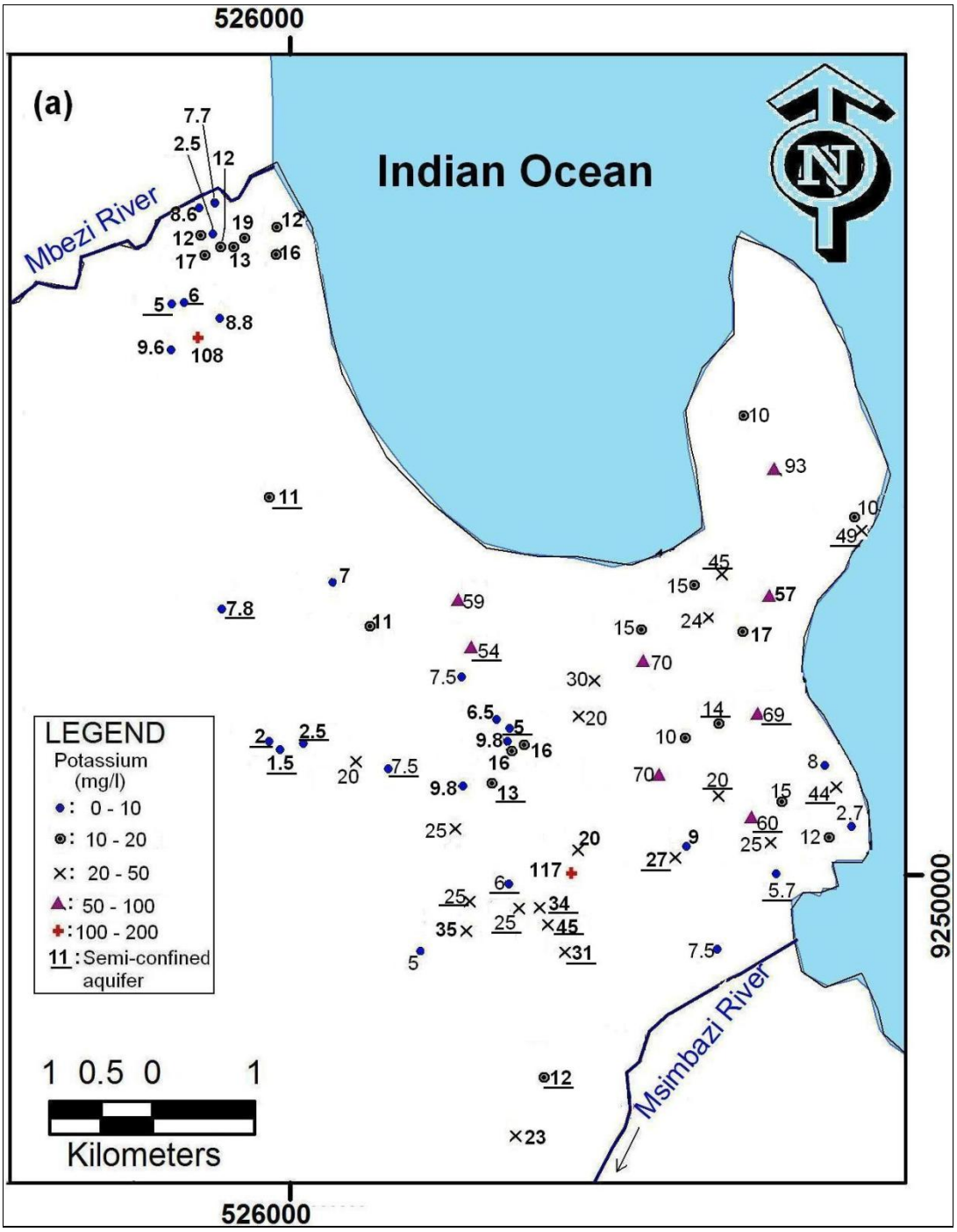

Figure 6.15: Spatial distribution of K^+ concentrations (mg/l) in the area between Mbezi River and Msimbazi River. Plain numbers and underlined numbers signify unconfined aquifer and semi-confined aquifer respectively.

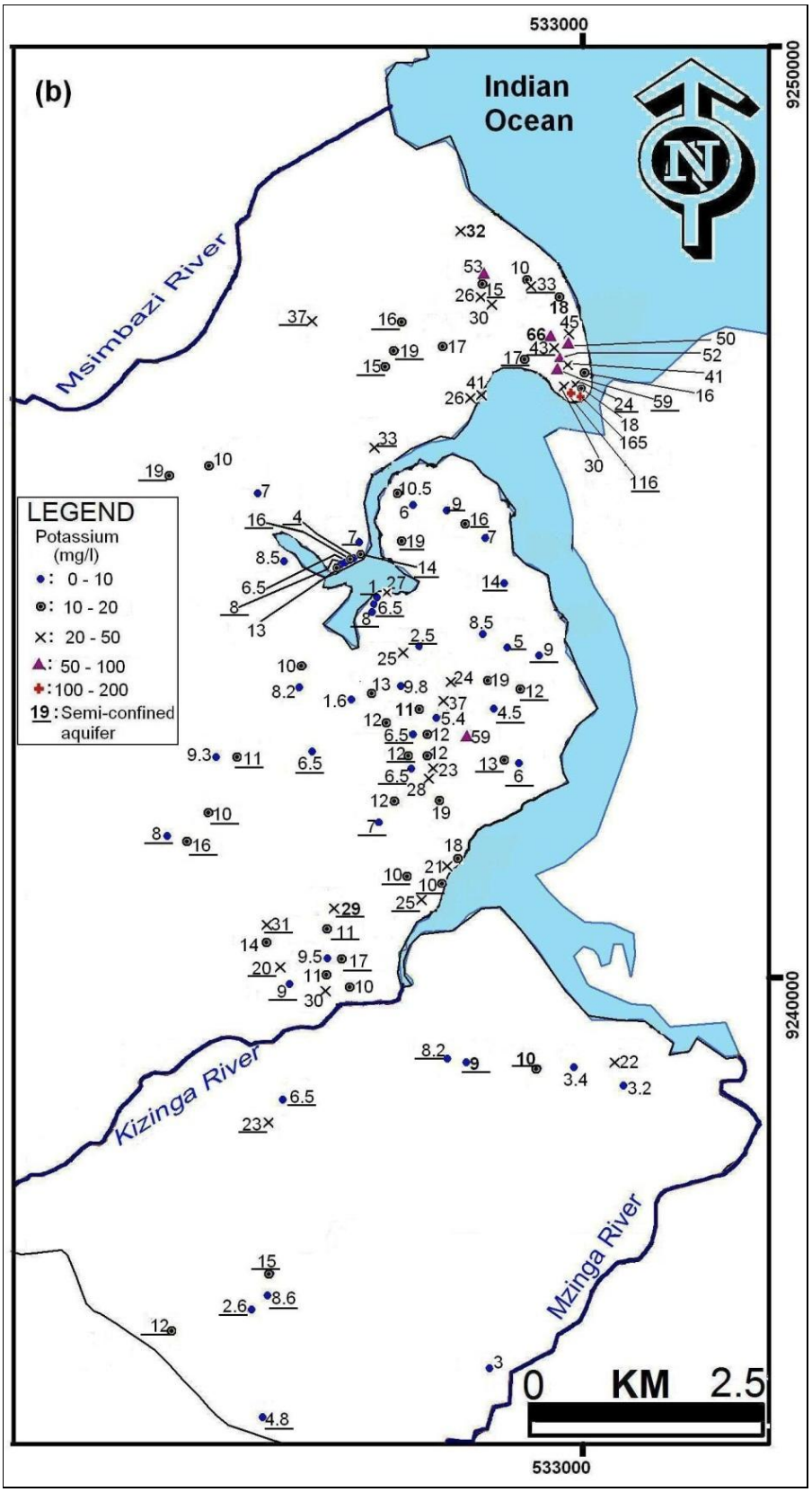

Figure 6.16: Spatial distribution of K^+ concentrations (mg/l) in the area between Msimbazi River and Mzinga River. Plain numbers and underlined numbers signify unconfined aquifer and semi-confined aquifer respectively.

6.4.1.7 Sulphate

Oxidation of sulphide ores (pyrite) and the dissolution of sulphate minerals (gypsum and anhydrite) are natural sources of sulphate (SO_4^{2-}) (Todd, 1980). Concentration of sulphate in natural water is usually less than 300 mg/l and can occur up to 200,000 mg/l in some brines (Todd, 1980). According to Appelo and Postma (1993) (Table 6.1), the sulphate ion concentration in seawater is 29.3 mmol/l (ca. 2837 mg/l). High concentrations can originate from industrial effluents or application of agricultural fertilisers (Matthess, 1982; Chapman and Kimstach, 1996).

The spatial distribution of sulphate from analysed groundwater samples in the study area is presented in Fig. 6.17(a-b). SO_4^{2-} represents on average 8.74% and 14.55% of all anions in the unconfined aquifer and semi-confined aquifer respectively. SO_4^{2-} ranges from 2.1–2857 mg/l and 0.66–703 mg/l in unconfined and semi-confined aquifers respectively (Table 6.3). 13.46% of samples from the unconfined aquifer and 4.39% of semi-confined aquifer water samples exceed the permissible limit for SO_4^{2-} of WHO (2004). The highest values of sulphate in the upper unconfined aquifer and semi-confined aquifer were observed in the water sample numbers 18’ and 41 with concentrations of 2857 mg/l (Fig. 6.17a) and 703 mg/l (Fig. 6.17b) respectively (Fig. 6.17a-b). High values of sulphate concentration (672 mg/l (Fig. 6.17a) and 1064 mg/l (Fig. 6.17b)) were also observed in sample numbers 176 and 132 collected from the boreholes located close to the coastline. Samples showing concentrations less than 100 mg/l are mostly observed in the south part of the study area away from the coastline (Fig. 6.17b). This indicates seawater has influenced groundwater samples collected near the coastline.

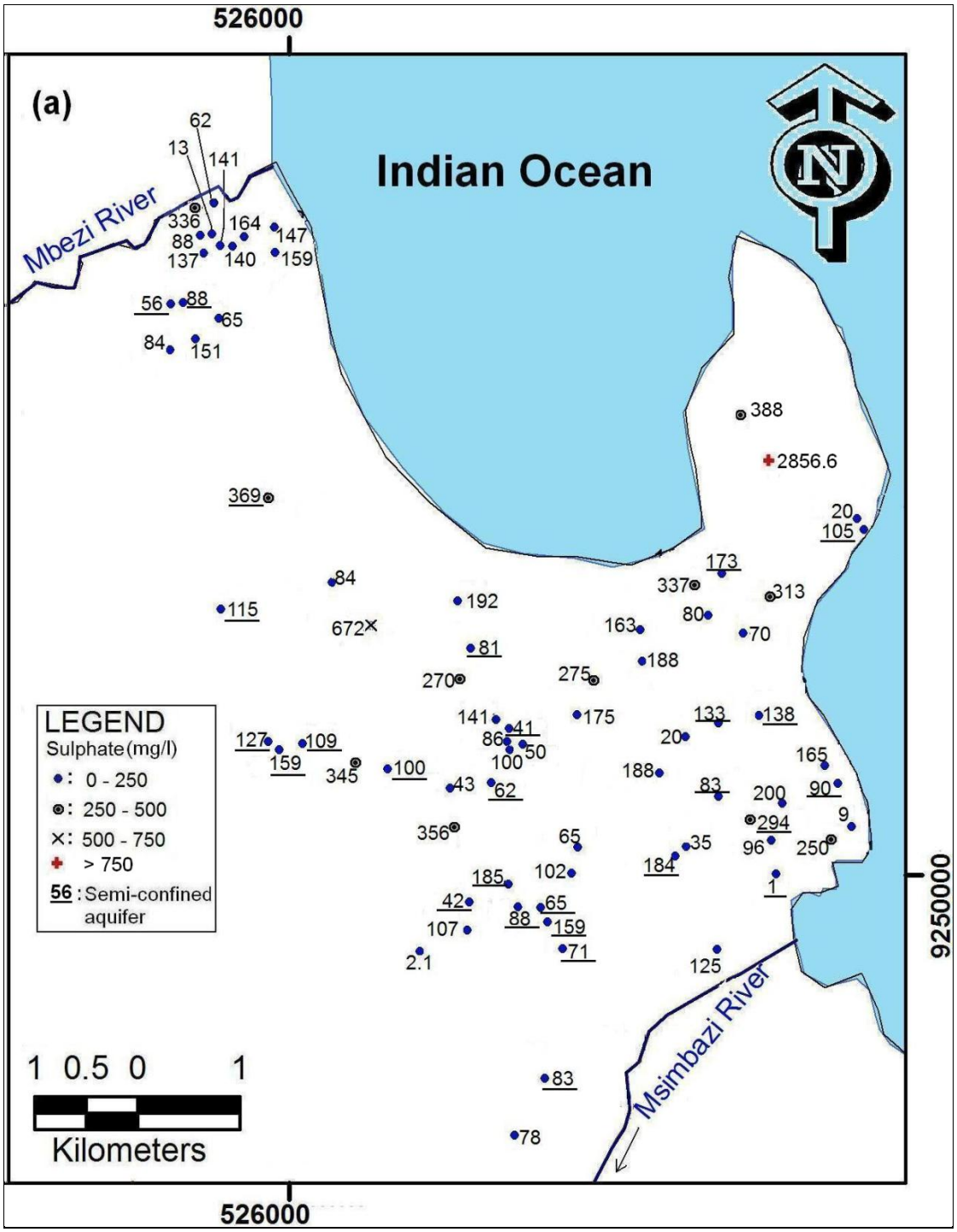

Figure 6.17(a): Spatial distribution of SO_4^{2-} concentrations (mg/l) in the area between Mbezi River and Msimbazi River. Plain numbers and underlined numbers signify unconfined aquifer and semi-confined aquifer respectively.

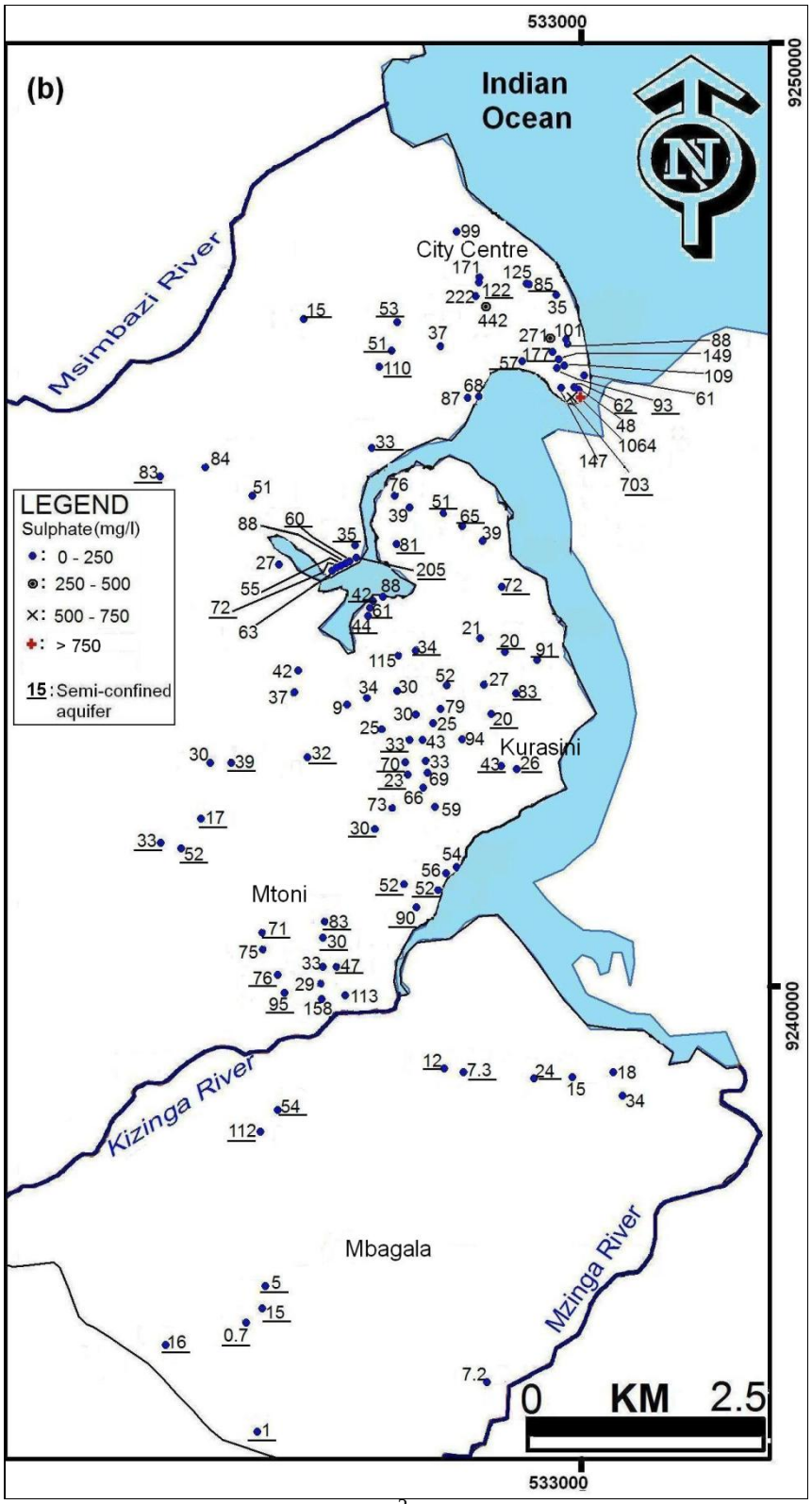

Figure 6.17(b): Spatial distribution of SO_4^{2-} concentrations (mg/l) in the area between Msimbazi River and Mzinga River. Plain numbers and underlined numbers signify unconfined aquifer and semi-confined aquifer respectively.

6.4.1.8 Bicarbonate

Limestone and dolomite are natural sources of bicarbonate (HCO_3^-) (Todd, 1980; Appelo and Postma, 1993). Concentration of bicarbonate in natural water is usually less than 500 mg/l (Todd, 1980). The dissolution of carbonate minerals (calcite and dolomite) increases the concentration of HCO_3^- in the groundwater. The dissolution of carbonates also leads to an increase of the pH.

The spatial distribution of bicarbonate from the analysed groundwater samples in the study area is presented in Fig. 6.18(a-b). HCO_3^- represents on average 18.76% and 30.39% of all anions in the unconfined aquifer and semi-confined aquifer respectively. HCO_3^- ranges from 7.9–798 mg/l and 5.5–585 mg/l in unconfined and semi-confined aquifers respectively (Table 6.3). High values of bicarbonate concentrations (> 500 mg/l) were observed in eight samples (numbers 96, 97, 98, 133, 134, 137, 139, 140) within the City Centre area (Fig. 6.18b) and three samples (numbers 8, 159, 160) to the north of Msimbazi River (fig. 1.18a). Low values of bicarbonate concentrations ranging from 5 to 28 mg/l are associated with samples 75-80, and were collected in the southern part of the study area at Mbagala (Fig. 6.18b). This signifies dissolution of carbonate minerals is less significant in this area located away from the coast. This is also supported by low pH values associated with mentioned samples, which show pH values between 5.7 and 6.5 (Fig. 6.8b). Toward the north, pH and HCO_3^- are observed to increase to a maximum value of 8.6 and 798 mg/l (around the City Centre) respectively.

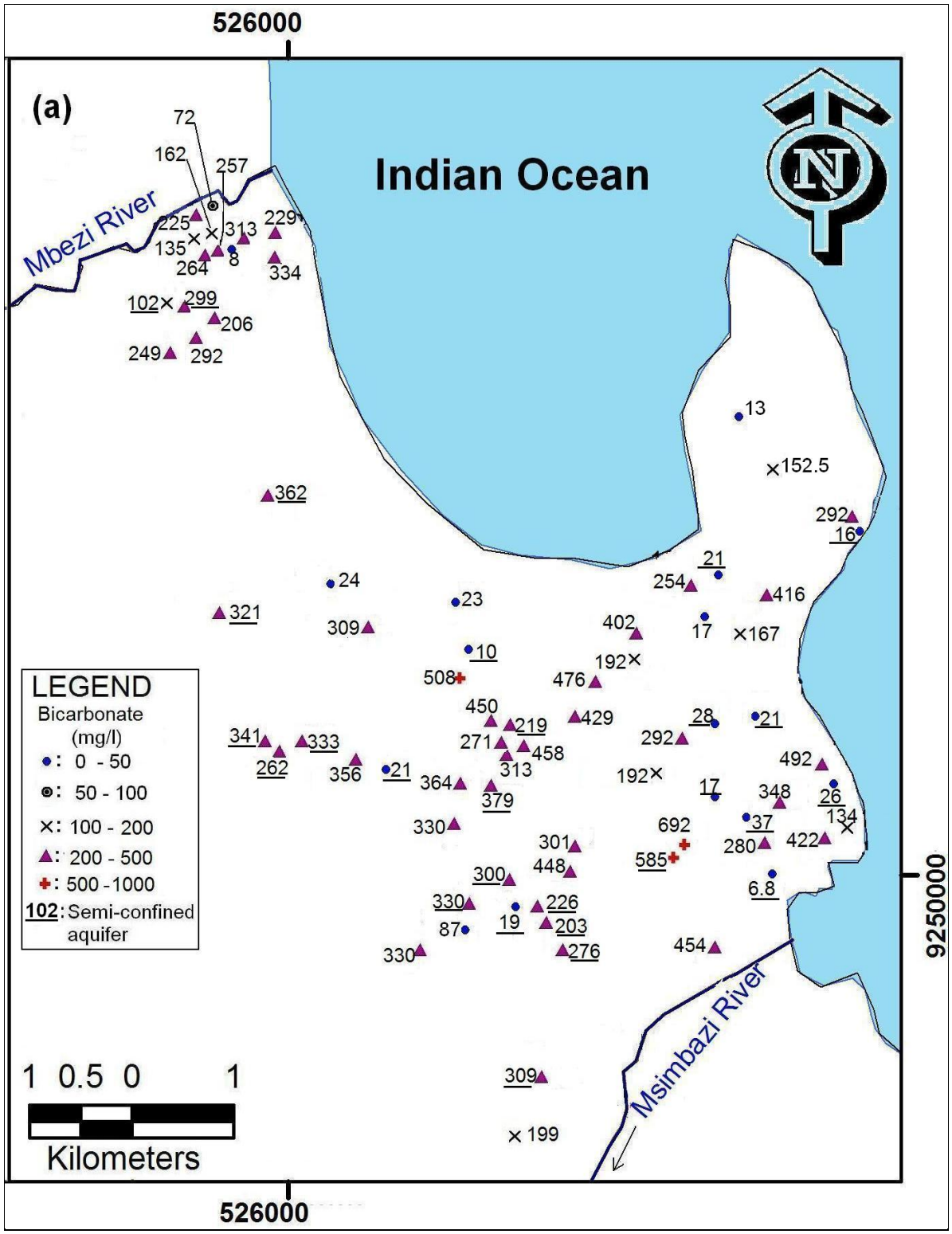

Figure 6.18(a): Spatial distribution of HCO_3^- concentrations (mg/l) in the area between Mbezi River and Msimbazi River. Plain numbers and underlined numbers signify unconfined aquifer and semi-confined aquifer respectively.

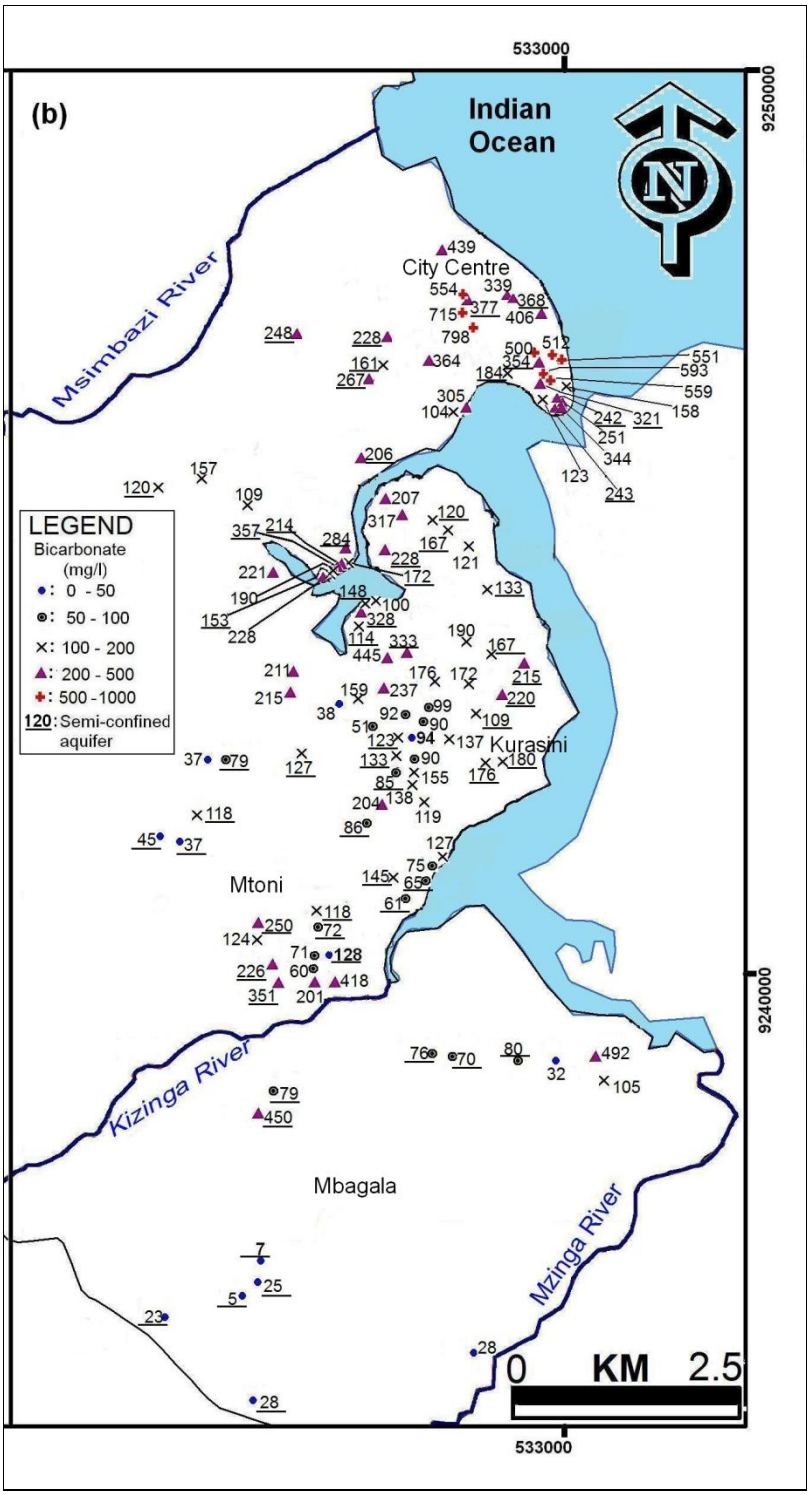

Figure 6.18(b): Spatial distribution of HCO_3^- concentrations (mg/l) in the area between Msimbazi River and Mzinga River. Plain numbers and underlined numbers signify unconfined aquifer and semi-confined aquifer respectively.

6.4.1.9 Chloride

Concentration of chloride (Cl^-) in natural water is usually less than 10 mg/l in humid areas and can occur up to 1000 mg/l in more arid regions and up to approximately 19,300 mg/l in seawater (Todd, 1980).

The spatial distribution of chloride from analysed groundwater samples in the study area is presented in Fig. 6.19 (a-c). Cl^- ranges from 6.4–15,478 mg/l and 14.1–4745 mg/l in unconfined and semi-confined aquifers respectively. 44.23% of samples from the unconfined aquifer and 27.47% of semi-confined water samples exceed the permissible limit for Cl^-.

Cl^- is the dominant anion in both the upper unconfined aquifer and lower semi-confined aquifer. Cl^- represents on average 67.59% of all anions in the unconfined aquifer and 45.22% in the semi-confined aquifer. High concentrations of chloride are observed in several samples representing boreholes/wells constructed near the coastline. Most boreholes/wells with high values of chloride concentrations are found within 2 km from the coastline. These include sample numbers 13 (15076 mg/l), 18 (15478 mg/l), 18’ (8171 mg/l) and 33 (10433 mg/l) indicated in Fig 6.19(b); numbers 41 (4745 mg/l) and 132 (4906 mg/l) indicated in Fig. 6.19(c). Chloride concentration shows a general increase down gradient to the east towards the coastline. Many samples show fresh water (< 150 mg/l) is present beyond 2 km from the sea, but within 1 km from the sea, many boreholes/wells are brackish (300-1000 mg/l) to brackish-salt (1000-10000 mg/l). This evident relation to distance from the sea clearly points to seawater intrusion for the cause of salinity.

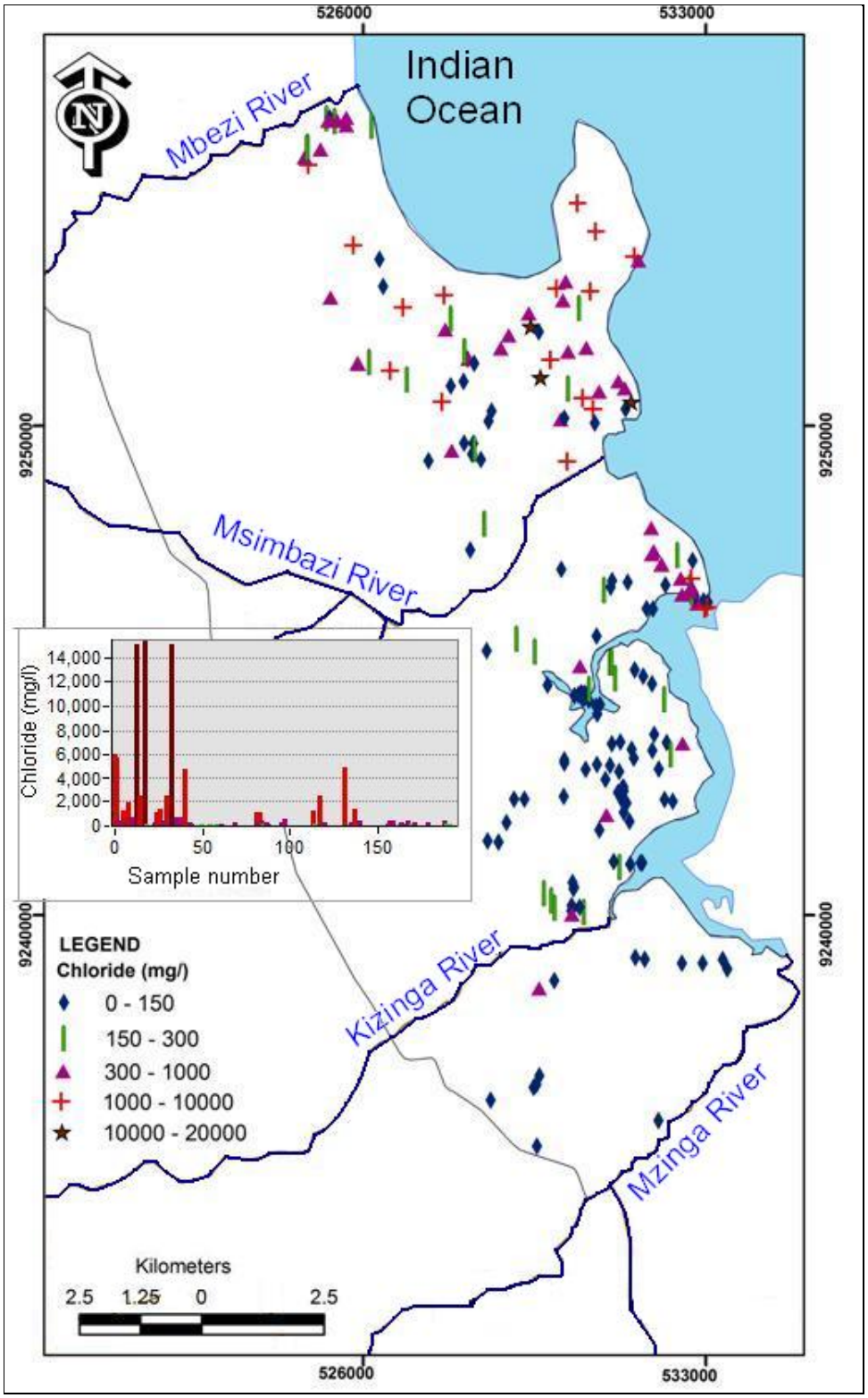

Figure 6.19(a): Chloride distribution in the area of analysed groundwater and overview of concentrations per sample number.

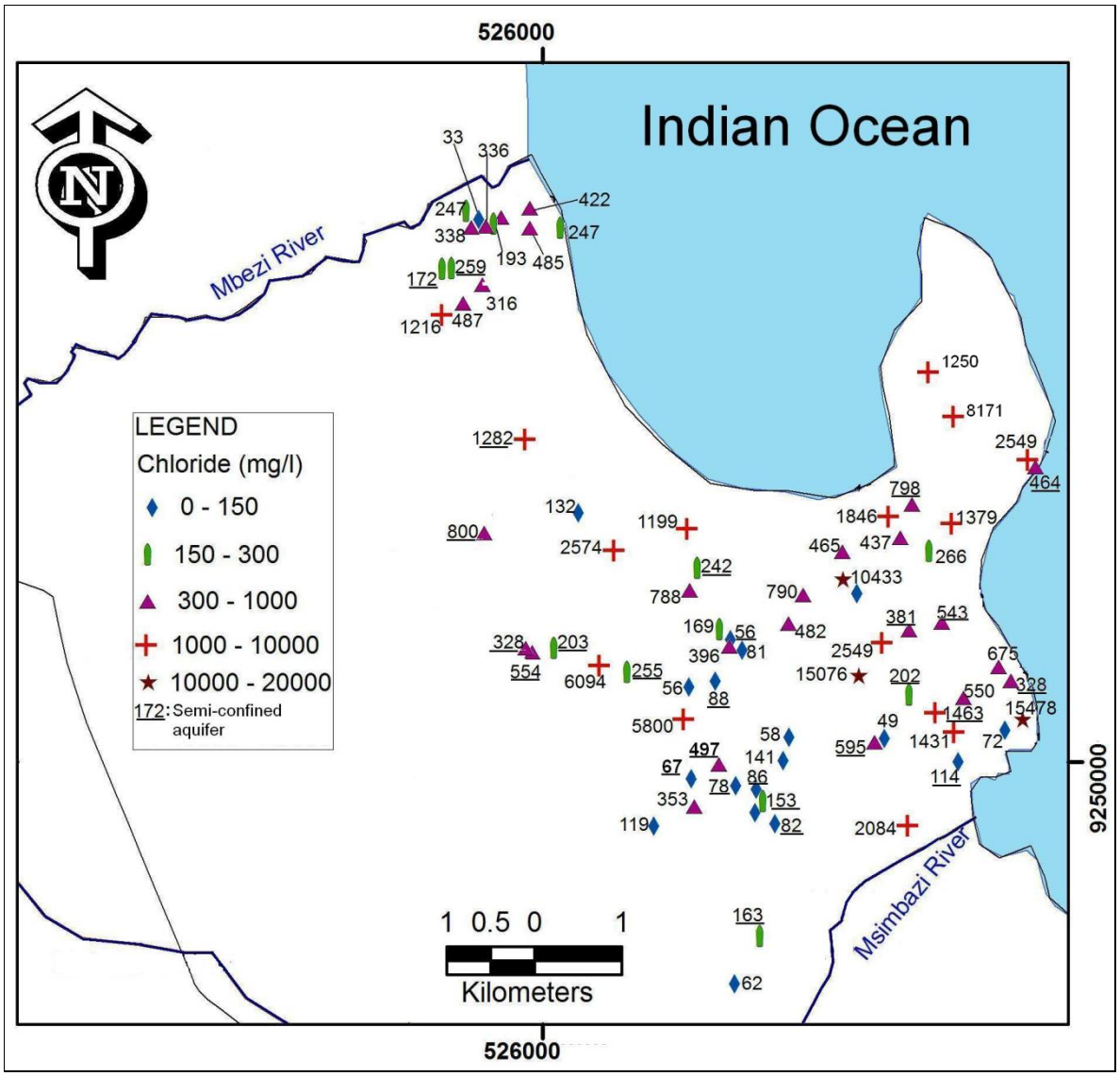

Figure 6.19(b): Spatial distribution of chloride concentrations (mg/l) in the area between Mbezi River and Msimbazi River. Plain numbers and underlined numbers signify unconfined aquifer and semi-confined aquifer respectively.

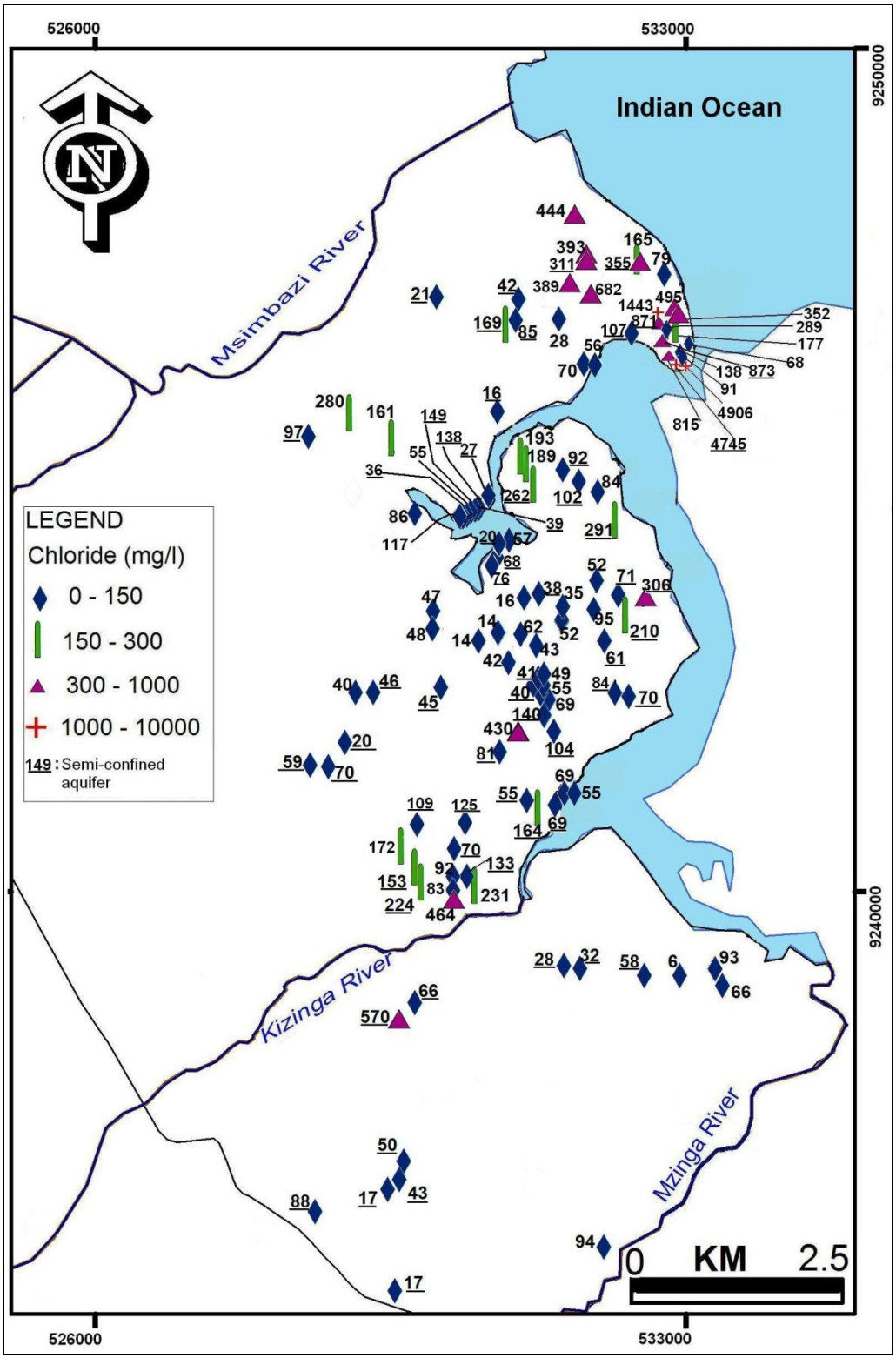

Figure 6.19(c): Spatial distribution of chloride concentrations (mg/l) in the area between Msimbazi River and Mzinga River. Plain numbers and underlined numbers signify unconfined aquifer and semi-confined aquifer respectively.

6.4.1.10 Nitrate

Nitrogen is a major component of the atmosphere occurring in many different forms which include nitrate, ammonia and elemental nitrogen. Concentration of nitrate (NO_3^-) in natural water is usually less than 10 mg/l (Todd, 1980). Excess concentration of nitrate may be caused by anthropogenic sources such as septic tanks/pit latrines and application of manure or fertilizers.

The spatial distribution of nitrate from analysed groundwater samples in the study area is presented in Fig. 6.20 (a-c). NO_3^- represents on average 4.91% and 9.82% of all anions in the unconfined aquifer and semi-confined aquifer respectively. NO_3^- ranges from 0.0–435 mg/l and 0.04–424 mg/l in unconfined and semi-confined aquifers respectively. 48.08% of samples from the unconfined aquifer and 35.16% of semi-confined aquifer samples are beyond the permissible NO_3^- limit of WHO (2004). Excessive nitrate concentrations in groundwater of the study area are the result of contamination by wastewater from pit latrines and leakage from septic tanks. High nitrate concentrations have been encountered in various parts of the aquifer especially in the high-density housing settlements. Nitrate levels of 50–100 mg/l within the City Centre can be related to the leaking from the unrehabilitated aging sewerage system. Nitrate values of 100-200 mg/l and > 200 mg/l in dense informal settlements reflect the existence of high to very high density of pit latrines respectively.

Boreholes exploiting deeper groundwater are expected to show good quality of water, due to overlying strata which provide some degree of protection from contamination. For example, if a thick layer of clay overlies the strata, then the aquifer vulnerability is reduced due to the protection offered by such low permeability material. Although results indicate that many boreholes/wells encountered with high nitrate values greater than permissible limit are located in the unconfined aquifer, groundwater pollution by nitrate is substantial in the semi-confined (lower) aquifer (Fig. 6.20d). These results suggest that the lower aquifer is less semi-confined. On the other hand, the presence of a number of boreholes in the study area screened in several units and sometimes connecting both aquifers and the aquitard and thus making water from the two aquifers to mix, could also contribute to high nitrate values observed in the semi-confined aquifer.

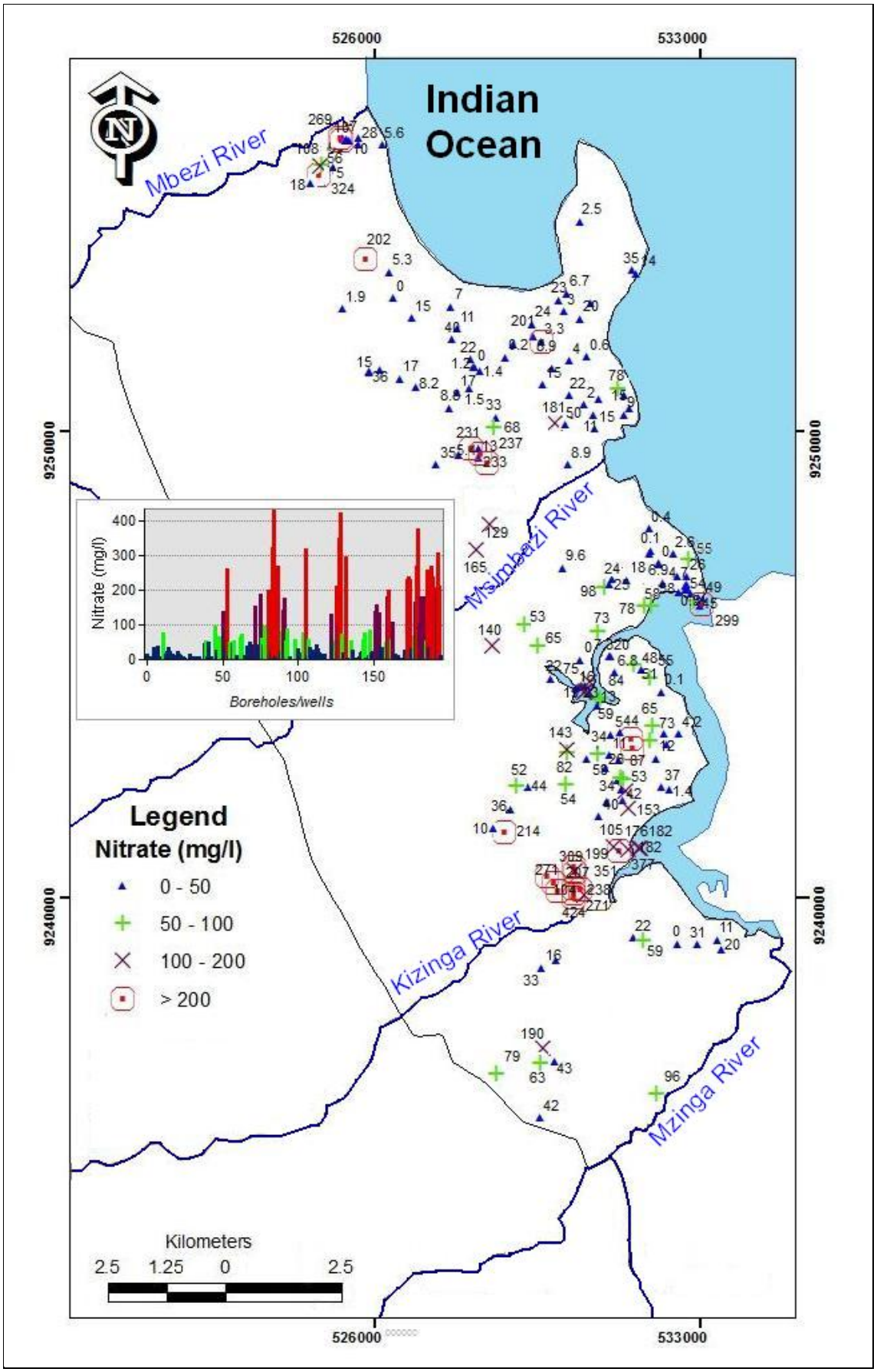

Figure 6.20(a): Nitrate distribution in the area of analyzed groundwater and overview of concentrations per sample number.

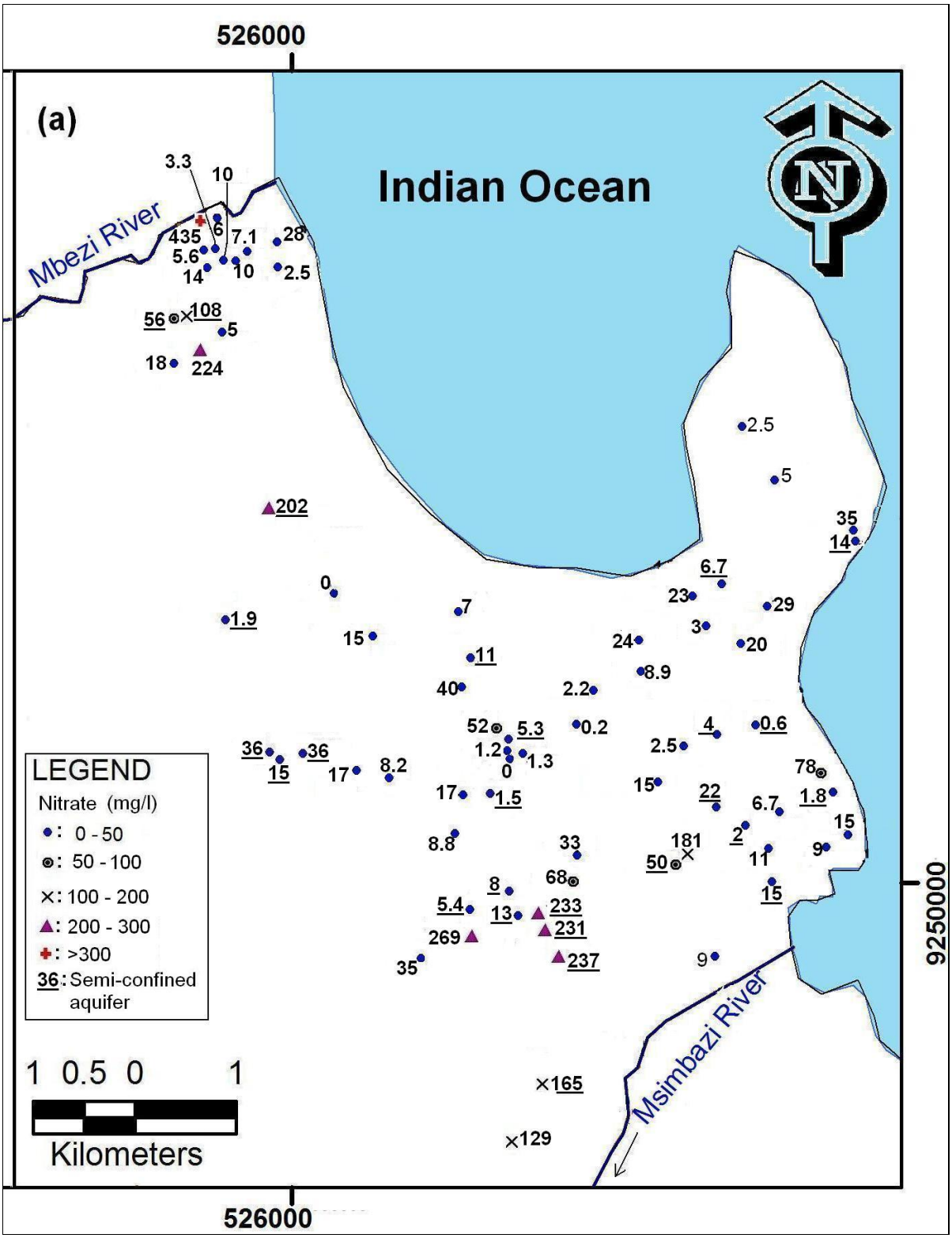

Figure 6.20(b): Spatial distribution of nitrate concentrations (mg/l) in the area between Mbezi River and Msimbazi River. Plain numbers and underlined numbers signify unconfined aquifer and semi-confined aquifer respectively.

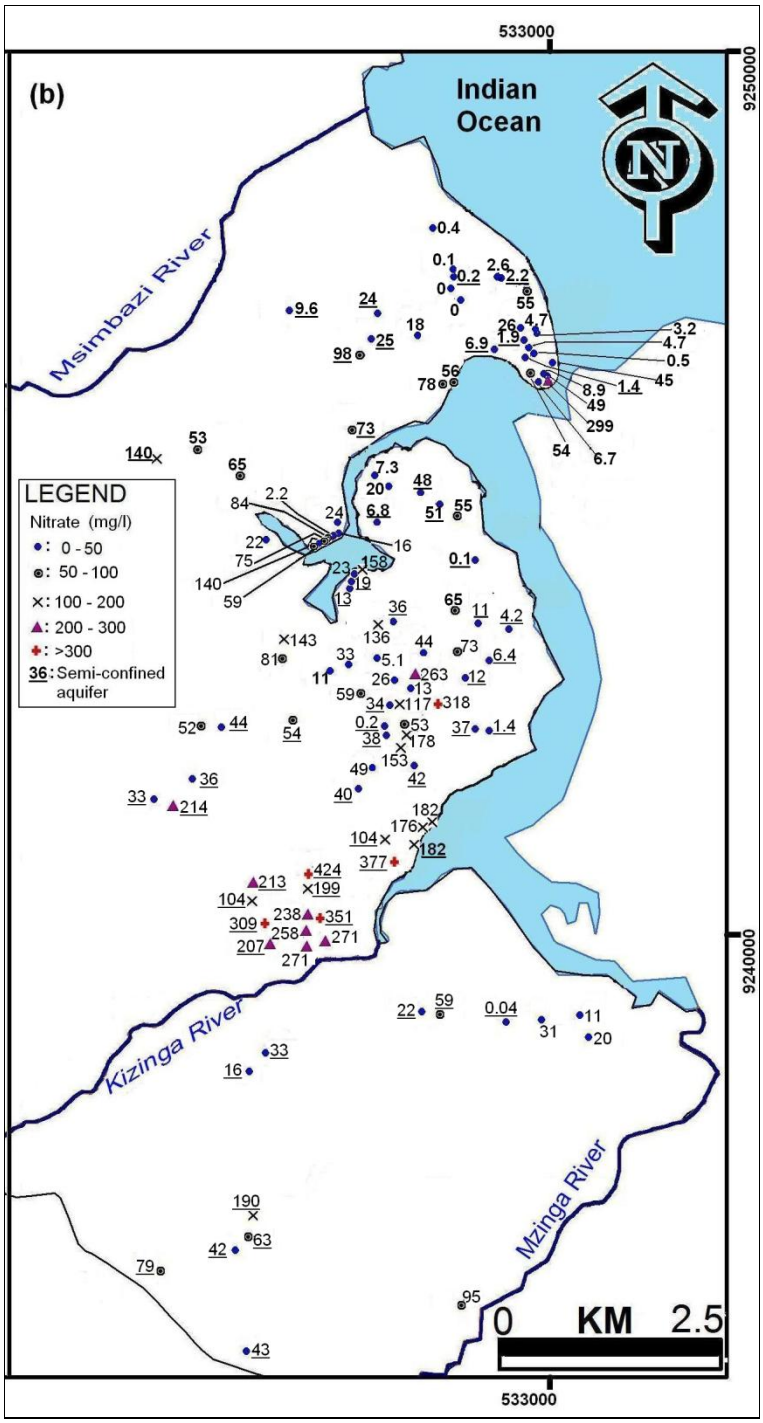

Figure 6.20(c): Spatial distribution of nitrate concentrations (mg/l) in the area between Msimbazi River and Mzinga River. Plain numbers and underlined numbers signify unconfined aquifer and semi-confined aquifer respectively.

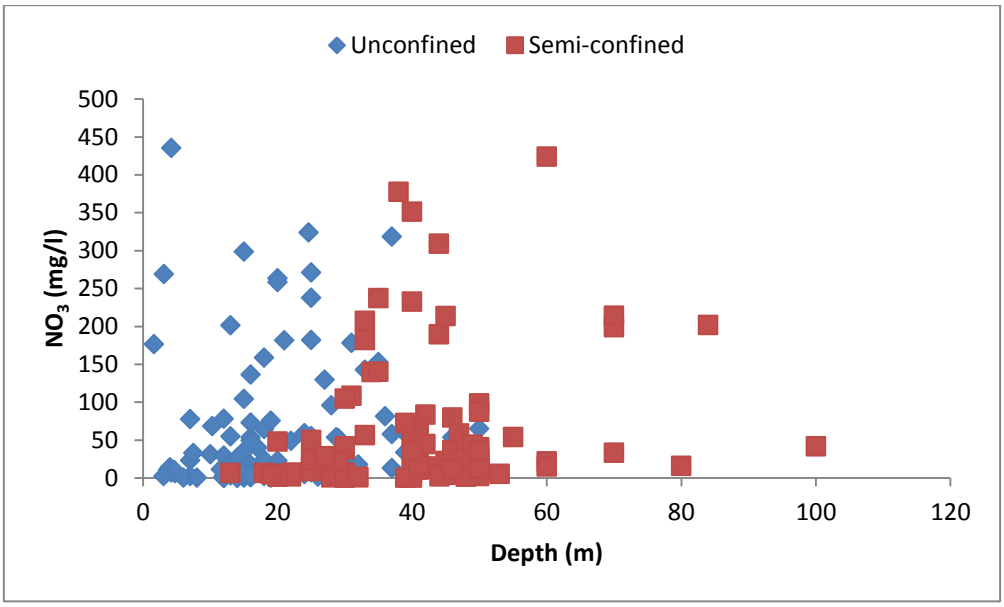

Figure 6.20(d): Variation of NO_3^- with depth.

6.4.2 Seawater intrusion and mixing processes

Calculation of any change in concentration ($m_{i,\ reaction}$; *cfr.* Equation 6.3) as a result of reactions (not of mixing) gives the deviation from the conservative mixture. It enables a comparison of the actual concentration of each constituent with its theoretical concentration for a freshwater-seawater mix calculated from the concentration of Cl^- analysed from water sample. The results of this calculation for selected major ions are presented in Appendix 6.3. Fig. 6.21(a) shows change in concentration ($m_{i,\ reaction}$) calculated for Na^+, Ca^{2+}, Mg^{2+}, K^+, HCO_3^- and SO_4^{2-} for all analysed samples.

The $m_{Na^+_{reaction}}$ is positive for a large number of samples. On the other hand, significant number of groundwater samples show a deficit of Na^+. The most visible process is cation exchange: in a coastal aquifer direct exchange is indicative of freshening (enrichment of saline waters with respect to Na^+), while reverse exchange (removal of Na^+ from solution) is evidence of active marine intrusion. The latter is associated with the release of Ca^{2+} to the solution. A reverse relationship between Na^+ and Ca^{2+} is observed predominantly in the highly saline groundwater, where samples with large negative values of m_{Na+},reaction generally show strong positive m_{Ca2+},reaction. Fig. 6.21(b) represents ΔNa^+ for all analysed samples with indication of areas showing deficit of Na^+. Large number of samples with negative values is found north of Msimbazi River, at Kawe, Msasani, Masaki and Oysterbay (fig. 6.21(b-i)): these samples are particularly those indicating highly saline water. The largest negative value for samples collected north of Msimbazi River is -38.55 mmol/l. To the south

of Msimbazi River, large number of samples has positive values (Fig. 6.21(b-ii)). Few samples indicate negative values. The largest negative value is -6.27 mmol/l located in City Centre at southern tip of peninsula in Mzinga estuary.

For $m_{K^+}{}_{reaction}$, most samples show values close to zero or positive. Seawater intrusion and cation exchange due to freshening are the possible extra sources of potassium.

$m_{mg^{2+}}{}_{reaction}$ is mostly close to zero or positive (for most water samples) due to more Mg^{2+} added by dissolution of Mg^{2+}-rich carbonate, or desorbed from the clay exchange complex during freshening. However, some groundwater samples show a deficit of Mg^{2+}. Fig. 6.21(a) also shows that $m_{HCO_3^-}{}_{reaction}$ is negative for most water samples signifying precipitation of carbonate minerals as a result of salinization: cation exchange adds Ca^{2+} to water already saturated with calcite. Calcite precipitation may also remove Mg^{2+} from solution. However, positive values of $m_{HCO_3^-}{}_{reaction}$ shown by some samples suggest some dissolution of carbonate minerals in the aquifer deposits.

For $m_{SO_4^{2-}}{}_{reaction}$, most water samples indicate values close to zero or positive. Excess of sulphate is most likely due to oxidation of pyrite. The oxidation of sulphide minerals such as pyrite (Fe_2S) is one of the important redox reactions within the unsaturated zone (Domenico and Schwartz, 1990) (Equation 6.8). On the other hand, only few samples show negative values signifying sulphate reduction.

$$4FeS_2 + 15O_2 + 14H_2O = 4Fe(OH)_3 + 16H^+ + 8SO_4^{2-} \qquad (6.8)$$

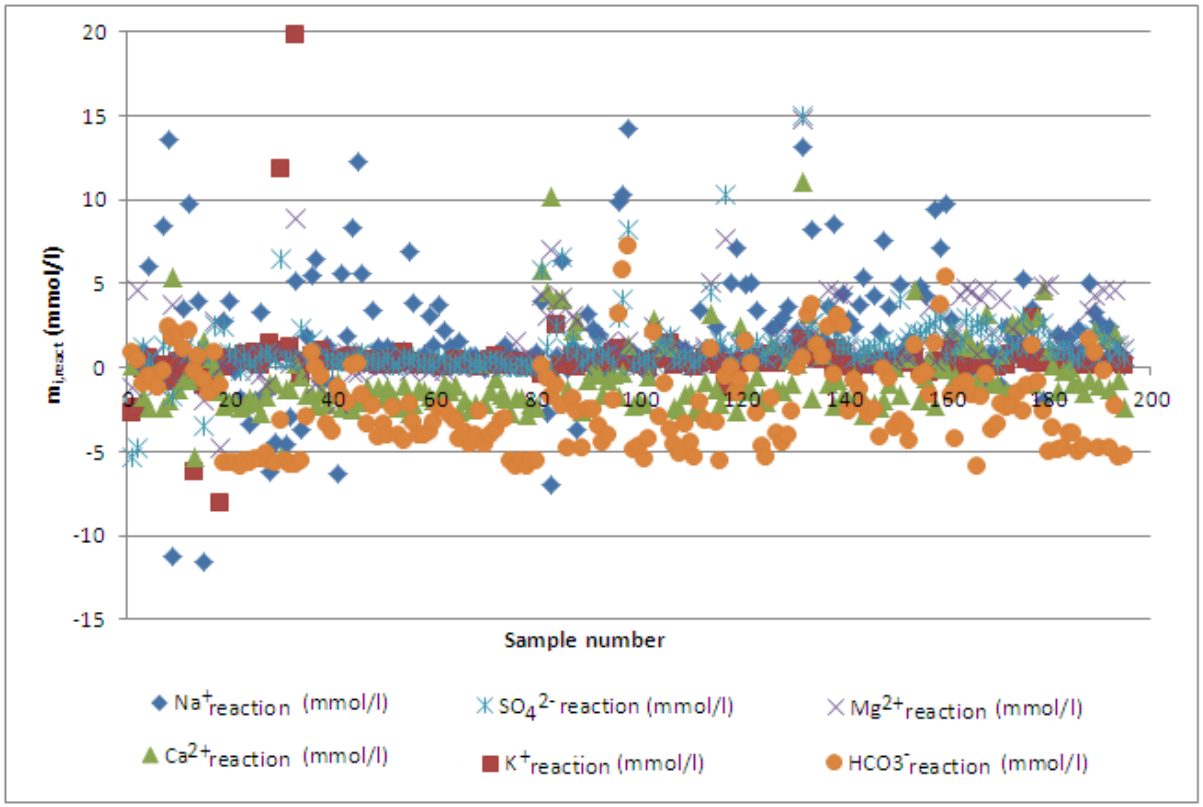

Figure 6.21(a): Diagram representing change in concentration for all analysed samples. React: Sample – Mix, showing effects of cation exchange and other reactions.

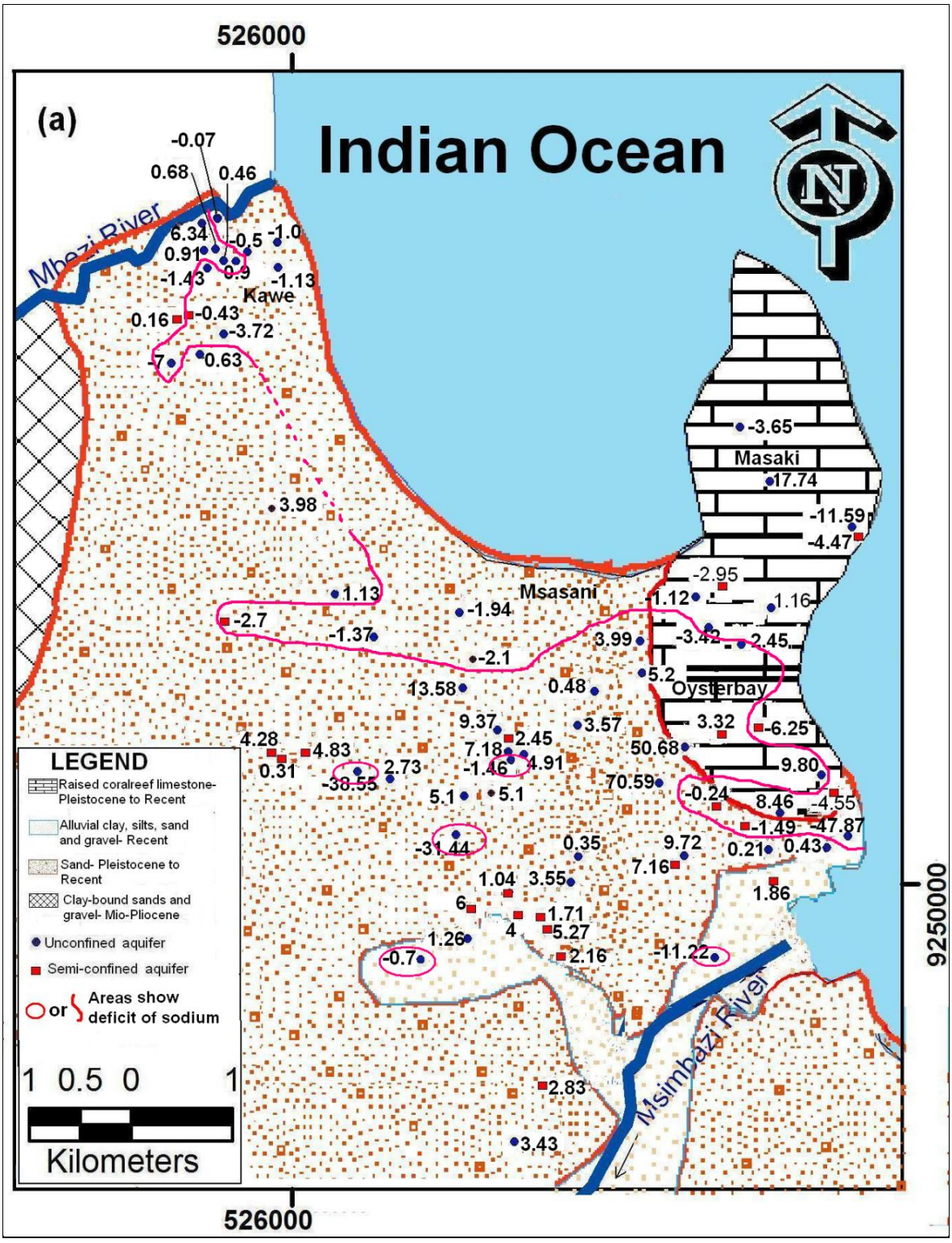

Figure 6.21(b-i): Spatial distribution of ΔNa^+ for all analysed samples (for both unconfined aquifer and semi-confined aquifer) in the area between Mbezi River and Msimbazi River with areas showing Na^+ deficit.

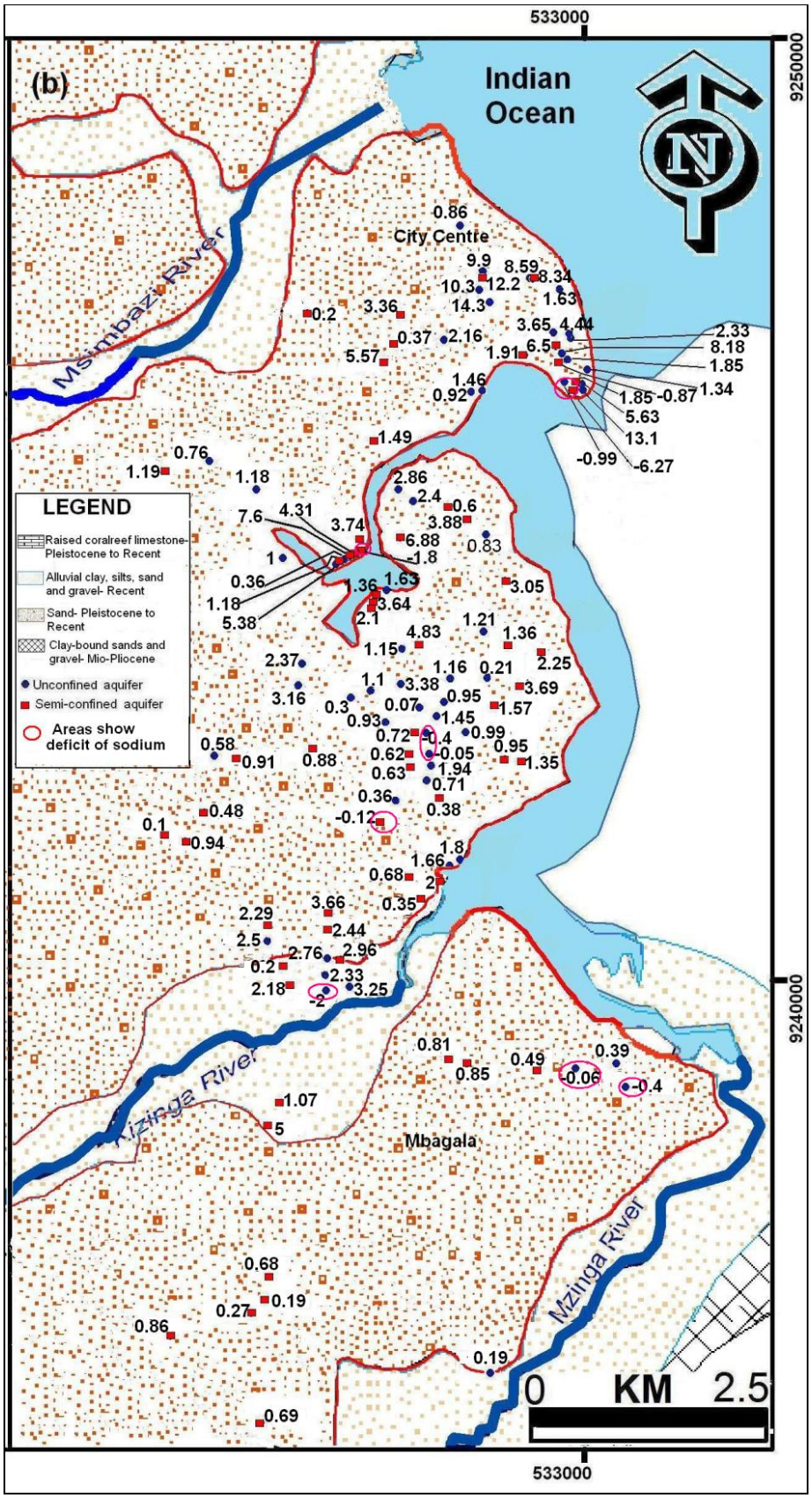

Figure 6.21(b-ii): Spatial distribution of ΔNa+ for all analysed samples (for both unconfined aquifer and semi-confined aquifer) in the area between Msimbazi River and Mzinga River with areas showing Na+ deficit.

6.4.3 Correlation coefficient

The correlation coefficient of the studied parameters is shown in Table 6.4. A significant correlation is observed between Na^+ and Cl^- (0.985) and between Mg^{2+} and Cl^- (0.911), due to seawater intrusion. Poor correlation (0.477) was observed between Ca^{2+} and Cl^-. When seawater intrudes into a coastal aquifer, Na^+ in the seawater typically replaces the Ca^{2+} on exchange sites, causing water to be supersaturated with respect to calcite. Calcite precipitation takes place during the cation exchange process which is the later effect from the seawater intrusion into the aquifer. The positive correlation of K^+ with both Cl^- (0.306) and SO_4^{2-} (0.546), which are all high in seawater, may be interpreted in the light of seawater intrusion as well. A positive correlation also exists between $Ca^{2+}$and Mg^{2+} (0.636): both ions have a common origin in regard to calcite and dolomite dissolution in the study area. A positive correlation exists between Ca^{2+} and SO_4^{2-} (0.572), K^+ and SO_4^{2-} (0.546) and as well between Mg^{2+} and SO_4^{2-} (0.421). The input of SO_4^{2-} to groundwater attributed to seawater intrusion is mostly located in the area near the coastline.

Table 6.4: Correlation matrices for all data (n = 196).

	Na	**Ca**	**Mg**	**K**	**Cl**	**SO_4**	**NO_3**	**HCO_3**
Na	1.0	0.415	0.841	0.328	0.985	0.321	0.025	0.078
Ca		1.0	0.636	0.257	0.477	0.572	0.226	0.256
Mg			1.0	0.293	0.911	0.421	0.13	0.109
K				1.0	0.306	0.546	0.22	0.196
Cl					1.0	0.323	0.013	0.051
SO_4						1.0	0.099	0.306
NO_3							1.0	-0.124
HCO_3								1.0

The hydrogeochemical results show that different processes determine major ionic composition of groundwater in the study area. The distribution pattern of major ions shows compositional variation in the groundwater samples. In general, the concentration of cations decreases in the order $Na^+ > Ca^{2+} > Mg^{2+} > K^+$ and of anions in the order $Cl^- > HCO_3^- > SO_4^{2-} > NO_3^-$. However, HCO_3^- dominates over Cl^- in some samples.

Based on the correlation coefficient among the major cations and anions, three main processes play a very important role in shaping the chemistry and the quality of the groundwater. These include: i) groundwater salinization indicated by positive correlation of Na^+, K^+, Mg^{2+}, Cl^- and SO_4^2, ii) dissolution of calcite/dolomite minerals in the aquifer matrix indicated by positive correlation of Ca^{2+}, Mg^{2+} and HCO_3^-, and iii) nitrate pollution which showed more or less no correlation with other ions indicating a separate source (i.e. anthropogenic factor).

6.4.4 Saturation indices

Saturation index (SI) calculations of some common minerals using the program PHREEQC (Parkhurst and Appelo, 1999) were employed to determine whether a mineral species is likely to dissolve or precipitate in the groundwater flow system. The saturation indices of some common carbonate (aragonite, calcite and dolomite), sulphate (gypsum and anhydrite) minerals and halite are summarized in Table 6.5 and details are provided in Appendix 6.4 and in spatial distribution maps: aragonite (Fig. 6.22a-b), calcite (Fig. 6.23a-b), dolomite (Fig. 6.24a-b), anhydrite (Fig. 6.25a-b), gypsum (Fig. 6.26a-b) and halite (Fig. 6.27a-b). All samples are undersaturated with respect to anhydrite (Fig. 6.25a-b), gypsum (6.26a-b) and halite (6.27a-b). These minerals were not observed in the study area. Aragonite, calcite and dolomite are distributed around saturation equilibrium (i.e. oversaturated to undersaturated) (Table 6.5). 40%, 40% and 42% of the samples were undersaturated respectively with respect to aragonite, calcite and dolomite. On the other hand, 44%, 53% and 54% of the samples were oversaturated respectively with respect to aragonite, calcite and dolomite. The processes of dissolution, precipitation and cation exchange are actively taking place within the groundwater system. The dissolution of minerals and exchange between cations can lead to the precipitation of minerals.

Table 6.5: Percentages of samples with saturation indices subdivided into 3 classes (undersaturated, in equilibrium, supersaturated) obtained from PHREEQC analysis.

Mineral	**SI < -0.1**	**SI = 0 (or ± 0.1)**	**SI >+0.1**
Aragonite (%)	40	16	44
Calcite (%)	40	7	53
Dolomite (%)	42	4	54
Anhydrite (%)	100	0	0
Gypsum (%)	100	0	0
Halite (%)	100	0	0

Saturation indices indicate the geology in the study area has a potential influence on the saturation status towards carbonate minerals. The area adjacent to the ocean is characterized by raised coral reef limestone and/or sand materials underlain by coral reef limestone. Most of the groundwater samples from the area adjacent to the ocean range from equilibrium to oversaturation with respect to carbonate minerals (calcite and dolomite) and most of them have pH approximately between 7.5 and 8.7. Away from the coastline, where the lithology is

dominated by sands and clay, most samples are undersaturated with respect to carbonate minerals. This is supported by Fig. 6.28 which shows the relation between the SI of carbonate minerals in different samples and their respective pH. Carbonate minerals become undersaturated below pH of 7.5 and above pH 7.5 they become oversaturated. Owing to undersaturated condition, carbonate minerals may have been dissolved and added to the groundwater. The dissolution of calcite and/or dolomite is a major hydrogeochemical process in the study area near the coastline and/or areas where the lithology is dominated by carbonate minerals. The more advanced dissolution of carbonates leads to a high HCO_3^- concentration and high pH.

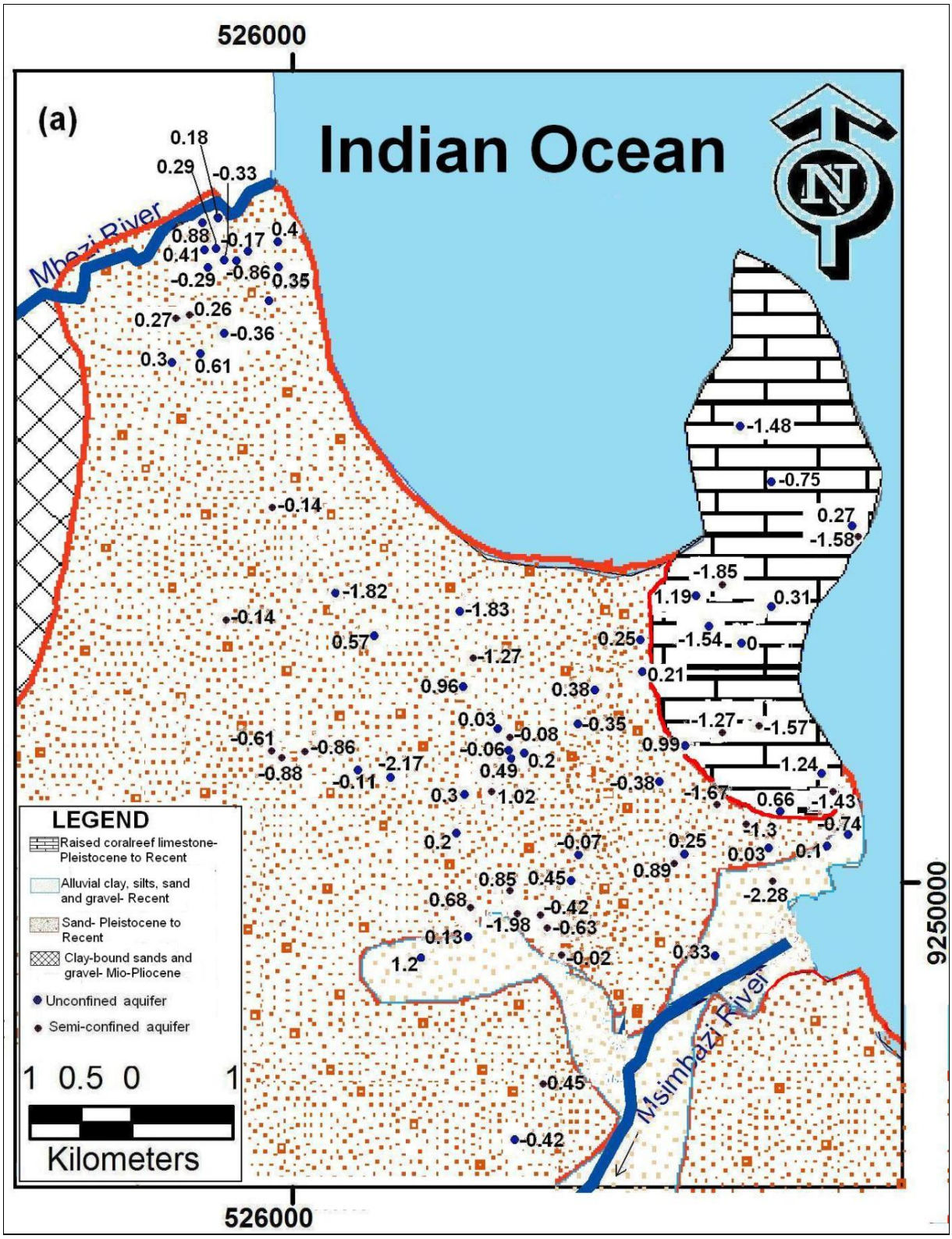

Figure 6.22(a): Spatial distribution of saturation indices of aragonite (for both unconfined aquifer and semi-confined aquifer) in the area between Mbezi River and Msimbazi River.

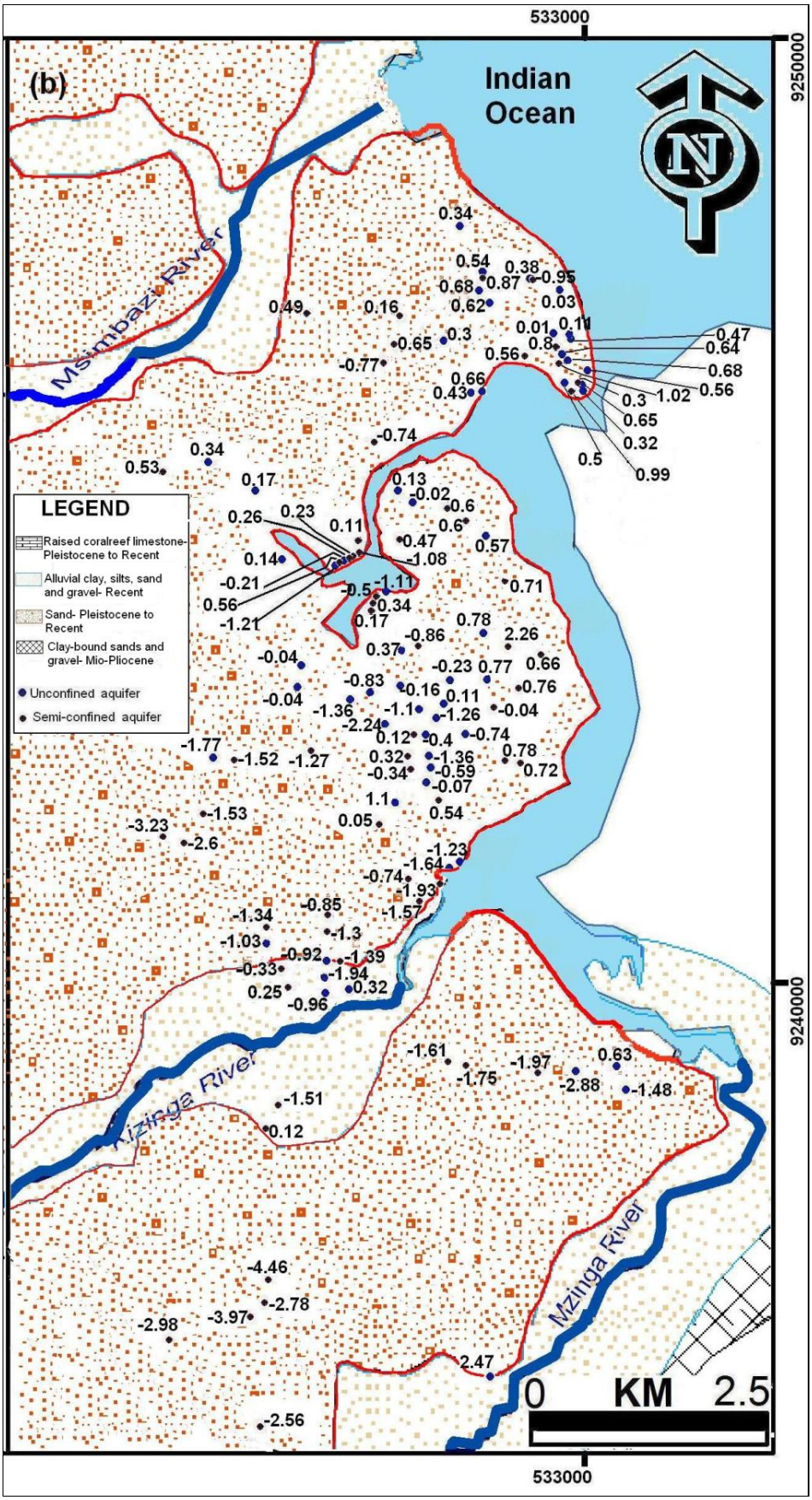

Figure 6.22(b): Spatial distribution of saturation indices of aragonite (for both unconfined aquifer and semi-confined aquifer) in the area between Msimbazi River and Mzinga River.

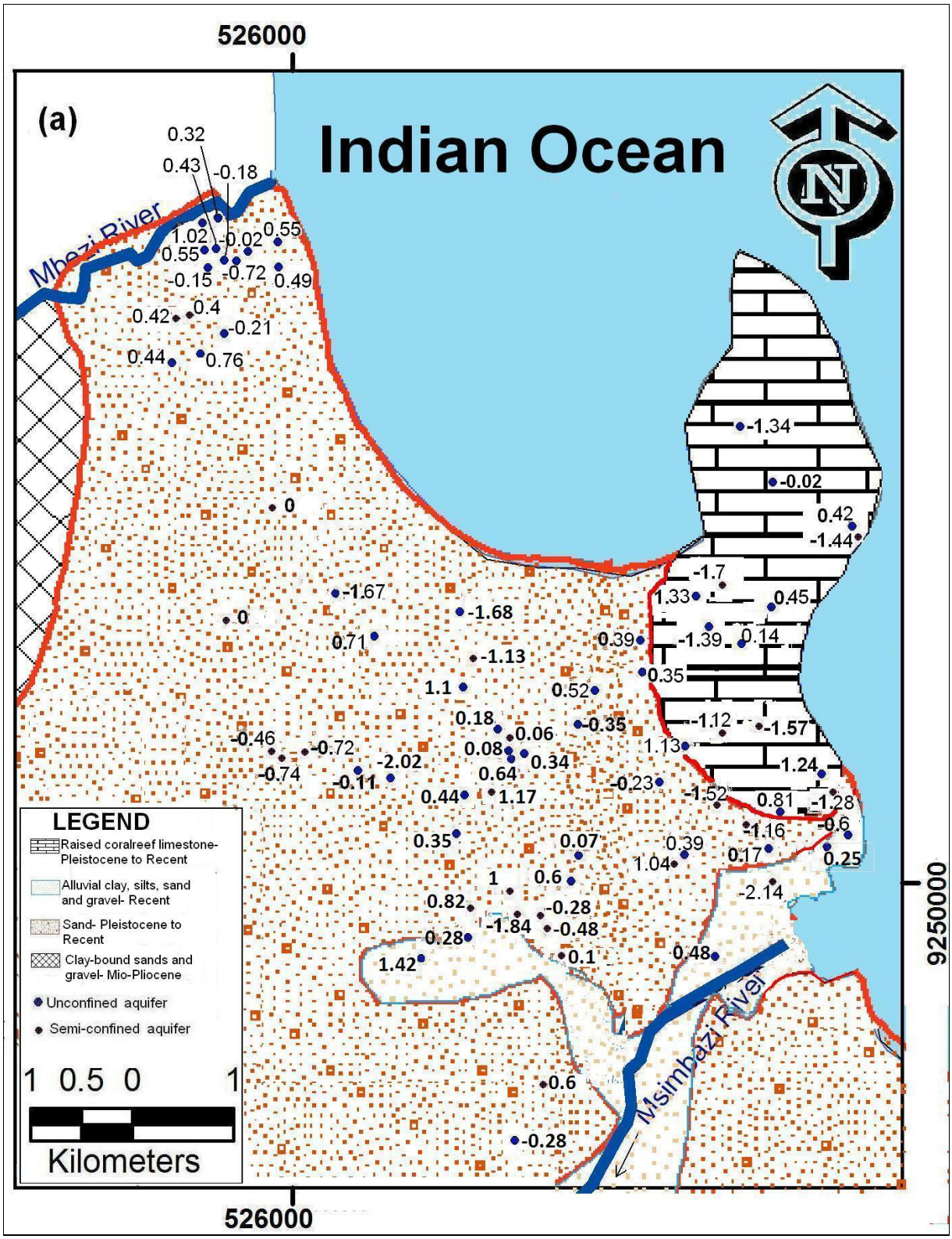

Figure 6.23(a): Spatial distribution of saturation indices of calcite (for both unconfined aquifer and semi-confined aquifer) in the area between Mbezi River and Msimbazi River.

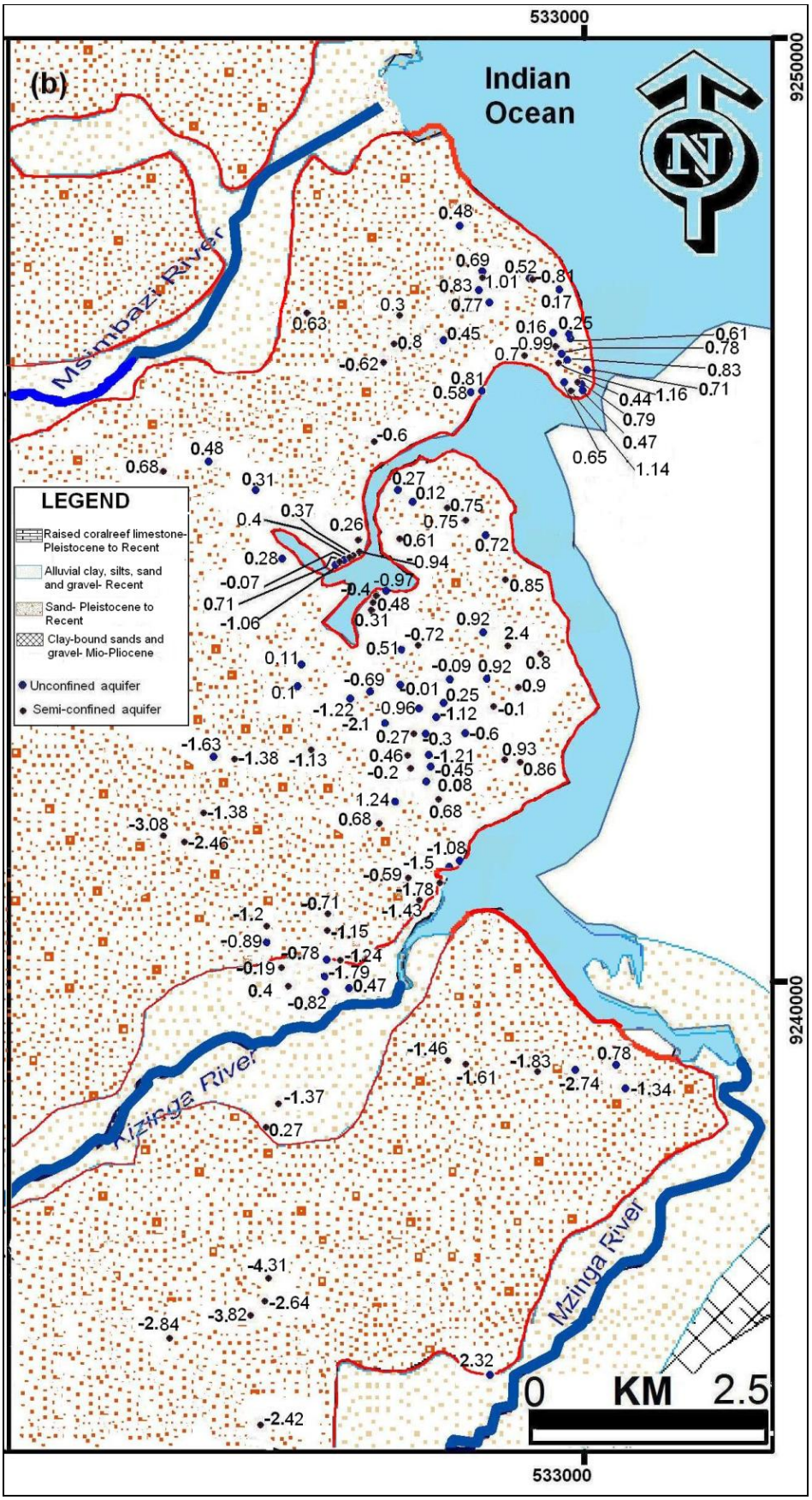

Figure 6.23(b): Spatial distribution of saturation indices of calcite (for both unconfined aquifer and semi-confined aquifer) in the area between Msimbazi River and Mzinga River.

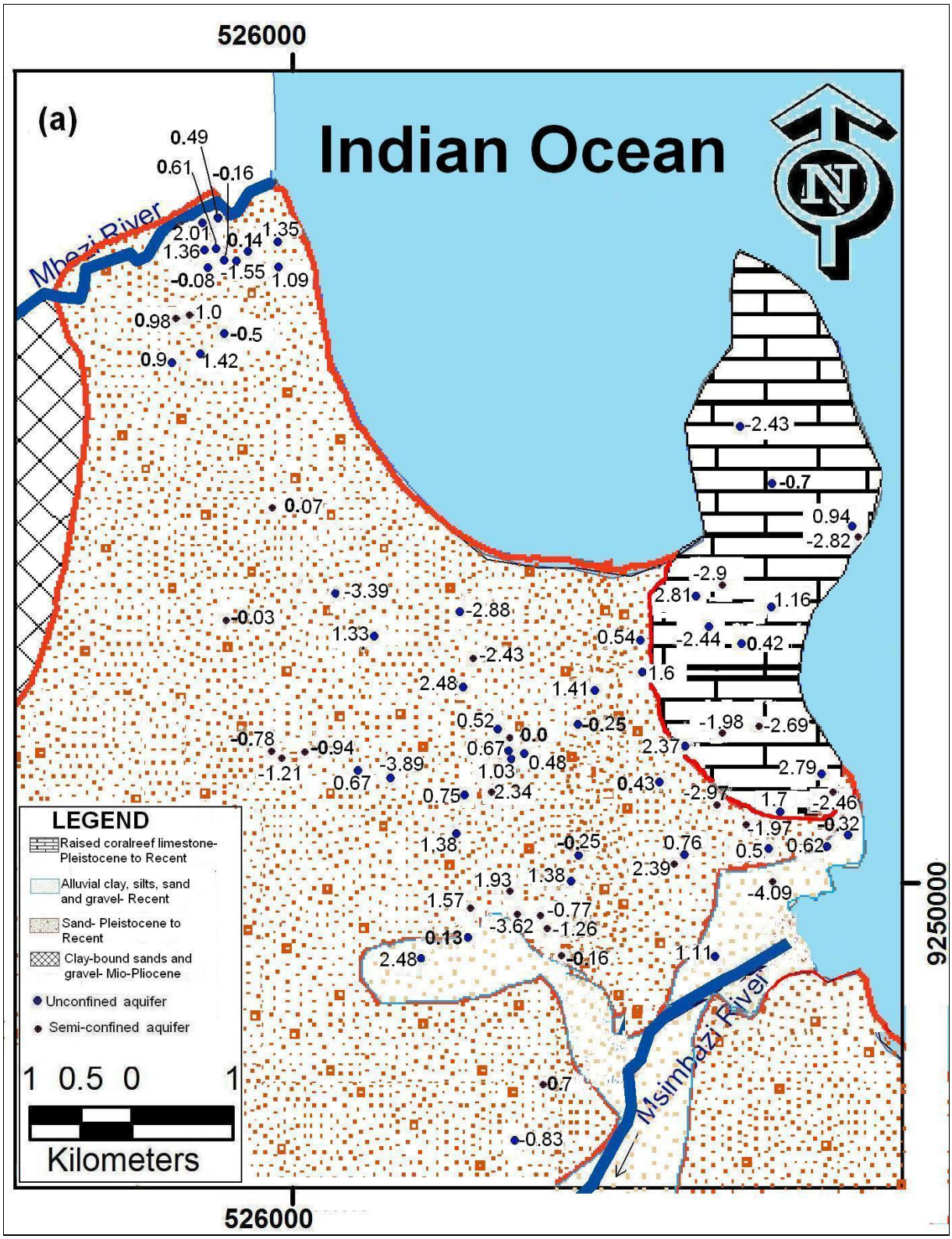

Figure 6.24(a): Spatial distribution of saturation indices of dolomite (for both unconfined aquifer and semi-confined aquifer) in the area between Mbezi River and Msimbazi River.

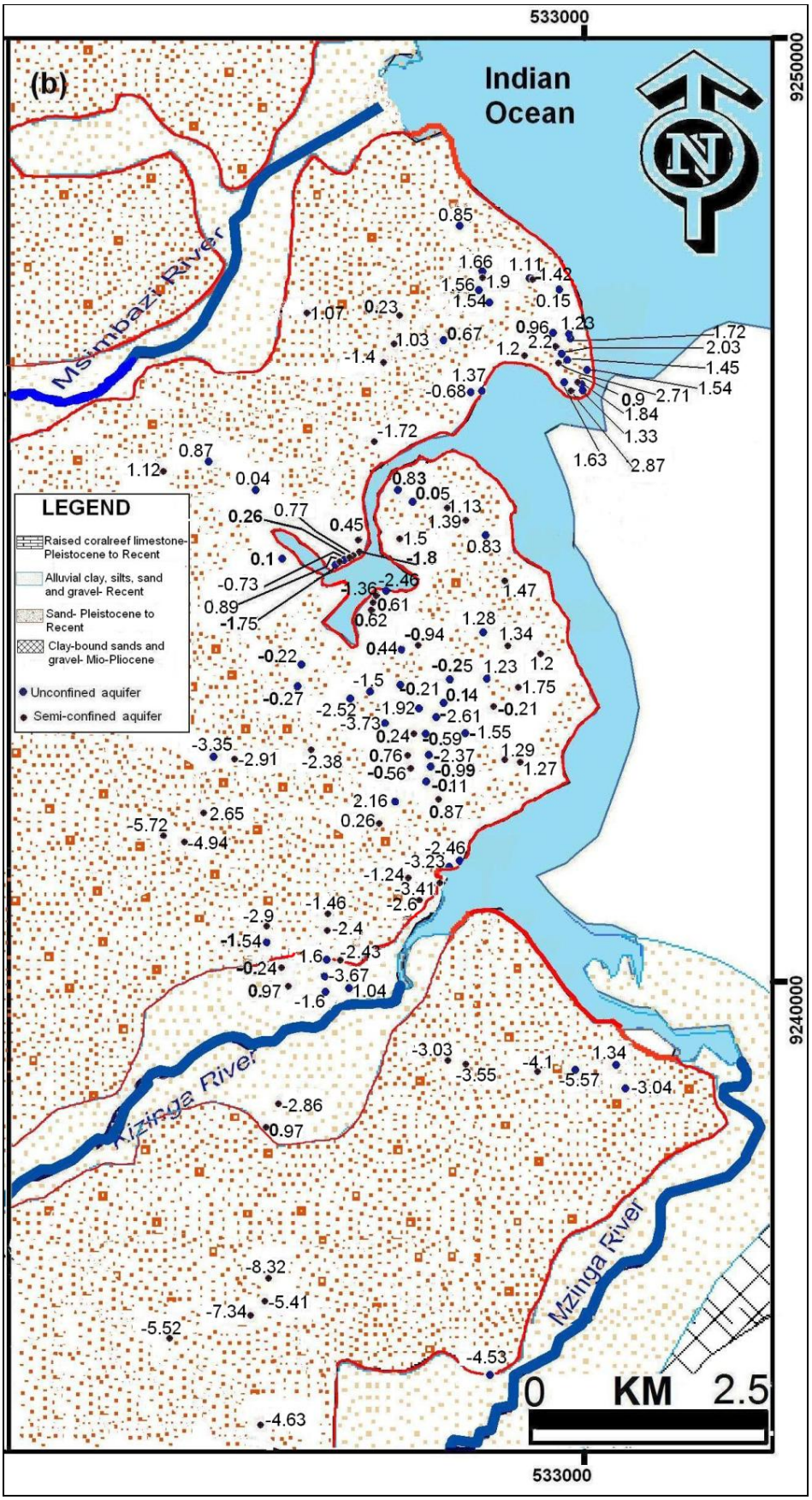

Figure 6.24(b): Spatial distribution of saturation indices of dolomite (for both unconfined aquifer and semi-confined aquifer) in the area between Msimbazi River and Mzinga River.

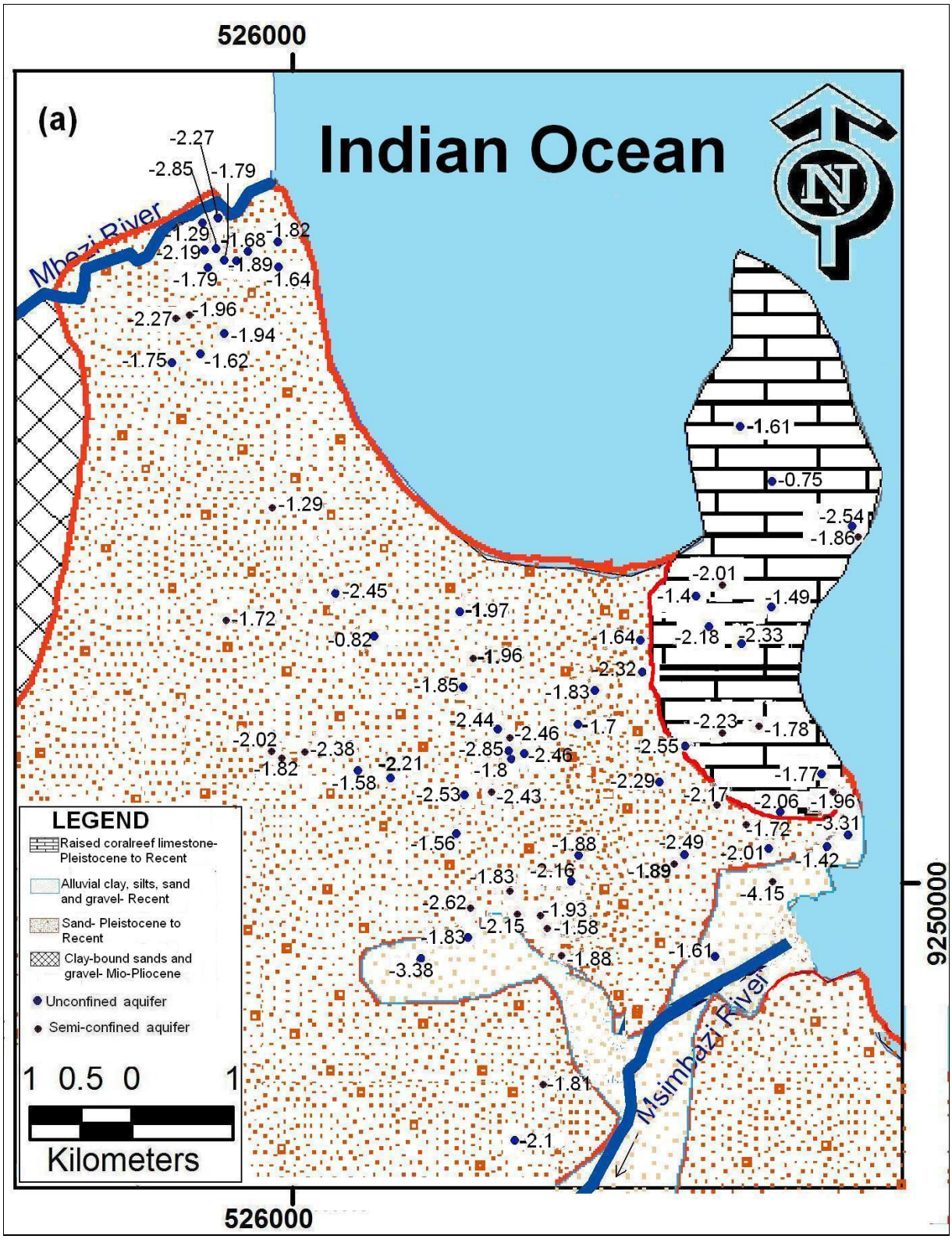

Figure 6.25(a): Spatial distribution of saturation indices of anhydrite (for both unconfined aquifer and semi-confined aquifer) in the area between Mbezi River and Msimbazi River.

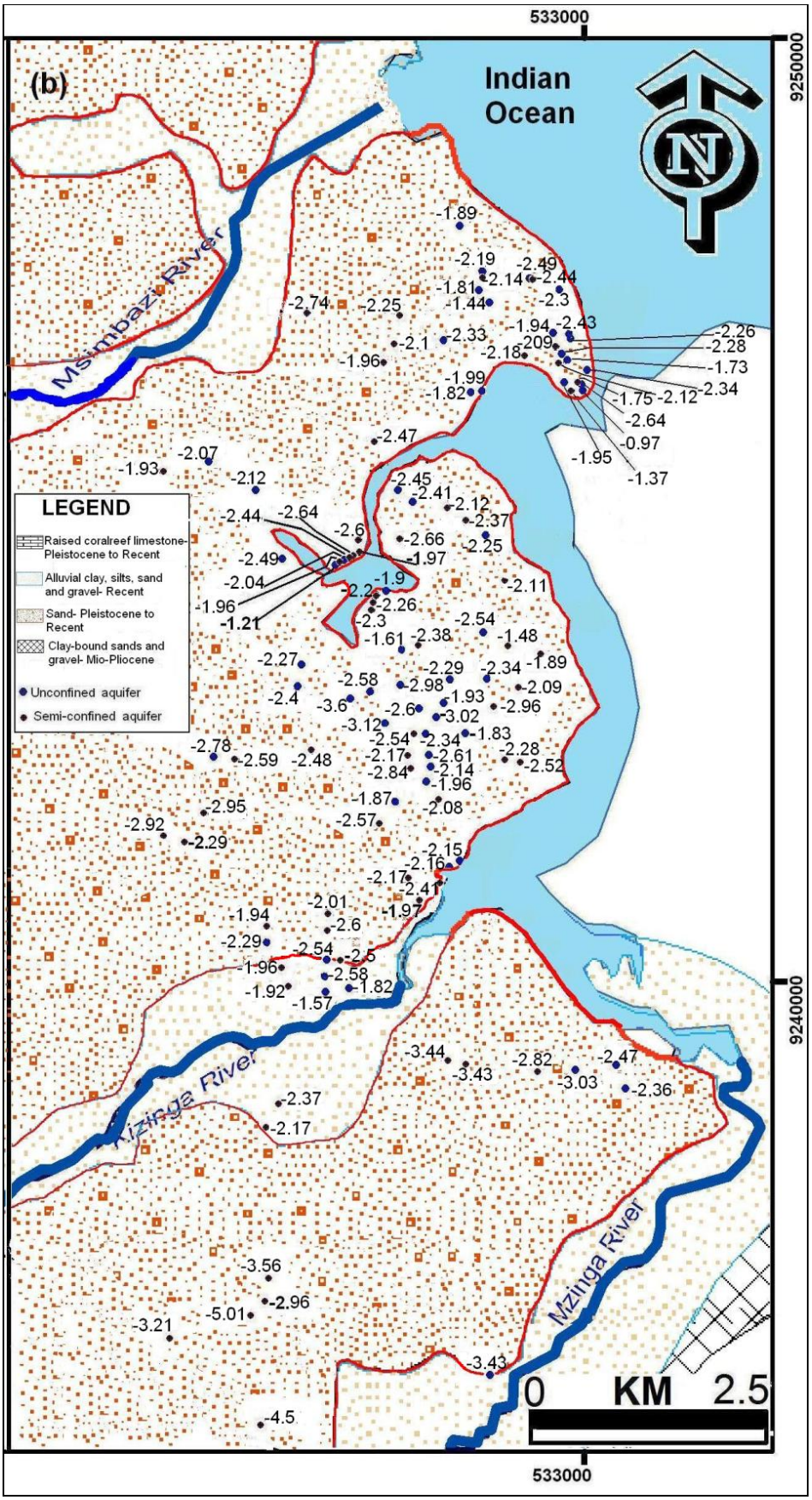

Figure 6.25(b): Spatial distribution of saturation indices of anhydrite (for both unconfined aquifer and semi-confined aquifer) in the area between Msimbazi River and Mzinga River.

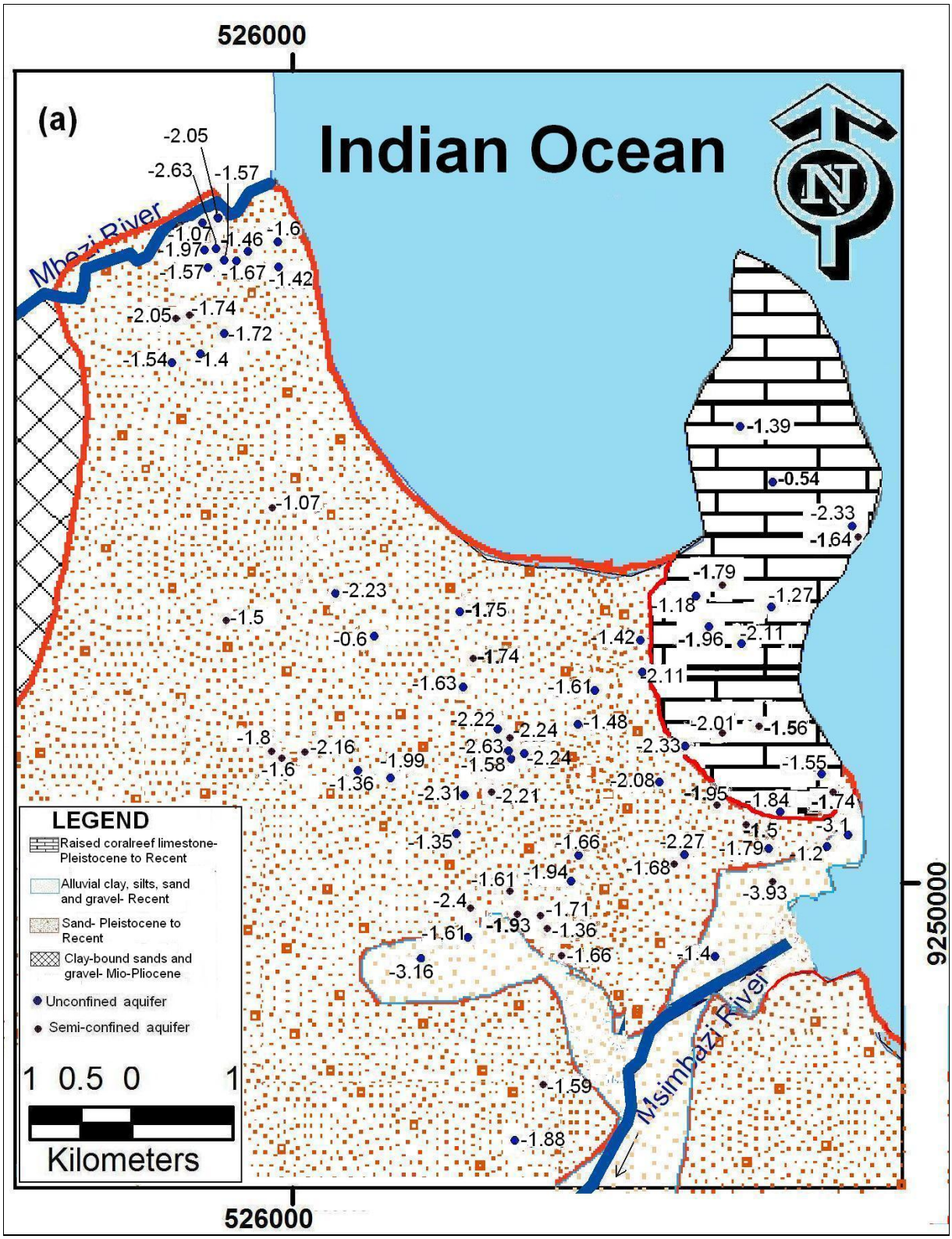

Figure 6.26(a): Spatial distribution of saturation indices of gypsum (for both unconfined aquifer and semi-confined aquifer) in the area between Mbezi River and Msimbazi River.

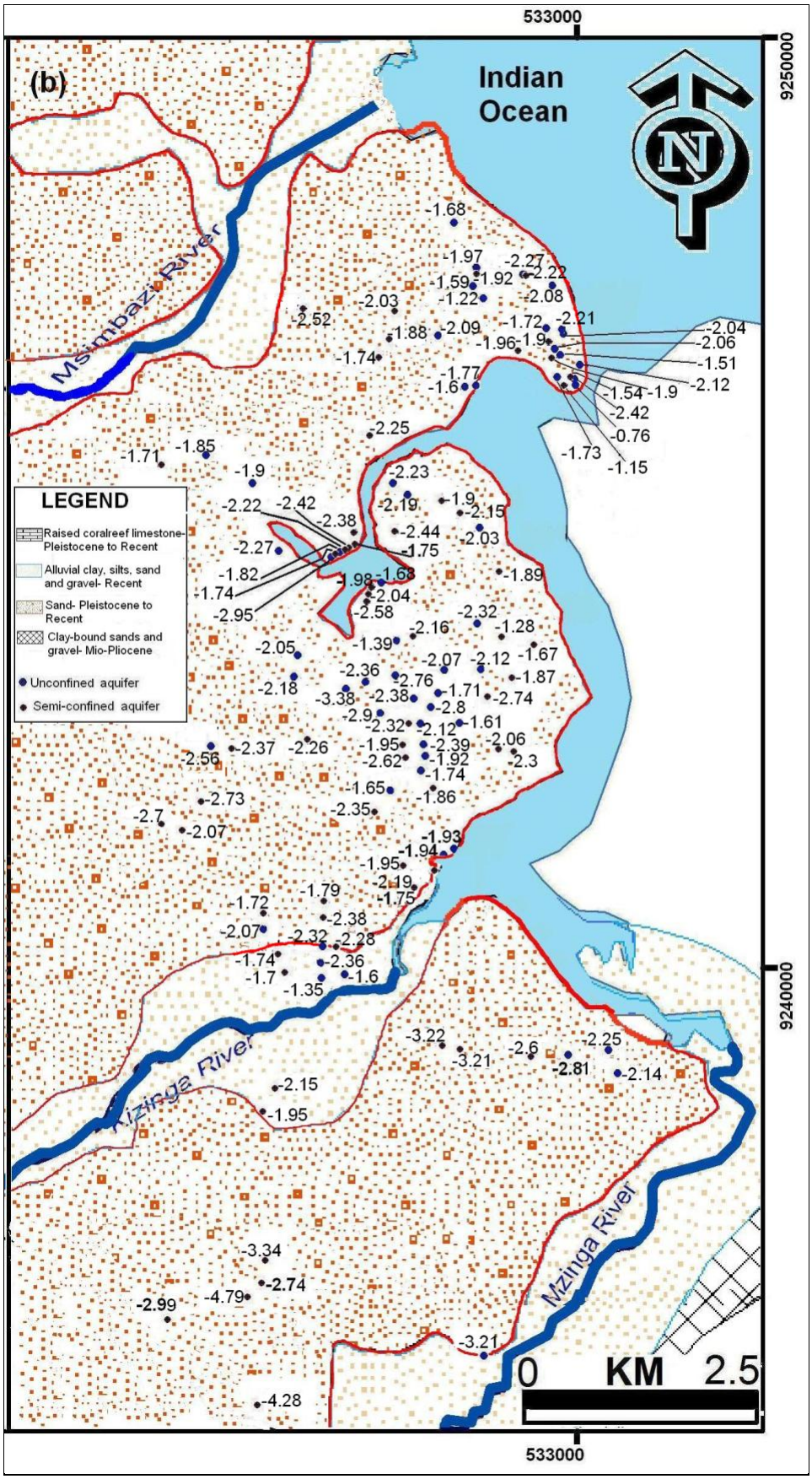

Figure 6.26(b): Spatial distribution of saturation indices of gypsum (for both unconfined aquifer and semi-confined aquifer) in the area between Msimbazi River and Mzinga River.

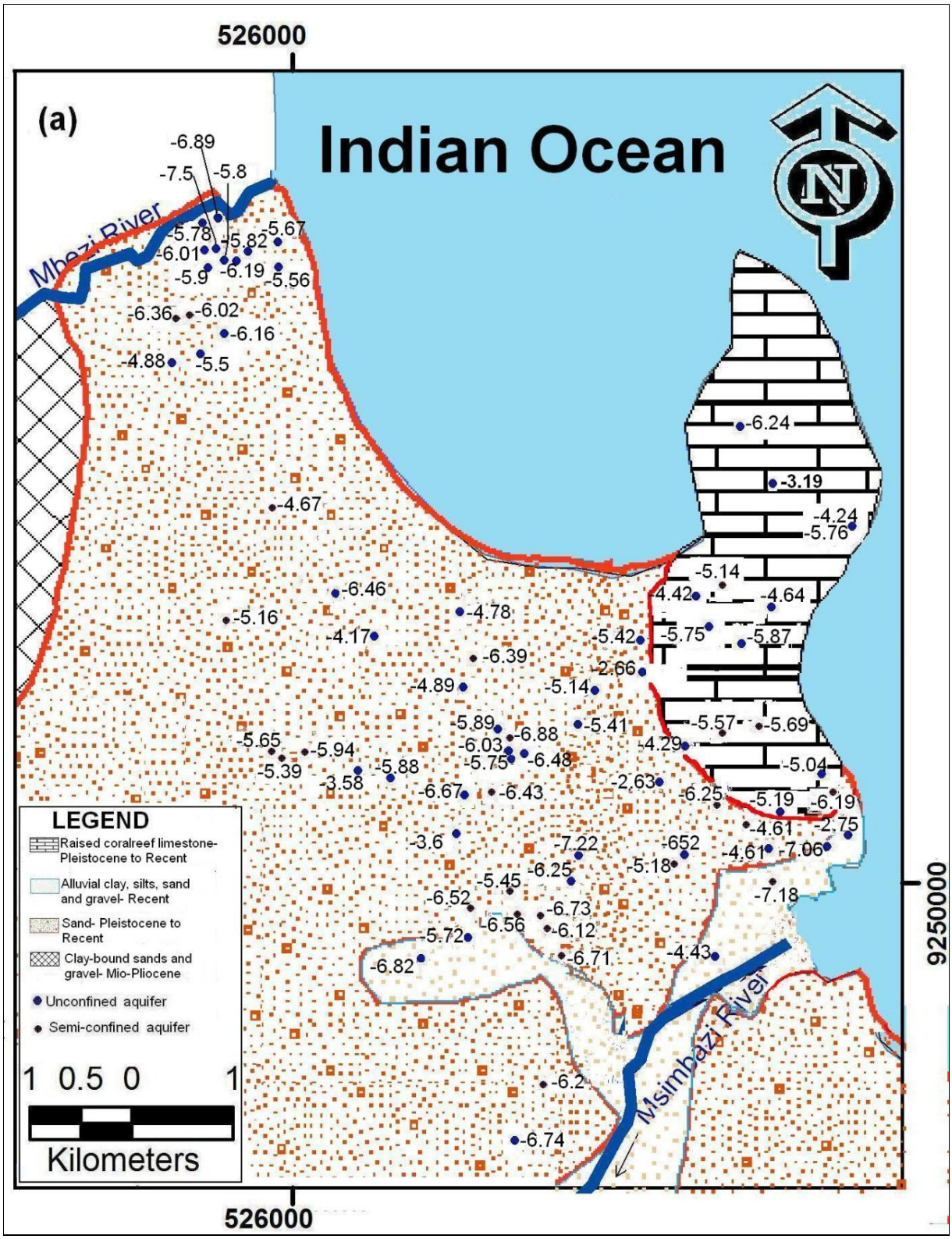

Figure 6.27(a): Spatial distribution of saturation indices of halite (for both unconfined aquifer and semi-confined aquifer) in the area between Mbezi River and Msimbazi River.

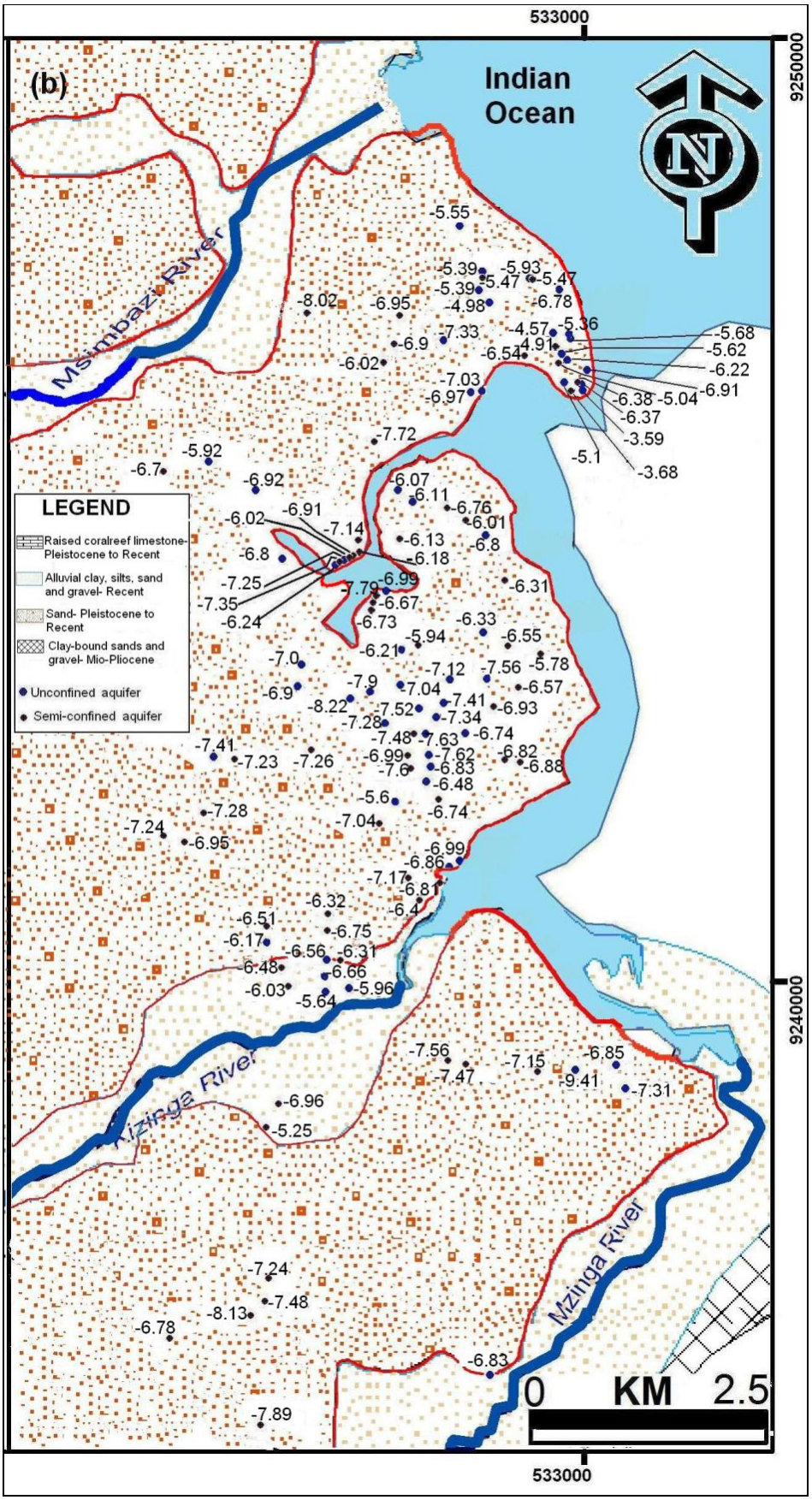

Figure 6.27(b): Spatial distribution of saturation indices of halite (for both unconfined aquifer and semi-confined aquifer) in the area between Msimbazi River and Mzinga River.

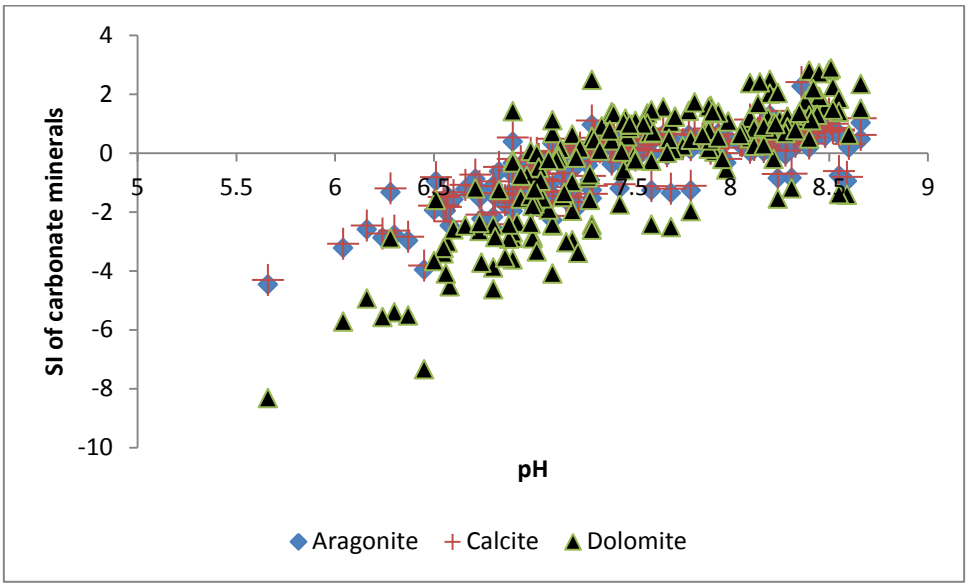

Figure 6.28: Relation between the SI of carbonate minerals and pH.

6.4.5 Bivariate scatter plots

In order to determine the processes that occurred in the groundwater, the concentration of the different ions is crucial. Bivariate scatter plots are used in order to display the relative concentrations of different ions against each other. Chemical composition of groundwater subjected to seawater intrusion tends to deviates from simple conservative seawater-freshwater mixing. Values from Table 6.1 which provide the compositions of freshwater and seawater were used in the plots to indicate the seawater ratio and the mixing line between freshwater and seawater for different ions.

In the bivariate diagram of Cl^-/HCO_3^- versus Cl^- (Fig. 6.29) some samples have much higher ratios compared to the others. The spatial distribution of Cl/HCO_3 ratio (both in unconfined and semi-confined aquifers) is provided in Fig. 6.31 (a-b). The ratio of Cl/HCO_3 ranges between 0.13 and 199. The effect of salinization of the groundwater was classified using the Cl^-/HCO_3^- - ratio: < 0.5 for unaffected groundwater, 0.5 – 6.6 for slightly and moderately affected, and > 6.6 for strongly affected groundwater (Revelle, 1941). Considering the values of Cl^- concentration and the ratio Cl/HCO_3, 15% of groundwater samples are unaffected, 69% of groundwater samples are slightly or moderately affected and 16% are strongly affected by salinization. Water samples which are strongly affected are mostly from the boreholes/wells

located near to the coastline (Fig. 6.30a-b): three samples (number 40, 41 and 132) of the most affected boreholes are located in City Centre (i.e. at southern tip of peninsula in Mzinga estuary) while the majority, accounting to 29 borehole/wells, are located to the north of Msimbazi River in areas which include Oysterbay, Masaki and Msasani, and locally Kawe. Water samples plotting in the lower ratios are mostly from boreholes/wells drilled away from the coastline.

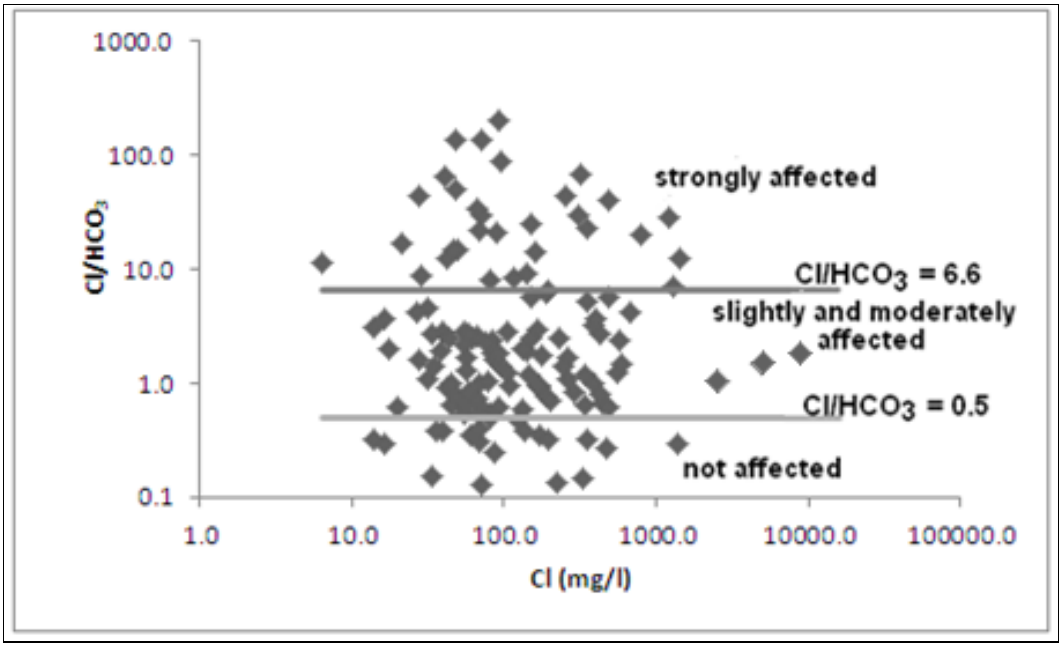

Figure 6.29: Cl/HCO_3 ratio versus Cl (mg/l).

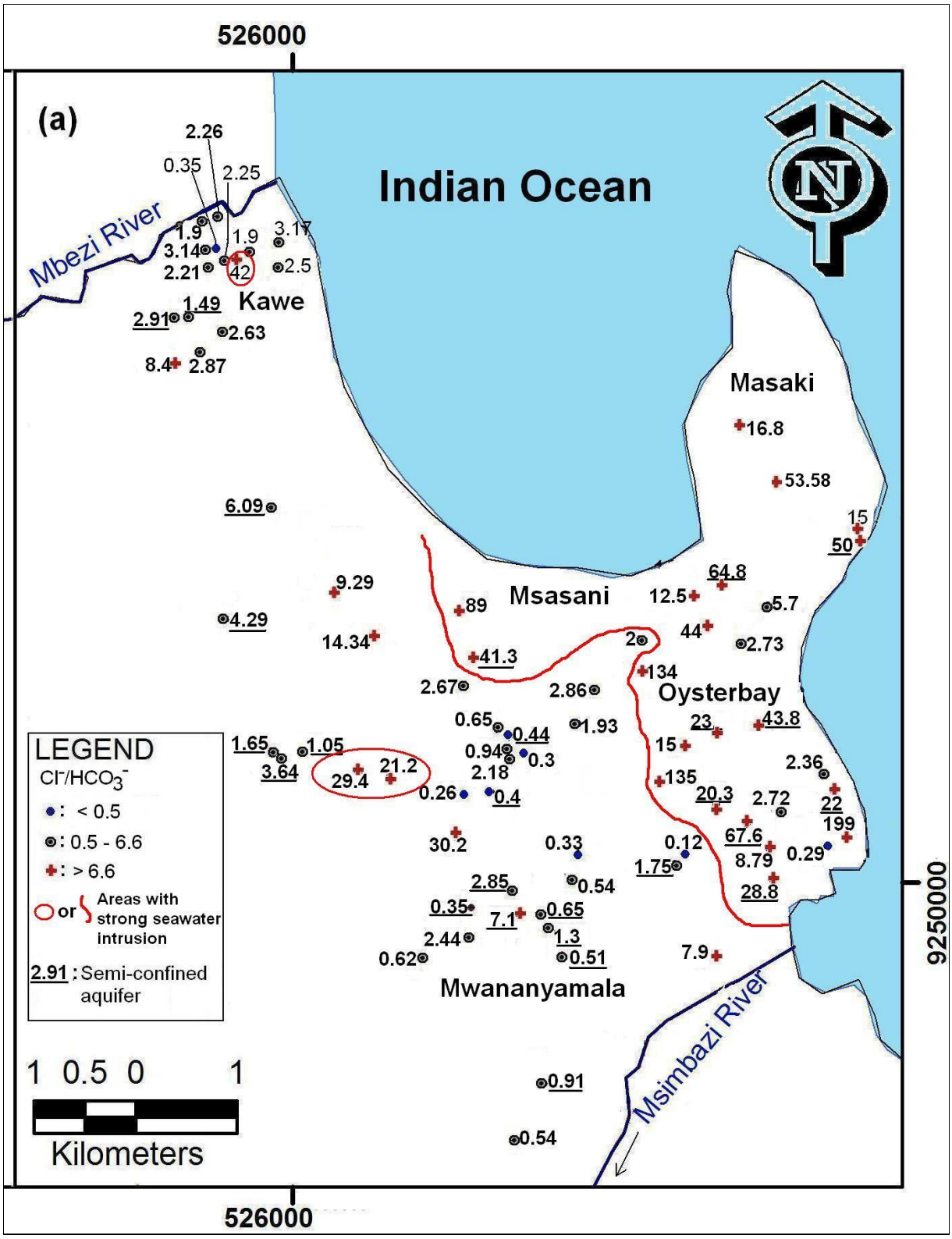

Figure 6.30(a): Spatial distribution of Cl/HCO_3 ratio (both in unconfined and semi-confined aquifers) in the area between Mbezi River and Msimbazi River with indication of areas with strong seawater intrusion.

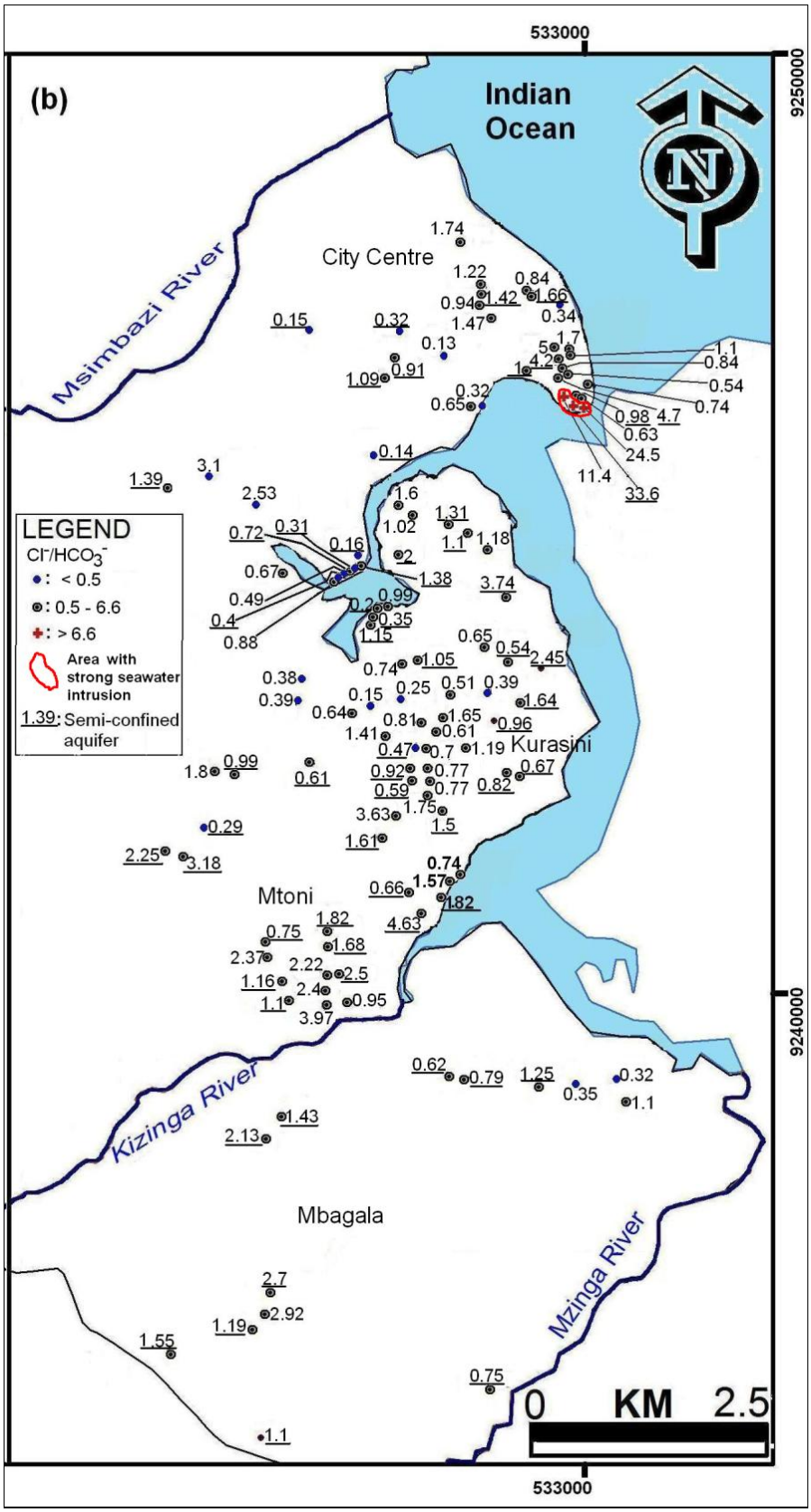

Figure 6.30(b): Spatial distribution of Cl/HCO_3 ratio (both in unconfined and semi-confined aquifers) in the area between Msimbazi River and Mzinga River with indication of area with strong seawater intrusion.

In Fig. 6.31(a), Na^+/Cl^- molar ratio is plotted against Cl^- in order to compare with the Na^+/Cl^- molar ratio of seawater (0.86) (HydroMetrics, 2008). The deviation of the calculated molar ratio of Na^+/ Cl^- from the Na^+/Cl^- molar ratio of seawater could be ascribed to ion exchange processes, indicating an excess or depletion of Na^+ relative to Cl^-. Excess Na^+ in water indicates freshening and it corresponds to samples with lower Cl^- (Fig. 6.31a). On the other hand, depletion of Na^+ in water indicates salinization and it corresponds to samples with high Cl^- (Fig. 6.31a). The Na^+/Cl^- ratio could reach unity due to the mixing of seawater and freshwater, which has a Na^+/Cl^- ratio greater than unity (Vengosh et al., 1999, cited in Ghabayen et al., 2006).

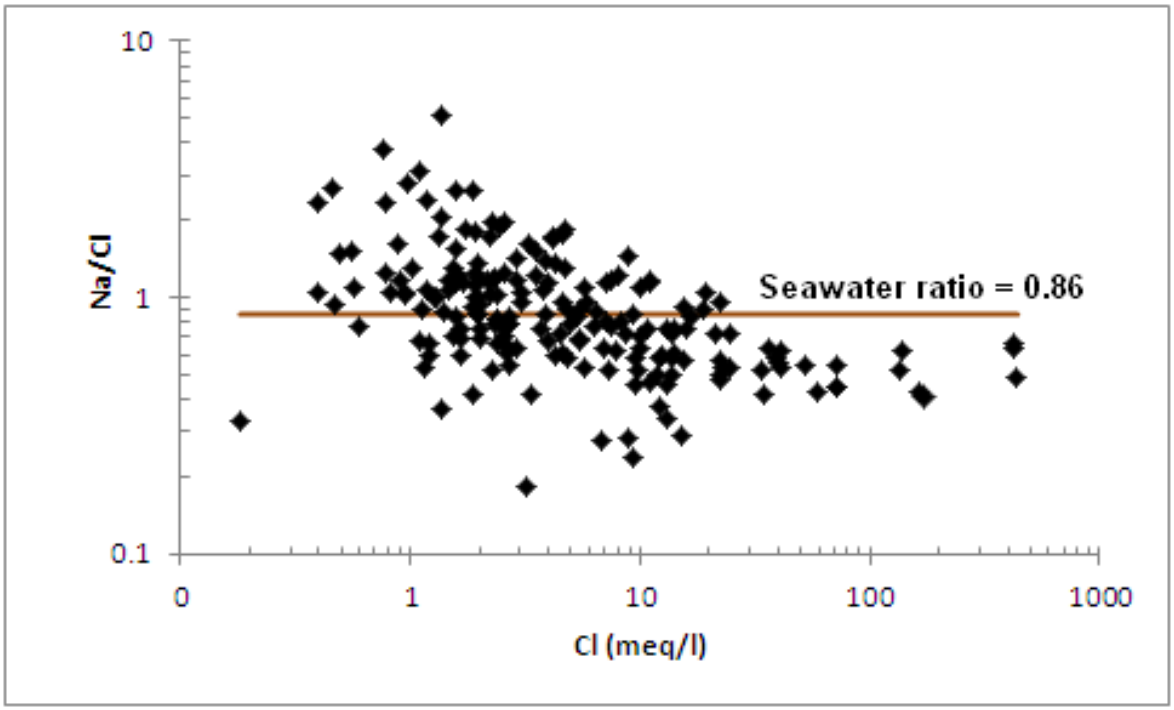

Figure 6.31(a): Log Na^+/Cl^- ratio vs. Cl^-.

Ratios of Ca^{2+}/Mg^{2+} (Fig. 6.31(b) and Ca^{2+}/Na^+ (Fig. 6.31c) are much higher than those of seawater, which indicate enrichment of Ca^{2+} by dissolution of carbonate minerals in the aquifer matrix and/or, for Ca^{2+}/Na^+, depletion of Na^+ and enrichment of Ca^{2+} due to cation exchange during mixing with seawater.

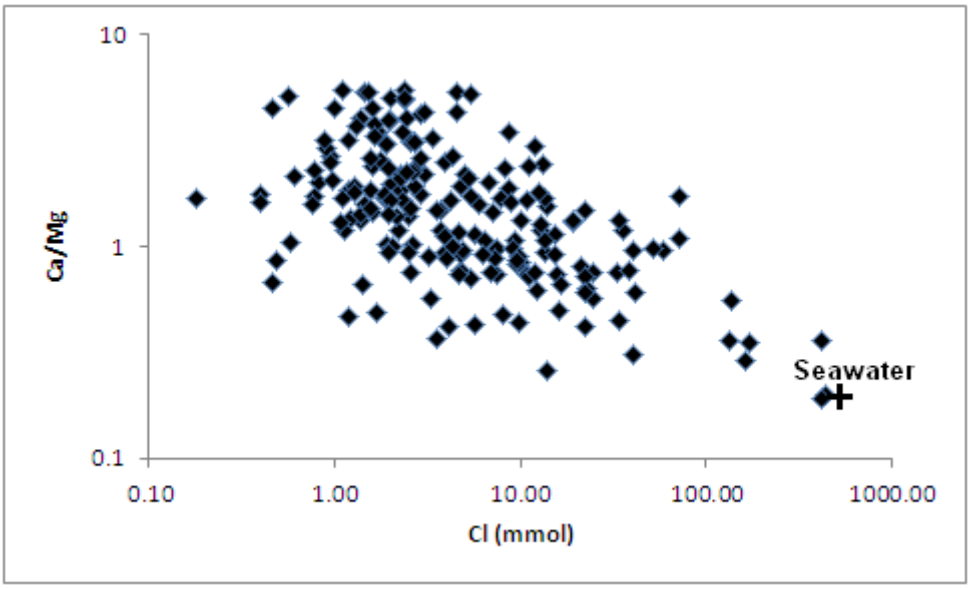

Figure 6.31(b): Log Ca^{2+}/Mg^{2+} ratio vs. Cl^-.

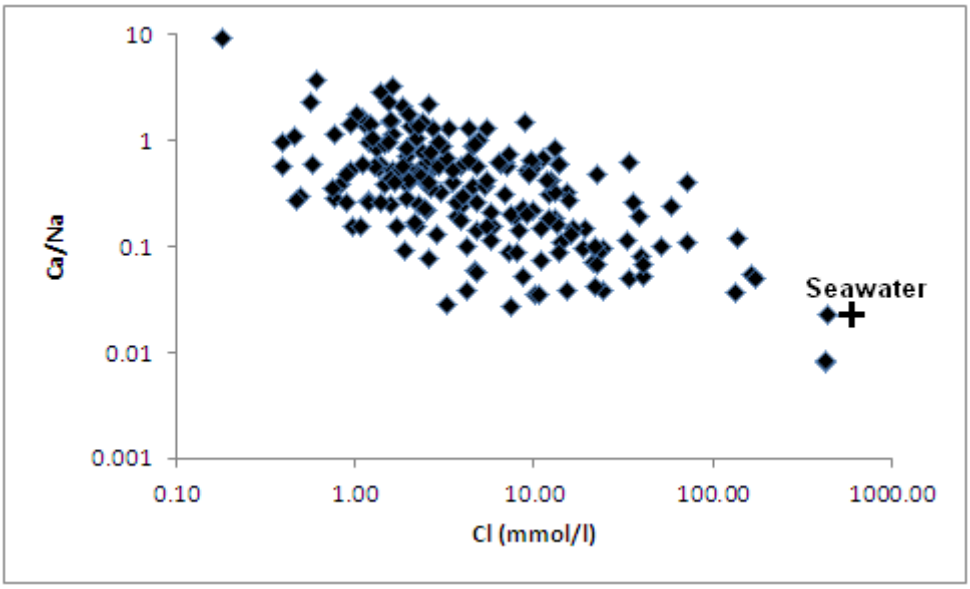

Figure 6.31(c): Ca^{2+}/Na^+ ratio vs. Cl^-.

A linear relation between Na^+ and Cl^- (Fig. 6.32(a)) represents simple mixing of the fresh groundwater with the seawater. Seawater-freshwater mixing is expected to show a linear increase in Na and Cl (Sanchez Martos et al., 1999). The seawater dilution line in Fig. 6.32(a) shows simple mixing of both end members freshwater and seawater as shown by the Na^+ and Cl^- ion concentration. A deviation from the mixing line could be ascribed to ion exchange processes, indicating an excess or depletion of Na^+ relative to Cl^- (Walraevens and Van

Camp, 2005). Excess Na^+ in water plotting above mixing line in Fig. 6.32(a) indicates freshening and it corresponds to samples with lower Cl^- in Fig. 6.32(a). On the other hand, depletion of Na^+ in water plotting below the mixing line in Fig. 6.32(a) indicates salinization and it corresponds to samples with high Cl^- in Fig. 6.32(a). The Na^+–Cl^- bivariate plot (Fig. 6.32(a) demonstrates a distinct strong correlation between Na^+ and Cl^- concentrations for most of the samples indicating saltwater intrusion, as admixture of the saline end member is increased. As already explained, under the conditions of saline intrusion, Na^+ in seawater replaces Ca^{2+} adsorbed onto the surface of clays and this result in a relative depletion of Na^+ in groundwater. Thus, Na^+ values for some samples are decreased due to cation exchange and are plotted below the mixing line.

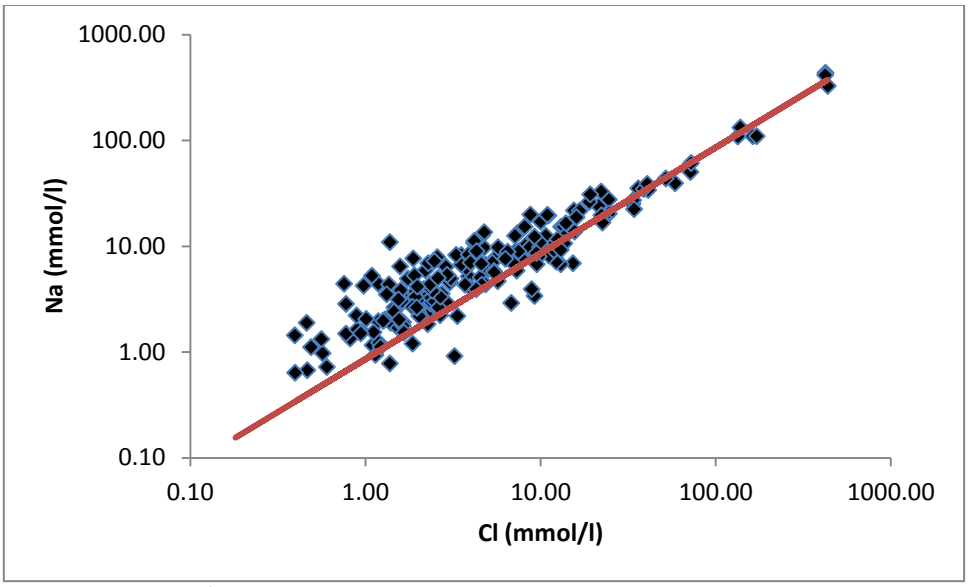

Figure 6.32(a): Log Na^+ versus Log Cl^- with mixing line between fresh water and seawater

In Fig. 6.32(b), Mg^{2+} is plotted versus Cl^{-}. A large number of samples are plotted above the seawater-freshwater mixing line. Most samples indicate higher magnesium concentration than they would have if their only source would be mixing with seawater. Apart from the effect of seawater intrusion, the possible extra source of magnesium can be cation exchange and the dissolution of dolomite (Reaction 6.12). The former occurs due to freshening whereby magnesium is released in the solution as it is exchanged for calcium. Weak linear relation exists between Ca^{2+} and Cl^- (Fig. 6.32c). Ca^{2+} values for most samples, mainly for lower Cl^-, are decreased and are plotted below the mixing line. Decrease of Ca^{2+} in freshening groundwater is associated with cation exchange, whereby Ca^{2+} is adsorbed and Na^+ is released. Excess Ca^{2+} in water plotting above mixing line in Fig. 6.32(c) indicates salinization

and it corresponds to samples with high Cl^-. On the other hand the possibility for addition of Ca^{2+} can occur through calcite dissolution or weathering of silicate minerals such as calcium plagioclase (anorthite) (Reaction 6.9) (Appelo and Postma, 1993).

$$\underset{Anorthite}{CaAl_2Si_2O_8} + 2H_2CO_3 + H_2O \rightarrow \underset{Kaolinite}{Al_2Si_2O_5(OH)_4} + 2HCO_3^- + Ca^{2+} \ldots\ldots\ldots (6.9)$$

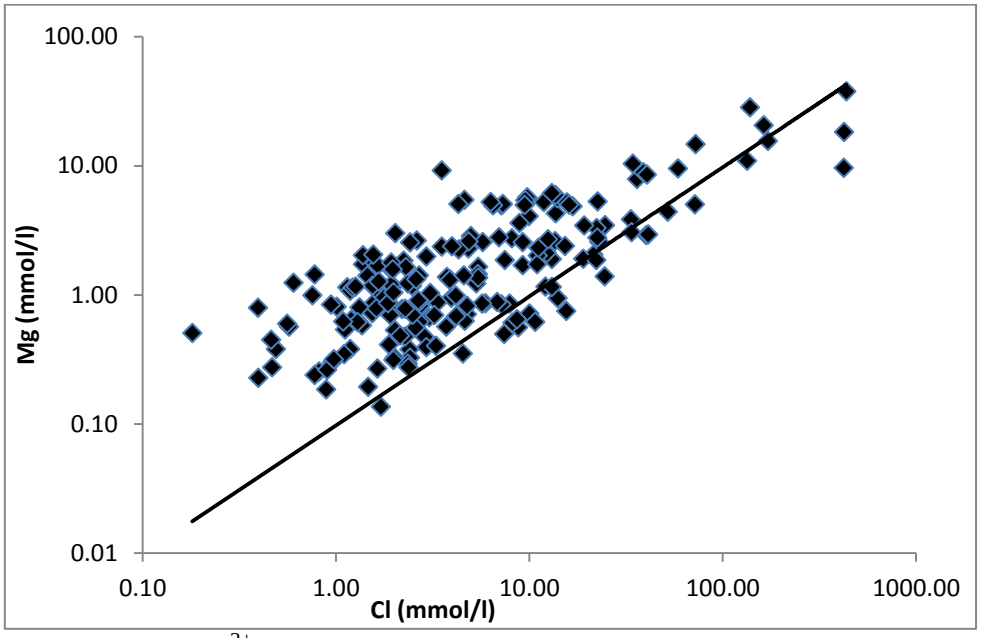

Figure 6.32(b): Log Mg^{2+} versus Log Cl^- with mixing line between fresh water and seawater.

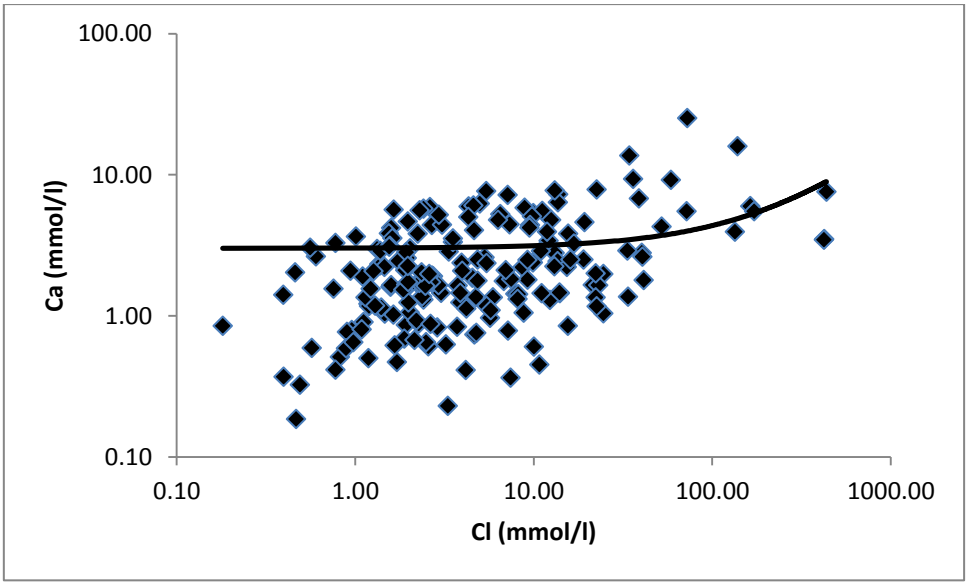

Figure 6.32(c): Log Ca^{2+} versus Log Cl^- with mixing line between fresh water and seawater.

In Fig. 6.32(d), K^+ is plotted against Cl^-. A large number of samples are plotted above the seawater-freshwater mixing line. Apart from the effect of seawater intrusion, the possible extra source of potassium can be cation exchange due to freshening. This is in line with the lower Cl^- concentrations that are mostly accompanying excess.

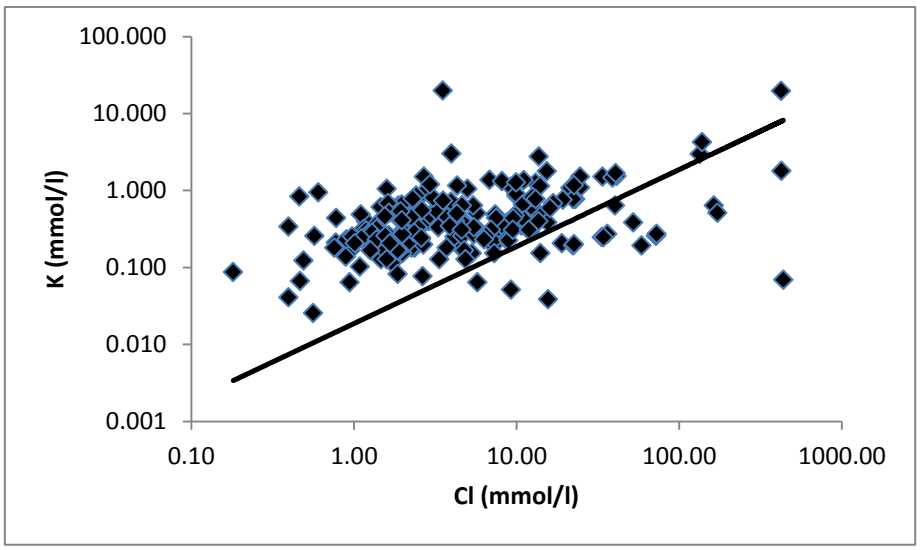

Figure 6.32(d): Log K^+ versus Log Cl^- indicating mixing line between fresh water and seawater.

Fig. 6.32(e) shows SO_4^{2-} versus Cl^-. A positive relation is visible, suggesting seawater influence, but there is a clear excess of sulphate. The main explanation for this excess of sulphate is pyrite oxidation (6.4.2; cfr. Equation 6.8). Samples plotting below the dilution line suggest SO_4^{2-} reduction.

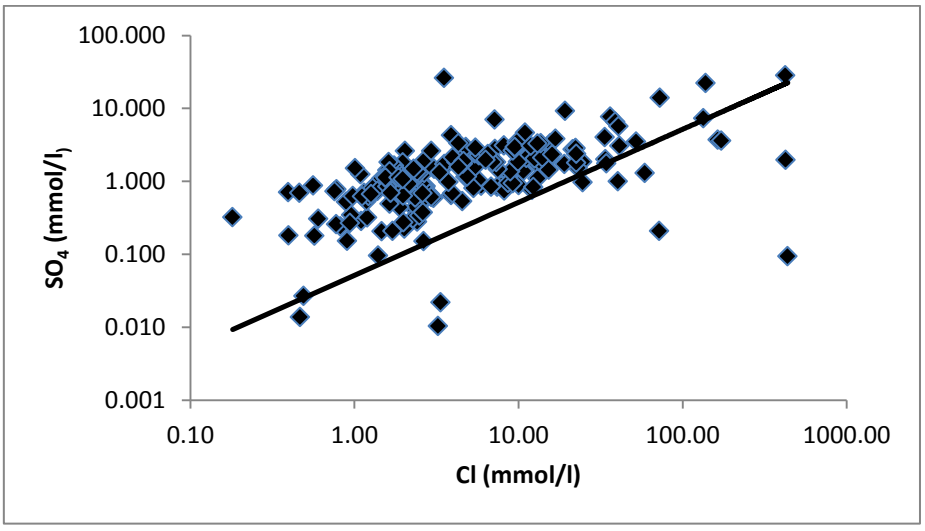

Figure 6.32(e): Log SO_4^{2-} versus Log Cl^- indicating mixing line between fresh water and seawater.

As already explained in section 6.4.1.4, the geochemistry of the aquifer system in the study area is also contributed by the dissolution of calcite. Fig. 6.33(a) shows the relationships 2:1 and 1:1 between HCO_3^- and Ca^{2+} respectively corresponding to the following reactions:
Typical dissolution of calcite by CO_2 in the unsaturated zone (Walraevens, 1990), results in a 2:1 relationship:

2:1 relationship

$$CaCO_3 + CO_2 + H_2O \rightarrow Ca^{2+} + 2HCO_3^- \qquad (6.10)$$

Whereas calcite dissolution by other acids apart from CO_2 (e.g. humic acids or due to cation exchange) results in a 1:1 relationship (Walraevens, 1990).

1:1 relationship

$$CaCO_3 + H^+ \rightarrow Ca^{2+} + HCO_3^- \quad \ldots\ldots\ldots\ldots\ldots\ldots\ldots\ldots\ldots\ldots\ldots\ldots\ldots\ldots\ldots\ldots\ldots\ldots (6.11)$$

According to Fig. 6.33(a), both reactions may play a role.

When dolomite is present, this mineral may dissolve under the influence of CO_2, according to the reaction:

$$CaMg(CO_3)_2 + 2CO_2 + 2H_2O \Leftrightarrow Ca^{2+} + Mg^{2+} + 4HCO_3^- \ldots\ldots\ldots\ldots\ldots\ldots\ldots (6.12)$$

If dolomite dissolves according to reaction 6.12, the relation of [Ca+Mg] to [HCO_3] should be linear, with a slope of 2 (Fig. 6.33b). Dolomite dissolution by other acids results in a 1:1 relationship:

$$CaMg(CO_3)_2 + 2H^+ \Leftrightarrow Ca^{2+} + Mg^{2+} + 2HCO_3^- \ldots\ldots\ldots\ldots\ldots\ldots\ldots\ldots\ldots\ldots\ldots (6.13)$$

In the study area groundwater samples are often highly enriched in (Ca^{2+} + Mg^{2+}) relative to HCO_3^-. If all calcium and magnesium were derived from calcite and dolomite dissolution, samples would plot along the equiline. Many points fall far below the equiline, signifying an additional source of (Ca^{2+} + Mg^{2+}), and especially Mg^{2+} (comparing also Fig. 6.33(a)). Looking at higher Mg^{2+}concentrations (> 10 mmol/l) in Fig. 6.32(b) and higher Ca^{2+}

concentrations (>10 mmol/l) in Fig. 6.33(a), higher (Ca^{2+} + Mg^{2+}) concentrations (> 10 mmol/l) in Fig. 6.33(b) are mainly due to Mg^{2+} caused by enrichment due to seawater admixture.

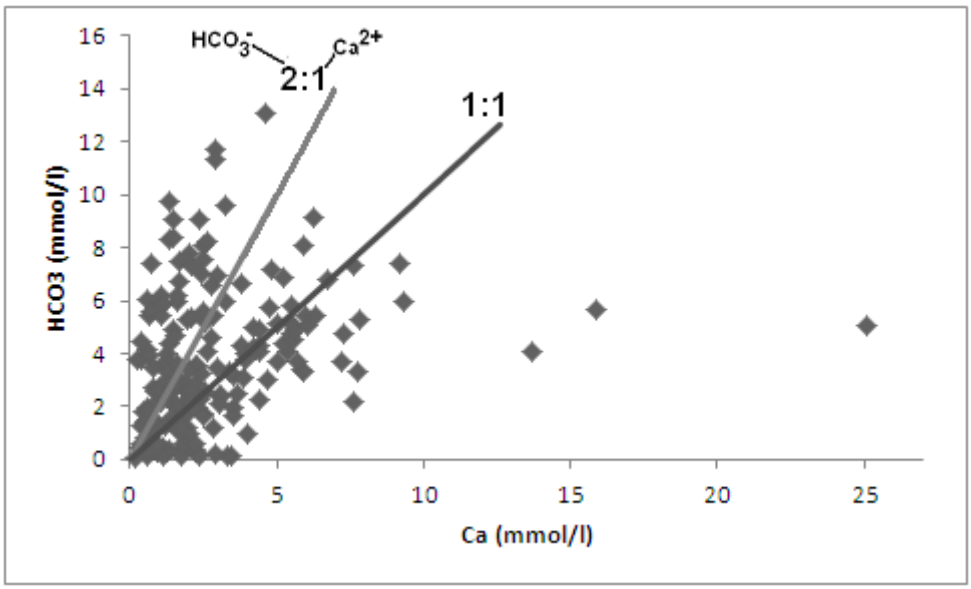

Figure 6.33(a): Scatter diagram of HCO_3^- versus Ca^{2+}.

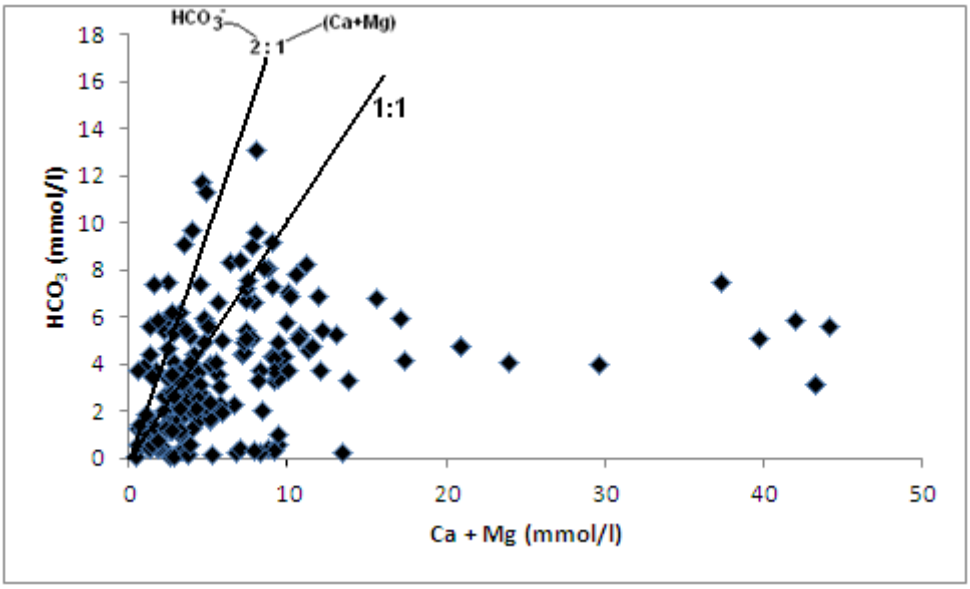

Figure 6.33(b): Scatter diagram of (HCO_3) versus (Ca+Mg) for groundwater from the study area.

6.4.6 Groundwater classification

Groundwater samples were classified according to Stuyfzand (1986) and Piper's (1944) classification systems (Appendix 6.5).

6.4.6.1 Piper diagram

Hydrochemical diversity among the groundwater samples in the study area is exposed by the Piper diagram (Fig. 6.34a). From the analysis of the Piper diagram it is clear that several water types (Appendix 6.5) are present in the groundwater reservoir in the study area. The spatial distribution of water types according to Piper diagram is presented in Fig. 6.35(a-b). Although the Piper diagram shows many water types are present in the groundwater system, five dominant groups can be identified. Group A is mainly dominated by Ca–HCO_3, Ca-Na-Cl-HCO_3 and Ca-Mg-HCO_3 (Fig. 6.34a). The freshwater's end member has a $CaHCO_3$ major ion composition and is part of group A. Group B consists mainly of NaCl type which makes up a large proportion of the groundwater types. The seawater's end member has a NaCl major ion composition, and belongs to group B. Group C is an intermediate between both end members. It is more dominated by Na–Ca–Cl, indicating freshwater-seawater mixing (Walraevens and Van Camp, 2005). Group D which is dominated by Na–HCO_3 gives an indication of groundwater freshening (Walraevens and Van Camp, 2005). Group E consists of mg-Ca-Na-Cl, Ca-Na-Cl-HCO_3 or Ca-Na-HCO_3–Cl, and Ca-Mg-Na-HCO_3–Cl: these water types indicate mixed water type that has evolved from Ca-HCO_3 (recharge water) mixing with seawater.

The dashed line central in the Piper diagram represents the freshwater-seawater simple mixing line. The left side represents the freshwater end member whereas the right side represents the seawater (NaCl) end member. If the chemical composition of groundwater in the study area was only influenced by a simple mixing process between freshwater and seawater, water samples would have plotted along the straight line connecting the background freshwater and seawater. However, cation exchange reactions play a significant role in influencing the chemical compositions of coastal aquifers affected by seawater intrusion (Appelo and Postma, 1993). When samples plot above the mixing line, it indicates salinization is present, whereas water samples plotting below the mixing line indicate freshening. Samples with Na–Ca–Cl water type plotting above the mixing line (signifying effect of salinization) are dominant in the unconfined aquifer compared to the semi-confined aquifer. Samples from both unconfined

and semi-confined aquifer, plotting below the mixing line, are signifying both mixing and freshening processes.

Dissolution of calcite and dolomite in recharge areas results in fresh Ca–HCO_3 and Ca–Mg–HCO_3 groundwater types. Groundwater evolution in the study area shows a curved path of hydrogeochemical evolution which begins from the Ca-HCO_3 water type, advancing through the Na-Ca-Cl water type to Na-Cl water type. Seawater intrusion results in Na^+ uptake by the exchange sites, releasing Ca^{2+}, and delivering the CaCl groundwater type as an intermediate water type, before the NaCl type. On the other hand, in the fresh waters, Na^+ is enriched indicating freshening of the aquifer as Ca^{2+} is replacing Na^+ on the exchange complex. Formation of $NaHCO_3$ water types provides evidence of freshening. Brackish and saline groundwater samples appearing in the mixing line have a Na–Ca–Cl major ion composition. Samples of most of the boreholes located close to the coastline plot in the NaCl area, while those located further from the coast (Fig. 6.35a-b) plot over a very large range.

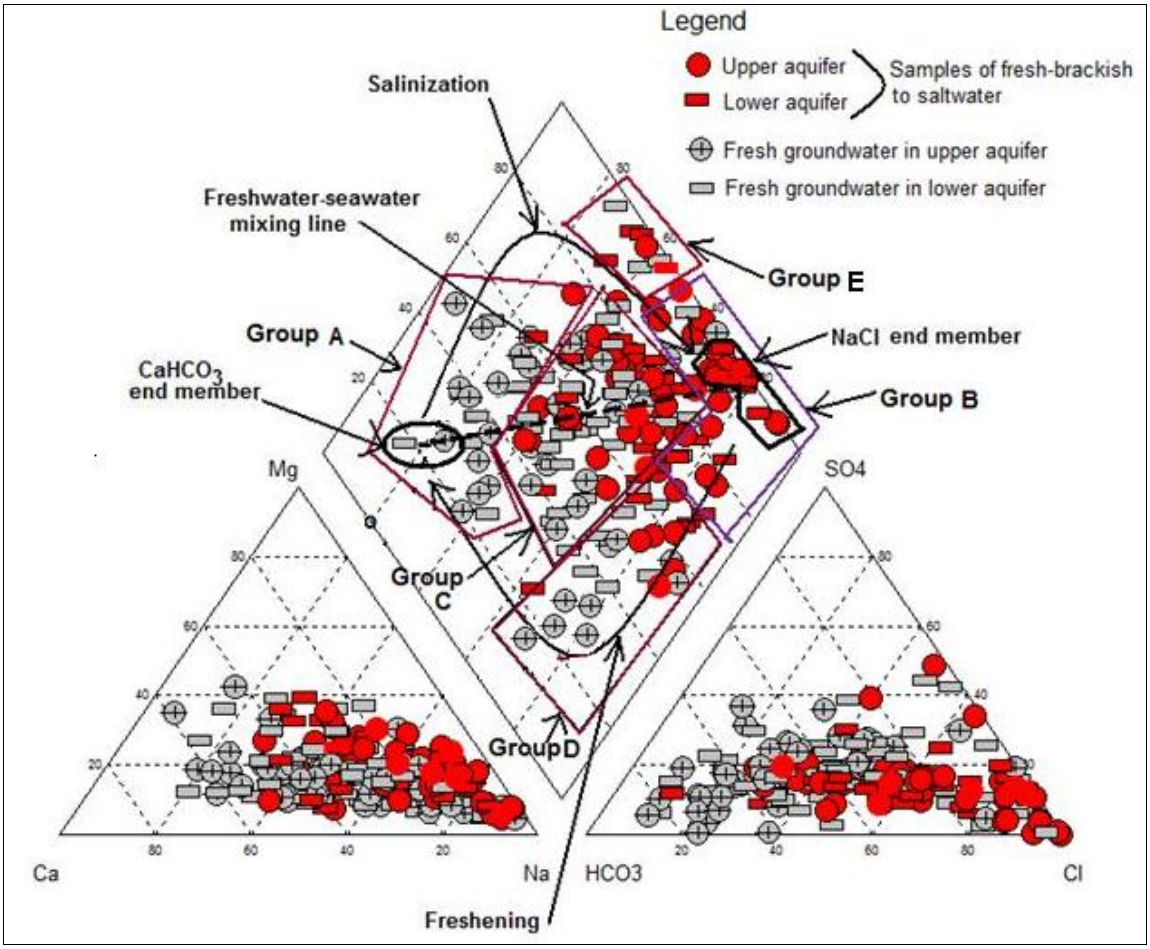

Figure 6.34(a): Piper plot with representation of major ions and groundwater types in the upper aquifer and in lower aquifer.

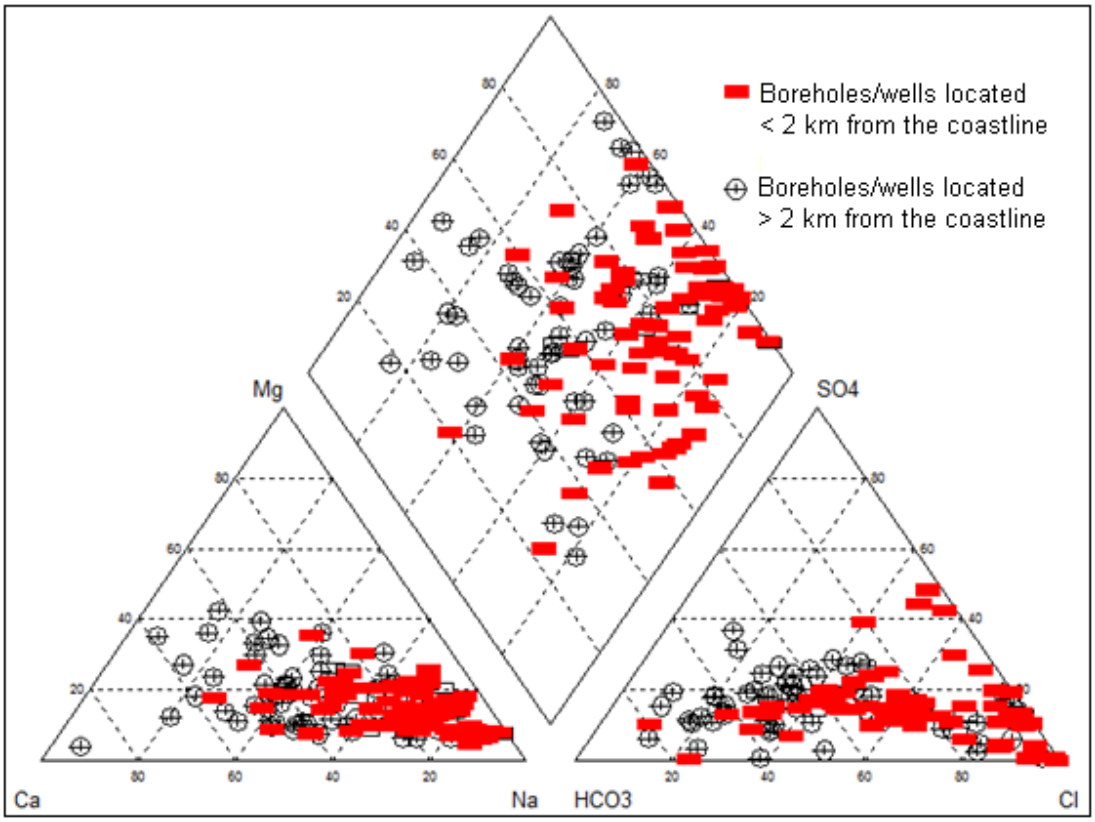

Figure 6.34(b): Piper plot showing boreholes/wells (for the first 134 samples) located in close proximity to the coastline (< 2 km) and further from coastline (> 2 km).

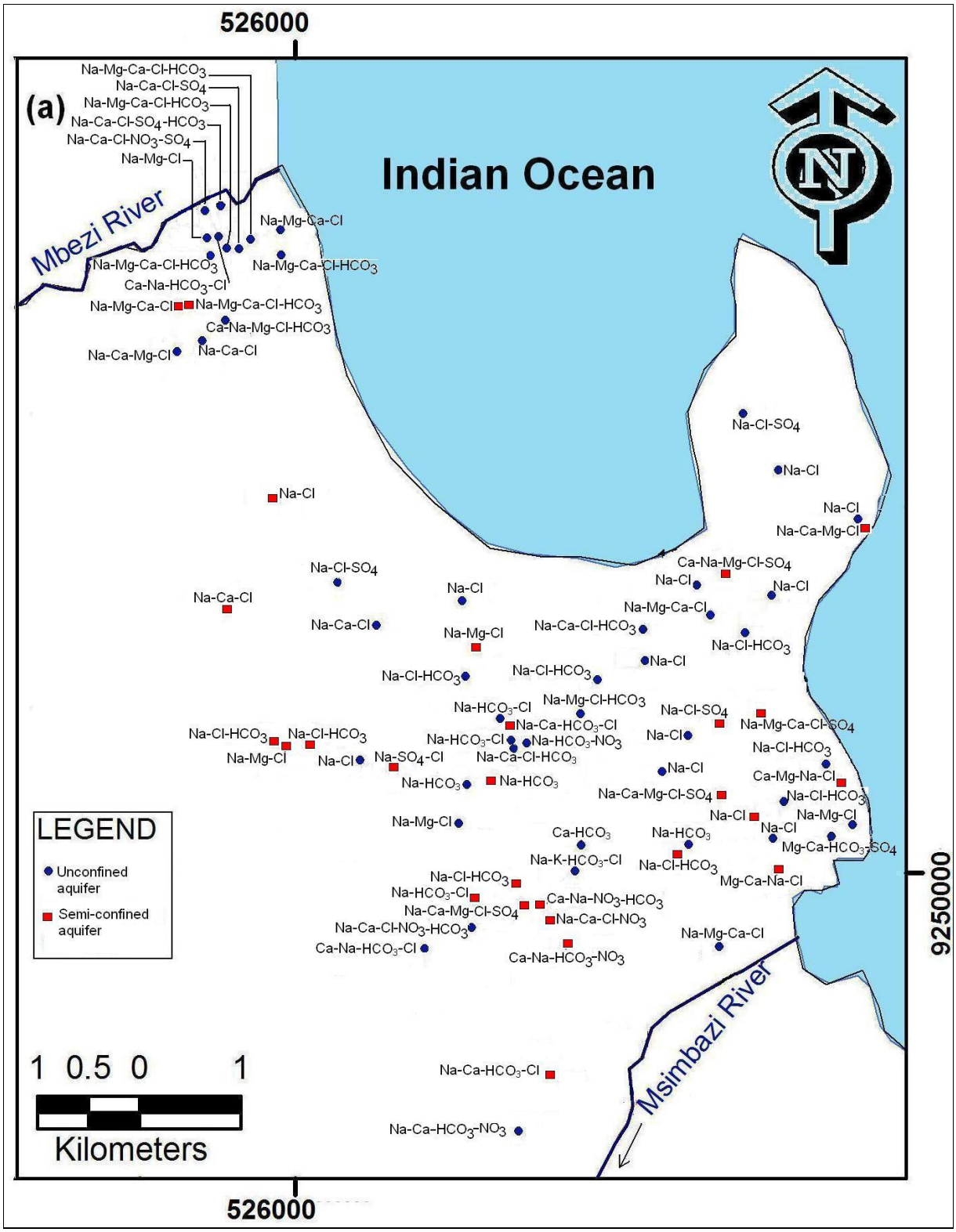

Figure 6.35(a): Spatial distribution of water types according to Piper (both in unconfined and semi-confined aquifers) in the area between Mbezi River and Msimbazi River.

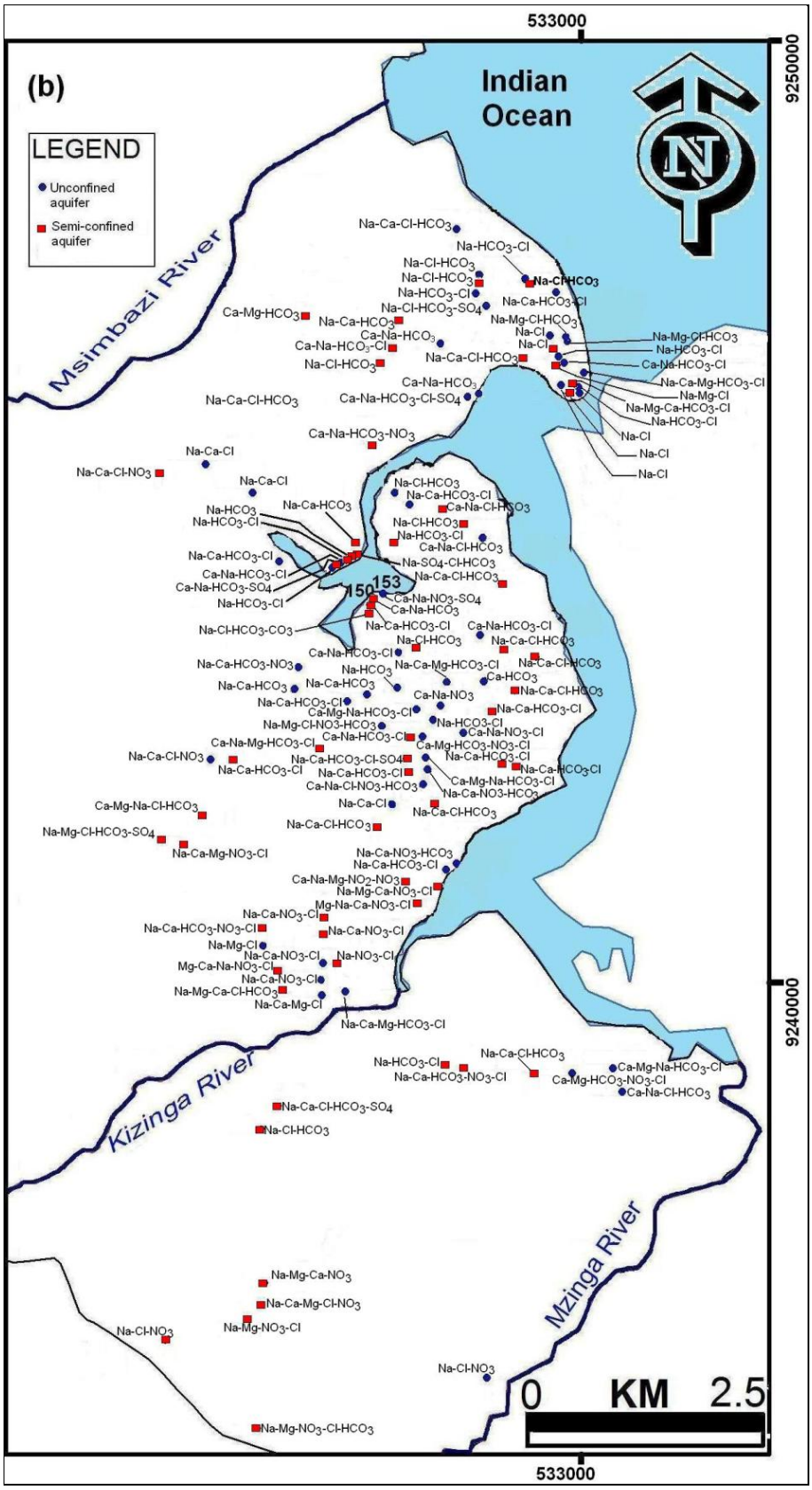

Figure 6.35(b): Spatial distribution of water types according to Piper (both in unconfined and semi-confined aquifers) in the area between Msimbazi River and Mzinga River.

6.4.6.2 Durov diagram

Fig. 6.36 is Durov plot of the groundwater samples showing water types and the geochemical evolutionary trend. The main purpose of the Durov diagram is to show clustering of data points to indicate samples that have similar compositions (Hem, 1989). The Durov diagram undoubtedly shows the modification of water types from fresh recharge-$CaHCO_3$ end member to saline-NaCl end member, where the end members are mixed in different proportions between the two water types. If a simple two component mixing model of seawater with unaffected groundwater is assumed, it is expected that the salinity affected groundwater analyses (fresh-brackish to saltwater) should plot on a straight line in the plotting field. It is, however, noticed that most of the samples fall distinctly away from the expected straight line joining both end members (freshwater-seawater mixing line). This indicates that the chemical composition of groundwater in the study area is influenced by other factors (e.g. cation exchange reactions) apart from a simple mixing process with seawater.

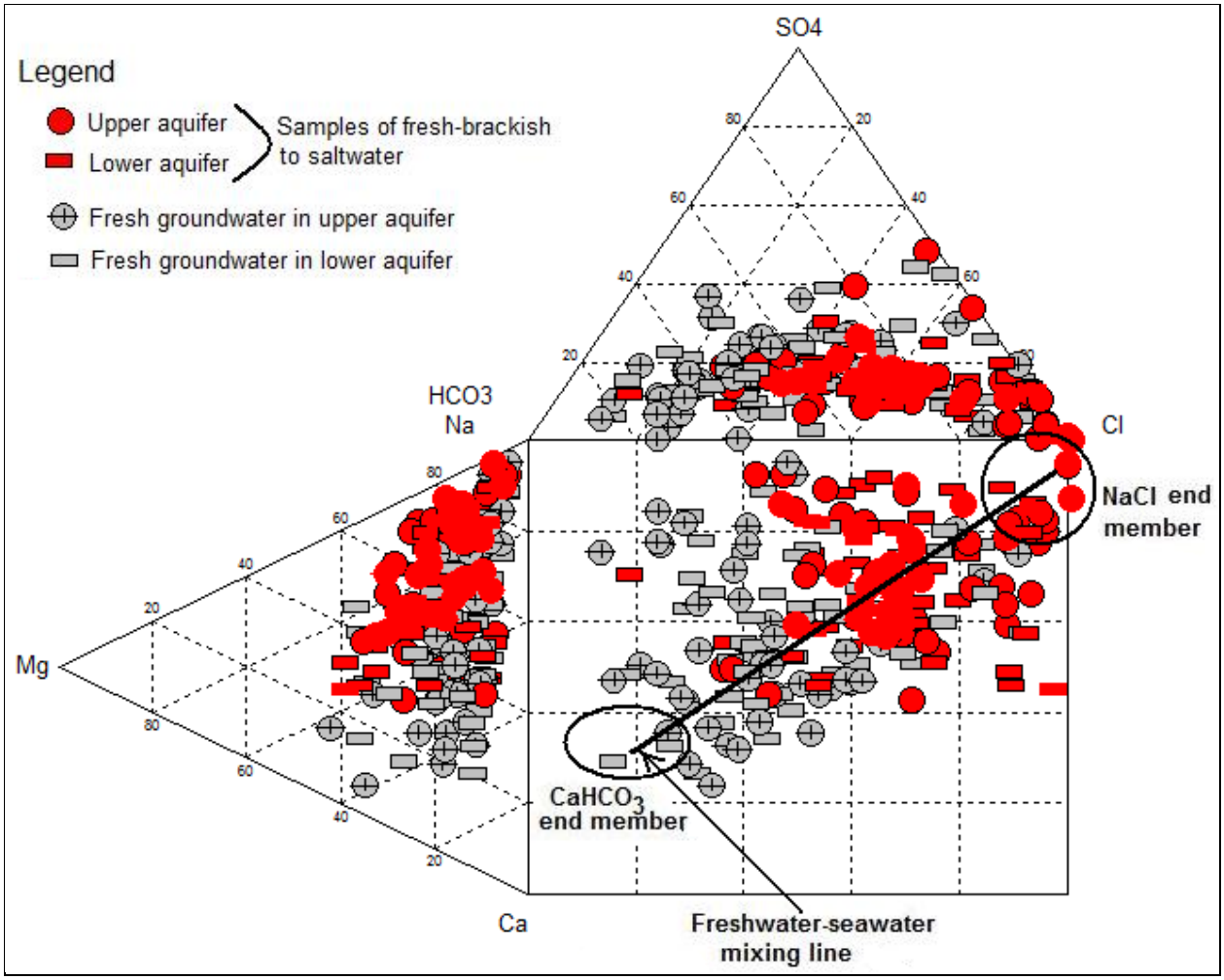

Figure 6.36: Durov plot of the groundwater samples showing water types and the geochemical evolutionary trend.

6.4.6.3 Stuyfzand water type classification

The chloride concentrations of the samples have a wide range from 6.42 mg/l to 15478 mg/l, ranging from fresh to salt main type (Table 6.6). The majority of the samples accounting to 53.33% are grouped as fresh (F). The second most important class is brackish for 21.54% of samples.

Table 6.6: Classification of water based on chloride concentration by Stuyfzand (1986) classification

Main type (code)	**Cl (mg/l)**	**Number of samples**	**%**
Fresh (F)	$Cl^- < 150$ mg/l	104	53.33
Fresh-Brackish (Fb)	150 mg/l < Cl^- < 300 mg/l Cl^-	30	15.38
Brackish (B)	300 mg/l < Cl^- < 1000 mg/l	42	21.54
Brackish salt (Bs)	1000 mg/l < Cl^- < 10000 mg/l	16	8.21
Salt (S)	$Cl^- > 10000$ mg/l	3	1.54

In the study area, the total hardness varies through a wide range from very soft (0.46 mmol/l) to extremely hard (90.6 mmol/l). However, it is clear that most of the samples are hard (30.3%), or very hard (27.7%) (Table 6.7). Generally, these high values of total hardness are related to the dissolution of carbonate (calcite and dolomite) yielding high concentrations of Ca^{2+} and Mg^{2+} (Appelo and Postma, 1993). However, Mg^{2+} is also caused by enrichment due to seawater admixture.

Table 6.7: Classification of water based on hardness by Stuyfzand (1986) classification

Type (code)	**Total hardness (mmol/l)**	**number of samples**	**%**
Very soft (*)	0-0.5	1	0.5
Soft (0)	0.5 – 1	6	3.0
Moderately hard (1)	1-2	20	10.3
Hard (2)	2-4	59	30.3
Very hard (3)	4-8	54	27.7
Extremely hard (4)	8-16	41	21.0
Extremely hard (5)	16-32	6	3.1
Extremely hard (6)	32-64	7	3.6
Extremely hard (7)	64-128	1	0.5

Groundwater was classified into several categories based on dominant cation and anion, i.e., Sodium-Chloride, Sodium-Bicarbonate, Calcium-Bicarbonate, Magnesium-Bicarbonate,

Sodium-Mix and Calcium-Mix. Most of shallow wells close to the shoreline have "Brackish-saline extremely hard NaCl" to "Brackish very hard CaCl" water. The spatial distribution of Stuyfzand (1986) water type classification from analysed groundwater samples in the study area is presented in Fig. 6.37(a-b).

Appendix 6.5 shows the Stuyfzand (1986) classification results of the groundwater samples analyzed from the study area. It is observed that most samples have a positive cation exchange code. This would refer to freshening. However, the concept supposes that the only fresh water cation is Ca^{2+}, while Mg^{2+} is only contributed by the seawater end member. In the study area, this assumption is not valid: part of the Mg^{2+} derives from dolomite dissolution. Therefore in the study area, the corrected sum of marine cations is increased by the dolomite-derived Mg^{2+}, upgrading the cation exchange code. Water samples, affected by active salinization, can therefore show equilibrium, or even a positive cation exchange code, instead of the expected negative code. Dissolution of calcite, dolomite and/or Mg^{2+} bearing calcite is an important process in most groundwaters (Al Farrah et al. 2011; Morse and Mackenzie 1990). The same process of saltwater intrusion has been established in many other coastal regions (Trabelsi et al. 2012; Ahmed et al. 2012; Reddy 2012). A study conducted in Libya (Al Farrah et al. 2011) gives a comparable example to this study: the water types indicate that groundwater chemistry is changed by cation exchange reactions during the mixing process between freshwater and seawater.

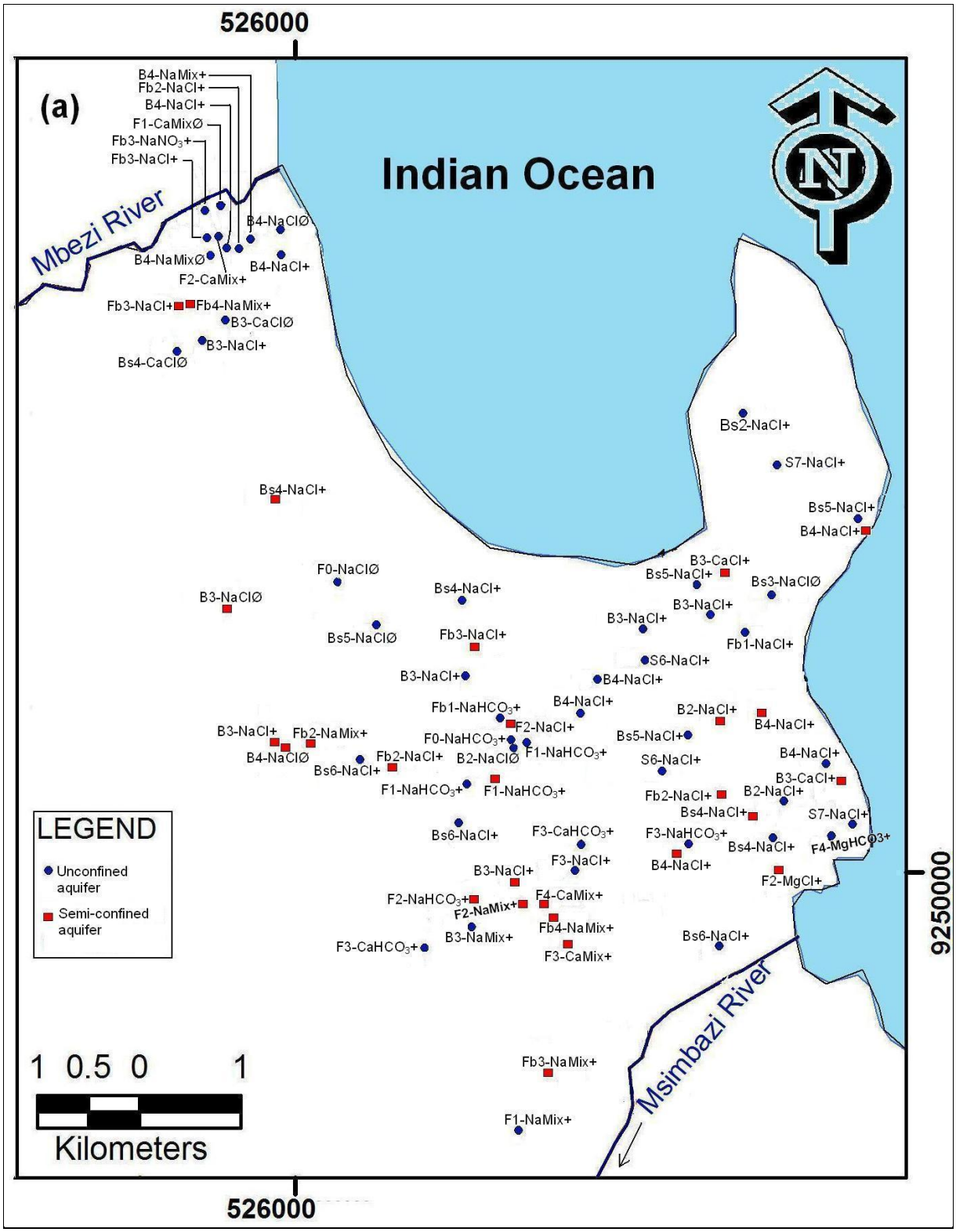

Figure 6.37(a): Spatial distribution of Stuyfzand (1986) water type classification (both in unconfined and semi-confined aquifers) in the area between Mbezi River and Msimbazi River.

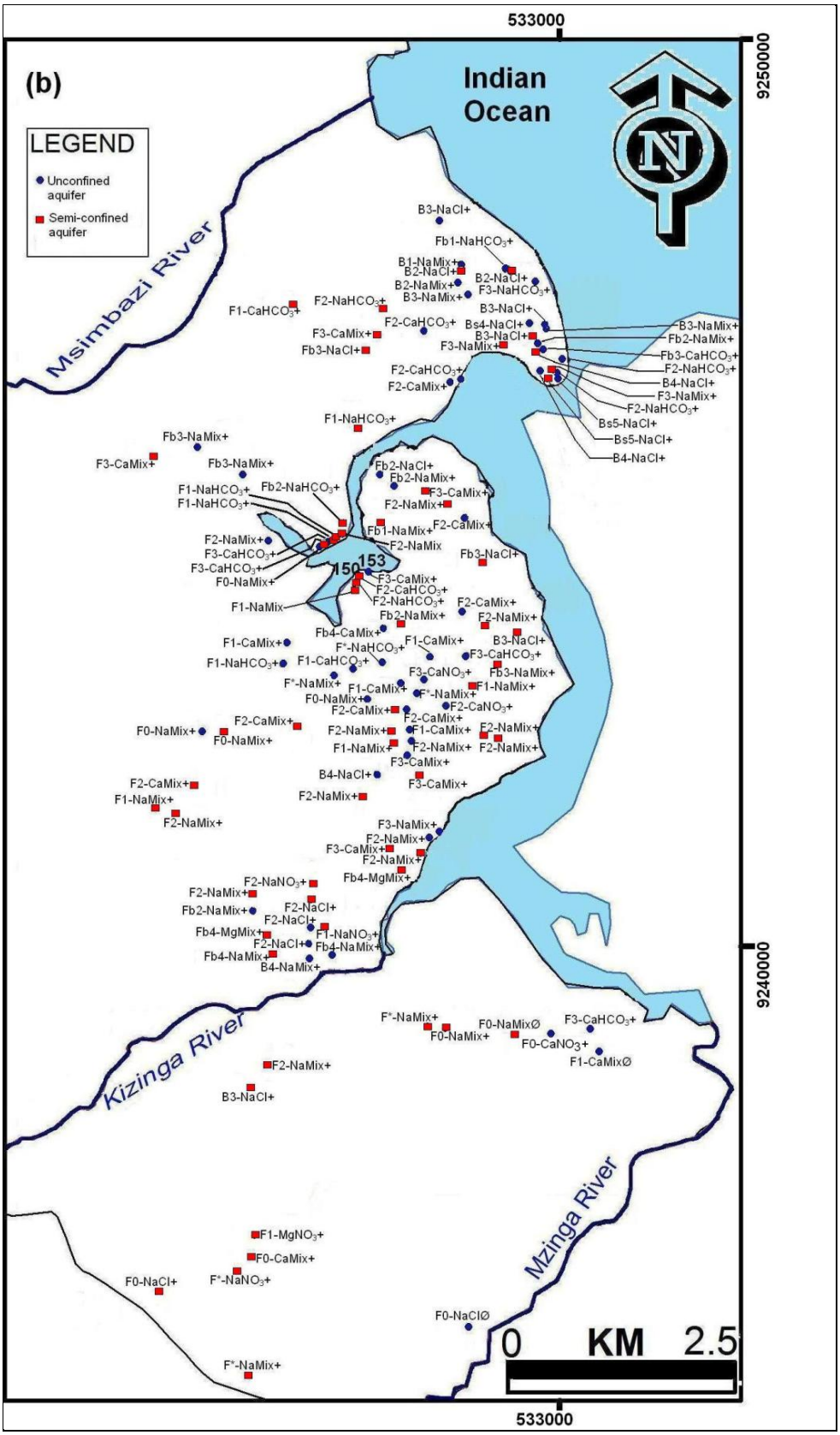

Figure 6.37(b): Spatial distribution of Stuyfzand (1986) water type classification (both in unconfined and semi-confined aquifers) in the area between Msimbazi River and Mzinga River.

6.4.7 Processes affecting groundwater quality

Hydrogeochemical data on dissolved major cations and anions analysed in 196 groundwater samples from Dar es Salaam quaternary coastal aquifer (DQCA) reveal the main processes responsible for their geochemical evolution. Based on the analytical results, mainly involving water type classification according to Stuyfzand (1986), graphical illustration methods (bivariate scatter plots, ionic ratios diagrams, Piper diagram and Durov diagram) and maps showing the spatial distribution of water quality parameters in the study area, the main processes affecting groundwater quality have been deduced: mixing with seawater end member, cation exchange during salinization, dissolution of calcite and dolomite minerals in the aquifer matrix, and nitrate pollution mainly caused by the use of on-site sewage disposal systems, in particular pit latrines and septic tanks, as well as by the leaking sewerage system in the City Centre.

Stuyfzand classification clearly shows the significant geochemical differences between the area near the coastline and the area away from the coastline. Groundwater was classified into several categories by subtype, i.e., Sodium-Chloride, Sodium-Bicarbonate, Calcium-Bicarbonate, Magnesium-Bicarbonate, Sodium-Mix and Calcium-Mix. Most of shallow wells close to the shoreline have "Brackish-saline extremely hard NaCl" to "Brackish very hard CaCl" water. Groundwater types are from the inland toward the coast: CaMix, NaMix, and NaCl, showing increasing influence of salinity. Hydrochemical diversity among the groundwater samples in the study area is exposed by the Piper diagram. Groundwater evolution in the study area shows a curved path of hydrogeochemical evolution which begins from the Ca-HCO_3 water type, advancing through the Na-Ca-Cl water type to Na-Cl water type. Seawater intrusion results in Na^+ uptake by the exchange sites, releasing Ca^{2+}, and delivering the CaCl groundwater type. On the other hand, in the fresh waters, Na^+ is enriched indicating freshening of the aquifer as Ca^{2+} is replacing Na^+ on the exchange complex. Formation of $NaHCO_3$ water types provides evidence of freshening. Brackish and saline groundwater samples appearing in the mixing line on the Piper diagram have a Na–Ca–Cl major ion composition. Dissolution of calcite and dolomite in recharge areas results in fresh Ca–HCO_3 and Ca–Mg–HCO_3 groundwater types. Further along flow paths, Ca^{2+} and Na^+ ion exchange causes groundwater evolution to Na–HCO_3 type.

The saturation index for most of the groundwater samples shows mostly a tendency to precipitation for calcite and dolomite in the aquifer system. Saturation indices indicate the geology in the study area has a potential influence on the saturation status towards carbonate minerals. Most of the groundwater samples from the area adjacent to the coastline range from equilibrium to oversaturation with respect to carbonate minerals (calcite and dolomite). However, all groundwater samples are undersaturated with respect to sulphate minerals (gypsum and anhydrite) and halite.

From the calculated ionic ratios, it can be deduced that the chemical composition of groundwater in the study area is influenced by seawater intrusion. From the graph showing the relationship between Cl^-/HCO_3^- ratio versus Cl^- (Fig. 6.29) and the spatial distribution map of Cl/HCO_3 ratio (Fig. 6.30a-b), it is evident that the boreholes inland have a much lower ratio compared to the boreholes located near the coastline: this signifies saltwater intrusion into the aquifer at boreholes close to the coastline. On the other hand, groundwater samples with Na^+/Cl^- ratio less than that of seawater (0.86) (Fig. 6.31a) are attributed to depletion of Na^+ caused by cation exchange. This process is associated with saltwater intrusion in coastal aquifers. Ratios of Ca^{2+}/Mg^{2+} (Fig. 6.31b) and Ca^{2+}/Na^+ (Fig. 6.31c) are much higher than those of seawater, which indicates enrichment of Ca^{2+} by dissolution of carbonate minerals in the aquifer matrix and/or depletion of Na^+ due to cation exchange during mixing with seawater.

Contamination by seawater leads to the elevated Cl^- and EC values. High electrical conductivity (EC) and chloride (Cl^-) concentration values decrease away from the coastline. Fresh groundwater that is not affected by pollution is characterized by low values of EC, Cl^- and Ca–Mg–HCO_3 water type. The latter represents freshwater that has recently infiltrated into the zone of recharge, while the EC and Cl^- show a gradual increase from the west (recharge areas) towards the lowlands (discharge areas). Along the coastline, high values of EC and Cl^- are attributed to salinization by seawater intrusion. The groundwater EC and Cl^- values range from 138.4–2,200 μS/cm and 6.2–353 mg/l at distances greater than 2 km away from the coastline, to about 760–19,200 μS/cm and 72–15,478 mg/l at a distance of less than 2 km from the coastline, respectively. The former are related to areas such as Mbagala, Mtoni, Kurasini, Ilala and Mwananyamala, whereas the latter are related mainly to the areas close to the coastline such as City Centre, Oysterbay, Msasani and Masaki.

Groundwater samples collected in most of the boreholes drilled more inland show good quality of water in regard to salinity. Most of the boreholes near the coastline are drilled at shallow depth to minimize the possibility of meeting saline water. In areas close to the coastline such as Msasani, Oysterbay and City Centre, in 60% of sampled boreholes, drilling depths range from 10 to 20 meters. These boreholes are located within a distance of 1.5 km from the ocean. Samples from these boreholes show elevated chloride and sodium concentrations and comprise about 83% of the total of samples which are beyond the permissible chloride and sodium limits of WHO (2004) (Table 6.3). Due to their high solute concentrations, they are not suitable for domestic purposes, as they do not comply with the limits set by the WHO.

6.4.8 Suitability of groundwater quality for different uses

Groundwater in Dar es Salaam is used for domestic, industrial and irrigation purposes. The domestic water used for drinking should comply with WHO standards. Irrigation water is tested based on the Sodium Adsorption Ratio (SAR), EC, Soluble Sodium Percent (SSP), Cl^- and SO_4^{2-}. These evaluations will be made in the following part. Required groundwater quality for industrial purposes depends on the different industrial uses, and cannot be generalized. However, high salinity is undesirable.

6.4.8.1 Groundwater quality for drinking purposes

The parameters of concern in this study were chloride and nitrates levels in the drinking water. High chloride concentrations have been recorded in 71 boreholes/wells (equivalent to 36.41% of all samples). Chloride values down to 250 mg/l have adverse effect on the potable water (WHO, 2004). Mixing of seawater and fresh groundwater is the main process for the on-going saline water intrusion in the study area leading to the groundwater quality degradation. Furthermore, high levels of nitrate observed both in unconfined aquifer and semi-confined aquifer due to lack of proper sanitation do not comply with the limits set by WHO. NO_3^- ranges from 0.0–435.4 mg/l and 0.0–423.9 mg/l in unconfined and semi-confined aquifers respectively. 48.08% of samples from the unconfined aquifer exceed the permissible limit of WHO (2004) and 35.16% of semi-confined water samples are beyond the permissible limit.

Improper disposal of solid and liquid wastes, is leading to groundwater contamination. From the results of water analysis it is observed that many boreholes/wells located in the

unconfined boreholes have been affected by nitrate comparing to those located in the semi-confined aquifer (Table 6.3). This implies that the unconfined aquifer is more vulnerable to anthropogenic pollution than the lower aquifer. This is of particular concern to the people who use shallow drinking water wells (most of them located in the unconfined aquifer) that can be easily contaminated. About 75% of the city's residents live in unplanned and un-serviced settlements. General characteristics of these settlements include high population density, overcrowding, haphazardly laid out infrastructure and poor provision of basic services such as water supply and sanitation. Mainly residents living in these settlements use shallow wells for water supply and as well use pit latrines/septic tanks which are usually poorly constructed, causing health and major environmental problems.

6.4.8.2 Groundwater quality for irrigation purposes

The United States Department of Agriculture (USDA) (1954) classifies irrigation water with respect to its Sodium Adsorption Ratio (SAR). SAR is calculated from the following formula, all concentrations expressed in milli-equivalents per litre:

$$SAR = \frac{Na^{+}}{\frac{Ca^{2+} + Mg^{2+}}{2}}$$

The sodium hazard is low if the amount of calcium plus magnesium is high compared with the amount of sodium. Table 6.8 shows both the criteria for water irrigation classification based on SAR and the results obtained. The waters having SAR values less than 10 are considered as excellent, 10 to 18 as good, 18 to 26 as fair, and above 26 are unsuitable for irrigation use (USDA, 1954) (Table 6.8). The calculated SAR (Appendix 6.6) ranges from 0.11 to 93.40 in groundwater in the study area and almost all samples fall into excellent and good classes, except 9 samples which fall into doubtful and unsuitable class (Table 6.8). The outcome of USDA (1954) water irrigation classification on the basis of electrical conductivity (EC) is also indicated in Table 6.8. A great majority of samples in the study area fall into high salinity water (53%) and very high salinity water (25%) classes (Table 6.8).

Table 6.8: Classification of irrigation water according to USDA (1954).

Parameter	Range	Water Class	Number of samples	Percentage of total
SAR	<10	Excellent	160	81.63
	10-18	Good	27	13.78
	18-26	Doubtful	3	1.53
	>26	Unsuitable	6	3.06
EC (micro mhos/cm)	100 - 250	Low salinity water	4	2.04
	250 -750	Medium salinity water	39	19.90
	750 - 2250	High salinity water	103	52.55
	>2250	Very high salinity water	50	25.51

Fig. 6.38 represents the outcome. Water classification for irrigation in the study area was further defined according to USSL's diagram (US Salinity Laboratory Staff, 1954), which is widely used for rating irrigation waters: water can be grouped up to 16 classes (Fig. 6.8). It uses SAR (vertical axis) and EC (horizontal axis). The conductivity (horizontal axis) is classified into low (C1), medium (C2), high (C3) and very high (C4) salinity zones. The SAR (vertical axis) is subdivided into four classes, with decreasing limiting values as EC increases: low (S1), medium (S2), high (S3) and very high (S4) sodium hazard. The overall results based on the use of USSL's diagram are presented in Appendix 6.6. Table 6.9 shows the summary of groundwater classification based on USSL diagram. The results show that 61.73% of all samples from the study area were graded as suitable for irrigation use, while 13.78% as unsuitable in specific conditions. 24.49% of samples were regarded as unsuitable. Groundwater samples classified as C2-S1, C3-S1, C3-S2 and C4-S4 are the dominant classes.

Soluble Sodium Percentage (%Na), defined as the ratio of sodium to the total of cations, is also used to evaluate sodium hazard (Khodapanah et al. 2009). The %Na determines the ratio of sodium to total cations including sodium, potassium, calcium and magnesium. The %Na is calculated as follows:

$$\%Na = \frac{Na}{Na+K+Ca+Mg} X\ 100$$

All concentration values are expressed in milli-equivalents/l.

The values for %Na in the study area range from 5.96 to 90.60%. It is observed that 76 samples have very high sodium percentage (above 60%) (Table 6.10).

Table 6.9: Summary of groundwater classification based on USSL diagram (n=196).

No.	Category	No. of samples	Salinity/sodium hazard	Status for irrigation	%
1	C_1-S_1	4	Low salinity hazard-low sodium hazard	Suitable	61.73
2	C_2-S_1	39	Medium salinity hazard-low sodium hazard	Suitable	
3	C_3-S_1	78	High salinity hazard-low sodium hazard	Suitable	
4	C_4-S_1	4	Very high salinity hazard-low sodium hazard	Suitable in specific conditions	13.78
5	C_3-S_2	23	High salinity hazard-medium sodium hazard	Suitable in specific conditions	
6	C_4-S_2	14	Very high salinity hazard-medium sodium hazard	Unsuitable	24.49
7	C_3-S_3	7	High salinity hazard-high sodium hazard	Unsuitable	
8	C_3-S_4	1	High salinity hazard- very high sodium hazard	Unsuitable	
9	C_4-S_3	12	Very high salinity hazard-high sodium hazard	Unsuitable	
10	C_4-S_4	14	Very high salinity hazard-very high sodium hazard	Unsuitable	

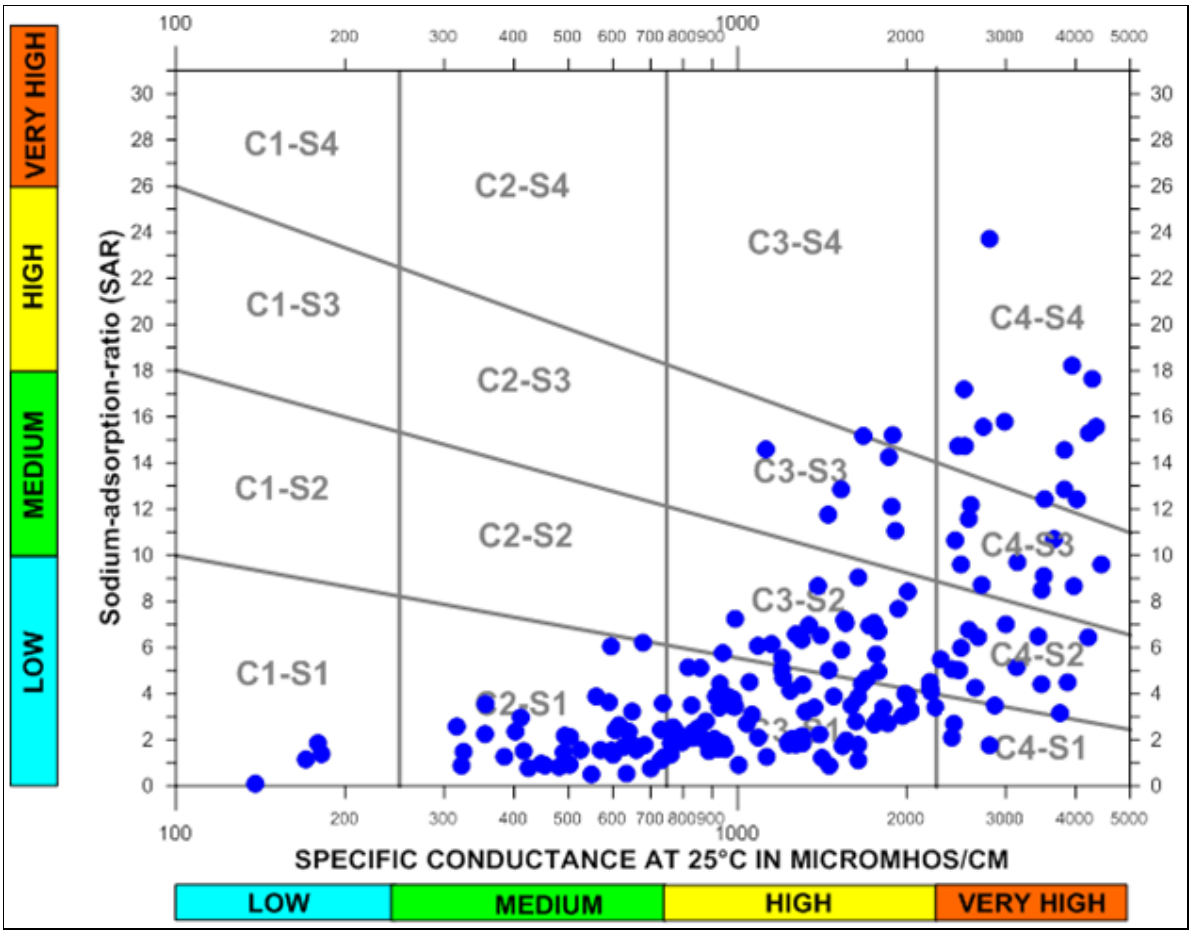

Figure 6.38: USSL (US Salinity Laboratory Staff, 1954) classification of irrigation water in relation to salinity and sodium hazard.

Table 6.10: Classification of water based on percent sodium (%Na).

Parameter	Range	Water Class	Number of samples	Percentage of total
%Na	< 20	Excellent	5	2.55
	20 - 40	Good	50	25.52
	40 - 60	Permissible	64	32.65
	60 - 80	Doubtful	61	31.12
	> 80	Unsuitable	16	8.16

Other parameters such as chloride and sulphate have been also used for assessment of suitability of water for irrigation (Sagnak, 1991). It is observed that 125 samples with respect to chloride concentration fall into excellent and good classes, while 24 samples fall into permissible class. 46 samples are considered to be doubtful or unsuitable (Table 6.11). For sulphate concentration, 185 samples fall into excellent and good classes, while 7 samples fall into permissible class. Only four samples are considered to be doubtful or unsuitable (Table 6.11).

Table 6.11: Irrigation water classes based on chloride and sulphate contents

Parameter	Range	Water Class	Number of samples	Percentage of total
Cl^- (mg/l)	< 142	Excellent	101	51.53
	142 - 249	Good	24	12.24
	249 - 426	Permissible	24	12.24
	426 - 710	Precaution usable	18	9.19
	>710	Unsuitable	29	14.80
SO_4^{2-} (mg/l)	<192	Excellent	174	88.78
	192 - 336	Good	11	5.61
	336 - 575	Permissible	7	3.57
	575 - 960	Precaution usable	2	1.02
	>960	Unsuitable	2	1.02

6.4.9 Groundwater quality at Kimbiji well

Dar es Salaam City had long been struggling with the unreliable Ruvu River as its main source of water and a rapidly growing demand for water. Due to unreliability of water from Ruvu River and due to the fact that Dar es Salaam Quaternary coastal aquifer (DQCA) is already overexploited, the discovery of the Kimbiji aquifer, found at considerable depths under the city, created prospects of an improved water supply. In view of the potential existence of a deep groundwater aquifer about 40 km west of Dar es Salaam (Fig. 2.13) which

can contribute to the water supply problem in Dar es Salaam (URT, 2007; Ruden, 2007), important follow-up questions remain. These questions related to the Kimbiji aquifer include:

i) Aquifer geometry: spatial and vertical extent of the aquifer system which include continuity under Dar es Salaam and interaction with DQCA;
ii) Aquifer recharge: recharge mechanism and quantities;
iii) Groundwater flow pattern: head gradients and flow directions, hydraulic interaction between deep and shallow aquifer zones including risks of cross-flows if future production and monitoring wells are improperly constructed;
iv) Sustainable abstraction rates and how the aquifer might be best developed;
v) Possible locations and interactions between freshwater and saltwater in coastal areas or offshore under present conditions and following medium-term aquifer development;
vi) Groundwater quality distribution within aquifer, both horizontally and with depth: possibility of more saline water at depth.

Groundwater sampling at Kimbiji well was conducted during this study at point PW1 (Fig. 2.13) and analysed in the Laboratory for Applied Geology and Hydrogeology of Ghent University, Belgium (Appendix 6.7). Compared to WHO international standards (2004), the water is well below allowable limits on all parameters except for HCO_3^- parameter. Some vital results are shown in Table 6.12. Generally, groundwater is potable in its natural state, only requiring disinfection before being delivered for household consumption.

Table 6.12: Hydrochemical parameters of groundwater at Kimbiji well (Neogene aquifer).

Parameter	**WHO international standards (2004)**	**Kimbiji well**
Ca^{2+} (mg/l)	200	1.49
Mg^{2+} (mg/l)	150	2.1
Na^+ (mg/l)	200	157
K^+ (mg/l)	200	6.5
SO_4^{2-} (mg/l)	250	14.54
HCO_3^- (mg/l)	240	301.95
Cl^- (mg/l)	250	66.12
NO_3^- (mg/l)	50	2.77
EC (µS/cm –25 ^oC)	1500	867
pH	6.5-9.2	8.62
TDS	600	581.6

6.4.10 Conclusions and Recommendations

6.4.10.1 Conclusions

Water samples from 196 groundwater boreholes/wells with depths ranging from 1.66 m to100 m below ground surface were tested. Results indicate that the Dar es Salaam quaternary coastal aquifer (DQCA) is experiencing contamination primarily by seawater intrusion due to overexploitation and the use of on-site sewage disposal systems, in particular pit latrines and septic tanks. Dissolution of calcite/dolomite minerals in the aquifer matrix in the recharge areas, as well as cation exchange modify the concentration of ions in groundwater.

High electrical conductivity (EC) and chloride (Cl^-) concentration values decrease from the coastline to inland. Fresh groundwater that is not affected by pollution is characterized by low values of EC and Ca–Mg–HCO_3 or Ca-HCO_3 water type. Hydrogeochemical data of unconfined samples are dominated by Na-Ca-Cl type with Cl^- as the dominant anion, due to the effect of seawater intrusion. The semi-confined groundwaters are slightly to moderately mineralized and are of Na-HCO_3 type induced mainly by ion exchange reactions. Based on Stuyfzand (1986) classification, over 50% of groundwater samples are categorized as hard and very hard.

The findings show that DQCA, bordering the Indian Ocean, is vulnerable to the influence of seawater intrusion, and is heavily affected by human influence due to groundwater overpumping. Overabstraction of groundwater to meet fresh water demand has contributed to the deterioration of the water quality by seawater intrusion. From the results, it is evident that most boreholes located close to the coastline, due to their high solute concentrations, are not suitable for domestic purposes. The increase of salinization limits the application of groundwater for both domestic and irrigation purposes. Furthermore, high levels of nitrate observed both in the unconfined aquifer and semi-confined aquifer due to lack of proper sanitation, do not comply with the limits set by WHO. Sulphate is another contaminant encountered in groundwater samples. The source of sulphates in groundwater is partly due to seawater (especially for boreholes/wells located near the coastline), oxidation of pyrite, improper disposal of solid and liquid wastes from industries and agricultural fertilizers.
The salinity and sodicity hazards of groundwater of DQCA were mainly classified as high salinity with medium sodicity problems. Other factors such as soil and crop types need to be

considered, since they play an important role in deciding on the suitability of water for irrigation.

6.4.10.2 Recommendations

Urban and industrial development continue to expand in the coastal areas of Dar es Salaam. These research results are useful for making better groundwater protection and exploitation plans for limiting the increasing saltwater intrusion and anthropogenic aquifer contamination. Application of rational groundwater management practices, including the decrease of pumping rates, is crucial in attaining the sustainability of groundwater resources in the study area.

All sewage should be treated before being discharged into the environment. In order to improve and expand the sanitation services, devoted efforts are needed to enhance intersectoral coordination and cooperation, and frameworks facilitating stakeholder participation

Decreasing of groundwater supply from the Quaternary aquifer can be compensated by exploitation of the Kimbiji Neogene aquifer which shows good quality of water. However important questions pertaining to the aquifer geometry, source of water recharge to the aquifer, groundwater flow pattern, groundwater quality and sustainable abstraction rates must be dealt with. Furthermore, establishing a groundwater monitoring program close to the coast is equally important, based on which, measures may be taken to avoid the advancement of seawater intrusion on a large scale.

7 SIMULATION OF SEAWATER INTRUSION IN COASTAL AQUIFER IN RESPONSE TO GROUNDWATER ABSTRACTION

7.1 Modelling of seawater intrusion in coastal aquifers

Seawater intrusion is a common contamination problem in coastal areas. It affects, mainly, arid and semi-arid zones, where high population and urbanization are coupled to scarce water resources and resorting to intense exploitation of groundwater. Numerical models provide effective tool to understand groundwater problems.

The seawater intrusion mechanism in coastal aquifers generally causes the occurrence of a freshwater zone over a seawater zone. Intrusion of saline water occurs where saline water dislocates or mixes with fresh water in an aquifer. Groundwater overexploitation through the wells that are located near the shoreline is a major cause of seawater intrusion. Seawater, because of its higher density (1.025 g/ml), goes inland under a relatively low density freshwater (1.0 g/ml). Density dependent flow or variable density flow is the term that classifies the flow pattern influenced by density differences in the fluid system (Lebbe, 1996; Vandenbohede, 2008). Proper simulation of density-dependent phenomena in groundwater flow and transport relies on coupled models that incorporate the constitutive relationship between solute concentration and density (Paniconi et al., 2001). Darcy's law presented in equation 7.1 is the foundation of groundwater flow models.

$$q = -K\nabla h \qquad 7.1$$

Where: q = the flow rate, K = hydraulic conductivity, and ∇h = the hydraulic gradient.

The horizontal and vertical components q_{hi} and q_{vi} of the Darcian velocity at a point i are presented in equations 7.2 (Lebbe, 1996).

$$q_{hi} = K_{h_{fi}} \frac{\mu_f}{\mu_i} \frac{\partial h_{fi}}{\partial x} \quad q_{vi} = K_{v_{fi}} \frac{\mu_f}{\mu_i} \left(\frac{\partial h_{fi}}{\partial z} + \frac{\delta_i - \delta_f}{\delta_f} \right) \qquad 7.2$$

K_{hfi} and K_{vfi} are the horizontal and vertical conductivity for freshwater, δ_f and δ_i are the densities of the freshwater and of the water at point i and μ_f and μ_i are their dynamic

viscosities, $\partial h_{fi}/\partial x$ and $\partial h_{fi}/\partial z$ are the vertical and the horizontal freshwater head gradients and $(\delta_i - \delta_f)/\delta_f$ is the buoyancy at point i.

Under natural conditions, aquifer recharge is in equilibrium with groundwater discharge (Fig. 7.1). Near the shoreline, this equilibrium shows a salt-water wedge inland, under the freshwater, because of the higher density of the seawater. When groundwater is pumped from coastal aquifers, freshwater that is discharging into the sea is intercepted, disrupting the natural equilibrium. In order to manage saltwater intrusion, it is important to first understand, among others, the physical mechanisms by which saltwater intrusion occurs. The understanding of saltwater intrusion mechanisms will help to establish sustainable groundwater development scenarios. Saltwater intrusion causes the zone of diffusion (mixing zone between fresh and saltwater) to migrate landward and/or locally upward. This research presents simulation of seawater intrusion in a coastal aquifer in response to groundwater abstraction, inspired by the case of Dar es Salaam aquifer.

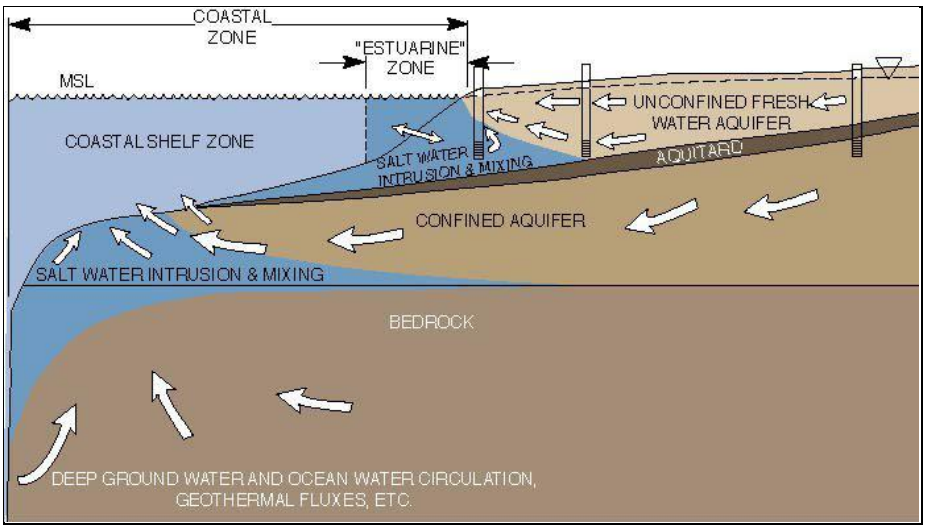

Figure 7.1: Cross-sectional views of the coastal zone, illustrating the types and pathways of fluid movements (Buddemeier, 1996).

7.2 Objective of the modelling

The objective of the modelling was to assess how a coastal aquifer system, such as the Dar es Salaam aquifer, responds to abstraction and whether the groundwater abstraction will induce seawater intrusion. It was intended to simulate typical coastal pumping situations. Average conditions in the Dar es Salaam Quaternary Aquifer system were used as input to the model.

It is a conceptual model for the problem-based learning on the impact of groundwater overpumping causing salinization. Specific objectives include:

i) to simulate typical coastal pumping situations
ii) to study the impact of distance between pumping and shoreline
iii) to study the impact of depth of pumping wells
iv) to study the impact of the existence of a semi-pervious layer in the aquifer system

7.3 SEAWAT code description

The SEAWAT program was developed to simulate three-dimensional, variable-density, transient groundwater flow in porous media and was first published by Guo and Bennett (1998). The source code for SEAWAT was developed by combining MODFLOW and MT3DMS into a single program that solves the coupled flow and solute-transport equations (Guo and Langevin, 2002). The SEAWAT program has been substantially improved since it was first published. Major improvements from the previous version of SEAWAT by Guo and Bennett (1998), include (Guo et al., 2002): i) reformulation of the flow equation based on the conservation of mass, ii) modification of stress packages to allow variable-density sources and sinks, and iii) incorporation of an implicit coupling procedure between the flow and solute-transport equations.

As documented in Langevin et al. (2003), the first version of SEAWAT was developed using MODFLOW-88 (McDonald and Harbaugh, 1988) and MT3D (Zheng, 1996). The second version of SEAWAT documented by Guo and Langevin (2002) and published by the U.S. Geological Survey (USGS) used MT3DMS (Zheng, 1996), including improvements in the representation of the flow equation and boundary fluxes comparing to MT3D (Langevin et al., 2003). The third version of SEAWAT, referred to as SEAWAT-2000 (Langevin et al., 2003), is a combined version of MODFLOW-2000 (Harbaugh et al., 2000) and MT3DMS. The SEAWAT code follows a modular structure, and thus, new capabilities can be added with only minor modifications to the main program (Guo and Langevin, 2002).

SEAWAT uses an implicit finite-difference approximation to solve the groundwater flow equation, and contains several alternative methods for solving the solute-transport equation, including implicit and explicit finite-difference methods (Langevin et al., 2004). With the explicit procedure, the flow equation is solved first for each time step, and the resulting

advective velocity field is then used for solving the solute-transport equation. This procedure for alternately solving the flow and transport equations is repeated until the stress periods and simulation are complete. Example of this is the study by Paritsis (2005), comprising MT3DMS runs for a time step, and then MODFLOW runs for the same time step using the last concentrations from MT3DMS to calculate the density terms in the flow equation (Paritsis, 2005). For the next time step, velocities from the current MODFLOW solution are used by MT3DMS to solve the transport equation: for most simulations, the one-step lag does not introduce significant error and the error can be reduced by decreasing the length of the time step (Paritsis, 2005). With the implicit procedure for coupling, the flow and transport equations are solved multiple times for the same time step until the maximum difference in fluid density between consecutive iterations is less than a user-specified tolerance.

Governing equations for the 3-D density-dependent miscible flow and transport equations (Guo and Langevin, 2002) for a coastal aquifer may be written as follows (Guo and Langevin, 2002):

Flow equation $$-\nabla\ \rho q\ +\ \rho q_s\ =\ \frac{\partial\ \rho\theta}{\partial t} \quad 7.3$$

Transport equation $$-\nabla\ D(\nabla \mathrm{c}) - \nabla\ vc\ +\ \frac{q_s}{\theta} C_s\ =\ \frac{\partial C}{\partial t} \quad 7.4$$

Where ∇ is the gradient operator:

$$\frac{\partial}{\partial x} + \frac{\partial}{\partial y} + \frac{\partial}{\partial z};\ q_x = \frac{k_x}{\mu}\frac{\partial P}{\partial x}\ ;\ q_y = \frac{k_y}{\mu}\frac{\partial P}{\partial y}\ ;\ q_z = \frac{k_z}{\mu}\ \frac{\partial P}{\partial z} + \rho g\ ;$$

ρ is the variable fluid density [M L^{-3}]; q is the specific discharge vector [L T^{-1}]; ρ is the density of water entering from a source or leaving through a sink [M L^{-3}]; q_s is the volumetric flow rate per unit volume of aquifer representing sources/sinks [T^{-1}]; θ is porosity [-]; t is time [T]; c is solute concentration [M L^{-3}]; q_x, q_v, q_z are the individual components of specific discharge; μ is the dynamic viscosity [M L^{-1} T^{-1}]; k_x, k_y, k_z represent intrinsic permeabilities [L^2] in the three coordinate directions; g is the gravitational constant [LT^2] and treated here as positive scalar quantity; P is the fluid pore pressure [$ML^{-1}T^{-2}$]; D is the dispersion coefficient [L^2T^{-1}]; v represents the seepage velocity [LT^{-1}]; θ is porosity; and C_s is concentration of water entering from a source or leaving through a sink [ML^{-3}].

SEAWAT which is a public-domain computer program is well suited for the modelling objectives of this study. Thus SEAWAT code has been chosen in this study to simulate the variable-density groundwater flow under the different pumping scenarios.

7.4 Model setup and input

7.4.1 Model discretization and grid

The model is a schematic generalized cross-section model perpendicular to the coastline with an average reservoir buildup and boundary conditions, based on the case of Dar es Salaam aquifer (Fig. 7.2). The model domain encloses an area 2500 m long (2000 m inland and 500 m into the sea) and average reservoir thickness of 150 m. The model domain consists of 100 columns and 30 rows, and one layer simulated with or without an intercalated semi-pervious layer, reflecting the effect of the intercalated semi-pervious layer in the coastal Dar es Salaam Quaternary Aquifer system, which in some places is present, while in others it is not.

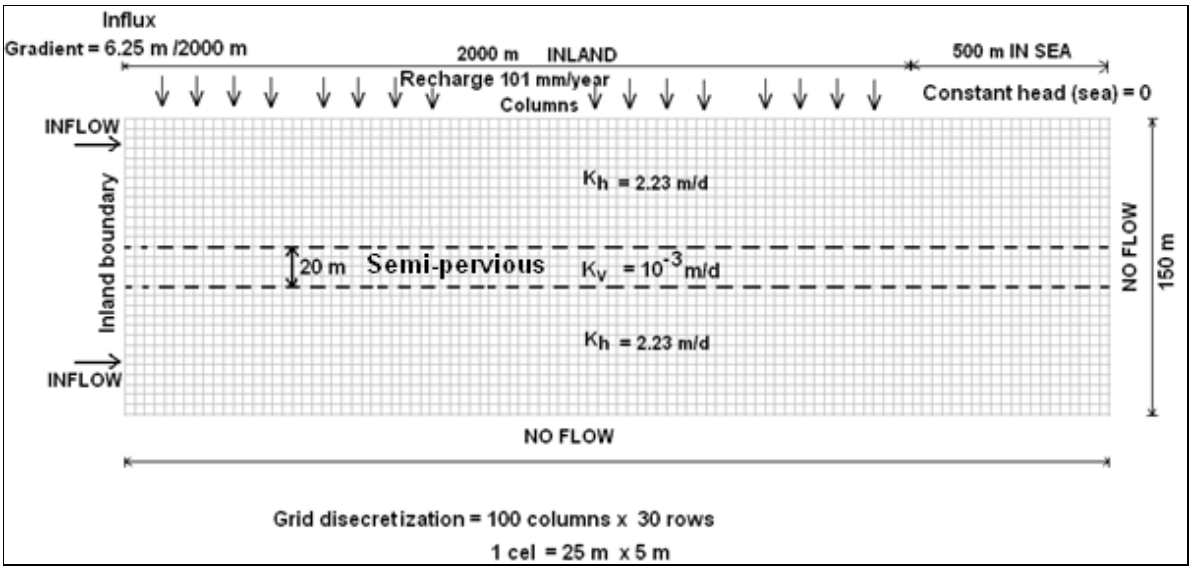

Figure 7.2: Schematization of the aquifer system in the model and boundary conditions.

7.4.2 Hydraulic parameters

The value of hydraulic conductivity of 2.23 m/day was taken from the previous study from the regional groundwater flow model of Dar es Salaam aquifer (Van Camp et al., 2013). In the scenario with a semi-pervious layer, a 20 m thick layer, halfway in the aquifer is added with a vertical hydraulic conductivity of 0.001 m/d (Fig. 7.2). The porosity of 0.30 is uniform and longitudinal dispersivity is 2 m. Ratio of vertical to horizontal dispersivity is 0.1.

7.4.3 Boundary conditions

The boundary conditions of the aquifer bottom (substratum) are set to no-flux, while the aquifer top is a recharge boundary by direct infiltration, with recharge value of 101 mm/year, taken from the regional groundwater flow modeling study of Dar es Salaam aquifer (Van Camp et al., 2013). The east boundary, 500 m from the coast, within the Indian Ocean, is approximated as zero-flux border. The west boundary (inland side) is subject to constant freshwater inflow, estimated based on the piezometric contour gradient of 6.25m/2000 m. This gradient is derived from the regional groundwater flow model, which was calibrated on measured piezometric levels (Van Camp et al., 2013). At the sea side, the aquifer system is in contact with the seawater body at the reference salt concentration of 35 grams/liter.

In the simulations, a pumping rate of 1.5 m^3/d/m was chosen. As the model is two dimensional, its rate cannot be straightforward recalculated to extraction rates on a regional scale. The used value was chosen only to obtain a clear seawater intrusion effect within the simulated time period of 100 years. Higher rates will increase the intrusion effect and reduce the time span in which intrusion develops.

7.4.4 Initial seawater distribution

The starting concentration distribution for each scenario was calculated during a “spin up” simulation with pre-pumping boundary conditions, until a near steady state salinity distribution was obtained. This needed 200 to 300 years of time to be established. Next, upon pumping, an increased saltwater wedge develops into the inland part of the aquifer. The absence or presence of a semi-pervious layer in the aquifer has a remarkable effect on the development of this wedge, both in size and in shape.

7.5 Studied scenarios

Table 7.1 represents different scenarios which were considered in the simulation. Symbols have been provided in the table to facilitate identification of figures that were generated in the simulation. Two types of simulations were considered: i) single layer aquifer (150 m thick), and ii) occurrence of semi-pervious layer (20 m thick) at the depth between 65 m and 85 m. For both cases, simulations were performed for a constant rate of pumping (1.5 m^3/day/m) for a period of over 100 years.

Table 7.1: Pumping scenarios (Key: SU: pumping from upper part of the aquifer, SL: pumping from lower part of the aquifer, and, SWU: pumping from upper layer above the semi-pervious layer).

PUMPING SCENARIOS	**SIMULATION WITHOUT SEMI-PERVIOUS LAYER**			**SIMULATION WITH SEMI-PERVIOUS LAYER**
Distance	500 m from the shore line	1000 m from the shore line	1500 m from the shore line	500 m from the shore line
Pumping rate	1.5 m^3/day/m	1.5 m^3/day/m	1.5 m^3/day/m	1.5 m^3/day/m
Year 0	Pre-pumping (PRE-1)			Pre-pumping (PRE-2)
20 years	SU-500m-20y	SU-1000m-20y	SL-1500m-20y	SWU-500m-20y
40 years	SU-500m-40y	SU-1000m-40y	SL-1500m-40y	SWU-500m-40y
60 years	SU-500m-60y	SU-1000m-60y	SL-1500m-60y	SWU-500m-60y
80 years	SU-500m-80y	SU-1000m-80y	SL-1500m-80y	SWU-500m-80y
100 years	SU-500m-100y	SU-1000m-100y	SL-1500m-100y	SWU-500m-100y

7.5.1 Aquifer setup without semi-pervious layer

7.5.1.1 Pumping at 500 m distance from the shoreline in upper part of aquifer

Fig. 7.3a presents the pre-pumping situation of the aquifer setup without semi-pervious layer. From the pre-pumping situation (Fig. 7.3a), it can be observed that, even without pumping, a seawater wedge is present inland (about 400 m from shoreline), due to density driven flow. Fig. 7.3b presents a scenario whereby the pumping well is located at 500 m distance from the shoreline in the upper part of the aquifer. As a result of pumping, the interface rises towards the pumping well causing interface upconing, as is well observed after 20 years of constant pumping at a rate of 1.5 m^3/day/m (Fig. 7.3b), and the seawater wedge has advanced for another 200 m inland, additional to the pre-pumping situation. Continuous pumping causes the interface to rise to successively higher levels and within 40 years of pumping the saltwater interface is already reaching the well (Fig. 7.3c). After 28 years of pumping, the chloride concentration in the well had increased from 0 to 250 mg/l (corresponding to 0.454 g/l salinity), which is the limit for drinking water (WHO, 2004; EU, 1998) (Fig. 7.3g). Beyond 28 years of pumping, water quality is not suitable for drinking. Within 20 years of pumping,

water quality has changed from fresh to fresh-brackish due to upconing which is caused by movement of brackish water (from the freshwater/seawater interface) to the pumping well (Fig. 7.3b). The effect of pumping observed after 40 years (Fig. 7.3c) to 60 years (Fig. 7.3d) is causing water quality to change from fresh-brackish to brackish. Due to constant pumping beyond 80 years (Figs. 7.3e-f), it can be observed that seawater is completely invading the well. Fig. 7.3g indicates high values of salinity of 5.7 g/l and 7 g/l after 80 years and 100 years of constant pumping respectively.

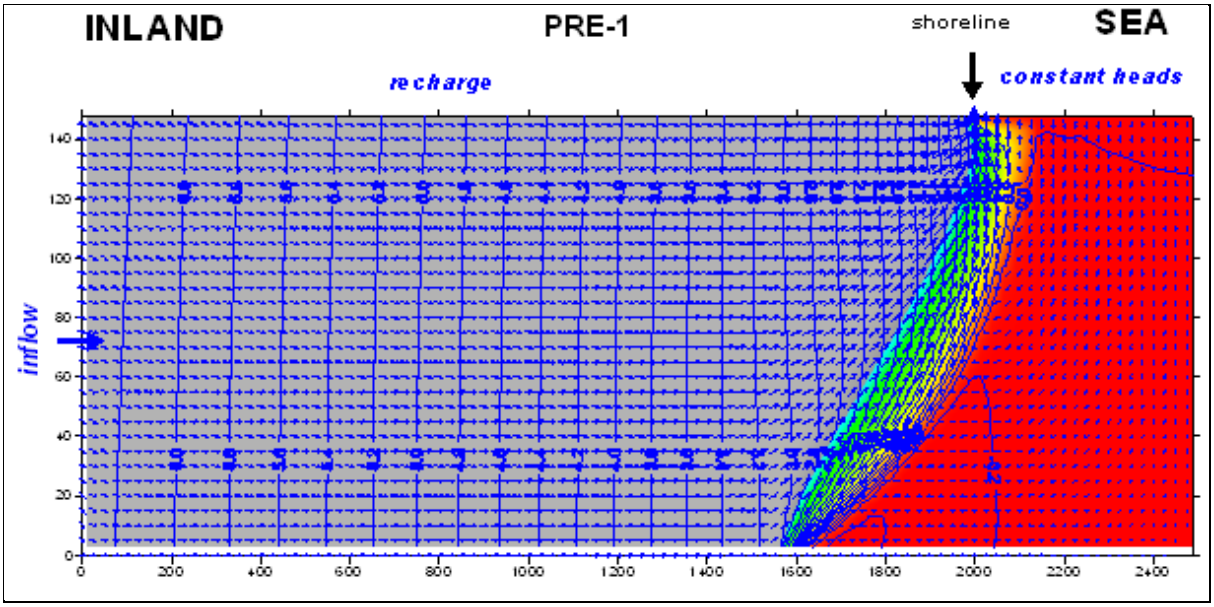

Figure 7.3(a): Pre-pumping situation (= year "zero"). Steady-state concentration distribution after 200 years of simulation. Aquifer setup without semi-pervious layer.

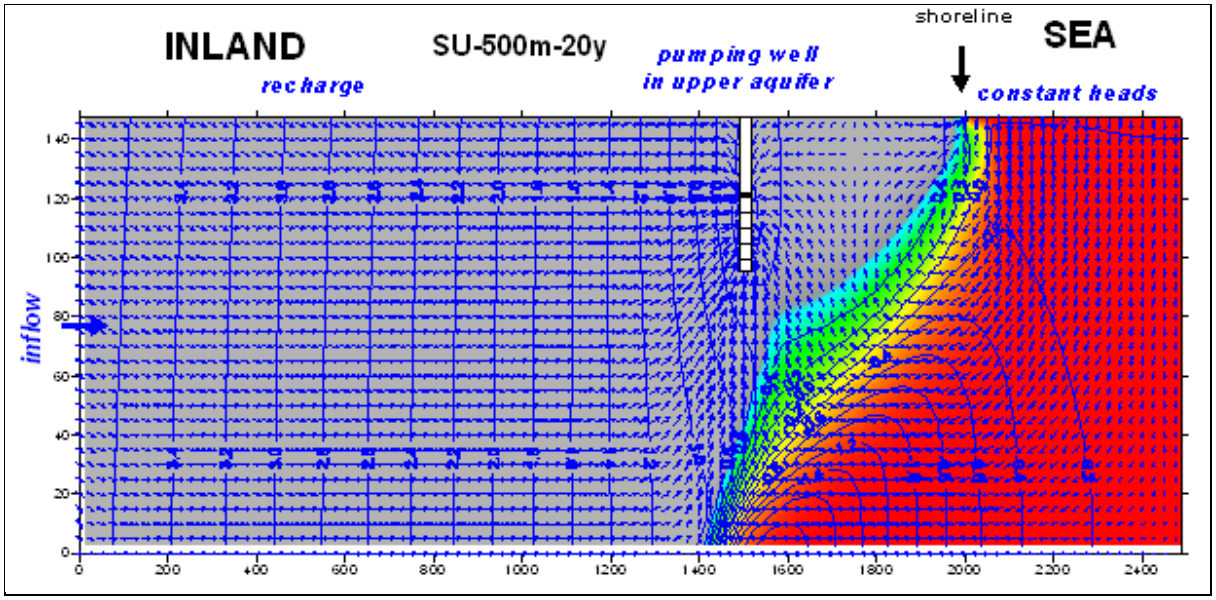

Figure 7.3(b): Situation after 20 years of pumping in upper part of the aquifer for the well located at 500 m from the shoreline. Aquifer setup without semi-pervious layer.

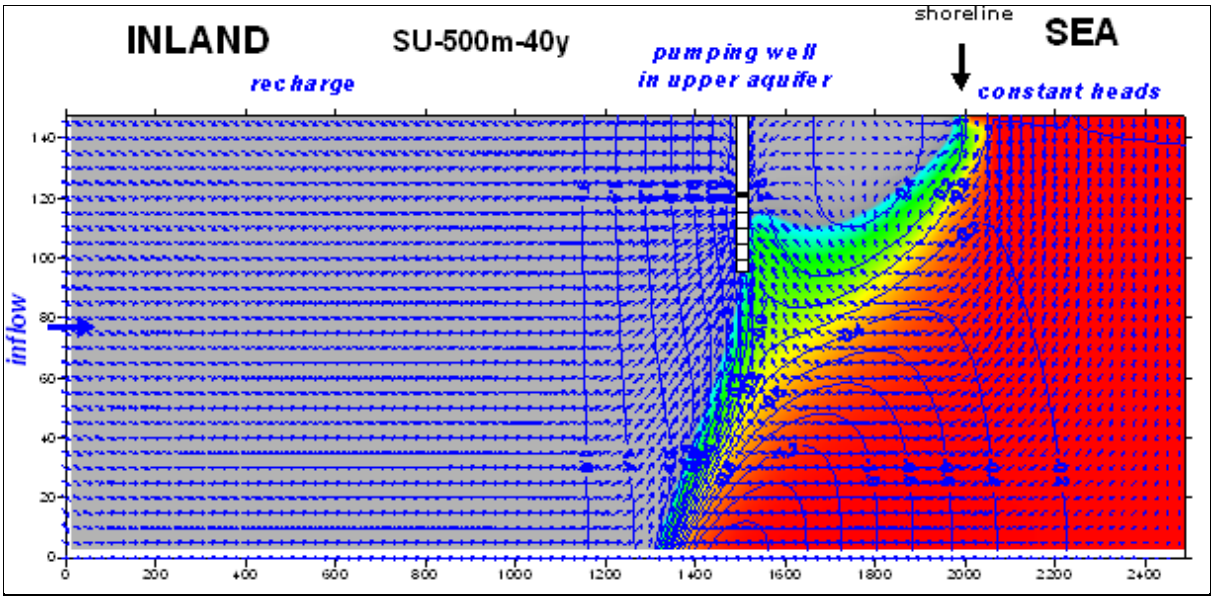

Figure 7.3(c): Situation after 40 years of pumping in upper part of the aquifer for the well located at 500 m from the shoreline. Aquifer setup without semi-pervious layer.

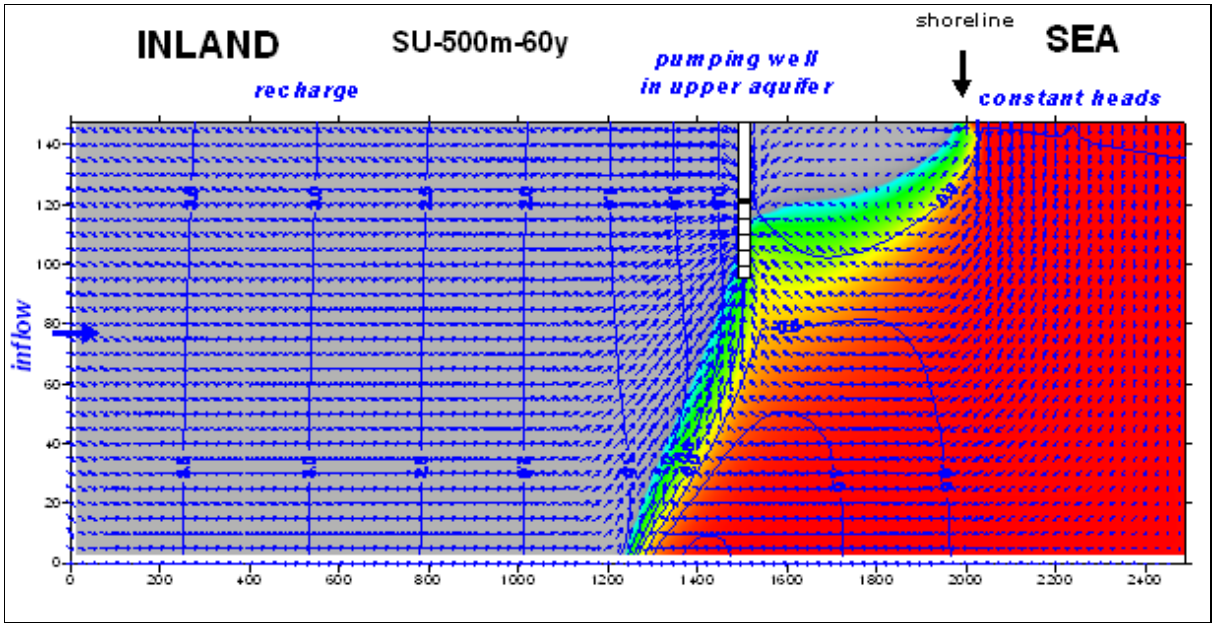

Figure 7.3(d): Situation after 60 years of pumping in upper part of the aquifer for the well located at 500 m from the shoreline. Aquifer setup without semi-pervious layer.

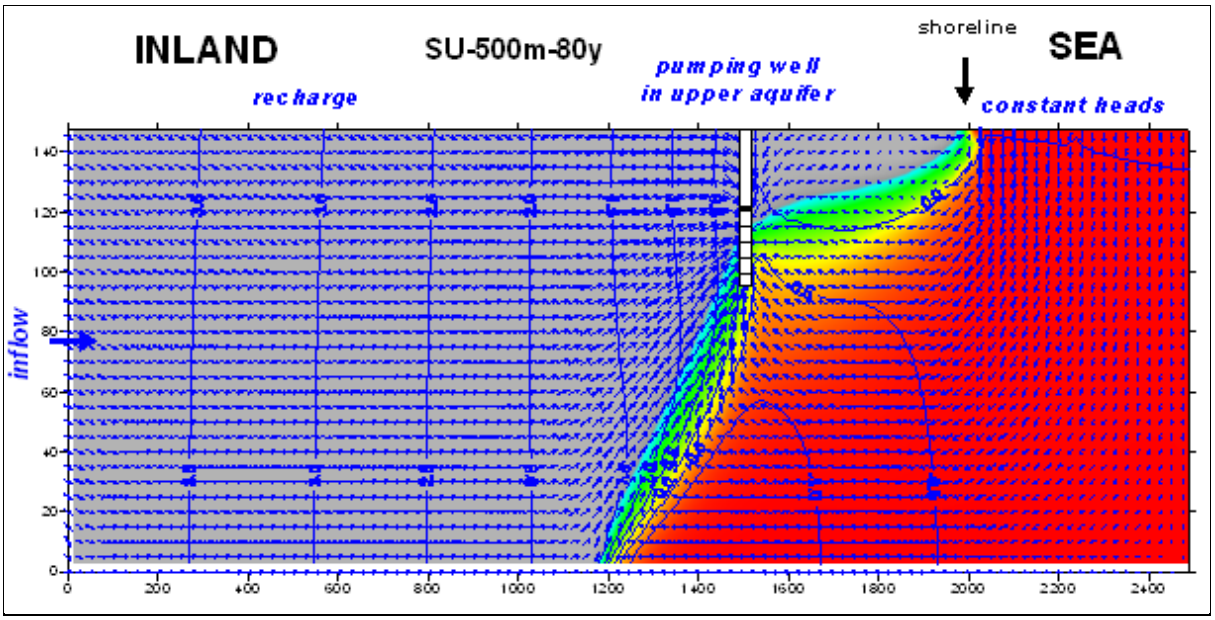

Figure 7.3(e): Situation after 80 years of pumping in upper part of the aquifer for the well located at 500 m from the shoreline. Aquifer setup without semi-pervious layer.

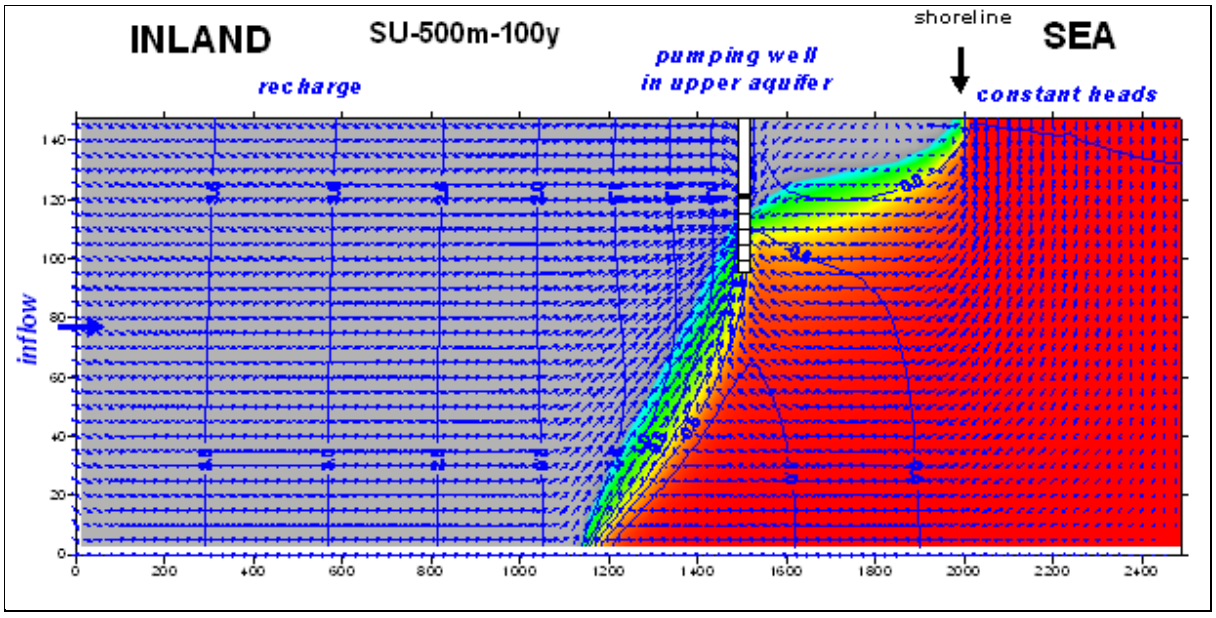

Figure 7.3(f): Situation after 100 years of pumping in upper part of the aquifer for the well located at 500 m from the shoreline. Aquifer setup without semi-pervious layer.

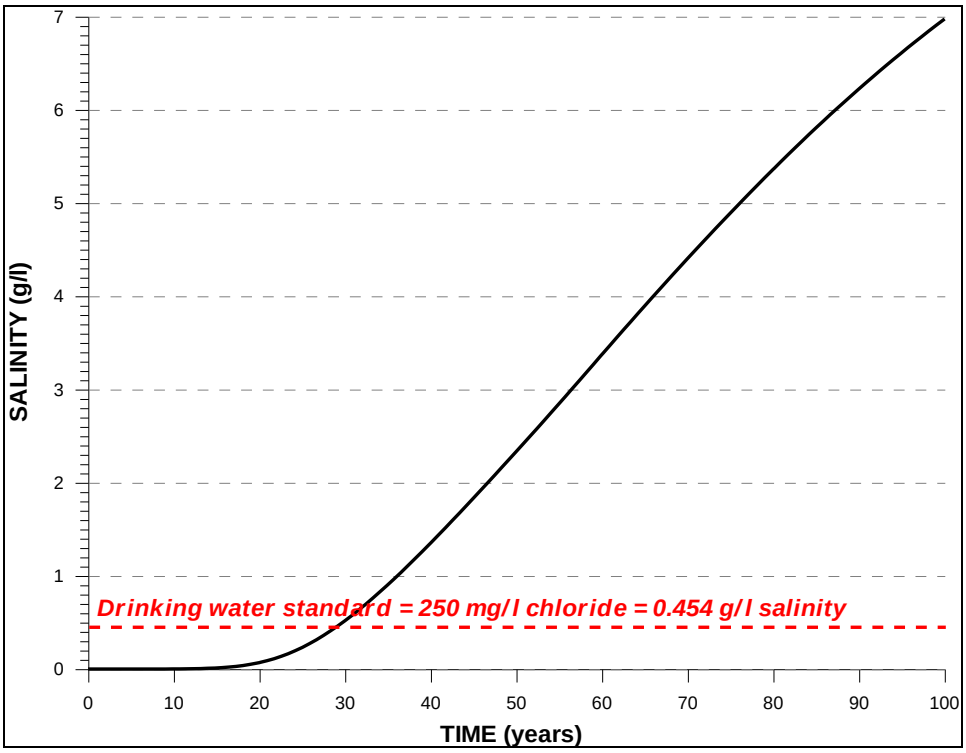

Figure 7.3(g): Evolution of salinity (TDS) in a pumping well located at 500 m from the shoreline and tapping water from the upper part of the aquifer for the case of single layer setup (without semi-pervious layer). Drinking Water Standard = 250 mg/l chloride (0.454 g/l salinity) (WHO, 2004; EU, 1998).

7.5.1.2 Pumping at 1000 m distance from the shoreline in upper part of aquifer

In this scenario the pumping well is located in the upper part of the aquifer, around 600 m inland from the tip of the saltwater wedge, present in the pre-pumping situation. Fig. 7.4(a) shows conditions after 20 years of constant pumping. The seawater wedge has advanced 300 m more compared to the pre-pumping situation (Fig. 7.3a). For the case where the well is located 500 m from the shoreline, advancement of the seawater wedge for 300 m is occurring only after 40 years (Fig. 7.3c). This means that, with increasing distance of the pumping well from the shoreline, the seawater wedge, in the first stage, advances more laterally toward the direction of the well, before upconing begins. This situation can clearly be seen in the salinity evolution in Fig.7.4 (f). Salinity starts to increase in the well after 52 years, compared to the first change of salinity which was documented already after 16 years (Fig. 7.3g) of pumping, when the well is located at 500 m from the shoreline. In the well at 500 m from the shoreline, the value of salinity exceeded the limit of the drinking water standard (WHO, 2004; EU, 1998) after 28 years of pumping (Fig. 7.3g), whereas in the well located at 1000 m from the shoreline, this is happening after 80 years of pumping (Fig. 7.4f). In the latter case it takes many years for the change in salinity to be noticed in the pumping well, but afterward it

increases fast. Yet, salinity is increasing in the aquifer, long before this is observed in the well. This suggests that groundwater monitoring is important not only in the upper part of the aquifer, but also in its lower part, in order to detect a lateral advancement of the seawater wedge. After 40 years of pumping (Fig. 7.4b), the seawater wedge has penetrated 500 m more inland compared to the pre-pumping situation. Upconing is observed in Fig. 7.4 (c) after 60 years of pumping and salinity increase in the well starts after 52 years of pumping (Fig. 7.4f). Continued pumping causes upconing of the fresh-salt interface to rise to successively higher levels reaching the well (Fig. 7.4d). After 80 years of pumping, the seawater wedge has advanced for 700 m more, compared to the pre-pumping situation. More upconing is observed in Fig. 7.4 (e) after 100 years, when the seawater wedge has advanced for 800 m more inland. Within a period of 48 years (52-100 years of pumping), the salinity has changed from almost zero up to 1.45 g/l (Fig. 7.4f): this same evolution happened in a period of 24 years (16-40 years of pumping) for the well located at 500 m from the shoreline. For the latter, the salinity level of 1.45 g/l was reached within the first 40 years of pumping, whereas for the former, it was attained after 100 years of pumping.

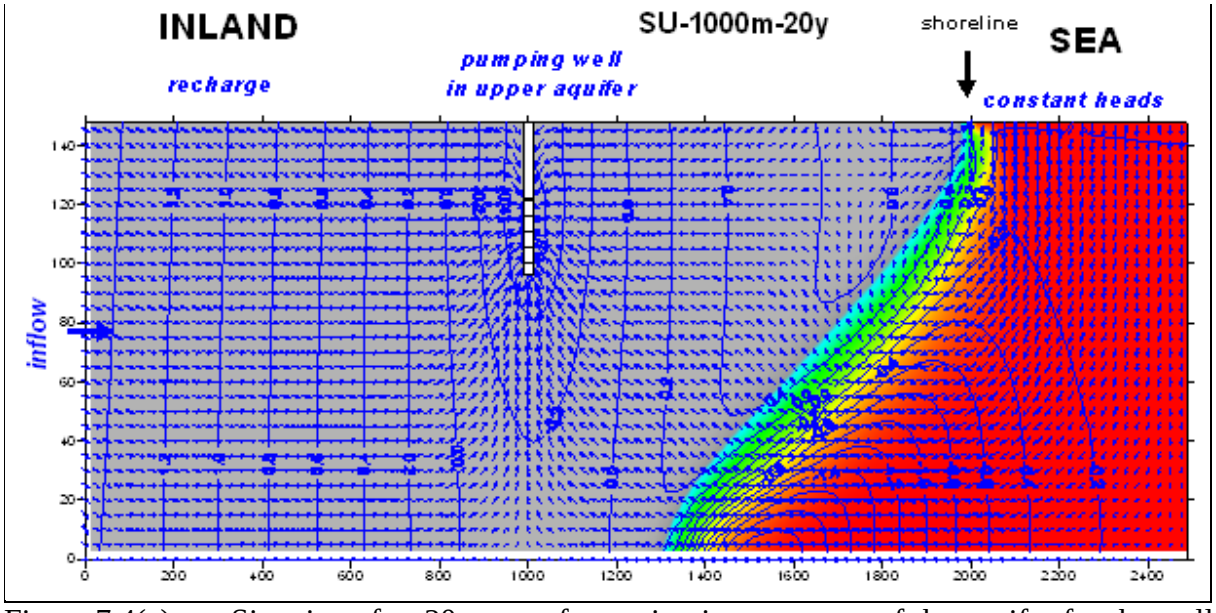

Figure 7.4(a): Situation after 20 years of pumping in upper part of the aquifer for the well located at 1000 m from the shoreline. Aquifer setup without semi-pervious layer.

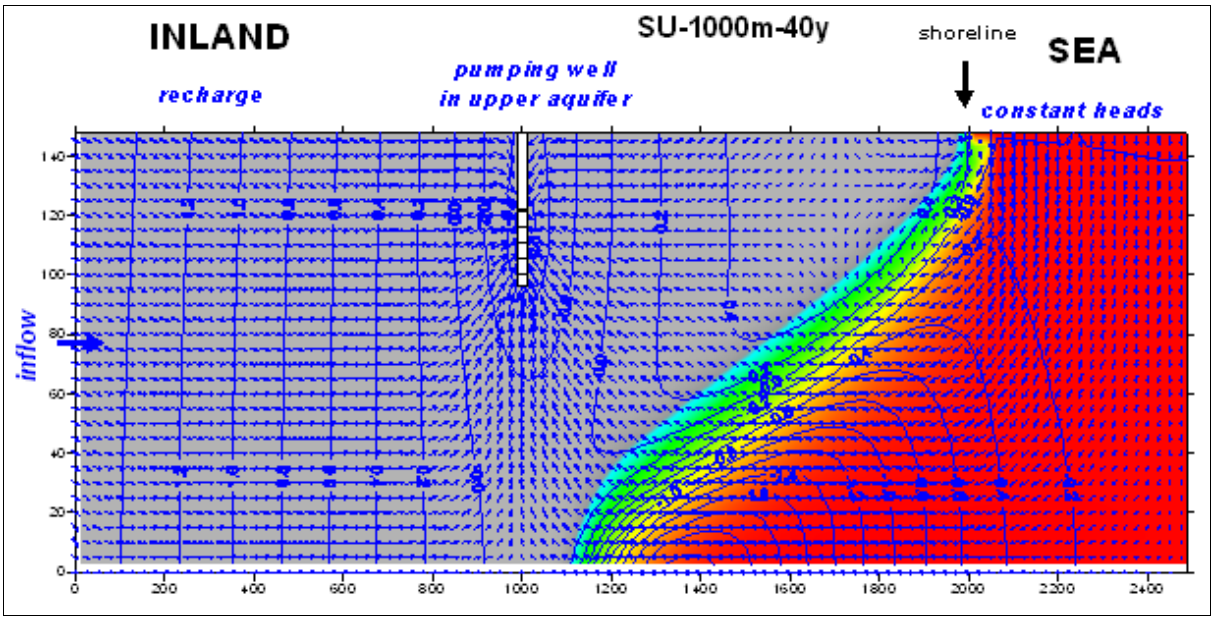

Figure 7.4(b): Situation after 40 years of pumping in upper part of the aquifer for the well located at 1000 m from the shore line. Aquifer setup without semi-pervious layer.

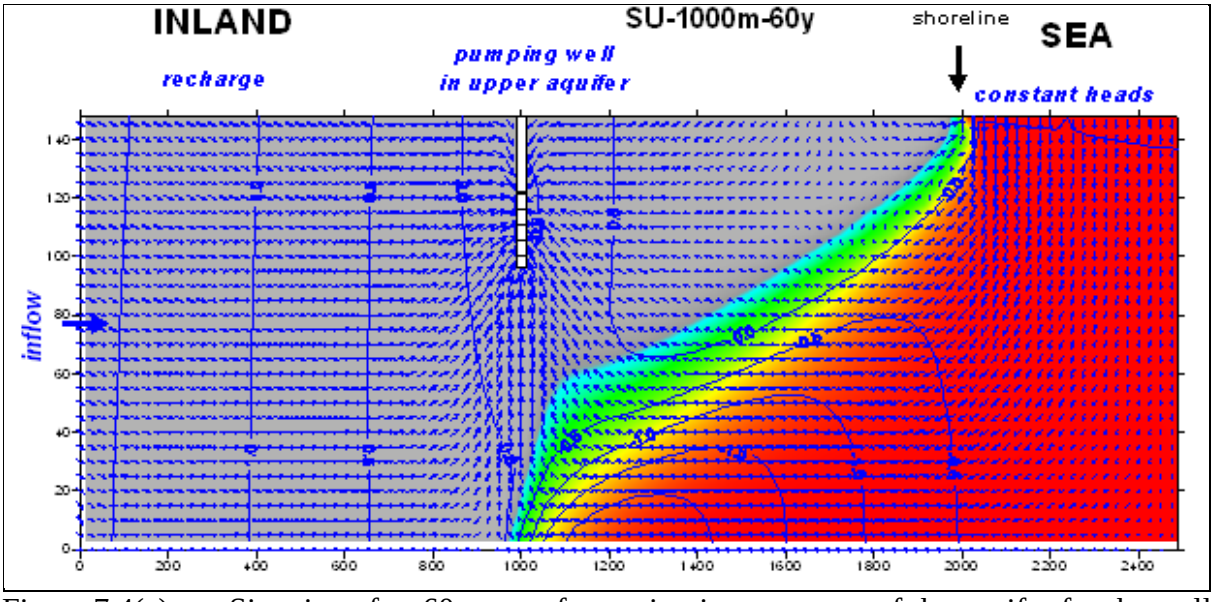

Figure 7.4(c): Situation after 60 years of pumping in upper part of the aquifer for the well located at 1000 m from the shoreline. Aquifer setup without semi-pervious layer.

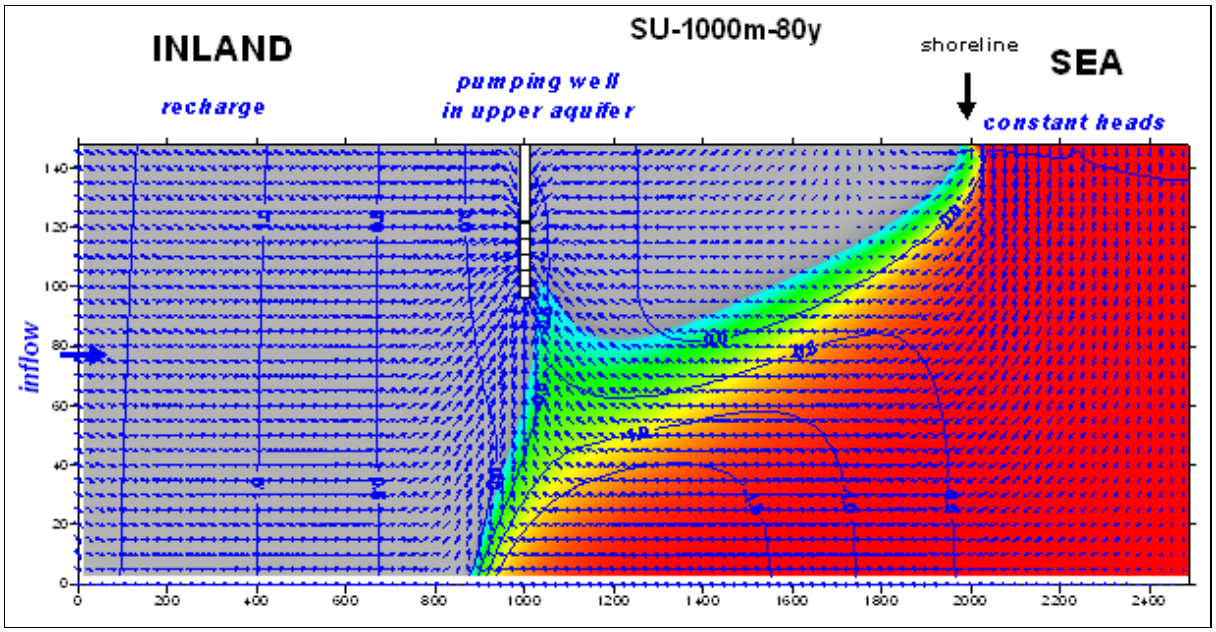

Figure 7.4(d): Situation after 80 years of pumping in upper part of the aquifer for the well located at 1000 m from the shoreline. Aquifer setup without semi-pervious layer.

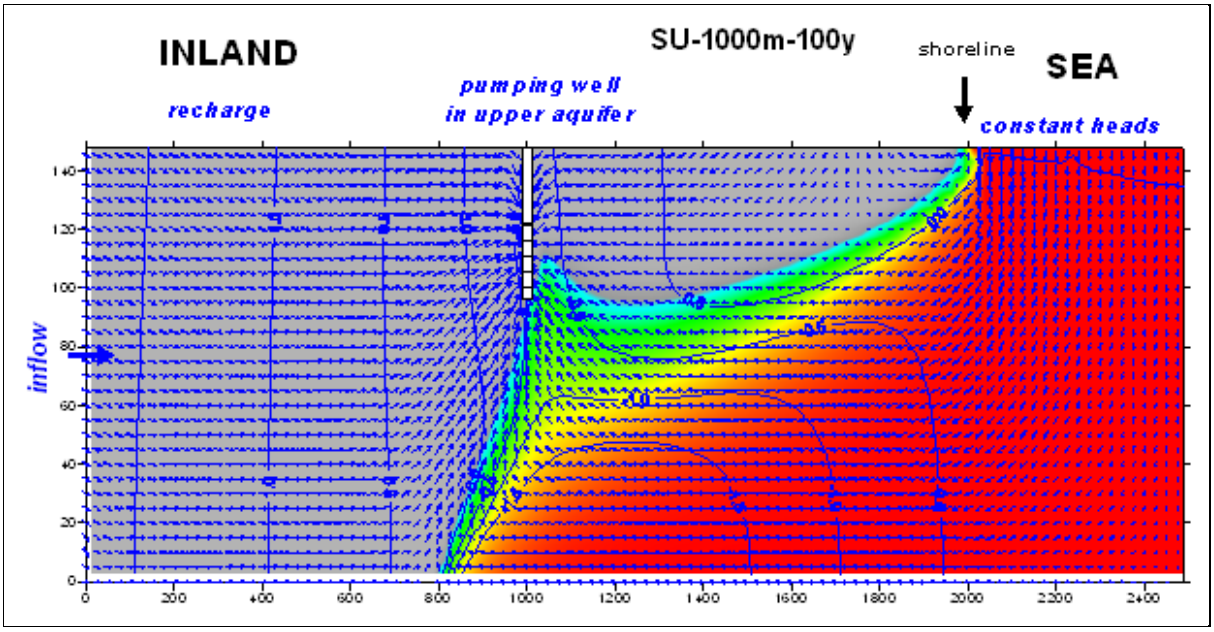

Figure 7.4(e): Situation after 100 years of pumping in upper part of the aquifer for the well located at 1000 m from the shoreline. Aquifer setup without semi-pervious layer.

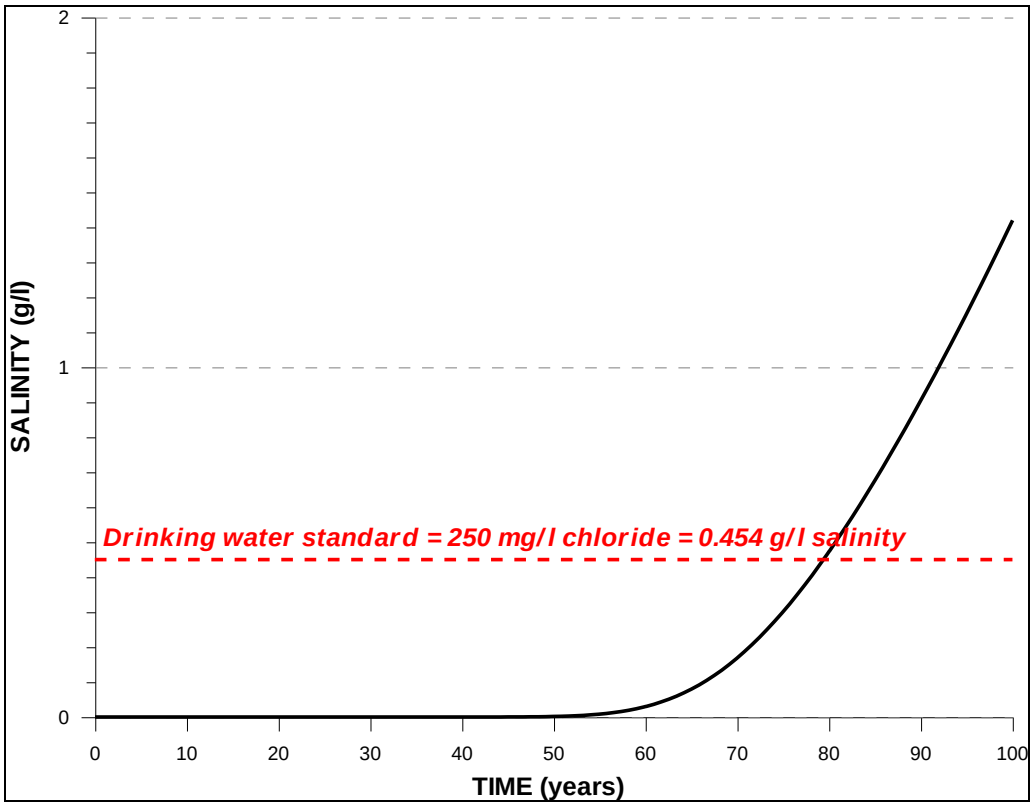

Figure 7.4(f): Evolution of salinity (TDS) in a pumping well located at 1000 m from the shoreline and tapping water from the upper part of the aquifer for the case of single layer setup (without semi-pervious layer). Drinking Water Standard = 250 mg/l chloride (0.454 g/l salinity) (WHO, 2004; EU, 1998).

7.5.1.3 Pumping at 1500 m distance from the shoreline in lower part of aquifer

In this scenario, the pumping well is located in the deep part of the aquifer around 1 km inland from the tip of the seawater wedge present in the pre-pumping situation. The seawater wedge is progressively advancing inland (Figs. 7.5a-d) as a result of pumping, until it reaches the well after 100 years of pumping (Fig. 7.5e). Salinity starts to increase in the well after 72 years (Fig. 7.5f), compared to the first change of salinity which was documented after 16 years (Fig. 7.3g) and 52 years (Fig. 7.4f) of pumping when the well is located at 500 m and 1000 m from the shoreline respectively. Increasing the distance of a pumping well from the shoreline provides the opportunity for longer pumping without seawater contamination in the well. However, the aquifer becomes polluted. Additionally, locating a well in the lower part of the aquifer facilitates further lateral movement of the seawater wedge compared to the situation when the well is located in the upper part of the aquifer and closer to the shoreline. Fig. 7.5(f) indicates the salinity exceeds the drinking water standard (WHO, 2004; EU, 1998) after 90 years of pumping. It takes many years for any change in salinity to be noticed in the pumping well, but afterward the evolution goes very fast. Yet, saltwater intrusion in the aquifer progresses since the onset of pumping. Within a relatively short period of 28 years

(72-100 years of pumping), the salinity in the well has changed from 0 to 1.6 g/l (Fig. 7.5f). The seawater wedge has penetrated inland to reach the well at 1500 m from the shoreline after 100 years (Fig. 7.5e). This again suggests that groundwater monitoring is important not only in the upper part of the aquifer but also in its lower part, in order to detect a lateral advancement of the seawater wedge.

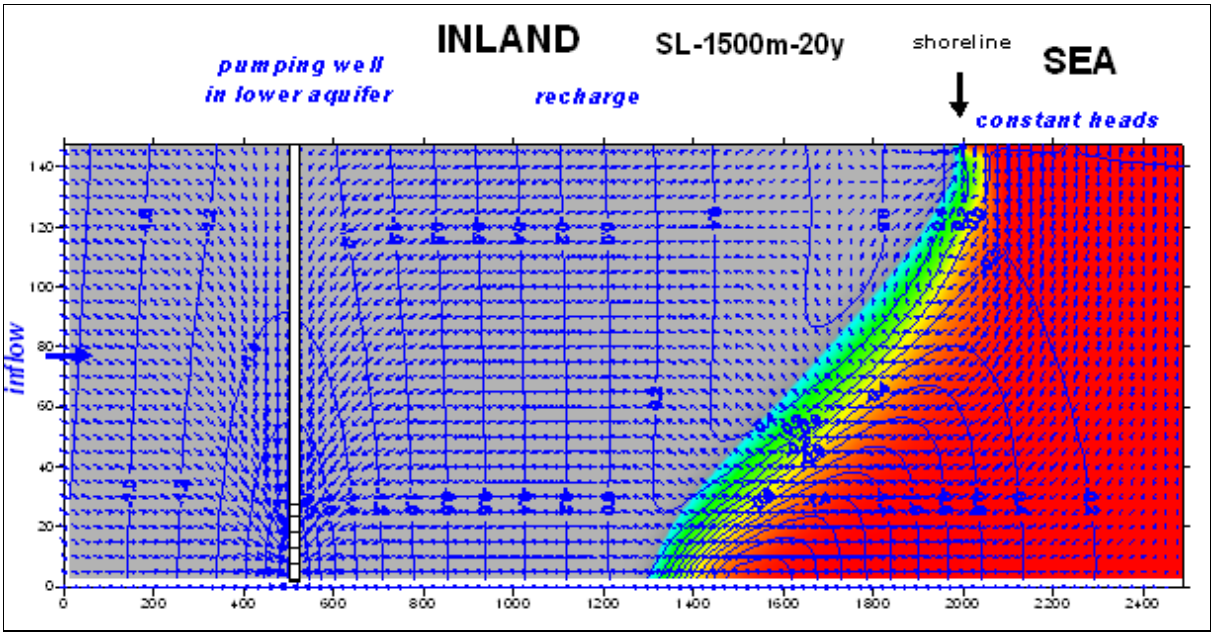

Figure 7.5(a): Situation after 20 years of pumping in lower part of the aquifer for the well located at 1500 m from the shoreline. Aquifer setup without semi-pervious layer.

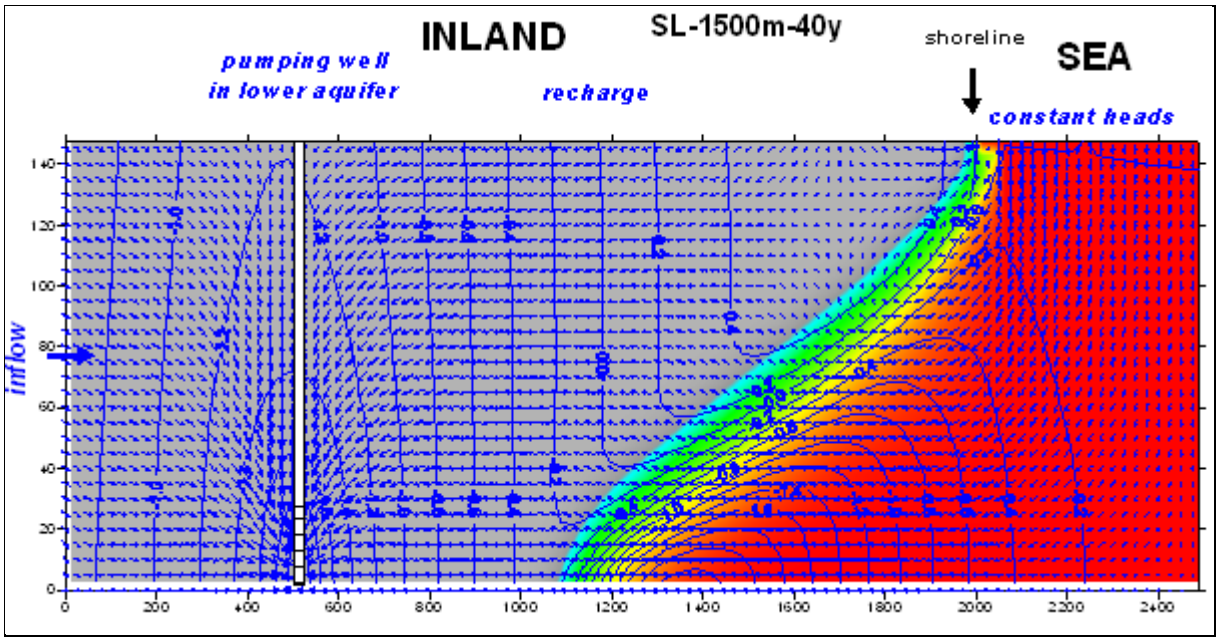

Figure 7.5(b): Situation after 40 years of pumping in lower part of the aquifer for the well located at 1500 m from the shoreline. Aquifer setup without semi-pervious layer.

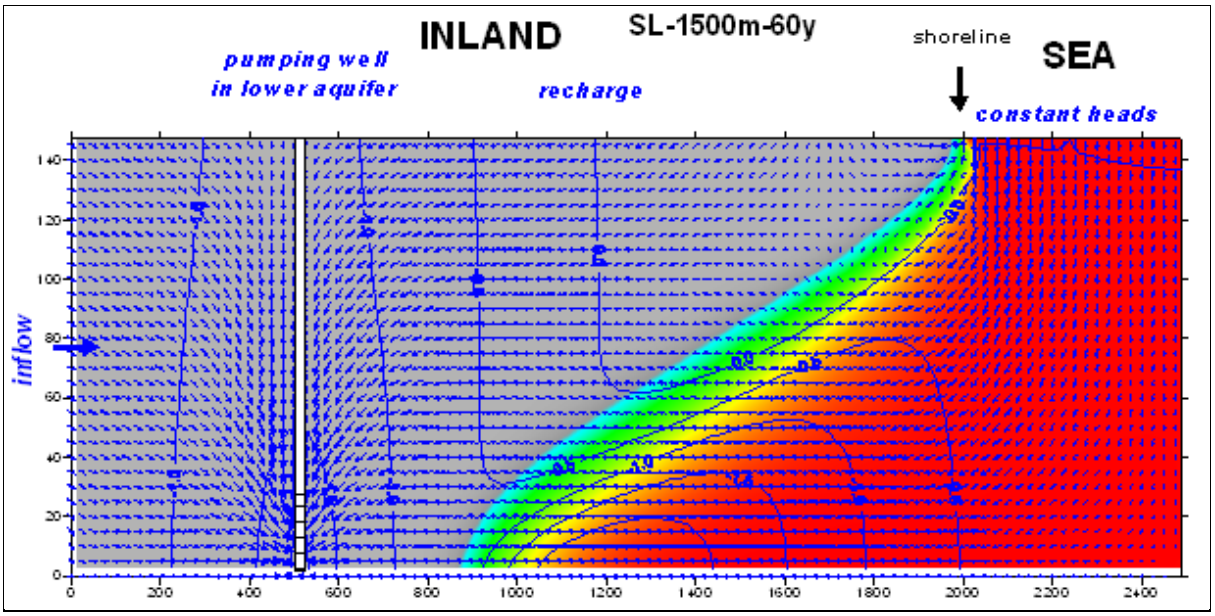

Figure 7.5(c): Situation after 60 years of pumping in lower part of the aquifer for the well located at 1500 m from the shoreline. Aquifer setup without semi-pervious layer.

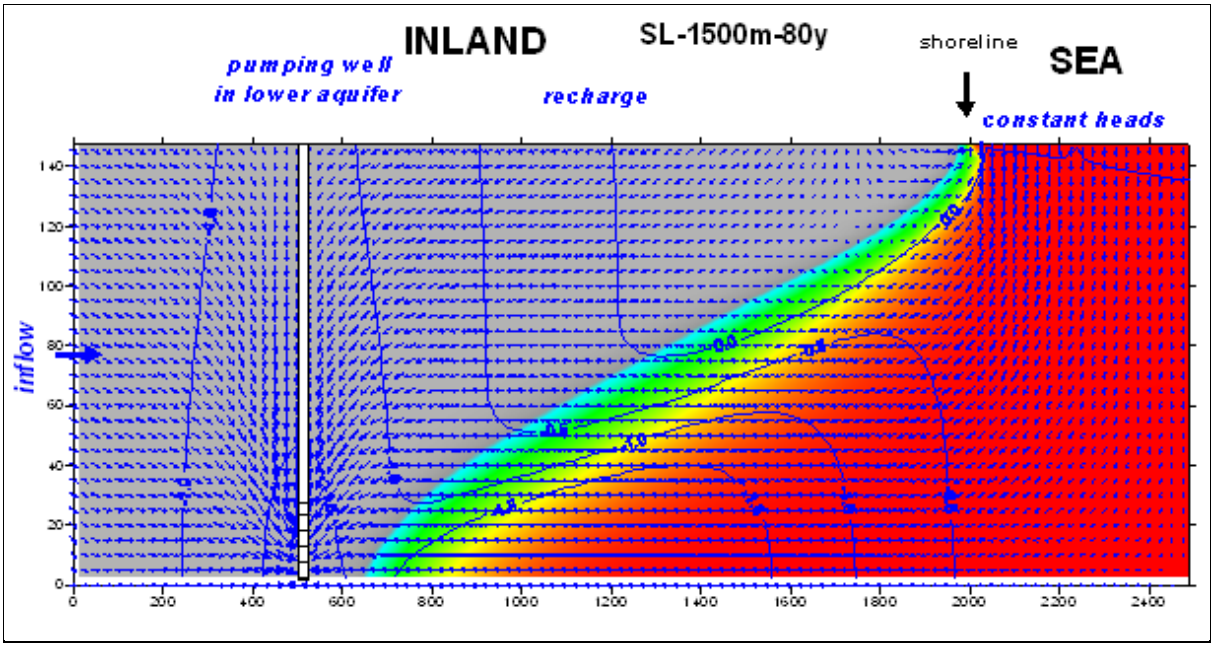

Figure 7.5(d): Situation after 80 years of pumping in lower part of the aquifer for the well located at 1500 m from the shoreline. Aquifer setup without semi-pervious layer.

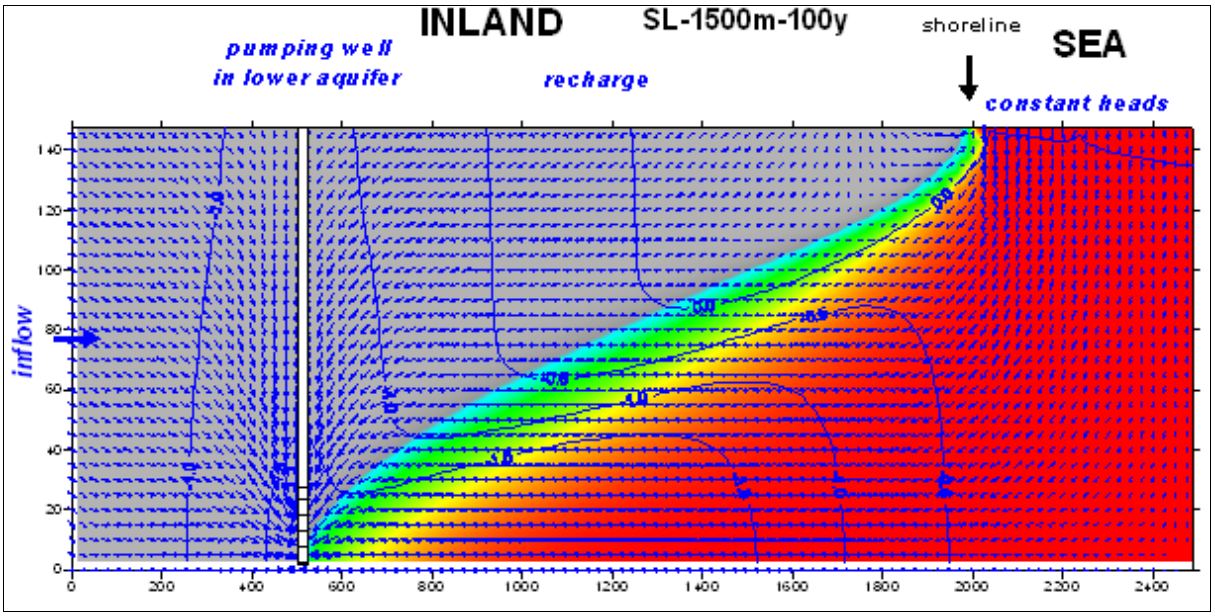

Figure 7.5(e): Situation after 100 years of pumping in lower part of the aquifer for the well located at 1500 m from the shoreline. Aquifer setup without semi-pervious layer.

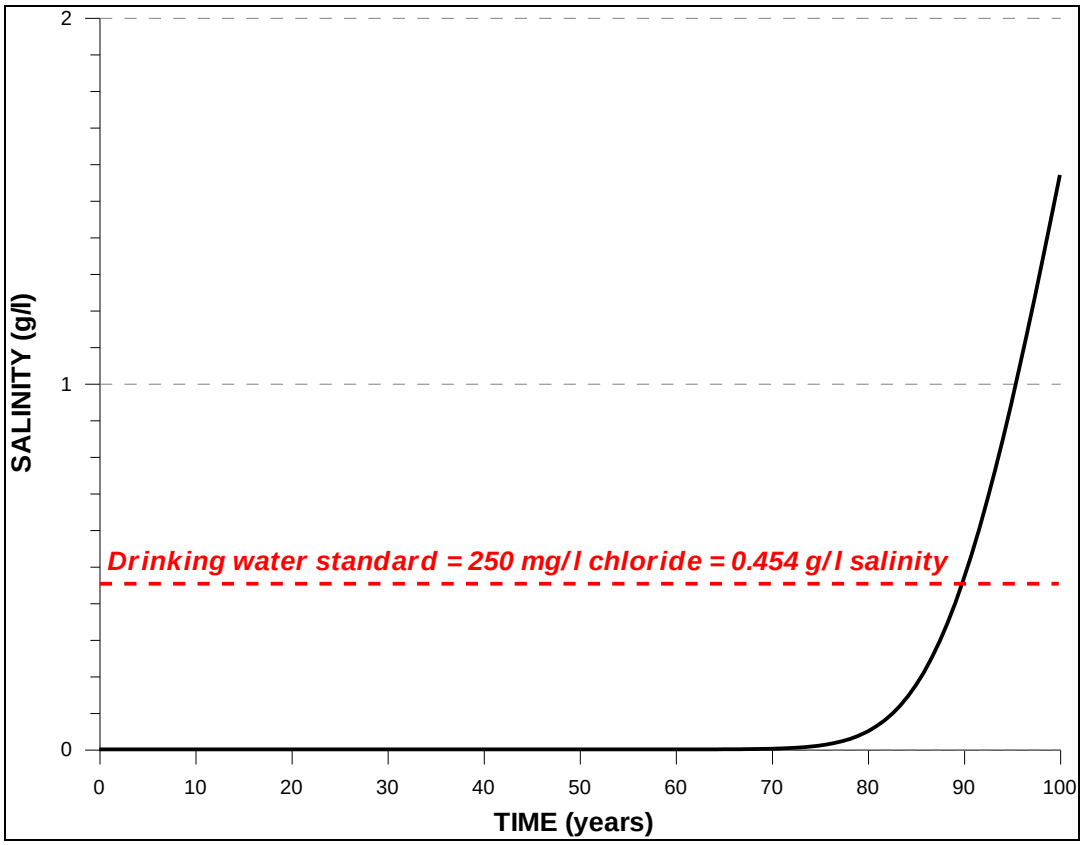

Figure 7.5(f): Evolution of salinity (TDS) in a pumping well located at 1500 m from the shoreline and tapping water from the lower part of the aquifer for the case of single layer setup (without semi-pervious layer). Drinking Water Standard = 250 mg/l chloride (0.454 g/l salinity) (WHO, 2004; EU, 1998).

7.5.2 Aquifer setup with semi-pervious layer

This part presents the simulation results which involved the aquifer setup with semi-pervious layer located between 65 and 85 m depth, and the pumping well located at 500 m distance from the shoreline in the upper part of aquifer. In the pre-pumping situation (Fig. 7.6a), it can be observed that even without pumping, a seawater wedge is present inland, due to density driven flow. Different from the situation observed in the single layer aquifer without semi-pervious layer (Fig. 7.3a), in the presence of a semi-pervious layer (which divides the aquifer, creating upper and lower layers) (Fig. 7.6a), freshwater pushes the seawater back in the upper part of the lower aquifer, but a saline wedge still develops near the bottom of the aquifer. In the lower aquifer seawater intrusion is extensive (over 500 m) inland, compared to the upper aquifer, where no saltwater wedge is intruding inland. As a result of pumping in the upper part of the aquifer, salinity starts to increase in the well in a relatively quick way, compared to the situation of a single layer aquifer. Within 20 years of pumping (Fig. 7.6b) seawater has already advanced for 500 m mainly laterally to the well (in the upper part) in the upper aquifer, and at the same moment the seawater wedge in the lower aquifer is pushed back for over 200 m at the bottom of the aquifer, because of a change in tilt of the fresh/salt water interface. The semi-pervious layer prevents upconing of the deep saline wedge. However, wells can become salinized in a short time by lateral intrusion. Fig. 7.6 (g) indicates that, only after 3 years of pumping, salinity is already at the limit of the drinking water standard (WHO, 2004; EU, 1998), whereas this situation happened after 28 years (Fig. 7.3g) when the semi-pervious layer is not taken into account. The rate of increase of salinity is very high within the first ten years of pumping (salinity has increased to 0.9 g/l), whereas for the next 50 years, the same increase of the amount of salinity (0.9 g/l) is observed (1.8 g/l reached after 60 years of pumping) (Fig. 7.6g). The gradual increase of salinity in this second stage is due to the fact that the seawater is less advancing. While the first stage of intrusion occurred mainly in the upper part of the aquifer, it is now progressively sinking down to the bottom of the upper aquifer (Figs. 7.6 c-e). Fig. 7.6(f) is indicating that the well is pumping seawater after 100 years of pumping. On the other hand, the seawater wedge in the lower part of the aquifer has constantly progressed, starting after 20 years of pumping, until it has penetrated inland over a distance of 400 meters from the shoreline (Fig. 7.6f).

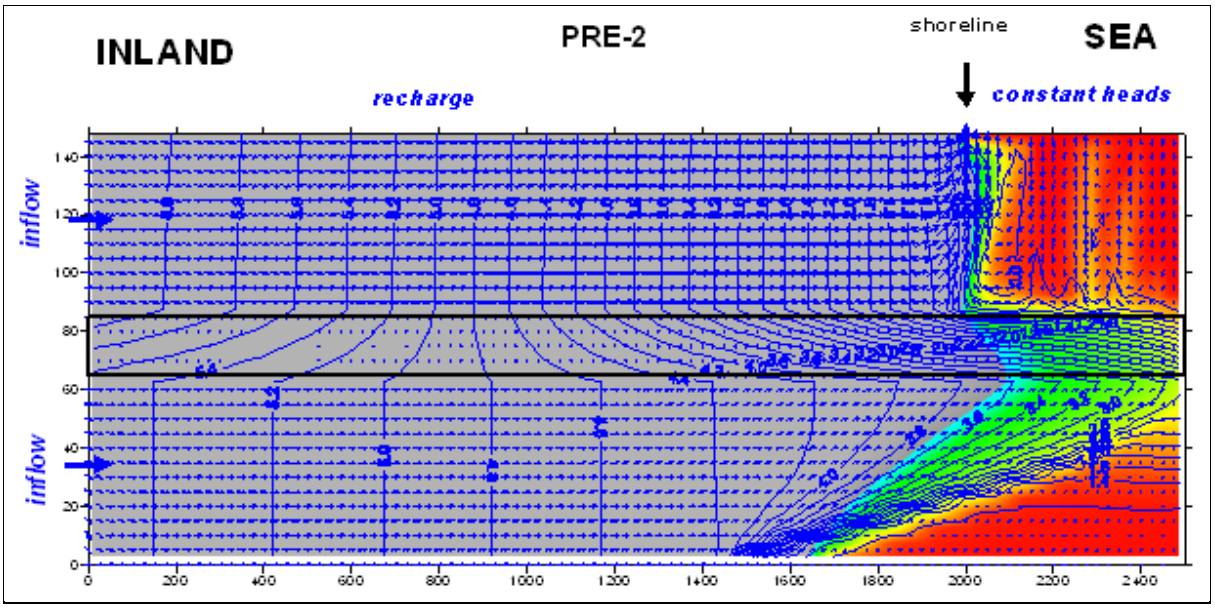

Figure 7.6(a): Pre-pumping situation (= year "zero"). Steady-state concentration distribution after 300 years of simulation. Aquifer setup with semi-pervious layer between 65 and 85 m depth.

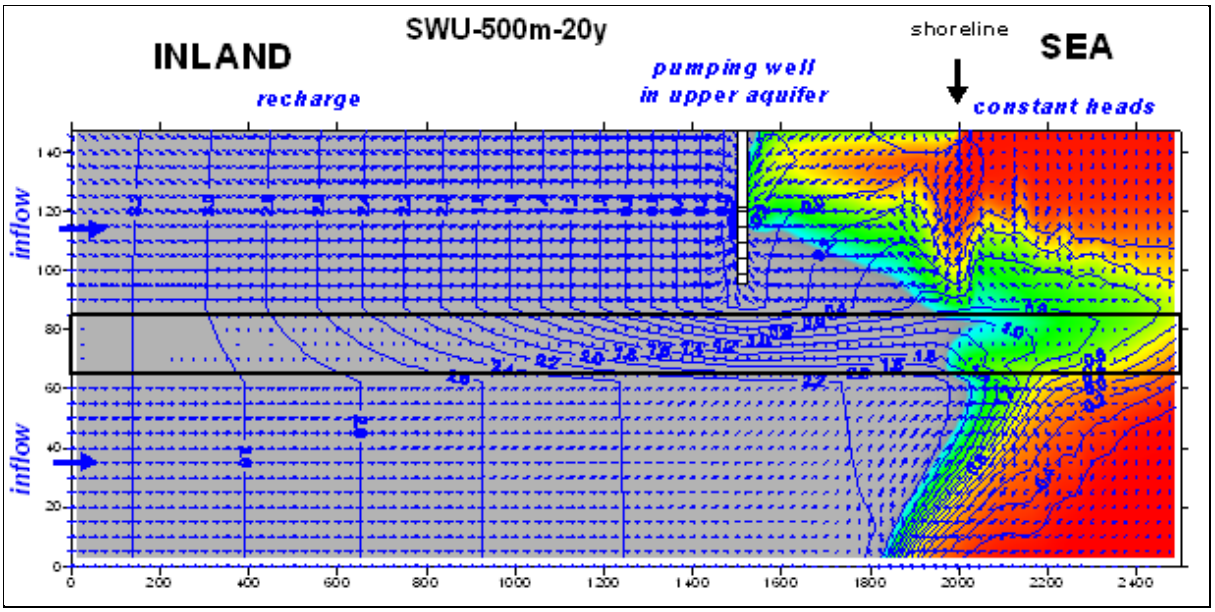

Figure 7.6(b): Situation after 20 years of pumping in upper aquifer for the well located at 500 m from the shoreline. Aquifer setup with semi-pervious layer between 65 and 85 m depth.

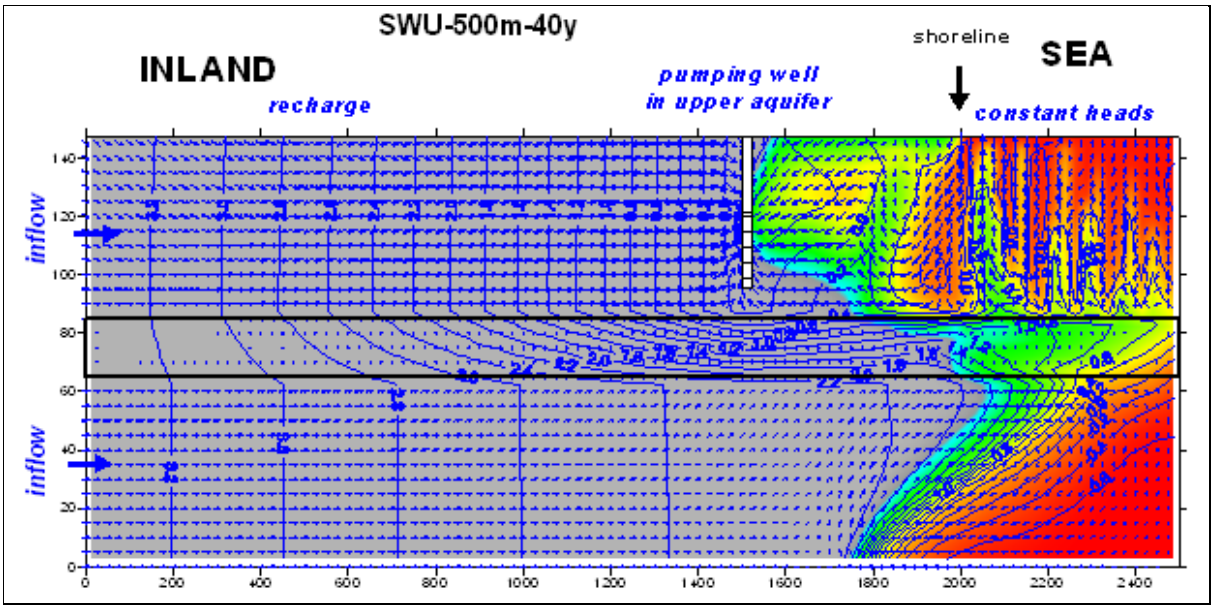

Figure 7.6(c): Situation after 40 years of pumping in upper aquifer for the well located at 500 m from the shoreline. Aquifer setup with semi-pervious layer between 65 and 85 m depth.

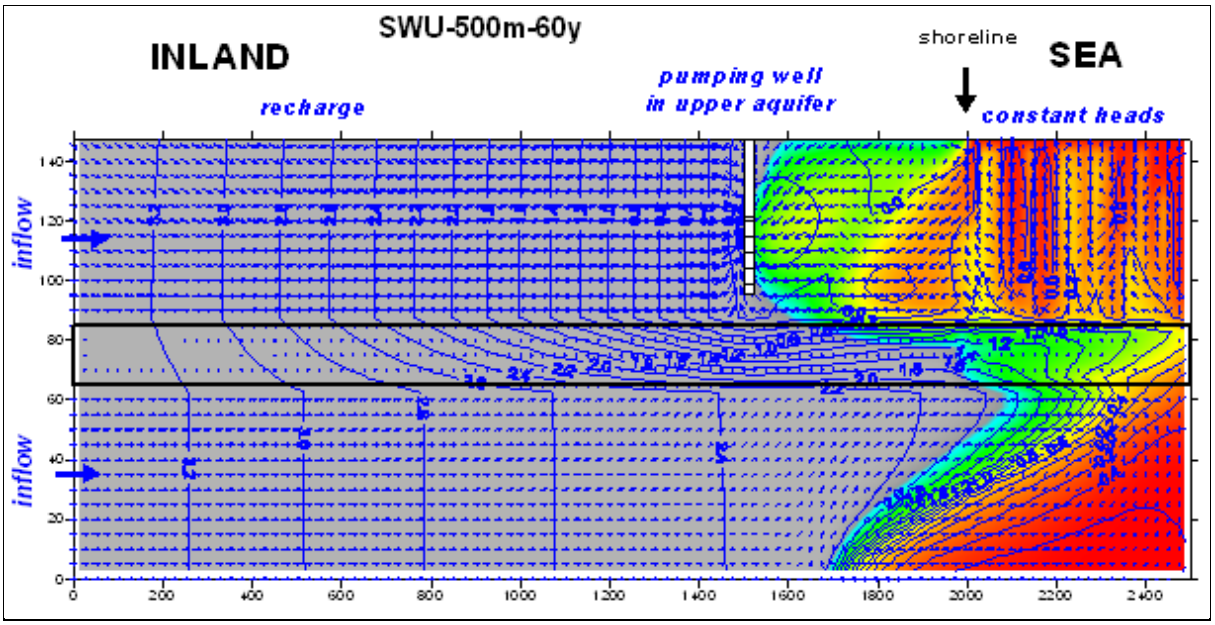

Figure 7.6(d): Situation after 60 years of pumping in upper aquifer for the well located at 500 m from the shoreline. Aquifer setup with semi-pervious layer between 65 and 85 m depth.

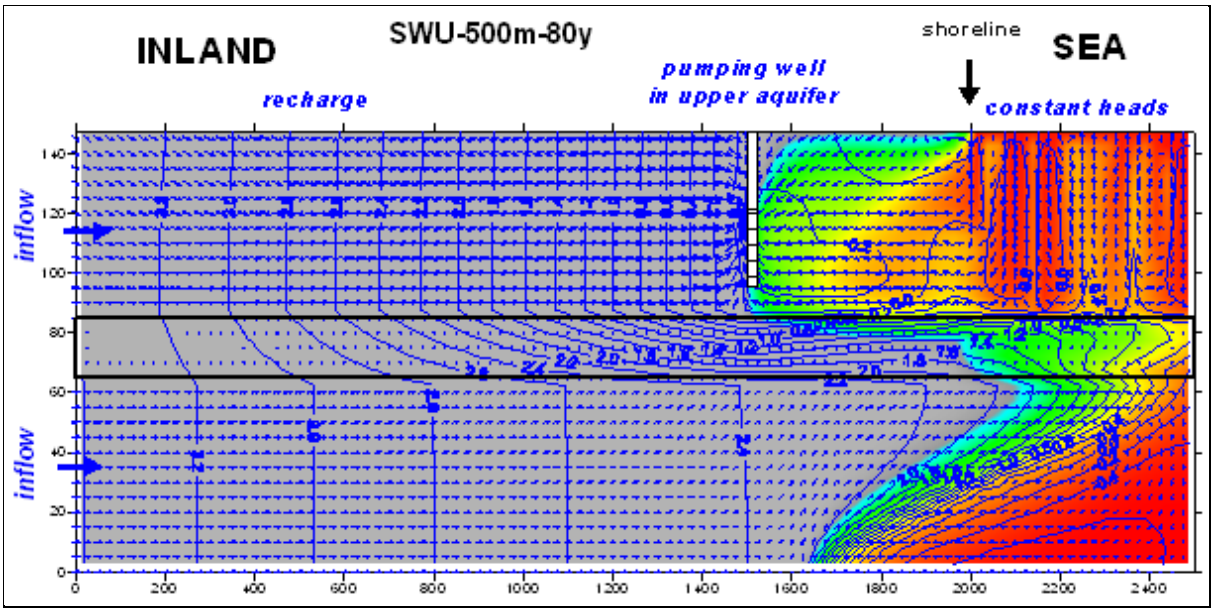

Figure 7.6(e): Situation after 80 years of pumping in upper aquifer for the well located at 500 m from the shoreline. Aquifer setup with semi-pervious layer between 65 and 85 m depth.

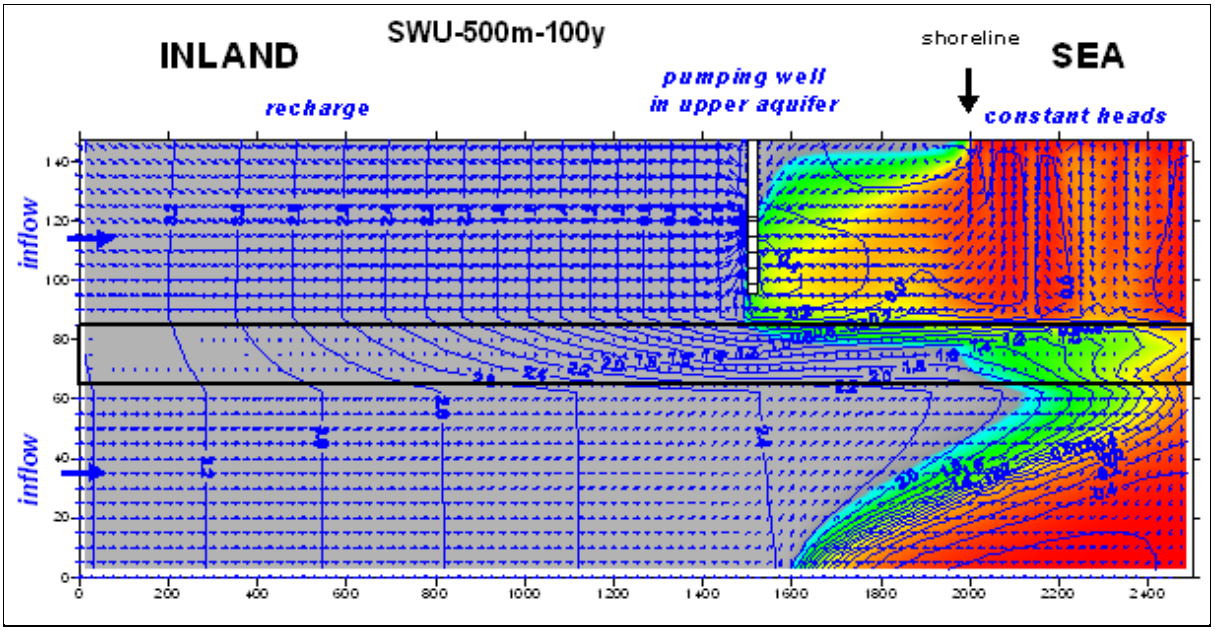

Figure 7.6(f): Situation after 100 years of pumping in upper aquifer for the well located at 500 m from the shoreline. Aquifer setup with semi-pervious layer between 65 and 85 m depth.

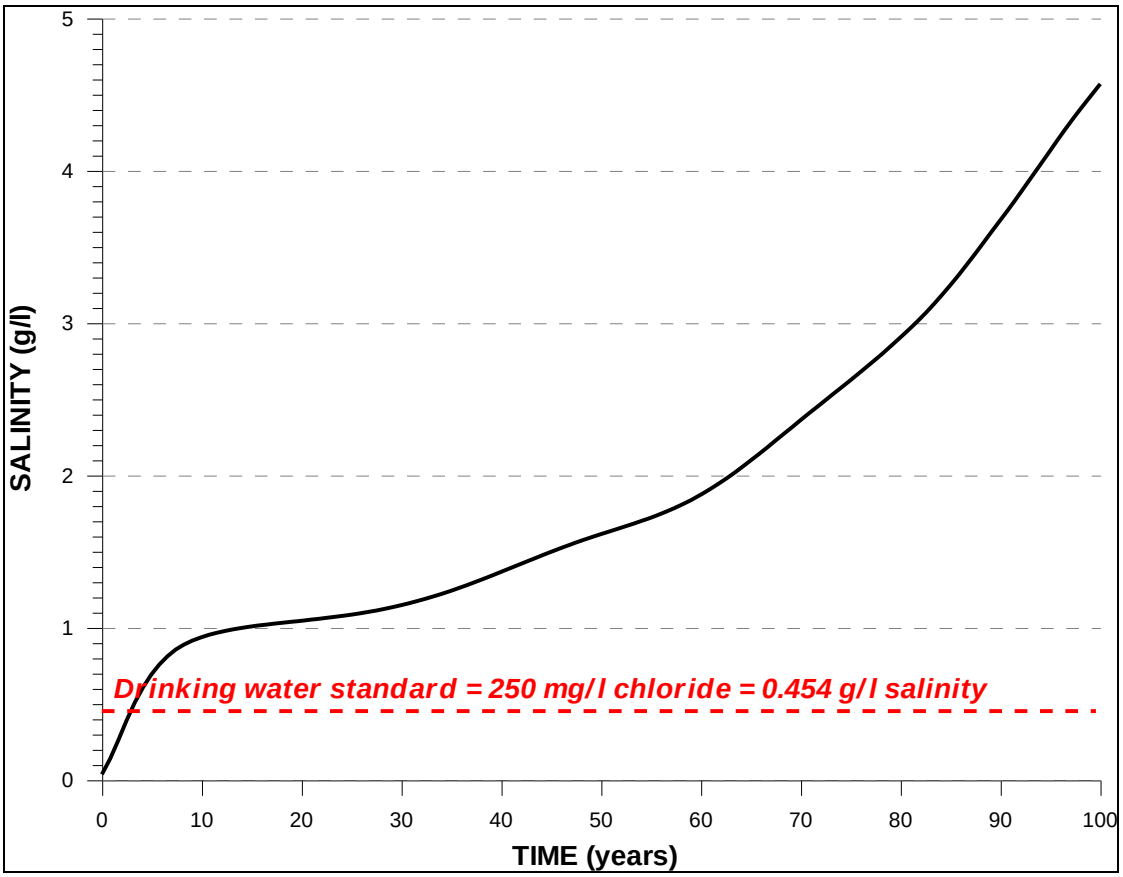

Figure 7.6(g): Evolution of salinity (TDS) in a pumping well located at 500 m from the shoreline and tapping water from the upper aquifer for the case of multi-layer setup (with semi-pervious layer). Drinking Water Standard = 250 mg/l chloride (0.454 g/l salinity) (WHO, 2004; EU, 1998).

7.6 Conclusions and recommendations

7.6.1 Conclusions

7.6.1.1 Pre-exploitation

- Even without pumping, a seawater wedge is present inland, due to density driven flow.
- If no semi-pervious layer is present, the wedge penetrates around 400 m inland near the bottom of the aquifer system, decreasing with depth.
- If a semi-pervious layer is present, halfway the aquifer, freshwater will push the seawater back in the upper part of the lower aquifer, but a saline wedge will still develop near the bottom of the aquifer, penetrating to about 540 m inland. In the upper aquifer few seawater will intrude.

7.6.1.2 Exploitation scenarios

- If no semi-pervious layer is present, pumping in the upper part of the aquifer close to the shoreline, above the saline wedge, will cause upconing of the deep saline wedge (Fig. 7.7a). Salinisation of the wells is mainly by upconing and not by shallow intrusion of seawater.

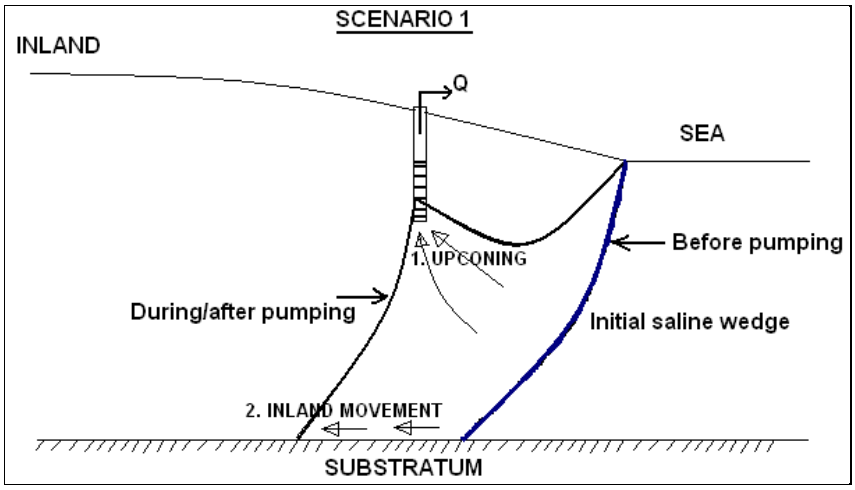

Figure 7.7(a): Scenario 1: Groundwater salinization is mainly by upconing.

- If no semi-pervious layer is present, pumping in the upper part of the aquifer inland from the deep saline wedge, will first cause a further inland penetration of the saline wedge near the bottom of the aquifer, and then an upward upconing of the pronounced wedge (Fig. 7.7b)

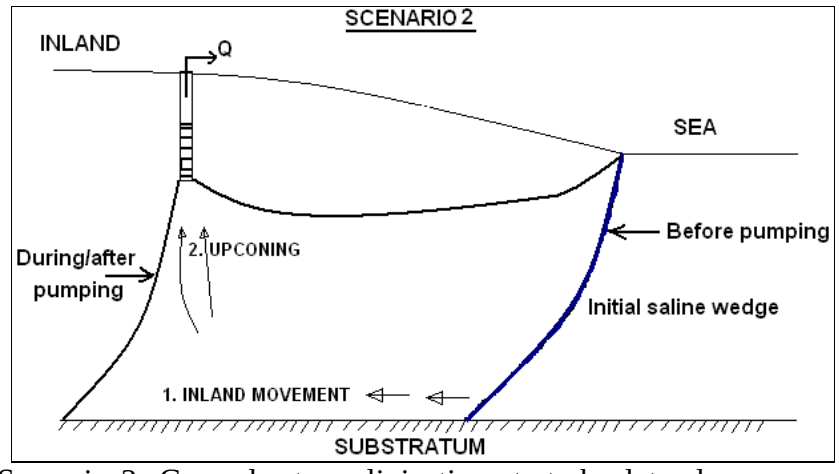

Figure 7.7(b): Scenario 2: Groundwater salinization starts by lateral movement followed by upconing.

- If no semi-pervious layer is present, pumping in the lower part of the aquifer inland from the deep saline wedge, will cause a further inland penetration of the saline wedge towards the pumping wells (Fig. 7.7c). It can take a long time before salt water is found in the wells (dependent on the distance from the wedge) and the saltwater will be diluted with freshwater, attracted from the upper part of the aquifer.

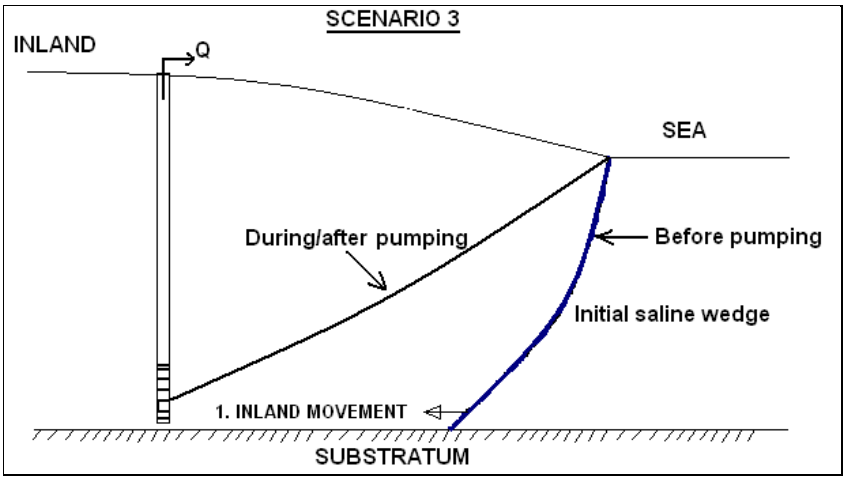

Figure 7.7(c): Scenario 3: Groundwater salinization is by lateral movement.

- If a semi-pervious layer is present, halfway the aquifer, pumping in the upper aquifer above the seawater wedge (which is situated near the bottom of the lower aquifer), will cause lateral intrusion of seawater (Fig. 7.7d). The semi-pervious layer prevents upconing of the deep saline wedge (Fig. 7.7d). However, wells can become salinized in a short time. Already after only a few years chloride concentrations may be above the drinking water limit, also for wells at half a km from the shoreline.

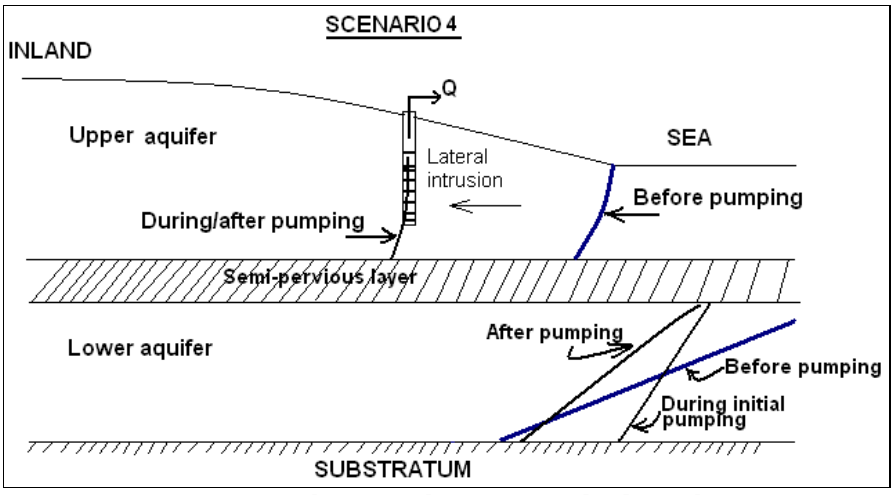

Figure 7.7(d): Scenario 4: Groundwater salinization is by lateral movement.

7.6.2 Recommendations

In this study, a conceptual basis was established for understanding the saltwater transport processes occurring as the effect of pumping in the Dar es Salaam Quaternary coastal aquifer. These conceptual simulations are prototypes for future field studies, and they provide insight into the density driven transport processes that would occur in a coastal aquifer due to overexploitation of groundwater. A further study is needed in order to develop a management model of the aquifer to control saltwater intrusion.

Groundwater pumping near the coast should be avoided to help control the saltwater wedge. Furthermore, groundwater monitoring in the deep part of the aquifer to detect lateral movement of the saline wedge inland is recommended.

8 CONCLUSIONS AND RECOMMENDATIONS

In this final chapter, the main findings and conclusions have been summarised focusing on the primary objective of the research and research questions. Recommendations and areas for further investigation were also outlined.

The primary objective of this research was to investigate groundwater quantity and quality by understanding the hydrogeological settings and hydrogeochemical processes of the coastal aquifer in Dar es Salaam. The following were research questions:

i) How is water supply provision currently being met within the study area?
ii) How much groundwater (m^3/year) can be extracted sustainably?
iii) What are the major factors and issues affecting groundwater quality?
iv) What is the current state of groundwater quality near the coastline?
v) In which areas the problem of seawater intrusion is mostly to be acute?
vi) How are sanitation practices related to groundwater quality?
vii) What are the main gaps in data, information or knowledge needed to promote sustainable groundwater management?

8.1 Conclusions

This part provides a summary of the main findings of this thesis. The main conclusions of this thesis are as follows:

8.1.1 Water supply and sanitation situation for Dar es Salaam City

Dar es Salaam City faces fundamental environmental pressures caused by high population growth, rapid urbanization and inadequate water sector services reflecting on improper management of water resources. There is an acute water shortage to meet the water demand of the population. Struggle to overcome these challenges has come at a tremendous cost to an overexploitation of Dar es Salaam Quaternary coastal aquifer (DQCA). The DQCA has experienced heavy pumping since 1997 when boreholes drilling began to expand quickly following the weakening of the surface water supply. Over 50% of the residents depend on groundwater for domestic, irrigation and industrial usage. Over 10,000 boreholes/wells exist, owned and managed by a variety of public and private institutions and individuals. Despite

the significant importance of groundwater in Dar es Salaam City, threats exist, which include: i) groundwater over-abstraction that leads to the intrusion of seawater in fresh water aquifers, and ii) poor sewerage system and industrial disposal. About 75 percent of the residents in Dar es Salaam City live in unplanned and unserviced settlements and about 80 percent of residents living in these settlements use pit latrines, which are usually poorly constructed causing health and major environmental problems.

8.1.2 Water balance

A study of the water balance of DQCA has been found to be very relevant and useful. The seasonal and annual distributions of important water balance parameters such as rainfall, potential evapotranspiration, actual evapotranspiration, water surplus, water deficit, have been calculated and discussed to provide a better understanding of the hydro-climatic background of the study area. Water balance for DQCA was calculated according to the method of Thornthwaite and Mather. The groundwater replenishment under natural infiltration is about 186 mm (72.17 x 10^6 m^3 $year^{-1}$) indicating that only 16.7% of the long term average annual precipitation of 1114 mm ends up as groundwater recharge. Estimated total groundwater abstraction is approximately 69.3 x 10^6 m^3 $year^{-1}$. The water balance of the catchment suggests an average sustainable yield of 28.67 x 10^6 m^3 $year^{-1}$ (calculated as 40% of natural groundwater recharge) which leaves a shortfall of 40.63 x 10^6 m^3 $year^{-1}$. This clearly shows the unbalanced situation which leads to important water level decline and water quality deterioration. When the extracted volumes of water are greater than the recharge, even on local base, a salinisation process begins in the aquifer as the seawater flows towards inland.

8.1.3 Aquifer characterization and groundwater flow

The study area is characterized by alternating layers of sands, clays, gravel and coral limestone of various degree of weathering. Within the unconsolidated Quaternary sand deposits, the presence of the semi-pervious unit (clay, sandy clay and silts) allows two productive aquifers both of Quaternary age to be distinguished: an upper unconfined sand aquifer and a lower semi-confined sand aquifer. The lower aquifer overlies the substratum formed by Mio-Pliocene clay-bound sands. Closer to the coastline, there exists the limestone aquifer, comprising reef limestone of Pleistocene to Recent age, which is often in contact with

the sandy aquifer, either underlying it or connected laterally. However, sandy aquifers are the most important in Dar es Salaam for supplying groundwater. The upper unconfined sand aquifer varies in thickness from 1 m near the ocean to about 25 m inland. The semi-confined aquifer varies greatly, from about 3 to 50 m. The thickness of the impervious layer separating the two aquifers also varies greatly, from about 6 to 35 m. Due to the sandy nature of the subsoil in many parts of the city, sinking of boreholes/wells is easy and this has led to the increased supply of groundwater to complement the reticulated supply by surface water.

The study quantified the variability of transmissivity and hydraulic conductivity. Analysis results of existing raw pumping test data and new pumping test data show the average transmissivity and hydraulic conductivity values of 44.87 m^2/d and 1.83 m/d respectively for the upper unconfined aquifer. The semi-confined aquifer showed average value of 49.60 m^2/d and 1.17 m/d for transmissivity and hydraulic conductivity respectively. The transmissivity and conductivity values vary reflecting the type of lithology in which the well is constructed.
The water table contour map showed the elevation and configuration of the water table at the time the measurements were taken. The highest water levels are found in the west and southwest of the study area. The groundwater flows toward northeast and east, where the ocean represents the natural discharge area. The direction of groundwater flow is similar in both unconfined and semi-confined aquifers. Piezometric data indicate a general lowering of the piezometric level especially in areas close to the coastline.

In the study area groundwater levels change for many reasons. Some changes are due to natural phenomena and others are caused by human activities. The influence of evapotranspiration is more important in the wells located at Mnazi Mmoja Primary School and Temeke Municipal Garden. Fluctuations of the groundwater level for boreholes located near to the coastline indicate that variations of sea levels affect the groundwater level directly. The effect of the tides is strong near the coastline and becomes weak inland. Apart from the influence of evapotranspiration and tides, groundwater resources are mostly at great risk from the results of human activities, and an increase in population which leads to high demand of fresh water. Improper disposal of sewage was observed in the study area to recharge the groundwater, and is a potential source of groundwater contamination.

Monitoring data show a strong relationship between the rainfall amount and groundwater level. At the onset of the major rainy season, the groundwater level is low and as the season

sets in, the groundwater level rapidly increases. The use of Divers in this research for groundwater level monitoring has proven to be extremely valuable. Interpretation of data for daily fluctuation of groundwater level identified changes in water levels caused by major rainfall events, tides, evapotranspiration, and human activities. The provision of continuous time-series water level measurements is a significant improvement and has enhanced understanding of groundwater resources in the study area. Monitoring data show a strong relationship between the rainfall amount and groundwater level. At the onset of the major rainy season, the groundwater level is low and as the season sets in, the groundwater level rapidly increases. The fluctuations of the groundwater level for boreholes located near to the coastline indicate that variations of sea level affect the groundwater level.

8.1.4 Seawater intrusion zones

The study used the application of the resistivity survey supported by hydrogeological investigation and hydrogeochemical parameters of groundwater to identify fresh-, brackish-, and saline-water zones in the study area. Zone where seawater intrusion has taken place, and the fresh water zone were marked. Hydrochemical/lithological cross-sections indicate the trend of electrical conductivity (EC) and chloride concentration decreasing from the ocean to inland. VES curves and resistivity profiles have shown a decrease of resistivity by going deeper and towards the coastline respectively. This therefore substantiates that there is seawater intrusion in the area close to the coastline. Most vertical electrical soundings (VES) carried out near to the coastline had a 3-layer geoelectric section: the top layer consists of the unsaturated zone, the intermediate layer consists of fresh-water saturated limestone or sands and the bottom layer is saltwater saturated.

Geophysical data supported by groundwater hydrogeochemical data and hydrochemical/lithological sections, have enabled to draw a map showing the depth of the fresh water/saltwater interface. Cross sections have shown the presence of salt water near the coastline and the boundary between fresh and saline waters is marked. Salt water was found mostly in the area within 2 km of the coastline, and the depth to the interface is ranging from 1.3 m to 20 m. Away from the coastline, the interface (if present) is at greater depth that could not be reached by the instrument/lower-power equipment used. However, toward the south of the study area, the VES executed at Kurasini (located 4 km from the sea/mouth of Mzinga Creek to the sea), showed freshwater/interface at a greater depth (43 m). Towards the west of

the study area (about 2.7 km from the coastline) the resistivity logging at point B13 was conducted up to the depth of 37 m but the saltwater interface (if present) was not reached. The findings that salinity decreases with increasing distance from the coast and that salinity increases with increasing depth, indicate that seawater intrusion causes the salinization. The results of VES and resistivity logging indicate area affected by saltwater intrusion include City Centre, Oysterbay, Masaki, Msasani, Kawe, some parts of Mikocheni and Kijitonyama.

8.1.5 Groundwater quality

The physicochemical parameters pH, electrical conductivity, total dissolved solids (TDS), calcium (Ca^{2+}), magnesium (Mg^{2+}), sodium (Na^{+}), potassium (K^{+}), bicarbonate (HCO_3^{-}), chloride (Cl^{-}), sulphate (SO_4^{2-}) and nitrate (NO_3^{-}) were analysed to know the present groundwater quality as well as the possible source of ions in the groundwater. The distribution pattern of major ions shows compositional variation in the groundwater samples. The concentration of cations decreases in the order $Na^{+} > Ca^{2+} > Mg^{2+} > K^{+}$ and of anions in the order $Cl^{-} > HCO_3^{-} > SO_4^{2-} > NO_3^{-}$. Na^{+} and Cl^{-} are the dominant cation and anion respectively. However, HCO_3^{-} dominates over Cl^{-} in some samples.

8.1.5.1 Sources of ions in groundwater

Relationships between major cations and anions were employed to deduce the probable sources of different ions in groundwater. The hydrogeochemical results show that different processes determine major ionic composition of groundwater in the study area.

8.1.5.1.1 Ionic ratios

From the calculated ionic ratios, it was deduced that the chemical composition of groundwater in the study area is influenced by seawater intrusion. Graphs showing the relationship between Cl^{-}/HCO_3^{-} ratio versus Cl^{-} and Na^{+}/Cl^{-} ratio distinguished mixing mechanisms with saline water from chemical reactions in the groundwater system. From the graph showing the relationship between Cl^{-}/HCO_3^{-} ratio versus Cl^{-} and spatial distribution map of Cl/HCO_3 ratio, it is evident that the boreholes located away from the coastline have a much lower ratio compared to the boreholes located toward the coastline: this is signifying saltwater intrusion into the aquifer at boreholes close to the coastline. On the other hand groundwater samples

with Na^+/Cl^- ratio less than that of seawater (0.86) are attributed to depletion of Na^+ caused by cation exchange. This process is associated with saltwater intrusion in coastal aquifers. Ratios of Ca^{2+}/Mg^{2+} and Ca^{2+}/Na^+ are much higher than those of seawater, which indicate enrichment of Ca^{2+} by dissolution of carbonate minerals in the aquifer matrix and/or depletion of Na^+ due to cation exchange during mixing with seawater.

8.1.5.2 Piper diagram

Hydrochemical diversity among the groundwater samples in the study area is exposed by the Piper diagram. Piper diagram shows several water types are present in the groundwater system: five dominant groups can be id entified. Group A is mainly dominated by Ca–HCO_3, Ca-Na-Cl-HCO_3 and Ca-Mg-HCO_3. The freshwater's end member has a $CaHCO_3$ major ion composition and is part of group A. Group B consists mainly of NaCl type which makes up a large proportion of the groundwater types. The seawater's end member has a NaCl major ion composition. Group C is an intermediate between both end members and is dominated by Na–Ca–Cl, indicating freshwater-seawater mixing. Group D which is dominated by Na–HCO_3 signifies groundwater freshening. Group E consists of mg-Ca-Na-Cl, Ca-Na-Cl-HCO_3 or Ca-Na-HCO_3–Cl, and Ca-Mg-Na-HCO_3–Cl: these water types indicate mixed water type that has evolved from Ca-HCO_3 (recharge water) mixing with seawater.

Samples with Na–Ca–Cl water type plotting above the mixing line (signifying effect of salinization) are dominant in the unconfined aquifer compared to the semi-confined aquifer. Samples from both unconfined and semi-confined aquifer, plotting below the mixing line, are signifying both mixing and freshening processes. Dissolution of calcite and dolomite in recharge areas results in fresh Ca–HCO_3 and Ca–Mg–HCO_3 groundwater types. Further along flow paths, Ca^{2+} and Na^+ ion exchange causes groundwater evolution to Na–HCO_3 type. Groundwater evolution in the study area shows a curved path of hydrogeochemical evolution which begins from the Ca-HCO_3 water type, advancing through the Na-Ca-Cl water type to Na-Cl water type. Seawater intrusion results in Na^+ uptake by the exchange sites and releasing Ca^{2+}. On the other hand, in the fresh waters, Na^+ is enriched indicating freshening of the aquifer as Ca^{2+} is replacing Na^+ on the exchange complex. Formation of $NaHCO_3$ water types provides evidence of freshening. Brackish and saline groundwater samples appearing in the mixing line have a Na–Ca–Cl major ion composition. Samples of most of the boreholes

located close to the coastline plot in the NaCl area while those located further from the coast appear to plot over a very large range.

8.1.5.3 Durov diagram

The Durov diagram undoubtedly shows the modification of water types from fresh recharge-$CaHCO_3$ end member to saline-NaCl end member, where the end members are mixed in different proportions between the two water types. Most of the samples fall distinctly away from the expected straight line joining both end members (freshwater-seawater mixing line). This indicates that the chemical composition of groundwater in the study area is influenced by other factors (e.g. cation exchange reactions) apart from a simple mixing process with seawater.

8.1.5.4 Stuyfzand water type classification

Stuyfzand classification clearly shows the significant geochemical differences between the area near the coastline and the area away from the coastline. Groundwater was classified into several categories by subtype, i.e., Sodium-Chloride, Sodium-Bicarbonate, Calcium-Bicarbonate, Magnesium-Bicarbonate, Sodium-Mix and Calcium-Mix. Most of shallow wells close to the shoreline have "Brackish-saline extremely hard NaCl" to "Brackish very hard CaCl" water. Groundwater types are from the inland toward the coast: CaMix, NaMix, and NaCl, showing increasing influence of salinity.

8.1.6 Processes affecting groundwater quality

Results from the hydrogeochemical investigation in the study area indicate that the DQCA is experiencing contamination primarily by seawater intrusion and the use of on-site sewage disposal systems, in particular pit latrines and septic tanks. Seawater intrusion is limited to the area nearby the coast, whereas pollution by sewage is more widely spread. Dissolution of calcite/dolomite minerals in the aquifer matrix as well as cation exchange also modify the concentration of ions in groundwater.

8.1.6.1 Groundwater use for drinking

Most boreholes located close to the coastline, due to their high solute concentrations, are not suitable for domestic purposes. Contamination by seawater leads to the elevated Cl^- and EC values. The groundwater EC and Cl^- values range from 138.4–2,200 µS/cm and 6.2–353 mg/l at distances greater than 2 km away from the coastline to about 760–19,200 µS/cm and 72–15,478 mg/l at a distance of less than 2 km from the coastline, respectively. The former are related to areas such as Mbagala, Mtoni, Kurasini, Ilala and Mwananyamala, whereas the latter are related mainly to the areas close to the coastline such as City Centre, Oysterbay, Masaki, Msasani and some parts of Mikocheni. The increase of salinization limits the application of groundwater for drinking/domestic purposes. 44.23% of samples from the unconfined aquifer exceed the permissible limit of WHO (2004) and 27.47% of semi-confined water samples are beyond the permissible limit. Furthermore, high levels of nitrate observed both in unconfined aquifer and semi-confined aquifer due to lack of proper sanitation do not comply with the limits set by WHO. NO_3^- ranges from 0.0–435.4 mg/l and 0.0–423.9 mg/l in unconfined and semi-confined aquifers respectively. 48.08% of samples from the unconfined aquifer exceed the permissible limit of WHO (2004) and 35.16% of semi-confined water samples are beyond the permissible limit.

8.1.6.2 Groundwater use for irrigation

Sodium Adsorption Ratio (SAR), Soluble Sodium Percent (SSP or %Na), Electrical Conductivity (EC) and other parameters such as chloride and sulphate were used for irrigation suitability assessment. Groundwater suitability was interpreted by using the US Salinity Laboratory (USSL) diagram. The results show that 60% of all samples from the study area were graded as suitable for irrigation use, while 12% as suitable under specific conditions and 28% as unsuitable. Few samples were classified as C1S1 (low salinity-low sodium) whereas samples classified as C2S1 (moderate salinity-low sodium), C3S1 (high salinity-low sodium), C3S2 (high salinity-medium sodium) and C4S4 (very high salinity-very high sodium) were the dominant classes. C3S3 (high salinity-high sodium) and C4S3 (very high salinity-high sodium) groundwater classes represent a transition from C3S2 to C4S4.

8.1.6.3 Groundwater use for industrial purposes

Required groundwater quality for industrial purposes depends on the different industrial uses, and cannot be generalized. However, high salinity is undesirable.

8.1.7 SEAWAT Intrusion modelling of DQCA

In this study, a conceptual basis was established for understanding the saltwater transport processes occurring as the effect of pumping in the DQCA. These conceptual simulations conducted are prototypes for future field studies, and they provide insight into the density driven transport processes that would occur in a coastal aquifer due to overexploitation of groundwater.

8.1.7.1 Pre-exploitation

Even without pumping, a seawater wedge is present inland, due to density driven flow. In a situation where the aquifer system does not consist a semi-pervious layer, a seawater wedge penetrates around 400 m inland near the bottom of the aquifer system. If a semi-pervious layer is present, halfway the aquifer, freshwater will push the seawater back in the upper part of the lower aquifer, but a saline wedge will still develop near the bottom of the aquifer penetrating to about 540 m inland. In the upper aquifer less seawater will intrude.

8.1.7.2 Exploitation scenarios

In the situation where a semi-pervious layer is not present in the aquifer system, pumping in the upper part of the aquifer close to the shoreline, above the saline wedge, will cause upconing of the deep saline wedge. Salinisation of the wells is mainly by upconing and not by shallow intrusion of seawater. On the other hand, pumping in the upper part of the aquifer inland from the deep saline wedge, will first cause a further inland penetration of the saline wedge near the bottom, and then an upward upconing of the pronounced wedge: groundwater salinization starts by lateral movement followed by upconing. If no semi-pervious layer is present and pumping is conducted in the lower part of the aquifer, inland from the deep saline wedge, this will cause a further inland penetration of the saline wedge towards the pumping wells. Groundwater salinization is by lateral movement. It can take a long time before salt

water is found in the wells (dependent on the distance from the wedge) and the saltwater will be diluted with freshwater, attracted from the upper part of the aquifer.

In the situation where a semi-pervious layer is present, halfway the aquifer, pumping in the upper aquifer above the seawater wedge (near the bottom of the lower aquifer), will cause lateral intrusion of seawater. The semi-pervious layer prevents upconing of the deep saline wedge. However, wells can become salinized in a short time. Already after only a few years chloride concentrations may be above the drinking water limits, also for wells at half a km from the shoreline.

8.1.8 Groundwater management

Generally, there has been a lack of a sustained systematic groundwater quality monitoring program in the study area. Groundwater quality data available in the Ministry of Water and Irrigation (MoWI) involves mainly the water quality analysis conducted at the time that the boreholes were drilled. Boreholes lack long term monitoring data. Long term monitoring data covering key elements of the hydrological cycle such as groundwater quality, groundwater fluctuations and water-level trends are very important for management and for evaluating the implications of changes in use.

The use of geophysics for groundwater studies has been stimulated in part by a desire to reduce the risk of drilling dry holes and also to offset the costs associated with poor groundwater production. Despite of the success of the resistivity survey for both groundwater resource mapping and groundwater quality evaluation, the use of geophysics in Tanzania is still often not adequate. Partly this is because of poor publicity of the potential use of geophysics, practical implementation difficulties and financial limitations. Regrettably it is occasionally because of in-appropriate use of geophysics, ending by getting misleading and/or wrong results.

8.2 Recommendations

In light of the above conclusions, which involved a multitude of parameters at different spatial levels, many recommendations can be drawn out of this research. However, the recommendations listed here support groundwater management and future studies:

- Over-exploitation of groundwater should be avoided especially near the coast to prevent seawater intrusion. Sustainable groundwater management is needed and will require restriction of well development and appropriate monitoring of potential saltwater intrusion, particularly near the coastline.
- DQCA can be a sustainable source of freshwater if correctly managed and exploited according to recharge, well pattern and local hydrogeological characteristics. Given the highly specialized nature of the field of seawater intrusion expertise, there is great need for the training of hydrogeologists/hydrogeophysicists for effective monitoring, evaluation and management of coastal aquifers.
- Developing and understanding the application of seawater-intrusion assessment tools, including both modeling and field based utilities, is equally important. Furthermore, community and professional education in coastal groundwater hydrology need to be enhanced for effective monitoring, evaluation and management of coastal aquifers in Tanzania.
- Increase of borehole drilling that goes unchecked affects the protection of the groundwater resource. The excessive pumping to meet the increasing water demand for domestic, industrial and agricultural purposes is the main reason of saltwater intrusion in DQCA. This necessitates the reduction in pumping to eliminate the on-going problem of saltwater intrusion. The evaluation suggests that the total pumping should be reduced by 59% to eliminate the problem of saltwater intrusion.
- Currently, groundwater monitoring is considered inadequate to provide data needed to support groundwater management. This study recommends further investigation of water level measurements in the area by installation of piezometers and regular measurements. This will help to control the groundwater exploitation. Sustainable abstraction from the aquifer system will require monitoring boreholes to appropriately monitor potential saltwater intrusion, particularly near the coastline. Furthermore, groundwater monitoring in the deep part of the aquifer to detect lateral movement of the saline wedge inland is recommended.

- There is a need of establishment of a warning system for drop in piezometric head and the encroachment of saltwater by placement of piezometers along the edge of the sea. Accordingly monitoring wells should be strategically established inland to monitor groundwater fluctuation and quality. By continuously monitoring the head and the water quality, it will be possible to detect some long-term trends and to devise management strategies.
- More pumping tests are needed to have a better understanding of aquifer properties.
- Raised and lined pit latrines and other low-cost technologies should be considered to minimize potential of groundwater pollution. Septic tanks and soakaways should be properly constructed to be better managed with more quality assurance and control. Improving and expanding the sanitation services is very important for groundwater protection. All kind of sewage should be treated before being discharged into the environment.
- Artificial groundwater recharge (AGR) is recommended. As urban and industrial development continues to expand around the coastal areas of Dar es Salaam, so will the demand for freshwater. Utilizing runoff (which otherwise drains off) and grey water will bring great benefits for improving groundwater levels, providing a barrier for seawater intrusion and prevention of diseases and floods by deviating peak flows. By implementing artificial groundwater recharge, excess water in the catchment area can be collected and allowed to infiltrate, to increase groundwater storage in rainy seasons to be utilized later in dry seasons. However, a detailed study is needed to determine sites and design structures for artificial groundwater recharge. Future work should also focus on designing a test programme which includes chemical and physical modelling of recharge options, and measurement of recharge rates. Close follow-up of infiltrated water quality to prevent aquifer pollution is crucial. However, detailed study is needed to determine sites and design structures for artificial groundwater recharge. Future work should also focus on designing a test programme which includes chemical and physical modelling of recharge options, and measurement of recharge rates. The main environmental issue associated with AGR is the degradation of subsurface environment and groundwater due to the transport of pathogenic viruses with the recycled water. Close follow-up of infiltrated water quality to prevent aquifer pollution is crucial.

9 REFERENCES

Adams, S., Titus, R., Pietersen, K., Tredoux, G. and Harris, C. (2001). Hydrochemical characteristics of aquifers near Sutherland in the Western Karoo, South Africa. Journal of Hydrology 241: 91–103. www.elsevier.com/locate/jhydrol.

Ahmed, M.A., Abdel Samie, S.G. and Badawy, H.A. (2012). Factors controlling mechanisms of groundwater salinization and hydrogeochemical processes in the Quaternary aquifer of the Eastern Nile Delta, Egypt. Environ Earth Sci. doi:10.1007/s12665-012-1744-6.

Ahrens, C.D. (2007). Meteorology today: an introduction to weather, climate and the environment (8th edition). UK: Thomson Learning.

Al Farrah, N., Martens, K. and Walraevens, K. (2011). Hydrochemistry of the Upper Miocene–Pliocene Quaternary aquifer complex of Jifarah Plain, NW-Libya. Geol Belg 14(3–4):159–174.

Alexander, C.S. (1968). The marine terraces of the northeast coast of Tanganyika. Zeitschrift fur Geomorphologie, Supplement band 7, 133-154.

Allen, D.M and Matsuo, G.P. (2002). Results on the Groundwater Geochemistry Study on Hornby Island, British Columbia. Burnaby, B.C., Simon Fraser University. p. 9-12.

Allen, G.R., Pereira, L.S., Raes, D. and Smith, M. (1998). Crop evapotraspiration – Guidelines for computing crop water requirements – FAO irrigarion and drainage paper 56. FAO, Rome, Italy.

Alley, W.M. and Leake, S.A. (2004). The journey from safe yield to sustainability. Ground Water, 42(1): 12–16.

APHA (1992). Standard Methods for the Examination of Water and Wastewater. 18th edition, American Public Health Association (APHA), American Water Works Association (AWWA) and Water Pollution Control Federation (WPCF), Washington, D.C.

Appelo, C.A.J. and Postma, D. (2005). Geochemistry, groundwater and pollution (second ed.). Netherland: A.A Balkema.

Appelo, C.A.J. and Postma, D. (1993). Geochemistry, groundwater and pollution. A.A., Balkema, Rotterdam, 526 p.

Avaşar, H. (2006). Control, optimization and monitoring of portland cement (PC 42.5) quality at the ball mill. MSc thesis, Izmir Institute of Technology, Turkey.

Back, W. and Hanshaw, B.B. (1965). Chemical geohydrology. In Chow V.T. ed. Advances in Hydroscience 2, 49-109. Academic Press, New York.

Bakundukize, C. (2012). Hydrogeological and Hydrogeochemical Investigation of a Precambrian Basement Aquifer in Bugesera Region (Burundi). PhD Thesis, Ghent University, Belgium. 430 pp.

Barker, A.P., Newton, R.J. and Bottrell, S.H. (1998). Processes affecting groundwater chemistry in a zone of saline intrusion into an urban aquifer. Applied Geochemistry 13, 735-749

Bauer, P., Supper, R., Zimmermann, S. and Kinzelbach, W. (2006). Geoelectrical imaging of groundwater salinization in the Okavango Delta, Botswana, Journal of Applied Geophysics, Vol.60: 126–141.

Baulies, X. and Szejwach, G. (1998). LUCC data requirements workshop survey of needs, gaps and priorities on data for land-use/land-cover change research organized by IGBP/IHDP-LUCC AND IGBP-DIS, Barcelona, Spain, 11-14 November 1997 LUCC report series no. 3.

Baumann, E., Ball, P. and Beyene, A. (2005). Rationalization of Drilling Operations in Tanzania. Review of the Borehole Drilling Sector in Tanzania. http://www.rwsn.ch/documentation/skatdocumentation.2008-08-25.3938556797/file

Bear, J. (2007). Hydraulics of groundwater. Dover Publications, Mineola, 569p.

BGS (2005). Mineral profile: cement raw materials, British Geological Survey (BGS), Natural Environment Research Council.

Buddemeier, R.W. (1996). Groundwater flux to the Ocean: Definitions, data, applications, uncertainties. In: Buddemeier, R. W. (ed.), Groundwater Discharge in Coastal Zone: Proceedings of an International Symposium. LOICZ Reports and Studies No. 8, LOICZ, Texel, The Netherlands, pp. 16-21.

Burgess, N.D., Mwasumbi, L.B., Hawthorne, W.J., Dickinson, A and Doggett, R.A. (1992). Preliminary assessment of the distribution, status and biological importance of coastal forests in Tanzania. Biological Conservation, 62, 205 – 218.

CABI (2007). The Agricultural groundwater revolution: opportunities and threats to development. ISBN-13:978 1 84593 172 8.

Calmbach, L. (1997). AquaChem 3.6.2, Hydrogeochemical data analysis, plotting and modeling, Waterloo Hydrogeologic, Ontario, Canada.

Cardoso da Silva, Jr.G., Carlos, E. and de Carvalho Lange, I. (2003). Hydrogeology of study of mangrove area around Guanabara bay, Rio de Janeiro, Brazil, Unuaro do Instito de Geociencias, UFRJ, Volume, 26, 92-100.

Chapman, D. (1996). Water Quality Assessments. A guide to the use of biota, sediments and water in environmental monitoring, (2nd ed). Chapman and Hall, London.

Chenini, I. and Khemiri, S. (2009). Evaluation of groundwater quality using multiple linear regression and structural equation modeling. Int. J. Environ. Sci. Tech., 6(3): 509-519.

Clarke, G.P. and Dickinson, A. (1995). Status Reports for 11 Coastal Forests in Coast Region, Tanzania. Frontier-Tanzania Technical Report No. 17. The Society for Environmental Exploration, London, UK and the University of Dar es Salaam, Dar es Salaam, Tanzania.

Cooper, H.H. and Jacob, C.E. (1946). A generalized graphical method for evaluating formation constants and summarizing well field history. American Geophysical Union Transactions, 27: 526-534.

Craig, D.S.A. (2008). The Saline Interface of Shallow Unconfined Aquifer, Rangitikei Delta. MSc thesis, Victoria University of Wellington, New Zealand.

Custodio, E. (1985). Saline intrusion. In: Hydrogeology in the Service of Man. Memoires of the 18th Congress of the International Association of Hydrogeologists. Cambridge, pp. 65-90

Custodio, E. (2002). Aquifer overexploitation: what does it mean? Hydrogeol. J., 10, 254–277, 2002.

Davis, N.S. and De Wiest, R.J. (1966). Hydrogeology. John Wiley and Sons, Inc. New York. Xi, 43p.

DAWASA: Dar es Salaam Water and Sewerage Authority (2007). Development of a Future Water Source for Dar es Salaam – Water Source Development Master Plan, Final Version: Prepared by Norconsult, Water Resource Assessment (WRA) and Norwegian Institute for Water Research (NIVA) for DAWASA.

De Castro, M.C. and Singer, B. (2003). Migration, Urbanization and Malaria: A Comparative Analysis of Dar es Salaam, Tanzania and Machadinho, Rondônia, Brazil. Paper prepared for Conference on African Migration in Comparative Perspective, Johannesburg, South Africa, 4-7 June, 2003.

De Moor, G. and De Breuck, W. (1969). De freatische waters in het Oostelijk Kustgebied en in de Vlaamse vallei. Natuurwet. Tijdschr., 51(1-2): 3-68, + 8 annexes.

De Witte, I. (2012). Characterization of status of Dar es Salaam aquifer in view of salt-water intrusion and nitrate contamination. MSc. thesis, Ghent University, Belgium, 141p.

Dejager, N. (2011). Groundwater characterisation of a coastal aquifer in Dar es Salaam, Tanzania: Identification of sources of groundwater pollution. MSc. thesis, Ghent University, Belgium, 118p.

Domenico, P.A. and Schwartz, F.W. (1990). Physical and chemical hydrogeology. John Wiley and Sons, 824p.

Dongus, S. and Nyika, I. (2000) vegetable production on open spaces in Dar es Salaam–Spatial Changes from 1992 to 1999. City Farmer, Vancouver. http://www.cityfarmer.org/daressalaam.html

Douglas, B.C. (1992). Global sea level acceleration. Journal of Geophysical Research, 97: 12699-12706.

Driscoll, F.G. (1986). Groundwater and Wells. (2nd ed.), Johnson Filtration Systems Inc., St. Paul, Minnesota, USA.

Duffield, G.M. (2007). AQTESOLV for Windows Version 4.5 User's Guide, HydroSOLVE, Inc., Reston, Virginia. http://www.hydrosys.net/myplus/bbs/table/hydrosyssoft/upload/2720aqtw20070719.pdf

Dunne, T., Moore, T.R., and Taylor, C.H. (1975). Recognition and prediction of runoff-producing zones in humid regions. Hydrological Sciences Bulletin. 20(3):305-327.

Dupuit, J. (1863). Etudes théoriques et pratiques sur le mouvement des eaux dans les canaux découverts et à travers les terrains perméables [Theoretical and practical studies on the movement of water in open channels and through permeable rocks]. Editions Dunod Paris.

Durov, S.A. (1948). Natural waters and graphic representation of their composition. Dokl. Akad. Nauk SSSR. V. 59. 87-90

El Moujabber, M., Bou Samra, B., Darwish, T. and Atallah, T. (2006). Comparison of different indicators for groundwater contamination by seawater intrusion on the Lebanese coast. Water Resources Management, 20: 161-180.

EPA: Environmental Protection Agency (2004). European Communities. Drinking water regulation, 2000 (S. I. 439 of 2000), a handbook on implementation for sanitary authorities, 155 p.

FAO: Food and agriculture Organization (2003). Groundwater management- the search for practical approaches. Publishing Management Service, Information Division, FAO, Rome, Italy.

Ferris, J.G., Knowles, D.B., Brown, R.H. and Stallman, R.W. (1962). Theory of aquifer tests. US Geol, Survey Water Supply Paper 153-E.

Fetter, C.W. (2001). Applied Hydrogeology, 4th Edition, Prentice Hall, 2001, 598 p.

Foster, S.S.D., Morris, B.L. and Lawrence, A.R. (1993). Effects of Urbanization on groundwater recharge, in Wilkinson, W.B., (ed), Groundwater Problems in Urban Areas, Proceeding of Institution of Civil Engineers, June 1993, London, p. 43 – 63.

Foster, S.S.D., Morris, B.L. and Chilton, P.J. (1999). Groundwater in urban development- review of linkages and concerns. In: Impacts of Urban Growth on Surface Water and Groundwater Quality (Proceedings of IUGG 99 Symposium HS5, Birmingham, July 1999). IAHS Publ. no. 259, 1999.

Freeze, R.A. and Cherry, J.A. (1979). Groundwater. Prentice-Hall, Inc., Englewood Cliffs, New Jersey.

Ghabayen, S.M.S., McKee, M. and Kemblowski, M. (2006). Ionic and isotopic ratios for identification of salinity sources and missing data in the Gaza aquifer. Journal of Hydrology 318, pp 360-373.

Gleick, P.H. (1993). Water in crisis. A guide to world's fresh water resources, Oxford University Press, Oxford, UK

Gribovszki, Z., Szilagyi, J. and Kalicz, P. (2010). Diurnal fluctuations in shallow groundwater levels and stream flow rates and their interpretation: a review. Journal of Hydrology, 385, 371-383.

GST: Geological Survey of Tanganyika (1963). Geological map of Dar es Salaam Region, Quarter Degree Sheet 186, 1:125,000: First Edition.

Guo, W. and Bennett, G.D. (1998). "Simulation of saline/fresh water flows using MODFLOW." in Poeter, E., and others, MODFLOW '98 Conference, Golden, Colorado, 1998, Proceedings: Golden, Colorado, v. 1, p. 267-274.

Guo, W. and Langevin, C.D. (2002). User's guide to SEAWAT: A computer program for simulation of three-dimensional variable-density ground-water flow." U.S. Geological Survey Techniques of Water-Resources Investigations, book 6, chapter A7, 77 p.

Guo, W., Langevin, C.D. and Bennett, G.D. (2002). Improvements to SEAWAT and Applications of the Variable-Density Modeling Program in Southern Florida. In Proceedings of the MODFLOW 2001 and Other Modeling Odysseys Conference, E. Poeter and others (eds.), Colorado School of Mines, Golden, Colorado, v. 2, p. 621-627. http://fl.water.usgs.gov/numerical/scientists/langevin.html

Hamm, S.Y., Cheong, J.Y., Jang, S., Jung, C.Y. and Kim, B.S. (2005). Relationship between transmissivity and specific capacity in the volcanic aquifers of Jeju Island, Korea. Hydrogeology Journal, 310(1-4): 111-121.

Hamon, W.R. (1961). Estimating potential evapotranspiration: Journal of the Hydraulics Division, Proceedings of the American Society of Civil Engineers, v. 87, p. 107–120.

Hantush, M.S. (1961a). Drawdown around a partially penetrating well, Jour. of the Hyd. Div., Proc. of the Am. Soc. of Civil Eng., vol. 87, no. HY4, pp. 83-98.

Hantush, M.S. (1961b). Aquifer tests on partially penetrating wells, Jour. Of the Hyd. Div., Proc. of the Am. Soc. of Civil Eng., vol. 87, no. HY5, pp. 171-194.

Harbaugh, A.W., Banta, E.R., Hill, M.C. and McDonald, M.G. (2000). MODFLOW-2000, the U.S. Geological Survey modular ground-water model – User guide to modularization concepts and the ground-water flow process: U.S. Geological Survey Open-File Report 00-92, 121 p.

Hargreaves, G.L. and Samani, Z.A. (1982). Estimating potential evapotranspiration. Journal of Irrigation and Drainage Engineering, 108(3): 225–230.

Haurwitz, B. (1956). 'The geographical distribution of the solar semidiurnal pressure oscillation, Meteorol. Pap. 2 (5), New York University.

Hem, J.D. (1989). The Study and Interpretation of the Chemical Characteristics of Natural Water. 3rd edn. USGS Water Supply Paper 2254, US Geological Survey.

Howell, K.M. (1981). Pugu Forest Reserve: biological values and development. African Journal of Ecology, 19: 73-81.

HydroMetrics, L.L.C. (2008). Seawater Intrusion Response Plan Sea Side Basin, Monterey Country California. Prepared for Seaside Basin Watermaster. http://www.seasidebasinwatermaster.org/Other/Final_Draft.pdf)

IWM: Integrated Watershed Management – Navigating Ontario's Future (2009). A Water Budget Overview for Ontario. www.conservationontario.ca

Irmak, S: Evapotranspiration. Department of Biological Systems Engineering University of Nebraska-Lincoln. http://watercenter.unl.edu/downloads/ResearchInBrief/IrmakSuatET.pdf

Jeen, S., Kim, J., Yum, B., and Chang, H. (2001). Hydrogeochemical characteristics of groundwater in a mid-western coastal aquifer system, Korea. Geoscience Journal, 5, 339-348.

JICA: Japan International Cooperation Agency (2008). The study on the groundwater resources development and management in the Internal Drainage Basin in the United Republic of Tanzania. Final Report. Ministry of Water and Irrigation. Dar es Salaam.

Johnson, A. I., Moston, R. P. and Versaw, S. F. (1966). Laboratory study of aquifer properties and well design for an artificial recharge site: U.S. Geological Sure by Water Supply Paper, no. 1615-H, pp. H23-H25.

Kajato, H. K. (1982). Gas strike spurs: Search for Oil in Tanzania, Oil and Gas Journal, 1 23, pp. 123-131.

Kapilima, S. (2003). Tectonic and sedimentary evolution of the coastal basin of Tanzania during the Mesozoic times. Tanz. J. Sci. Vol. 29(1), pp. 1-16.

Kashaigili, J.J. (2010). Assessment of groundwater availability and its current and potential use and impacts in Tanzania. Report Prepared for the International Water Management Institute (IWMI).

Kaushal, S.S., Groffman, P.M., Likens, G.E., Belt, K.T., Stack, W.P., Kelly, V.R., Band, L.E. and Fisher, G.T. (2005). Increased salinization of freshwater in the northern eastern of the United States. National Academy of Sciences of the USA 102(38), 13517 – 13520.

Kazmann, R. G. (1956). Safe yield in ground-water development, reality or illusion?: Journal of the Irrigation and Drainage Division, ASCE, v. 82, no. IR3, Proc. Paper 1103, November 1956, 12.

Kebede, S.A. and Nicholls, J.R. (2010). Population and assets exposure to coastal flooding in Dar es Salaam (Tanzania): vulnerability to climate extremes. University of Southampton, United Kingdom. http://www.tzdpg.or.tz/uploads/media/Dar es Salaam_City-Analysis_Final-Report_1_.pdf

Kehew, A.E. (2001). Applied Chemical Hydrogeology, Prentice Hall (2001) ISBN 0- 13-270927-9 368 pp

Kent, P.E., Hunt, J.A. and Johnstone, M.A. (1971). The geology and geophysics of coastal Tanzania. Geophysical paper no. 6, Natural Environment Research Council, Institute of Geological Sciences, London, 101pp.

Khodapanah, L., Sulaiman, W.N.A., and Khodapanah, N. (2009). Groundwater Quality Assessment for Different Purposes in Eshtehard District, Tehran, Iran. European Journal of Scientific Research, 36(4), 543-553.

Kirsch, R. (2009). Petrophysical Properties of Permeable and Low Permeable Rocks. In: Groundwater Geophysics: Tool for Hydrogeology, Kirsch, R. (Ed.). 2nd Edn., Springer, Berlin, Heidelberg.

Kombe, W. (2005). Land use dynamics in peri-urban areas and their implications on the urban growth and form: the Case of Dar es Salaam, Tanzania, Habitat International 29, 113-135.

Krasny, J. (1993). Classification of transmissivity magnitude and variation. Ground Water, 31(2): 231-236.

Kruseman, G.P. and de Ridder, N.A. (1970). Analysis and evaluation of pumping test data./nf. Inst. Land Reclam. Improv. Neth., Bull. 11.

Kruseman, G.P. and de Ridder, N.A. (1994). Analysis and evaluation of pumping test data (2nd edition). Wageningen: ILRI.

Kulindwa, K., Jambiya, G. and Sosovele, H. (2005). Poverty and the Environment: The Case of Informal Sand mining, Quarrying and Lime-making activities in Dar es Salaam, Tanzania. In Researching Poverty in Tanzania; problems, policies and perspectives. REPOA, Dar es Salaam.

Kumar, C. P. (2006). Management of Groundwater in Salt Water Ingress Coastal Aquifers. In: Groundwater Modelling and Management (Eds. N. C. Ghosh and K. D. Sharma), Capital Publishing Company, New Delhi, pp. 540-560. http://www.angelfire.com/nh/cpkumar/publication/gwman.pdf

Kumar, D., Ahmed, S., Krishnamurthy, N.S. and Dewandel, B. (2006). Reducing ambiguities in vertical electrical sounding interpretations: A geostatistical application, J. Appl. Geophy. 62(1): 16-32.

Langevin, C. (2003). Simulation of submarine ground water discharge to a marine estuary: Biscayne Bay, Florida. Ground Water, 41/6, 758-771.

Langevin, C.D., Shoemaker, W.B., Guo, W. (2003). MODFLOW-2000, the U.S. Geological Survey modular ground-water model—Documentation of the SEAWAT-2000 version with the Variable Density Flow process (VDF) and the Integrated MT3DMS Transport Process (IMT): U.S. Geological Survey Open File Report 03- 426, Tallahassee FL, 43 pp. http://fl.water.usgs.gov/PDF_files/ofr03_426_langevin.pdf

Langevin, C.D., Swain, E.D., Wolfert, M.A. (2004). Simulation of integrated surface-water/fround-water flow and salinity for a coastal wetland and adjacent estuary: US Geological Survey Open-File Report 2004-1097. http://www.dtic.mil/cgi-bin/GetTRDoc?AD=ADA439842

Lashkaripour, Ghafoori, M. and Dehghani, A. (2005). Electrical resistivity survey for predicting Samsor aquifer properties, southeast Iran. Geophysical Research Abstracts (7) (Europian Geosciences Union).

Lebbe, L. C. (1996). Regression modelling of freshwater heads and borehole resistivities observed on the shore. Calibration and Reliability in Groundwater Modelling (Proceedings of the ModelCARE 96 Conference held at Golden, Colorado, September 1996). IAHS Publ. no. 237.

Lenoir, J.L., Liégeois, J.P., Theunissen, K., Klerkx, J. (1994). The Palaeoproterozoic Ubendian shear belt in Tanzania: geochronology and structure. Journal of African Earth Sciences, 19, 169-184.

Lerner, D. N., Issar, A. S. and Simmers, I. (1990) Groundwater recharge: a guide to understanding and estimating natural recharge. International Contributions to Hydrogeology, Vol. 8. International Association of Hydrogeologists, Verlag Heinz Heise.

Lerner, D.N. (1997). Too much or too little: Recharge in urban areas. In Groundwater in the Urban Environment: Problems, processes and management, (eds. P.J. Chilton et al.) pp. 41-47, Balkema, Rotterdam.

Levanon, E., Yechieli, Y., Shalev, E., Friendman, V., Gvirtzman, H. (2012). Reliable monitoring of fresh-saline water interface in coastal aquifers. 22nd Salt Water Intrusion Meeting (SWIM): Saltwater Intrusion in Aquifers: Challenges and Perspectives, Rio de Janeiro, Brazil 2012. p. 2008.

Lindzen, R.S. and Chapman, S. (1969). Atmospheric tides. Space Science Reviews, 10, 3-188.

Lloyd, J. W. (1986). A review of aridity and groundwater. Hydrological Processes, 1, 63-78.

Lohman, S.W. (1972). Ground-water hydraulics. US Geol. Survey Prof. Paper 708.

Loke, M.H. (1999). Electrical imaging surveys for environmental and engineering studies. A practical guide to 2-D and 3-D surveys.

Lupala, J.M. (2002). Urban types in rapidly urbanising cities. Analysis of formal and informal settlements in Dar es salaam, Tanzania. PhD Thesis, Trita-ARK 1651-0216 ; 02/030-SE, ISBN 91-7323-030-8, Royal Institute of Technology, KTH, Sweden.

Mace, R. E. (1997). Determination of transmissivity from specific capacity tests in a Karst aquifer. GroundWater, 25(5): 738-742.

Maimone, M. (2004): Defining and managing sustainable yield, Ground Water, 42(6), 809–814. http://info.ngwa.org/gwol/pdf/042979897.pdf

Mather, J.R. (1979). Use of the climatic water budget to estimate streamflow, *in* Mather, J.R., ed., Use of the climatic water budget in selected environmental water problems, J.R. Mather (Editor). Publications in Climatology, v. 32, no. 1, p. 1–52.

Mato, R.A.M. (2002). Groundwater Pollution in Urban Dar es Salaam, Tanzania: assessing Vulnerability and Protection Priorities. University Press, Eindhoven University of Technology, The Netherlands.

Mato, R.A.M. and Mjwahuzi, M. (2010). Groundwater Governance Case Study: Tanzania, Groundwater use, characterization and vulnerability. http://xa.yimg.com/kq/groups/22477246/889666431/name/Aquifer+characteristics.pdf

McDonald, M.C. and Harbaugh, A.W. (1988) A modular three dimensional finite-difference groundwater flow model. Techniques of Water-Resources Investigations of the U.S. Geol. Surv., vol. 6, p. A1.

McDonald, M.G. and Harbaugh, A.W. (1988). A modular three dimensional finite-difference ground water flow model, volume 6 of "Techniques of Water-Resources Investigation of the United States Geological Survey", chapter A1, Scientific Software Group.

Milly, P. C. D. (1994). Climate, soil water storage, and the average annual water balance, Water Resources Research, Vol. 30, 2143–2156.

Mjemah, I.C. (2007). Hydrogeological and Hydrogeochemical Investigation of a Coastal aquifer in Dar es Salaam, Tanzania. PhD thesis, Ghent University, Belgium, 222 pp.

Mjemah, I.C., Van Camp, M., Martens, K. and Walraevens, K. (2011). Groundwater exploitation and recharge rate estimation of a quaternary sand aquifer in Dar es Salaam area, Tanzania. Springer, Environmental Earth Sciences Journal. 63 (3), pp. 559-569 (DOI: 10.1007/s12665-010-0723-z)

Mng'ong'o, O. (2004). A browning process: The case of Dar es Salaam city. Doctoral Dissertation, Royal Institute of Technology, Stockholm, Sweden.

Mnzava, J. (1986). The distribution, chemistry and origin of saline groundwaters in Dar es Salaam area. MSc thesis, Geology Dept, University of Dar es Salaam, Tanzania.

Morris, B.L., Lawrence, A.R., Chilton, P.J.C., Adams, B., Calow, R.C., and Klinck, B.A. (2003). Groundwater and its susceptibility to degradation: A global assesment of the problem and options for management. Early Warning and Assesment Report Series, RS.03-3. United Nations Environment Programme, Nairobi, Kenya.

Mpanda, S. (1997). Geological development of the East African coastal basin of Tanzania. PhD thesis, University of Stockholm, Sweden, 121 pp.

Msindai, K. (1988). Engineering geological aspects of soil and rocks in the Dar es Salaam region, Tanzania. Institute of quaternary geology, University of Turku, Finland.

MTL Consulting Company Limited (2010). Scoping report and terms of reference (ToR) for portland cement manufacturing factory at Wazo Hill, Dar es Salaam, Tanzania.

Mtoni, Y. (2003). Problems and strategies of groundwater protection in Dar es Salaam: Community participation approach. Serie: Trita-LWR. Master Thesis, 1651-064X ; 03-28, Royal Institute of Technology, KTH, Sweden.

Mtoni, Y., Mjemah, I.C. and Walraevens, K. (2010). Towards Effective Pollution Control of Dar es Salaam Quaternary Sand Aquifer: A Challenge to Achieve Sustainable Development. In: Proceedings of the IAHR International Groundwater Symposium, Valencia, Spain, 22-24 September, 2010.

Mtoni, Y., Mjemah, I.C., Bakundukize, C., Van Camp, M., Martens, K. and Walraevens, K. (2013). Saltwater intrusion and nitrate pollution in the coastal aquifer of Dar es Salaam, Tanzania. Springer, Environmental Earth Sciences (DOI: 10.1007/s12665-012-2197-7).

Mtoni, Y., Mjemah, I.C., Msindai, K., Van Camp, M. and Walraevens, K. (2012). Saltwater Intrusion in the Quaternary Aquifer of the Dar es Salaam Region, Tanzania. Geologica Belgica 15/1-2: 16-25.

Mtoni, Y., Mjemah, I.C., Van Camp, M. and Walraevens, K. (2011). Enhancing Protection of Dar es Salaam Quaternary Aquifer: Groundwater Recharge Assessment. Springer, Environmental Earth Sciences, Advances in Research of Aquatic Environment volume 1, pp 299-306 (DOI 10.1007/978-3-642-19902-8).

Mtoni, Y., Mwiturubani, D.A., Msonde, A. and Mwassaga, S. (2006). Social and Environmental impact of river and pit sand mining activities along the Mbezi and Mpiji rivers, Dar es Salaam, Tanzania, Kinondoni Integrated Coastal Area Management Programme (KICAMP), Tanzania

Muhongo, S., Kapilima, S., and Mtoni, Y. (2000). Geological development and mineral resources management of the coastal basin of Tanzania. Proceedings of the International Conference On Sustainable Integrated Coastal Management, Maputo (Mozambique), UNESCO/IOC, Workshop Report No. 165, pp. 209-216.

Muhongo, S., Tuisku, P. and Mtoni, Y. (1999). Pan-African pressure – temperature evolution of the Merelani area in the northeast Tanzania. Journal of Africa Earth Sciences, Vol. 29, No.2 pp. 353-365.

Murray, K.S. (1996). Hydrology and geochemistry of thermal waters in the Upper Napa Valley, California. Groundwater, 34 (6), 1115-1124.

Mutakyahwa, M.K.D. (1987). Fluvio-deltaic environment and in situ pedogenesis of Middle Miocene kaolinitic sandstones of the Pugu coastal area of Tanzania. Journal of African Earth Sciences, Volume 6, Issue 2, Pages 229-242.

Napacho, Z.A. and Manyele, S.V. (2010). Quality assessment of drinking water in Temeke District (part II): Characterization of chemical parameters. African Journal of Environmental Science and Technology Vol. 4(11), pp. 775-789.

NEMC: National Environment Management Council (2009). State of the coast report Tanzania mainland: people and the environment.

Neuman, S.P. (1975). Analysis of pumping test data from anisotropic unconfined aquifers considering delayed gravity response. Water Resources Research, 11(2): 329-342.

Ngoye, E. and Machiwa, J.F. (2004). The Influence of Land-Use Patterns in the Ruvu River Watershed on Water Quality in the River System. Physics and Chemistry of the Earth 29(15-18):1161-1166.

Nimmo, J.R. (2009). Vadose Water. In: Gene E. Likens, (Editor) Encyclopedia of Inland Waters. Volume 1, pp. 766-777 Oxford: Elsevier.

Nkotagu, H. (1989). Geochemistry of shallow groundwater at Kigamboni peninsula along Dar es Salaam coastal strip Tanzania. Journal of African Earth Sciences, 9, 739-748.

Norconsult (2007). Development of a Future Water Source for Dar es Salaam, Tanzania. Pre-design and Environmental report, Phase 2. Part 2: Review of Social and Environmental Factors.

Nowroozi, A.A., Horrocks, S.B. and Henderson, P. (1999). Saltwater intrusion into the freshwater aquifer in the eastern shore of Virginia: a reconnaissance electrical resistivity survey, J. of Applied Geophysics, Vol. 42: 1–22.

Obikoya, I.B. and Bennell, J.M. (2012). Geophysical investigation of fresh-saline water interface in the coastal area of Abergwyngregyn. Journal of Environmental protection, 3: 1039-1046.

Paniconi, C., Khalaifi, I., Lecca, G., Giacomelli, A. and Tarhouni, J. (2001). A modelling study of seawater Intrusion in Korba Coastal Plain, Tunisia; Physics and Chemistry of the Earth, Vol 26 N° 4:345-351.

Papadopoulou, M.P., Karatzas, G.P., Koukadaki, M.A. and Trichakis, Y. (2005). Modelling the saltwater intrusion phenomenon in coastal aquifers – a case study in the industrial zone of Herakleto in Crete. Global NEST Journal. 7(2), 197-203.

Paritsis, S.N. (2005). Simulation of Seawater Intrusion into the Tymbaki Aquifer, South. Central Crete, Greece, Study implemented on behalf of the Department of Department of Management of Water Resources of the Region of Crete. http://www.uni-muenster.de/Umweltforschung/medis/pub/tymbaki.pdf

Parkhurst, D.L., Appelo, C.A.J. (1999). User's Guide to Phreeqc (version 2) – A Computer Program for Speciation, Batch-Reaction, One-Dimensional Transport, and Inverse Geochemical Calculation. USGS Water Resources Investigation Report 99-4259, 310 pp.

Pearson, P.N., Nicholas, C.J., Singano, J.M., Bown, P.R., Coxall, H.K., Van Dongen, B.E., Huber, B.T., Karega, A., Lees, J.A., Msaky, E., Pancost, R.D., Pearson, M. and Roberts, A.P (2004). Paleogene and Cretaceous sediment cores from the Kilwa and Lindi areas of coastal Tanzania: Tanzania Drilling Project Sites 1–5. Journal of African Earth Sciences 39: 25–62.

Penman, H.L. (1948). Natural evaporation from open water, bare soil and grass. Proceedings of the Royal Society of London, A193: 120-146.

Penman, H.L. (1956). Evaporation: an introductory survey. Netherlands J. Agr. Sci. 4, 9–29.

Piper, A. m. (1953): A graphic procedure I the geo-chemical interpretation of water analysis, USGS Groundwater Note no, 1953, 12.

Pirttijärvi, M. (2005). DCINV: 1-D interpretation of electrical (DC) soundings software. Oulu, Finland.

Plummer, L.N. (1975). Mixing of seawater with calcium carbonate groundwater. Geological Soc America, Memoir 142:219-36.

Polemio, M., Casarano, D. and Limoni, P.P. (2010). Apulian coastal aquifers and management criteria In: SWIM 21 - 21st Salt Water Intrusion Meeting. Edited by: MT Condesso de Melo, L Lebbe, JV Cruz, R Coutinho, C Langevin, A Buxo. 203-206

Polemio, M., Limoni, P.P., Mitolo, D. and Santaloia, F. (2002). Characterisation of Ionian-Lucanian coastal aquifer and seawater intrusion hazard. 17th SWIM Meeting, Delft, 424- 434

Ponce, M.V. (2007). Sustainable Yield of Groundwater. http://ponce.sdsu.edu/groundwater_sustainable_yield.html. Accessed on March 13, 2011

Raes, D., Steduto, P., Siao, T.C. and Fereres, E. (2010). Reference Manual, Chapter 2, AquaCrop, Version 3.1 January 2010. http://www.fao.org/nr/water/docs/aquacrop3_1/AquaCropV31Chapter2.pdf. Accessed on February 23, 2011

Rao, S.V.N., Sreenivasulu, V., Bhallamudi, S.M., Thandaveswara, B.S., and Sudheer, K.P. (2004). Planning groundwater development in coastal aquifers: Hydrological Sciences Journal 49, no. 1:155-170.

Reddy, A.G.S. (2012). Evaluation of hydrogeochemical characteristics of phreatic alluvial aquifers in southeastern coastal belt of Prakasam district, South India Environ Earth Sci. doi:10.1007/ s12665-012-1752-6

Revelle, R. (1941). Criteria for recognition of sea water in groundwaters. Trans. Amer. Geophys. Union. V. 22, pp. 593-597.

Reynolds, J.M. (1997). An Introduction to Applied and Environmental Geophysics. Chichester, John Wiley and Sons Ltd. 796 pp.

Ritter, M.E. (2006). The physical environment: An introduction to Physical Geography. http://www.uwsp.edu/geo/faculty/ritter/geog101/textbook/title_page.html.

Rosegrant, M.W, Cai, X. and Cline, S.A. (2002). Global water outlook to 2025: Averting an impending crisis. International Food Policy Research Institute. Washington, D.C. USA and International Water Management Institute. Colombo Sri Lanka. 26 pp.

Rosen, M., Jones, S. (1998). Controls of the chemical composition of groundwater from alluvial aquifers in the 414 Wanaka and Wakatipu basins, Central Otago, New Zealand. Hydrogeol. J, 6, 264-281.

Ruden, F. (2007). The discovery of a regional Neogene aquifer in coastal Tanzania. Coastal aquifers: Challenges and solutions, 1, 363-372.

Rygaard, M., Binning, P.J. and Albrechtsen, H.J. (2011). Increasing urban water self-sufficiency: New era, new challenges', Journal of Environmental Management, vol. 92, no. 1, pp. 185-194.

Sagnak, C. (1991). Groundwater pollution originated from Geological formation: Example of Konya-Çumra-Karapinar plain with GIS Application. Department of Geotechnical Services DSI, Ankara, Turkey.

Sanchez Martos, F., Pulido Bosch, A. and Calaforra, Jm. (1999). Hydrogeochemical processes in an arid region of Europe (Almeria, SE Spain). Applied Geochemistry, 14, 735-745.

Seckler, D., Molden, D. and Barker, R. (1998b). Water Scarcity in the Twenty-first Century. International Water Management Institute, Colombo, Sri Lanka.

Seckler, D.W., Amarasinghe, U., Molden, D., de Silva, R. and Barker, R. (1998a). World Water Demand and Supply, 1990–2025: Scenarios and Issues. Research Report 19, International Water Management Institute, Colombo, Sri Lanka.

Seward, P., Xu, Y. and Brendonck., L. (2006). Sustainable groundwater use, the capture principle, and adaptive management, Water SA, 32(4), 473–482.

Shingwela, E. (2009). Site selection for establishing new water pipeline for Dar es Salaam City from Rufiji River Tanzania. MSc. Thesis**,** Carinthia University, Austria, 75pp.

Sophocleous, M. (1997). Managing water resources systems: why "safe yield" is not sustainable. Ground Water, 35(4): 561.

Sophocleous, M. (2000): From safe yield to sustainable development of water resources: The Kansas experience, Journal of Hydrology, 235, 27–43.

Starpoint Software (1996). Infinite Extent: Aquifer pumping test analysis software version 3.2 User's Guide, Starpoint Software Inc.

Stavric, V. (2004). Aquifer overexploitation and groundwater mining. BALWOIS, Ohrid, Republic of Macedonia. http://balwois.com/balwois/administration/full_paper/ffp-458.pdf

Stuyfzand, P.J. (1986). A new hydrogeochemical classification of water types: principles and application to the coastal dunes aquifer system of the Netherlands. Proceedings 9th Salt Water Intrusion Meeting (SWIM), Delft (The Netherlands), 641-656.

Stuyfzand, P.J. (1993). Hydrochemistry and hydrology of the coastal dune area of the Western Netherlands. PhD dissertation, Free University (VU), Amsterdam, 90-74741-01-0: 366 pp.

Taylor, M.J. (2009). Report on the Ushirombo mineral exploration property of Tanzanian Royalty Exploration Corporation in the Bukombe district, Shinyanga region of the United Republic of Tanzania, East Africa. NI 43-101 Report.

Theis, C.V. (1935). The relationship between the lowering of the piezometric surface and the rate and duration of discharge of a well using groundwater storage. Am. Geophys. Union Trans. 16, pp. 519–524.

Theis, C.V., Brown, R. H. and Meyer, R.R. (1963). Estimating the transmissivity of aquifers from specific capacity of wells. In: Bental, R. (Ed.), Methods of determining permeability, transmissivity, and drawdown. U.S. Geological Survey Water Supply Paper, 1536(I): 331-340.

Thomas, H. E. (1955). Water rights in areas of groundwater mining: Washington: U.S. Dept. of the Interior, Geological Survey, Circular 347, 10 p.

Thomasson, H. J., Olmstead, F. H. and LeRoux, E. R. (1960). Geology, water resources, and usable ground water storage capacity of part of Solano County, CA: U.S. Geological Survey Water Supply Paper, 1464, 693 p.

Thornthwaite, C.W. and Mather, J.R. (1955). The water balance. Laboratory of Climatology, No. 8, Centerton New Jersey.

Thornthwaite, C.W. and Mather, J.R. (1957). Instructions and tables for computing potential evapotranspiration and the water balance. Publications in Climatology, Vol.10 (3), pp.183 – 311 Laboratory of Climatology, Drexel Institute of Technology, Centerton, New Jersey, USA.

Thornthwaite, C.W. (1948). An approach toward a rational classification of climate. Geographical Review, 38: 55–94.

Todd, D. K. (1959). Groundwater hydrology. John Wiley and Sons, New York, 336 p.

Todd, D.K. (1974). Salt-water intrusion and its control. Journal of American Water Works Association, 66(3): 180-187.

Todd, D.K. (1980). Groundwater Hydrology, 2nd Ed. John Wiley, New York: 535 pp.

Tong, S.T.Y. and Chen, W. (2002). Modeling the Relationship Between Land Use and Surface Water Quality. Journal of Environmental Management 66(4):377-393.

UNEP (2003). Environmentally sound technologies for sustainable development. International Environmental Technology Centre. Division of Technology, Industry and Economics United Nations Environment Programme.

UN-HABITAT (2007). Evaluation report: Water for African Cities (WAC), Dar es Salaam Project.
www.unhabitat.org/.../5415_26650_7541_WAC_Dar_es_Salaam_Project_Evaluation_Report8-2007.doc

UN-HABITAT (2008). State of the World's Cities- Harmonious Cities.

UN-HABITAT (2009). Regional and Technical Cooperation Division, Tanzania, Dar es Salaam City Profile.

UN-HABITAT (2010a). Citywide Action Plan for Upgrading Unplanned and Unserviced Settlements in Dar es Salaam, Tanzania.

UN-HABITAT (2010b). Informal settlements and finance in Dar es Salaam, Tanzania.

URT: United Republic of Tanzania (2007). Development of a Future Water Source for Dar es Salaam: Pre-design and Environment Report, Phase 2. Ministry of Water and Irrigation.

URT: United Republic of Tanzania (1990). National Health Policy, Ministry of Health,

URT: United Republic of Tanzania (1997). National Environmental Policy, Vice President Office, Dar es Salaam.

URT: United Republic of Tanzania (2000). National Human Settlements Development Policy, Dar es Salaam, Tanzania

URT: United Republic of Tanzania (2002a). National Water Policy (NAWAPO), Ministry of Water and Livestock Development, Dodoma.

URT: United Republic of Tanzania (2002b). Population and Housing Census, National Bureau of Statistics, Dar es Salaam.

URT: United Republic of Tanzania (2003): Integration of Population Variables in Development Planning United Nations Population Fund and Demographic Training Unit, Dar es Salaam.

URT: United Republic of Tanzania (2004a). Dar es Salaam City Profile, Dar es Salaam City Council, Tanzania.

URT: United Republic of Tanzania (2004b). National Environmental Management Act (EMA), Vice President Office, Dar es Salaam.

URT: United Republic of Tanzania (2009). Water Resources Management Act, Ministry of Water and Irrigation, Dar es Salaam.

US Salinity Laboratory Staff (1954). Diagnosis and improvement of saline and alkali soils", in US Department of Agricultural Hand Book, vol. 60, p. 147, US Department of Agricultural

Van Camp, M. and Walraevens, K. (2009). Recovery scenarios for deep over-exploited aquifers with limited recharge: Methodology and application to an aquifer in Belgium. Environmental Geology. 56(8). p.1505-1516.

Van Camp, M., Mjemah, I.C., Al Farrah, N. and Walraevens, K. (2013). Modeling approaches and strategies for data-scarce aquifers: example of the Dar es Salaam aquifer in Tanzania. Hydrogeology Journal 21:341-356. DOI 10.1007/s10040-012-0908-5.

Vandenbohede, A. (2008). Visual MOCDENS3D: visualisation and processing software for MOCDENS3D, a 3D density dependent groundwater flow and solute transport model. User Manual v2008a. Research Unit Groundwater Modelling, Ghent University.

Vandenbohede, A., Courtens, C., Lebbe, L. and De Breuck, W. (2010). Fresh-salt water distribution in the Central Belgian coastal pain: an update. Geologica Belgica 11/3: 163-169.

Vander Leeden, F., Troise, F. and Todd, D. (1990). The Water Encyclopaedia, 2nd edition, Lewis Publishers.

Vâzquez-suné, E. (2003). Urban groundwater: Barcelona City Case Study. PhD Thesis, Universitat Politecnica De Katalunya, Barcelona, Spain, 134 pp.

Vengosh, A., Spivack, A.J., Artzi, Y., Ayalon, A. (1999). Geochemical and boron, strontium, and oxygen isotopic constraints on the origin of the salinity in groundwater from the Mediterranean coast of Israel. Water Resour. Res. 35, 1877–1894.

Voudouris, K., Kazakis, N., Polemio, M. and Kareklas, K. (2010). Assessment of intrinsic vulnerability using the DRASTIC model and GIS in the Kiti aquifer, Cyprus. Europian Water 30: 13-24.

Wadie AST, Abduljalil GADS (2010). Assessment of hydrochemical quality of groundwater under some Urban areas within Sana'a Secretariat. Ecletica quimica. www.SCIELO.BR/EQ. 35(1): 77-84.

Walraevens, K. and Van Camp, M. (2005). Advances in understanding natural groundwater quality controls in coastal aquifers. 18 Salt Water Intrusion Meeting (SWIM). Cartagena 2004, Spain, 451-460.

Walraevens, K. (1990). Hydrogeology and hydrochemistry of the Ledo-Paniselian semi-confined aquifer in East- and West-Flanders. Acad. Analecta 52(3): 11-66.

Walraevens, K., Lebbe, L., De Ceukelaire, M., Van Houtte, E. and De Breuck, W. (1993). Influence on groundwater quality of the Paleozoic Brabant Massif in Belgium due to overexploitation. Groundwater Quality Management (Proceedings of the GQM 93 Conference held at Tallinn, September 1993). IAHS Publ. no. 220, 1994.

Walraevens, K., Lebbe, L., Van Camp, M., Angius,, Serra, M.A., Vacca,, A., Massidda, R. and De Breuck, W. (1993). Salt/fresh-water flow and distribution in a cross-section at Oostduinkerke (western coastal plain of Belgium). Study and modelling of Saltwater Intrusion into Aquifers. Proceedings 12th Saltwater Intrusion.

Walraevens, K., Martens, K. and De Breuck, W. (1994). Salt/fresh-water distribution in the polder area near Axel (Zealand-Flanders). Proceedings of the 13th Salt-Water Intrusion Meeting, Cagliari (1994). pp. 321 – 334

Ward, A. D. and Trimble, S. W. (2004). Environmental Hydrology, 2nd edn, CRC Press LLC, Florida.

Weight, W.D. (2008). Hydrogeology field manual. Second edition, The McGraw-Hill Compagnies Inc. 751 p.

Westenbroek, S.M., Kelson, V.A., Dripps, W.R., Hunt, R.J., and Bradbury, K.R. (2010). Modified Thornthwaite-Mather Soil-Water-Balance code for estimating groundwater recharge: US. Geological Survey Techniques and Methods 6- A31, 60 p.

Whitehead, E., Hiscock, K.M. and and Dennis, P.F. (1999). Evidence for sewage contamination of the Sherwood Sandstone aquifer beneath Liverpool, UK. In: Impacts of Urban Growth on Surface Water and Groundwater Quality (Proceedings of IUGG 99 Symposium HS5, Birmingham, July 1999). IAHS Publ. no. 259, 1999.

Wigley, T.M.L. and Plummer, L.N. (1976). Mixing of carbonate waters. Geochim. Cosmochim. Acta 40:989-995.

Winter, T.C., Harvey, J.W., Franke, O.L. and Alley, W.M. (1998). Ground water and surface

Wolock, D.M., and McCabe, G.J. (1999). Effects of potential climatic change on annual runoff in the conterminous United States: Journal of the American Water Resources Association, v. 35, p. 1,341–1,350.

World Health Organization (2004). Guidelines for Drinking Water Quality, Vol. 1. Recommendations (3rd edn). WHO, Geneva.

Yanda, P. Z. and Munishi, P. K. T. (2007). Hydrologic and land use/cover change analysis forthe Ruvu River (Uluguru) and Sigi River (East Usambara) watersheds. http://easternarc.or.tz/downloads/Uluguru/Final%20Report%20Revised_20_04_2007.pdf

Zaporozec, A. (ed.) (2004). Groundwater contamination inventory: a methodological guide with a model legend for groundwater contamination inventory and risk maps. IHP-VI, series on groundwater, 2. UNESCO, Paris, France.

Zheng, C. (1996). MT3D-A modular three-dimensional transport model for simulation of advection, dispersion and chemical reactions of contaminants in groundwater systems: S.S. Papadopulos & Associates, Inc., Bethesda, Md.

Zohdy, A.A.R., Eaton, G.P. and Mabey, D.R. (1974). Application of surface geophysics to groundwater investigation, U.S.G.S. Techniques of Water-Resource Investigation, Book 2.